

**Alteration of organic geochemical molecular composition by the
process of petroleum expulsion**

Dissertation

zur Erlangung des Doktorgrades

der Mathematisch-Naturwissenschaftlichen Fakultät

der Christian-Albrechts-Universität zu Kiel

vorgelegt von:

Florian Maximilian Panitz

Kiel, 2019

Erster Gutacher: Prof. Dr. Lorenz Schwark

Zweiter Gutachter: Dr. Michael Erdmann

Tag der mündlichen Prüfung: 15.11.2019

Alteration of organic geochemical molecular composition by the process of petroleum expulsion

Florian Maximilian Panitz

Abstract

A series consisting of 134 samples from six different North Sea exploration wells (15/3-8, 15/3-9 T2, 24/9-1, 34/7-23 A, 34/7-23 S, 34/10-36) penetrating organic-rich shales of the Upper Jurassic Draupne (Kimmeridge Clay) Formation and coals and shales of the Middle Jurassic Hugin Formation has been analyzed for bulk properties and molecular composition in order to investigate molecular fractionation effects associated with petroleum expulsion. In addition, a geochromatographic retardation experiment including a natural Draupne source rock column, a tracer stock solution, and a synthetic oil has been performed to examine the interaction of selected organic compounds, i.e. phenanthrenes, dibenzofuran, dibenzothiophenes, and carbazoles, with minerals and organic material. Petroleum expulsion can be considered as the final stage of primary migration, which describes the initial phase of petroleum migration in a petroleum system that is generally defined as the discharge of oil and gas from a source rock into adjacent reservoir rocks. In the past, this process has been associated with substantial molecular fractionation between polar-rich source bitumen and low polar, hydrocarbon-enriched oils. However, to date, the processes operating during petroleum expulsion and especially the expulsion behavior of individual organic compounds remain highly elusive. In particular, it is largely unknown to what extent petroleum expulsion affects well-established, organic geochemical maturity (e.g. the methylphenanthrene index, MPI 1) or migration parameters (e.g. the benzocarbazoles ratio, BC ratio), which play major roles in the petroleum exploration business. The evaluation of the large dataset showed that samples from well 15/3-8, 15/3-9 T2 and 24/9-1 are thermally mature and therefore suitable to investigate catagenic expulsion fractionation. By contrast, analysis of source rock material from well 34/7-23 A, 34/7-23 S and 34/10-36 revealed a significantly lower thermal maturity. Consequently, samples from these immature sections were unsuitable to study the process of expulsion fractionation but allowed to characterize the source rock in a state prior to expulsion. A compositional comparison between source bitumens and reservoir extracts for oils from the wells 15/3-8, 24/9-1, 34/7-23 S and the Draupne scenario of well 15/3-9 T2 points to an origin from nearby source intervals and hence to a genetic

Abstract

relationship. This is strongly supported by the intra-formational character of the reservoir beds, which largely rules out contribution of different sources. On the other hand, the molecular composition of reservoir petroleum from well 34/7-23 A and from the Hugin scenario of well 15/3-9 T2 indicates an external source, most likely mature parts of the Draupne Formation. Characterization of the organic facies has shown that most Draupne source rock samples contain a mixed type II/III kerogen typical of marine environments. By contrast, source rock material from the Hugin Formation was found to contain greater proportions of land plant material, whereby the coals were likely deposited in coastal swamps and the shales in marine transitional environments. Except for the Hugin section, facies variations were demonstrated to be small within individual expulsion scenarios. Based on the maturity assessment, the oil-source rock correlation, and the palaeofacies characterization, the following natural sections turned out to be suitable for the investigation of petroleum expulsion: both profiles from well 15/3-8, the Draupne section of well 15/3-9 T2, and both scenarios from well 24/9-1. The results of this study indicate that molecular fractionation of organic compounds during petroleum expulsion essentially depends on the polarity and the molecular shape of the expelled components. The most important molecular fractionation effects associated with petroleum expulsion that were observed in this study comprise: (1) a preferential expulsion of phenanthrenes relative to dibenzothio-phenes, dibenzofurans, and carbazoles, (2) a preferential release of alkylated compared to non-alkylated aromatics, and (3) a preferential expulsion of nitrogen-shielded vs. nitrogen-exposed C₂ carbazoles. Furthermore, there are indications of a faster migration of *n*-relative to *iso*-alkanes. In addition, the results of this work suggest a robust applicability of the methylphenanthrene index as source rock maturity indicator, since a good correlation between the thermal maturity and the MPI 1 was observed throughout the study area. However, a comparison between the MPI 1 values of source rock bitumen and adjacent reservoir extracts suggests that the MPI 1 values of the reservoir units are influenced by petroleum expulsion in that methylated phenanthrenes are preferentially expelled compared to phenanthrenes, which seems to cause higher MPI 1 values in the reservoir. Individual methylphen-anthrene isomers do, however, not appear to be sensitive to expulsion fractionation. The same applies to the methylated dibenzothiophenes and the methylated carbazoles. Conversely, close examination of the distribution of methyl dibenzofurans indicates a preferential migration of the 2- and the 3- over the 1- and the 4-isomer. A fractionation of aliphatic biomarkers, i.e. steranes

Abstract

or hopanes, was not observed. Also, no clear expulsion-related trends were documented for the benzocarbazoles ratio, which seems to be a very complex parameter that depends on various factors and therefore needs to be applied with caution. However, the results of this work indicate that the benzocarbazoles ratio of a source rock is at least partially controlled by the thermal maturity, as suggested by a relatively good correlation with the Rock-Eval T_{max} and the triaromatic steroid ratio. The data obtained from the geochromato-graphic experiment principally support the findings from the natural scenarios. In particular, phenanthrenes were found to be more efficiently released than dibenzothiophenes, dibenzofuran and carbazoles, the partially nitrogen-shielded 1,4-dimethylcarbazole was shown to migrate slightly faster than its nitrogen-exposed counterparts, and carbazoles were most strongly retained by the source rock column. Interestingly, the experiment additionally points to a preferential migration of benzo[a]- relative to benzo[c]carbazole, but yet in substantially lower absolute quantities. With respect to natural systems, this implies that the first oil expelled from a source rock has a very high benzocarbazoles ratio, which then decreases over time. Concerning the Hugin case scenario, this study was able to show that both coals and shales do, despite sufficient maturity, either not or only marginally contribute to the reservoir petroleum in the surrounding sandstones and that expulsion has probably occurred primarily via a volatile gas/condensate phase, as has been suggested previously. A special feature of source rock samples from the Hugin Formation is the enrichment of benzo[b]carbazole, which could have application potential for oil-source rock correlations.

Keywords: Expulsion; Primary migration; Molecular fractionation; Geochromatography; Organic geochemistry; Draupne (Kimmeridge Clay) Formation; Hugin Formation

Alteration of organic geochemical molecular composition by the process of petroleum expulsion

Florian Maximilian Panitz

Zusammenfassung

Eine Serie bestehend aus 134 Proben aus sechs verschiedenen, sowohl organikangereicherte Tonsteine der oberjurassischen Draupne (Kimmeridge Clay) Formation, als auch organikreiche Tonsteine und Kohlen der mitteljurassischen Hugin Formation enthaltenden Nordsee-Explorationsbohrungen (15/3-8, 15/3-9 T2, 24/9-1, 34/7-23 A, 34/7-23 S, 34/10-36) wurde zur Untersuchung molekularer Fraktionierungseffekte bei der Petroleumexpulsion bulk- und molekulargeochemisch analysiert. Daneben wurde unter Verwendung einer natürlichen Erdölmuttergesteinssäule der Draupne Formation, einer Tracer-Stammlösung und eines synthetischen Öls ein geochromatographisches Retardationsexperiment durchgeführt, um die Interaktion ausgewählter organischer Verbindungen, speziell Phenanthrenen, Dibenzofuran, Dibenzothiophenen und Carbazolen mit Mineralien und organischem Material zu untersuchen. Petroleumexpulsion kann als finaler Prozess der primären Migration, des ersten, initialen Migrationsstadiums von Petroleum innerhalb eines Petroleumsystems verstanden werden und bezeichnet generell die Abgabe von Öl und Gas aus einem Mutter- in angrenzende Speichergesteine. In der Vergangenheit wurde dieser Prozess oft mit signifikanter molekularer Fraktionierung zwischen Muttergesteinsbitumen und Rohölen in Verbindung gebracht, wobei das Bitumen des Muttergesteins für gewöhnlich mit hochpolaren Komponenten angereichert ist und Öle im Vergleich dazu einen erheblichen Anteil gering polarer Kohlenwasserstoffe enthalten. Trotz allem sind die während der Expulsion ablaufenden Prozesse und dabei insbesondere das Verhalten einzelner organischer Verbindungen bis heute nur unzureichend verstanden. Weitestgehend unbekannt ist vor allem, inwieweit sich der Expulsionsprozess auf etablierte organisch-geochemische Maturitäts- (z.B. den Methylphenanthrenindex, MPI 1) oder Migrationsparameter (z.B. das Benzocarbazol-verhältnis, BC Ratio) auswirkt, die eine wesentliche Rolle bei der Petroleum-exploration spielen. Die Auswertung des umfangreichen Datensatzes ergab, dass Proben aus den Bohrungen 15/3-8, 15/3-9 T2 und 24/9-1 thermisch reif und daher geeignet sind um katagenetische Expulsionsfraktionierungsprozesse zu untersuchen. Im Gegensatz

Zusammenfassung

dazu offenbarte die Analyse des Muttergesteinsmaterials aus den Bohrungen 34/7-23 A, 34/7-23 S und 34/10-36 eine deutlich geringere thermische Reife. Aufgrund dessen erlaubten Proben aus diesen unreifen Sektionen nicht die Untersuchung von expulsionsgesteuerten Fraktionierungsprozessen, gestatteten jedoch die Charakterisierung des Muttergesteins vor Einsetzen der Expulsion. Ein kompositioneller Vergleich von Muttergesteinsbitumen und Reservoirextrakten deutet für Öle aus den Bohrungen 15/3-8, 24/9-1, 34/7-23 S sowie dem Draupne Szenario aus Bohrung 15/3-9 T2 jeweils auf eine Herkunft aus nahen Muttergesteinsintervallen hin. Dies wird maßgeblich durch den intraformationellen Charakter der Reservoirintervalle bekräftigt, welcher Beiträge anderer Quellen nahezu ausschließt. Demgegenüber muss bei Reservoirölen aus Bohrung 34/7-23 A und dem Hugin Szenario aus Bohrung 15/3-9 T2 von einer fremden Quelle ausgegangen werden, wobei die molekulare Zusammensetzung einen Ursprung aus der Draupne Formation nahelegt. Eine Charakterisierung der organischen Fazies zeigte, dass der überwiegende Teil des Muttergesteinsmaterials der Draupne Formation ein Typ II/III Kerogen gemischten Ursprungs enthält, was typisch für marine Ablagerungsräume ist. Dagegen wurden für Muttergesteine aus der Hugin Formation größere Mengen an Landpflanzenmaterial nachgewiesen, wobei die Kohlen höchstwahrscheinlich in Küstensümpfen und die organikreichen Tonsteine in einer marinen Übergangs-umgebung abgelagert wurden. Abgesehen vom Hugin Profil konnte gezeigt werden, dass Faziesvariationen innerhalb einzelner Expulsionsszenarien nur gering ausgeprägt sind. Basierend auf der Abschätzung der thermischen Reife, der Öl-Muttergesteinskorrelation und der Paläofaziescharakterisierung stellten sich folgende Szenarien als geeignet für die Untersuchung von Petroleumexpulsion heraus: beide Profile aus Bohrung 15/3-8, die Draupne Sektion aus Bohrung 15/3-9 T2 und beide Szenarien aus Bohrung 24/9-1. Die Ergebnisse dieser Arbeit deuten darauf hin, dass die molekulare Fraktionierung organischer Verbindungen bei der Petroleumexpulsion in besonderer Weise von der Gestalt und der Polarität der abgegebenen Verbindungen abhängt. Die wichtigsten im Rahmen dieser Studie beobachteten molekularen Fraktionierungseffekte bei der Petroleumexpulsion umfassen: (1) die bevorzugte Abgabe von Phenanthrenen im Verhältnis zu Dibenzothiophenen, Dibenzofuranen und Carbazolen, (2) eine präferenzielle Abgabe von alkylierten gegenüber nicht-alkylierten Aromaten und (3) eine bevorzugte Expulsion stickstoff-abgeschirmter vs. stickstoffexposierter C₂-alkylierter Carbazole. Zusätzlich gibt es Anzeichen einer schnelleren Migration

Zusammenfassung

kettenförmiger gegenüber isoprenoidaler Alkane. Die Ergebnisse dieser Studie deuten ferner auf eine robuste Anwendbarkeit des Methylphenanthrenindex als Reifeindikator für Erdölmuttergesteine hin, da über das gesamte untersuchte Gebiet hinweg eine gute Korrelation zwischen thermischer Reife und MPI 1 beobachtet wurde. Dennoch legt ein Vergleich der MPI 1 Werte in Mutter- und angrenzenden Speichergesteinen den Schluss nahe, dass die MPI 1 Werte innerhalb der Reservoireinheiten dahingehend einem Expulsionseinfluss unterliegen, als dass methylierte Phenanthrene bevorzugt abgegeben werden, was letztlich zu höheren MPI 1 Werten im Reservoir führt. Einzelne Methylphenanthren-isomere scheinen dabei allerdings nicht fraktioniert zu werden. Dies gilt gleichermaßen für methylierte Dibenzothiophene und methylierte Carbazole. Im Gegensatz dazu deutet eine genaue Untersuchung der Methyl-dibenzofuranverteilung auf eine präferenzielle Abgabe des 2- und 3- gegenüber des 1- und 4-Isomers hin. Eine Fraktionierung aliphatischer Biomarker, speziell Sterane und Hopane, wurde nicht beobachtet. Ebenso wurden keine eindeutig expulsiionsgesteuerten Trends für das Benzocarbazolverhältnis dokumentiert, welches ein sehr komplexer Parameter zu sein scheint, der von vielen Faktoren abhängt und daher mit Vorsicht angewendet werden sollte. Die Ergebnisse dieser Arbeit deuten dennoch darauf hin, dass das Benzocarbazolverhältnis zumindest teilweise von der thermischen Reife kontrolliert wird, was durch gute Korrelationen mit dem Rock-Eval T_{max} Parameter und dem triaromatischen Steroidverhältnis deutlich wird. Die Daten des geochromato-graphischen Experiments unterstützen im Allgemeinen die Ergebnisse aus den natürlichen Szenarien. Im Speziellen konnte gezeigt werden, dass Phenanthrene effizienter abgegeben wurden als Dibenzothiophene, Dibenzofuran und Carbazole, das partiell stickstoffabgeschirmte 1,4-Dimethylcarbazol schneller migrierte als seine stickstoffexponierten Analoge und Carbazole am stärksten von der Muttergesteins-säule zurückgehalten wurden. Interessanterweise weist das Experiment darüber hinaus auf eine bevorzugte Migration von Benzo[a]- relativ zu Benzo[c]carbazol hin, allerdings in substantiell geringeren absoluten Mengen. Hinsichtlich natürlicher Systeme impliziert dies, dass das erste Öl, das von einem Muttergestein abgegeben wird, ein sehr hohes Benzocarbazolverhältnis aufweist, welches dann im Laufe der Zeit abnimmt. In Bezug auf das Hugin Szenario konnte in dieser Studie gezeigt werden, dass sowohl die Tonsteine, als auch die Kohlen trotz hinreichender Maturität entweder gar nicht, oder nur sehr marginal zum Reservoirpetroleum innerhalb der umliegenden Sandsteine beitragen und die

Zusammenfassung

Expulsion aus den Muttergesteins-intervallen wahrscheinlich primär, wie auch teilweise in früheren Studien vorgeschlagen, in einer volatilen Gas-/Kondensatphase erfolgt. Ein besonderes Merkmal von Muttergesteinsproben der Hugin Formation ist die Anreicherung von Benzo[b]carbazol, welches Anwendungspotenzial für Öl-Muttergesteinskorrelationen besitzen könnte.

Schlüsselworte: Expulsion; Primäre Migration; Molekulare Fraktionierung; Geochromatographie; Organische Geochemie; Draupne (Kimmeridge Clay) Formation; Hugin Formation

Acknowledgements

Acknowledgements

First, I would like to express my gratitude to my primary supervisor Prof. Dr. Lorenz Schwark for his excellent guidance through the complex field of petroleum geology. In many fruitful discussions, he helped analysing the data and always provided promising interpretation approaches. Moreover, he carefully checked the measurement qualities and therefore guaranteed both data reliability, as well as an efficient working progress. Without his great support, this work would not have been possible.

Equinor (formerly Statoil) is gratefully acknowledged for funding this project, thus offering me the opportunity for this PhD thesis. In particular, I am indebted to my co-supervisor Dr. Michael Erdmann and Dr. Ulrich Berner for their great support and guidance throughout the study, as well as the warm welcome in Norway. Moreover, I would also like to thank Marcel Naumann, Arne Steen and Aaron Howie for their assistance concerning sample collection and treatment, as well as detailed information on the lab equipment.

Dr. Martin Stockhausen is thanked for both his assistance during the sample preparation, as well as his technical support. From his experience and knowledge in petroleum geology this work benefitted a lot.

I would also like to thankfully acknowledge Dr. Wolfgang Ruebsam, who guided me through the first steps as a scientific researcher and always had time to answer both administrative and geochemical questions. Furthermore, he is thanked for detailed instructions on the technical equipment, which helped to avoid analytical mistakes and therefore led to an efficient laboratory phase.

Nicole Haeuser is gratefully mentioned for her assistance in the laboratory, particularly concerning the group-type separation of crude oils and source rock extracts via solid-phase extraction.

The technical staff, i.e. Petra Fiedler, Vanessa Grote, Eyke Kirchhof and Marieke Muijsers are mentioned for their great support in the laboratory. Through their supervision of the analytical devices and many advices and instructions, they also contributed to a high degree to this study.

Lastly, Dr. Bernhard Krooss from the RWTH Aachen University is thankfully acknowledged for conducting most of the Rock-Eval pyrolysis measurements.

This thesis is dedicated to my parents, considering their incredible support in altogether nine years of studying, including three years of PhD thesis writing. Thank you!

Table of Contents

Table of Contents

| | |
|---|------|
| Abstract | ii |
| Zusammenfassung | iii |
| Acknowledgements | iv |
| Table of Contents | v |
| List of Tables | vi |
| List of Figures | vii |
| Abbreviations | viii |
| 1. Introduction | 1 |
| 2. Petroleum system dynamics | 3 |
| 2.1 Source rock deposition..... | 3 |
| 2.2 Types of kerogen..... | 5 |
| 2.2.1 Type I kerogen..... | 5 |
| 2.2.2 Type II kerogen..... | 6 |
| 2.2.3 Type III kerogen..... | 6 |
| 2.2.4 Type IV kerogen..... | 7 |
| 2.3 Kerogen maturation stages..... | 7 |
| 2.3.1 Diagenesis..... | 7 |
| 2.3.2 Catagenesis..... | 8 |
| 2.3.3 Metagenesis..... | 9 |
| 2.4 Petroleum movement and accumulation..... | 9 |
| 2.4.1 Expulsion and primary migration..... | 9 |
| 2.4.2 Secondary migration..... | 10 |
| 2.4.3 Tertiary migration..... | 11 |
| 2.4.4 Petroleum entrapment..... | 11 |
| 3. Primary migration – state of the art | 13 |
| 3.1 Potential mechanisms..... | 13 |
| 3.1.1 Primary migration via separate petroleum droplets..... | 14 |
| 3.1.2 Primary migration via organic aggregates..... | 14 |
| 3.1.3 Primary migration via dissolution of compounds in pore water..... | 15 |
| 3.1.4 Primary migration via molecular diffusion..... | 16 |
| 3.1.5 Primary migration via hydrocarbon bulk phase flow..... | 17 |
| 3.1.6 Primary migration as interrelated event sequence..... | 19 |
| 3.2 Factors that influence primary migration..... | 20 |
| 3.2.1 Pressure regime..... | 20 |
| 3.2.2 Temperature..... | 21 |
| 3.2.3 Source rock composition..... | 22 |
| 3.2.4 Porosity and permeability..... | 23 |
| 3.2.5 Phase transitions..... | 26 |
| 3.3 Reasons for molecular redistribution..... | 27 |
| 3.3.1 Diffusive fractionation..... | 28 |
| 3.3.2 Natural chromatography..... | 30 |
| 3.3.3 Kerogen absorption..... | 32 |
| 3.4 Expulsion-related compositional changes..... | 35 |
| 3.4.1 General considerations: types of natural crude oils..... | 36 |
| 3.4.2 Gross compositional differences between source bitumens and crude oils..... | 38 |
| 3.4.3 Principal expulsion sequences..... | 40 |
| 3.4.4 Expulsion trends in natural systems..... | 41 |
| 3.4.5 Experimentally simulated fractionation effects..... | 48 |
| 3.5 Kinetic concepts..... | 54 |
| 3.6 Experimental approaches..... | 56 |
| 3.6.1 Open system pyrolysis..... | 57 |
| 3.6.2 Anhydrous closed system pyrolysis..... | 59 |

Table of Contents

| | |
|--|------------|
| 3.6.3 Hydrous closed system pyrolysis..... | 60 |
| 3.6.4 Experimental investigation of molecular diffusion..... | 61 |
| 3.6.5 Column flow experiments..... | 61 |
| 3.6.6 Solvent-swelling experiments..... | 62 |
| 4. Geological background of the study area | 63 |
| 4.1 Evolution of North-West Europe..... | 63 |
| 4.1.1 Palaeozoic..... | 63 |
| 4.1.2 Mesozoic..... | 65 |
| 4.1.3 Cenozoic..... | 65 |
| 4.2 Geology of the North Sea region..... | 66 |
| 4.3 Depositional history and source rock characteristics of the Draupne (Kimmeridge Clay) Formation..... | 69 |
| 4.3.1 Distribution and stratigraphy..... | 69 |
| 4.3.2 Source rock characteristics..... | 71 |
| 4.3.3 Palaeoenvironment..... | 73 |
| 4.4 The Hugin Formation..... | 74 |
| 4.4.1 Distribution and stratigraphy..... | 74 |
| 4.4.2 Source rock characteristics..... | 76 |
| 4.4.3 Palaeoenvironment..... | 77 |
| 5. Material and methods | 80 |
| 5.1 Sample set..... | 81 |
| 5.1.1 Well 15/3-8..... | 81 |
| 5.1.2 Well 15/3-9 T2: Draupne section..... | 82 |
| 5.1.3 Well 15/3-9 T2: Hugin section..... | 82 |
| 5.1.4 Well 24/9-1..... | 82 |
| 5.1.5 Well 34/7-23 A..... | 83 |
| 5.1.6 Well 34/7-23 S..... | 83 |
| 5.1.7 Well 34/10-36..... | 83 |
| 5.2 Bulk geochemistry..... | 84 |
| 5.2.1 Elemental analysis..... | 84 |
| 5.2.2 Rock-Eval pyrolysis..... | 85 |
| 5.3 Molecular geochemistry..... | 85 |
| 5.3.1 Bitumen extraction..... | 85 |
| 5.3.2 Extract separation..... | 91 |
| 5.3.3 Gas chromatography-mass spectrometry..... | 92 |
| 5.4 Geochromatographic experiment..... | 94 |
| 6. Results | 97 |
| 6.1 Natural expulsion scenarios..... | 97 |
| 6.1.1 Bulk data..... | 97 |
| 6.1.2 Molecular geochemical data..... | 118 |
| 6.2 Geochromatographic experiment..... | 164 |
| 6.2.1 Compound elution..... | 164 |
| 6.2.2 Mass balance approach..... | 166 |
| 7. Discussion | 169 |
| 7.1 Bulk characterization..... | 169 |
| 7.2 Palaeofacies characterization..... | 175 |
| 7.2.1 Type of organic material..... | 175 |
| 7.2.2 Depositional conditions..... | 180 |
| 7.3 Maturity assessment..... | 184 |
| 7.4 Oil-source rock correlation..... | 190 |
| 7.5 Implications from the geochromatographic experiment..... | 202 |
| 7.6 Identifying fractionation effects in the natural case scenarios..... | 207 |
| 7.6.1 System C ₁ phenanthrenes-C ₁ dibenzofurans-C ₁ dibenzothiophenes..... | 207 |
| 7.6.2 System C ₁ phenanthrenes-C ₁ carbazoles-C ₁ dibenzothiophenes..... | 209 |

Table of Contents

| | |
|---|------------|
| 7.6.3 System C ₁ carbazoles-C ₁ dibenzofurans-C ₁ dibenzothiophenes..... | 210 |
| 7.6.4 Distribution of methylated dibenzofurans..... | 212 |
| 7.6.5 Distribution of methylated carbazoles..... | 213 |
| 7.6.6 Nitrogen-shielded vs. nitrogen-exposed C ₂ carbazoles..... | 215 |
| 7.6.7 Higher vs. lower alkylated compounds and implications for the MPI 1..... | 217 |
| 7.6.8 Fractionation effects among aliphatics..... | 223 |
| 7.7 Influences on the benzocarbazoles ratio..... | 230 |
| 8. Conclusions and further research | 235 |
| References | 239 |
| Appendix | 248 |
| (1) Data..... | 248 |
| Bulk data..... | 248 |
| Molecular geochemical data (I): Saturates..... | 252 |
| Molecular geochemical data (II): Aromatics..... | 256 |
| Molecular geochemical data (III): Carbazoles..... | 260 |
| Molecular geochemical data (IV): Ternary systems I..... | 261 |
| Molecular geochemical data (IV): Ternary systems II..... | 265 |
| (2) Analytics overview..... | 269 |
| Eidesstattliche Erklärung | 271 |

List of Tables

List of Tables

| | |
|--|-----|
| <u>Table 1</u> : Organofacies types (modified after Pepper and Corvi, 1995a)..... | 23 |
| <u>Table 2</u> : Sample list..... | 86 |
| <u>Table 3</u> : List of standards..... | 93 |
| <u>Table 4</u> : Composition of the tracer solution (in DCM)..... | 96 |
| <u>Table 5</u> : Peak identification..... | 123 |
| <u>Table 6</u> : Tracer concentrations over time..... | 165 |
| <u>Table 7</u> : Mass balance results..... | 168 |
| <u>Table 8</u> : Transformation ratio constants (after Banerjee et al., 1998)..... | 178 |

Appendix

List of Figures

List of Figures

| | |
|--|-----|
| <u>Figure 1</u> : Pathways for marine carbon recycling and transfer (from Harvey, 2006)..... | 4 |
| <u>Figure 2</u> : Kerogen formation scheme (modified after Killops and Killops, 2005)..... | 5 |
| <u>Figure 3</u> : Kerogen maturation stages and hydrocarbon products (modified after Peters et al., 2005a)..... | 8 |
| <u>Figure 4</u> : Potential primary migration mechanisms (after Tissot and Welte, 1984)..... | 14 |
| <u>Figure 5</u> : Consecutive sequence of primary migration (modified after Mann et al., 1997)..... | 19 |
| <u>Figure 6</u> : Elements of sediment compaction (modified after Bjørlykke, 2015a)..... | 24 |
| <u>Figure 7</u> : Concept of geochromatographic separation (modified after Krooss et al., 1991)..... | 31 |
| <u>Figure 8</u> : Solubility parameter δ for different compounds (modified after Ritter, 2003)..... | 34 |
| <u>Figure 9</u> : Classification scheme of crude oils (modified after Selley, 1998)..... | 37 |
| <u>Figure 10</u> : Composition of source bitumens vs. crude oils for different lithologies (modified after Tissot and Welte, 1984)..... | 39 |
| <u>Figure 11</u> : Map of the Norwegian Continental Shelf (modified after the Norwegian Petroleum Directorate, 2016)..... | 64 |
| <u>Figure 12</u> : Illustration of the North Sea triple rift system (modified after Zanella et al., 2003)..... | 67 |
| <u>Figure 13</u> : Structural configuration of the North Sea (modified after Faleide et al., 2015)..... | 68 |
| <u>Figure 14</u> : Upper Jurassic stratigraphy of the study area (modified after Fraser et al., 2003)..... | 70 |
| <u>Figure 15</u> : Mesozoic-Cenozoic stratigraphy of the South Viking Graben (modified after Folkestad and Satur, 2008)..... | 75 |
| <u>Figure 16</u> : Potential formation model of the Middle Jurassic Hugin 2 unit (from Folkestad and Satur, 2008)..... | 78 |
| <u>Figure 17</u> : Lab work scheme..... | 80 |
| <u>Figure 18</u> : Geological map of the Norwegian North Sea (modified after the Norwegian Petroleum Directorate, 2017)..... | 84 |
| <u>Figure 19</u> : Lithostratigraphic columns of the investigated expulsion scenarios..... | 90 |
| <u>Figure 20</u> : Extraction cell structures..... | 92 |
| <u>Figure 21</u> : Evolution of the extract yield of sample K012448..... | 93 |
| <u>Figure 22</u> : Setup of the geochromatographic retardation experiment..... | 95 |
| <u>Figure 23</u> : Expulsion scenario A: bulk geochemical depth profiles..... | 98 |
| <u>Figure 24</u> : Expulsion scenario B: bulk geochemical depth profiles..... | 101 |
| <u>Figure 25</u> : Expulsion scenario C: bulk geochemical depth profiles..... | 103 |
| <u>Figure 26</u> : Expulsion scenario D: bulk geochemical depth profiles..... | 105 |
| <u>Figure 27</u> : Expulsion scenario E: bulk geochemical depth profiles..... | 108 |
| <u>Figure 28</u> : Expulsion scenario F: bulk geochemical depth profiles..... | 110 |
| <u>Figure 29</u> : Expulsion scenario G: bulk geochemical depth profiles..... | 112 |
| <u>Figure 30</u> : Expulsion scenario H: bulk geochemical depth profiles..... | 114 |
| <u>Figure 31</u> : Expulsion scenario I: bulk geochemical depth profiles..... | 117 |
| <u>Figure 32</u> : Expulsion scenario A: Selected molecular geochemical depth profiles..... | 120 |
| <u>Figure 33</u> : Expulsion scenario A: Exemplary ion chromatograms..... | 121 |
| <u>Figure 34</u> : Expulsion scenario B: Selected molecular geochemical depth profiles..... | 126 |

List of Figures

| | |
|--|-----|
| <u>Figure 35</u> : Expulsion scenario B: Exemplary ion chromatograms..... | 127 |
| <u>Figure 36</u> : Expulsion scenario C: Selected molecular geochemical depth profiles..... | 131 |
| <u>Figure 37</u> : Expulsion scenario C: Exemplary ion chromatograms..... | 132 |
| <u>Figure 38</u> : Expulsion scenario D: Selected molecular geochemical depth profiles..... | 135 |
| <u>Figure 39</u> : Expulsion scenario D: Exemplary ion chromatograms..... | 136 |
| <u>Figure 40</u> : Expulsion scenario E: Selected molecular geochemical depth profiles..... | 141 |
| <u>Figure 41</u> : Expulsion scenario E: Exemplary ion chromatograms..... | 142 |
| <u>Figure 42</u> : Expulsion scenario F: Selected molecular geochemical depth profiles..... | 145 |
| <u>Figure 43</u> : Expulsion scenario F: Exemplary ion chromatograms..... | 146 |
| <u>Figure 44</u> : Expulsion scenario G: Selected molecular geochemical depth profiles..... | 150 |
| <u>Figure 45</u> : Expulsion scenario G: Exemplary ion chromatograms..... | 151 |
| <u>Figure 46</u> : Expulsion scenario H: Selected molecular geochemical depth profiles..... | 155 |
| <u>Figure 47</u> : Expulsion scenario H: Exemplary ion chromatograms..... | 156 |
| <u>Figure 48</u> : Expulsion scenario I: Selected molecular geochemical depth profiles..... | 160 |
| <u>Figure 49</u> : Expulsion scenario I: Exemplary ion chromatograms..... | 161 |
| <u>Figure 50</u> : Geochromatographic experiment: concentrations of tracer molecules over time..... | 164 |
| <u>Figure 51</u> : Geochromatographic experiment: recovery rates of the tracer molecules..... | 167 |
| <u>Figure 52</u> : Total organic carbon vs. extract yield for the investigated expulsion scenarios..... | 170 |
| <u>Figure 53</u> : Total organic carbon vs. production index..... | 171 |
| <u>Figure 54</u> : Total organic carbon vs. the Rock-Eval S ₁ | 172 |
| <u>Figure 55</u> : Rock-Eval S ₂ vs. Rock-Eval S ₁ | 174 |
| <u>Figure 56</u> : Oxygen index vs. hydrogen index..... | 176 |
| <u>Figure 57</u> : T _{max} vs. hydrogen index..... | 177 |
| <u>Figure 58</u> : Ternary system C ₂₇ -C ₂₈ -C ₂₉ 5 α ,14 β ,17 β (H)-steranes (20S+20R) for the source rock samples..... | 179 |
| <u>Figure 59</u> : Pristane/phytane vs. dibenzothiophene/phenanthrene..... | 181 |
| <u>Figure 60</u> : Total organic carbon vs. total sulfur..... | 182 |
| <u>Figure 61</u> : Phytane/ <i>n</i> C ₁₈ vs. pristane/ <i>n</i> C ₁₇ | 183 |
| <u>Figure 62</u> : T _{max} -MPI 1 maturity correlation..... | 185 |
| <u>Figure 63</u> : T _{max} -C ₃₀ diahopane ratio maturity correlation..... | 186 |
| <u>Figure 64</u> : T _{max} - $\beta\beta/(\beta\beta+\alpha\alpha)$ C ₂₉ steranes maturity correlation..... | 188 |
| <u>Figure 65</u> : T _{max} -TA(I)/TA(I + II) maturity correlation..... | 189 |
| <u>Figure 66</u> : 22S/(22S+22R) C ₃₂ $\alpha\beta$ hopanes vs. 20S/(20S+20R) C ₂₉ $\alpha\alpha\alpha$ steranes..... | 190 |
| <u>Figure 67</u> : Ternary system C ₂₇ -C ₂₈ -C ₂₉ 5 α ,14 β ,17 β (H)-steranes (20S+20R) for all samples..... | 191 |
| <u>Figure 68</u> : C ₂₇ diasteranes/C ₂₉ regular steranes vs. the steranes/hopanes ratio..... | 192 |
| <u>Figure 69</u> : Ternary system showing the relative distributions of methylphenanthrenes..... | 195 |
| <u>Figure 70</u> : Ternary system showing the relative distributions of methyl dibenzothiophenes..... | 197 |
| <u>Figure 71</u> : $\beta\beta/(\beta\beta+\alpha\alpha)$ C ₂₉ steranes vs. the C ₃₀ diahopane ratio..... | 199 |
| <u>Figure 72</u> : Geochromatographic experiment: ternary system showing the relative distributions of C ₂ carbazoles, dimethyldibenzothiophenes, and methylphenanthrenes..... | 203 |
| <u>Figure 73</u> : Geochromatographic experiment: Ternary diagram showing the relative distributions of C ₂ carbazoles, dimethyldibenzothiophenes, and 2-ethyldibenzofuran..... | 204 |

List of Figures

| | |
|---|-----|
| <u>Figure 74</u> : Geochromatographic experiment: evolution of the benzocarbazoles ratio over time..... | 205 |
| <u>Figure 75</u> : Geochromatographic experiment: evolution of the 9-/1-methylphenanthrene ratio over time..... | 206 |
| <u>Figure 76</u> : Ternary system C ₁ phenanthrenes-C ₁ dibenzofurans-C ₁ dibenzothiophenes..... | 208 |
| <u>Figure 77</u> : Ternary system C ₁ phenanthrenes-C ₁ carbazoles-C ₁ dibenzothiophenes..... | 210 |
| <u>Figure 78</u> : Ternary system C ₁ carbazoles-C ₁ dibenzofurans-C ₁ dibenzothiophenes..... | 211 |
| <u>Figure 79</u> : Ternary system showing the relative distributions of methyl dibenzofurans..... | 213 |
| <u>Figure 80</u> : Ternary system showing the relative distributions of methyl carbazoles..... | 214 |
| <u>Figure 81</u> : Ternary system 1,8-dimethylcarbazole-2,7-dimethylcarbazole-1,3-dimethylcarbazole..... | 216 |
| <u>Figure 82</u> : Methylphenanthrene index vs. the $\beta\beta/(\beta\beta+\alpha\alpha)$ C ₂₉ sterane ratio..... | 219 |
| <u>Figure 83</u> : (2+3-methylphenanthrene)/(1+9-methylphenanthrene) vs. the $\beta\beta/(\beta\beta+\alpha\alpha)$ C ₂₉ sterane ratio..... | 221 |
| <u>Figure 84</u> : T _{max} vs. the (2+3-methylphenanthrene)/(1+9-methylphenanthrene) ratio..... | 222 |
| <u>Figure 85</u> : C ₃₁ /C ₃₂ homohopanes vs. 22S/(22S+22R) C ₃₂ hopanes..... | 224 |
| <u>Figure 86</u> : $\beta\beta/(\beta\beta+\alpha\alpha)$ vs. 20S/(20S+20R) C ₂₉ steranes..... | 226 |
| <u>Figure 87</u> : C ₂₇ diasteranes/C ₂₉ regular steranes vs. the $\beta\beta/(\beta\beta+\alpha\alpha)$ C ₂₉ sterane ratio..... | 227 |
| <u>Figure 88</u> : $\beta\beta/(\beta\beta+\alpha\alpha)$ C ₂₉ steranes vs. the ratio between the C ₂₇ and the C ₂₉ $\alpha\beta\beta$ steranes..... | 228 |
| <u>Figure 89</u> : Ternary diagram showing the relative distributions of benzocarbazoles..... | 231 |
| <u>Figure 90</u> : T _{max} -benzocarbazoles ratio maturity correlation..... | 232 |
| <u>Figure 91</u> : TA(I)/TA(I + II)-benzocarbazoles ratio maturity correlation..... | 233 |

Abbreviations

Abbreviations

ASE= Accelerated Solvent Extraction
BC ratio= Benzocarbazoles Ratio
CAMP= Central Atlantic Magmatic Province
Carb= Carbazole
CNS= Elemental Analysis
DBF= Dibenzofuran
DBT= Dibenzothiophene
DCM= Dichloromethane
DOM= Dissolved Organic Material
GC-MS= Gas Chromatography-Mass Spectrometry
HC= Hydrocarbons
HI= Hydrogen Index
HPLC= High Performance Liquid Chromatography
MD= Measured Depth
MDR= Methyl dibenzothiophene Ratio
MeOH= Methanol
MPI 1= Methylphenanthrene Index
MSSV= Microscale Sealed Vessel Pyrolysis
NCS= Norwegian Continental Shelf
NPD= Norwegian Petroleum Directorate
NSO= Heteroatomic Compounds
OI= Oxygen Index
OM= Organic Material
OSI= Oil Saturation Index
Ph= Phytane
Phen= Phenanthrene
PI= Production Index
POM= Particulate Organic Material
Pr= Pristane
R_o= Vitrinite Reflectance
RSFP= Reservoir Source Fractionation Parameter
SIM= Selected Ion Monitoring
SPE= Solid-Phase Extraction
TC= Total Carbon
THGP= Total Hydrocarbon Generation Potential
TIC= Total Inorganic Carbon
Tm= Trisnorhopane
TN= Total Nitrogen
TOC= Total Organic Carbon
TR= Transformation Ratio
Ts= Trisnorneohopane
TS= Total Sulfur
TVD= True Vertical Depth

1. Introduction

Since the Industrial Revolution, the significance of fossil fuels considerably increased as the world's energy demand began to rise severely. Still, coal, gas and oil account for much of the global energy consumption each year and will at least remain important until the end of this century. Hence, to guarantee energy supply in the nearest future, especially considering a rapidly growing world population, research on and exploration of petroleum systems is essential to provide resources for future generations. According to Peters et al. (2005a), petroleum is a conventional term referring to solid, liquid and gaseous materials predominantly composed of carbon and hydrogen. Natural petroleum systems comprise a source rock, a place where petroleum is generated from organic matter by pressure and temperature, a carrier bed, which represents the interval between source and reservoir rock and, lastly, a trap structure consisting of a reservoir rock and a sealing, impermeable cap rock. In sedimentary rocks, organic material generally occurs in three forms, (1) bitumen, (2) kerogen, and (3) hydrocarbon gases (e.g. Tissot and Welte, 1984; Killips and Killips, 2005; Peters et al., 2005a). While bitumen represents either solid or liquid hydrocarbon deposits soluble in organic solvents (e.g. Tissot and Welte, 1984; Killips and Killips, 2005), kerogen is defined as macromolecular, polymer-like organic matter insoluble in nonoxidizing acids, organic solvents and water (e.g. Behar and Vandenbroucke, 1987; Larter and Horsfield, 1993). Principally, sedimentary organic molecules can be subdivided into bio- and geomarkers. While biomarkers are geochemical fossils structurally related to biological precursors (e.g. Killips and Killips, 2005; Peters et al., 2005a), geomarkers, on the other hand, represent non-source related molecular remains with no clear linkage to living organisms. In the last century, pioneer work and technical advances in chromatography, mass spectro-metry and pyrolysis techniques provided the opportunity to study organic material on a molecular level, hence opening up the possibility to identify and investigate such marker molecules and the processes determining their chemical and physical properties. Over time, research led to extensive knowledge about petroleum generation, accumulation and flow in the subsurface, ultimately leading to the discovery of new, exploitable reservoirs. For example, much effort has been put into the modelling of petroleum systems (e.g. Behar et al., 1992; Pepper and Corvi, 1995a, b; Stainforth, 2009), the understanding of petroleum movement from source rocks into reservoirs (secondary migration) (e.g. Li et al., 1998; Leythaeuser et al., 2000), and the correlation of oils and source rocks (e.g.

1. Introduction

Dow, 1974; Zhang et al., 2000). However, the flow of petroleum within a source rock (primary migration), including the processes operating during the discharge into adjacent carrier beds (expulsion) received comparatively little interest. This is surprising, considering the fact that such data are essential for basin modelling and petroleum exploration. Indeed, previous studies on expulsion and primary migration have revealed striking compositional differences between source bitumens (polar-rich) and crude oils (hydrocarbon-rich) (e.g. Mackenzie et al., 1983; Leythaeuser et al., 1984a, 1988a, b). This study aims to provide further insights into molecular fractionation effects associated with petroleum expulsion. Therefore, 134 samples representing nine different natural expulsion scenarios were collected from six conventional exploration wells (15/3-8, 15/3-9 T2, 24/9-1, 34/7-23 A, 34/7-23 S, 34/10-36) penetrating organic-rich shales and adjacent sandstones of the Upper Jurassic Draupne (Kimmeridge Clay) Formation and coals of the Middle Jurassic Hugin Formation in exploration areas offshore Norway. In addition, a geochromatographic retardation experiment using powdered, pre-extracted Draupne source rock material from well 15/3-8, a tracer stock solution, and a synthetic oil was performed to investigate the interaction of selected, frequently occurring and routinely applied organic compounds with kerogen and minerals of an oil window-mature source rock column. Due to their significance in the petroleum exploration business, the focus of this work was laid on phenanthrenes, dibenzo-thiophenes (sulfur-substituted), dibenzofurans (oxygen-substituted) and carbazoles (nitrogen-substituted). As not part of the retardation experiment, aliphatics played a rather subordinate role. In the following, first petroleum systems in general and the state of knowledge on primary migration will be reviewed, after which the geological evolution of the study area and in particular the depositional histories and source rock characteristics of the Draupne and the Hugin Formation will be discussed in more detail. Thereafter, the reader will be introduced into the sample set and the analytical procedures that were applied to generate the data, as well as the concept and setup of the geochromatographic experiment. Then, after having presented the results of both the natural case scenarios and the geochromatographic experiment, the data will be discussed in order to identify the influence of primary migration on different organic compounds and compound groups in the context of facies variability and thermal maturity. The thesis ends with a conclusions section in which the most important findings will be summarized.

2. Petroleum system dynamics

The following chapter aims to summarize the most essential elements and processes of a petroleum system. By definition, a petroleum system comprises an organic-rich source rock, often referred to as “black shale” (Tourtelot, 1979), a porous, highly permeable reservoir rock, e.g. sandstone, and a sealing, impermeable cap rock, commonly a low porosity material like clay or salt, hindering migrating petroleum from further movement (e.g. Tissot and Welte, 1984; Selley, 1998; Peters et al., 2005a). Considering the regional geologic framework, petroleum may accumulate in a variety of different trap structures, consequently leading to multiple forms of oil and gas pools. The key elements of a petroleum system include, (i) the deposition of a source rock with a sufficient amount of organic material (OM), usually >0.5 wt.% total organic carbon (TOC) (Peters et al., 2005a and references therein), (ii) the successive thermal alteration of the organic material during sedimentary burial via the stages of diagenesis, catagenesis and metagenesis, (iii) the expulsion of petroleum from the source rock into adjacent carrier beds, and (iv) the subsequent migration into a reservoir rock.

2.1 Source rock deposition

The initial stage in the evolution of a petroleum system is the deposition of a source rock that has the potential to generate hydrocarbons in the subsurface. Therefore, it has to contain a sufficient amount of organic material, commonly associated with oxygen depleted depositional conditions since oxygen serves as the preferential terminal electron acceptor during biological decomposition (e.g. Didyk et al. 1978; Bordenave, 1993). The places most prone to the deposition of bituminous sediments involve large lakes, restricted basins and upwelling areas (Demaison and Moore, 1980). Most of today’s effective oil source rocks are of marine or, alternatively, lacustrine origin because both marine and lacustrine organisms are molecularly enriched in hydrogen compared to oxygen, favoring the release of paraffinic oil and gas during burial (Behar and Vandenbroucke, 1987). By contrast, terrigenous plants contain greater amounts of oxygenated functional groups and polyaromatic structures, leading to higher gas yields (Behar and Vandenbroucke, 1987). As illustrated in Fig. 1, the vast majority of the organic material in marine environments is produced in the photic zone through photosynthesis by primary producing organisms. Most biomass becomes, however, almost immediately recycled following the food chain,

2. Petroleum system dynamics

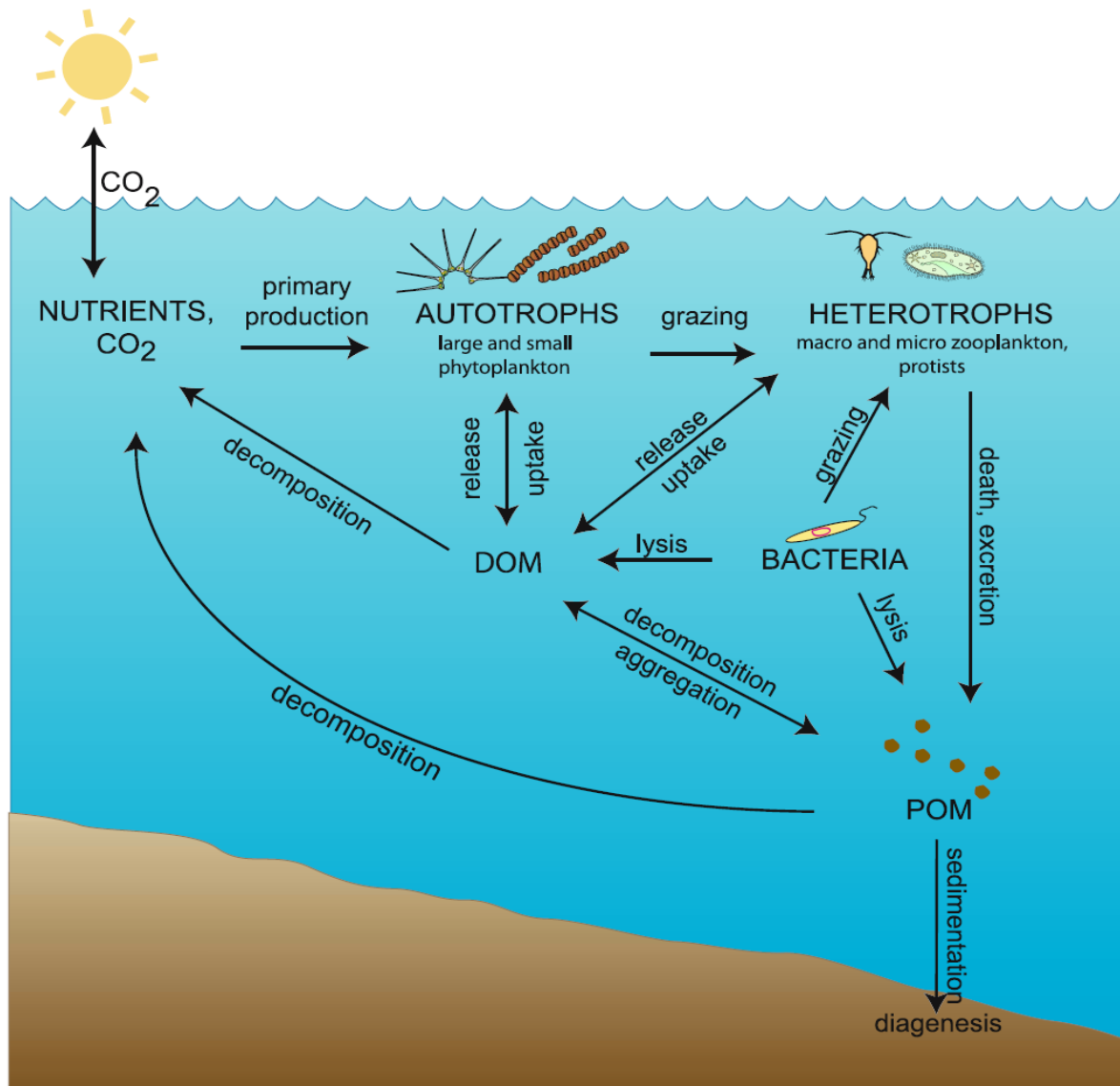


Fig. 1. Schematic pathways for marine carbon recycling and transfer (from Harvey, 2006). The formation of a petroleum source rock requires the deposition of a sufficient amount of organic material, usually associated with oxygen-deficient depositional conditions facilitated by extensive biodegradation and poor water mass exchange. Deposited organic material afterwards passes through the diagenesis. Abbreviations: DOM= Dissolved Organic Material; POM= Particulate Organic Material.

hence causing nutrient remobilization. Nevertheless, some material is exported to the sea floor as organic detritus, usually via organic aggregates and fecal pellets. On its way down, the particulate organic material (POM) becomes progressively scavenged by oxygen-consuming microorganisms. After having reached the seafloor, diagenesis is initiated by progressive sedimentary burial, which is accompanied by increasing pressure and temperature. Following, for example, Tissot and Welte (1984) and Killips and Killips (2005), kerogen is during this stage successively formed via condensation of humic substances (Fig. 2). In addition, resistant biomacromolecules, sulphur-rich macromolecules, and low molecular weight biomolecules derived either from biomacromolecules or low molecular weight biomolecules contribute to the complex kerogen matrix, too (Killips and Killips, 2005).

2. Petroleum system dynamics

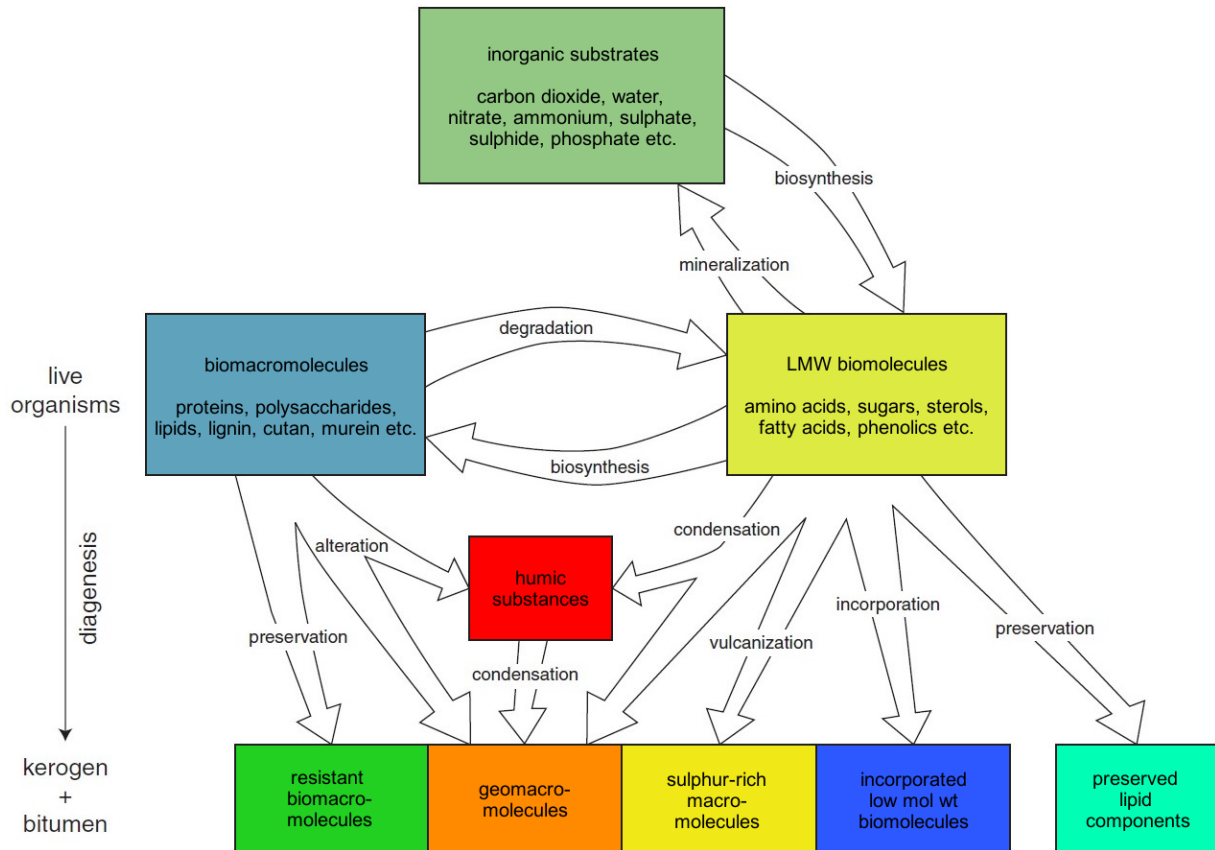


Fig. 2. Kerogen formation scheme (modified after Killops and Killops, 2005). Kerogen can be considered as a complex, macromolecular geopolymer comprising both biogenic precursor molecules and humic substances. It is formed during diagenesis, the earliest stage of kerogen maturation.

2.2 Types of kerogen

On the basis of elemental analysis and in consideration of both the depositional setting and the organic input, altogether four different kerogen types are differentiated. Those are, (i) type I kerogen, (ii) type II kerogen, (iii) type III kerogen, and (iv) type IV kerogen (e.g. Kubala et al., 2003; Killops and Killops, 2005; Peters et al., 2005a; Vandenbroucke and Largeau, 2007).

2.2.1 Type I kerogen

Type I kerogens comprise highly oil-prone material with high H/C and low O/C ratios of predominantly algal origin (e.g. Tissot and Welte, 1984; Killops and Killops, 2005; Peters et al., 2005a; Bjørlykke, 2015a). In general, type I kerogens are enriched in aliphatic structures and do not contain greater quantities of heteroatomic bonds and polyaromatic nuclei (Tissot and Welte, 1984; Killops and Killops, 2005). Usually, paraffinic dominate over cyclic compounds and oxygen occurs almost exclusively in ester bonds (Tissot and Welte, 1984). Type I kerogens are typical of lacustrine environments, which has been reported, for instance, for the Eocene Green River

2. Petroleum system dynamics

Formation, U.S.A. (e.g. Ingram et al., 1983; Horsfield et al., 1994). Although comparatively rare, lacustrine petroleum systems are in some parts of the world of high economic significance, e.g. in Brazil, China and Indonesia, as underlined by Pepper and Corvi (1995a). Type I kerogens are, however, not limited to freshwater settings, as stated by Bjørlykke (2015a).

2.2.2 Type II kerogen

Similar to type I kerogens, type II kerogens are characterized by high H/C and low O/C ratios, but largely originate from marine environments. Phytoplankton, zoo-plankton and bacteria are the major contributors to the organic material (e.g. Tissot and Welte, 1984; Peters et al., 2005a; Bjørlykke, 2015a). Usually, type II kerogens represent mixtures of both algal and terrigenous organic material in paralic marine depositional systems (Peters et al., 2005a). Heteroatomic bonds, polyaromatic nuclei and cyclic structures are more essential than in type I kerogens, but not as they are in type III kerogens (Tissot and Welte, 1984). The side chains in type II kerogens typically have less than 20 carbon atoms and are linked predominantly via esters and amides (Behar and Vandenbroucke, 1987). Type II kerogens containing between 8 and 14% of incorporated sulphur are termed type IIS kerogens, respectively (Orr, 1986). According to Peters et al. (2005a), black shales containing predominantly type II kerogens constitute most effective source rocks worldwide, hence making them economically extremely important. Prominent examples for type II organic-matter containing source rocks are the Lower Toarcian (Lower Jurassic) Posidonia Shale, Germany (e.g. Moldowan et al., 1986; Röhl et al., 2001), and the Upper Jurassic Kimmeridge Clay Formation, UK (e.g. Williams, 1986; Leythaeuser et al. 1988a; Ramanampisoa and Disnar, 1994).

2.2.3 Type III kerogen

In contrast to the kerogen types described above, type III kerogens display relatively low H/C and high O/C ratios attributable to a mostly terrigenous source (e.g. Tissot and Welte, 1984; Peters et al., 2005a). The kerogen is mainly composed of poly-aromatic domains, resulting in a low oil generation potential (Tissot and Welte, 1984; Behar and Vandenbroucke, 1987). Due to the formation of a microporous solid during burial, most liquid hydrocarbons generated from type III kerogens during catagenesis become trapped until they are cracked into gas, consequently making these kerogens

2. Petroleum system dynamics

predominantly gas-prone (Behar and Vandenbroucke, 1987). Tissot and Welte (1984) and Killips and Killips (2005) underscored that the structure of type III kerogen includes high amounts of oxygenated functional groups, particularly carboxylic acids and ketones, but, remarkably, virtually no ester bonds. Humic coals are typical examples of type III kerogens (e.g. Peters et al., 2005a).

2.2.4 Type IV kerogen

The last type, type IV kerogens, largely represent oxidized and reworked organic material from higher plants with very low oil generation potential (e.g. Killips and Killips, 2005; Peters et al., 2005a), which was first recognized by Harwood (1977) regarding dry-gas-generative Pennsylvanian coals. Type IV kerogens can be considered as “dead carbon” (Peters et al., 2005a).

2.3 Kerogen maturation stages

After deposition, the organic material passes through three steps of alteration, chronologically termed diagenesis, catagenesis and metagenesis (Fig. 3) (e.g. Tissot and Welte, 1984; Vandenbroucke et al., 1993; Rullkötter, 1993; Selley, 1998; Killips and Killips, 2005; Peters et al., 2005a). They will be briefly described in the following.

2.3.1 Diagenesis

Diagenesis represents the earliest stage of sedimentary burial characterized by low temperature alterations of the immature organic material and very scarce hydro-carbon generation (Vandenbroucke et al., 1993). The most essential processes affecting the organic material comprise the microbially-mediated loss of nitrogen, which is mainly released as ammonia (NH_3), the continuous loss of oxygen due to the cracking of heteroatomic bonds and successive, maturity induced structural transformations via highly complex reaction schemes (Behar and Vandenbroucke, 1987; Vandenbroucke et al., 1993). In environments marked by elevated rates of bacterial sulfate reduction, significant amounts of sulfur may become incorporated into the organic material forming organic sulfur compounds (OSCs) (Sinninghe Damsté et al., 1990; Schwark et al., 1998). Both, the end of the diagenesis and the beginning of the catagenesis are not strictly defined and strongly depend on the regional temperature regime and geological framework.

2. Petroleum system dynamics

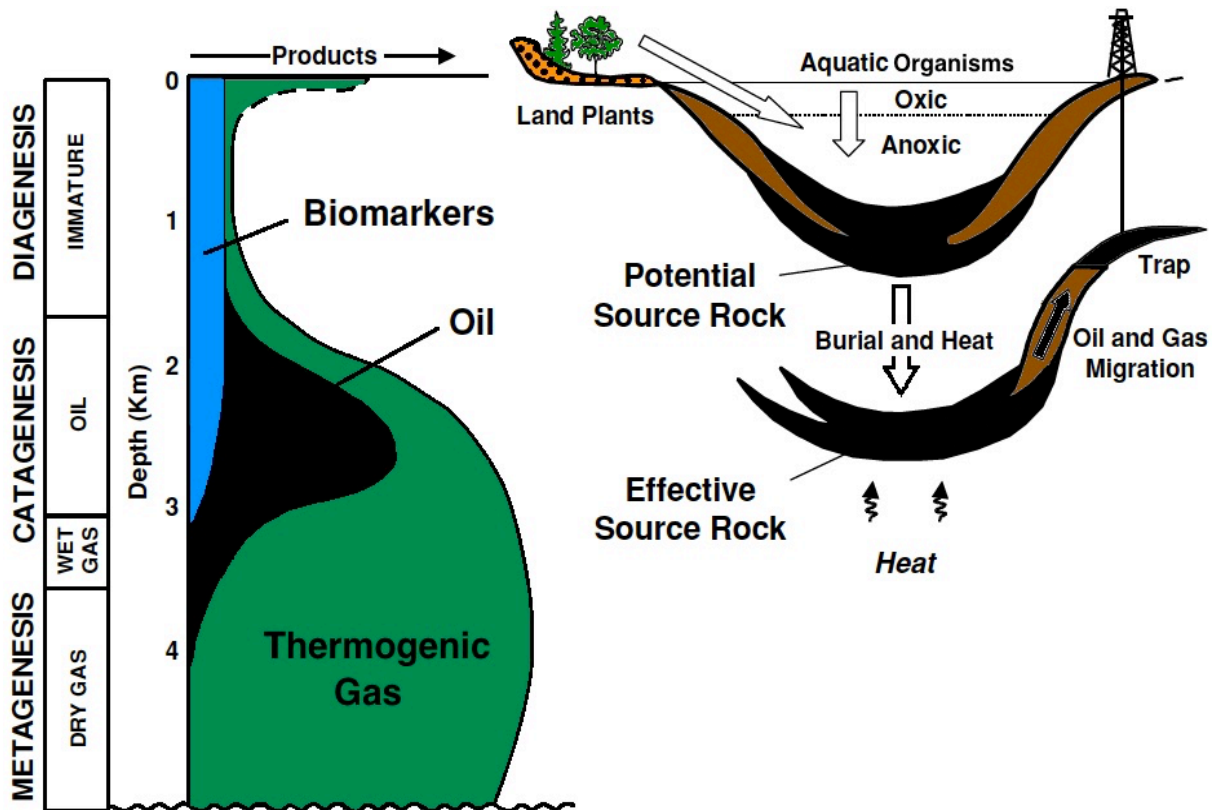


Fig. 3. Kerogen maturation stages and hydrocarbon products (modified after Peters et al., 2005a). During burial, organic material passes through three alteration stages, ultimately leading to the generation of oil and gas in the subsurface.

2.3.2 Catagenesis

The catagenesis kerogen maturation stage is characterized by the substantial loss of hydrogen, due mostly to thermal cracking of covalent C-C bonds (Vandenbroucke et al., 1993). Therefore, during catagenesis significant volumes of hydrocarbons are generated in the subsurface from the thermal breakdown of kerogen (e.g. Vandenbroucke et al., 1993; Rullkötter, 1993). Besides, Behar et al. (2008) and Behar et al. (2010) reported that considerable volumes of hydrocarbons may be generated by the release and subsequent cracking of heavy heteroatomic (NSO) compounds. Biodegradation is negligible since temperature has notably increased and microbial activity has thus become restricted. According to Killips and Killips (2005), the catagenesis stage is primarily characterized by thermally mediated rearrangements of the kerogen structure leading to a more compact and ordered configuration with minimal molecular stress. It is noteworthy that most hydrocarbons are generated in a relatively narrow temperature range from about 100 to 150 °C, a zone referred to as oil window (e.g. Quigley and Mackenzie, 1988; Killips and Killips, 2005), which roughly corresponds to a vitrinite reflectance (R_o) of around 0.5-0.7 to 1.3% (Tissot and Welte, 1984). The vitrinite reflectance is a conventional maturity parameter in

2. Petroleum system dynamics

petroleum geology that is based on the thermal alteration of vitrinite, a common maceral constituent of kerogens (e.g. Peters et al., 2005a). Since petroleum expulsion takes place during the catagenesis, it will be the main subject of interest in the following sections.

2.3.3 Metagenesis

The third and last step of kerogen maturation is associated with the generation of large volumes of gas, chiefly hydrogen, hydrogen sulfide, methane (CH₄), and nitrogen (N₂) through carbon structure rearrangement and cracking-recondensation reactions of aromatic heterocycles (Vandenbroucke et al., 1993). As a result, a highly carbon-enriched, polymer-like residuum is formed, the so-called pyrobitumen (Bernard et al., 2012a, b; Stockhausen, 2015). Vandenbroucke et al. (1993) pointed out that during the metagenesis stage the kerogen matrix is reorganizing towards a graphitic structure providing maximum compactness. In general, the metagenesis follows on the catagenesis stage at a vitrinite reflectance above ~2.0% (e.g. Tissot and Welte, 1984; Killops and Killops, 2005). Since most oil has already been expelled before during the catagenesis, gas is the main product generated throughout the metagenesis stage. Proceeding sedimentary burial leads to graphitization and metamorphism (Killops and Killops, 2005).

2.4 Petroleum movement and accumulation

After having described the process of petroleum formation, the next subchapter addresses its subsequent passage into a reservoir rock. Essentially, three types of petroleum migration can be differentiated. Those are in consecutive sequence: (1) primary, (2) secondary, and (3) tertiary migration (e.g. Killops and Killops, 2005). A summary and mathematical examination of the processes operating during petroleum movement is given by England et al. (1987).

2.4.1 Expulsion and primary migration

Among the three migration types, primary migration is of special importance for this study. It comprises both the flow of petroleum within the pore space of a fine-grained source rock, as well as the discharge of oil and gas from the source into adjacent carrier beds, a process that is termed expulsion (e.g. Tissot and Welte, 1984; Vandenbroucke, 1993; Mann et al., 1997; Selley, 1998; Peters et al., 2005a). As

2. Petroleum system dynamics

mentioned in the beginning, former research has provided clear evidence that petroleum expulsion is associated with substantial molecular fractionation between crude oils and source bitumens (Mackenzie et al., 1983; Sajgo et al., 1983; Leythaeuser et al., 1988a, b; Zhusheng et al., 1988; Price and Clayton, 1992; Kelemen et al., 2006a; Esemé et al., 2007; among others). Therefore, redistribution processes operating during primary migration principally have the potential to impact well-established, bio- and geomarker-based ratios, including traditional organic geochemical maturity and migration proxies. Consequently, knowing precisely the effects of primary migration on the molecular composition of petroleum is crucial for a successful hydrocarbon exploration. Since this work aims to provide further insights into expulsion-related fractionation effects, expulsion and primary migration will be discussed in more detail in an individual chapter (see 3.).

2.4.2 Secondary migration

The term secondary migration refers to the movement of petroleum from a source into a reservoir rock (e.g. Tissot and Welte, 1984; England et al., 1987; Selley, 1998; Killops and Killops, 2005; Peters et al., 2005a) and must be considered as two- or three-phase flow (Bjørlykke, 2015b). The principal driving force of secondary migration is buoyancy, counteracted by capillary forces dependent on pore throat radiuses (e.g. Tissot and Welte, 1984; Vandenbroucke, 1993; Bjørlykke, 2015b). Hence, for secondary petroleum migration into potential trap structures, buoyancy needs to exceed capillary forces. The buoyancy force can be expressed by the following equation (from Bjørlykke, 2015b):

$$F1 = (\rho_w - \rho_o) * H \quad (1)$$

$F1$ represents the buoyancy force, H the height of the petroleum column and ρ_w and ρ_o symbolize the densities of water and petroleum, respectively. Bjørlykke (2015b) pointed out that secondary migration preferentially proceeds along pathways with the lowest capillary resistance and especially where petroleum is concentrated. Since the saturation levels for oil and gas are crucial with respect to permeability, hydrocarbon flow is initiated particularly at places where petroleum reaches elevated concentrations and therefore permeability is increased and capillary pressure reduced. Furthermore, the pressure-driven hydrodynamic flow of water, provided it is not too strong and long-lasting, may also be critical (Tissot and Welte, 1984; Bonilla and Engel,

2. Petroleum system dynamics

1986). On the other hand, the strength of the counteracting capillary forces largely depends on the interplay between grain surface and fluids and can under assumption of normal water-wet conditions be described as (from Bjørlykke, 2015b):

$$F_2 = \frac{(2\gamma * \cos\phi)}{R} \quad (2)$$

In this equation, F_2 refers to the capillary resistance, γ to the interfacial tension between the petroleum and the water phase, ϕ to the wetting angle and R to the pore throat radius. As a consequence, the larger the pore throats, the weaker the capillary resistance. In petroleum systems, fluids and gases conventionally segregate due to density differences with gas over oil over water. To pass the pore throats, oil globules tend to deform elongately, thus leading to an increase in buoyant force (Tissot and Welte, 1984; Selley, 1998). The migration distance of petroleum is highly variable, ranging from several hundreds of meters to more than one hundred kilometers (e.g. Tissot and Welte, 1984; Vandenbroucke, 1993; Larter et al., 1996; Killops and Killops, 2005).

2.4.3 Tertiary migration

In the third migration type, previously accumulated petroleum moves from one trap to another or, instead, to a seep (e.g. Killops and Killops, 2005; Peters et al., 2005a). Thus, it is likely that this type of migration is facilitated by regional tectonic features, for example faults and fractures, which may provide pathways for migration. Killops and Killops (2005) pointed out that the densest petroleum compounds in a reservoir may become progressively displaced by less dense fluids, particularly gas, when passing the spill point, a process that can heavily alter hydrocarbon density sequences in reservoirs. Hence, tertiary migration is an essential mechanism operating in petroleum systems and should always be considered when dealing with petroleum movement in the subsurface.

2.4.4 Petroleum entrapment

Over geological timescales, petroleum may accumulate in pools underneath so-called cap rocks or seals, which are usually that fine-grained that capillary pressures exceed petroleum buoyancy forcing (e.g. Tissot and Welte, 1984; Selley, 1998; Killops and Killops, 2005). In general, a cap rock represents a virtually impermeable layer of rock

2. Petroleum system dynamics

preventing petroleum stored in an underlying reservoir from leakage and further migration (e.g. Peters et al., 2005a). Sedimentary rocks that are suitable as seals comprise particularly evaporites and shales (e.g. Grunau, 1987; Schlömer and Krooss, 1997). According to Tissot and Welte (1984), potential reservoir rocks typically exhibit porosities between 5 and 30%, thus making sandstones, siltstones and carbonates most suitable for accumulating hydrocarbons. Furthermore, the permeability of reservoir rocks should ideally vary between 1 and 1000 mD (Killops and Killops, 2005).

3. Primary migration – state of the art

3. Primary migration – state of the art

The flow of petroleum within and out of a source rock is called primary migration. Despite decades of research (e.g. Mackenzie et al., 1983; Tissot and Welte, 1984; Leythaeuser et al., 1984a, b; 1988a, b, c; Ungerer, 1990; Pepper and Corvi, 1995a, b; Selley, 1998; Esemé et al., 2006, 2007; Kelemen et al., 2006a, b; Stockhausen, 2015), it is still among the least understood processes operating in petroleum systems. Former studies have, however, revealed that primary migration, in particular the expulsion of hydrocarbons from a source rock into the pore space of a higher permeable secondary migration system, is accompanied by substantial molecular redistribution (Mackenzie et al. 1983; Sajgo et al., 1983; Leythaeuser et al., 1984a, b; 1988a, b, c; Lafargue et al. 1990; Li et al., 1997; Esemé et al., 2006, 2007; among others). The following chapter intends to review the current level of knowledge on expulsion and primary migration by summarizing, (i) the potential mechanisms that have been considered in the past by which generated petroleum compounds may be passed through the source rock, (ii) the most essential factors controlling primary migration and causing compositional change, (iii) the most prominent molecular redistribution effects that have been observed so far, (iv) the basic kinetic concepts established to model kerogen degradation and petroleum formation (generation and expulsion) during sedimentary burial, and (v) the principal experimental approaches developed to simulate organic matter maturation and primary migration in the subsurface.

3.1 Potential mechanisms

The first section of this chapter aims to briefly recapitulate the possible ways by which petroleum may migrate from its place of generation to adjacent reservoir rocks. A comprehensive overview of the potential mechanisms operating during primary migration can be found in Tissot and Welte (1984). The following subchapter gives a short summary based on the overview of these researchers. According to Tissot and Welte (1984), primary migration can principally take place in five different ways: (1) as separate petroleum bubbles or globules, (2) via colloidal and micellar solutions, (3) as molecular solution, (4) via molecular diffusion, and (5) as bulk petroleum phase (Fig. 4). Furthermore, these potential mechanisms can be grouped into two classes, whereby the first category significantly depends on the flow of pore waters and comprises the transport of petroleum compounds as bubbles or globules, via colloidal

3. Primary migration – state of the art

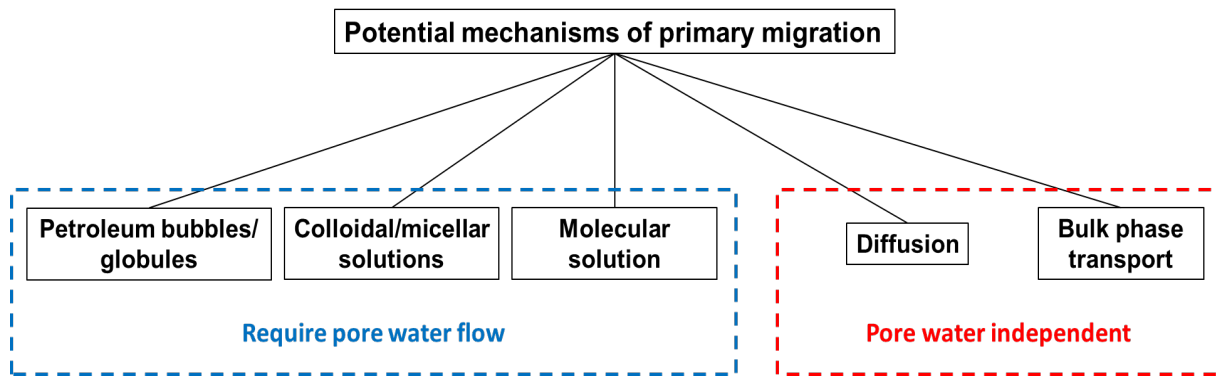


Fig. 4. Potential mechanisms of primary migration (after Tissot and Welte, 1984). Petroleum bulk phase transport can be considered as the most efficient form of primary migration. Note, however, that the predominant expulsion mode may vary from one source rock to another depending on local circumstances.

and micellar solution, and as molecular solution. By contrast, the second group of possible primary migration mechanisms is largely independent of pore water currents and consists of molecular diffusion and hydrocarbon bulk phase flow. Which mechanism potentially operates in an actively generating and expelling source rock strongly relies on local factors, meaning the predominant expulsion mechanism may vary from one source rock to another (e.g. Killops and Killops, 2005).

3.1.1 Primary migration via separate petroleum droplets

Following Tissot and Welte (1984), there is hypothetically the possibility that source rocks can expel petroleum compounds via separate, mostly elongated globules or bubbles, provided they can pass the small pore throats of the source rock and overcome the high capillary pressures. This way of expulsion is supposed to require an active pore water current but, however, considered as highly unlikely, even at later stages of thermal maturation when source rocks are typically pervaded by fractures (Tissot and Welte, 1984). Tissot and Welte (1984) argued that this is due primarily to the small pore diameters of commonly very fine grained, argillaceous source rocks and the extreme displacement pressures that would be needed to pass oil and gas as bubbles/globules through such narrow pore throats.

3.1.2 Primary migration via organic aggregates

Another possible variant of primary migration is the movement of petroleum compounds as colloidal and micellar aqueous solutions (Tissot and Welte, 1984; Selley, 1998 and references therein). Thereby, colloids symbolize macromolecular organic assemblages (10-10.000 Å) usually consisting either of identically structured compounds, or, alternatively, of a combination of smaller, differently configured

3. Primary migration – state of the art

components (Tissot and Welte, 1984). In addition to such colloids, Tissot and Welte (1984) stated that some petroleum components, particularly organic acids, may concentrate in so-called micelles, which represent organic accumulations composed predominantly of polar compounds with both hydrophobic and hydrophilic sites. Following their argumentation, colloids and micelles are, in principle, capable of mobilizing most compounds that frequently occur in crude oils, even if they are not soluble in water. Though, on the other hand, they presented several convincing reasons against colloids and micelles as the principal transport mechanism of petroleum during primary migration. First, it was underlined that these petroleum aggregates are often too large to pass the small pore throats of a source rock, a fact that effectively limits this expulsion mode to around 2000 m burial depth and therefore far below oil window pressures and temperatures. Second, it was argued that the concentration of amphiphilic compounds, especially that of organic acids, which can form micelles under subsurface conditions is significantly reduced at the beginning of catagenesis. Third, it was pointed out that organic acids are prone to react with calcium and magnesium cations under the formation of salts, a process that basically counteracts the formation of micelles. Furthermore, fourth and last, it was emphasized that, apart from the fact that some polar petroleum compounds may interact with reactive surfaces of clay minerals and are thus removed from the aqueous solution, clay minerals principally also have the potential to electrically repel micelles and thus hinder migration. Taking these arguments into account, Tissot and Welte (1984) concluded that primary migration via colloids/micelles in an aqueous solution is problematic for mature source rocks and can therefore practically be ruled out as the predominant mode of primary migration.

3.1.3 Primary migration via dissolution of compounds in pore water

Petroleum compounds are principally able to dissolve in and to be transported by pore water, whereby the relative solubility reduces with increasing number of carbon atoms and salinity, as well as decreasing temperature (Tissot and Welte, 1984 and references therein). The basic concept of this form of primary migration is that generated organic compounds dissolve in the pore water of a source rock and are subsequently transported towards adjacent carrier rocks via a compaction-induced water current. Therefore, a constant flow of pore water is, like for the mechanisms described before, a prerequisite for this mode of transport, too. According to Tissot and Welte (1984),

3. Primary migration – state of the art

there are, however, a number of arguments against this form of molecular solution as the major transport mechanism of organic compounds during primary migration. The most striking evidence against such a mode of primary migration is that natural crude oils are typically strongly enriched in paraffins, particularly *n*-alkanes, as will be described later (see 3.4), which is in strong contrast to the solubilities of these compounds in water (Tissot and Welte, 1984 and references therein). Based solely on the aqueous solubilities of petroleum compounds, one would expect a natural crude oil to be generally depleted in *n*- and *iso*-alkanes. On the other hand, following this idea, aromatic hydrocarbons and polar NSO compounds would occur in much higher abundances in crude oils than they actually do, considering the fact that these components are typically only low to moderately concentrated in unaltered, natural crudes (see 3.4). Consequently, following Tissot and Welte (1984), the movement of oil and gas via molecular solution in pore water is rather unlikely to represent the predominant transport mechanism of organic components during primary migration.

3.1.4 Primary migration via molecular diffusion

The fourth potential transport mechanism of oil and gas during primary migration is molecular diffusion (Tissot and Welte, 1984; Killips and Killips, 2005; among others). It is generally independent of the presence and flow of pore water and takes place chiefly along concentration gradients from areas of higher to areas of lower chemical potential (Tissot and Welte, 1984). Hence, generated petroleum compounds tend to diffuse away from the place of generation (high concentration) to areas of low concentration, i.e. organic-lean intervals, regardless of the spatial direction. Molecular diffusion has also been suggested as one major reason for compositional fractionation upon primary migration (see 3.3.1) (e.g. Stainforth and Reinders, 1990; Thomas and Clouse, 1990c). The diffusive transport of petroleum compounds is supposed to be most efficient over relatively short migration distances and, therefore, for example, of particular importance close to the edges of a source rock or near fractures, which may act as migration avenues. Concerning diffusively charged gas reservoirs, Tissot and Welte (1984) mentioned that the composition of hydrocarbon gases expelled from a source rock essentially depends on the concentration of these compounds at the time of generation, the diffusion rates of individual molecules, and, lastly, the diffusion distance and thus the thickness of the source rock. Although these aspects were mentioned with regard to the diffusion of gases from source rocks towards reservoirs,

3. Primary migration – state of the art

it is likely that the same factors need to be considered for the diffusive movement of liquid petroleum compounds, too, as subsequent research has provided evidence that bitumen can indeed diffuse through the source rock, particularly through the kerogen network (Stainforth and Reinders, 1990; Thomas and Clouse, 1990a, b, c). In their evaluation of the importance of the different possible primary migration mechanisms, Tissot and Welte (1984) concluded that molecular diffusion is indeed an important transport mechanism during primary migration, particularly for gases, but it does, however, probably not represent the principal form of mass transfer during primary migration, which is responsible for the formation of large oil and gas pools.

3.1.5 Primary migration via hydrocarbon bulk phase flow

Since all previously described possible primary migration mechanisms appear rather unlikely to account for the large number of oil and gas accumulations worldwide, the most likely form of primary migration is pressure-driven hydrocarbon bulk phase flow, as stated by several authors (e.g. Tissot and Welte, 1984; England et al., 1987; Killops and Killops, 2005; Ziegs et al., 2017). Essentially, in this variant of primary migration, generated petroleum compounds continuously accumulate in the pore space of a source rock and are subsequently transported to adjacent carrier beds under the influence of lithostatic pressure. Tissot and Welte (1984) accentuated that this process requires a minimum petroleum saturation of the pore space, a continuous generation of bitumen from the kerogen, low amounts of free pore water, and, lastly, sufficient load pressure, which is typically the case throughout the catagenesis kerogen maturation stage. Moreover, they emphasized that oil-wet particle surfaces can potentially reduce the petroleum saturation threshold that is necessary for discrete bulk phase transport. As a consequence, oil-wet surfaces may strongly facilitate primary migration and enable hydrocarbon bulk phase flow at relatively early stages of thermal maturation. Correspondingly, Killops and Killops (2005) mentioned that petroleum can only be effectively expelled from a source rock if sufficient hydrocarbons are generated from the kerogen and accumulate in the pore space, which usually contains only trace amounts of free pore water under catagenesis temperature and pressure conditions. According to Tissot and Welte (1984), primary migration via hydrocarbon bulk phase flow may generally proceed in two different ways. In the first variant, capillary pressures within the source rock are so high that the release of petroleum compounds into the pore space causes fracturing and ultimately drainage of the source rock. Following

3. Primary migration – state of the art

Tissot and Welte (1984), this scenario actually represents a discontinuous process consisting of a recurring sequence of five individual events: (1) pressure increase, (2) fracturing of the rock matrix, (3) decreasing pressure, (4) volume increase of the mobile phase, and (5) bulk flow. With respect to the second possible mode of discrete hydrocarbon phase movement, which can be considered as a continuous process, Tissot and Welte (1984) underscored that generated petroleum compounds are expelled without fracturing of the source rock. Following their argumentation, this form of bulk phase flow requires reduced capillary pressures, which may prevail, for example, in source rocks with wider pore throats or large, coherent networks of organic material. Similarly, Stainforth and Reinders (1990) suggested that the most prominent types of discrete hydrocarbon phase movement are on one hand focused flow along fractures, and, on the other hand, Darcy flow through the mineral matrix of a source rock. Regardless of which of these possible variants is eventually active, the moving petroleum can, though, be regarded as a discrete phase that passes the source rock (Tissot and Welte, 1984). Therefore, according to Tissot and Welte (1984), the petroleum current is very sensitive to geochromatographic interactions with the surrounding environment, which represents another possible fractionation mechanism of organic compounds during primary migration (see 3.3.2).

3.1.6 Primary migration as interrelated event sequence

Following Mann et al. (1997), it is most likely that primary migration is a process proceeding successively by, (1) petroleum generation from the kerogen, (2) molecular diffusion, either directly towards adjacent reservoirs or to internal migration avenues (e.g. fractures), (3) desorption from the kerogen and accumulation on the pore wall, and (4) aggregation into the pore space where petroleum bulk phase flow is primarily initiated by the pressure of the overburden load (Fig. 5). Thereby, according to Killops and Killops (2005), primary migration is closely linked to the saturation of adsorptive surfaces in a source rock and thus especially to the rate of petroleum generation. Note that it has also often been stated that petroleum generation and expulsion take place contemporaneously (e.g. Esemé et al., 2006 and references therein). Following this idea, it can be assumed that all individual

3. Primary migration – state of the art

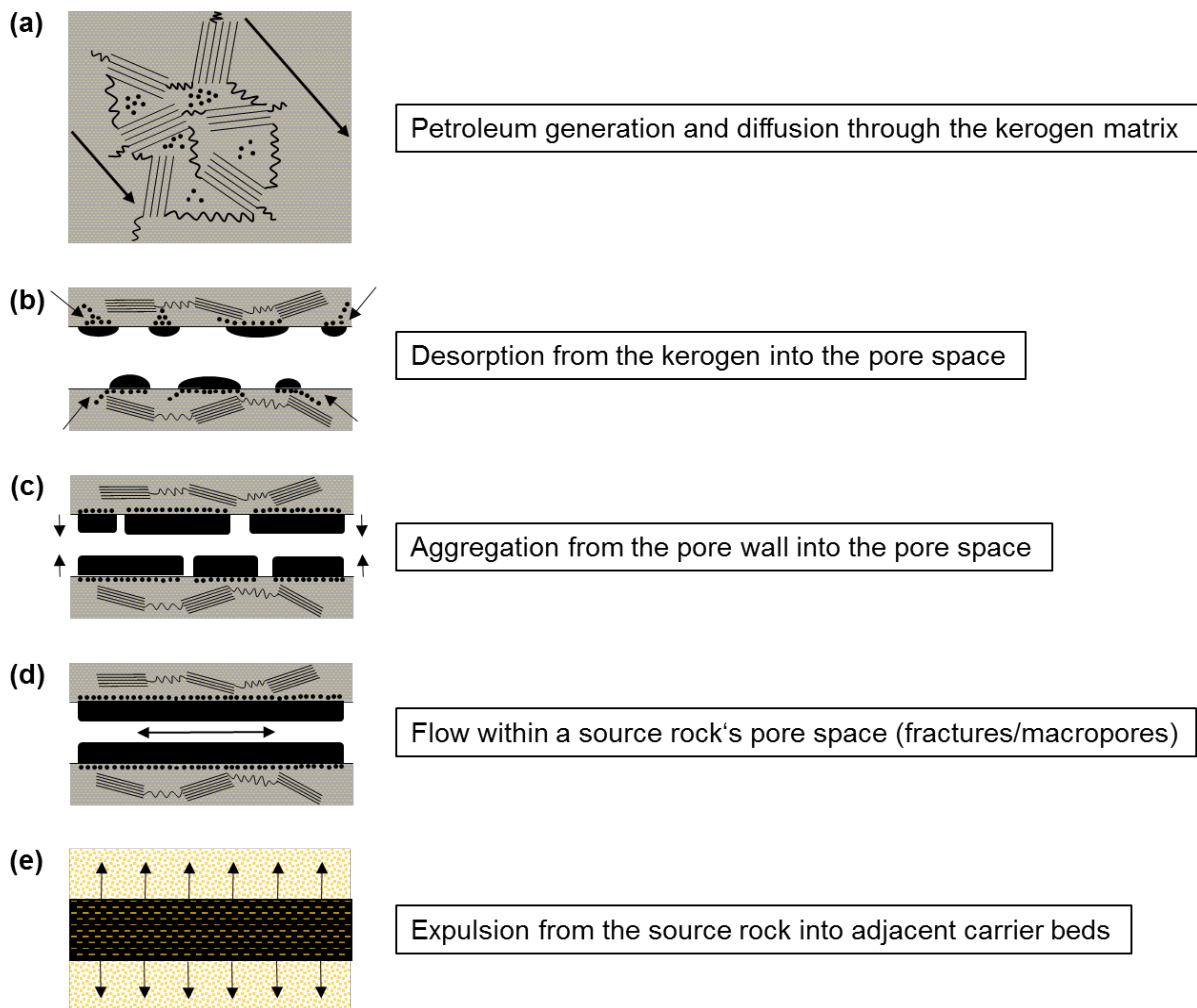


Fig. 5. Consecutive sequence of primary migration (modified after Mann et al., 1997). (a) Petroleum generation and diffusion through the kerogen network along concentration or pressure gradients. (b) Desorption from the kerogen and accumulation at the pore wall. (c) Aggregation into fractures or macro-pores. (d) Pressure-driven petroleum bulk phase flow within the source rock. (e) Expulsion into adjacent carrier beds.

processes that are supposed to constitute primary migration (generation, diffusion, desorption, aggregation, bulk phase flow) take place at the same time and merge into one another. Once after the generated petroleum has left the source rock, secondary migration sets in, transporting the expelled products to reservoirs or seeps.

3.2 Factors that influence primary migration

After having described the possible mechanisms by which generated petroleum can be transported from its place of generation to adjacent carrier rocks, the next section concentrates on the factors that principally control primary migration in the sub-surface. In summary, these are: (1) the pressure regime, (2) the temperature, (3) the organic and inorganic composition of the source rock, (4) the configuration of the pore space, and (5) burial-induced changes in the physicochemical characteristics of certain minerals, particularly clays.

3. Primary migration – state of the art

3.2.1 Pressure regime

As already indicated in the previous subchapter, compaction due to load pressure can be considered as the most critical factor initiating primary migration in petroleum systems (e.g. du Rouchet, 1981; Mackenzie et al., 1983, 1988; Durand, 1988; Lafargue et al., 1990, 1994; Mann et al., 1997; Stockhausen, 2015). As a source rock becomes progressively buried, compaction causes declining porosity and increasing internal pressure with depth, consequently generating a pressure-driven fluid flow which forces segregated petroleum compounds out of the source rock (e.g. Mackenzie et al., 1983; Mann et al., 1997). According to Stockhausen (2015), the load pressure, also called lithostatic pressure, can be calculated the following way (from Stockhausen, 2015):

$$p_l(z) = z * \rho_r * \vec{g} \quad (3)$$

with p_l representing the lithostatic pressure, z the depth, ρ_r the rock density and \vec{g} the gravitational acceleration. In nature, the lithostatic pressure typically increases by 0.3 kbar/km, thus reaching pressures of approximately 1 kbar in 3 km depth (e.g. Stockhausen, 2015). Besides, the hydrostatic pressure, also termed pore pressure, represents the pressure effective in the pore space of a rock. It strongly depends on the present pore fluids, in case of petroleum systems particularly the volumes of oil, gas and water. As a consequence, the discharge of fluid hydrocarbons from the kerogen into the pore space heavily impacts the pressure regime of a source rock (Hedberg, 1974; Ungerer, 1990; Mann et al., 1997; Berg and Gangi, 1999) and partially facilitates primary migration via overpressure-induced fractures, as will be discussed later (see 3.2.4) (e.g. Leythaeuser et al., 1988c; Littke et al., 1988; Ungerer, 1990; Stockhausen, 2015). Similar to equation (3), calculation of the hydro-static pressure is possible as follows (from Stockhausen, 2015):

$$p_h(z) = z * \rho_w * \vec{g} \quad (4)$$

In contrast, here p_h represents the pore pressure and ρ_w the pore fluid density instead of the lithostatic pressure and the rock density, respectively. Again, z and \vec{g} symbolize depth and gravitational acceleration. Following Stockhausen (2015), the pore pressure roughly amounts to a third of the lithostatic pressure and is thus typically in the magnitude of around 300 bar.

3.2.2 Temperature

3. Primary migration – state of the art

Temperature represents the second key factor that influences primary migration. In natural systems, it generally increases with depth and strongly depends on the respective geothermal gradient (rise of temperature with increasing depth), which is different from place to place. For example, rift areas favor early petroleum formation due to higher temperatures at earlier stages of burial. As mentioned before in chapter 2, typical oil window temperatures range from around 100 to 150 °C, corresponding to burial depths of approximately two to four kilometers, considering the regional geothermal conditions. With regard to source rocks, increasing temperatures usually result in kerogen cracking, followed by the thermal breakdown of heavy NSO compounds, both of which lead to substantial amounts of hydrocarbons (Behar et al., 2008, 2010). Besides, the temperature may have profound impact on the physico-chemical characteristics of pore fluids. For example, Stockhausen (2015) highlighted the temperature dependency of the pore fluid density, which is essential concerning petroleum expulsion. More specifically, it was mentioned that increasing temperatures lead to both enhanced dissolution of solid materials, and higher solubilities of gases, which might either increase or reduce the pore fluid density and thus the hydrostatic pressure. Similarly, Tissot and Welte (1984) emphasized that the temperature has striking influence on the volume, the viscosity and the solvent capacity of water, which plays a major role in the subsurface, particularly during petroleum formation (e.g. Lewan, 1997).

Another interesting study dealing inter alia with the influence of the temperature in petroleum systems was conducted by Bennett and Larter (1997). Essentially, these researchers investigated the relative impacts of crude oil composition, pressure, salinity, and temperature on oil/water partition coefficients of alkylphenols, organic compounds that have the potential to act as molecular petroleum migration tracers, i.e. they can be used to infer the distance that petroleum migrated in a sedimentary basin (e.g. Taylor et al., 1997; Galimberti et al. 2000). In short, they found that the partition coefficients for C₀-C₂ alkylphenols considerably decreased with increasing temperature, and increased with pore water salinity and concentration of polar NSO compounds in a crude oil. A pressure dependency was not recognized. The main conclusion regarding the temperature influence was that more alkylphenols dissolve in water at higher temperatures, an observation that might also be true for other organic tracers, thus accentuating the importance of temperature in petroleum systems and particularly during petroleum migration.

3. Primary migration – state of the art

3.2.3 Source rock composition

The molecular signature of a source rock fundamentally depends on the type and amount of organic material that has once been deposited in its respective environmental setting (e.g. Tissot and Welte, 1984; Ungerer, 1990; Pepper and Corvi, 1995a, b; Killops and Killops, 2005; Peters et al., 2005a, b). Therefore, expelled petroleum principally reflects the signature of its source rock, allowing for oil-source rock correlations even at large distances of secondary migration (e.g. Tissot and Welte, 1984; Peters et al., 2005a, b). However, biodegradation (e.g. Bailey et al., 1973; Huang et al., 2003; Peters et al., 2005a), mixing (e.g. Trinidade et al., 1992; Koopmans et al., 2002; Zhang et al., 2004), thermal maturity (e.g. Clegg et al., 1998a, b; Horsfield et al., 1998), facies variability (e.g. Pepper and Corvi, 1995a; Bakr and Wilkes, 2002), and fractionation effects due to primary or secondary migration (e.g. Larter et al., 2000; Zhang et al., 2013) may influence an oil's molecular composition and therefore complicate oil-source rock correlations. It has also been shown that the composition and quantity of clays in a source rock is essential with respect to petroleum migration (e.g. Espitalié et al., 1980; Carlson and Chamberlain, 1986; Charlesworth, 1986; Bonilla and Engel, 1988; Brothers et al., 1991). More specifically, clay minerals have been demonstrated to effectively retain petroleum compounds due to specific surface adsorption interactions. Hence, since petroleum source rocks are usually very rich in clays, it can be concluded that the respective clay mineralogy of a source rock is extremely important with respect to fractionation effects associated with petroleum expulsion.

Pepper and Corvi (1995a, b) aimed to improve basin analysis and to contribute to a better understanding of expulsion and primary migration using a kinetic model based on depositional environments. Therefore, they distinguished between five different global kinetic facies types, controlling fundamentally the expulsion behavior of a source rock, as well as the rates of oil and gas generation. These facies types comprise, (A) marine environments, either siliciclastic-poor, calcareous or evaporitic from any age, (B) marine, siliciclastic dominated depositional systems without age limitation, (C) lacustrine, Phanerozoic settings, (D) terrigenous, ever wet, waxy coastal areas from the Mesozoic on, (E) Mesozoic and more recent terrigenous, ever wet, resin- and wax-rich coastal environments, and, finally, (F) terrigenous, wax-poor coastal-related depositional systems either of late Palaeozoic age or younger (Table 1) (Pepper and

3. Primary migration – state of the art

Corvi, 1995a). The authors accentuated that the activation energies for oil generation significantly increase from facies type (A) to (F), meaning that most energy is required for oil generation from a pure terrigenous source, corresponding to observations in nature. Consequently, waxy, terrigenous kerogens are supposed to expel greater quantities of aromatic hydrocarbons than marine kerogens, which are predominantly composed of algal and bacterial remains.

As a final aspect regarding the importance of the source rock composition with respect to petroleum expulsion, consider also that both the mineralogy and the organic facies of a source rock may have direct influence on the effective mode of primary migration, which may vary from one source rock to another (e.g. Tissot and Welte, 1984; Killips and Killips, 2005).

3.2.4 Porosity and permeability

As discussed in section 3.1, it is widely accepted that pressure-driven, discrete petroleum bulk phase flow is the principal transport mechanism of oil and gas during primary migration (e.g. Tissot and Welte, 1984; England et al., 1987; Mackenzie et al., 1988; Leythaeuser et al., 1988a, b; Sandvik and Mercer, 1990; Ungerer, 1990; Mann et al., 1997; Esemé et al., 2012; Ziegls et al., 2017). Petroleum bulk phase flow is, however, limited by the porosity of the source rock, which constantly decreases with increasing depth (Fig. 6), accompanied by a rise in density and capillary

Table 1. Organofacies types (modified after Pepper and Corvi, 1995a)

| Organofacies | Environment | Predominant biomass | Sulphur incorporation | Depositional setting | Kerogen type |
|--------------|---|---|-----------------------|--|--------------|
| A | Aquatic, marine, siliceous or carbonate/evaporite | Marine algae, bacteria | High | Marine, upwelling zones, elastic-starved basins (any age) | Type IIS |
| B | Aquatic, marine, siliciclastic | Marine algae, bacteria | Moderate | Marine, clastic basins (any age) | Type II |
| C | Aquatic, non-marine, lacustrine | Freshwater algae, bacteria | Low | Tectonic nonmarine basins; minor on coastal plains (Phanerozoic) | Type I |
| D | Terrigenous, non-marine, waxy | Higher plant cuticle, lignin; bacteria | Low | Some ever-wet coastal plains (Mesozoic and younger) | Type IIIH |
| E | Terrigenous, non-marine, resin- and wax-rich | Higher plant cuticle, resin, lignin; bacteria | Low | Some ever-wet coastal plains (Mesozoic and younger) | Type IIIH |
| F | Terrigenous, non-marine, waxy | Lignin | Low | Coastal plains (Late Palaeozoic and younger) | Type III/V |

resistance (Maxwell, 1964; Tissot and Welte, 1984; Ozkaya, 1988; Esemé et al., 2012; Bjørlykke, 2015a). Permeability, which basically symbolizes a rock's fluid transport

3. Primary migration – state of the art

capacity, is therefore an important criterion to consider in the context of primary migration. A few years ago, Esemé et al. (2012) divided permeability into fracture and intergranular permeability. While the former refers to petroleum passage through the pore space, the latter denotes focused flow along cracks. Note that these two types roughly correspond to the two principal bulk flow variants of primary migration, which are: (1) concentrated passage along fractures, and (2) Darcy flow through the closed pore network (see 3.1.5) (Stainforth and Reinders, 1990). Based on permeability coefficients, expulsion flow rates and microscopic observations, Esemé et al. (2012) concluded that fracture permeability and therefore the first of the two possible bulk flow mechanisms represents the main pathway for petroleum expulsion. Their results gain support from the natural system data published earlier by Leythaeuser et al. (1988c) and Littke et al. (1988), who investigated several Posidonia Shale samples from the Hils syncline in northern Germany and noted numerous well-developed fractures within samples spanning the catagenesis kerogen maturation stage. These

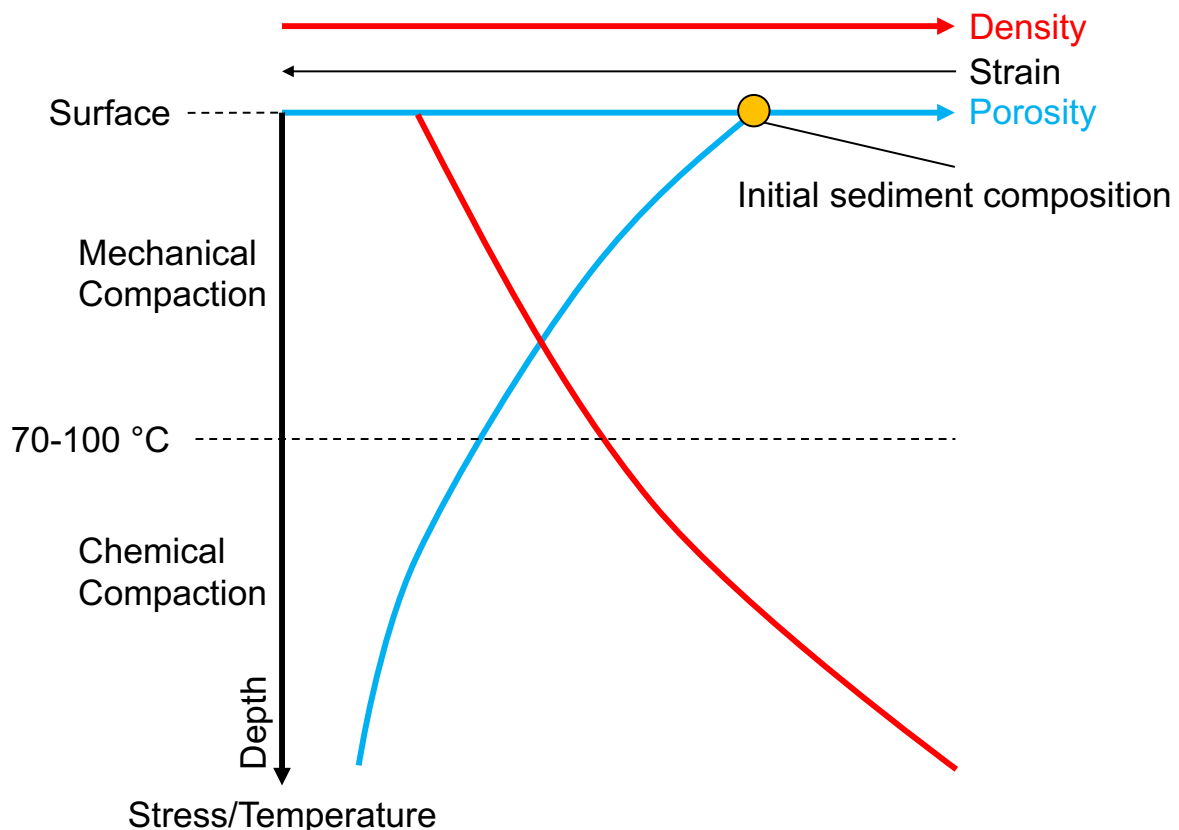


Fig. 6. Essential elements of sediment compaction (modified after Bjørlykke, 2015a). With increasing depth (burial), density increases, while porosity decreases. Mechanical compaction can generally be considered as a strain caused by burial stress. In contrast, chemical compaction is attributed to the dissolution and precipitation of minerals and mainly governed by temperature and time.

fractures were attributed to overpressuring due to oil and gas generation and interpreted as major expulsion avenues, as they were not discovered in under- and

3. Primary migration – state of the art

overlying stratigraphic units nor in corresponding immature sample material. Similarly, Esemé et al. (2012) reported that the porosity of various source rock samples from Permian to Miocene age significantly increased during high-temperature compaction experiments because of petroleum generation and expulsion. Since primary migration seems to proceed preferentially along fractures, it is necessary to take a closer look at their possible origins in source rocks.

In general, fractures in source rocks may evolve either in response to tectonic stress or expulsion fracturing, which can be ascribed to an increase in pore fluid pressure due to the release of generated petroleum compounds into the pore space (e.g. Leythaeuser et al., 1988a; Littke et al., 1988; Ozkaya, 1988; Guo et al., 2011; Stockhausen, 2015). Basically, the rise in pore pressure counteracts the porosity reduction caused by the lithostatic load (burial), thus triggering overpressure and fracture formation. Furthermore, Stockhausen (2015) pointed out that fractures do not only represent important pathways for primary migration, but also induce pressure gradients within source rocks accelerating the thermally-activated diffusion of bitumen through the kerogen matrix, which is believed to represent a major fractionation mechanism during primary migration (e.g. Stainforth and Reinders, 1990) (see 3.3.1). Ozkaya (1988) emphasized that petroleum generation-induced fracture propagation requires in total four conditions: (1) most organic material has to be focused in discrete, separate aggregates, (2) these aggregates need to fulfill a distinct length to thickness ratio of at least 6 mm length per 0.1 mm thickness, (3) some initial oil is necessary to attain kerogen permeability, and (4) a fracture network has to develop, permitting an effective drainage of petroleum compounds from the source rock.

Secondary porosity is another aspect that has to be considered with regard to the pore space of a source rock. In general, secondary porosity may evolve due mainly to either diagenetic alteration (e.g. dissolution of minerals) or mineral transformations (Bjørlykke and Høeg, 1997; Esemé et al., 2012), and may provide additional pore space, as well as structural weaknesses, which consequently lead to increased permeability and facilitate fracture propagation.

An interesting topic that also falls into the category porosity and permeability as factor influencing primary migration is maceral nanoporosity, which was investigated, for example, by Ritter and Grøver (2005). These authors examined the effects of vitrinite

3. Primary migration – state of the art

nanoporosity on the expulsion behavior of coals and concluded that both the distribution of nanopores, as well as the cross-link density may have considerable influence on the composition of expelled petroleum. Similarly, in a previous publication, Ritter (2003) proposed that nanopores account for a large proportion of a maceral's internal surface area and principally have the potential to cause both capillary condensation and molecular sieving, which both may contribute to compositional fractionation upon primary migration. Although Ritter and Grøver (2005) focused exclusively on coals, their results suggest, however, that nanoporosity needs to be considered in other maceral types, too, and thus in kerogens of greater economic significance, i.e. type II kerogens. Further investigations are necessary to assess such effects particularly in type II kerogens to provide closer insights into nanoscale adsorption/desorption processes.

3.2.5 Phase transitions

With proceeding burial, minerals tend to change their physicochemical properties due to phase transitions. Such changes are important with regard to petroleum generation and migration (e.g. Burst, 1969; Freed and Peacor, 1989; Selley, 1998; Stockhausen, 2015). More specifically, phase transitions may provide, (i) secondary porosity, (ii) impact the pressure regime, and (iii) add fluids to the pore space. As many petroleum source rocks, including the majority of source rock samples analyzed in this work, are argillaceous, clay mineral transformations can be regarded as the most important phase transitions with regard to petroleum formation. For example, Burst (1969) studied the gradual dehydration of clay minerals in argillaceous sediments from the Gulf Coast and reported that substantial volumes of water are released upon compaction, particularly throughout the catagenesis kerogen maturation stage. The author postulated that water derived from the dehydration of clay minerals significantly contributes to petroleum migration in the Gulf Coast region. In general, water in petroleum systems occurs in three forms: (1) free, either as fluid or gas, (2) structured, and (3) incorporated into the crystal lattice (Eseme et al., 2012), which become unstable at temperatures of 105, 150, and 350 °C, respectively. Clays typically comprise either free pore water or structured water interbedded between aluminosilicate layers (Powers, 1967; Selley, 1998). Dehydration temperatures of around 150 °C thereby fit well with the catagenesis kerogen maturation stage,

3. Primary migration – state of the art

indicating that substantial fluid volumes are released into the pore space during this temperature stage.

Recently, Stockhausen (2015) again drew attention to the significance of the conversion of smectite to illite, which is accompanied by the release of considerable volumes of water into the pore space of a source rock and therefore heavily impacts the pressure regime, as has been noted previously (e.g. Colten-Bradley, 1987; Freed and Peacor, 1989; Selley, 1998). The transformation seems to depend chiefly on temperature, time and lithostatic pressure (Colten-Bradley, 1987; Stockhausen, 2015) and is accompanied by a tremendous loss of volume and weight (Freed and Peacor, 1989; Stockhausen, 2015). Both the stoichiometry and the reaction kinetics are, however, still relatively poorly resolved, due particularly to the complex mineralogy of clay minerals. If considering reactive organic material, pressure, temperature and the omnipresence of mineral surfaces, the reaction becomes even more complicated. Following Selley (1998), the transformation of smectite to illite generally proceeds in two stages. First, free water is released upon compaction, after which structured water is mobilized at temperatures of around 100-110 °C. The author pointed, however, out that many prolific petroleum provinces lack smectitic clays and therefore the dewatering of clay minerals cannot be considered as the main reason for petroleum expulsion. Nonetheless, it certainly represents a major contributing factor, especially in petroleum systems involving argillaceous source rocks.

3.3 Reasons for molecular redistribution

Several fractionation mechanisms have been proposed in the past to explain the observed compositional differences between source bitumens and crude oils. Krooss et al. (1991) grouped these mechanisms into: (1) multiphase fractionation processes, comprising all chromatographic interactions between one or more bulk flowing mobile phases and surrounding stationary phases, and (2) single phase fractionation processes, which are not necessarily related to petroleum bulk flow. Summarized, the most important fractionation mechanisms operating during primary migration include: (i) the interaction of petroleum with minerals, (ii) the partitioning of petroleum compounds between oil, gas and water, (iii) kerogen absorption and adsorption, and (iv) diffusion of petroleum compounds through organic material (Ziegls et al., 2017).

3.3.1 Diffusive fractionation

3. Primary migration – state of the art

Molecular diffusion of petroleum compounds from places of higher to places of lower concentration or, alternatively, along pressure gradients, has been suggested as one of five principal transport modes of primary migration (see 3.1.4) (Tissot and Welte, 1984) and can be considered as a single phase separation process (Krooss et al., 1991). It is supposed to take place preferentially through the kerogen network of a source rock (Stainforth and Reinders, 1990; Thomas and Clouse, 1990a, b, c), and to be of particular importance during the early stages of petroleum formation. Furthermore, molecular diffusion can be regarded as the initial process transporting generated organic compounds from their place of origin to areas of lower concentration, i.e. to the pore space, internal migration avenues (e.g. fractures) or directly to adjacent reservoir rocks. Thereby, molecular diffusion is supposed to proceed via successive adsorption and desorption processes with smaller, lighter molecules being more easily transported than larger, heavier ones (Stainforth and Reinders, 1990; Thomas and Clouse, 1990b; Stockhausen, 2015). According to Killops and Killops (2005), diffusion and generation of hydrocarbons roughly proceed at the same rate, which, therefore, implies that diffusion will only take place if enough hydrocarbons are generated from the kerogen. This represents an important circumstance that has to be considered. Mathematically, diffusion can be expressed by Fick's law, which basically describes how a substance's concentration C changes with time t . D represents the diffusion coefficient (from Ungerer, 1990):

$$\frac{dC}{dt} = \text{div}(D \text{ grad } C) \quad (5)$$

Following Tissot and Welte (1984), the main reason for molecular redistribution during diffusion are differences in the value of the diffusion coefficient. Essentially, the diffusion coefficient relates the diffusive flux to the concentration gradient of a compound and is therefore principally a measure of particle movement. Note that the diffusion coefficient strongly relies on pressure and temperature, which further underpins the importance of these factors during primary migration. According to Tissot and Welte (1984), D rapidly decreases with increasing number of carbon atoms. In fact, this means that the higher the number of carbon atoms, the slower the diffusion, hence causing fractionation. In this respect, Ungerer (1990) mentioned that molecular diffusion is most efficient for gaseous hydrocarbons due to both greater solubilities and higher diffusion coefficients relative to liquid compounds. The data published by

3. Primary migration – state of the art

Thomas and Clouse (1990a, b, c) indicate that molecular diffusion of petroleum compounds through organic material can indeed account for at least some of the fractionation trends witnessed in nature (see 3.4). Correspondingly, Stainforth and Reinders (1990) proposed that pressure-forced petroleum bulk flow alone cannot adequately explain the frequently observed compositional changes during primary migration, consequently leading them to assume a critical role of molecular diffusion during the earliest stage of petroleum movement. Diffusion seems, however, to be rate-limiting only at short migration distances, as already mentioned in section 3.1.4 (Tissot and Welte, 1984; Mann et al., 1997). Furthermore, Thomas and Clouse (1990b) noted that diffusion processes through organic matter appear to be remarkably lithology dependent. They reported that a calcareous rock matrix facilitates diffusion through interaction with organic functionalities, whereas silicate minerals do not seem to heavily respond to functional groups. Hence, the diffusive transport of organic components through the kerogen matrix might proceed more readily in source rocks with elevated carbonate contents than in source rocks dominated by silicate minerals, which could be due to an easier formation of consistent kerogen networks. Besides, Stockhausen (2015) pointed out that the lithostatic pressure plays a key role in terms of molecular diffusion, too. In general, compaction provides a narrower pore space, which, in turn, supports diffusion networks. According to Stainforth and Reinders (1990), diffusion proceeds preferably along aliphatic compartments of kerogen. Therefore, since there is evidence that aliphatic hydrocarbons are preferentially expelled during primary migration (see 3.4) (e.g. Mackenzie et al., 1983; Tissot and Welte, 1984; Leythaeuser et al., 1988a), diffusion can be expected to weaken with ongoing thermal maturation because of changes in the adsorption/desorption characteristics of the kerogen. In this regard, Stockhausen (2015) underlined that such a scenario would almost perfectly fit natural fractionation effects, where aromatics are frequently later expelled than aliphatics, due probably to a decreasing adsorption potential of the kerogen.

In contrast to the diffusive transport of organic compounds through the kerogen, which seems highly reasonable, diffusion through water can largely be neglected since the majority of petroleum compounds is only very slightly or even insoluble in water (e.g. Tissot and Welte, 1984; Ungerer, 1990; Esemé et al., 2012). Indeed, Lewan (1997) did not document such effects in a series of hydrous pyrolysis experiments which served to evaluate the role of water in petroleum formation. Though, on the other hand,

3. Primary migration – state of the art

Lafargue and Barker (1988) and Bennett and Larter (1997) reported a strong impact of water washing during secondary migration and reservoiring, which can principally be considered as liquid-liquid chromatography (Krooss et al., 1991). For example, Lafargue and Barker (1988) showed that water washing had particular influence on the C₁₅ fraction, but also on dibenzothiophene. This clearly shows that water partitioning and diffusion of petroleum compounds through water need definitely to be taken into account when dealing with compositional changes upon petroleum migration. However, with regard to primary migration, Krooss et al. (1991) pointed out that liquid-liquid chromatographic processes are certainly limited because of both the commonly low permeability of source rocks and the comparatively low volumes of water required for petroleum generation.

3.3.2 Natural chromatography

Larter et al. (2000) defined the term “geochromatography” as migration-related compositional changes of petroleum attributed to compound-specific molecular interactions with minerals, solid organic matter and water. For a detailed review on this topic, the reader is referred to Krooss et al. (1991). Previous research has shown that geochromatographic interactions have profound impact on the composition of migrating petroleum (e.g. Bonilla and Engel, 1986, 1988; Larter et al., 1996, 2000; Li et al., 1997). Essentially, such effects cause petroleum compounds to become temporally separated with increasing migration distance, similar to a normal-phase chromatography routinely applied in organic geochemical laboratories. Krooss et al. (1991) described geochromatographic systems simply as systems comprising at least one stationary and one mobile phase, excluding single phase separation processes like diffusion and gravity segregation, which might be important over short migration distances. Therefore, according to Krooss et al. (1991), geochromatography is related to petroleum bulk phase flow and can be regarded as a multiphase fractionation process. Thereby, kerogen and minerals are supposed to represent the principal solid stationary phases in petroleum systems. In addition, pore water films and bitumen may act as liquid stationary phases. On the other hand, gas, water and hydrocarbon fluids generated in response to petroleum generation (i.e. oil) can be regarded as the major mobile phases (Fig. 7) (Krooss et al., 1991). According to Krooss et al. (1991), the level of chromatographic interaction between different phases chiefly depends on, (1) partition coefficient differences of compounds, (2) the presence of phases, and (3) the

3. Primary migration – state of the art

total amount of individual fractionation steps. Thereby, the principal interaction mechanisms between mobile and stationary phases involve adsorption, partitioning, ion exchange, and size exclusion, from which adsorption and size exclusion can be considered as most essential with respect to primary migration (Krooss et al., 1991). Among these, adsorption/desorption processes of petroleum compounds on solid organic matter and mineral phases have been proposed as the major reason for natural chromatographic effects (e.g. Tissot and Welte, 1984; Tannenbaum et al., 1986; Bonilla and Engel, 1988; Krooss et al., 1991), whereby the degree of interaction fundamentally depends on the polarity and molecular weight of the respective compound. With regard to size exclusion, pelitic rocks may represent molecular sieves for certain molecules, thus impacting a mobile phase's composition.

Clay minerals and their catalytic influence are of prime importance for geochromatography and have been studied intensely (e.g. Eltantawy and Arnold, 1972; Espitalié et al., 1980; Carlson and Chamberlain, 1986; Charlesworth, 1986; Tannenbaum et al., 1986; Bonilla and Engel, 1988; Brothers et al., 1991). Since petroleum source rocks are usually highly argillaceous, clay minerals like illite and montmorillonite typically represent important components of the inorganic matrix and can be expected to impact a source rock's expulsion behavior. Interestingly, the retention

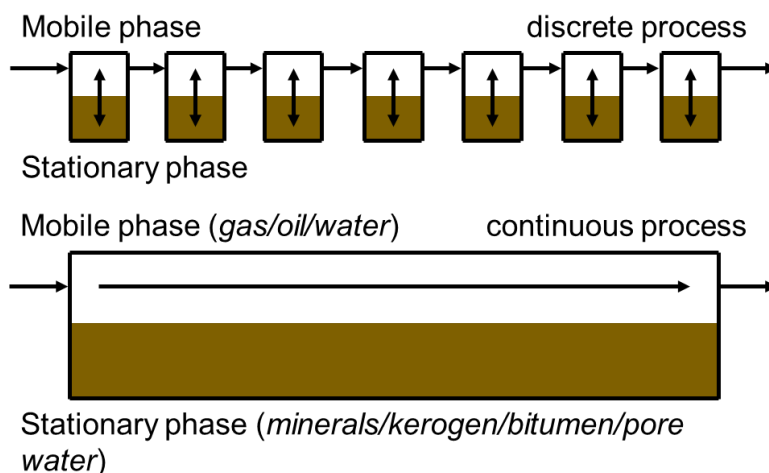


Fig. 7. Principal concept of geochromatographic separation (modified after Krooss et al., 1991). The chromatographic separation of petroleum compounds can be considered as a continuous process involving numerous individual equilibration and transport steps. While stationary phases in petroleum systems usually comprise minerals and kerogen (solid stationary phases) as well as sorbed layers of bitumen and pore water (liquid stationary phases), gas, oil and pore water represent the principle mobile phases (Krooss et al., 1991).

potential of clay minerals seems to intensify with decreasing water content, pointing to a crucial role of water in petroleum systems, as has been proposed by various researchers (e.g. Hoering, 1984; Krooss et al., 1991; Seewald, 1994; Stalker et al.,

3. Primary migration – state of the art

1994; Lewan, 1997; Stockhausen, 2015). Conversely, the retention potential of clay minerals appears to weaken with increasing water content, potentially because of a blocking of active sites by water molecules (Tannenbaum et al., 1986; Stockhausen, 2015).

Krooss et al. (1991) suggested that geochromatographic interactions are strongest at the very beginning of primary migration when generated petroleum is mostly isolated and finely disseminated, leading to large contact areas between minerals and petroleum and therefore strong atomic sorption. Moreover, they stated that primary migration can, like most processes in geological systems, theoretically be considered as a type of frontal chromatography. Following Krooss et al. (1991), frontal chromatography represents one of the three major types of chromatographic separation (displacement chromatography, elution chromatography, frontal chromatography) and describes a continuous material flow in which only the fastest moving components become temporarily separated from each other, leading to homogenization among later eluting compounds. With respect to petroleum migration, this means that compound sorption is strongest at the front of a migrating petroleum stream where compounds are subjected to reactive mineral surfaces. While liquid-solid geochromatography can be assumed to represent the most important geochromatographic fractionation mechanism during primary migration, gas-solid and gas-liquid interactions need, however, also to be considered (Krooss et al., 1991). Note that the concept of geochromatographic separation (Fig. 7) represents the basis for molecular migration tracers, compounds that partition between petroleum, water, rock and solid organic matter in a petroleum system depending on their chemical and physical properties. In general, concentration and isomerization changes of such molecules, chiefly NSO compounds, relative to their abundance and isomerization pattern in the retained source bitumen have successfully been applied to infer the migration distance of crude oils in sedimentary basins (e.g. Larter et al., 1996; Terken and Frewin, 2000; Zhang et al., 2004, 2013).

3.3.3 Kerogen absorption

It has been postulated that kerogen can be considered as a geopolymer that has the potential to absorb hydrocarbons (Sandvik et al., 1992; Larsen and Li, 1994, 1997a, b; Ritter, 2003; Kelemen et al., 2006a). Following this point of view, compositional fractionation between source bitumen and petroleum can at least in part be explained

3. Primary migration – state of the art

by the selective absorption of compounds in kerogen, a process that can be regarded in the context of the polymer solution theory. Essentially, it describes the interaction between solvents and macromolecular polymers, whereby the degree of interaction depends on the absorption capacity of the polymer. Principal evidence for the absorption of petroleum compounds in kerogen derives from the frequently observed relationships between extract yield and TOC (Sandvik et al., 1992), as well as between Rock-Eval S_1 and S_2 (see 3.5.1) (Ziegs et al., 2017). Rullkötter (1993) pointed, however, out that kerogen is a complex, heterogeneous substance instead of a single polymer. Therefore, it is questionable whether the polymer solution theory is fully applicable to natural kerogens. Indeed, Ritter (2003) mentioned that both compositional differences between source bitumen and crude oils from the North Sea, as well as coal-derived, hydrocarbon-enriched petroleum are not exclusively explainable by polymer absorption. However, the polymer solution theory seems to be a useful approach to examine the differential retention of certain molecules in kerogen. To test the applicability of the polymer solution theory to natural kerogens, Ritter (2003) calculated polymer solubility parameters, so-called “Hildebrand parameters”, for different petroleum compounds, attempting to evaluate their sensitivity to primary migration fractionation (Fig. 8). The author noted great variances within the aromatic fraction with significant implications concerning petroleum expulsion. Polymer solubility parameters can be calculated using the following equation (from Ritter, 2003):

$$\delta = \left[\frac{\Delta E - RT}{V_m} \right]^{\frac{1}{2}} \quad (6)$$

in which δ represents the solubility parameter, ΔE the energy required to vaporize a liquid and to overcome its van der Waals forces, the so-termed vaporization energy, R the universal gas constant, T the temperature, and V_m the molar volume. In general, the closer the δ value of a component to the δ of the kerogen, which is in the range of 9.5 to 10 (cal/cm³)^{1/2} according to Larsen and Li (1997b) and Ritter (2003), the higher its solubility and thus the stronger the retention (Fig. 8).

3. Primary migration – state of the art

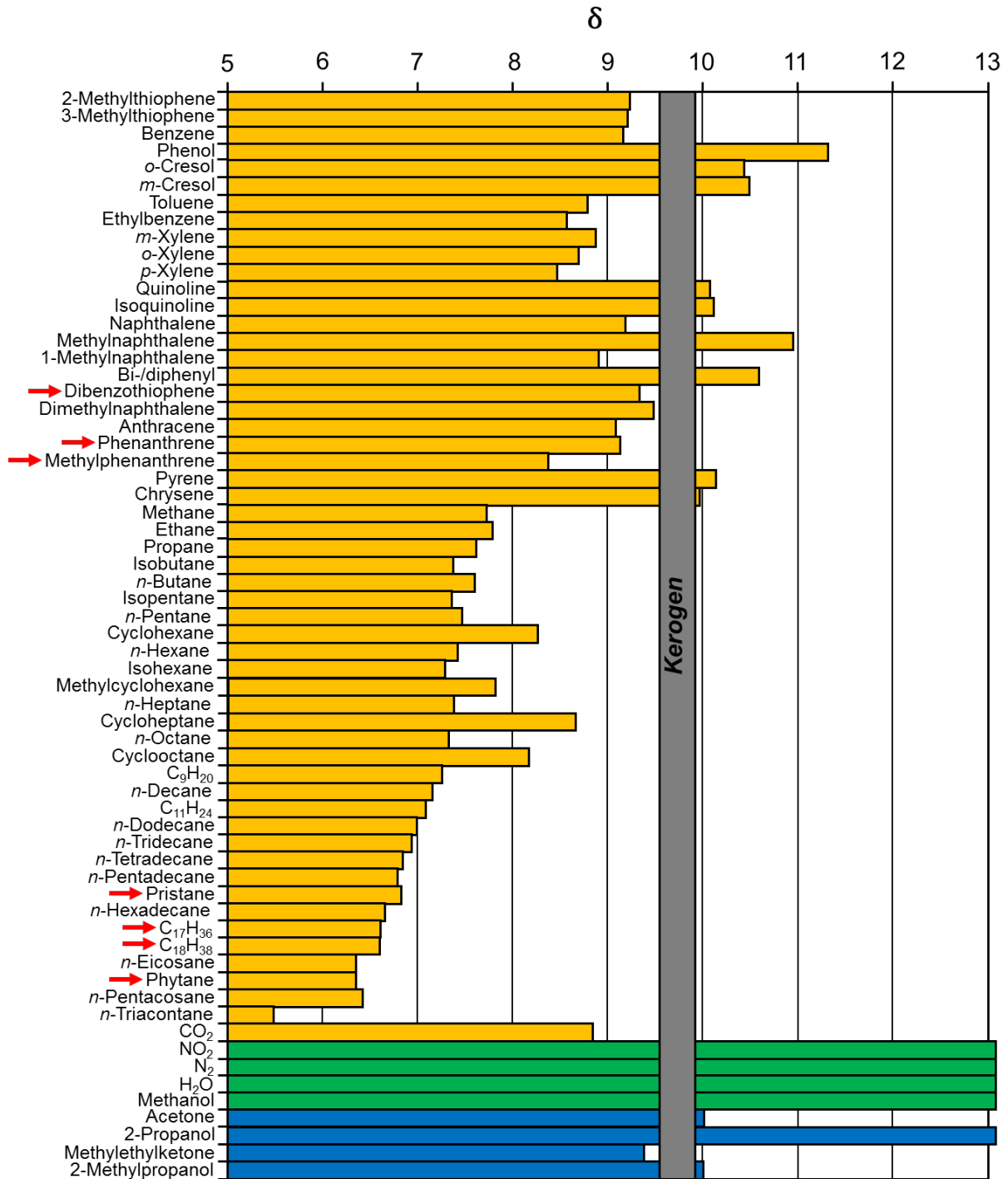


Fig. 8. Polymer solubility parameter δ for different compounds (modified after Ritter, 2003). Kerogen is supposed to have a δ in the range of approximately 9.5-10.0 (cal/cm^3)^{1/2} (Larsen and Li, 1997b; Ritter, 2003). Essentially, the closer a compound's δ to the δ of the kerogen, the better its solubility and the stronger the retention. The pattern indicates that due to their relatively high δ values aromatic petroleum compounds are preferentially retained in the kerogen matrix, whereas the aliphatic fraction is preferably released, corresponding to trends in natural systems. δ numbers are given for temperatures of 0 K. Compounds regarded in the context of this work are indicated by red arrows.

The true solubility parameter and hence the sorption capacity of kerogens can be investigated by means of solvent-swelling experiments (Sandvik et al., 1992; Larsen and Li, 1997a, b; Ritter, 2003; Kelemen et al., 2006a). Essentially, HCl/HF-isolated kerogens or, alternatively, ground and solvent-extracted coals become subjected to

3. Primary migration – state of the art

different solvents to determine the magnitude of expansion, which can be measured either gravimetric or volumetric (Green et al., 1984; Larsen and Li, 1997a, b; Sandvik et al., 1992). A kerogen's sorption capacity is related to its swelling ratio Q_V , which can be calculated from the volume of the solvent-swollen sample V_S relative to the volume of the initial, dry sample V_i (from Ritter, 2003):

$$Q_V = V_S/V_i \quad (7)$$

Larsen and Li (1997b) found that the thermal maturity has little influence on the absorption capacity of kerogens. Nevertheless, they showed that the swelling of kerogens tends to decrease with increasing maturity. This effect becomes, however, only noteworthy at very high levels of thermal maturity, as mentioned by Kelemen et al. (2006a). In general, it seems to apply that the higher the solubility parameter, the greater the kerogen swelling, regardless of the type of organic material (Kelemen et al., 2006a). Kelemen et al. (2006a) are of the opinion that a multicomponent equilibrium controlling the molecular fractionation between kerogen and petroleum is present during primary migration, which can be well described by an extended Flory-Rehner (rubber elasticity theory) and polymer solution theory approach. By applying this framework to solvent swelling data from selected type II and III kerogens, they were able to model the principal thermodynamic parameters that are required to describe this multicomponent equilibrium. Those are: (1) the solubility parameter (solvency behavior of a certain solvent), (2) the cross-link density (sum of all bond-concerning reactions that proceed during maturation), and (3) the native swelling (kerogen volume minimizing its elastic strain energy) (Kelemen et al., 2006a). Theoretically, these parameters make it possible to conclude about the solvent swelling behavior of different kerogen types and therefore to investigate fractionation effects between crude oils and retained source rock bitumens that are potentially related to kerogen absorption.

3.4 Expulsion-related compositional changes

After having described the potential transport mechanisms of primary migration, the most critical factors controlling primary migration in the subsurface, and the main reasons for molecular fractionation, the next subchapter addresses the principal compositional differences between source bitumens (retained) and crude oils (expelled) that are frequently observed in natural systems. Based on these differences,

3. Primary migration – state of the art

conclusions can be drawn about the selective retention of organic compounds in the source rock during petroleum generation and expulsion. For that reason, it is first necessary to look at the principal classes of natural crude oils, whose composition is not only, but significantly related to adsorption/desorption processes during primary migration. Thereafter, the section continues with an overview of the most striking compositional differences between crude oils and source rock bitumens with respect to saturates, aromatics, and resins/asphaltenes, which represent the three principal compound categories occurring in petroleum. Subsequently, expulsion sequences of individual components will be presented that have been deduced in the past from both natural case studies, as well as experimental approaches.

3.4.1 General considerations: types of natural crude oils

In total, six different crude oil categories have been defined in the past based on the relative abundances of paraffins, naphthenes (cycloalkanes), aromatics, and NSO compounds (Fig. 9) (e.g. Tissot and Welte, 1984; Selley, 1998; Killips and Killips, 2005). Those are: (1) paraffinic oils, (2) paraffinic-naphthenic oils, (3) naphthenic oils, (4) aromatic-intermediate oils, (5) aromatic-naphthenic oils, and (6) aromatic-asphaltic oils. According to Krooss et al. (1991), the composition of crude oils essentially depends on: (i) the thermal maturity and the organic facies of the source rock, as well as mixing between different oil families, (ii) degradation processes in the reservoir, and, most important with respect to this study, (iii) expulsion fractionation upon primary migration and/or redistribution processes during secondary migration. Detailed information and examples of the individual oil classes are given, for instance, by Tissot and Welte (1984). The following section gives a short overview based on the descriptions of these authors. Essentially, according to Tissot and Welte (1984), paraffinic crudes are oils with slightly elevated viscosity and low sulfur content that are characterized by a high content of *n*- and *iso*-alkanes, low quantities of resins and asphaltenes (<10%), and only minor proportions of aromatic hydrocarbons. Concerning paraffinic-naphthenic oils, Tissot and Welte (1984) stated that this category comprises moderately dense and viscous, low sulfur crudes composed mainly of *n*-, *iso*-, and cycloalkanes. Besides, they mentioned that the aromatic fraction typically constitutes between 25 and 40% of the total composition, resins and asphaltenes are on average moderately abundant, and sulfur aromatics are usually more common than in paraffinic oils. Since this oil class is supposed to

3. Primary migration – state of the art

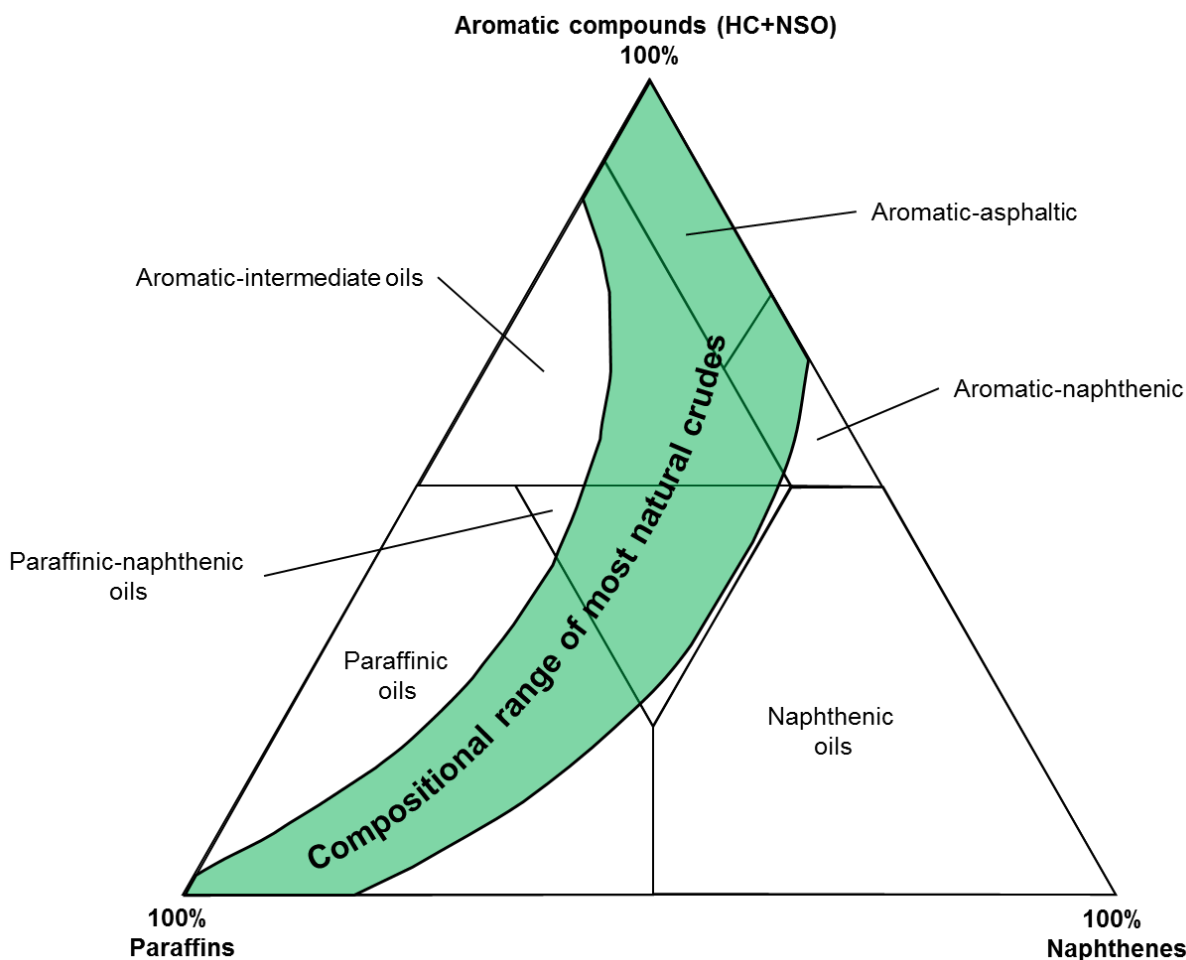


Fig. 9. Classification scheme of crude oils (modified after Selley, 1998). In total, six different oil categories can be distinguished based on the relative abundances of acyclic alkanes (paraffins), cycloalkanes (naphthenes), aromatic hydrocarbons and heteroatomic compounds. Compositional differences between the classes are partly attributable to petroleum expulsion.

be, inter alia, characteristic for the North Sea (e.g. Tissot and Welte, 1984; Kubala et al., 2003) and to originate mainly from source rocks comprising mixed proportions of marine and terrestrial organic material (Killops and Killops, 2005), there is a high probability that the reservoir extracts from the Viking Graben area in the northern North Sea analyzed in this work (see 5.) fall into this category. With respect to pure naphthenic oils, Tissot and Welte (1984) emphasized that these crudes refer mostly to biodegraded oils containing below 20% paraffins and low amounts of sulfur, whereby both paraffinic, as well as paraffinic-naphthenic oils represent possible precursors for naphthenic crudes. The fourth class, aromatic-intermediate oils, can be considered as a fundamentally important category as it comprises major petroleum reserves in, for instance, Saudi Arabia and Kuwait (Tissot and Welte, 1984). According to Tissot and Welte (1984), oils belonging to this category are relatively heavy and contain abundant aromatic hydrocarbons (40-70%), as well as elevated levels of resins and asphaltenes, which can partially exceed 30%. Moreover, it was mentioned that monoaromatic

3. Primary migration – state of the art

hydrocarbons are commonly rare, whereas sulfur-containing heterocycles represent major constituents of the aromatic fraction. With regard to the sulfur content, Tissot and Welte (1984) underlined that aromatic-intermediate oils tend to contain higher quantities of sulfur (>1%) than crude oils from the previous categories. The two remaining classes, aromatic-naphthenic and aromatic-asphaltic oils represent heavy degraded oils (e.g. Tissot and Welte, 1984; Killops and Killops, 2005). Essentially, following Tissot and Welte (1984), these two categories symbolize degraded, heavy and highly viscous oils with large proportions of aromatics, as well as resins and asphaltenes (25-60%), whereby aromatic-naphthenic oils are supposed to be formed through alteration of paraffinic and paraffinic-naphthenic oils, while aromatic-asphaltic oils likely originate mainly from the degradation of aromatic-intermediate oils. As stated by Tissot and Welte (1984), the major differences between the two groups of heavy degraded oils are that resins are generally more abundant in aromatic-naphthenic than in the aromatic-asphaltic oils and that the sulfur content of aromatic-naphthenic crudes is considerably lower than that of aromatic-asphaltic oils.

3.4.2 Gross compositional differences between source bitumens and crude oils

Irrespective of the oil category, several general observations concerning the composition of crude oils vs. source rock bitumens have been made in the past. Before going into detail, it is essential to regard first the basic composition of oils and source bitumens. Basically, both consist of three fractions: (1) hydrocarbons, which comprise saturates and aromatics, (2) resins, and (3) asphaltenes (e.g. Killops and Killops, 2005). With respect to the elemental composition, Killops and Killops (2005) underscored that carbon and hydrogen represent by far the most significant elements in crude oils and source bitumens. Furthermore, following these authors, nitrogen, oxygen and sulfur can be considered as the most important heteroatoms. In addition to these elements, oils and source rock bitumens contain trace quantities of metals, among which particularly nickel and vanadium are worth mentioning (Killops and Killops, 2005).

With regard to the principal compositional differences between oils and source bitumens, crude oils generally tend to be enriched in saturates and, to a minor extent, in low polar aromatics compared to source rock bitumens (e.g. Young and McIver, 1977; Lewan, 1993; Killops and Killops, 2005). Likewise, Tissot and Welte (1984) mentioned that there is a tendency that low polar compounds, i.e. saturates, are more

3. Primary migration – state of the art

efficiently expelled than polar NSO compounds, which are normally strongly retained in the source rock instead of being expelled. Also, these authors drew attention to compositional differences between shaly and carbonate lithologies and their associated crude oils, highlighting the importance of the source rock composition as key element for primary migration (Fig. 10). Briefly, with regard to shaly source rocks, paraffins were reported to represent the most abundant components, followed by resins and asphaltenes in moderate extents, and aromatics as least occurring fraction. On the other hand, it was stated that oils related to shaly source rocks show a strong enrichment of saturates, moderate proportions of aromatics and low concentrations of resins and asphaltenes, which seem to remain preferentially in the source rock. This distribution is fundamentally different to that of the source rock, where resins and asphaltenes are much more abundant than in the oil, suggesting that primary migration has profound impact on the relative abundances of hydro-carbons, resins, and asphaltenes in crude oils. A similar pattern was shown for carbonaceous source rocks and carbonate-derived crude oils, but with some

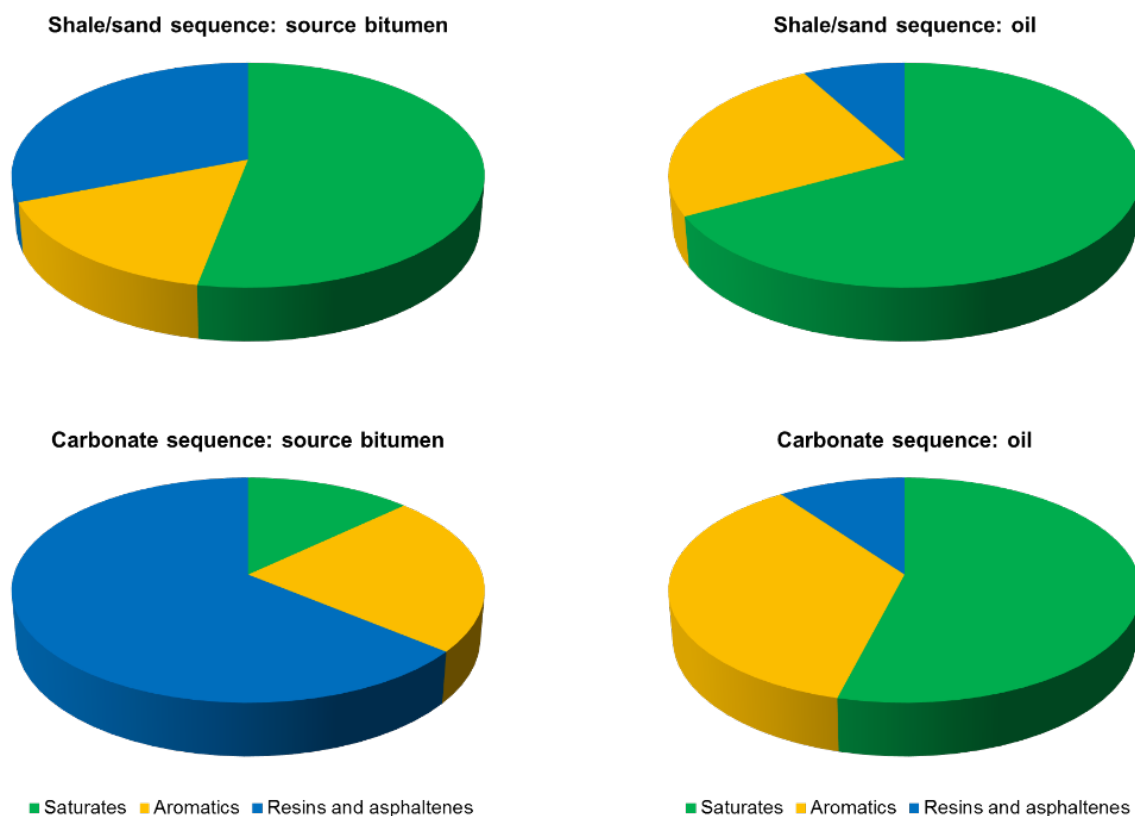


Fig. 10. Compositional comparison of source bitumens vs. crude oils for different lithologies (modified after Tissot and Welte, 1984). Note that crude oils show a tendency to be enriched in saturates relative to aromatics and NSO compounds. The latter are supposed to remain preferentially in the source rock due to stronger retention. Aromatics are classically moderately enriched in crude oils. In general, simple structured, low polarity molecules tend to leave the source rock more easily than complex, heavy compounds.

3. Primary migration – state of the art

conspicuous differences. More specifically, following Tissot and Welte (1984), source rocks with elevated carbonate content tend to contain high amounts of resins and asphaltenes, which often dominate over saturates and aromatics. In contrast to organic-rich shales, these fractions are supposed to be much less abundant, whereby aromatics are slightly more common than aliphatics. With respect to oils originating from carbonate source rocks, this pattern is, similar to that described before for shaly sequences, considerably different. In particular, saturates were reported to prevail over aromatics, resins and asphaltenes, and aromatics are usually higher concentrated in oils than in the source bitumen.

3.4.3 Principal expulsion sequences

As mentioned previously, former research has provided circumstantial evidence that primary migration is associated with profound molecular redistribution (e.g. Mackenzie et al., 1983; Leythaeuser et al., 1988a, b, c; Bennett et al., 2002; Esemé et al., 2006, 2007; Stockhausen, 2015). It has been suggested that compositional fractionation upon primary migration is chiefly attributable to different degrees of molecular interaction between petroleum compounds and kerogen or active mineral sites, mainly depending on the compound polarity (e.g. Tissot and Welte, 1984; Sandvik et al., 1992; Ritter, 2003; Kelemen et al., 2006b; Esemé et al., 2007; Stockhausen, 2015). Based on both observations in natural systems and experimental data, it has been proposed that organic compounds are principally expelled according to the following sequence: *n*-alkanes ≥ *iso*-alkanes > cycloalkanes > aromatics > polars, resins > asphaltenes (Mackenzie et al., 1983; Leythaeuser et al., 1988a, b, c; Lafargue et al., 1990; Sandvik et al., 1992; Pepper and Corvi, 1995b; Ritter, 2003; Esemé et al., 2006, 2007). This sequence remains, however, partly controversial, due primarily to contradictory results from laboratory simulations and natural case studies. For example, it is still uncertain if primary migration indeed fractionates *n*- and *iso*-alkanes, and causes redistribution among hopanes and steranes. In addition, potential expulsion-related fractionation effects among aromatic compounds are poorly resolved, too. Hence, a more simplified expulsion sequence can be formulated as: saturates > aromatic hydrocarbons > NSO compounds, with heavy, polar NSO molecules being most strongly retained in the source rock (e.g. Han et al., 2015, 2017). Despite these uncertainties, it is very likely that additional internal fractionation occurs among the individual categories, due probably to differences in the molecular chain length, the molecular structure and the

3. Primary migration – state of the art

polarity. Moreover, concerning NSO compounds, any variations in the amount and polarity of heteroatoms may also cause fractionation.

An interesting effect that concerns both the molecular structure and the polarity of a heteroatomic compound is molecular shielding. More specifically, various authors have suggested that a compound's retention capacity is principally dependent on the amount and position of alkyl substituents (Li et al., 1994, 1995; Yamamoto, 1992; Larter and Aplin, 1995; Smirnov and Frolov, 1997; Horsfield et al., 1998). In theory, this means that molecules with one or more functional groups adjacent to the polar functionality, so-called "shielded" isomers, are supposed to be less retained than those with an exposed functionality, which indicates that alkyl substituents do not interfere with the polar heteroatom.

3.4.4 Expulsion trends in natural systems

There are principally two different ways to investigate molecular redistribution effects upon primary migration: natural case studies and laboratory experiments. One strategy is to select, collect, and subsequently analyze samples from adequate, oil window-mature natural case scenarios. In this respect, the most promising sequences are intra-formation source rock-carrier bed couplets from mature, actively generating organic-rich units. Many of such case studies have been conducted in the past to understand the effects of expulsion and primary migration on the composition of crude oils. The most prominent studies of primary migration in natural systems were performed in the eighties by Mackenzie, Leythaeuser, and co-workers (e.g. Mackenzie et al., 1983, 1988; Leythaeuser and Schaefer, 1984; Leythaeuser et al., 1984a, b; Leythaeuser et al., 1988a, b, c). While these studies were kept rather general, i.e. focused mainly on gross differences between *n*-alkanes, isoprenoids and aromatic hydrocarbons, subsequent research went more into detail, concentrating for example explicitly on the expulsion behavior of biomarkers (steranes/hopanes) (e.g. Han et al., 2017), or selected organic tracer molecules like carbazoles (Li et al., 1995, 1997) and benzocarbazoles (Bennett et al., 2002). An important concept to consider with regard to expulsion in natural systems is that of the expulsion efficiency (Mackenzie et al., 1983; Cooles et al., 1986). Essentially, the petroleum expulsion efficiency represents the degree of compound depletion in source rock samples located close to adjacent reservoir layers relative to the concentration of these compounds in the center of the

3. Primary migration – state of the art

source rock (Mackenzie et al., 1983; Leythaeuser et al., 1988a, b). It ranges from 0 to 100%, whereby 0% symbolizes complete retention and 100% maximum expulsion.

One of the first and most important studies dealing with the compositional fractionation of organic compounds during petroleum expulsion from source into adjacent carrier rocks was conducted by Mackenzie et al. (1983). Essentially, these researchers examined early mature, type III organic matter-containing source rock-reservoir sequences from Svalbard, Norway, and proposed that petroleum expulsion has substantial impact particularly on small, light hydrocarbons. More specifically, it was found that *n*-alkanes up to *n*C₁₉ are preferentially expelled compared to the total bitumen content. Moreover, a significant depletion of C₁₅₊ components in both thin black shale layers, as well as at the edges of thicker source packages relative to reference samples from the centers of these thick units was documented, which they attributed to petroleum expulsion. Interestingly, their data did, however, not suggest differences in the absolute degree of expulsion between alkanes and aromatic hydrocarbons, implicating the total amounts of expelled alkanes and aromatics are roughly the same. Concerning differences between *n*- and *iso*-alkanes, Mackenzie et al. (1983) demonstrated that the expulsion efficiencies for pristane and phytane are lower than for *n*C₁₇ and *n*C₁₈, which represent the adjacently eluting *n*-alkanes.

In a more detailed study on the same sample material, Leythaeuser et al. (1984a) principally confirmed the results of Mackenzie et al. (1983). Essentially, it was reported that both thin shale layers, as well as the outer parts of thick source rock units are considerably depleted in petroleum compounds, particularly in light hydrocarbons, relative to the central parts of thick shale units, which are supposed to be largely unaffected by expulsion fractionation. Furthermore, significant fractionation among *n*- and *iso*-alkanes was attested with preferential expulsion of short- over long-chain *n*-alkanes, and a lower expulsion efficiency of pristane and phytane compared to *n*C₁₉ and *n*C₂₀. Note that the authors emphasized that these effects might have profound impact on the pristane/*n*C₁₇ ratio, which, although its significance has decreased over time, still represents a maturity indicator in petroleum geochemistry. In contrast to Mackenzie et al. (1983), Leythaeuser et al. (1984a) also presented data for steranes and hopanes. Based on the relative distributions of these biomarkers in source rock vs. reservoir samples, the authors concluded that steranes and hopanes do not undergo fractionation during primary migration, thus making them excellent tools for

3. Primary migration – state of the art

oil-source rock correlations, maturity estimation, and the determination of the organic facies type. In summary, Leythaeuser et al. (1984a) proposed that their observed fractionation trends are most probably related to adsorption/desorption processes between petroleum compounds and the source rock matrix, whereby the degree of retention significantly depends on the molecular structure of a component, its polarity, and steric hindrance effects.

A similar primary migration study but on different sample material was performed by Leythaeuser and Schaefer (1984). Basically, these researchers investigated rock material from a mature, Upper Carboniferous shale-carrier bed sequence from Germany and documented several well-pronounced geochemical trends, which they attributed to petroleum expulsion. First, similar to the expulsion studies described before, it was revealed that petroleum expulsion mainly occurred at the edges of the investigated source rock packages. Thereby, primary migration was accompanied by decreasing total extract yields, a decrease in the production index (see 3.6.1), as well as generally declining amounts of aliphatic and aromatic hydrocarbons. Concerning the distribution of *n*-alkanes, high expulsion efficiencies were calculated for *n*-alkanes $<nC_{26}$, pointing to a preferential expulsion of light hydrocarbons. Furthermore, a fractionation between pristane and nC_{17} in favor of nC_{17} was documented, indicating that *n*-alkanes move faster through the source rock than isoprenoids.

A few years later, Leythaeuser et al. (1988a, b) conducted a comprehensive two-part study on primary migration on mature source rock material from the Kimmeridge Clay Formation in the British North Sea. This study is very interesting for this work because comparable sample material was examined (see 5.). In the first part (Leythaeuser et al., 1988a), which focused mainly on the expulsion characteristics of *n*-alkanes and general differences in the distribution patterns of paraffins, aromatic hydrocarbons and polar heteroatomics, the authors revealed several conspicuous geochemical trends in approximation to nearby reservoir units. These were interpreted as effects of primary migration via petroleum bulk phase flow. In particular, it was reported that the total extract volumes notably decrease towards organic-lean intervals and the expulsion efficiencies for *n*-alkanes can reach values of 90% or greater, indicating *n*-alkanes are favorably expelled from the source rock compared to the rest of the source bitumen. Remarkably, no molecular redistribution among *n*-alkanes between nC_{15} and nC_{30} was documented, which was explained by discrete hydrocarbon phase movement. Another

3. Primary migration – state of the art

noteworthy tendency is that, consistent with results from earlier works, particularly the edges of the sampled source rock packages, as well as thin, intercalated organic-rich layers showed strong evidence for depletion, indicating that expulsion occurs predominantly from the outer parts of shale units. The main conclusion was that primary migration has substantially altered the original geochemical character of the Kimmeridge Clay Formation and therefore, without paying attention, false conclusions might be drawn with respect to the quality and the thermal maturity of source rock material. For example, if only the depleted edges of a source rock would be sampled, an investigator could falsely interpret the source rock as immature or gas-prone, although it actually contains a highly oil-prone kerogen type and is in the main stage of petroleum generation and expulsion. Hence, samples collected from the largely unaltered center of thick source units are probably most suitable to describe a source rock's geochemical character and to minimize the risk of false interpretations.

In contrast to the first part, the focus of the second part of the study (Leythaeuser et al., 1988b) was laid on the expulsion behavior of naphthalenes, phenanthrenes (both aromatic hydrocarbons), and benzothiophenes (sulfur aromatics). It is important to note that these compounds form the basis for several well-established organic geochemical maturity parameters, including the famous methylphenanthrene index (MPI 1), as well as the methyl dibenzothiophene ratio (MDR) (Radke, 1988 and references therein), and therefore their primary migration behavior is extremely important with respect to maturity estimations. Essentially, these ratios are defined as follows (from Radke, 1988):

$$MPI\ 1 = 1.5 * \frac{(2-MP + 3-MP)}{(P + 1-MP + 9-MP)} \quad (8)$$

$$MDR = \frac{(4-MDBT)}{(1-MDBT)} \quad (9)$$

whereby *P* stands for phenanthrene, *MP* for methylphenanthrene, and *MDBT* for methyl dibenzothiophene, respectively. Analogical to the trends observed in the first part of the study, Leythaeuser et al. (1988b) reported that the concentration of aromatic compounds also systematically decreased towards the edges of the thick source rock units, pointing to expulsion of these components into the adjacent reservoir units. Nevertheless, with regard to the absolute expulsion efficiencies, the values are much

3. Primary migration – state of the art

higher for *n*-alkanes than for aromatics, indicating that the latter are expelled to lesser degrees than saturates, which is in accordance with the composition of most natural crude oils. Additionally, among the investigated aromatics, the expulsion trends were more pronounced for naphthalenes than for phenanthrenes and benzothiophenes, suggesting that naphthalenes are generally easier expelled. The most important finding of the second part of the study was, however, that neither alkylnaphthalenes, alkylphenanthrenes nor alkylated sulfur aromatics were not found to undergo fractionation during primary migration. This is extremely important for maturity indicators based on these compounds, which, following Leythaeuser et al. (1988b), are therefore not affected by primary migration fractionation and can thus be applied to evaluate the thermal maturity of source rocks and their associated crude oils. In this context, it was mentioned that, for example, the MPI 1 in the reservoir probably reflect an average, mixed signal representing the maturation history of the source rock.

While the studies above can be regarded as a kind of basis for the investigation of primary migration and associated fractionation effects in natural systems, subsequent work concentrated particularly on the migration behavior of carbazoles, which represent pyrrolic nitrogen components that frequently occur in crude oils (e.g. Larter et al., 1996; Li et al., 1995, 1997; Clegg et al., 1997). What is important is that, although the factors influencing the distribution of these compounds in the sub-surface are still not completely understood, it seems that carbazoles can be applied to infer the migration distance of petroleum in sedimentary basins (e.g. Larter et al., 1996; Terken and Frewin, 2000; Zhang et al., 2004, 2013; Yang and Arouri, 2016). In this respect, one of the most popular organic geochemical ratios is the benzo-carbazoles ratio (BC ratio), which was established by Larter et al. (1996). It is defined as (from Larter et al., 1996):

$$BC \text{ ratio} = \frac{\textit{Benzo[a]carbazole}}{\textit{Benzo[a]carbazole} + \textit{Benzo[c]carbazole}} \quad (10)$$

Basically, these researchers proposed that the distribution of benzo[a]- and benzo[c]-carbazole varies with the migration distance of petroleum in a sedimentary basin, whereby benzo[a]carbazole seems to be preferentially retained by minerals and organic matter, ultimately resulting in a decrease of the BC ratio with increasing migration distance. Further investigations casted, however, doubt on the applicability of the ratio due to good correlations with organic facies and thermal maturity (Clegg et

3. Primary migration – state of the art

al., 1997, 1998a, b; Bakr and Wilkes, 2002; Zhang et al., 2013). Up to present, it is largely unresolved to what extent primary migration influences the distribution of carbazoles in the subsurface, and has thus an impact on the BC ratio, which has an outstanding importance in the petroleum exploration business. The investigation of a potential expulsion influence on the BC ratio was also part of this work. Promising studies on the impact of primary migration on the distribution of carbazoles were conducted, for example, by Li et al. (1995, 1997) and Bennett et al. (2002), who presented convincing evidence for substantial carbazole redistribution during primary migration, indicating these molecules are indeed fractionated upon petroleum expulsion. For instance, Li et al. (1995) examined the distributions of carbazoles in selected crude oils vs. associated source bitumens and reported several remarkable differences. The first thing that was observed was that alkylated carbazoles were generally more abundant in crude oils than alkylated benzocarbazoles, indicating that benzocarbazoles are preferentially retained compared to the more simply structured carbazoles. Second, the data showed that nitrogen-shielded carbazoles tended to be more enriched in crude oils than nitrogen-exposed isomers, suggesting that alkyl groups located adjacent to the polar group significantly restrict adsorption/desorption interactions and therefore favor expulsion. Furthermore, third and last, Li et al. (1995) noted that the higher the degree of alkylation, the greater the enrichment of the respective compound in the reservoir, which, in turn, implies that higher alkylated compounds move faster than non- or single-alkylated molecules, i.e. are preferentially expelled from the source rock. Correspondingly, in an ensuing study, Li et al. (1997) monitored pyrrolic nitrogen compounds of the Duvernay Formation in Alberta, Canada, over a wide range of thermal maturities. They observed an increase in the concentration of C₀-C₃ carbazoles, accompanied by an increase of the BC ratio with increasing maturity. In addition, they reported that the ratios of 1-/4-methylcarbazole and 1,8-/2,4-, as well as 1,3-/2,4-dimethylcarbazole first increased with maturity, and then significantly decreased at maturities exceeding 1.02% R_o. The authors concluded that both adsorption/desorption effects during primary migration, as well as the thermal maturity exert a strong influence on the distribution of carbazoles in the subsurface. To exclude artifacts due to secondary migration, the results were controlled by hydrous pyrolysis experiments following the standard procedure by Lewan et al. (1979) and Lewan (1993) (see 3.6.3). However, the study lacked sample material from the maturity interval between 0.74% and 1.02% R_o, which roughly corresponds to the peak oil

3. Primary migration – state of the art

window where most of the expulsion takes place. Therefore, the data should be regarded with caution. In a similar approach, Bennett et al. (2002) investigated fractionation effects of benzocarbazoles in a series of oil and source rock samples from the Kimmeridge Clay Formation, North Sea. They introduced the so-called reservoir source fractionation parameter (RSFP), which is defined as the ratio between the summed concentrations c of benzo[a]- and benzo[c]carbazole in reservoired petroleum, divided through the sum of both components in the retained source rock bitumen (from Bennett et al., 2002):

$$RSFP = \frac{c(\text{Benzo}[a]\text{carbazole} + \text{Benzo}[c]\text{carbazole})_{\text{Reservoired Petroleum}}}{c(\text{Benzo}[a]\text{carbazole} + \text{Benzo}[c]\text{carbazole})_{\text{Source Bitumen}}} \quad (11)$$

While ratios considerably less than 1 indicate substantial fractionation, values close to 1, on the other hand, suggest weak fractionation. The data indicate that benzocarbazoles are generally much higher concentrated in the source rock than in crude oils, pointing to a strong retention of benzocarbazoles during petroleum generation and expulsion. Thereby, their distribution pattern seems to be particularly controlled by the amount of organic material present in the source rock, as suggested by a good correlation between the total organic matter content of the source rock and the BC ratio. Interestingly, as an additional point, the distribution of benzocarbazoles in the source rock was found to be remarkably lithology dependent. In particular, shaly source rocks seem to retain benzocarbazoles more effectively than carbonate source rocks, indicating that the mineralogy of the source rock is extremely important with respect to primary migration. Note, however, that Bennett et al. (2002) focused exclusively on benzocarbazoles and did not consider alkylated carbazoles, which might have provided further insights. Since the studies cited above indicate that carbazoles undergo fractionation during primary migration, it can be assumed that other potential heteroatomic petroleum migration tracers, e.g. alkylbenzoquinolines (Yamamoto, 1992) and xanthenes (Oldenburg et al., 2002), are also influenced by expulsion fractionation. This remains, however, to be confirmed.

A last and very recent case study that should be described in this subchapter is that of Han et al. (2017), which concentrated particularly on the expulsion behavior of steranes and hopanes that is still open for discussion. Essentially, these workers analyzed mature source rock and reservoir samples from the Barnett Shale, U.S.A., and proposed that primary migration has negligible influence on the distribution patterns of

3. Primary migration – state of the art

biomarkers in their sample material, indicating that steranes and hopanes are very suitable to determine the thermal maturity and the organic facies of source rocks, and can in addition well be used for correlations between crude oils and source bitumens. These findings are in good agreement with those published earlier by Leythaeuser et al. (1984a), who also did not recognize compositional fractionation among steranes or hopanes upon petroleum expulsion. Nevertheless, since Seifert and Moldowan (1978, 1981) reported that the distribution of steranes in their sample material was considerably influenced by migration processes, it remains questionable whether biomarkers are indeed not redistributed upon migration. Both, additional field and experimental studies are necessary for clarification.

3.4.5 Experimentally simulated fractionation effects

The second possibility to investigate expulsion-related molecular redistribution effects are laboratory experiments. A brief summary of the potential techniques that can be used to simulate petroleum formation and primary migration in the laboratory can be found in section 3.6. The major advantage of experimental approaches compared to natural expulsion scenarios is that secondary factors, e.g. secondary migration, oil mixing or biodegradation, which need to be considered in natural systems, can be ruled out in experiments, thus simplifying the interpretation. On the other hand, there is, however, always some uncertainty if nature is reproduced correctly, due particularly to generally very fixed experimental conditions, which may deviate from those in natural petroleum systems. Nevertheless, despite some variance, experiments in the past were largely able to simulate at least the gross compositional differences between crude oils and source bitumens that are frequently observed in nature (see 3.4.2) (e.g. Lewan et al., 1979; Horsfield et al., 1989; Lafargue et al., 1990; Lewan, 1993; Stockhausen, 2015). Some of the most essential results are described in the following.

The first study that is important to mention in this context is that of Lewan et al. (1979), who established an experimental technique termed hydrous pyrolysis. Although it remains debated in how far nature is adequately reproduced, hydrous pyrolysis (see also Lewan, 1993) still counts as one of the most promising experimental approaches to simulate organic matter maturation and petroleum expulsion from source rocks. Essentially, Lewan et al. (1979) pyrolyzed immature, oil-prone Woodford Shale (U.S.A.) material in a pressure reactor in the presence of water and were able to generate a floating, oil-like pyrolyzate phase, whose composition was strikingly similar

3. Primary migration – state of the art

to that of a natural crude oil believed to originate from the Woodford Shale. In particular, Lewan et al. (1979) documented an almost equivalent distribution pattern of *n*-alkanes, a very similar gross geochemical composition, as well as comparable carbon isotope ($\delta^{13}\text{C}$) values in the artificial pyrolyzate vs. the natural crude oil. There were, however, also some differences. The first noteworthy discrepancy was that the pyrolyzate displayed a broader range of pristane/phytane ratios compared to the natural oil sample. Because the pristane/phytane ratio showed pronounced variations with time, this dissimilarity was attributed to the experimental runtime. Though, more important were the facts that the pyrolyzate on one hand contained considerably greater proportions of polar compounds, and, on the other hand, was mildly depleted in saturates compared to the natural crude. These variations were related to differences between the conditions in natural systems and the applied experimental setup, in which the sample material experienced much lower pressures and tremendously higher temperatures (200-250 °C) than in nature. Furthermore, it was mentioned that in natural systems many polar compounds may either be strongly retained in the source rock, or adsorbed due to chromatographic interactions during secondary migration.

Subsequent work using hydrous pyrolysis was generally in accordance with these findings (e.g. Lewan, 1983, 1993; Lewan et al., 1986). For example, in another experimental study, Lewan et al. (1986) performed hydrous pyrolysis experiments on shaly, oil-prone samples from the Permian Phosphoria Formation, U.S.A., in order to investigate the effects of thermal maturation on the distribution of regular steranes, diasteranes, and aromatic steroids. Similar to Lewan et al. (1979), their experiment revealed a high degree of similarity between the hydrous pyrolysis products and crude oils and source bitumens from the corresponding natural petroleum system, indicating hydrous pyrolysis experiments are indeed very suitable to simulate petroleum formation in the subsurface. In short, Lewan et al. (1986) documented maturity trends analogous to observations in natural systems and concluded that maturity parameters based on steroid-type hydrocarbons can, provided they are verified by other maturity indicators, well be applied to evaluate the thermal maturity of source rocks and crude oils in natural petroleum systems. With regard to effects attributable to primary migration, Lewan et al. (1986) reported similar sterane distributions in the pyrolyzate and the retained source rock bitumen, suggesting steranes are not fractionated during expulsion. Though, a preferential enrichment of mono- over triaromatic steroids was

3. Primary migration – state of the art

observed in the pyrolyzate phase, indicating that triaromatic steroids are preferentially retained in the source bitumen compared to monoaromatic steroids. In sum, despite some uncertainties that always exist in experimental approaches, hydrous pyrolysis seems to be generally appropriate for the investigation of molecular redistribution effects associated with petroleum expulsion. According to Lewan (1993), the main advantage of hydrous pyrolysis is that practically all components greater than five carbon atoms can be investigated, including a large suite of low-boiling, heteroatomic compounds that are often lost in corresponding anhydrous techniques. More specifically, it was accentuated that the pyrolyzate phases generated and expelled in equivalent anhydrous methods mostly do not sufficiently reproduce the composition of natural crude oils, e.g. contain significant quantities of alkenes, and, additionally, are often formed by processes that are rather unlikely to operate in natural petroleum systems. Indeed, in a later publication concentrating explicitly on the influence of water during petroleum generation and expulsion, Lewan (1997) came to the conclusion that water is extremely important during petroleum generation and expulsion.

Nevertheless, some promising anhydrous experiments have been conducted as well. For example, Lafargue et al. (1990) used anhydrous, confined pressure pyrolysis to investigate the influence of expulsion on the molecular composition of petroleum derived from the Schistes Carton, France, and the Kimmeridge Clay Formation from the North Sea and noted considerable redistribution effects as a result of primary migration. In particular, these were the preferential expulsion of saturated hydrocarbons relative to aromatic components, and a higher yield of *n*-alkanes relative to isoprenoids, trends that correspond well with observations in natural systems (e.g. Mackenzie et al., 1983; Leythaeuser et al., 1984a, 1988a). A subsequent, more recent anhydrous approach was performed by Esemé et al. (2007). These researchers investigated the molecular composition of pyrolyzates generated and expelled from six different source rock plugs during anhydrous, open system pyrolysis under controlled pressure conditions. Thereby, they focused specifically on the distribution patterns of *n*-alkanes, *iso*-alkanes, hopanes, phenanthrenes, and fatty acids and therefore in the main compounds that play an important role in the petroleum industry, in the initial source bitumens vs. the expelled pyrolyzates and the bitumens after the experiment. In essence, they were able to demonstrate a preferential expulsion of *n*- and *iso*-alkanes relative to triterpanes, aromatics, and polars, whereby the composition of the expelled products strongly depended on the type of the organic material in the

3. Primary migration – state of the art

respective source rock and inevitable evaporative losses due to open system conditions. Moreover, this sequence suggests that cyclic aliphatics, aromatic hydrocarbons, as well as heteroatomic compounds, including fatty acids, are preferentially retained in the source rock compared to the more simply structured acyclic saturates, which is in good accordance with the compositional differences between source bitumens and crude oils in natural systems. Primary migration-related redistribution effects within the individual compound groups, e.g. among triterpanes or phenanthrenes, were, however, not observed. Particularly interesting is that no fractionation between *n*- and *iso*-alkanes (pristane/*n*C₁₇, phytane/*n*C₁₈) was reported. Furthermore, molecular effects related to the lithology of the source rock were not documented either. Based on their data, Esemé et al. (2007) concluded that petroleum generation and expulsion take place contemporaneously, and, since the expelled pyrolyzate phases are principally composed of the full range of compounds generated throughout the experiments, the compositions of the expelled products probably reflect the whole maturation histories of the source rock samples. It should, however, be emphasized again that these and the results of Lafargue et al. (1990) were obtained by anhydrous pyrolysis. Therefore, since hydrous approaches appear to reproduce natural processes more accurately, it is questionable in how far their observations actually reflect natural processes.

One of the most promising experimental techniques to simulate primary migration in the subsurface was recently introduced by Stockhausen (2015), who developed an open hydrous pyrolysis system termed “Expulsinator”. The results obtained from “Expulsinator” experiments are to a large extent in agreement with nature, hence making this technique very suitable to investigate molecular fractionation effects associated with petroleum expulsion. Briefly, Stockhausen (2015) performed “Expulsinator” experiments on eight source rock samples with varying types of organic material. Essentially, the experiments revealed that, (1) short-chain were expelled preferentially to long-chain *n*-alkanes, (2) the ratio of *n*-alkanes to isoprenoids depended mainly on petroleum generation, (3) pristane was preferentially released compared to phytane, and (4) the lithology of the source rock had a strong impact on petroleum expulsion. Concerning the influence of the mineralogy, dense and robust source rocks were demonstrated to expel petroleum less efficient than source rocks with a low hardness, which was related to a greater fracturing resistance of the former, assuming that cracks represent important migration pathways during primary

3. Primary migration – state of the art

migration. Regarding the data, the author concluded that petroleum generation and expulsion are first initiated in type III kerogens, followed by type IIS, type II, and lastly type I kerogens. This sequence is partially contradictory to nature, where coals are usually considered as late expellers and to be predominantly gas-prone. Taking this into account, Stockhausen (2015) attributed the observed generation-expulsion sequence to a combination of a very good petroleum generation potential of the type III organic matter-containing source rock material and the experimental setup, which was constructed to provide excellent expulsion conditions.

In addition to the experimental approaches designed to investigate petroleum generation and expulsion on the whole, other laboratory techniques exist that concentrated explicitly on the impact of specific factors on the composition of petroleum. Concerning primary migration, these are molecular diffusion, geochromatography, and kerogen absorption (see 3.3). Larter et al. (2000) attempted to study geochromatographic separation processes (see 3.3.2) by means of a core-flood experiment in which a crude oil was passed through a water-wet siltstone column under subsurface conditions. Although the focus of this experiment was laid on secondary rather than on primary migration, it well allowed to examine the fractionation behaviour of different organic compounds upon migration, which may be transferable to primary migration. The authors reported that the aliphatic hydrocarbon fraction did not exhibit notable compositional changes upon migration, whereas, on the other hand, the NSO fraction underwent considerable fractionation when passing the siltstone column. Similar to the natural case studies conducted for instance by Leythaeuser et al. (1984a) and Han et al. (2017) (see above), the witnessed effects cast doubt on the applicability of aliphatic petroleum migration tracers (Seifert and Moldowan, 1978, 1981), as well as the molecular redistribution effects reported by Carlson and Chamberlain (1986) and Zhusheng et al. (1988), who noted migration-induced fractionation among aliphatic biomarkers. The results published by Larter et al. (2000) are, however, to some extent different compared to those published earlier by Bonilla and Engel (1986, 1988), who also attempted to investigate geochromatographic fractionation effects and passed a natural crude oil through a high-performance liquid chromatography (HPLC) column loaded with water-saturated quartz sand and varying proportions of montmorillonite. These authors noted a preferential migration of short- over long-chain *n*-alkanes, which intensified proportionally to the amount of clay minerals. Moreover, in both studies the NSO and the aliphatic fractions became increasingly ¹³C-depleted with increasing

3. Primary migration – state of the art

migration distance, whereas, on the other hand, the $\delta^{13}\text{C}$ values of the aromatic hydrocarbons did not show systematic changes. It is interesting to note that Bonilla and Engel (1988) additionally reported a chromatographic separation of methylphenanthrenes in favor of the 9- and 1-isomers with increasing migration distance. This has profound consequences with regard to the MPI 1 maturity parameter (equation 8), which, according to Bonilla and Engel (1988), would consequently decrease in the course of migration and therefore not be appropriate to determine the thermal maturity of crude oils. This is in strong contrast to the natural results published by Leythaeuser et al. (1988b), who did not observe redistribution effects among methylphenanthrenes in mature sample material from the British North Sea.

In a series of solvent swelling-experiments, Sandvik et al. (1992) attempted to investigate the differential retention of petroleum compounds in the kerogen matrix and therefore the role of kerogen absorption on the composition of expelled petroleum. The authors came to the conclusion that NSO compounds and aromatics are preferentially retained by the polymer-like kerogen, whereas acyclic isoprenoids and *n*-alkanes are favorably released. Additionally, isoparaffins were proposed to be more sensitive to absorption in organic material than *n*-alkanes. Furthermore, Sandvik et al. (1992) provided evidence that particularly the polar compounds are retained in the source rock, leading to expelled products enriched in saturates, consistent with observations in natural petroleum systems.

Fractionation effects related to molecular diffusion were investigated, for example, by Stainforth and Reinders (1990). Using a combination of laboratory experiments and numerical modeling, these authors concluded that light, small components are mobilized more readily than branched compounds, pointing to a preferential expulsion of *n*-alkanes relative to isoprenoids. Furthermore, concentration trends very similar to those reported in natural systems (Leythaeuser et al., 1988a) were obtained, indicating that molecular diffusion plays indeed a key role during primary migration and can be considered as a fundamental mechanism for compositional reorganization. Note also that compositional differences in the source bitumen were identified depending on the relative location in the source rock. Hence, source rock edges may display a different compositional signal than source rock centers.

3. Primary migration – state of the art

To sum up, laboratory experiments are very useful to get a better understanding of the processes operating during primary migration. In general, primary migration can be investigated either as a whole process, for instance by using the “Expulsinator” device (Stockhausen, 2015) or, alternatively, individual factors causing compositional differences between source bitumens and crude oils can be studied separately by very specialized experiments (e.g. diffusion experiments, column flow experiments, solvent-swelling experiments). However, results from experimental and natural studies are often contradictory. This may, on one hand, be related to sometimes unsuitable experimental conditions, but, on the other hand, also due to misinterpretations of natural trends, which could, for instance, also be influenced by secondary migration, staining or mixing effects. Therefore, further studies involving both natural and experimental approaches are necessary for a comprehensive understanding of primary migration and particularly the fractionation behavior of compounds with great significance in the petroleum industry.

3.5 Kinetic concepts

Kerogen decomposition and petroleum generation can be modelled using reaction kinetics based on pyrolysis experiments. Kinetic modelling plays, however, a subordinate role in this work since main emphasis is placed on expulsion-induced molecular fractionation effects. Therefore, only the basic concepts shall be summarized here. Briefly, kerogen degradation can be considered as a 1st order reaction (Ungerer, 1990; Behar et al., 1992; Pepper and Corvi, 1995b; Bjørlykke, 2015a), although alternative modes of nth order have been postulated, too (Sagert and Laidler, 1963a, b; Blakemore et al., 1973; Delvaux et al., 1990; Stainforth, 2009). Basically, this is due to the relationship between generated petroleum and residual organic matter during maturation, which points towards 1st order kinetics (Pepper and Corvi, 1995b). Kinetic models describe the kerogen decomposition over time, following the equation below (from Pepper and Corvi, 1995a):

$$\frac{dc}{dt} = -kc \quad (12)$$

dc/dt refers to the rate of kerogen conversion over time, c to the kerogen concentration and k to the rate constant. k is described by the Arrhenius law, which links the kerogen degradation to the frequency factor A , the activation energy E , the Universal

3. Primary migration – state of the art

Gas Constant R , as well as the temperature T , allowing petroleum geologists to model oil and gas generation in a sedimentary basin over geological timescales (e.g. Burnham and Braun, 1990; Ungerer, 1990; Pepper and Corvi, 1995b; Lewan et al., 2006; Stainforth, 2009; Wei et al., 2012). The Arrhenius law is defined as follows (from Pepper and Corvi, 1995a):

$$k = A * e^{\left(\frac{-E}{RT}\right)} \quad (13)$$

One of the most essential approaches to obtain kinetic parameters are hydrous pyrolysis experiments (see 3.6.3) (Lewan et al., 1979; Lewan, 1993). Such experiments bear the advantage that they explicitly focus oil generation, whereas alternative anhydrous approaches largely suffer carbon-carbon cross-linking and the formation of pyrobitumen, resulting in misleading data and inexact kinetic parameters (Lewan, 1997). However, they lack lithostatic pressure, making them partially incomparable to nature (Stockhausen, 2015). Basically, kinetic parameters can be determined using oil yields from time and temperature runs (Lewan et al., 2006). Considering the percentage of a reaction completed at a given temperature, reaction rate constants can be calculated, logarithmized and plotted against the temperature reciprocal to determine the activation energy from the slope and the frequency factor from the intercept of the Arrhenius equation (equation 13) (Lewan and Ruble, 2002; Lewan et al., 2006). Since A and E depend on the experimental procedure, different models exist, including several values for both parameters. Following Wei et al. (2012), A is related to the vibrational frequency of the reactants, whereas E is proportional to the bond energy. Hence, E crucially depends on the kerogen type, with kerogens containing large quantities of stable covalent C-C bonds requiring the highest activation energies. By contrast, E is lower for kerogens comprising chiefly weak heteroatomic bonds.

Stainforth (2009) underlined that conventional kinetic models are often not straightforward. Limitations arise due to, (i) unsuitable pyrolysis methods, (ii) oversimplification of natural systems, (iii) inadequate mathematical conversion of laboratory data, (iv) poor knowledge about primary migration, and (v) limited subsurface data. In particular, it was criticized that kinetic parameters often do not have true physical meanings, underscoring the complexity of kinetic modeling. As a result, prediction of natural heating rates is often inaccurate, leading to false conclusions concerning

3. Primary migration – state of the art

petroleum generation and expulsion. The author accentuated that adequate kinetic models need to consider chain and parallel reactions, n^{th} order reaction behavior, as well as an integrated model for primary migration involving the key factors described in 3.2.

3.6 Experimental approaches

A wide range of laboratory techniques for the investigation of petroleum formation has been published throughout the last decades (e.g. Espitalié et al., 1977; Lewan et al., 1979; Lewan, 1993; Monthioux et al., 1985; Horsfield et al., 1989; Lafargue et al., 1990, Liao et al., 2004). In general, such techniques include (i) open system pyrolysis, (ii) anhydrous closed system pyrolysis, (iii) hydrous closed system pyrolysis (Behar et al., 2010), and (iv) hydrous open pyrolysis (Stockhausen, 2015). Only few of them focused on primary migration. However, various types of experiments have been conducted to study explicitly the molecular effects of diffusion (see 3.3.1) (Stainforth and Reinders, 1990), geochromatography (see 3.3.2) (e.g. Bonilla and Engel, 1986; Greibrokk et al. 1994; Larter et al., 2000) and kerogen absorption (see 3.3.3) (Sandvik et al., 1992), which are supposed to represent the major reasons for molecular fractionation during primary migration. To provide a comprehensive over-view of primary migration the principal approaches mentioned above will be briefly described in the following. A detailed overview of different pyrolysis techniques as well as a discussion of their suitability for simulation of primary migration is given by Stockhausen (2015). Conventional pyrolysis methods suffer a number of limitations, comprising: (1) the absence of water, (2) the destruction or removal of the mineral matrix, (3) the lack of lithostatic pressure, (4) inappropriate temperature ranges, and (5) artifacts due to unsuitable experimental setups. Since petroleum generation, migration and accumulation in natural systems usually take millions of years of time, laboratory experiments, therefore, cannot entirely fit nature. Hence, any experimental approaches must necessarily be conducted at higher temperatures, partially above 300 °C (Lafargue et al., 1990, 1994; Lewan et al., 1979; Lewan, 1997; Esemé et al., 2006; Stockhausen, 2015). However, temperatures above 374.12 °C exceed the critical point of water, causing both experimental complications and result uncertainties, as emphasized by Stockhausen (2015).

3.6.1 Open system pyrolysis

3. Primary migration – state of the art

It has been suggested that petroleum systems can largely be considered as open systems, due primarily to the possibility of energy and mass exchange with the surrounding (Cooles et al., 1986; Pepper and Corvi, 1995b). To fit best to natural conditions, open system pyrolysis should ideally be conducted in attendance of water, lithostatic pressure and intact rock samples within a suitable open system device. This is, however, difficult to realize under conventional conditions with regard to the experimental setup but rather requires the use of an “Expulsinator” open pyrolysis device, as underlined by Stockhausen (2015).

Rock-Eval pyrolysis

The most prominent open system technique is Rock-Eval pyrolysis (Espitalié et al., 1977). This bulk flow approach is widespread in petroleum industry and basically serves to evaluate the source potential, the type of organic matter and the thermal maturity of a rock sample. Furthermore, the method enables the calculation of kinetic parameters required for basin modeling purposes (Schaefer et al., 1990; Erdmann and Horsfield, 2006). In short, between 10 and 100 mg of powdered rock material become thermo-vaporized in an oven under protective helium atmosphere. There-fore, the sample is progressively heated from 300 to about 600 °C, causing first the vaporization of free hydrocarbons, followed by artificial kerogen cracking at higher temperatures. Three peaks are measured, the S_1 peak, corresponding to the bitumen content of the sample, the S_2 peak, which represents hydrocarbons released from the thermal breakdown of the kerogen and, lastly, the S_3 peak, which correlates with the CO_2 released from the decomposition of oxygen-containing compounds. The data obtained from a Rock-Eval pyrolysis experiment allow for the calculation of the three well-established geochemical parameters production index (PI), hydrogen index (HI) and oxygen index (OI), which are useful with respect to kerogen classification and source potential assessment:

$$PI = \frac{S_1}{(S_1 + S_2)} \quad (14)$$

$$HI = \frac{S_2}{TOC} * 100 \quad (15)$$

$$OI = \frac{S_3}{TOC} * 100 \quad (16)$$

3. Primary migration – state of the art

Moreover, the total hydrocarbon generation potential (THGP) (Robison, 1997) can be expressed as:

$$THGP = S_1 + S_2 \quad (17)$$

Besides, the T_{max} parameter, which is measured at the acme of the S_2 peak corresponds to the temperature of the maximum pyrolysis yield and is therefore principally related to the thermal maturity of the sample. The T_{max} rises with increasing thermal maturity because more energy is required for kerogen decomposition at later stages of thermal maturation. In combination with the production index (equation 14), the T_{max} represents a relatively robust maturity parameter (Peters et al., 2005a). It should, however, always be verified with other maturity indicators, for example measured vitrinite reflectance data or molecular maturity proxies (Killops and Killops, 2005; Peters et al., 2005a). The T_{max} parameter can be converted into a vitrinite reflectance value $R_{o\text{ calculated}}$ using, for instance, the following equation (from Jarvie et al., 2007 and reference therein):

$$R_{o\text{ calculated}} = (0.018 * T_{max}) - 7.16 \quad (18)$$

Yet, the equation should be applied with caution since it can be problematic for type I kerogens containing abundant covalent C-C bonds, type IIS kerogens comprising many labile C-S bonds, and for immature and highly mature samples (Peters et al., 2005a). The reason to choose exactly this equation was that Peters et al. (2005a) stated that it produces good results for type II and III kerogens, which are expectable for the source rock samples examined in this work. Another important ratio based on Rock-Eval results is the oil saturation index (OSI) introduced by Jarvie (2012). Essentially, it relates the free bitumen content of a sample to its TOC value and therefore allows to estimate the degree of oil saturation in a sample (from Jarvie, 2012):

$$OSI = \frac{S_1}{TOC} * 100 \quad (19)$$

In petroleum exploration business the OSI serves to identify producible rock intervals. In particular, an oil crossover value of 100 mg oil/g TOC has been suggested to distinguish between producible and non-producible rock units (Jarvie, 2012).

The “Expulsinator”

3. Primary migration – state of the art

Recently, Stockhausen (2015) introduced a new pyrolysis method called “Expulsinator” to overcome the limitations of conventional approaches (see 3.6). The aim was to simulate primary migration and expulsion as close to natural conditions as possible. Basically, the “Expulsinator” can be considered as an open, hydrous pyrolysis system. It essentially consists of a central steel cell, a pressure stamp and a complex piping system interfaced with a controlling unit. The system utilizes intact source rock plugs with 5 cm diameter which become progressively subjected to catagenetic pressure conditions at elevated pyrolysis temperatures up to 360 °C. Products generated during the experiment are expelled into a porous artificial reservoir surrounding the rock plug. Subsequently, the products are flushed out of the reactor at regular time intervals using distilled water, mixed with small amounts of a modifier (*n*-hexane/isopropyl alcohol (85:15, v/v)) for quantitative flushing. The system allows quantitative sampling of liquids and gases.

Other open system approaches

Other open system pyrolysis techniques comprise (i) fixed-bed hydrolysis, (ii) pyrolysis coupled with gas chromatography, (iii) the self-purging reactor, and (iv) uni- and triaxial pressure pyrolysis (Stockhausen, 2015). Their description is, however, out of the scope of this work.

3.6.2 Anhydrous closed system pyrolysis

In contrast to Cooles et al. (1986), Lewan et al. (2006) suggested that a naturally maturing source rock can be regarded as a closed rather than an open system. These investigators argued that geological processes, in particular heating and migration usually proceed over large timescales, better represented by closed system pyrolysis where products generated are exposed for longer periods to pyrolysis temperatures. The second major group of pyrolysis techniques are anhydrous closed system approaches, in which samples are pyrolyzed in the absence of water. Experimental procedures of this type involve (i) microscale sealed vessel pyrolysis (MSSV), (ii) anhydrous closed small vessel pyrolysis, (iii) anhydrous gold bag pyrolysis, and (iv) confined pressure pyrolysis (Stockhausen, 2015). Due to the low relevance of these methodologies for this study, a description is omitted.

3.6.3 Hydrous closed system pyrolysis

3. Primary migration – state of the art

Various researchers have proposed that hydrous pyrolysis experiments are principally suitable to investigate primary migration (e.g. Lewan et al., 1979, 2006; Bonilla and Engel, 1986; Lewan, 1993). Lewan (1993) defined hydrous pyrolysis as a hydrothermal technique in which the pyrolyzed sample material is kept in contact with liquid water throughout the experiment. Such experiments are well-established in petroleum geology and inter alia serve to determine kinetic parameters for basin modeling. Stockhausen (2015) casted, however, doubt on the applicability of conventional hydrous pyrolysis experiments with respect to the investigation of primary migration. In particular, it was criticized that such approaches normally utilize rock chips or powder instead of untreated samples with intact rock matrices, causing a greater contact area between water and kerogen, which is in opposite to natural conditions. Therefore, Stockhausen (2015) concluded that some of the dynamics observed during conventional hydrous pyrolysis experiments rather reflect reservoir than primary migration processes. In general, two types of closed hydrous pyrolysis techniques can be distinguished: (1) hydrous gold bag pyrolysis, and (2) hydrous closed small vessel pyrolysis (Stockhausen, 2015). In the latter approach, which was established by Lewan et al. (1979), crushed or powdered source rock samples become heated in contact with liquid water within a reactor vessel, leading to artificial kerogen cracking, petroleum generation and finally expulsion. The volume of water required for the experiment can be calculated by means of steam tables and rock densities (Lewan, 1993). Helium is usually used as headspace gas. In contrast, hydrous gold bag experiments denote sample pyrolysis in small gold tubes, mostly under hydrostatic pressure (Monthieux et al., 1985; Stockhausen, 2015). Since gold is relatively temperature-resistant and behaves largely inert under catagenetic conditions, an experimental environment ideal for the investigation of petroleum generation and principally expulsion can be created.

3.6.4 Experimental investigation of molecular diffusion

Molecular diffusion of petroleum through the kerogen network can be considered as a major fractionation mechanism of organic compounds during primary migration (see 3.3.1). As described by Stainforth and Reinders (1990), molecular diffusion can be investigated by so-called “interdiffusion experiments” specifically adapted for rock samples. According to Stainforth and Reinders (1990), such experiments principally

3. Primary migration – state of the art

require two halves of one and the same source rock sample, from which one remains untreated, and the other is heated to 351 °C and kept isothermal for 17 h to induce petroleum generation. Thereafter, both halves become reunified and subjected to 40 MPa and 260 °C for 10 days to initiate molecular diffusion. After the experiment, high-resolution cross sections through the compressed halves principally enable the reconstruction of diffusion profiles from one half to the other. An alternative but very similar approach would be to powder, homogenize and split an organic-rich rock sample, and then completely solvent-extract one of the halves. Instead, it would also be possible to extract both halves and afterwards spike one part with a defined amount of tracer solution containing selected organic compounds. Subsequently, both halves are loaded into a closable steel cell separated by a glass wool filter, compacted and ultimately heated to the final temperature of 260 °C. After 10 days, high-resolution sampling and solvent-extraction of both sides would probably make it possible to reconstruct diffusion profiles and to get a better understanding of redistribution effects owing to molecular diffusion.

3.6.5 Column flow experiments

Geochromatography during petroleum migration, which can be regarded as another key mechanism causing compositional fractionation upon primary migration (see 3.3.2) (Krooss et al. 1991), was investigated via column flow experiments by various studies (e.g. Bonilla and Engel, 1986, 1988; Greibrokk et al. 1994; Larter et al., 2000). Essentially, natural crude oils were passed through columns filled with water-wet sand-/siltstone mixtures and optionally varying proportions of clay minerals to examine compositional redistribution associated with petroleum migration. As an alternative to a natural crude, it is also possible to use a synthetic oil with a defined chemical composition, which was done for example by Brothers et al. (1991). In general, two different ways exist to perform column flow experiments. While in the first approach oils are simply passed gravitationally through the column, the second variant is more complex and typically involves a heating device to simulate natural temperatures, and a pumping system, which forces the oil through the column.

3.6.6 Solvent-swelling experiments

The selective absorption of organic compounds by kerogen has been considered as a principal mode of fractionation during primary migration (see 3.3.3). This process can

3. Primary migration – state of the art

be examined by solvent-swelling experiments, which enable to investigate the absorption of organic compounds in macromolecular polymers, with respect to petroleum systems particularly in kerogen. Solvent-swelling experiments have been conducted, for example, by Green et al. (1984), Sandvik et al. (1992) and Larsen and Li (1994, 1997a, b). As mentioned in subsection 3.3.3, coals or isolated kerogens can be swollen by organic solvents to determine the respective swelling ratio Q_V , which is related to the solubility parameter δ and thus the absorption capacity. In general, the swelling of polymers can be measured through comparison of either volumes or weights of the untreated vs. the solvent-swollen sample (Green et al., 1984).

4. Geological background of the study area

4. Geological background of the study area

Most of Norway's petroleum resources are located on the Norwegian Continental Shelf (NCS) (Fig. 11), which can be subdivided into three major territories: (1) the North Sea, (2) the Mid-Norwegian continental margin, and (3) the western Barents Sea (Faleide et al., 2015). In the North Sea sector, the Viking Graben area is of particular importance, as it represents one of the largest oil provinces in western Europe. The following chapter addresses the geological evolution of the study area and its principal structural configuration. Further emphasizes will be put on depositional history and petroleum source rock characteristics of the formations studied in this work, namely the Upper Jurassic Draupne and the Middle Jurassic Hugin Formation.

4.1 Evolution of North-West Europe

A comprehensive overview of the geological history of North-West Europe, including the evolution of the Norwegian Continental Shelf, can be found, for example, in Coward et al. (2003). In the following chapter a short overview will be presented.

4.1.1 Palaeozoic

The evolution of North-West Europe started in the Ordovician (~460 Ma). At that time, the ancient landmasses Avalonia, Baltica and Laurentia were separated by the Iapetus Ocean and the Tornquist Sea, which began to close in the course of the Caledonian Orogeny from around the Middle Ordovician to the Lower Devonian (Zanella et al., 2003). The Caledonian Orogeny was initiated by convergent plate tectonics and can be considered as one of two major Palaeozoic accretionary events that formed large parts of the landscape of northern Europe (Coward et al., 2003). The second key event was the Variscan Orogeny that took place from about 400 to 300 Ma and culminated in the formation of the Appalachian orogen in North America. Essentially, both orogenies represented long-term, north-westerly orientated phases of convergent plate tectonics and continental accretion, accompanied by continental escape in north-east direction (Coward et al., 2003). During the Devonian a proto-Viking Graben structure evolved in the area of the northern North Sea as a result of the formation of a large pull-apart basin, which most likely developed in response to the collapse of the Caledonian mountain belt (Coward et al., 2003; Zanella et al., 2003). It is important to note that several major faults and sub-basins developed all

4. Geological background of the study area

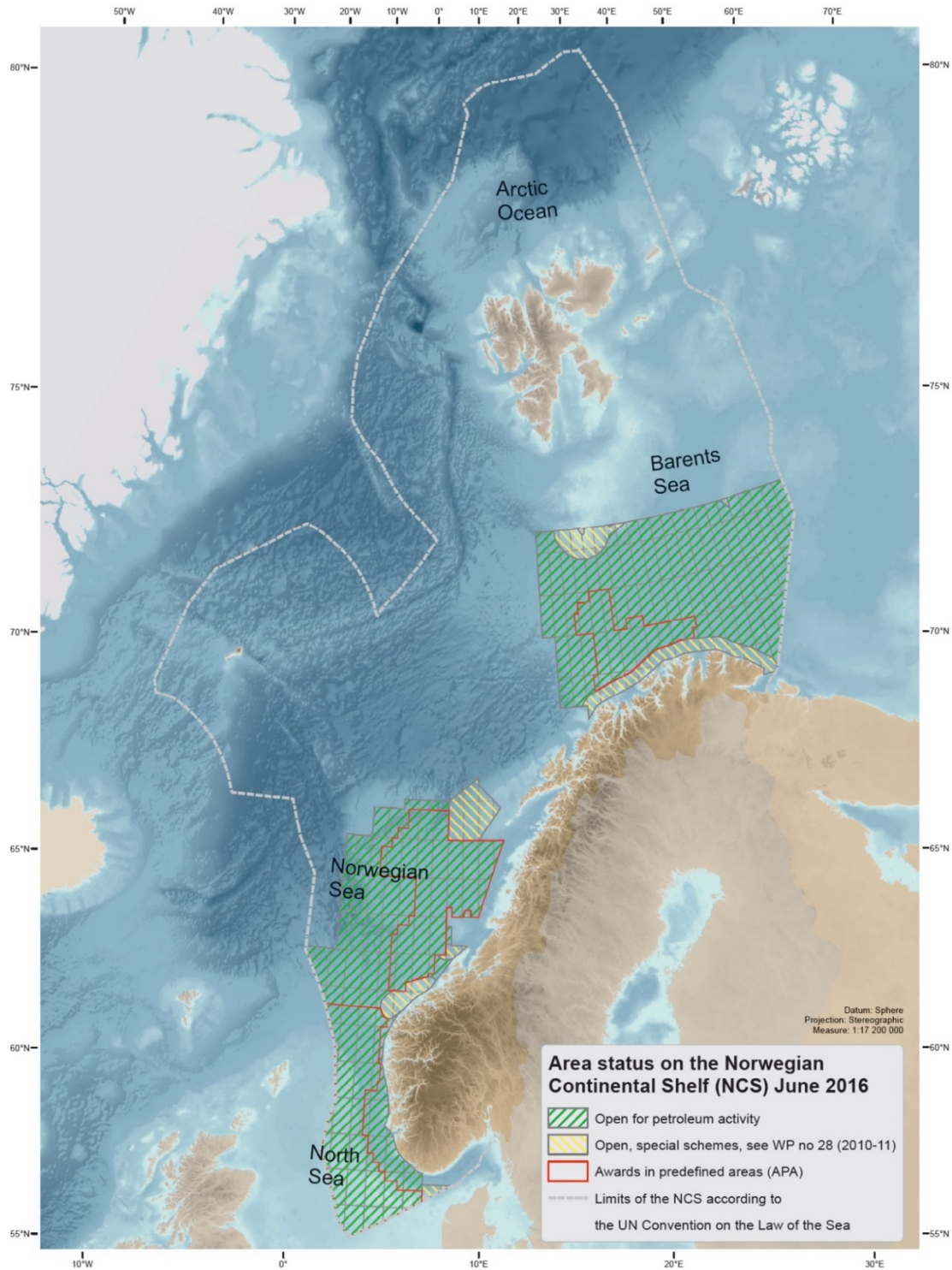


Fig. 11. Map of the Norwegian Continental Shelf (modified after the Norwegian Petroleum Directorate, 2016; www.npd.no/Global/Norsk/4-Kart/Sokkelkart2016/Kontinentalsockelkart_2016.pdf, 15.05.2017). Presently, there are three territories open for petroleum exploration: the North Sea, the Norwegian Sea and the Barents Sea. Norway (mainland) is shown in dark brown color.

through the Devonian. Most of these faults became reactivated in the Mesozoic (Coward et al., 2003; Zanella et al., 2003). These faults and sub-basins significantly contributed to the structure of the North Sea seen today.

4. Geological background of the study area

4.1.2 Mesozoic

The Mesozoic can be regarded as a period of intense reworking of Precambrian and Palaeozoic crustal domains, particularly south and southwest of Britain, west of Norway, in the central part of Europe and in the central region of the North Sea where rift systems altered Variscan and Caledonian basement (Coward et al., 2003). Nevertheless, some parts of North-West Europe remained unaffected by rifting, for example large areas of the North Sea and regions west of the UK (Coward et al., 2003). The Mesozoic was characterized by the existence of the supercontinent Pangea, which began to break up in the Upper Triassic. The breakup of Pangaea was accompanied by the emplacement of the Central Atlantic Magmatic Province (CAMP) (e.g. Marzoli et al., 1999; Golonka, 2007). The associated opening of the Atlantic Ocean can be considered as one of the most important tectonic events in the Mesozoic. Regarding North-West Europe, the opening of the Atlantic Ocean initiated the formation of a number of transform faults that were partly transferred into continental rift structures and oceanic basins of the western Tethys palaeo-ocean (Coward et al., 2003). Magmatic activity and oceanic spreading climaxed during the Lower Cretaceous, ultimately leading to the separation of Europe and North America, accompanied by the closure of the Tethyan Ocean and the Alpine orogeny (Coward et al., 2003). To the north, spreading in the Atlantic Ocean was limited by rift systems in the Labrador Sea and the Bay of Biscay, which evolved approximately in the Middle Cretaceous (Coward et al., 2003). At the same time, following Coward et al. (2003), both sea floor spreading in the North Atlantic and rifting in the North Sea weakened, resulting in post-rift subsidence and local basinal inversion.

4.1.3 Cenozoic

The early to middle Paleogene period was characterized by a new pulse of oceanic spreading in the North Atlantic, probably due to a mantle plume (White, 1988; Coward et al., 2003; Zanella et al., 2003). During the Eocene, Greenland separated from Europe, along with a propagation of the Atlantic spreading ridge into the Arctic (Coward et al., 2003). This was accompanied by the development of new shear zones, which locally initiated basinal inversion. With respect to the subsequent Neogene period, it has been suggested that it was as a major uplift phase (Japsen and Chalmers, 2000). As a consequence, sediment loading in the northern European extensional basins increased, leading to further subsidence (Coward et al., 2003).

4. Geological background of the study area

4.2 Geology of the North Sea region

The North Sea can be regarded as an intracratonic basin situated on thinned continental lithosphere (Faleide et al., 2015). According to Zanella et al. (2003) and Faleide et al. (2015), the North Sea largely overlies Caledonian basement and has experienced three major phases of crustal extension and thermal subsidence: (1) at the end of the Carboniferous, (2) throughout the Permian-Triassic transition, and (3) during the Upper Jurassic. Among these, the latter stage is assumed to have been mainly responsible for the structure of the North Sea today. Essentially, the initial structuring has been traced back to the Palaeozoic, in which the Caledonian orogeny led to strong crustal deformation. In the Carboniferous and Devonian early rifting pulses produced major strike-slip faults in the area. Furthermore, the most significant post-Palaeozoic structuring events comprise Permian-Triassic crustal extension, Middle Jurassic volcanic activity and uplift, and rifting extending from the end of the Jurassic to the Lower Cretaceous, which, during the final stages, was accompanied by a change of the extension direction. In addition, post-rift subsidence, tectonic inversion, and the uplift of basin flanks can be considered as the primary structuring processes of the subsequent Cenozoic era (Zanella et al., 2003).

The Viking Graben represents an important structural element of the northern North Sea (Zanella et al., 2003) and consists of three major north to northeast-trending sectors, termed North, Central and South Viking Graben. The Viking Graben denotes the northern arm of the North Sea triple rift comprising the Central Graben in the south, the Moray Firth basins in the west and the Viking Graben in the north (Fig. 12). The Viking Graben structure merges northwards into the Sogn Graben and is surrounded by the East Shetland Basin, the Tampen Spur and the Horda Platform (Fig. 13), which have been related to crustal extension in the Upper Jurassic (Christiansson et al., 2000; Faleide et al., 2015). However, there is evidence that the Viking Graben superimposes on an older Permian-Triassic rift system flanked by the East Shetland Platform and the Øygarden Fault Zone, which is marked by rotated fault blocks and sedimentary basins in half-graben arrangement (Christiansson et al., 2000; Faleide et al., 2015). According to Zanella et al. (2003), the Viking Graben represents an asymmetric graben structure in which the most essential faults are orientated east to east-south-east. Similar to the Viking Graben, the Moray Firth basins are asymmetric, too. However, within the Moray Firth basins the major faults

4. Geological background of the study area

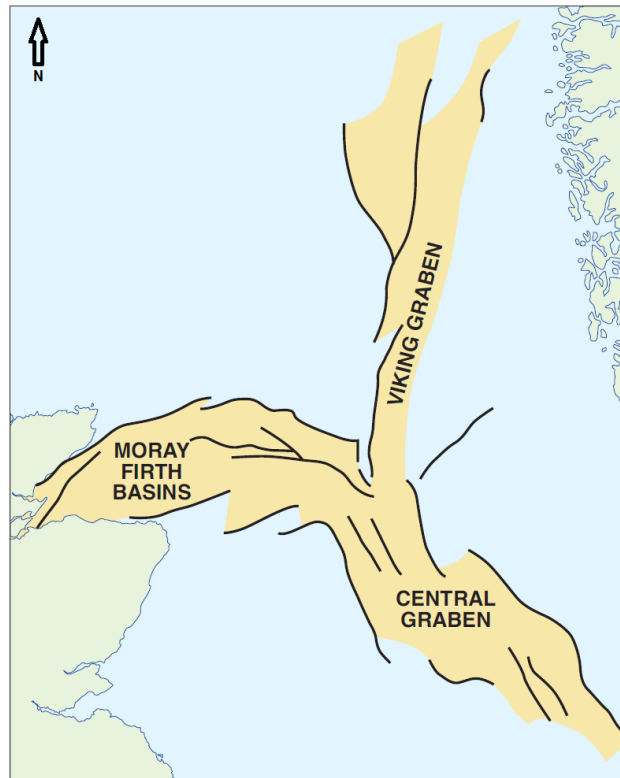


Fig. 12. Simplified illustration of the North Sea triple rift system (modified after Zanella et al., 2003). Although multiple geological processes have shaped the structural configuration of the North Sea over the Earth's history, the present-day arrangement was mainly created during a major rifting event in the Upper Jurassic.

are directed rather to the south-east and south-south-east, which is different to the Viking Graben. Concerning the Central Graben, Zanella et al. (2003) emphasized that both the degree of symmetry is higher than in the Viking Graben and the Moray Firth basins, and most of its structure is influenced by halokinesis. For example, it was mentioned that the majority of pre-Jurassic faults are overprinted by salt tectonics, complicating the reconstruction of tectonic activity during the Triassic and Palaeozoic. The presence of large amounts of Permian Zechstein salt represents a striking difference between the Central Graben, the Moray Firth basins and the central and northern parts of the Viking Graben (Glennie et al., 2003; Zanella et al., 2003). While the structural arrangement of the latter two is predominantly marked by fault block rotation, salt diapirism can be regarded as the principal mode of structuring in the Central Graben.

With respect to petroleum reservoir structures in the North Sea, two principal classes of traps have been defined: syn-rift and post-rift traps (Zanella et al., 2003). Basically, syn-rift traps involve reservoir strata deposited prior to the major phase of crustal extension in the Upper Jurassic, whereas post-rift traps commonly include Cretaceous to Cenozoic sediments formed after the main structuring event. The two

4. Geological background of the study area

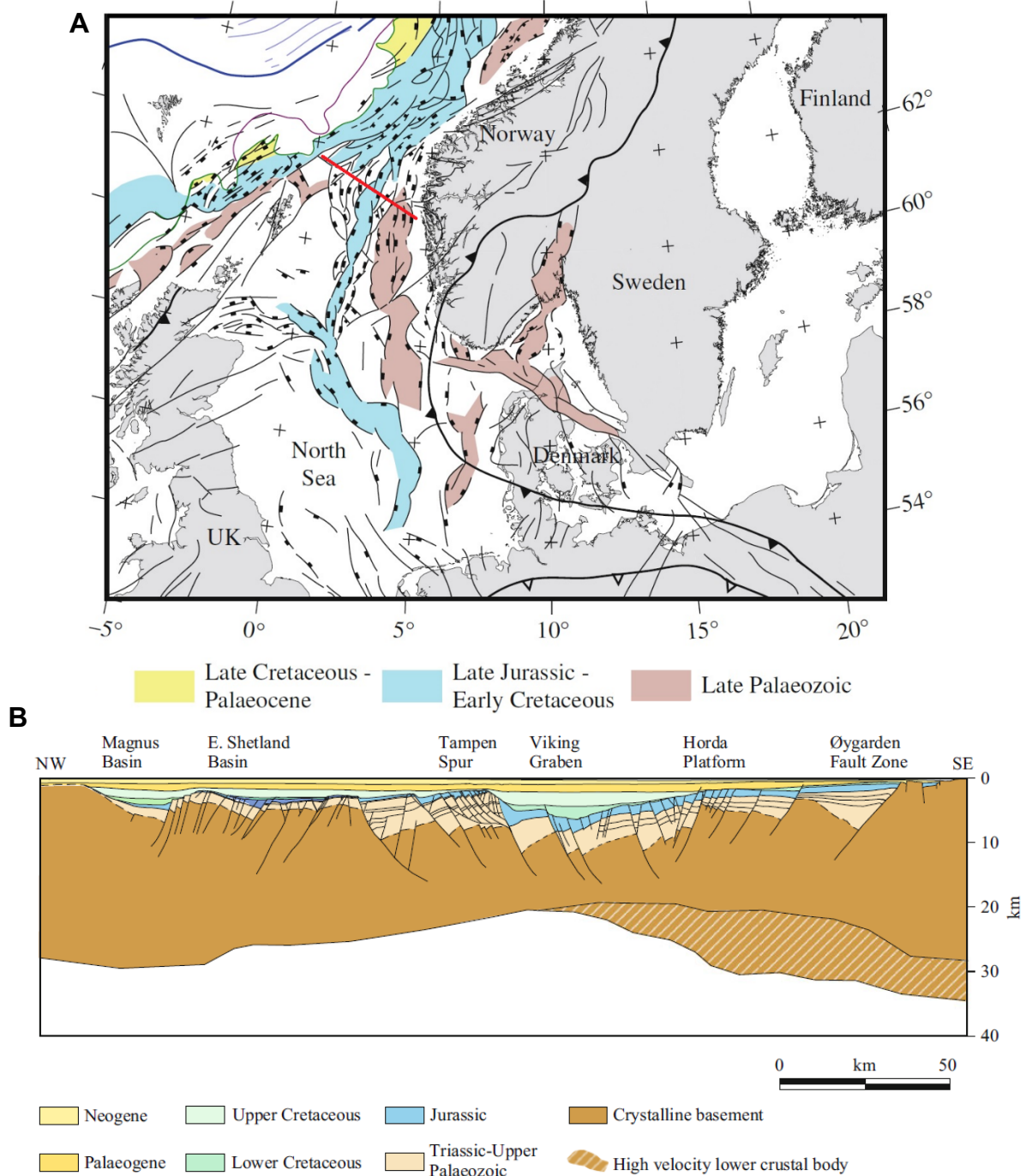


Fig. 13. Principal structural configuration of the North Sea (modified after Faleide et al., 2015). A: Map showing the basic geology of the North Sea region. The transect shown in B is indicated as a red line. B: Schematic cross section (NW-SE) through the northern part of the Viking Graben. The Viking Graben represents the northern part of the North Sea triple rift system consisting of the Central Graben (south), the Moray Firth basins (west) and the Viking Graben.

types of traps falling into the first category are footwall and hanging-wall traps, from which the former represents the most essential reservoir type in the North Sea (Fraser et al., 2003; Zanella et al., 2003). While in footwall traps hydrocarbons accumulate at the top of rotated fault blocks, hanging-wall traps, by contrast, symbolize structures in which petroleum concentrates mainly at the side of rotated fault blocks (Fraser et al., 2003; Zanella et al., 2003). On the other hand, hydrocarbon traps belonging to the

4. Geological background of the study area

second class (post-rift traps) are mainly associated with salt tectonics and basin inversion, but have, however, also been related to sediment compaction and subsequent deformation over protuberant subsurficial structural elements, e.g. fault blocks (Zanella et al., 2003). Typically, salt-related traps occur either alongside or above salt diapirs, whereby salt or superimposing, low-permeable claystones generally act as cap rocks (Zanella et al., 2003). With respect to inversion traps, these structures were largely formed during the Cenozoic and are commonly associated with compressional deformation related to the reactivation of Jurassic faults (Fraser et al., 2003; Zanella et al., 2003). According to Zanella et al. (2003), this kind of post-rift traps are relatively rare, due primarily to the low level of tectonic stress prevailing over most of the Cenozoic, a period mainly characterized by thermal subsidence. Nevertheless, tectonic inversion partially had strong influence on the configuration of pre-Cenozoic reservoirs, as stated by Fraser et al. (2003). While salt- and inversion-related traps represent the most significant forms of post-rift traps, sediment compaction over structural highs and therefore the third mechanism of post-rift trap formation in the North Sea generally leads to the formation of smooth anticlines (Zanella et al., 2003). According to Fraser et al. (2003), footwall, hanging-wall and salt-related traps together make up more than 90% of the entire petroleum exploration successes in the North Sea, whereas inversion-related traps are mostly of minor significance.

4.3 Depositional history and source rock characteristics of the Draupne (Kimmeridge Clay) Formation

It has been shown that the Upper Jurassic, organic-rich Draupne (Kimmeridge Clay) Formation is a major source rock for oil and gas in the North Sea region (e.g. Cooper et al., 1995; Isaksen and Ledje, 2001; Isaksen et al., 2002; Kubala et al., 2003; Keym et al., 2006). The Viking Graben area has reached oil window maturities approximately in the Upper Cretaceous (Kubala et al., 2003).

4.3.1 Distribution and stratigraphy

The Draupne Formation is distributed widespread across the Norwegian continental shelf and extends over large parts of the British North Sea as stratigraphically equivalent Kimmeridge Clay Formation. The formation is present onshore in eastern and southern England (Williams, 1986). It consists of predominantly carbonate-lean, dark colored claystones of 50 to more than 1200 m in thickness (Kubala et al., 2003). In the Norwegian part of the North Sea the formation belongs to the Viking Group,

4. Geological background of the study area

which corresponds to the Humber Group in the British sector (Fig. 14). The formation was deposited during Kimmeridgian to Ryazanian times in the Upper Jurassic to Lower Cretaceous (Fig. 14), particularly in response to a major transgressional phase in the Upper Jurassic (Fraser et al., 2003).

Tyson et al. (1979) identified four principal types of lithology within the Kimmeridge Clay Formation in its type section in Dorset, UK: (1) clays, (2) bituminous shales, (3) oil shales, and (4) coccolithic limestones. While the clays are characterized by abundant fossil remains of ammonites, bivalves, fish and reptiles as well as a diverse microfauna that consists of coccolithophorids, dinoflagellates and some acritarchs. Macro- and microfauna is much rarer in the bituminous mudstone facies, where the macrofauna is mostly distributed in separate layers. Evidence for benthic life is almost absent in the oil shales and the coccolithic limestones, which are characterized by elevated TOC contents and high concentrations of Cu, Ni, Mo, P, I and Br. Later, Oschmann (1988) extended Tyson's facies model and distinguished between five major facies types: (1) the marly and silty clays, (2) the shales, (3) the bituminous shales, (4) the oil shales, and (5) the coccolithic limestones. According to this classification scheme, the marly and silty clays comprise organic-lean, partly bioturbated mudstones that mainly consists of quartz and bioclasts with a diverse faunal community. By contrast, the shale facies is clearly microlaminated and contains slightly higher amounts of organic material and a less but still diverse

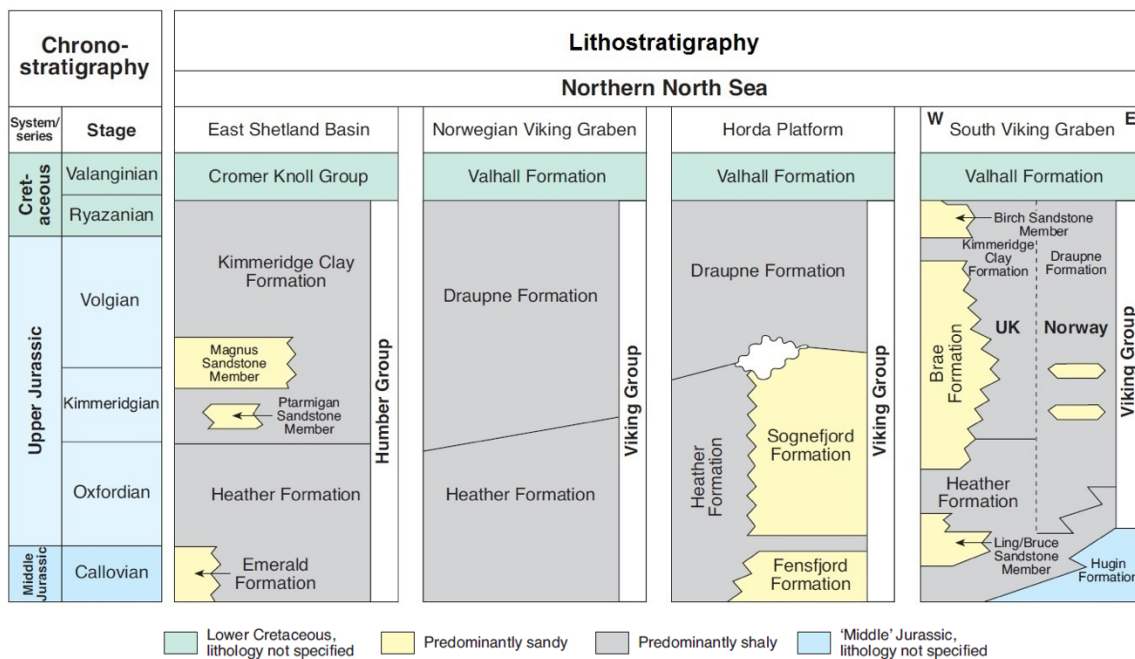


Fig. 14. Upper Jurassic stratigraphy of the study area (modified after Fraser et al., 2003).

4. Geological background of the study area

benthic fauna, which decreases in diversity towards the bituminous shales. The bituminous shale facies itself is marked by a distinct microlamination, elevated amounts of organic material and a low-diversity, but somewhat abundant faunal community. The highest TOC values are reached within the oil shales, which consist of dark, exceptionally finely laminated mudstones. Evidence for benthic life is generally rare and the mineralogy is dominated by clays, though calcite and pyrite are common, too. The last facies type, the coccolithic limestones, consists of CaCO₃-enriched mudstones that comprise an alternating, finely laminated sequence of clay- and organic-rich layers with white, coccolithophoride-rich layers. Like in the oil shales, benthic life is mostly absent.

Fraser et al. (2003) mentioned that the Draupne (Kimmeridge Clay) Formation can occur in two different stratigraphic arrangements. In general, the formation might either superimpose on older, sandy coastal shelf deposits, or, alternatively, cover or alternate with sandstones representing a basin-margin, submarine-fan environment. In the first case, it may additionally form a major cap rock for underlying reservoirs, which might be important for petroleum exploration business. Continuous mapping of the distribution of the Draupne (Kimmeridge Clay) Formation across the North Sea has revealed that the formation is under-represented or even absent on several structural highs, for example on the Forties-Montrose High (Central Graben) and the Utsira High (South Viking Graben), which was interpreted either as a condensing or an erosional effect (Kubala et al., 2003).

4.3.2 Source rock characteristics

The Draupne (Kimmeridge Clay) Formation predominantly contains a marine, liptinitic type II kerogen and is therefore highly oil-prone (e.g. Erdmann and Horsfield, 2006; Keym et al., 2006). Nevertheless, various studies documented a strong facies variability, pointing to local differences in the petroleum generation potential (Cooper et al., 1995; Isaksen and Ledje, 2001; Keym et al., 2006). For example, Cooper et al. (1995) identified altogether eight different kerogen types within the Draupne (Kimmeridge Clay) Formation and, therefore, drew attention to related problems concerning accurate oil-source rock correlations. In a subsequent study, Isaksen and Ledje (2001) attempted to compare the source rock quality in the eastern and the western part of the Viking Graben and reported an overall good petroleum generation potential, which is mostly the case for the Draupne (Kimmeridge Clay) Formation. However, they

4. Geological background of the study area

recognized a more gas-prone kerogen type on the western flank, owing probably to a stronger terrestrial influence at the time of deposition. Further-more, Keym et al. (2006) found evidence for a more stable type II/III organic facies type in the North Viking Graben and concluded that petroleum generation continues into greater depths than previously assumed. The strong facies variability of the Draupne (Kimmeridge Clay) Formation is fairly well expressed in its range of Rock-Eval HI values, which vary from about 150 mg HC/g TOC, representative of a terrigenously influenced type III kerogen, to approximately 600 mg/g TOC, corresponding to marine type II organic matter (Kubala et al., 2003). According to Kubala et al. (2003), the TOC contents of the Draupne (Kimmeridge Clay) Formation are typically in the range of 2 to more than 10%, depending on the local depositional conditions. Concerning the regional distribution of kerogen types, the authors stated that organic-rich shales from the graben areas are typically characterized by mixed type II/III kerogens, while source rock material from distant platform regions predominantly contains a type III/IV, low-quality organic facies.

The maturity of the Draupne (Kimmeridge Clay) Formation generally ranges from highly immature to post-oil window and, with respect to the heating rate, an average geothermal gradient of 34.6 °C/km has been established for the North Sea region (Kubala et al., 2003). Regarding the standard geothermal gradients in the Viking Graben study area, higher values have been reported for the northern (>40 °C/km) than for the southern part (26-40 °C/km) (Kubala et al., 2003). Previous work has revealed that the Draupne (Kimmeridge Clay) Formation is immature onshore England (Williams, 1986), but buried to catagenesis depths in large parts of the North Sea, particularly in the Viking Graben area (Kubala et al., 2003). Spatial maturity differences are commonly closely related to the geological history of the North Sea (see 4.1), in which particularly Upper Jurassic rifting and subsequent Cretaceous and Cenozoic thermal subsidence resulted in the formation of individual sub-basins with unique maturation histories. Another interesting point regarding the maturity of the formation is that, if its thickness is very high, significant maturity differences may occur between the base and the top of one and same section (Kubala et al., 2003). In fact, this would imply that in such cases the lower part of the formation would begin to generate and expel petroleum earlier than younger sections, which might not yet have reached the oil window.

4.3.3 Palaeoenvironment

4. Geological background of the study area

Geochemical and palaeontological evidence suggest that the Draupne (Kimmeridge Clay) Formation was deposited within restricted, rift-related shallow marine sub-basins during Upper Jurassic sea level rise (Fraser et al., 2003). Most organic material originates from marine sources with varying proportions of land plant material (Kubala et al., 2003). Concerning the Viking Graben area, which was investigated in this work, Isaksen and Ledje (2001) reported a greater input of terrestrial organic material on the western than on the eastern part of the graben. With regard to the vertical facies distribution, it seems that particularly the lower part of the Draupne (Kimmeridge Clay) Formation is enriched in terrigenous organic material and consequently has a lower source potential (Kubala et al., 2003), which could be interpreted as a transition from proximal to distal conditions in the course of the Upper Jurassic. Overall high TOC contents and mostly scarce to absent benthic life within large parts of the formation clearly indicate oxygen-depleted to anoxic bottom water conditions and restricted water mass circulation, favoring organic matter preservation and black shale sedimentation. Coccolithophorids were found to be the principal primary producing organisms, as evidenced for example by Gallois (1976) and Tyson et al. (1979). Sulfur within the Draupne (Kimmeridge Clay) Formation is mostly bound in framboidal pyrite (Kubala et al., 2003), indicating that the formation was deposited within a marine environment comprising abundant reactive iron.

Based on observations in Boulonnais, France, and Dorset, UK, Oschmann (1988) developed a dynamic depositional model for the Kimmeridge Clay Formation. Essentially, anoxic bottom water conditions were mainly controlled by a monsoon-driven water current-counter current system in the North Atlantic region, which ultimately led to the development of a stratified water column and oxygen-deficient bottom waters. Moreover, both the regional bathymetric conditions, as well as elevated sedimentation rates need to be taken into account, too (Fraser et al., 2003). The palaeo-water depth at the time of deposition of the Draupne (Kimmeridge Clay) Formation is not well known. While, for example, Oschmann (1988) suggested that the palaeo-water depth ranged close to the storm wave base, perhaps between 50 and 100 m, Goff (1983) inferred, based on modelling results, a water depth between 500 and 700 m in the Viking Graben area.

Concerning the deposition of Upper Jurassic reservoir rocks, which are also import-

4. Geological background of the study area

ant for this study, Fraser et al. (2003) stated that coastal shelf and deep-water fan sandstones represent the two major types of Upper Jurassic reservoirs in the North Sea. Furthermore, following these authors, their distribution, quality and thickness are mainly governed by: (1) the development of the accommodation space over time (uplift-subsidence balance), (2) the sediment supply (e.g. via rivers, turbidites), (3) the principal lithological composition of the hinterland, and (4) the degree of erosion after deposition.

4.4 The Hugin Formation

Compared to the Draupne (Kimmeridge Clay) Formation, the Middle Jurassic Hugin Formation so far has received comparatively little interest, which is surprising considering both its thickness and composition consisting essentially of coals, organic-rich shales and sandstones. Indeed, Kubala et al. (2003) mentioned that coals and shales of the Hugin Formation may represent important Middle Jurassic source rocks in the North Sea region. In addition, Folkestad and Satur (2008) stated that the formation acts as an important reservoir unit in the South Viking Graben.

4.4.1 Distribution and stratigraphy

The Hugin Formation is part of the Vestland Group and was deposited approximately during the Callovian to early Oxfordian in the Middle Jurassic (Folkestad and Satur, 2008) and is composed of sandstones alternating with coals beds and organic-rich shales (Husmo et al., 2003). The formation can be found in the southern Viking Graben, is superimposed on the Sleipner Formation, and passes upwards into the Viking Group, which consists of the Heather and the Draupne (Kimmeridge Clay) Formation (Fig. 15) (Husmo et al., 2003; Folkestad and Satur, 2008). The thickness of the Hugin Formation varies from around 5 to more than 200 m and is typically influenced by halokinesis (Folkestad and Satur, 2008).

Folkestad and Satur (2008) distinguished between two major lithological units within the Hugin Formation: Hugin 1 and Hugin 2. While the sedimentary structure of the basal Hugin 1 unit points to a deposition during a period of active rifting in the Viking Graben, the younger Hugin 2 unit, by contrast, is characterized by a stacked sedimentary sequence documenting an aggrading to retrograding environment. Concerning the Hugin 2 unit, Folkestad and Satur (2008) identified in total seven different facies associations, from which three were classified as regressive due to

4. Geological background of the study area

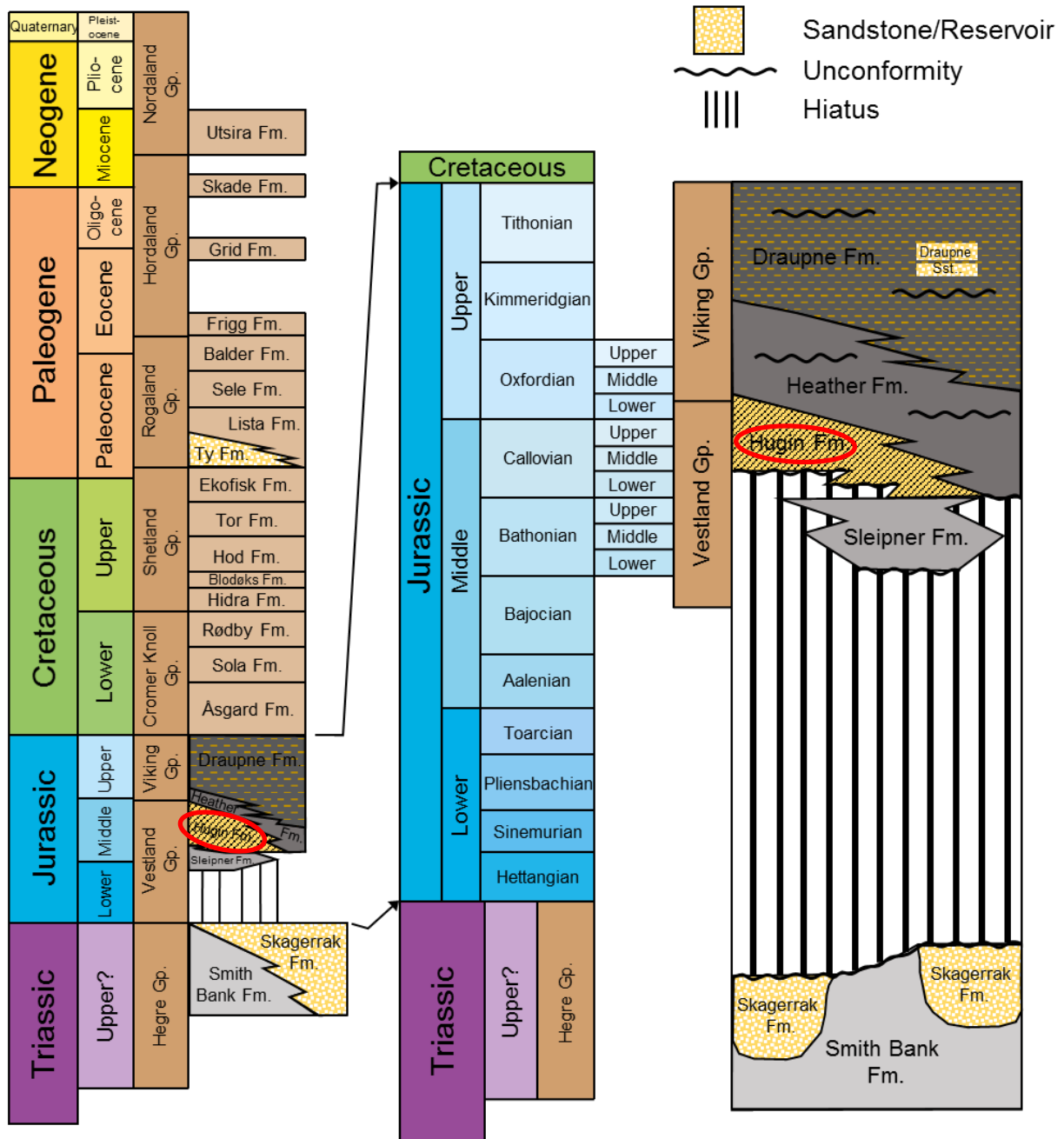


Fig. 15. Principal Mesozoic-Cenozoic stratigraphy of the South Viking Graben (modified after Folkestad and Satur, 2008). The Hugin Formation is highlighted in red.

pronounced coarsening upward trends, and four were related to transgressive conditions because of well-developed fining-upward tendencies. Note that the deposits corresponding to regressive units actually represent highstand systems tracts probably associated with periods of only low sea level rise and rapid subsidence of the basin. Sediments deposited under these conditions comprise offshore mudstones, shoreface sediments and mouthbars. Conversely, the trans-gressive facies associations involve tidal channels, tidal dunes, as well as deposits from tidal flats and salt marshes.

4.4.2 Source rock characteristics

4. Geological background of the study area

Coals and shales of the Hugin Formation have been shown to represent good petroleum source rocks and to be thermally mature throughout the study area (Isaksen et al., 1998). In general, coals are defined as rocks containing more than 50% organic carbon (e.g. Peters et al., 2005a) and are widely believed to be predominantly gas-prone (e.g. Killops and Killops, 2005; Peters et al., 2005a). However, in the past some oils were correlated with coaly sources as well (e.g. Petersen et al., 1996, 2000) and it is controversial under which circumstances and to what extent coals can generate and expel liquid hydrocarbons (e.g. Fleet and Scott, 1994; Wilkins and George, 2002).

With respect to the Hugin coals, the organic content can reach up to 80% (Isaksen et al., 1998). Interestingly, their Rock-Eval hydrogen indices are typically in the range of 200 to 400 mg HC/g TOC and therefore also fairly high (Isaksen et al., 1998). Consequently, conventional hydrogen index vs. oxygen index plots (pseudo-Van Krevelen diagrams) are misleading because such high HI values would rather point to mixed type II/III organic matter than to humic coals, which are mainly composed of vascular land plant material rich in oxygen-functionalized compounds (Killops and Killops, 2005) expected to have low HI values. In purpose to study the petroleum generation and expulsion characteristics of humic coals in general, Isaksen et al. (1998) analyzed the maceral composition of a number of Hugin coal samples from the South Viking Graben and revealed a highly heterogeneous character. They found that coals of the Hugin Formation principally consist of 25-90% vitrinite, 5-70% inertinite and 5-25% liptinite and therefore display a broad compositional range. Furthermore, through conduction of pyrolysis-gas chromatography they were able to show that the composition of the organic material is dominated by aromatic rather than aliphatic components, which did not change significantly throughout the experiments. It was concluded that, although the Hugin Formation is thermally mature and theoretically has the potential to generate liquid hydrocarbons, the formation expelled hydrocarbons predominantly via a volatile gas/condensate phase. According to Rullkötter (1993), the frequently observed paradox between high TOC values, elevated hydrogen indices and limited oil expulsion of many coals has been ascribed primarily to their microporous structure, which acts as trap for liquid hydrocarbons. Based on this idea, most generated non-volatile hydrocarbons become cracked to gas during progressing thermal maturation. Similarly, Behar and Vandenbroucke (1987) suggested that type III kerogens contain dense aromatic kerogen networks that largely prevent the expulsion of liquid hydrocarbons. By contrast, in a subsequent review article by Wilkins

4. Geological background of the study area

and George (2002), it was stated that the low expulsion capacity of coals is mainly related to the strong sorption of generated bitumen on the organic matter. These authors emphasized that the pores of vitrinites are, unlike previously thought, not interconnected and therefore atomic sorption of oil on the kerogen network is likely more essential than structural trapping. Following their argumentation, expulsion of oil from coals may be possible if coals either display low thicknesses and alternate with reservoir strata, or are highly oil-prone and thus capable of generating large volumes of hydrocarbons exceeding the expulsion threshold. Regarding the considerable discrepancy between TOC and HI values in their sample material, Isaksen et al. (1998) suggested that for rocks containing elevated amounts of land plant material, the HI represents an alteration indicator rather than a proxy for the oil generation potential. Indeed, Wilkins and George (2002) underlined that the HI is a very complicated parameter that is strongly influenced by the composition of macerals within a sample and therefore does not simply correlate with the generation and expulsion of hydrocarbons.

Apart from the coal beds, organic-rich shales of the Hugin Formation can be expected to contain a mixed type II/III kerogen comprising material from both marine and terrigenous sources (Folkestad and Satur, 2008).

4.4.3 Palaeoenvironment

The Hugin Formation developed in the course of a rift-related, transgressional phase in the Upper Bathonian (Folkestad and Satur, 2008) and was deposited mainly in response to a southward retrogradation of the Brent Delta, which created a broad, shallow marine coastal plain environment (Husmo et al., 2003). According to Folkestad and Satur (2008), the Hugin Formation has previously been described either as (i) marine shoreface including sediments from beach barriers, lagoons and coastal plains, or (ii) as delta-plain/delta-front environment. However, sedimentary structures interpreted as tidal channel or tidal flat deposits suggest considerable tidal influence as well (Husmo et al., 2003; Folkestad and Satur, 2008). Following the argumentation of Isaksen et al. (1998), the coal deposits of the Hugin Formation largely originate from peat-forming mires, which probably represented a characteristic

4. Geological background of the study area

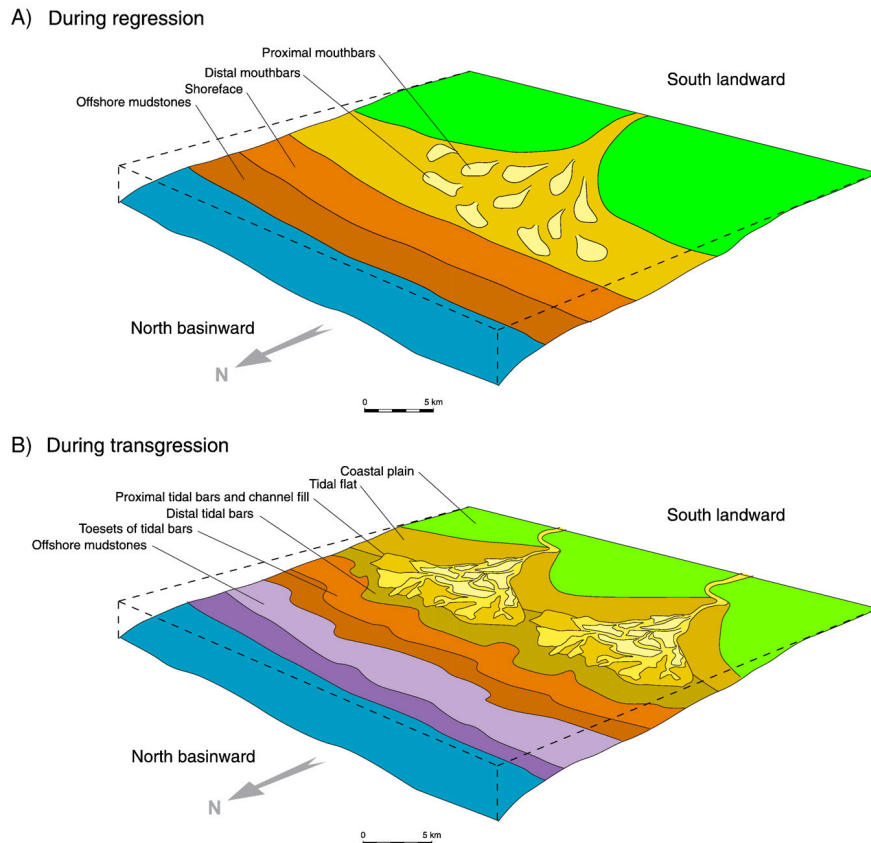


Fig. 16. Potential formation model of the Middle Jurassic Hugin 2 unit (from Folkestad and Satur, 2008). Essentially, palaeo-environment and sequence stratigraphy of the Hugin Formation were mainly controlled by sea level fluctuations. While during regressive units representing periods of low sea level rise (highstand systems tracts) a deltaic dominated environment developed (A), a tidal-estuarine controlled environment formed during periods of faster rising sea level (transgressive systems tracts) (B). No lowstand systems tracts were identified due to rapid subsidence of the basin relative to sea level evolution.

morphological feature of the coastal plain environment. Likewise, Folkestad and Satur (2008) believe that the Hugin coal beds were mainly formed in mires and swamps marked by high input rates of terrigenous organic matter and limited contribution of clastic sediments. In addition, these authors suggested that the organic-rich mudstones of the Hugin Formation were, in contrast to the coals, deposited in salt marshes under anoxic, quiet water conditions close to land plant-rich hinterland regions.

While Folkestad and Satur (2008) interpreted the sequence stratigraphy of the Hugin Formation mainly as the result of a variation of transgressive and highstand systems tracts, Husmo et al. (2003), by contrast, are of the opinion that the sequence stratigraphy of the Middle Jurassic was primarily controlled by fluvial sediment supply from the hinterland and regional tectonic activity instead of sea level fluctuations. They argued that the Sleipner and the Hugin Formation, which basically document the retrogradation of the Brent Delta, are principally age-equivalent to the Middle to Upper

4. Geological background of the study area

Jurassic sandy Krossfjord and Fensfjord formations in different regions of the basin and therefore regressive and transgressive sedimentary elements were deposited simultaneously. Folkestad and Satur (2008) provided, however, evidence for pronounced regression-transgression cycles within the Hugin Formation and developed a dynamic depositional model for the upper Hugin 2 unit (Fig. 16). Essentially, highstand systems tracts considered as regressive units led to the development of a deltaic-dominated depositional environment including offshore mudstones, shoreface and mouthbar deposits, whereas, on the other hand, faster rates of sea level rise (transgressive conditions) resulted in a tidal dominated estuarine environment with tidal channels, tidal dunes, tidal flats and salt marshes.

5. Material and methods

This section gives an overview of the sample material and the experimental procedures. The study investigates sample material from reservoir (carrier) and thermally immature to generative organic-rich rocks of the Upper Jurassic Draupne Formation, as well as sandstones, coals and shales of the Middle Jurassic Hugin Formation from the Viking Graben area in the North Sea (see above). The lab work comprised, (i) elemental analysis, (ii) Rock-Eval pyrolysis, (iii) bitumen extraction, (iv) extract separation, and (v) compound analysis, identification and quantification via gas chromatography-mass spectrometry (GC-MS) (Fig. 17). Besides, a geochromatographic retardation experiment involving pre-extracted source rock material from the Draupne Formation (well 15/3-8), a synthetic oil, and selected organic tracers was conducted to investigate molecular fractionation effects related to geochromatography.

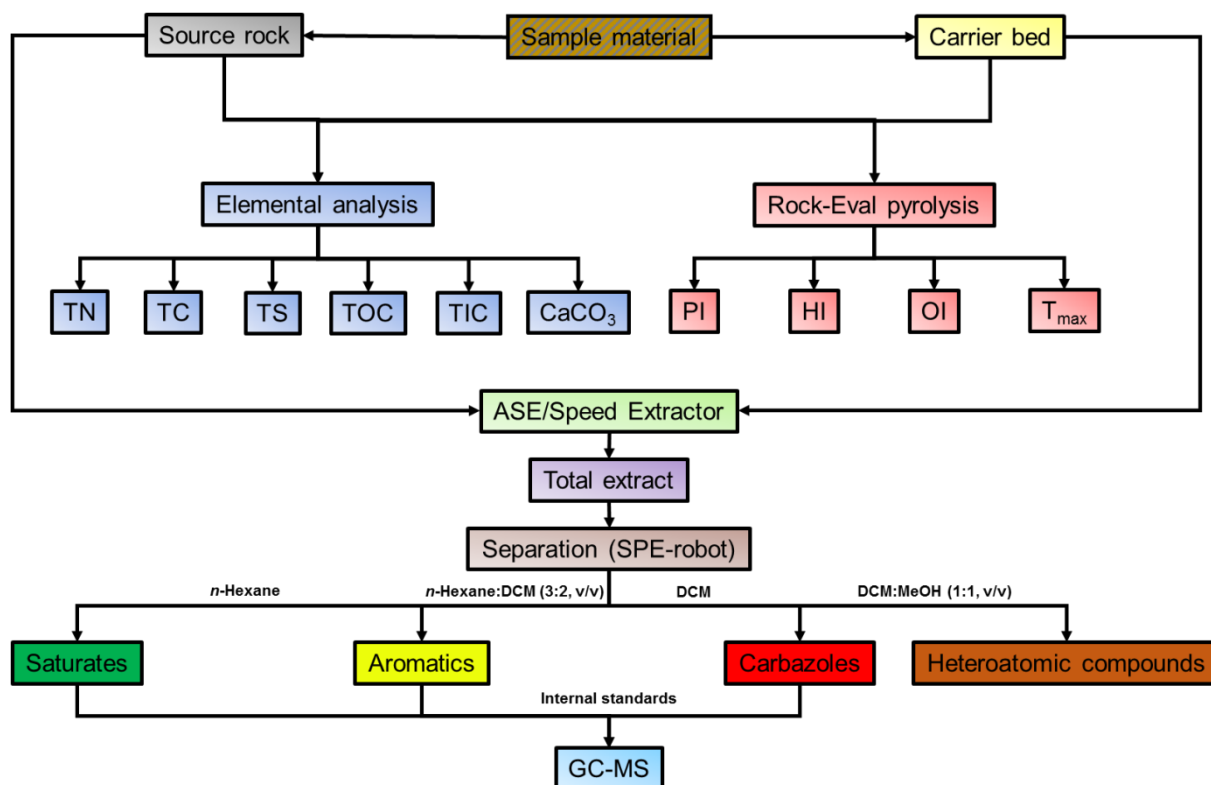


Fig. 17. Simplified lab work scheme. Source rock and reservoir (carrier bed) samples were subjected to elemental analysis, Rock-Eval pyrolysis and molecular geochemistry to determine bulk properties, source potential and molecular signature. The latter comprised bitumen extraction and subsequent separation into aliphatics (saturates), aromatics, carbazoles and heteroatomic compounds using different organic solvents and solvent mixtures. The molecular composition was analyzed via gas chromatography-mass spectrometry (GC-MS) after addition of internal standards. The heteroatomic compounds were not analyzed. Besides, a geochromatographic experiment (not shown) involving a Draupne source rock column, a synthetic oil, and a tracer solution was conducted. Abbreviations: ASE= Accelerated Solvent Extraction; TN= Total Nitrogen; TC= Total Carbon; TS= Total Sulfur; TOC= Total Organic Carbon; TIC= Total Inorganic Carbon; CaCO₃= Carbonate Content; PI= Production Index; HI= Hydrogen Index; OI= Oxygen Index; SPE= Solid-Phase Extraction; DCM= Dichloromethane; MeOH= Methanol; GC-MS= Gas Chromatography-Mass Spectrometry.

5. Material and methods

5.1 Sample set

Overall sample information is summarized in Table 2. In total, 134 samples were collected from six conventional drill cores (15/3-8, 15/3-9 T2, 24/9-1, 34/7-23 A, 34/7-23 S, 34/10-36) located in the Norwegian North Sea (Fig. 18). Information on the drill cores were obtained from the website of the Norwegian Petroleum Directorate (NPD) (www.npd.no/en/), including FactPages (<http://factpages.npd.no/factpages/Default.aspx?culture=en>) and FactMaps (http://gis.npd.no/factmaps/html_21/). Nine expulsion scenarios were examined, (A) a high-resolution section (1 m) comprising a small source rock interval intercalated between two reservoir units (15/3-8), (B) a second high-resolution profile (1 m) including two sandstone carrier intervals sandwiched between source rock strata (15/3-8), (C) 10 m of alternating source and carrier beds (15/3-9 T2, Draupne core), (D) a 30 m sequence involving one shaly and two coaly source units intercalated by reservoir beds (15/3-9 T2, Hugin Formation), (E) 5 m of black shale interrupted by three heterolithic layers (24/9-1), (F) a third high-resolution profile (1 m) comprising a distinct carrier unit enclosed by thick source strata (24/9-1), (G) 40 m of sandstone reservoir superimposed on 50 m of black shale (34/7-23 A), (H) 6 m of source rock interrupted by 60 cm of carrier bed (34/7-23 S) and, finally, (I) a low resolution profile (10 m) characterized by a distinct sandstone unit surrounded by massive black shale strata (34/10-36) (Fig. 19). All samples originate from depths either close to (34/7-23 A, 34/7-23 S, 34/10-36) or corresponding to (15/3-8, 15/3-9 T2, 24/9-1) the natural oil window in the North Sea basin, where peak oil generation takes place at about 130-140 °C in an average depth of approximately 3.5 km (Bjørlykke, 2015b). Three samples (K011198, K012306, K012482) turned out to be biodegraded based on molecular evidence. All samples were collected in close proximity to petrophysical data points. The depths are given as measured depths (MDs) and fit, except for well 34/7-23 A and 34/7-23 S, where the measured depths are significantly higher, well with the true vertical depths (TVDs).

5.1.1 Well 15/3-8

Well 15/3-8 penetrated the western margin of the Gudrun gas and condensate field (South Viking Graben) in 2006 and served to evaluate the quality of intra-Draupne reservoirs. Paratherm, a paraffin-based fluid system served as drilling mud. Two high-resolution profiles were sampled. For the first expulsion scenario, 17 samples (7x shale, 2x heterolithic, 8x reservoir) were collected within a small interval ranging from

5. Material and methods

4209 to 4210 m drilling depth (K011188-K011198; Table 2). The section is characterized by a thin black shale unit (~25 cm) in the central part surrounded by two sandstone carrier beds, from which the lower one contains another thin source layer (~3 cm) close to the bottom. The second high-resolution profile was placed between 4290 and 4291 m drilling depth (K012431-K012450; Table 2) and comprised in total 20 samples (13x shale, 1x heterolithic, 6x reservoir). It is marked by two reservoir units (~26 cm and ~5 cm) enclosed by organic-rich shales.

5.1.2 Well 15/3-9 T2: Draupne section

Well 15/3-9 T2 was drilled with oil-based, low equivalent circulating density-high temperature high pressure drilling mud (OBM-Low ECD-HTHP) in 2010 in purpose to confirm considerable petroleum accumulations in intra-Draupne sandstones and to investigate the eastward expansion of the Gudrun gas and condensate field. Moreover, it was aimed to collect information about the underlying, coaly-deltaic Hugin Formation. The well is located on the Brynhild Prospect in the South Viking Graben and comprised a Draupne as well as a Hugin core. A series of 16 samples (7x shale, 1x heterolithic, 8x reservoir) was collected between 4126 and 4136 m drilling depth (K011228-K011239; Table 2) from the Draupne core. The sampled section is characterized by a relatively thick reservoir unit (~3 m) superimposed on a rapidly alternating source rock-carrier bed sequence.

5.1.3 Well 15/3-9 T2: Hugin section

A second set of 20 samples (4x shale, 8x coal, 2x heterolithic, 6x reservoir) ranging from 4480 to 4510 m drilling depth (K012425-K011254; Table 2) was collected from the Hugin core of well 15/3-9 T2. The examined profile is marked by two coal beds alternating with organic-rich shales and sandstone carrier units.

5.1.4 Well 24/9-1

Well 24/9-1 was drilled in the Vana Sub-basin (South Viking Graben) in 1976 and served to improve structural resolution in the central Viking Graben. A water-based mud was chosen for drilling. Two expulsion scenarios were sampled. The first of the two scenarios includes 17 samples (12x shale, 5x heterolithic) located in an interval ranging from 4444 to 4450 m drilling depth (K012451-K012467; Table 2). The sampled section consists of three heterolithic layers surrounded by compact black shale units.

5. Material and methods

The second profile comprises 9 samples (7x shale, 2x reservoir) and is located between 4456.3 and 4457.3 m drilling depth (K012468-K012476; Table 2). It is characterized by a conspicuous reservoir interval sandwiched between dense organic-rich shales.

5.1.5 Well 34/7-23 A

Exploration well 34/7-23 A is located on the Vigdis Oilfield on the Tampen Spur south of the Snorre Field (North Viking Graben) and was drilled in 1994. Potassium mud (KCl mud), a water mud system served as drilling fluid. A total number of 16 samples (6x shale, 3x heterolithic, 7x reservoir) was chosen between 3204 to 3291 m drilling depth (K011212-K011227; Table 2). Note, however, that, according to the Norwegian Petroleum Directorate, the true vertical depths are, as mentioned before, much lower and range only from about 2619.5 to 2678 m.

5.1.6 Well 34/7-23 S

Well 34/7-23 S can be considered as a sidetrack of well 34/7-23 A and is therefore also located on the Vigdis Oilfield on the Tampen Spur. A section was selected where a distinct carrier bed is enclosed by thick black shale strata. In total, 13 samples (10x shale, 3x reservoir) were taken between 3130 and 3136 m drilling depth (K011199-K011211; Table 2). Again, as pointed out above, the true vertical depths in this section are, according to the information provided by the Norwegian Petroleum Directorate, considerably lower (~2652.6-2659.3 m).

5.1.7 Well 34/10-36

Well 34/10-36 was drilled on the Gullfaks Sør structure in the North Viking Graben in 1992 and served on one hand to evaluate the production potential of intra-Draupne sandstones and, on the other hand, to identify the gas-oil and oil-water contacts as well as the pressure regime in the Brent Group. A water-based mud served as drilling fluid. Altogether, six samples (5x shale, 1x reservoir) were collected between 3042 and 3054 m drilling depth to identify compositional changes in approximation to a small sandstone unit (~20 cm) at the bottom of the sequence (K012477-K012482; Table 2).

5. Material and methods

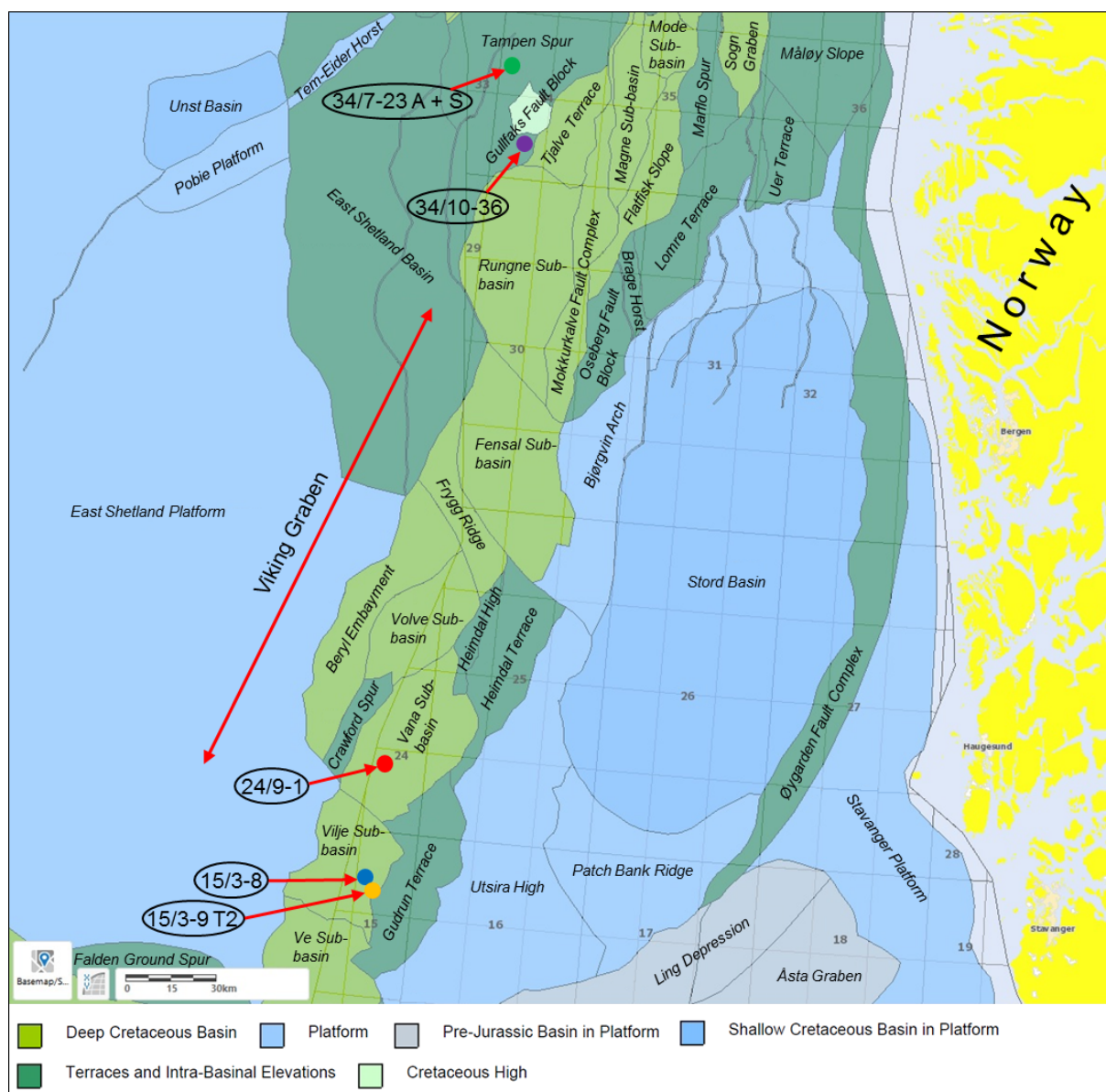


Fig. 18. Simplified geological map of the Norwegian North Sea showing the positions of the investigated wells (modified after the Norwegian Petroleum Directorate, 2017; http://gis.npd.no/factmaps/html_21/, 13.07.2017). While well 15/3-8 and well 15/3-9 T2 are located on the western flank of the Gudrun Terrace in the South Viking Graben, well 34/7-23 A, 34/7-23 S and well 34/10-36 are situated on the Tampen Spur in the northern Viking Graben. Well 24/9-1 is located in the center of the Vana Sub-basin in the South Viking Graben. Exploration quadrant numbers are indicated in light grey.

5.2 Bulk geochemistry

5.2.1 Elemental analysis

Elemental analysis (CNS) was conducted on all samples in order to determine the total nitrogen (TN), total carbon (TC), total sulfur (TS), total organic carbon (TOC), total inorganic carbon (TIC) and the carbonate content. While TN, TC and TS were directly measured on powdered sample material using a Vario EL III elemental analyzer (Elementar Analysensysteme GmbH) operating with helium as carrier gas, the TOC contents were determined on decalcified samples using an ELTRA CS-580A

5. Material and methods

carbon/sulfur analyzer working with oxygen as carrier gas. Decalcification was achieved by treating the samples with excess hydrochloric acid (10% and 25%) to remove calcium carbonate and dolomite, after which they were dried at room temperature for 48 h. The total inorganic carbon was calculated by subtracting TOC from TC:

$$TIC [\text{wt. \%}] = TC [\text{wt. \%}] - TOC [\text{wt. \%}] \quad (20)$$

Accuracy and reproducibility were checked by running replicate analysis of laboratory standards (sulfanilic acid, CaCO_3) and duplicate analysis of samples and were better than 0.1 wt.% (1σ) for carbon and sulfur and 0.02 wt.% (1σ) for nitrogen. The carbonate content was calculated by multiplying the TIC by 8.33 (stoichiometry of calcite, CaCO_3):

$$\text{Carbonate content} [\text{wt. \%}] = TIC [\text{wt. \%}] * 8.33 \quad (21)$$

5.2.2 Rock-Eval pyrolysis

Rock-Eval pyrolysis (see 3.5.1) was performed at the RWTH Aachen University using a Rock Eval 6 analyzer from Vinci Technologies with Helium as carrier gas following the procedure described by Espitalié et al. (1977). Between 10 and 100 mg of powdered sample material (TOC-dependent) were weight into steel crucibles, sealed, and injected into the pyrolysis chamber via an autosampler. Data verification was achieved through duplicates every tenth sample and a Posidonia Shale in-house standard containing 7.65 wt.% TOC at a T_{max} of 426 °C. PI, HI and OI were calculated according to the equations (14), (15) and (16) shown in section 3.6.1. The Rock-Eval data was validated on selected samples at Equinor in Bergen, Norway.

5.3 Molecular geochemistry

5.3.1 Bitumen extraction

Accelerated Solvent Extraction (ASE)

The majority of the sample material was extracted using Accelerated Solvent Extraction (ASE). About 5 g of powdered sample material (coals: ~2 g) were put into steel cells and extracted at 75 °C and 50 bar for 30 min using an ASE 200 device from Dionex using a mixture of dichloromethane (DCM) and methanol (MeOH) (93:7, v/v) as the solvent. The steel cells were filled as follows: (a) metal filter, (b) sealing

5. Material and methods

Table 2. Sample list

| Sample ID | Well | Depth (MD) [m] | Age/Formation | Lithology | Available volume [g] | Extraction method |
|-----------|-----------|----------------|----------------------------|--------------|----------------------|--------------------------------|
| K011188 | 15/3-8 | 4209.06 | Upper Jurassic/Draupne Fm. | Sandstone | 34.02 | Speed extractor |
| K011189 | 15/3-8 | 4209.19 | Upper Jurassic/Draupne Fm. | Sandstone | 52.98 | Speed extractor |
| K011190 | 15/3-8 | 4209.33 | Upper Jurassic/Draupne Fm. | Sandstone | 25.06 | Speed extractor |
| K012302 | 15/3-8 | 4209.36 | Upper Jurassic/Draupne Fm. | Shale | 25.05 | Accelerated Solvent Extraction |
| K011191 | 15/3-8 | 4209.39 | Upper Jurassic/Draupne Fm. | Shale | 46.72 | Accelerated Solvent Extraction |
| K011192 | 15/3-8 | 4209.41 | Upper Jurassic/Draupne Fm. | Shale | 37.77 | Accelerated Solvent Extraction |
| K011193 | 15/3-8 | 4209.49 | Upper Jurassic/Draupne Fm. | Shale | 31.62 | Accelerated Solvent Extraction |
| K011194 | 15/3-8 | 4209.56 | Upper Jurassic/Draupne Fm. | Shale | 38.69 | Accelerated Solvent Extraction |
| K011195 | 15/3-8 | 4209.61 | Upper Jurassic/Draupne Fm. | Shale | 37.29 | Accelerated Solvent Extraction |
| K011196 | 15/3-8 | 4209.63 | Upper Jurassic/Draupne Fm. | Sandstone | 51.98 | Speed extractor |
| K012303 | 15/3-8 | 4209.72 | Upper Jurassic/Draupne Fm. | Sandstone | 17.28 | Accelerated Solvent Extraction |
| K011197 | 15/3-8 | 4209.81 | Upper Jurassic/Draupne Fm. | Sandstone | 69.57 | Speed extractor |
| K012304 | 15/3-8 | 4209.84 | Upper Jurassic/Draupne Fm. | Shale | 10.39 | Accelerated Solvent Extraction |
| K012305 | 15/3-8 | 4209.85 | Upper Jurassic/Draupne Fm. | Heterolithic | 22.62 | Accelerated Solvent Extraction |
| K012430 | 15/3-8 | 4209.88 | Upper Jurassic/Draupne Fm. | Sandstone | 17.52 | Accelerated Solvent Extraction |
| K012306 | 15/3-8 | 4209.92 | Upper Jurassic/Draupne Fm. | Sandstone | 37.62 | Accelerated Solvent Extraction |
| K011198 | 15/3-8 | 4209.98 | Upper Jurassic/Draupne Fm. | Sandstone | 46.33 | Speed extractor |
| K012431 | 15/3-8 | 4290.02 | Upper Jurassic/Draupne Fm. | Source rock | 18.30 | Accelerated Solvent Extraction |
| K012432 | 15/3-8 | 4290.05 | Upper Jurassic/Draupne Fm. | Source rock | 16.23 | Accelerated Solvent Extraction |
| K012433 | 15/3-8 | 4290.10 | Upper Jurassic/Draupne Fm. | Source rock | 8.62 | Accelerated Solvent Extraction |
| K012434 | 15/3-8 | 4290.15 | Upper Jurassic/Draupne Fm. | Source rock | 24.79 | Accelerated Solvent Extraction |
| K012435 | 15/3-8 | 4290.23 | Upper Jurassic/Draupne Fm. | Source rock | 23.93 | Accelerated Solvent Extraction |
| K012436 | 15/3-8 | 4290.25 | Upper Jurassic/Draupne Fm. | Heterolithic | 17.66 | Accelerated Solvent Extraction |
| K012437 | 15/3-8 | 4290.28 | Upper Jurassic/Draupne Fm. | Sandstone | 29.90 | Accelerated Solvent Extraction |
| K012438 | 15/3-8 | 4290.30 | Upper Jurassic/Draupne Fm. | Source rock | 17.28 | Accelerated Solvent Extraction |
| K012439 | 15/3-8 | 4290.35 | Upper Jurassic/Draupne Fm. | Source rock | 20.95 | Accelerated Solvent Extraction |
| K012440 | 15/3-8 | 4290.38 | Upper Jurassic/Draupne Fm. | Source rock | 25.31 | Accelerated Solvent Extraction |
| K012441 | 15/3-8 | 4290.40 | Upper Jurassic/Draupne Fm. | Sandstone | 22.06 | Accelerated Solvent Extraction |
| K012442 | 15/3-8 | 4290.45 | Upper Jurassic/Draupne Fm. | Sandstone | 30.82 | Accelerated Solvent Extraction |
| K012443 | 15/3-8 | 4290.50 | Upper Jurassic/Draupne Fm. | Sandstone | 45.00 | Accelerated Solvent Extraction |
| K012444 | 15/3-8 | 4290.60 | Upper Jurassic/Draupne Fm. | Sandstone | 28.51 | Accelerated Solvent Extraction |
| K012445 | 15/3-8 | 4290.62 | Upper Jurassic/Draupne Fm. | Sandstone | 39.04 | Accelerated Solvent Extraction |
| K012446 | 15/3-8 | 4290.65 | Upper Jurassic/Draupne Fm. | Source rock | 21.61 | Accelerated Solvent Extraction |
| K012447 | 15/3-8 | 4290.70 | Upper Jurassic/Draupne Fm. | Source rock | 35.79 | Accelerated Solvent Extraction |
| K012448 | 15/3-8 | 4290.80 | Upper Jurassic/Draupne Fm. | Source rock | 45.60 | Accelerated Solvent Extraction |
| K012449 | 15/3-8 | 4290.85 | Upper Jurassic/Draupne Fm. | Source rock | 24.92 | Accelerated Solvent Extraction |
| K012450 | 15/3-8 | 4290.90 | Upper Jurassic/Draupne Fm. | Source rock | 21.24 | Accelerated Solvent Extraction |
| K011228 | 15/3-9 T2 | 4126.85 | Upper Jurassic/Draupne Fm. | Sandstone | 63.93 | Speed extractor |
| K011229 | 15/3-9 T2 | 4128.20 | Upper Jurassic/Draupne Fm. | Sandstone | 51.10 | Speed extractor |
| K011230 | 15/3-9 T2 | 4129.20 | Upper Jurassic/Draupne Fm. | Sandstone | 53.87 | Speed extractor |
| K011231 | 15/3-9 T2 | 4129.80 | Upper Jurassic/Draupne Fm. | Shale | 42.24 | Accelerated Solvent Extraction |

(continued on next page)

5. Material and methods

Table 2. Sample list (continued)

| Sample ID | Well | Depth (MD) [m] | Age/Formation | Lithology | Available volume [g] | Extraction method |
|-----------|-----------|----------------|----------------------------|-------------|----------------------|--------------------------------|
| K011232 | 15/3-9 T2 | 4131.10 | Upper Jurassic/Draupne Fm. | Shale | 42.63 | Accelerated Solvent Extraction |
| K011233 | 15/3-9 T2 | 4131.45 | Upper Jurassic/Draupne Fm. | Shale | 42.93 | Accelerated Solvent Extraction |
| K012421 | 15/3-9 T2 | 4131.55 | Upper Jurassic/Draupne Fm. | Sandstone | 38.50 | Accelerated Solvent Extraction |
| K012422 | 15/3-9 T2 | 4132.40 | Upper Jurassic/Draupne Fm. | Shale | 18.99 | Accelerated Solvent Extraction |
| K011234 | 15/3-9 T2 | 4132.50 | Upper Jurassic/Draupne Fm. | Sandstone | 79.34 | Speed extractor |
| K012423 | 15/3-9 T2 | 4132.65 | Upper Jurassic/Draupne Fm. | Sandstone | 10.10 | Accelerated Solvent Extraction |
| K012424 | 15/3-9 T2 | 4132.80 | Upper Jurassic/Draupne Fm. | Shale | 32.88 | Accelerated Solvent Extraction |
| K011235 | 15/3-9 T2 | 4133.90 | Upper Jurassic/Draupne Fm. | Sandstone | 94.66 | Speed extractor |
| K011236 | 15/3-9 T2 | 4135.15 | Upper Jurassic/Draupne Fm. | Shale | 39.11 | Accelerated Solvent Extraction |
| K011237 | 15/3-9 T2 | 4135.40 | Upper Jurassic/Draupne Fm. | Sandstone | 31.34 | Speed extractor |
| K011238 | 15/3-9 T2 | 4135.50 | Upper Jurassic/Draupne Fm. | Shale | 63.78 | Accelerated Solvent Extraction |
| K011239 | 15/3-9 T2 | 4135.90 | Upper Jurassic/Draupne Fm. | Sandstone | 49.58 | Speed extractor |
| K012425 | 15/3-9 T2 | 4482.10 | Middle Jurassic/Hugin Fm. | Coal | 10.67 | Accelerated Solvent Extraction |
| K011240 | 15/3-9 T2 | 4482.20 | Middle Jurassic/Hugin Fm. | Coal | 60.71 | Accelerated Solvent Extraction |
| K011241 | 15/3-9 T2 | 4483.30 | Middle Jurassic/Hugin Fm. | Coal | 28.61 | Accelerated Solvent Extraction |
| K011242 | 15/3-9 T2 | 4484.20 | Middle Jurassic/Hugin Fm. | Coal | 47.38 | Accelerated Solvent Extraction |
| K011243 | 15/3-9 T2 | 4485.40 | Middle Jurassic/Hugin Fm. | Sandstone | 60.61 | Speed extractor |
| K011244 | 15/3-9 T2 | 4488.40 | Middle Jurassic/Hugin Fm. | Sandstone | 64.68 | Speed extractor |
| K011245 | 15/3-9 T2 | 4492.40 | Middle Jurassic/Hugin Fm. | Sandstone | 39.81 | Speed extractor |
| K011246 | 15/3-9 T2 | 4494.35 | Middle Jurassic/Hugin Fm. | Sandstone | 31.25 | Speed extractor |
| K012426 | 15/3-9 T2 | 4496.50 | Middle Jurassic/Hugin Fm. | Sandstone | 56.55 | Accelerated Solvent Extraction |
| K012427 | 15/3-9 T2 | 4497.25 | Middle Jurassic/Hugin Fm. | Shale | 31.41 | Accelerated Solvent Extraction |
| K011247 | 15/3-9 T2 | 4498.45 | Middle Jurassic/Hugin Fm. | Shale | 18.61 | Accelerated Solvent Extraction |
| K011248 | 15/3-9 T2 | 4500.45 | Middle Jurassic/Hugin Fm. | Shale | 21.52 | Accelerated Solvent Extraction |
| K011249 | 15/3-9 T2 | 4501.50 | Middle Jurassic/Hugin Fm. | Coal | 32.18 | Accelerated Solvent Extraction |
| K011250 | 15/3-9 T2 | 4502.10 | Middle Jurassic/Hugin Fm. | Coal | 28.97 | Accelerated Solvent Extraction |
| K012428 | 15/3-9 T2 | 4502.40 | Middle Jurassic/Hugin Fm. | Coal | 11.59 | Accelerated Solvent Extraction |
| K011251 | 15/3-9 T2 | 4502.70 | Middle Jurassic/Hugin Fm. | Coal | 19.82 | Accelerated Solvent Extraction |
| K012429 | 15/3-9 T2 | 4504.50 | Middle Jurassic/Hugin Fm. | Sandstone | 25.16 | Accelerated Solvent Extraction |
| K011252 | 15/3-9 T2 | 4505.20 | Middle Jurassic/Hugin Fm. | Shale | 21.21 | Accelerated Solvent Extraction |
| K011253 | 15/3-9 T2 | 4506.30 | Middle Jurassic/Hugin Fm. | Shale | 35.66 | Accelerated Solvent Extraction |
| K011254 | 15/3-9 T2 | 4507.50 | Middle Jurassic/Hugin Fm. | Sandstone | 44.40 | Speed extractor |
| K012451 | 24/9-1 | 4444.80 | Upper Jurassic/Draupne Fm. | Source rock | 12.22 | Accelerated Solvent Extraction |
| K012452 | 24/9-1 | 4445.10 | Upper Jurassic/Draupne Fm. | Sandstone | 25.04 | Accelerated Solvent Extraction |
| K012453 | 24/9-1 | 4445.30 | Upper Jurassic/Draupne Fm. | Sandstone | 33.92 | Accelerated Solvent Extraction |
| K012454 | 24/9-1 | 4445.70 | Upper Jurassic/Draupne Fm. | Source rock | 25.01 | Accelerated Solvent Extraction |
| K012455 | 24/9-1 | 4446.30 | Upper Jurassic/Draupne Fm. | Source rock | 14.27 | Accelerated Solvent Extraction |
| K012456 | 24/9-1 | 4446.85 | Upper Jurassic/Draupne Fm. | Source rock | 23.60 | Accelerated Solvent Extraction |
| K012457 | 24/9-1 | 4447.30 | Upper Jurassic/Draupne Fm. | Source rock | 16.49 | Accelerated Solvent Extraction |
| K012458 | 24/9-1 | 4447.60 | Upper Jurassic/Draupne Fm. | Source rock | 20.66 | Accelerated Solvent Extraction |
| K012459 | 24/9-1 | 4447.75 | Upper Jurassic/Draupne Fm. | Source rock | 20.77 | Accelerated Solvent Extraction |

(continued on next page)

5. Material and methods

Table 2. Sample list (continued)

| Sample ID | Well | Depth (MD) [m] | Age/Formation | Lithology | Available volume [g] | Extraction method |
|-----------|-----------|----------------|----------------------------|--------------|----------------------|--------------------------------|
| K012460 | 24/9-1 | 4447.90 | Upper Jurassic/Draupne Fm. | Heterolithic | 39.08 | Accelerated Solvent Extraction |
| K012461 | 24/9-1 | 4447.95 | Upper Jurassic/Draupne Fm. | Source rock | 32.02 | Accelerated Solvent Extraction |
| K012462 | 24/9-1 | 4448.10 | Upper Jurassic/Draupne Fm. | Source rock | 19.48 | Accelerated Solvent Extraction |
| K012463 | 24/9-1 | 4448.40 | Upper Jurassic/Draupne Fm. | Source rock | 9.15 | Accelerated Solvent Extraction |
| K012464 | 24/9-1 | 4448.60 | Upper Jurassic/Draupne Fm. | Source rock | 10.18 | Accelerated Solvent Extraction |
| K012465 | 24/9-1 | 4448.90 | Upper Jurassic/Draupne Fm. | Heterolithic | 13.02 | Accelerated Solvent Extraction |
| K012466 | 24/9-1 | 4449.00 | Upper Jurassic/Draupne Fm. | Sandstone | 34.36 | Accelerated Solvent Extraction |
| K012467 | 24/9-1 | 4449.10 | Upper Jurassic/Draupne Fm. | Source rock | 18.19 | Accelerated Solvent Extraction |
| K012468 | 24/9-1 | 4456.40 | Upper Jurassic/Draupne Fm. | Source rock | 19.23 | Accelerated Solvent Extraction |
| K012469 | 24/9-1 | 4456.45 | Upper Jurassic/Draupne Fm. | Sandstone | 21.20 | Accelerated Solvent Extraction |
| K012470 | 24/9-1 | 4456.50 | Upper Jurassic/Draupne Fm. | Sandstone | 33.57 | Accelerated Solvent Extraction |
| K012471 | 24/9-1 | 4456.55 | Upper Jurassic/Draupne Fm. | Source rock | 16.70 | Accelerated Solvent Extraction |
| K012472 | 24/9-1 | 4456.65 | Upper Jurassic/Draupne Fm. | Source rock | 15.79 | Accelerated Solvent Extraction |
| K012473 | 24/9-1 | 4456.80 | Upper Jurassic/Draupne Fm. | Source rock | 12.85 | Accelerated Solvent Extraction |
| K012474 | 24/9-1 | 4456.85 | Upper Jurassic/Draupne Fm. | Source rock | 18.19 | Accelerated Solvent Extraction |
| K012475 | 24/9-1 | 4456.90 | Upper Jurassic/Draupne Fm. | Source rock | 19.28 | Accelerated Solvent Extraction |
| K012476 | 24/9-1 | 4457.10 | Upper Jurassic/Draupne Fm. | Source rock | 23.31 | Accelerated Solvent Extraction |
| K011212 | 34/7-23 A | 3204.05 | Upper Jurassic/Draupne Fm. | Sandstone | 44.61 | Speed extractor |
| K011213 | 34/7-23 A | 3207.10 | Upper Jurassic/Draupne Fm. | Sandstone | 58.78 | Speed extractor |
| K011214 | 34/7-23 A | 3210.55 | Upper Jurassic/Draupne Fm. | Sandstone | 76.07 | Speed extractor |
| K011215 | 34/7-23 A | 3215.80 | Upper Jurassic/Draupne Fm. | Sandstone | 49.80 | Speed extractor |
| K011216 | 34/7-23 A | 3220.40 | Upper Jurassic/Draupne Fm. | Sandstone | 57.91 | Speed extractor |
| K011217 | 34/7-23 A | 3225.50 | Upper Jurassic/Draupne Fm. | Sandstone | 31.08 | Speed extractor |
| K011218 | 34/7-23 A | 3234.30 | Upper Jurassic/Draupne Fm. | Sandstone | 54.45 | Speed extractor |
| K011219 | 34/7-23 A | 3240.45 | Upper Jurassic/Draupne Fm. | Heterolithic | 92.71 | Accelerated Solvent Extraction |
| K011220 | 34/7-23 A | 3247.30 | Upper Jurassic/Draupne Fm. | Heterolithic | 93.20 | Accelerated Solvent Extraction |
| K011221 | 34/7-23 A | 3254.50 | Upper Jurassic/Draupne Fm. | Heterolithic | 73.66 | Accelerated Solvent Extraction |
| K011222 | 34/7-23 A | 3260.25 | Upper Jurassic/Draupne Fm. | Shale | 78.89 | Accelerated Solvent Extraction |
| K011223 | 34/7-23 A | 3266.25 | Upper Jurassic/Draupne Fm. | Shale | 70.67 | Accelerated Solvent Extraction |
| K011224 | 34/7-23 A | 3271.30 | Upper Jurassic/Draupne Fm. | Shale | 71.29 | Accelerated Solvent Extraction |
| K011225 | 34/7-23 A | 3277.40 | Upper Jurassic/Draupne Fm. | Shale | 76.10 | Accelerated Solvent Extraction |
| K011226 | 34/7-23 A | 3283.60 | Upper Jurassic/Draupne Fm. | Shale | 44.50 | Accelerated Solvent Extraction |
| K011227 | 34/7-23 A | 3290.90 | Upper Jurassic/Draupne Fm. | Shale | 80.06 | Accelerated Solvent Extraction |
| K011199 | 34/7-23 S | 3130.25 | Upper Jurassic/Draupne Fm. | Shale | 58.91 | Accelerated Solvent Extraction |
| K011200 | 34/7-23 S | 3131.50 | Upper Jurassic/Draupne Fm. | Shale | 38.90 | Accelerated Solvent Extraction |
| K011201 | 34/7-23 S | 3132.50 | Upper Jurassic/Draupne Fm. | Shale | 48.35 | Accelerated Solvent Extraction |
| K011202 | 34/7-23 S | 3132.90 | Upper Jurassic/Draupne Fm. | Shale | 63.60 | Accelerated Solvent Extraction |
| K011203 | 34/7-23 S | 3133.20 | Upper Jurassic/Draupne Fm. | Shale | 42.93 | Accelerated Solvent Extraction |
| K011204 | 34/7-23 S | 3133.35 | Upper Jurassic/Draupne Fm. | Sandstone | 100.15 | Speed extractor |
| K011205 | 34/7-23 S | 3133.55 | Upper Jurassic/Draupne Fm. | Sandstone | 98.93 | Speed extractor |
| K011206 | 34/7-23 S | 3133.80 | Upper Jurassic/Draupne Fm. | Sandstone | 74.43 | Speed extractor |

(continued on next page)

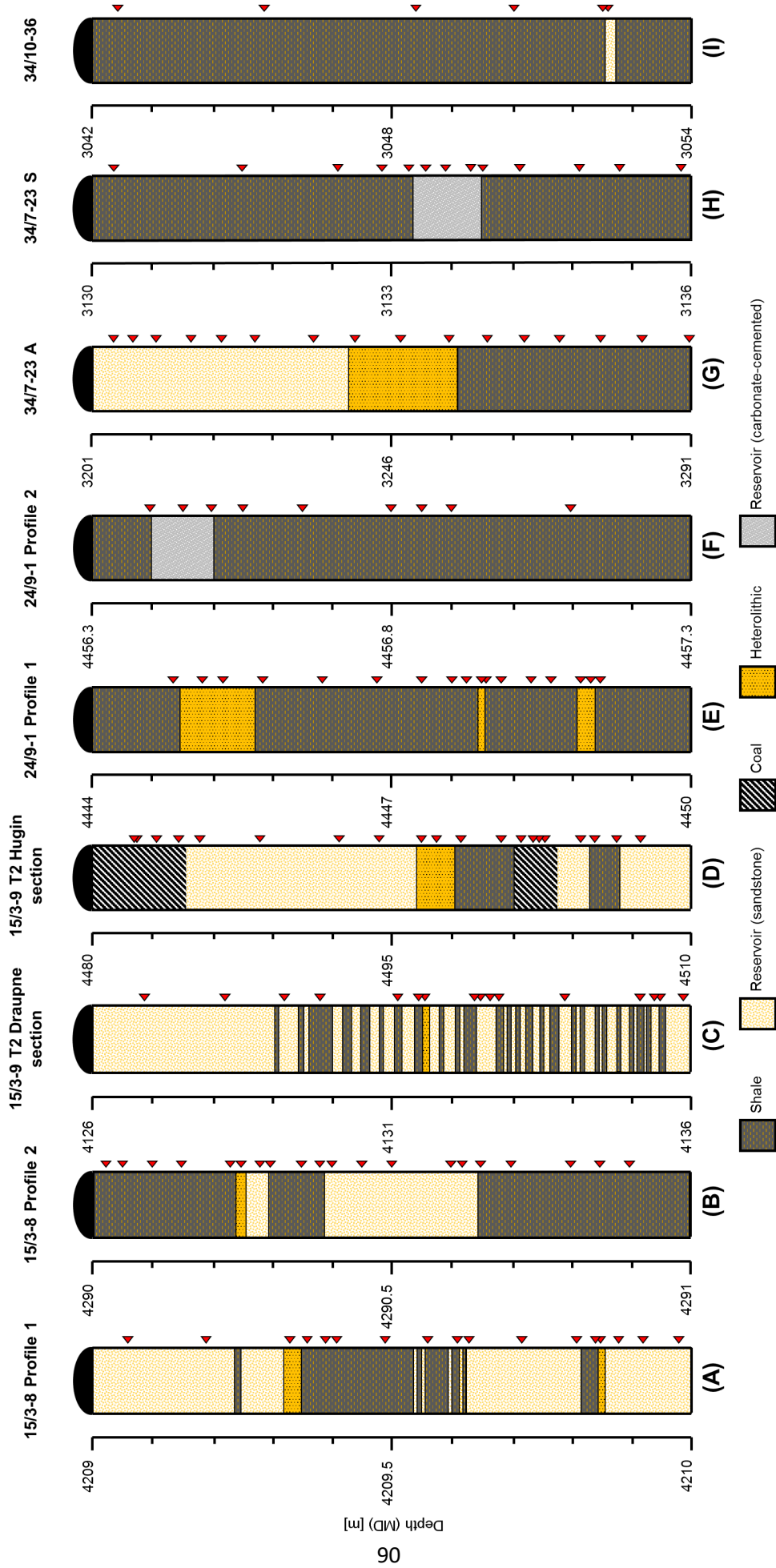
5. Material and methods

Table 2. Sample list (*continued*)

| Sample ID | Well | Depth (MD) [m] | Age/Formation | Lithology | Available volume [g] | Extraction method |
|-----------|-----------|----------------|----------------------------|-------------|----------------------|--------------------------------|
| K011207 | 34/7-23 S | 3133.90 | Upper Jurassic/Draupne Fm. | Shale | 47.54 | Accelerated Solvent Extraction |
| K011208 | 34/7-23 S | 3134.30 | Upper Jurassic/Draupne Fm. | Shale | 44.87 | Accelerated Solvent Extraction |
| K011209 | 34/7-23 S | 3134.90 | Upper Jurassic/Draupne Fm. | Shale | 32.25 | Accelerated Solvent Extraction |
| K011210 | 34/7-23 S | 3135.30 | Upper Jurassic/Draupne Fm. | Shale | 52.55 | Accelerated Solvent Extraction |
| K011211 | 34/7-23 S | 3135.90 | Upper Jurassic/Draupne Fm. | Shale | 58.64 | Accelerated Solvent Extraction |
| K012477 | 34/10-36 | 3042.50 | Upper Jurassic/Draupne Fm. | Source rock | 22.92 | Accelerated Solvent Extraction |
| K012478 | 34/10-36 | 3045.45 | Upper Jurassic/Draupne Fm. | Source rock | 14.62 | Accelerated Solvent Extraction |
| K012479 | 34/10-36 | 3048.50 | Upper Jurassic/Draupne Fm. | Source rock | 20.41 | Accelerated Solvent Extraction |
| K012480 | 34/10-36 | 3050.45 | Upper Jurassic/Draupne Fm. | Source rock | 12.31 | Accelerated Solvent Extraction |
| K012481 | 34/10-36 | 3052.25 | Upper Jurassic/Draupne Fm. | Source rock | 20.06 | Accelerated Solvent Extraction |
| K012482 | 34/10-36 | 3052.35 | Upper Jurassic/Draupne Fm. | Sandstone | 20.88 | Accelerated Solvent Extraction |

General sample information showing for each sample its ID, the corresponding well name, the depth, the age, the formation, the volume available for analyses and the extraction method. Altogether, 134 core samples were collected from six exploration wells (15/3-8; 15/3-9 T2; 24/9-1; 34/7-23 A; 34/10-36) located on the Norwegian continental shelf in purpose to investigate the molecular effects of petroleum expulsion. The extraction conditions were as follows: T= 75 °C; p= 50 bar; solvent mixture: dichloromethane:methanol (93:7, v/v). The depths are given as measured depths (MDs) and are mostly in good agreement with the true vertical depths (TVDs). Note, however, that the true vertical depths for samples from well 34/7-23 A (~2619.5-2678 m) and well 34/7-23 S (~2652.6-2659.3 m) are, according to the information provided by the Norwegian Petroleum Directorate, much lower than the measured depths.

5. Material and methods



5. Material and methods

Fig. 19. Simplified lithostratigraphic columns of the investigated expulsion scenarios. The sample positions are indicated by red arrows. Note that all columns have different scales. A: 15/3-8, 4209-4210 m, 17 samples. B: 15/3-8, 4290-4291 m, 20 samples. C: 15/3-9 T2, 4126-4136 m, 16 samples. D: 15/3-9 T2, 4480-4510, 20 samples. E: 24/9-1, 4444-4450 m, 17 samples. F: 24/9-1, 4456-4458 m, 9 samples. G: 34/7-23 A, 3201-3291 m, 16 samples. H: 34/7-23 S, 3130-3136 m, 13 samples. I: 34/10-36, 3042-3054 m, 6 samples. The depths are given as measured depths (MDs) and are, according to the Norwegian Petroleum Directorate (NPD), mostly in good agreement with the true vertical depths (TVDs). Only scenario G from well 34/7-23 A (~2619.5-2678 m TVD) and scenario H from well 34/7-23 S (~2652.6-2659.3 m TVD) are located much shallower than indicated by the measured depths.

ring, (c) metal fitting, (d) filter, (e) pre-extracted glass wool, (f) pre-extracted glass beads, (g) filter, (h) glass wool (i) pre-extracted glass beads mixed with sample powder, (j) pre-extracted glass wool (Fig. 20). After two extraction runs, the bitumen extracts were concentrated within a Büchi Syncore solvent evaporator coupled to a Büchi V-700 vacuum pump at 60 °C and 850 mbar for one hour. Additional extractions did not yield notable volumes of extract, as shown by test runs (Fig. 21). Subsequently, the concentrated extracts were carefully pipetted into pre-weighed vials and backweight after the solvent evaporated completely to determine the total liquid extract (mg/g TOC). Afterwards, the vials were refilled with DCM and prepared for group-type separation (see 5.3.2).

Speed Extractor

Selected reservoir samples (Schwark, personal communication, 2016, 2017) were extracted by means of a Büchi E-914 speed extractor, which is comparable to ASE. A mixture of dichloromethane and methanol (93:7, v/v) served as the solvent. The system operated at 75 °C and 50 bar for one hour, similar to the ASE procedure described above. The steel cells were filled as follows (base to top): (a) screw-cap, (b) metal filter, (c) pre-extracted glass wool, (d) pre-extracted glass beads, (e) pre-extracted glass beads mixed with sample powder, (f) pre-extracted glass beads, (g) pre-extracted glass wool, (h) filter (Fig. 20). After two extraction runs, the extract yields were concentrated within a solvent evaporator (Büchi), transferred into pre-weighed vials and afterwards prepared for group type separation.

5.3.2 Extract separation

The bulk extracts were separated into aliphatics, monoaromatics, aromatics, carbazoles and heteroatomic compounds using solid-phase extraction (SPE). The fractions were eluted with 7 ml *n*-hexane, 9 ml *n*-hexane, 6.5 ml *n*-hexane/DCM (3:2, v/v), 6.5 ml DCM and 14.5 ml DCM/MeOH (1:1, v/v), respectively, utilizing a LC Tech

5. Material and methods

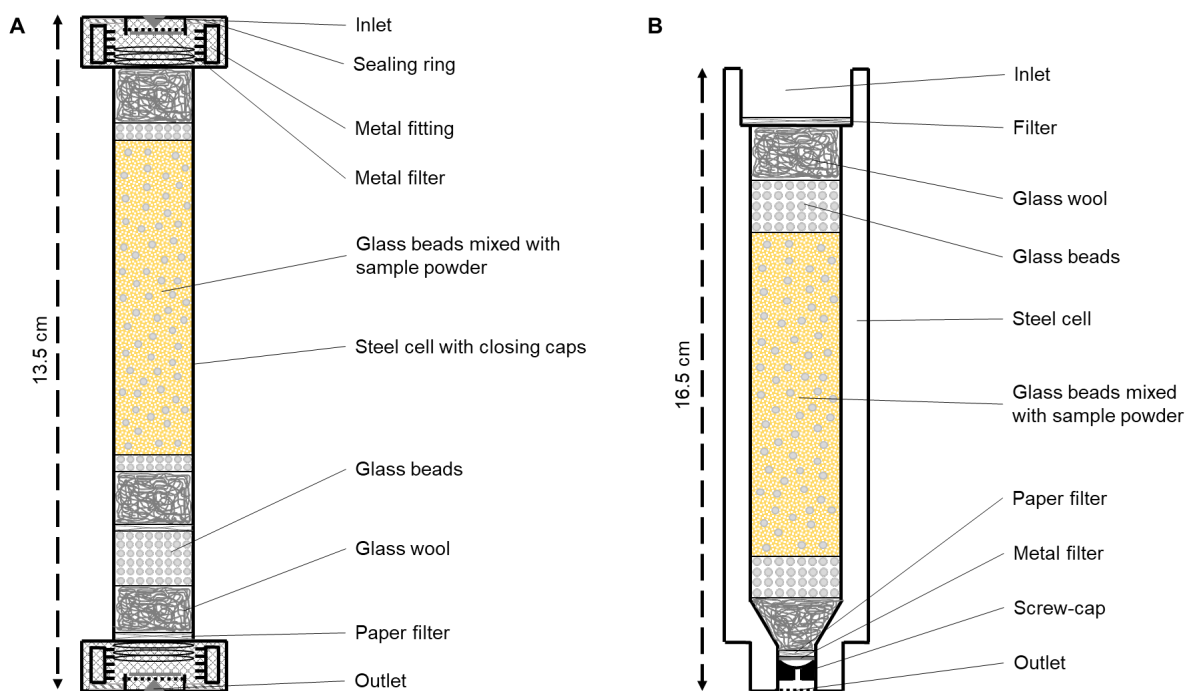


Fig. 20. Extraction cell structures. A: Simplified setup of an Accelerated Solvent Extraction (ASE) steel cell. B: Schematic configuration of a Büchi E-914 speed extractor cell. Note that both extraction cells contain sample powder mixed with glass beads to provide optimum flushing conditions.

Freestyle robot operating automatically (Haeuser, personal communication, 2016). Aromatics and monoaromatics were unified after the procedure. To remove elemental sulfur, excess HCl-activated copper filings were added to each aliphatic fraction. The elemental sulfur reacted with the copper filings under the formation of Copper(I) sulfide (Cu_2S) and was thus removed from the sample:



The concentration of individual compounds was determined using internal standards, i.e. deuterated tetracosane (tetracosane-d50) for the aliphatic fractions, deuterated pyrene (pyrene-d10) for the aromatic fractions and a 1:1 (v/v) mixture of 9-ethylcarbazole, 9-phenylcarbazole and 3,6-di-tert-butylcarbazole for the carbazole fractions (Table 3). The heteroatomic compounds were not analyzed. All standards were checked for purity by gas chromatography-mass spectrometry (GC-MS) (see below) before addition to the samples.

5.3.3 Gas chromatography-mass spectrometry

Aliphatics, aromatics and carbazoles were analyzed for their molecular composition using GC-MS. While the aliphatic fractions were measured using an Agilent

5. Material and methods

Table 3. List of standards

| Fraction | Standard 1 | Standard 2 | Standard 3 |
|------------|-----------------------------------|------------------------------------|---|
| Aliphatics | Tetracosane-d50: 0.1 µg/µl | - | - |
| Aromatics | Pyrene-d10: 0.1 µg/µl | - | - |
| Carbazoles | 9-Ethylcarbazole: 106.32 ng/10 µl | 9-Phenylcarbazole: 101.63 ng/10 µl | 3,6-Di-tert-butylcarbazole: 102.02 ng/10 µl |

Technologies 7890A GC System interfaced with an Agilent Technologies 5975B inert XL EI/CI MSD mass spectrometer, the aromatic and carbazole fractions were analyzed by means of an Agilent Technologies 7820A GC system connected to an Agilent Technologies 5975 Series MSD mass spectrometer. The first GC system was equipped with a 30 m x 0.25 mm x 0.25 µm Phenomenex Zebron ZB-1 fused silica capillary column coated with 100% dimethylpolysiloxane. Aromatics and carbazoles were eluted using a 30 m x 0.25 mm x 0.25 µm Agilent HP-5 fused silica capillary column coated with (5% phenyl-)-methylpolysiloxane. Helium served as carrier gas. With respect to the aliphatic hydrocarbons, the oven temperature was programmed from 60 °C for 5 min at the beginning to 140 °C at 10 °C/min and subsequently heated to the final temperature of 325 °C at a constant rate of 3 °C/min, which was kept isothermal for 15 min. Concerning the aromatic fractions, the starting temperature of 60 °C was held for 5 min, then raised to 140 °C at a rate of 10 °C/min and afterwards smoothly ramped to the final temperature of 325 °C at 3 °C/min, which was held for 8 min. The carbazole fractions were injected at 60 °C, held there for 2 min, then heated to 150 °C at 10 °C/min, then raised to 210 °C at 1.5 °C/min and

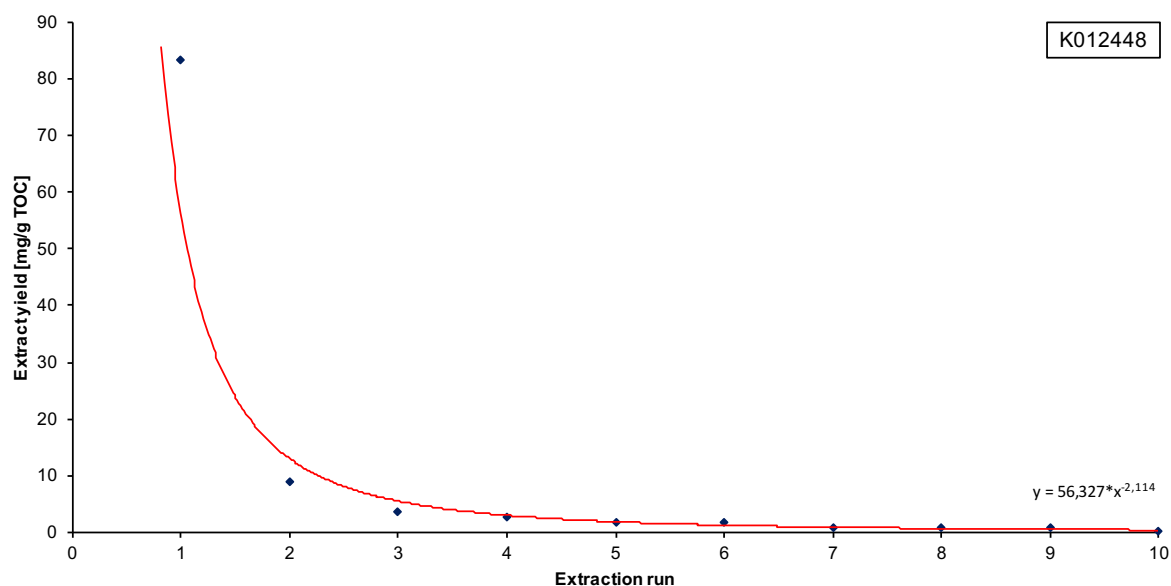


Fig. 21. Diagram showing the evolution of the extract yield of sample K012448 (source rock; Draupne Formation; well 15/3-8; 4290.80 m measured depth) over ten extraction runs. Note that the majority of the bitumen is extracted throughout the first two runs, whereas further extraction runs did not yield significant amounts of extract. The extraction conditions were as follows: T= 75 °C, p= 50 bar, solvent mixture: dichloromethane:methanol (93:7, v/v).

5. Material and methods

finally increased to the end temperature of 320 °C at a rate of 8 °C/min where the temperature remained constant for 13 min. The aliphatic fractions were analyzed in selected ion monitoring (SIM) mode with an ionization energy of 70 eV. The following ions were monitored: 85, 98, 191, 205, 217, 218, 231, 259. Full scan runs were conducted where necessary. Aromatics and carbazoles were measured in full scan mode at 70 eV. SIM analyses were performed on selected samples to improve measurement qualities. Peak integration was carried out manually utilizing the Agilent Technologies GC/MSD ChemStation Software under the use of published mass spectra and the comparison of retention times. 5 Å molecular sieving of *n*-alkanes following the procedure described by Grice et al. (2008) was conducted on selected aliphatic fractions to reduce noise and increase biomarker concentrations. Note, however, that pure cyclohexane instead of the mixture of cyclohexane and *n*-pentane (12:88, v/v) applied by Grice et al. (2008) was used in this study.

5.4 Geochromatographic experiment

In addition to the investigation of the natural case scenarios, a geochromatographic retardation experiment (Fig. 22) was conducted to examine explicitly the influence of geochromatography on selected organic compounds and compound groups. Therefore, a 13-component tracer solution (solved in DCM) consisting of 2-ethyl dibenzofuran, 9-methylphenanthrene, 1-methylphenanthrene, 4,6-dimethyldibenzothiophene, 2,8-dimethyldibenzothiophene, 1,4-dimethylcarbazole, 3-ethylcarbazole, 2,7-dimethylcarbazole, 3,6-dimethylcarbazole, benzo[def]carbazole, benzo[a]carbazole, 3,6-di-tert-butylcarbazole, and benzo[c]carbazole (Table 4) was passed gravitation-ally through a finely ground, compacted, pre-extracted (ASE, Soxhlet), oil window-mature, and 10% water saturated Draupne source rock column (20 cm x 1 cm, 15 cm filling height) from North Sea well 15/3-8 via a synthetic oil as defined below. The water saturation was achieved volumetrically. The organic tracers were chosen to represent compounds and compound groups that are routinely applied in the petroleum exploration business to evaluate, for example, the thermal maturity of oils and source rocks (e.g. dibenzothiophenes, phenanthrenes), the migration distance of crude oils in a sedimentary basin (e.g. carbazoles), the organic facies of a source rock (e.g. dibenzothiophenes, furans, phenanthrenes), or are frequently used as instruments for oil-source rock correlations. The synthetic oil was composed of isooctane, xylene, methanol, isopropanol, and tetrahydrofuran (45:35:10:5:5, v/v) and

5. Material and methods

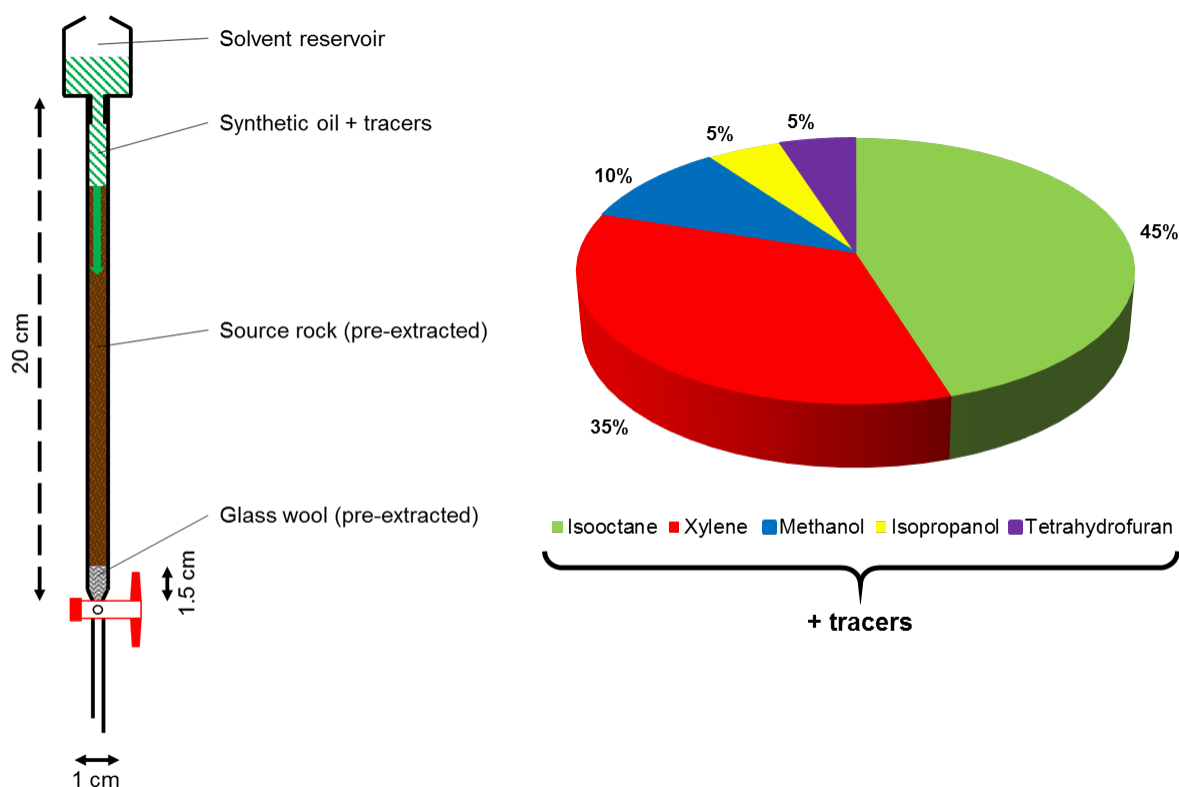


Fig. 22. Simplified setup of the geochromatographic retardation experiment. Essentially, a tracer stock solution (2 ml) containing selected organic compounds (Table 4) was flowed gravitationally through a powdered, compacted, solvent-extracted, and 10% water-saturated (ASE, Soxhlet) Draupne source rock column (20 cm x 1 cm, 15 cm filling height) from well 15/3-8, Norwegian North Sea, via a synthetic oil to investigate the influence of geochromatography on the tracer solution. Altogether, 32 fractions of different volumes (0.8-8.0 ml) were collected, desulfurized, and prepared for GC-MS analysis. 10 μ l of 9-phenylcarbazole (10 μ g/ml) were added to each fraction as internal quantification standard.

thus principally resembled the basic chemical composition (saturates, aromatics, heteroatomic compounds) of a natural crude oil. Based on the densities of the constituents and their respective proportions in the synthetic oil, its average density was calculated to be 0.77 g/cm³. Both oil and tracer solution were checked for purity by GC-MS before the experiment. The method was the same as for the eluates and the tracer solution (see below). Basically, 2 ml of tracer solution were added to the unconditioned source rock column and left in place until the DCM evaporated completely, which was optically visible. Subsequently, the column was flushed with synthetic oil and maintained oil-wet throughout the experiment. To avoid photo-oxidation, the column was coated with aluminium foil. In total, 32 eluates of different volumes (0.8-8.0 ml) were collected, desulfurized (equation 22), and prepared for GC-MS measurement. 10 μ l of 9-phenylcarbazole (10 μ g/ml) were added to each fraction, as well as to an aliquot of the tracer mixture as internal quantification standard. Except for the 2-ethyl dibenzofuran and the 3-ethylcarbazole, the response factors of the quantified components were similar to that of the internal standard. For the 2-ethyl dibenzofuran and the 3-ethylcarbazole, a correction was carried out. Each

5. Material and methods

Table 4. Composition of the tracer solution (in DCM)

| Component | Concentration [$\mu\text{g/ml}$] |
|------------------------------|------------------------------------|
| 2-Ethylidibenzofuran | 3.16 |
| 9-Methylphenanthrene | 3.99 |
| 1-Methylphenanthrene | 5.73 |
| 4,6-Dimethyldibenzothiophene | 3.83 |
| 2,8-Dimethyldibenzothiophene | 3.99 |
| 1,4-Dimethylcarbazole | 9.61 |
| 3-Ethylcarbazole | 8.10 |
| 2,7-Dimethylcarbazole | 7.83 |
| 3,6-Dimethylcarbazole | 8.32 |
| Benzo[def]carbazole | 7.24 |
| Benzo[a]carbazole | 7.59 |
| 3,6-Di-tert-butylcarbazole | 8.54 |
| Benzo[c]carbazole | 6.73 |

fraction and the tracer solution were analyzed for their molecular compositions using an Agilent Technologies 7820A GC system coupled with an Agilent Technologies 5977B Series MSD mass spectrometer. The GC system was equipped with a 30 m x 0.25 mm x 0.25 μm DB-5 fused silica column (Agilent) coated with (5% diphenyl)-dimethylpolysiloxane. The fractions were injected at 60 °C and held isothermal for 5 min, after which the oven temperature was raised to 140 °C at 10 °C/min, followed by a second heating step of 3 °C/min to the final temperature of 325 °C, which was kept for 8 min. The data were acquired in full scan mode. Helium served as carrier gas. Peak identification was done via the comparison of retention times and the use published mass spectra.

6. Results

After having described the general dynamics of a petroleum system, the current level of knowledge on primary migration, the geological evolution of the study area, including the depositional histories of the Draupne and the Hugin Formation, as well as the experimental procedures, the following chapter intends to present the dataset that was obtained as part of this work and therefore forms the basis for discussion. In the first part, the most essential trends observed in the natural case scenarios will be described, after which the results obtained from the geochromatographic experiment will be shown in the second part.

6.1 Natural expulsion scenarios

Part one of the chapter concentrates on the bulk and molecular geochemical results obtained from the nine natural expulsion scenarios (Fig. 19).

6.1.1 Bulk data

Bulk geochemical parameters are essential regarding the principal classification of source rocks, the determination of the organic facies, and for quantitative estimations concerning petroleum generation and expulsion. In particular, data obtained from bulk geochemical analyses theoretically allow to conclude about the depositional conditions, the kerogen type, the thermal maturity, and the bitumen content of a source rock. The bulk data summarized here comprise the results of the elemental analysis (TOC, TN, TS, TIC, carbonate content), the Rock-Eval pyrolysis (S_1 , HI, OI, PI, T_{max}), as well the solvent extraction procedure (bulk extract yields).

15/3-8 Profile 1 (expulsion scenario A)

As described in the previous chapter, the first analyzed section was a high-resolution profile (1 m) from well 15/3-8 (Fig. 18, 19). It ranges from 4209 to 4210 m drilling depth and consists of a well-defined source rock unit surrounded by two sandstone reservoir packages above and below, and a thin organic-rich layer close to the bottom. The bulk data are illustrated in Fig. 23.

With regard to the CNS results, the TOC values are in the range of 0.36 to 10.32 wt.%, the TN content varies between 0.01 and 0.29 wt.%, and the TS values extend from 0.22 to 10.02 wt.%. Both the TN and TS curves closely follow the TOC trend. As

6. Results

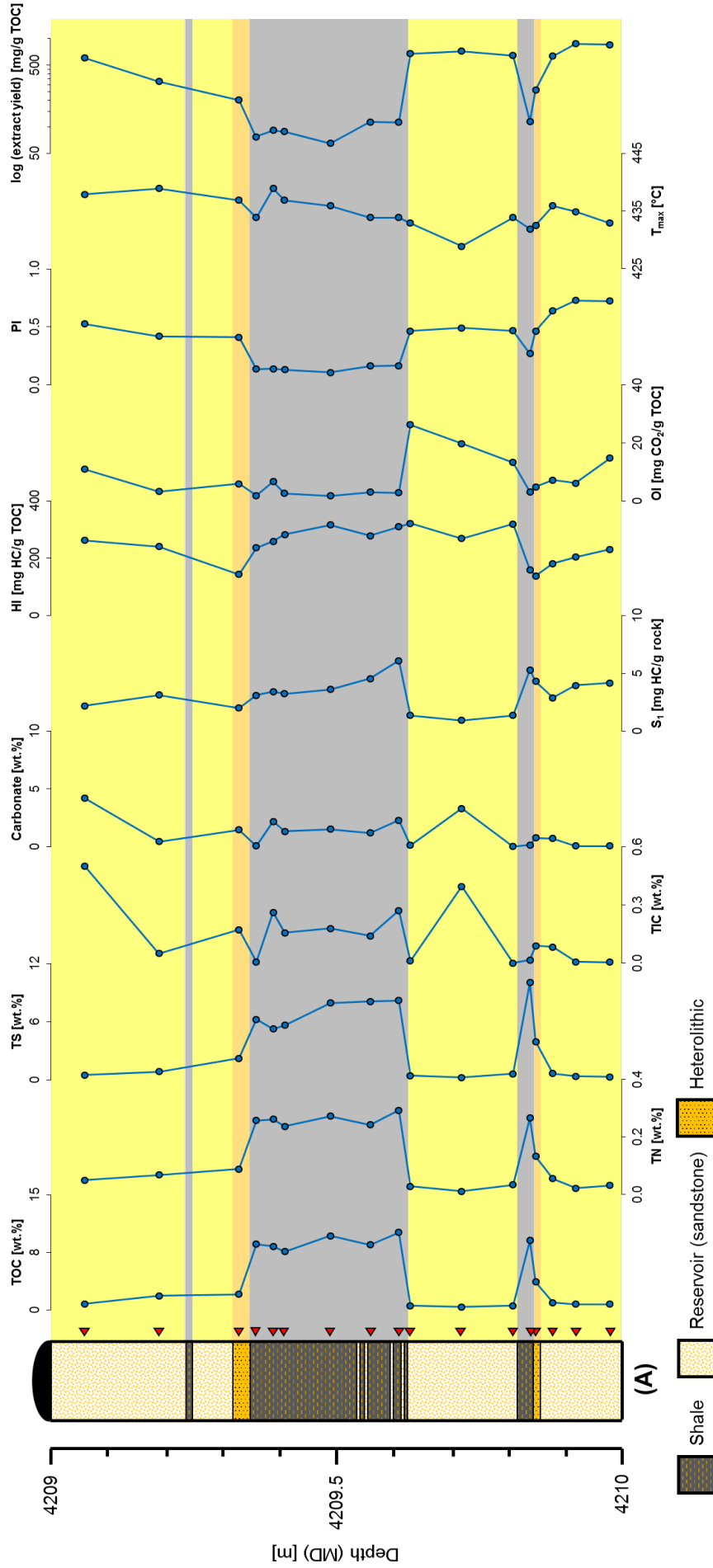


Fig. 23. Expulsion scenario A (North Sea well 15/3-8, 4209-4210 m drilling depth): bulk geochemical depth profiles. The depth is given as measured depth (MD) and comparable to the true vertical depth (TVD). One tick on the depth axis represents 0.1 m. Abbreviations: TOC= Total Organic Carbon; TN= Total Nitrogen; TS= Total Sulfur; TIC= Total Inorganic Carbon; HI= Hydrogen Index; OI= Oxygen Index; PI= Production Index.

6. Results

expected, the highest values are reached in the thick source rock interval in the center, as well as in the thin layer at the bottom of the section. Concerning the inorganic carbon and thus the carbonate content, it was shown that approximately 0.05 to 4.17 wt.% carbon are bound in carbonate minerals. With respect to the data from the Rock-Eval pyrolysis, the S_1 values plot in total between 0.92 and 6.09 mg HC/g rock, maximize in the organic-rich shales, and show a slightly bell-shaped trend within the central source unit. The HI of the source rock samples ranges from 159 to 315 mg HC/g TOC, and averages at 262 mg HC/g TOC. Note that the lowest value was measured in the thin layer in the lower half of the section. In contrast to the HI, the OI values of the shale units are generally low and display a narrow range from 2 to 7 mg CO₂/g TOC. Both HI and OI values are negligible for the sandstone samples and are only shown for completeness. Regarding the PI, the values vary between 0.11 and 0.73, and are highest within the sandstones. By contrast, the PI of the shaly samples is comparatively low and averages at around 0.16. Note again that the thin layer at the bottom of the profile displays a higher PI value than samples from the central source unit. With regard to the T_{max} parameter, the values remain relatively constant over the profile and, for the shale samples, totally extend from 432 to 439 °C with a mean value of 436 °C. As for the HI and OI, the T_{max} values can be neglected for the sandstones, too. Interestingly, the T_{max} of the sampled thin layer is slightly lower (432 °C) than the mean value of the central source package (436 °C). With respect to the solvent extraction results, the TOC-normalized extract yields of scenario A display a broad range over the profile and are plotted logarithmically for better visualization. In total, the extract volumes fluctuate between 65 and 872 mg/g TOC, whereby the highest values are attained in the sandstone units. Compared to the sandstones, the source rock samples exhibit only low to moderate extract yields (65-115 mg/g TOC), which, for the central shale unit, were found to increase towards the edges until a small decrease immediately before the sandstone contact. Although slightly elevated in the thin layer, the extract yields of thin layer and central source unit are still in the same order of magnitude.

In summary, based on the bulk parameters described above, active petroleum expulsion from the central source bed and the thin layer into the surrounding sandstone units can be expected. More specifically, the TOC values suggest sufficient organic richness, the T_{max} thermal maturity within in the oil-window, and the PI, as well as the extract yield curves the presence of a hydrocarbon phase in the carrier beds. Though,

6. Results

at this point it is not possible to identify the origin of this hydrocarbon phase. Although it is likely that, due to the intraformational character of the carrier beds, the fluids originate from the adjacent shale units, lateral migration from another source cannot completely be ruled out.

15/3-8 Profile 2 (expulsion scenario B)

The second examined expulsion scenario is also part of North Sea well 15/3-8 but, in contrast to scenario A, located 80 m deeper in a depth of 4290 to 4291 m (Fig. 18, 19). As described above, the profile covers 1 m of drill core and consists of three distinct source rock and two reservoir units. Fig. 24 shows the bulk geochemical depth profiles.

Regarding the CNS data, the trends are overall quite similar to the previous expulsion scenario. In particular, the TOC (0.28-7.49 wt.%), TN (0.03-0.24 wt.%) and TS (0.28-12.43 wt.%) values are highest in the source intervals, and drop to almost zero in the sandstone horizons. Again, the TN graph strongly resembles the TOC curve. However, this time the TS trend is shaped slightly different, but is still very similar to the TOC and TN graphs. With respect to the inorganic carbon content, all samples were found to contain less than 5 wt.% carbonate. Concerning the Rock-Eval results, the S_1 data plot in an area between 0.92 and 3.87 mg HC/g rock and, similar to the first profile, reach maximum values within the source intervals. However, in contrast to scenario A, the S_1 trend is shaped more irregular, especially in the upper part of the profile where the S_1 values seem to decrease towards the small reservoir layer. With regard to the HI values, the absolute numbers are considerably smaller in the upper (81-126 mg HC/g TOC) than in the lower half (169-231 mg HC/g TOC) of the section, and on average (143 mg HC/g TOC) significantly smaller than in the previous scenario (262 mg HC/g TOC). The OI values are generally quite low (3-4 mg CO₂/g TOC) and thus in a similar range as in scenario A. Again, the HI, OI and T_{max} values of the sandstones can be neglected and are shown only for completeness. With regard to the PI, the total values range from 0.18 to 0.55 and, as already observed in the previous scenario, are highest in the sandstone intervals. Conversely, the PI reaches mean values of only 0.26 in the source rock material, whereby samples collected from the upper half of the section exhibit on average higher PIs (0.30) than samples originating from the lower part (0.20). Similar to the previous profile, the T_{max} data show a fairly constant trend across the profile. The

6. Results

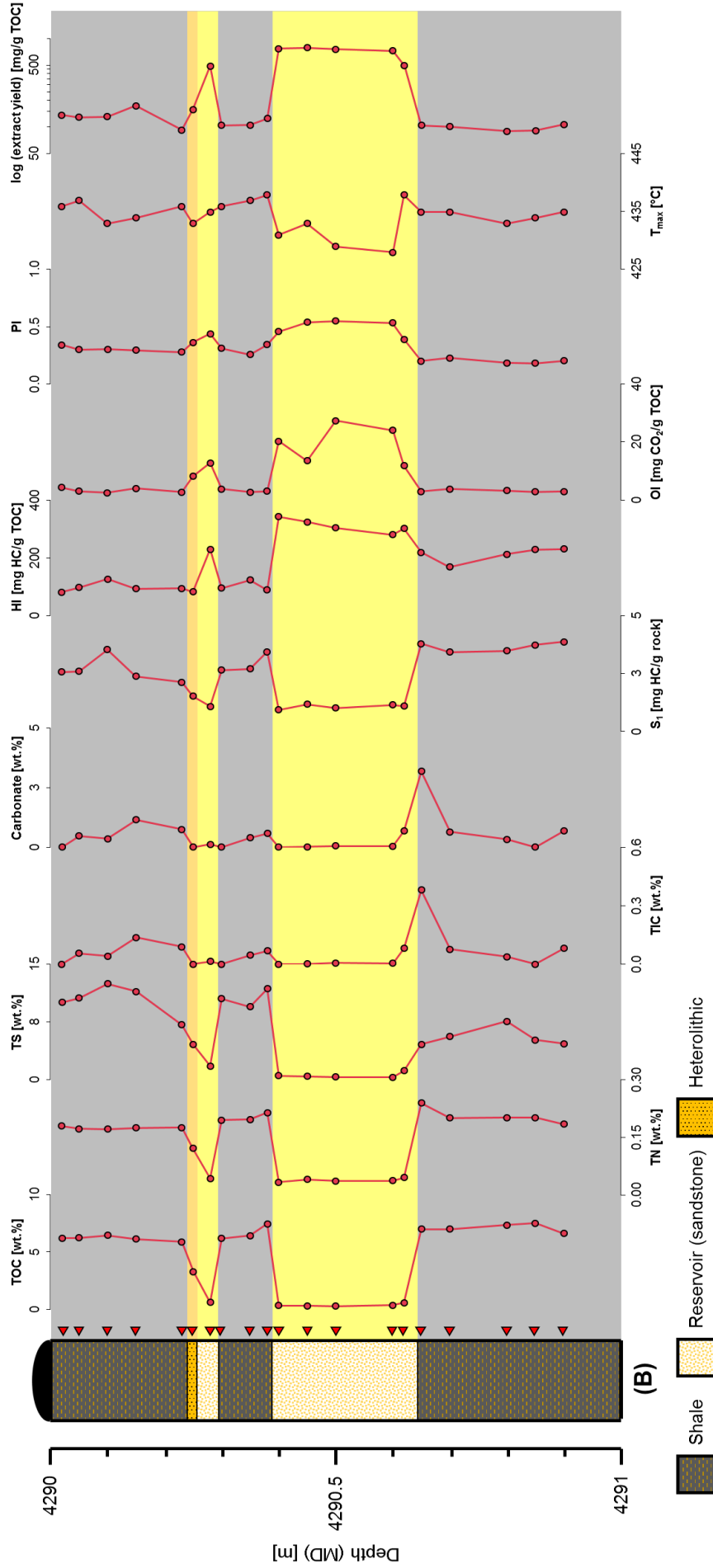


Fig. 24. Expulsion scenario B (North Sea well 15/3-8, 4290-4291 m drilling depth): bulk geochemical depth profiles. The depth is given as measured depth (MD) and comparable to the true vertical depth (TVD). One tick on the depth axis represents 0.1 m. Abbreviations: TOC= Total Organic Carbon; TN= Total Nitrogen; TIC= Total Inorganic Carbon; HI= Hydrogen Index; OI= Oxygen Index; PI= Production Index.

6. Results

values average at 435 °C, which fits well with the results of scenario A. The extract yield trend is, however, less pronounced than in scenario A. In general, the TOC-normalized extract yields of scenario B plot between 89 and 783 mg/g TOC and hence show a great variety. Nevertheless, in accordance with the previous section, the largest extract volumes were again recovered from the sandstones. For the shale samples, the data average at 114 mg/g TOC, which is slightly higher than in the first section. Furthermore, somewhat higher extract yields were obtained in the upper (124 mg/g TOC) than in the lower half (98 mg/g TOC) of scenario B.

Similar to the previous profile from the same well, scenario B seems, on the basis of the bulk parameters, also to be suitable to examine natural petroleum expulsion. In particular, TOC values above 5 wt.% indicate the presence of adequate amounts of organic material in the shale units, the T_{max} points to a maturity within the oil-window, and PI and extract yields suggest the presence of petroleum in the carrier beds. Yet, the lower HI values compared to the former section hint at a lower generation potential, which may point to differences in the organic facies. Again, the origin of the reservoir fluids is, at this point, still unclear.

15/3-9 T2 Draupne section (expulsion scenario C)

The third expulsion scenario that was examined originates from North Sea well 15/3-9 T2 and was placed between 4126 and 4136 m drilling depth in strata of the Draupne Formation (Fig. 18, 19). The 10 m profile is characterized by a strongly alternating sequence of organic-rich shales and sandstone beds, superimposed by a relatively thick reservoir unit at the top of the section. The bulk data are presented in Fig. 25.

The TOC content varies in total between 0.19 and 9.53 wt.%, whereby the highest values were as expected measured in the source rock intervals. As already observed in the previous scenarios, there are again strong similarities between the TOC, the TN (0.02-0.36 wt.%), and the TS (0.24-8.03 wt.%) curves. The inorganic carbon content of scenario C ranges between 0 and 1.61 wt.%, which corresponds to carbonate contents of up to 13.38 wt.%. With respect to the Rock-Eval parameters, the S_1 values range from 0.49 to 12.17 mg HC/g rock, the HI extends from 167 to 293 mg HC/g TOC (shale samples), and the OI is in the magnitude of 1 to 4 mg CO₂/g TOC (shale samples). Concerning the PI, the data display a total variety from 0.17 to

6. Results

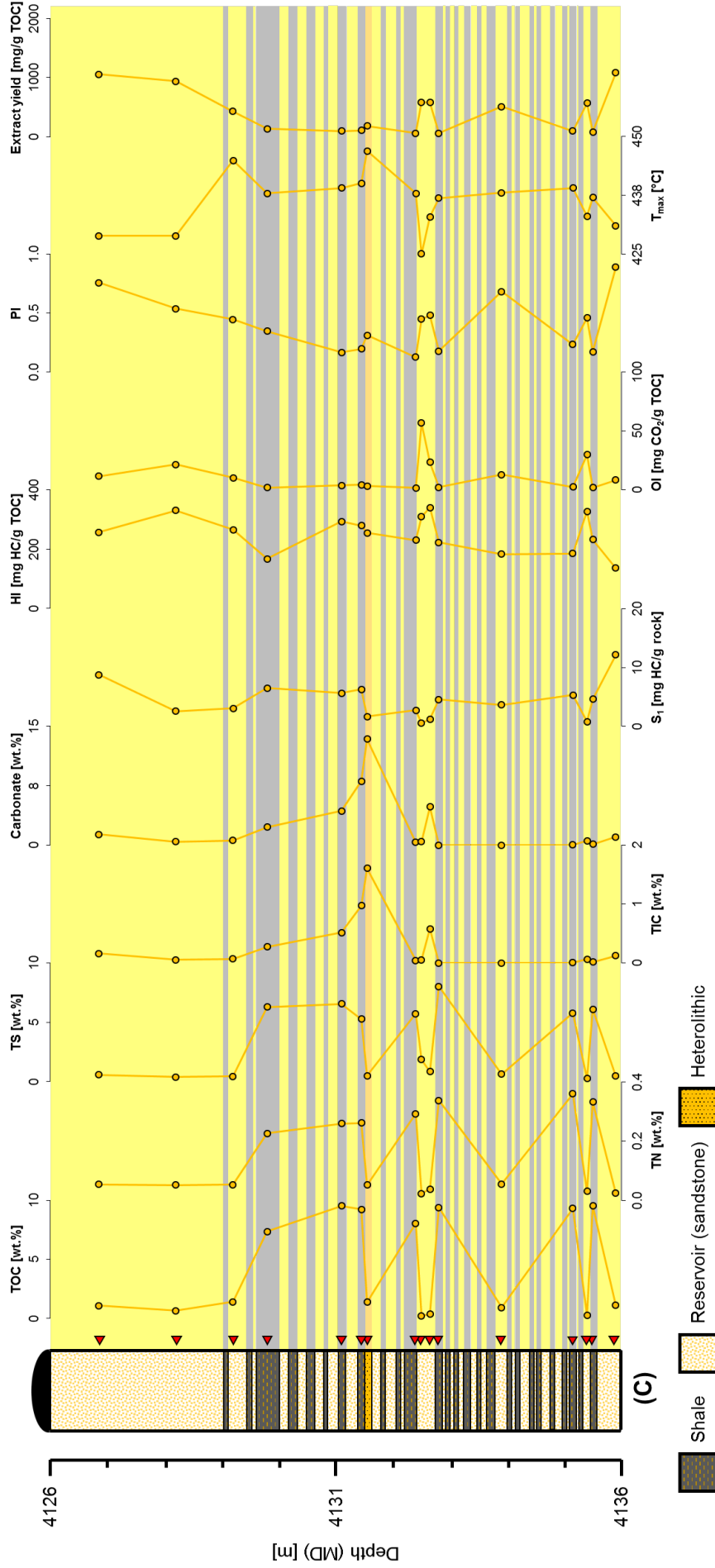


Fig. 25. Expulsion scenario C (North Sea well 15/3-9 T2, Draupne core, 4126-4136 m drilling depth): bulk geochemical depth profiles. The depth is given as measured depth (MD) and comparable to the true vertical depth (TVD). One tick on the depth axis represents 1 m. Abbreviations: TOC= Total Organic Carbon; TN= Total Nitrogen; TS= Total Sulfur; TIC= Total Inorganic Carbon; HI= Hydrogen Index; OI= Oxygen Index; PI= Production Index.

6. Results

0.89, whereby mean values of 0.20 and 0.59 were determined for the shale and sandstone samples, respectively. Only 3 °C difference in the T_{max} values of the source rock samples was measured (437-440 °C), which leads to a constant trend over the profile. Again, HI, OI, and T_{max} parameter can be neglected for the sandstone (reservoir/carrier bed) samples. With regard to the TOC-normalized extract yields (56-1083 mg/g TOC), the lowest volumes were extracted from the shale samples, whereas, on the other hand, the sandstones yielded the highest amounts of extract. In comparison to the previous scenarios, the extract yields of the source rock samples are on average lower (88 mg/g TOC) than in scenario A (94 mg/g TOC) and B (114 mg/g TOC).

To sum up, like in the two profiles before, the bulk parameters of the Draupne section of well 15/3-9 T2 suggest sufficient source rock richness, quality and thermal maturity to study petroleum expulsion. Besides, PI and extract yield values indicate the presence of hydrocarbons in the intercalated reservoir strata, which could originate from the adjacent, oil window-mature organic-rich shales. However, at this point an external origin might also be possible.

15/3-9 T2 Hugin section (expulsion scenario D)

Expulsion scenario D was sampled from the Hugin core of well 15/3-9 T2 and denotes a 30 m profile situated between 4480 and 4510 m drilling depth (Fig. 18, 19). The section consists of two distinct coal beds, two shaly units, and three intercalated sandstone intervals. Fig. 26 summarizes the bulk data.

First, with regard to the CNS results, it is clearly visible that the coals exhibit the highest TOC contents, which can partly exceed 80 wt.%. Thereby, the average TOC content of the upper coal bed (80.99 wt.%) is somewhat higher than that of the lower coal unit (63.64 wt.%). With respect to the shales, the TOC contents are generally much lower and typically range between 2 and 8 wt.%. In addition, values around 1 wt. % were measured in the sandstone units. A similar trend is visible for the TN values (0.01-1.85 wt.%), which also maximize in the coal samples. The TS data show, however, a slightly different trend. In contrast to the TOC and the TN curves, the highest sulfur contents were measured in the shaly units, particularly in the upper one. Remarkably, compared to the shales, the TS values in both coal units are relatively low. Values close to zero are approached in the sandstones. Note that the

6. Results

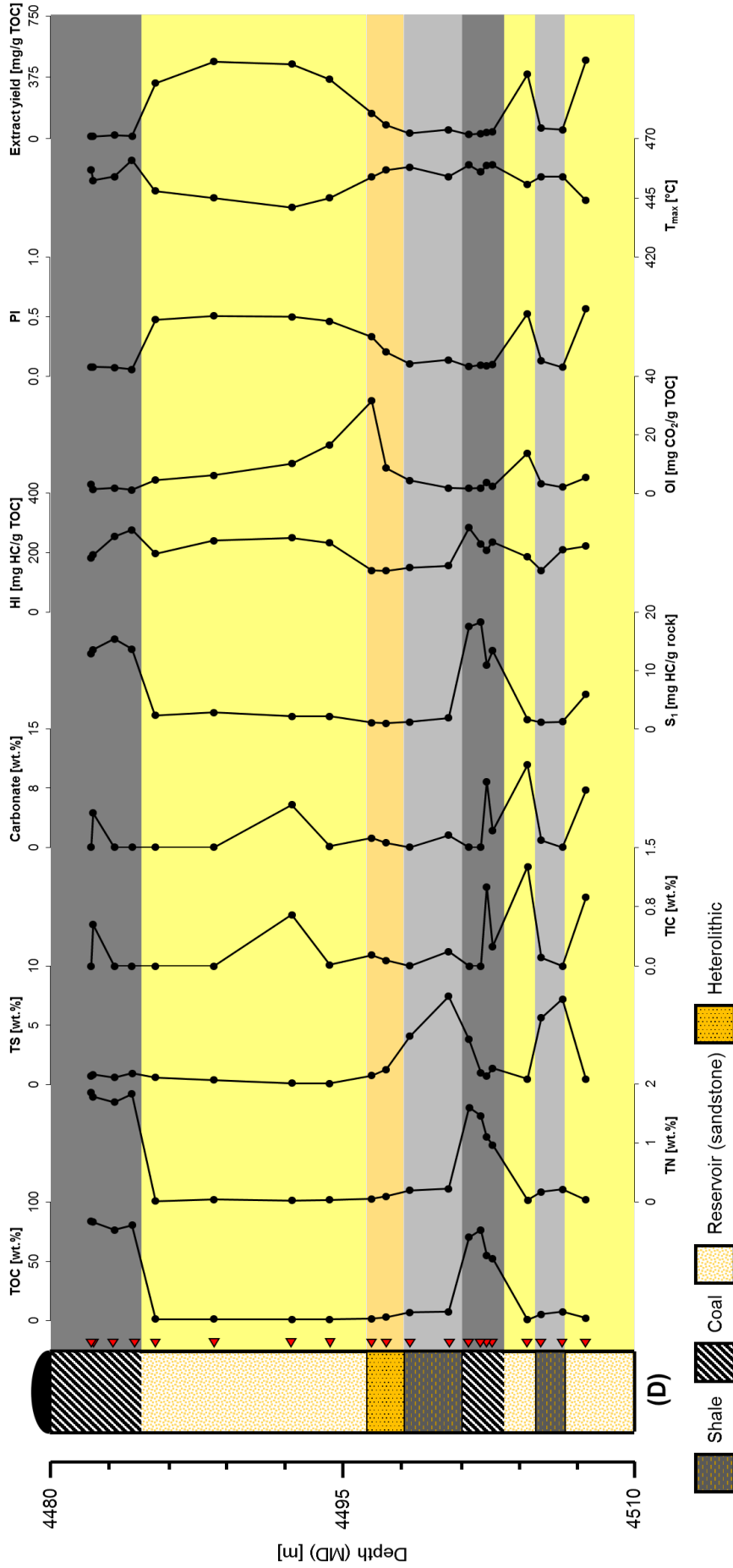


Fig. 26. Expulsion scenario D (North Sea well 15/3-9 T2, Hugin core, 4480-4510 m drilling depth); bulk geochemical depth profiles. The depth is given as measured depth (MD) and comparable to the true vertical depth (TVD). One tick on the depth axis represents 3 m. Abbreviations: TOC= Total Organic Carbon; TN= Total Nitrogen; TS= Total Sulfur; TIC= Total Inorganic Carbon; HI= Hydrogen Index; OI= Oxygen Index; PI= Production Index.

6. Results

sulfur content shows a decreasing trend in the upper shale unit in approximation to the overlying sandstone interval. Lastly, concerning the CNS data, it was revealed that the TIC values and hence the percentage of carbon fixed in carbonate minerals is generally low to moderate (0.00-10.46 wt.%) throughout the section. Looking at the Rock-Eval parameters, the S_1 data generally scatter between 1.01 and 18.22 mg HC/g rock. However, in contrast to the previous sections, the highest values were measured in the coal samples. In comparison, the S_1 values of the shale and sandstone samples are rather low, whereby on average slightly higher values were measured in the reservoir units (2.59 mg HC/g rock) than in the shales (1.30 mg HC/g rock). Regarding the HI and OI data of the source rock material, the HI extends from 139 to 283 mg HC/g TOC, whereas the OI displays much lower values of only 1 to 9 mg CO₂/g TOC. Note that the average HI values of the upper (226 mg HC/g TOC) and the lower (239 mg HC/g TOC) coal bed are remarkably high and fit well with the data published by Isaksen et al. (1998). Compared to the coals, the HI values of the shales are substantially lower and fall between 139 and 209 mg HC/g TOC, with an average value of 159 mg HC/g TOC. Concerning the PI, the absolute numbers vary from 0.06 to 0.56. While the highest values were obtained in the sandstone intervals (0.33-0.56), the PI reaches mean values of only 0.08 in the coaly and 0.13 in the shaly source rock material. When looking at the T_{max} curve, it becomes clear that the T_{max} values of scenario D are overall much higher than in the previous sections. In particular, the T_{max} averages at 456 °C and is thus significantly higher than in scenario A, B, and C. With regard to the total extract yields, the data range from 13.6 to 477.5 mg/g TOC. More specifically, the largest volumes were extracted from the sandstones (156-338 mg/g TOC), whereas the shales (34-83 mg/g TOC) and coals (14-41 mg/g TOC) yielded comparatively low amounts of extract. Note that the extract yields of the lower coal unit (34 mg/g TOC) were on average almost twice as high as those of the upper coal unit (16 mg/g TOC).

In brief, the bulk parameters of the Hugin scenario suggest a greater facies variability and thermal maturity than in the previous sections. As the profile is rich in organic material and the thermal maturity is likely within the oil window, petroleum expulsion can be expected to have occurred from both the organic-rich shales and the coals into the surrounding sandstone intervals, which are, considering the PI and extract yield data, filled with hydrocarbons. Though, as in the scenarios before, no conclusions can be made at this point about the origin of these hydrocarbons. Also, potential

6. Results

impregnation of the coals by reservoir fluids must be considered because of their porous structure.

24/9-1 Profile 1 (expulsion scenario E)

Expulsion scenario E consists of a virtually homogeneous source rock column, only interrupted by three distinct heterolithic units. The section comprises 6 m of drill core from North Sea well 24/9-1 and is located in a drilling depth of 4444 to 4450 m (Fig. 18, 19). An overview of the bulk data is provided in Fig. 27.

With respect to the CNS results, the TOC content ranges between 2.81 and 7.81 wt.%, the TN values extend from 0.10 to 0.36, and the TS curve approaches maxima and minima of 1.71 and 5.53 wt.%, respectively. Both the TOC and the TN curve show basically the same course. The heterolithic units can well be recognized by their lower TOC content compared to the surrounding black shale strata. Surprisingly, they also show very high TIC values, indicating the heterolithic units are carbonate-cemented. Indeed, the carbonate content reaches levels of up to 63.67 wt.% in the upper heterolithic unit, whereas, on the other hand, the proportion of carbonate in the surrounding shales generally ranges close to zero. Furthermore, expulsion scenario E is characterized by S_1 values in the range of 1.81 to 5.44 mg HC/g rock, HIs of 47 to 208 mg HC/g TOC, OIs between 3 and 9 mg CO₂/g TOC, and PIs in the magnitude of 0.22 to 0.51 (HI and OI values are only relevant for the shale samples). Concerning the T_{max} data of the pure source rock material, the maximum pyrolysis yield temperatures average at 446 °C, which is higher than in the scenario A, B, and C, but lower than in the Hugin section (scenario D). Regarding the extract yields, somewhat higher volumes were on average recovered from the heterolithic units (180 mg/g TOC) than from the shales (139 mg/g TOC), whereby the total numbers vary from 98 to 221 mg/g TOC. Thus, the total range is much narrower than in the previous sections.

In summary, bulk geochemical analysis of the first profile sampled in well 24/9-1 suggest sufficient organic richness, quality and thermal maturity to investigate petroleum expulsion. However, as no real carrier horizons are present and the heterolithic units actually have a low source potential and appear to be carbonate-cemented and therefore quite dense, it is questionable in how far this scenario actually allows to investigate petroleum expulsion.

6. Results

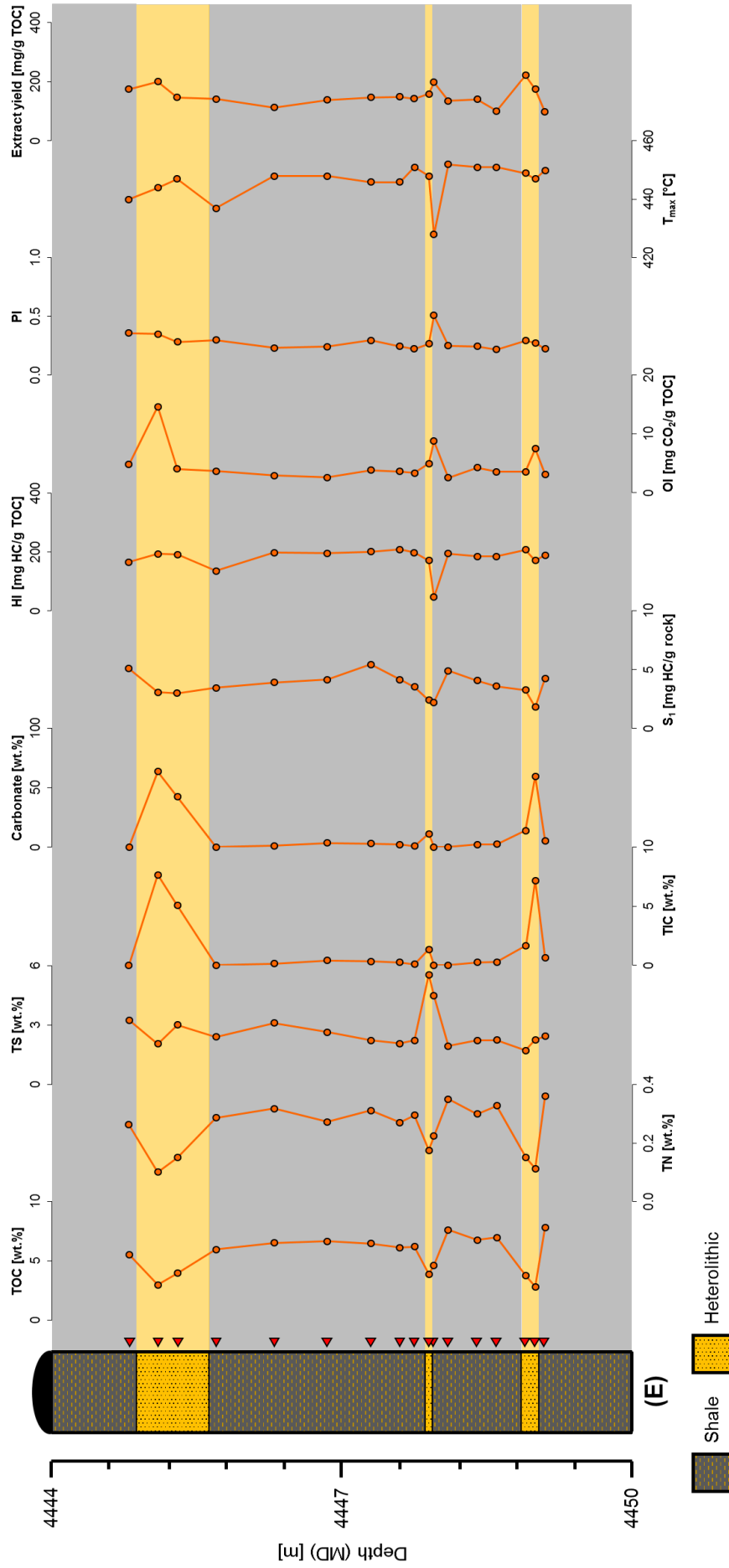


Fig. 27. Expulsion scenario E (North Sea well 24/9-1, 4444-4450 m drilling depth); bulk geochemical depth profiles. The depth is given as measured depth (MD) and comparable to the true vertical depth (TVD). One tick on the depth axis represents 0.6 m. Abbreviations: TOC= Total Organic Carbon; TN= Total Nitrogen; TS= Total Sulfur; TIC= Total Inorganic Carbon; HI= Hydrogen Index; OI= Oxygen Index; PI= Production Index.

6. Results

24/9-1 Profile 2 (expulsion scenario F)

Similar to section E, expulsion scenario F represents an almost pure source rock column (1 m), which is only intercalated by a distinct (~10 cm) reservoir horizon in the upper half. In contrast to the previous scenario, it does, however, not appear to be heterolithic. Section F also originates from North Sea well 24/9-1 and was positioned between 4456.3 and 4457.3 m drilling depth (Fig. 18, 19). The bulk geochemical results are illustrated in Fig. 28.

Looking at the CNS data, the TOC values of section F vary in total from 0.84 to 7.39 wt.% and are expectedly lowest in the reservoir unit. With regard to the shale samples, the TOC contents are quite constant over the profile and average at 6.76 wt.%, which is very similar to the mean TOC value of expulsion scenario E (6.43 wt.%) located around 6 m higher in the same well. The nitrogen content (0.04-0.34 wt.%) again closely follows the TOC trend, whereas the sulfur curve (1.28-5.55 wt.%) is shaped slightly different and climaxes in lower half of the profile. Concerning the inorganic carbon content (0.00-9.41 wt.%), the data clearly indicate that the reservoir interval is carbonate-cemented (65.35-78.39 wt.%). On the other hand, similar to the previous expulsion section, the surrounding shales do contain only trace quantities of carbonate (0.00-1.12 wt.%). Concerning the results of the Rock-Eval measurements, a quite irregular trend was revealed for the S_1 values, which extend in total from 0.85 to 4.98 mg HC/g rock, whereby the curve maximizes in the lower half of the profile. Conversely, the lowest S_1 values (0.85-1.56 mg HC/g rock) were measured in the reservoir unit. With respect to the HI data of the source rock material (46-171 mg HC/g TOC), the values are arranged in a zigzag course and average at 104 mg HC/g TOC, which is significantly below those of scenario E (175 mg HC/g TOC) in the same well. The OI values of scenario F plot between 3 and 9 mg CO₂/g TOC. Regarding the PI, the data curve remains fairly constant across the profile, whereby the total values range from 0.24 to 0.44. With respect to the shales, the PI averages at 0.35. Note that the PIs of the reservoir unit are in the same order of magnitude as those of the shale samples, which is in contrast to the profiles sampled in quadrant 15. Surprisingly, the T_{max} values are highly variable throughout section F (433-447 °C) and average at only 438 °C, which is lower than the mean value of the previous scenario (446 °C), but still higher than the data measured in scenario A, B, and C. With regard to the extract yield curve, the highest values were obtained in the

6. Results

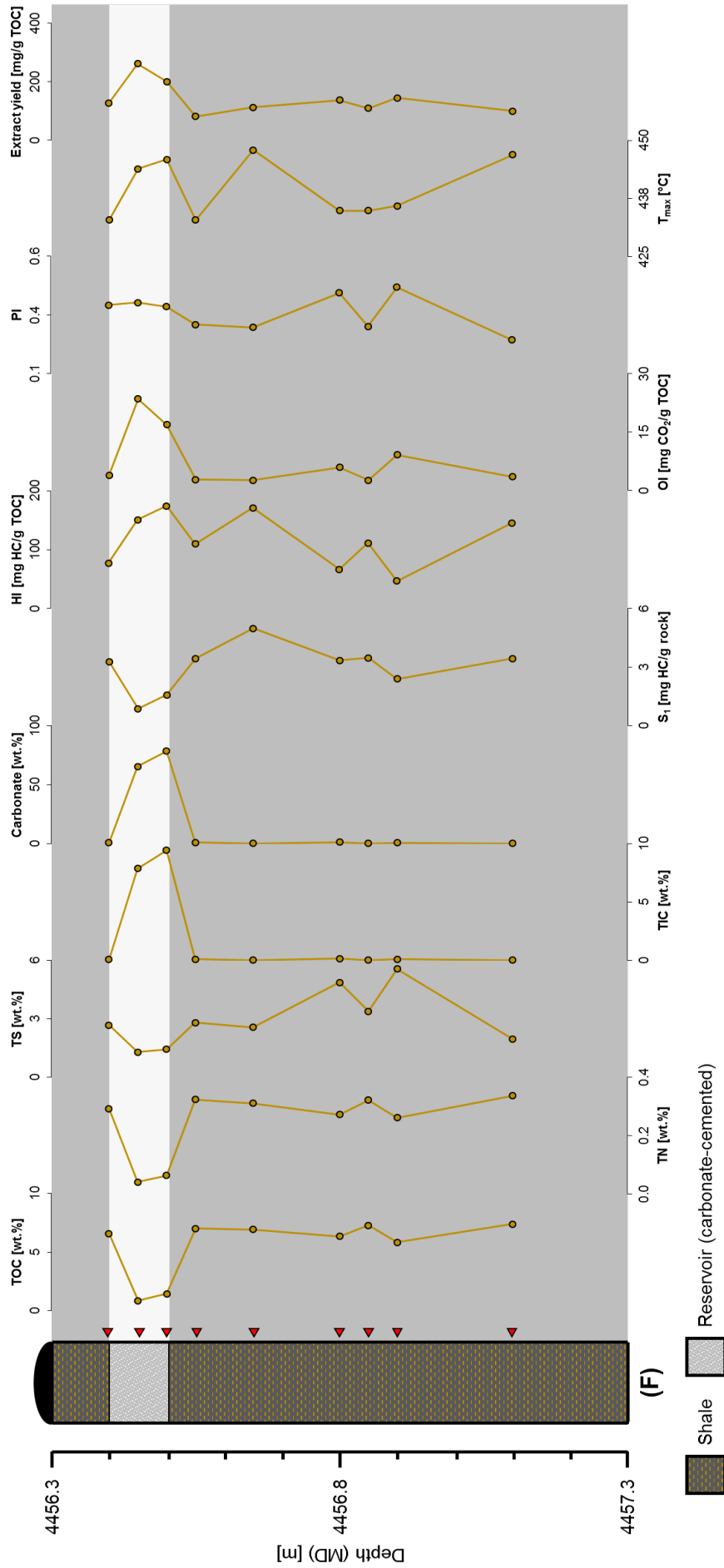


Fig. 28. Expulsion scenario F (North Sea well 24/9-1, 4456.3-4457.3 m drilling depth): bulk geochemical depth profiles. The depth is given as measured depth (MD) and comparable to the true vertical depth (TVD). One tick on the depth axis represents 0.1 m. Abbreviations: TOC= Total Organic Carbon; TN= Total Nitrogen; TIC= Total Sulfur; HI= Hydrogen Index; OI= Oxygen Index; PI= Production Index.

6. Results

reservoir unit (200-261 mg/g TOC), whereas, by contrast, the shaly samples yielded significantly less amounts of extract (80-144 mg/g TOC). Although the shale samples of scenario F yielded on average slightly lower volumes of extract (115 mg/g TOC) than those of scenario E (139 mg/g TOC), the numbers are, however, still comparable. Note that the average volumes of extract recovered from shales of well 24/9-1 are mostly higher than those of analogous material from quadrant 15.

As for the first profile from well 24/9-1, which is located only a few meters above in the same drill core, the bulk geochemical parameters for profile 2 indicate appropriate organic richness and quality, as well as thermal maturity to study petroleum expulsion. In contrast to the first section from well 24/9-1, a quite distinct reservoir horizon is visible in the upper part of the profile, which contains a hydrocarbon phase. As thick black shale units are present above and below, it appears very likely that this phase is derived directly from the surrounding shales. However, as this horizon is strongly carbonate-cemented and thus very dense and compact, expulsion may perhaps not have been that efficient as would be the case for sandstone intervals with low carbonate content.

34/7-23 A (expulsion scenario G)

Expulsion scenario G comprises a long, low-resolution profile from North Sea well 34/7-23 A and is located in the northern part of the Viking Graben (Fig. 18, 19). The section was placed between 3201 and 3291 m drilling depth, which, according to the information provided by the Norwegian Petroleum Directorate, corresponds to a true vertical depth of around 2619.5 to 2678 m. The profile is marked by a thick source rock package at the bottom of the section, a heterolithic middle part, and a massive reservoir unit at the top. A bulk geochemical overview is given in Fig. 29.

The TOC content of scenario G fluctuates in total between 1.44 and 7.94 wt.%, maximizes in the middle part of the source rock unit, and gradually decreases towards the reservoir. An equivalently-shaped curve is, once more, visible for the nitrogen content, which is in the range of 0.01 to 0.24 wt.%. Regarding the TS values, the data totally extend from 0.59 to 6.18 wt.% and climax in the source rock package, where the sulfur content averages at 4.96 wt.%. Similar to the TOC and TN curves, a progressively decreasing trend is evident in the direction of the overlying reservoir. Concerning the amount of inorganically-bound carbon, the TIC and the

6. Results

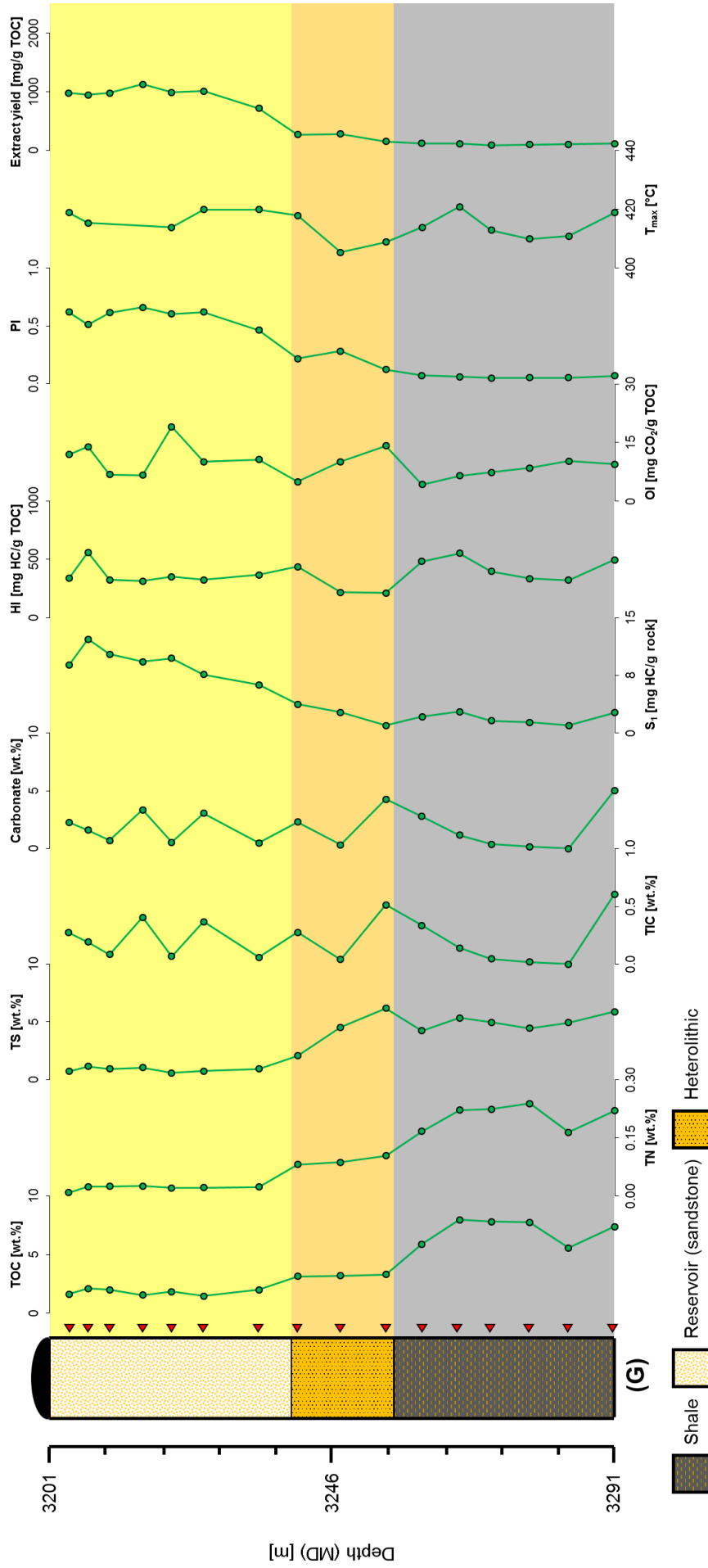


Fig. 29. Expulsion scenario G (North Sea well 34/7-23 A, 3201-3291 m drilling depth): bulk geochemical depth profiles. The depth is given as measured depth (MD), but corresponds to a true vertical depth (TVD) of only ~2619.5-2678 m. One tick on the depth axis represents 9 m. Abbreviations: TOC= Total Organic Carbon; TN= Total Nitrogen; TS= Total Sulfur; TIC= Total Inorganic Carbon; HI= Hydrogen Index; OI= Oxygen Index; PI= Production Index.

6. Results

corresponding carbonate graphs display a zigzag pattern, indicating the carbonate content is generally variable but mostly below 5 wt.%. With regard to the Rock-Eval data, the S_1 values vary from 0.99 to 12.17 mg HC/g rock, the HI and OI of the source rock material are in the magnitude of 320 to 551 mg HC/g TOC and 4 to 10 mg CO_2 /g TOC, the PI ranges from 0.05 to 0.66, and the T_{max} of the shale samples scatters between 410 and 421 °C. With respect to both the S_1 and PI, significantly higher values were determined in the reservoir than in the source rock unit. Moreover, while the OI remains relatively constant within the source unit, the HI, on the other hand, shows a great variability. Note that the T_{max} values, which are on average fairly low in the source rock section (415 °C), closely follows the HI trend. Lastly, concerning the TOC-normalized extract yields, average volumes of 107, 235 and 963 mg/g TOC were extracted from the shale package, the heterolithic middle section, and the reservoir unit, respectively. Thereby, the extract volumes do not markedly change in the source rock column (88-121 mg/g TOC), but significantly increase in approximation to the reservoir, especially in the heterolithic middle section.

Based on the bulk parameters, the Draupne Formation in well 34/7-23 A principally meets all requirements to generate hydrocarbons in the subsurface. However, the T_{max} values are very low, which indicates that the section is still thermally immature and has not yet reached the oil-window. On the other hand, this raises the question about the origin of the reservoir petroleum, which hence could originate from a different source.

34/7-23 S (expulsion scenario H)

The penultimate natural case scenario originates from North Sea well 34/7-23 S and therefore from a borehole right next to well 34/7-23 A (Fig. 18). The section is located between 3130 and 3136 m drilling depth, which, following the Norwegian Petroleum Directorate, represents a true vertical depth of approximately 2652.6 to 2659.3 m (Fig. 19). As described in chapter 5, the section essentially consists of a distinct, central reservoir interval surrounded by massive shale packages. The results of the elemental analysis, the Rock-Eval pyrolysis, and the solvent extraction procedure are shown in Fig. 30.

As evident from the CNS data, the TOC content of scenario H varies from 5.28 to

6. Results

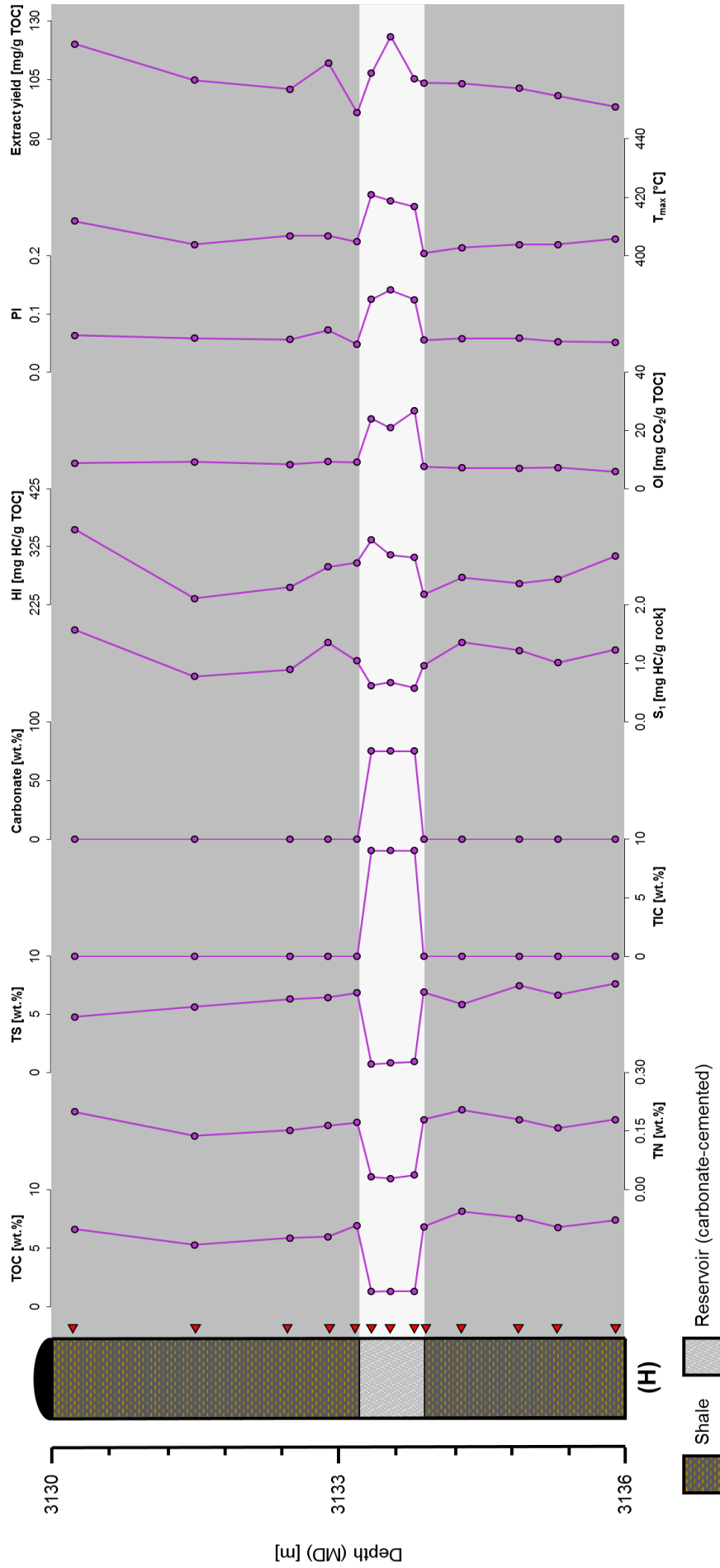


Fig. 30. Expulsion scenario H (North Sea well 34/7-23 S, 3130-3136 m drilling depth): bulk geochemical depth profiles. The depth is given as measured depth (MD), but corresponds to a true vertical depth (TVD) of only ~2652.6-2659.3 m. One tick on the depth axis represents 0.6 m. Abbreviations: TOC= Total Organic Carbon; TN= Total Nitrogen; TS= Total Sulfur; TIC= Total Inorganic Carbon; HI= Hydrogen Index; OI= Oxygen Index; PI= Production Index.

6. Results

8.12 wt.% and average at 6.73 wt.% in the shale samples. Regarding the TN values, the trend again closely resembles the TOC curve, whereby the total numbers are in the range of 0.03 to 0.20 wt.%. In contrast to the TOC and TN graphs, the TS curve, which itself extends from 0.69 wt.% in the reservoir horizon to 7.62 wt.% in the lower shale package, displays a slightly greater variability across the profile, but looks, however, still quite similar to the former trends. The percentage of TIC and thus the proportion of carbonate is, except for the reservoir unit, generally very low throughout the section, implicating the organic-rich shales do not contain significant proportions of inorganically-fixed carbon. By contrast, the carbonate content of the reservoir unit is constantly high and averages at 75.17 wt.%, suggesting the reservoir unit is carbonate-cemented. With regard to the Rock-Eval results, it is first visible that the S_1 curve is relatively irregular over the profile. Overall, the S_1 data range from 0.58 to 1.57 mg HC/g rock, whereby the lowest values of on average 0.62 mg HC/g rock are attained in the central reservoir unit. With respect to the HI curve, the data are in the magnitude of 235 to 354 mg HC/g TOC and are generally variable across the profile. However, the average HI values of the upper (286 mg HC/g TOC) and the lower source rock unit (270 mg HC/g TOC) are roughly the same. In opposite, the OI curve, which totally extends from 6 to 9 mg CO₂/g TOC in the source rock material, stays relatively constant over the profile. A similar tendency is observable for the PI (0.05-0.14), which reaches mean values of 0.06 in the source rock packages. Yet, the highest PI values of scenario H (0.12-0.14) were determined in the reservoir unit. Concerning the T_{max} curve, the absolute values of the source rock samples average at 405 °C and are thus in a similar range as before in scenario G. However, they are substantially lower than the T_{max} values measured in scenario A, B, C, D, E, and F. Looking at the extract yield data, one can see that, despite a slight zigzag pattern, the absolute values (91-123 mg/g TOC) are relatively stable across the profile. Note, however, that the largest volume of extract was recovered from the central part of the reservoir unit.

As for the previous profile, the bulk data of source rock samples from well 34/7-23 S also indicate sufficient amounts of organic carbon, as well as appropriate organic matter quality to generate hydrocarbons. Though, like the previous section from well 34/7-23 A, the profile appears to be very immature and has thus probably not yet reached the catagenesis maturation stage. Interesting in this context is the presence of a hydrocarbon phase in the carbonate-cemented and hence relatively dense carrier interval, which, due to the presence of source rock units above and below, seems

6. Results

unlikely to originate from an external source. More probable explanations for this phenomenon would therefore be, for example, contamination or pre-catagenetic expulsion of a kind of pre-mature oil phase.

34/10-36 (expulsion scenario I)

The last examined natural profile, expulsion scenario I, is also located in quadrant 34 in the northern region of the Viking Graben. However, in contrast to the two previous scenarios, the section is part of well 34/10-36, which is located slightly south of well 34/7-23 A and 34/7-23 S (Fig. 18), and was placed in a depth of 3042 to 3054 m and therefore around 400 m deeper than the two previous profiles (Fig. 19). Note that, unlike in the two sections before, the measured depths in scenario I fit well with the true vertical depths. The approximately 12 m thick profile consists of a massive, virtually homogenous source rock column, which is only interrupted by a small sandstone carrier bed close to the bottom. The bulk geochemical results are summarized in Fig. 31.

Concerning the CNS data, the TOC content of section I altogether varies between 0.75 wt.% in the reservoir interval to 6.94 wt.% in the shale package. Within the source rock strata, the TOC values frequently exceed 5 wt.% and exhibit a relatively low variance. Again, the TN curve, which ranges from 0.03 to 0.22 wt.%, basically mirrors the TOC graph and thus represents an almost 1:1 image. With respect to the TS values, the data plot between 0.46 and 5.85 and maximizes in the lower half of the profile. As expected, the lowest value was measured in the carrier bed sample. For the shaly material, the sulfur content usually remains below 5 wt.% throughout most of the section. Regarding the inorganic carbon content, the TIC data extend from 0 to 4.09 wt.%, which corresponds to a carbonate content of 0 to 34.05 wt.%. Thereby, the calcium carbonate content of the shale samples is generally close to zero, whereas the carrier bed contains considerable quantities of carbonate and thus seems to be carbonate-cemented. Looking at the Rock-Eval parameters, the S_1 data of section H are in the range of 0.26 to 2.97 mg HC/g rock. While the lowest value was measured in the reservoir unit, an average S_1 of 2.09 mg HC/g rock was determined for the source rock package. A similar trend is also visible for the HI, which fluctuates between 273 and 574 mg HC/g TOC in the source rock material. With regard to the OI, the data remain relatively constant over the profile. In total, the

6. Results

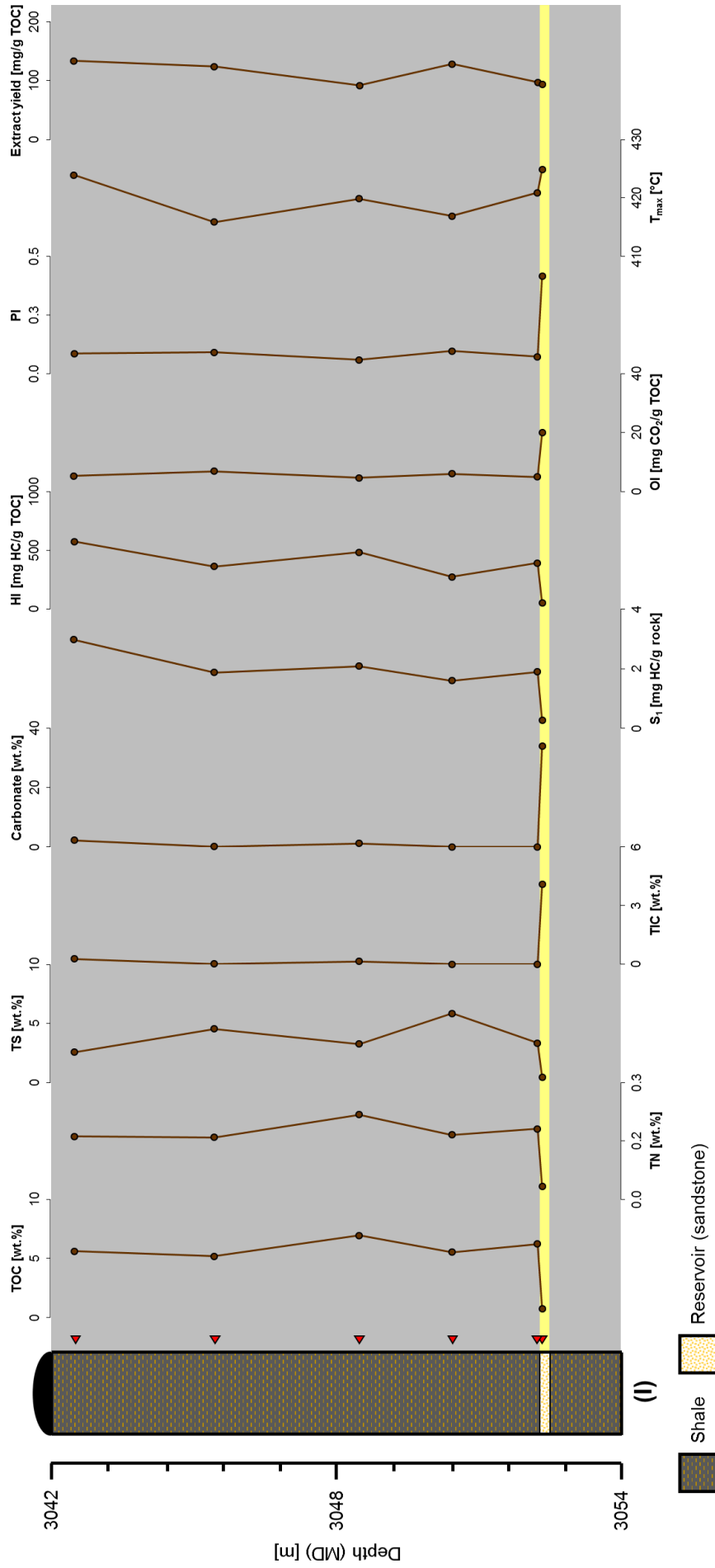


Fig. 31. Expulsion scenario I (North Sea well 34/10-36, 3042-3054 m drilling depth): bulk geochemical depth profiles. The depth is given as measured depth (MD) and comparable to the true vertical depth (TVD). One tick on the depth axis represents 1.2 m. Abbreviations: TOC= Total Organic Carbon; TN= Total Nitrogen; TS= Total Sulfur; TIC= Total Inorganic Carbon; HI= Hydrogen Index; OI= Oxygen Index; PI= Production Index.

6. Results

data scatter between 4 and 7 mg CO₂/g TOC and therefore displays a pretty narrow variance. Concerning the PI, the data generally fall in an area between 0.06 and 0.42, but stay relatively constant at about 0.08 within the source rock column. As in most sections before, the highest PI was again determined in the reservoir strata. Pertaining to the T_{max} data, an average value of 419 °C was measured for the source rock material. However, if looking at the T_{max} curve, it is clearly recognizable that the absolute values are not constant across the section. Instead, there is a discrepancy of 9 °C between the lowest (416 °C) and highest value (424 °C) measured in section I. With respect to the solvent extraction results, the extract yields of the source rock material are on average slightly higher (115 mg/g TOC) than the extract volume recovered from the reservoir unit (93 mg/g TOC). Hence, the TOC-normalized extract yields of source rock samples from scenario H are overall higher than those of organic-rich shales from scenario A, C, D, G, and H, but, on the other hand, lower than those of black shale strata from scenario E. Extract volumes in the same range were recovered from organic-rich shales from scenario B and F.

In summary, although the TOC and the HI point to a high petroleum generation potential, it is, due to the still quite low T_{max} values, questionable if the section is sufficiently mature to investigate petroleum expulsion. However, as the T_{max} values are on average somewhat higher than those measured in the two previous profiles from quadrant 34, a slightly greater thermal maturity can be inferred. Regarding the PI and the extract yield curves, it is likely that the small sandstone interval at the bottom of the sequence contains a hydrocarbon phase, but with yet unclear origin. Nevertheless, as the sandstone interval is, similar to the situation in well 34/7-23 S, enclosed by thick source strata, an origin from external sources does not appear very likely. Instead, the hydrocarbon phase could, for instance, also represent a pre-mature expulsion product or some kind of contamination.

6.1.2 Molecular geochemical data

The primary interest of this study is to provide new insights into expulsion-related molecular redistribution effects. Thereby, in accordance with the conducted geo-chromatographic experiment, which involved a tracer stock solution with defined molecular composition (Table 4), the work focused mainly on the migration behavior of aromatic tracer molecules, i.e. phenanthrenes, dibenzofurans (oxygen-substituted), dibenzothiophenes (sulfur-substituted), and carbazoles (nitrogen-substituted). All of

6. Results

these compounds play an important role in the petroleum exploration business, for example for maturity estimations, oil-source rock correlations, the determination of organic facies types, and the calculation of crude oil migration distances. The ratios shown in the following were chosen because they were assigned the highest probability to reveal potentially expulsion-related compositional differences between source and carrier rocks.

15/3-8 Profile 1 (expulsion scenario A)

Fig. 32 illustrates the most essential molecular geochemical depth profiles of expulsion scenario A. Correspondingly, Fig. 33 presents ion chromatograms of selected, representative samples (source rock vs. reservoir). The trends shown in Fig. 32 comprise the *n*-heptadecane/pristane ratio (nC_{17}/Pr), the ratio of C_{30} dia-hopane against C_{30} diahopane and C_{30} regular hopane ($C_{30}dia/(C_{30}dia+C_{30}\alpha\beta)$), the ratio of short- ($C_{20}+C_{21}$) against long-chain ($C_{20}+C_{21}+C_{26}+C_{27}+C_{28}$) triaromatic steroids ($TA(I)/TA(I + II)$), the methylphenanthrene index (MPI 1), and the ratios of 9- to 1-methylphenanthrene (9-/1-MPhen), C_1 -alkylated dibenzothiophenes against methylphenanthrenes ($C_1 DBT/C_1 Phen$), C_1 -alkylated dibenzofurans to C_1 -alkylated phenanthrenes ($C_1 DBF/C_1 Phen$), methyl dibenzofurans vs. methyl dibenzothiophenes ($C_1 DBF/C_1 DBT$), methylphenanthrenes to phenanthrene ($C_1 Phen/Phen$), C_1 -alkylated dibenzothiophenes vs. dibenzothiophenes, methyl dibenzofurans against dibenzofuran ($C_1 DBF/DBF$), methylated carbazoles to carbazole ($C_1 Carb/Carb$), shielded (1,8-, 1,3-, 1,6-, 1,7-, 1,4-, 1,5-dimethylcarbazole) vs. exposed (2,7-, 2,4-, 2,5-dimethylcarbazole) C_2 -alkylated carbazoles and the amount of benzo[a]- relative to benzo[c]carbazole (BC ratio). Therefore, the diagrams mostly comprise compounds and compound groups that were analogously investigated in the geo-chromatographic experiment (see 5.4). Among the shown plots, the diahopane ratio (Isaksen, 2004), the triaromatic steroid ratio (Riolo et al., 1986), as well as the methylphenanthrene index (e.g. Radke, 1988) represent famous and well-established molecular maturity parameters, which are principally applicable within the oil window. The two lowermost samples of scenario A were found to be biodegraded based on molecular evidence (unresolved complex mixture, "hump") and therefore excluded from the following comments.

The first trend that is presented is the *n*-heptadecane/pristane ratio and hence the ratio of the *n*- vs. the nearest eluting *iso*-alkane. For expulsion scenario A, the

6. Results

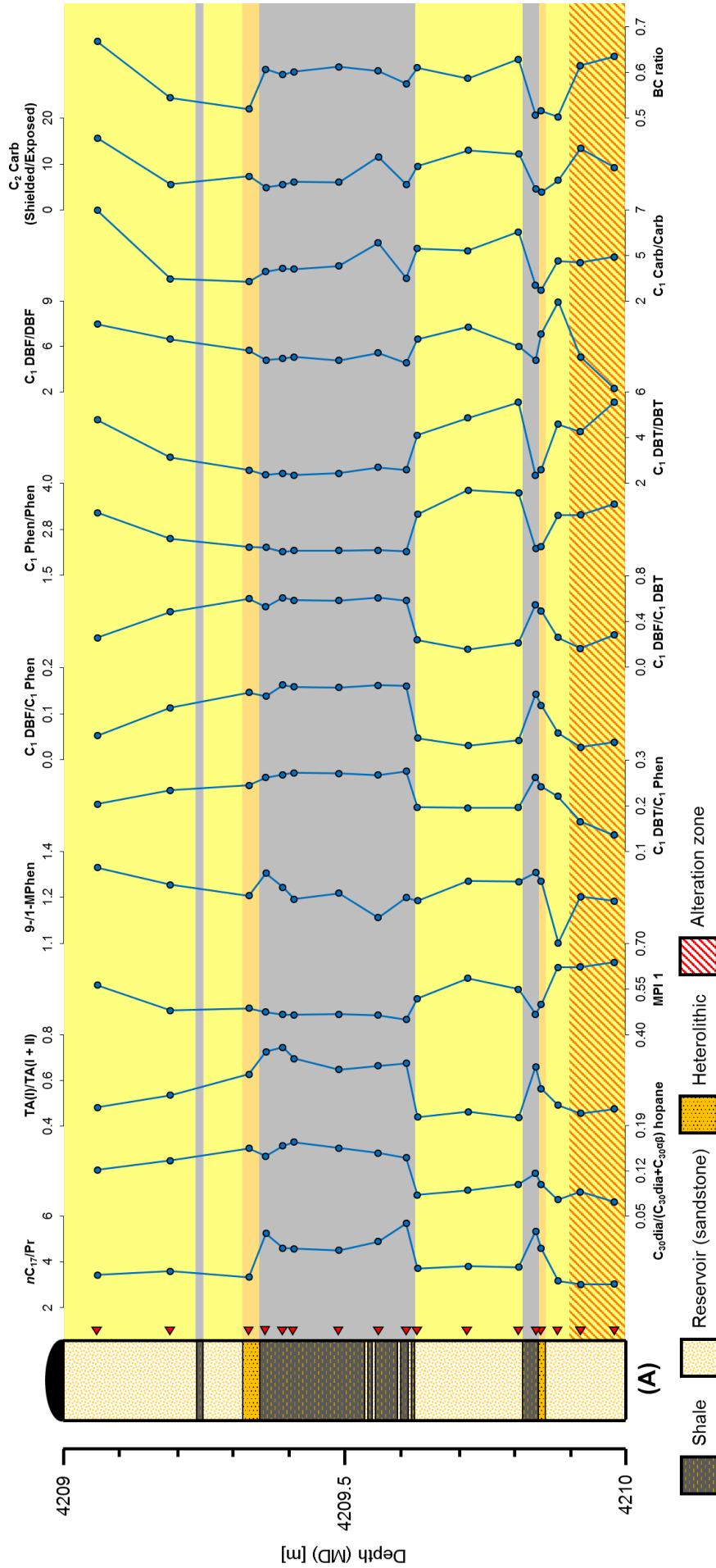
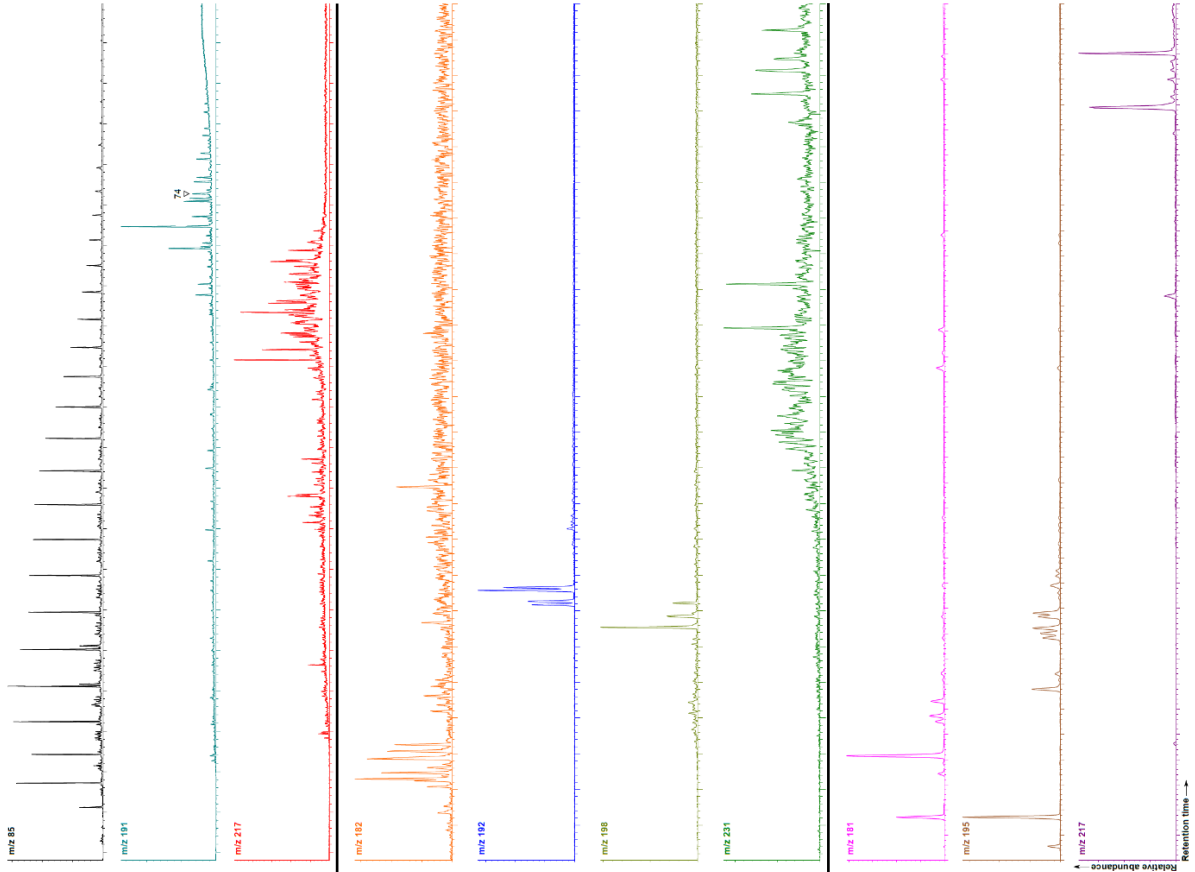


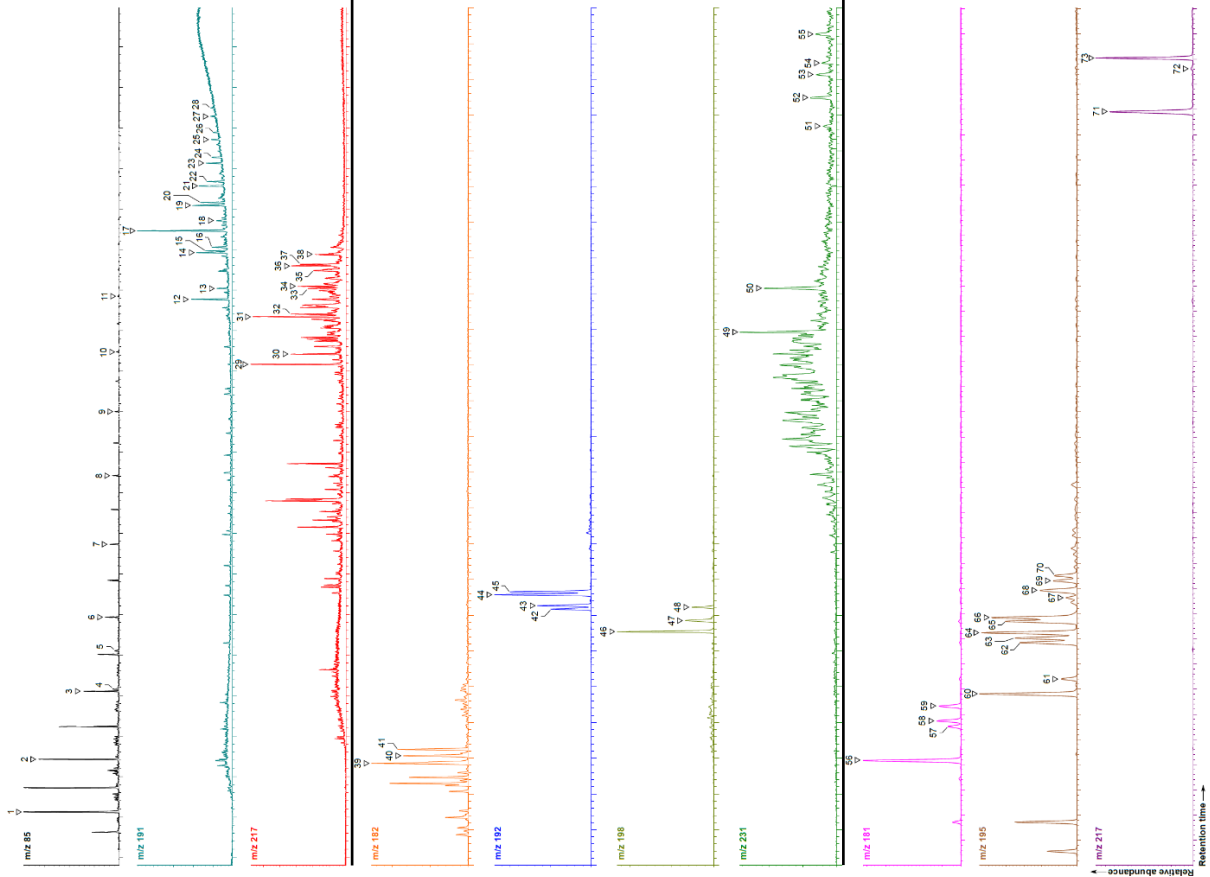
Fig. 32. Selected molecular geochemical depth profiles of expulsion scenario A, North Sea well 15/3-8, 4209-4210 m drilling depth. The depth is given as measured depth (MD) and comparable to the true vertical depth (TVD). One tick on the depth axis represents 0.1 m. Abbreviations: $nC_{17}/Pr = n$ -Heptadecane/Pristane; $C_{30dia}/(C_{30dia}+C_{30\beta}) = C_{30}$ Diahopane/(C_{30} Diahopane+ C_{30} Hopane); $TA(I)/TA(I+II) =$ Short-/Long-Chain Triaromatic Steroid Ratio ($(C_{20}+C_{21})/(C_{20}+C_{21}+C_{26}+C_{27}+C_{28})$); MPI 1 = Methylphenanthrene Index; 9-/1-MPhen = 9-Methylphenanthrene/1-Methylphenanthrene; $C_1 DBT/C_1 Phen = C_1$ -alkylated Dibenzofurans/ C_1 -alkylated Phenanthrenes; $C_1 DBF/C_1 Phen = C_1$ -alkylated Dibenzofurans/ C_1 -alkylated Phenanthrenes; $C_1 DBT/DBT = C_1$ -alkylated Dibenzofurans/Dibenzothiophenes; $C_1 Phen/Phen = C_1$ -alkylated Phenanthrenes/Phenanthrene; $C_1 DBT/DBT = C_1$ -alkylated Dibenzofurans/Dibenzothiophenes; $C_1 Carb/Carb = C_1$ -alkylated Carbazoles/Carbazole; $C_2 Carb (Shielded/Exposed) =$ Shielded/Exposed C_2 -alkylated Carbazoles (1,3-, 1,6-, 1,7, 1,4-, 1,5-Dimethylcarbazole)/(2,7-, 2,4-, 2,5-Dimethylcarbazole); BC ratio = Benzocarbazoles Ratio.

6. Results

Reservoir



Shale



6. Results

Fig. 33. Exemplary ion chromatograms of a selected source (K011193) vs. a carrier bed sample (K011197) for expulsion scenario A. The ion chromatograms shown comprise alkanes (m/z 85), hopanes (m/z 191), steranes (m/z 217), methyldibenzofurans (m/z 182), methylphenanthrenes (m/z 192), methyldibenzothiophenes (m/z 198), triaromatic steroids (m/z 231), methylcarbazoles (m/z 181), C₂-alkylated carbazoles (m/z 195), and benzocarbazoles (m/z 217). The most essential compounds are indicated by numbered arrows. Peak identification can be found in Table 5.

nC_{17}/Pr ratio of the non-degraded samples is in the range of 2.66 to 5.18. Thereby, the highest values were observed in the source beds, whereas, on the other hand, the reservoir units generally display much lower values. Interestingly, the nC_{17}/Pr curve is bell-shaped within the central source unit with the two highest values being reached at the edges (4.75 and 5.18 for the upper and lower border, respectively). Note that, due to different response factors, both components were integrated from the total ion current chromatogram (not shown in Fig. 33) instead of the m/z 85 ion chromatogram. When regarding the trendline for the C₃₀ diahopane ratio, it is evident that the values are generally higher in the source than in the adjacent reservoir units, which is most pronounced for the central source bed. In general, the data vary between 0.08 and 0.16, whereby average values of 0.15 and 0.10 are reached in the source and the reservoir beds, respectively. A very similar pattern is observable for the TA(I)/TA(I + II) ratio, which displays a total range of 0.39 to 0.70 and maximizes in the source rock units. The average values calculated for shales (0.64) and sandstones (0.42) thereby differ by an order of around 0.2. Note also that the triaromatic steroid curve is kind of bell-shaped within the central black shale unit. With respect to the MPI 1 data (0.45-0.62), the trend is not as clear as before for the two previous maturity indicators. While on one hand the reservoir zone at the top and the central source unit exhibit comparable MPI 1 values (0.52 and 0.47, respectively), the differences are, on the other hand, much greater in the lower half of the section where the reservoir units display an average MPI 1 value of 0.57, which is clearly higher as the values determined in the organic-rich shales. Thus, a tendency towards higher MPI 1 values in the reservoir is visible in expulsion scenario A. Concerning only the ratio of 9- to 1-methylphenanthrene (1.10-1.31), no clear trend is noticeable over the profile. Rather, the 9-/1-MPhen data exhibit a zigzag pattern and average at 1.24 in both source and carrier rocks. Looking at the ratio of methyldibenzothiophenes to methylphenanthrenes, the absolute numbers range in total from 0.20 to 0.28, climax in the source rock strata, and reach lowest levels in the reservoir units. Therefore, the data indicate that the carrier units are depleted in dibenzothiophenes relative to the shale samples. An almost equivalently-shaped curve is visible for the

6. Results

Table 5. Peak identification

| Peak | Compound | Abbreviation | Formula |
|------|---|---|---------------------------------|
| 1 | <i>n</i> -Tridecane | <i>n</i> C ₁₃ | C ₁₃ H ₂₈ |
| 2 | <i>n</i> -Pentadecane | <i>n</i> C ₁₅ | C ₁₅ H ₃₂ |
| 3 | <i>n</i> -Heptadecane | <i>n</i> C ₁₇ | C ₁₇ H ₃₆ |
| 4 | Pristane | Pr | C ₂₄ H ₄₄ |
| 5 | Phytane | Ph | C ₂₅ H ₄₆ |
| 6 | <i>n</i> -Nonadecane | <i>n</i> C ₁₉ | C ₁₉ H ₄₀ |
| 7 | <i>n</i> -Heneicosane | <i>n</i> C ₂₁ | C ₂₁ H ₄₄ |
| 8 | <i>n</i> -Tricosane | <i>n</i> C ₂₃ | C ₂₃ H ₄₈ |
| 9 | <i>n</i> -Pentacosane | <i>n</i> C ₂₅ | C ₂₅ H ₅₂ |
| 10 | <i>n</i> -Heptacosane | <i>n</i> C ₂₇ | C ₂₇ H ₅₆ |
| 11 | <i>n</i> -Nonacosane | <i>n</i> C ₂₉ | C ₂₉ H ₆₀ |
| 12 | 18 α (H)-22,29,30-Trisnorhopane | Ts | C ₂₇ H ₄₆ |
| 13 | 17 α (H)-22,29,30-Trisnorhopane | Tm | C ₂₇ H ₄₆ |
| 14 | 17 α ,21 β (H)-30-Norhopane | C ₂₉ q β S Hopane | C ₂₉ H ₅₀ |
| 15 | 18 α ,21 β (H)-30-Norhopane | C ₂₉ Ts | C ₂₉ H ₅₀ |
| 16 | 17 α (H)-Diahopane | C ₃₀ Diahopane | C ₃₀ H ₅₂ |
| 17 | 17 α ,21 β (H)-Hopane | C ₃₀ q β S Hopane | C ₃₀ H ₅₂ |
| 18 | 17 β ,21 α (H)-Hopane | C ₃₀ q α S Hopane | C ₃₀ H ₅₂ |
| 19 | 17 α ,21 β (H)-Homohopane 22S | C ₃₁ q β S Hopane | C ₃₁ H ₅₄ |
| 20 | 17 α ,21 β (H)-Homohopane 22R | C ₃₁ q β R Hopane | C ₃₁ H ₅₄ |
| 21 | 17 α ,21 β (H)-Bisnorhopane 22S | C ₃₂ q β S Hopane | C ₃₂ H ₅₆ |
| 22 | 17 α ,21 β (H)-Bisnorhopane 22R | C ₃₂ q β R Hopane | C ₃₂ H ₅₆ |
| 23 | 17 α ,21 β (H)-Trishomohopane 22S | C ₃₃ q β S Hopane | C ₃₃ H ₅₈ |
| 24 | 17 α ,21 β (H)-Trishomohopane 22R | C ₃₃ q β R Hopane | C ₃₃ H ₅₈ |
| 25 | 17 α ,21 β (H)-Tetrakishomohopane 22S | C ₃₄ q β S Hopane | C ₃₄ H ₆₀ |
| 26 | 17 α ,21 β (H)-Tetrakishomohopane 22R | C ₃₄ q β R Hopane | C ₃₄ H ₆₀ |
| 27 | 17 α ,21 β (H)-Pentakishomohopane 22S | C ₃₅ q β S Hopane | C ₃₅ H ₆₂ |
| 28 | 17 α ,21 β (H)-Pentakishomohopane 22R | C ₃₅ q β R Hopane | C ₃₅ H ₆₂ |
| 29 | 13 β ,17 α (H)-Diacholestane 20S | C ₂₇ q β S Diasterane | C ₂₇ H ₄₈ |
| 30 | 13 β ,17 α (H)-Diacholestane 20R | C ₂₇ q α R Diasterane | C ₂₇ H ₄₈ |
| 31 | 5 α ,14 β ,17 β (H)-Cholestane 20R | C ₂₇ q β R Sterane | C ₂₇ H ₄₈ |
| 32 | 5 α ,14 β ,17 β (H)-Cholestane 20S | C ₂₇ q β S Sterane | C ₂₇ H ₄₈ |
| 33 | 5 α ,14 β ,17 β (H)-24-Methylcholestane 20R | C ₂₈ q β S Sterane | C ₂₈ H ₅₀ |
| 34 | 5 α ,14 β ,17 β (H)-24-Methylcholestane 20S | C ₂₈ q β S Sterane | C ₂₈ H ₅₀ |
| 35 | 5 α ,14 α ,17 α (H)-24-Ethylcholestane 20S | C ₂₉ q α S Sterane | C ₂₉ H ₅₂ |
| 36 | 5 α ,14 β ,17 β (H)-24-Ethylcholestane 20R | C ₂₉ q β R Sterane | C ₂₉ H ₅₂ |
| 37 | 5 α ,14 β ,17 β (H)-24-Ethylcholestane 20S | C ₂₉ q β S Sterane | C ₂₉ H ₅₂ |

Table 5. Peak identification (continued)

| Peak | Compound | Abbreviation | Formula |
|------|---|---|---|
| 38 | 5 α ,14 α ,17 α (H)-24-Ethylcholestane 20R | C ₂₉ q α R Sterane | C ₂₉ H ₅₂ |
| 39 | 4-Methyldibenzofuran | 4-MDBF | C ₁₃ H ₁₀ O |
| 40 | 2-Methyldibenzofuran + 3-Methyldibenzofuran | 2-MDBF + 3-MDBF | C ₁₃ H ₁₀ O/C ₁₃ H ₁₀ O |
| 41 | 1-Methyldibenzofuran | 1-MDBF | C ₁₃ H ₁₀ O |
| 42 | 3-Methylphenanthrene | 3-MP | C ₁₅ H ₁₂ |
| 43 | 2-Methylphenanthrene | 2-MP | C ₁₅ H ₁₂ |
| 44 | 9-Methylphenanthrene | 9-MP | C ₁₅ H ₁₂ |
| 45 | 1-Methylphenanthrene | 1-MP | C ₁₅ H ₁₂ |
| 46 | 4-Methyldibenzothiophene | 4-MDBT | C ₁₅ H ₁₀ S |
| 47 | 2-Methyldibenzothiophene + 3-Methyldibenzothiophene | 2-MDBT + 3-MDBT | C ₁₃ H ₁₀ S/C ₁₃ H ₁₀ S |
| 48 | 1-Methyldibenzothiophene | 1-MDBT | C ₁₃ H ₁₀ S |
| 49 | C ₂₀ Triaromatic Steroid | C ₂₀ TAS | C ₂₀ H ₂₀ |
| 50 | C ₂₁ Triaromatic Steroid | C ₂₁ TAS | C ₂₁ H ₂₂ |
| 51 | C ₂₆ Triaromatic Steroid 20S | C ₂₆ TAS | C ₂₆ H ₃₂ |
| 52 | C ₂₆ Triaromatic Steroid 20R + C ₂₇ Triaromatic Steroid 20S | C ₂₆ TAS 20R + C ₂₇ TAS 20S | C ₂₆ H ₃₂ /C ₂₇ H ₃₄ |
| 53 | C ₂₈ Triaromatic Steroid 20S | C ₂₈ TAS 20S | C ₂₈ H ₃₆ |
| 54 | C ₂₇ Triaromatic Steroid 20R | C ₂₇ TAS 20R | C ₂₇ H ₃₄ |
| 55 | C ₂₈ Triaromatic Steroid 20R | C ₂₈ TAS 20R | C ₂₈ H ₃₆ |
| 56 | 1-Methylcarbazole | 1-MCarb | C ₁₃ H ₁₁ N |
| 57 | 3-Methylcarbazole | 3-MCarb | C ₁₃ H ₁₁ N |
| 58 | 2-Methylcarbazole | 2-MCarb | C ₁₃ H ₁₁ N |
| 59 | 4-Methylcarbazole | 4-MCarb | C ₁₃ H ₁₁ N |
| 60 | 1,8-Dimethylcarbazole | 1,8-Dimethylcarb | C ₁₄ H ₁₃ N |
| 61 | 1-Ethylcarbazole | 1-Ethylcarb | C ₁₄ H ₁₃ N |
| 62 | 1,3-Dimethylcarbazole | 1,3-Dimethylcarb | C ₁₄ H ₁₃ N |
| 63 | 1,6-Dimethylcarbazole | 1,6-Dimethylcarb | C ₁₄ H ₁₃ N |
| 64 | 1,7-Dimethylcarbazole | 1,7-Dimethylcarb | C ₁₄ H ₁₃ N |
| 65 | 1,4-Dimethylcarbazole + 4-Ethylcarbazole | 1,4-Dimethylcarb + 4-Ethylcarb | C ₁₄ H ₁₃ N |
| 66 | 1,5-Dimethylcarbazole + 3-Ethylcarbazole | 1,5-Dimethylcarb + 3-Ethylcarb | C ₁₄ H ₁₃ N |
| 67 | 2,6-Dimethylcarbazole | 2,6-Dimethylcarb | C ₁₄ H ₁₃ N |
| 68 | 2,7-Dimethylcarbazole | 2,7-Dimethylcarb | C ₁₄ H ₁₃ N |
| 69 | 2,4-Dimethylcarbazole | 2,4-Dimethylcarb | C ₁₄ H ₁₃ N |
| 70 | 2,5-Dimethylcarbazole | 2,5-Dimethylcarb | C ₁₄ H ₁₃ N |
| 71 | Benzo[a]carbazole | BaC | C ₁₆ H ₁₁ N |
| 72 | Benzo[b]carbazole | BbC | C ₁₆ H ₁₁ N |
| 73 | Benzo[c]carbazole | BcC | C ₁₆ H ₁₁ N |
| 74 | Gammacerane | Gammacerane | C ₃₀ H ₅₂ |

6. Results

same ratio but with methyl dibenzofurans (C_1 DBF/ C_1 Phen). Here, calculation of the ratio revealed that it varies between 0.03 and 0.16. Similar to the previous graph, the values maximize in the source rock samples and are lowest in the three reservoir intervals, suggesting the reservoir petroleum is depleted in oxygen-substituted aromatics compared to the adjacent source bitumen. If calculating the ratio between methyl dibenzofurans and methyl dibenzothiophenes (C_1 DBF/ C_1 DBT), which is in the magnitude of 0.16 to 0.61, the data suggest that dibenzofurans are generally more abundant in the source than in the reservoir units. Conversely, as the C_1 DBF/ C_1 DBT ratio is lowest in the reservoir, the carrier bed petroleum seems to be more enriched in dibenzothiophenes than in dibenzofurans. Regarding differences between alkylated vs. non-alkylated phenanthrenes (C_1 Phen/Phen), dibenzothiophenes (C_1 DBT/DBT), dibenzofurans (C_1 DBF/DBF), and carbazoles (C_1 Carb/ Carb), the data plot between 2.13 to 3.81, 2.34 to 5.53, 4.22 to 8.91, and 2.61 to 6.96, respectively. All trends show principally the same course: elevated values are reached in the carrier units, whereas the source rock intervals are comparatively depleted in alkylated over non-alkylated compounds. The trend looks, however, less clear for the C_1 -alkylated carbazoles against carbazole, which is due mainly to an outlier in the lower half of the central source unit. The penultimate plot that is shown in Fig. 32 comprises the ratio of nitrogen-shielded vs. nitrogen-exposed C_2 -alkylated carbazoles. C_2 -alkylated compounds were chosen because of both a higher evaporation resistivity and stronger molecular shielding compared to C_1 carbazoles. The C_2 Carb (Shielded vs. Exposed) curve ranges from 3.84 to 15.67 and looks principally similar to the C_1 Carb/Carb trend described before. Remarkably, it also contains an outlier, which is located at the same position as in the previous diagram. If comparing the average values of sandstones (10.37) and shales (6.27), the reservoir intervals seem to be enriched in shielded C_2 carbazoles compared to the source rock units. This is particularly apparent in the lower half of the diagram, but, however, less clear in the upper part above the central source unit. The last ratio that is illustrated in Fig. 32 is the benzocarbazoles ratio (Larter et al., 1996), for which the data falls in an area between 0.45 to 0.62. Interestingly, the trend is quite irregular over the profile and only marginal differences between source rock (average value: 0.54) and reservoir intervals (average value: 0.54) were ascertained. Note, however, that the BC ratio sharply drops at the transition from the central source towards the upper reservoir unit and from the thin layer towards the lowermost carrier bed, whereas it remains quite stable in the sandstone interval located

6. Results

directly underneath the central source package. Note also that the BC ratio of the thin source rock layer close to the bottom of the section (0.46) is significantly lower than the BC ratios calculated for the central source unit (0.52-0.56).

Concerning the relative distributions of alkanes (m/z 85), hopanes (m/z 191), steranes (m/z 217), methyldibenzofurans (m/z 182), methylphenanthrenes (m/z 192), methyldibenzothiophenes (m/z 198), triaromatic steroids (m/z 231), methylcarbazoles (m/z 181), C₂-alkylated carbazoles (m/z 195), and benzocarbazoles (m/z 217) in source vs. reservoir material (Fig. 33), a high degree of similarity is visible. However, there are some important differences. First, the reservoir unit is clearly enriched in *n*-alkanes, particularly in long-chain, waxy components. Second, the ratio of trisnorhopane (Ts) to trisnorhopane (Tm) is much lower in the reservoir than in the source unit. Third, rearranged steranes are generally more abundant in source than in reservoir samples and, last, the reservoir units contain gammacerane, which is not or only marginally present in the source rock samples and could indicate contribution of a different source.

In general, however, the observed trends fit relatively well with the expectations, especially because dibenzofurans and dibenzothiophenes appear to be more enriched in the source than in the reservoir intervals, there are no significant differences in the 9-/1-methylphenanthrene ratio between shale and sandstone samples, and nitrogen-shielded carbazoles seem to be slightly enriched in the carrier beds compared to nitrogen-exposed carbazoles. Yet, a discrepancy in the maturity signal of the reservoir petroleum is apparent, which could be related to petroleum expulsion. While the C₃₀ diahopane ratio and the triaromatic steroids both indicate lower thermal maturity of the reservoir petroleum compared to the source bitumen, which seems likely considering that early mature petroleum probably leaves the source rock before late mature petroleum, the MPI 1 curve suggests the opposite.

15/3-8 Profile 2 (expulsion scenario B)

Analogous to the previous section, Fig. 34 shows the most essential molecular geochemical parameters of expulsion scenario B. Again, corresponding ion chromatograms (source vs. reservoir) are subsequently illustrated in Fig. 35. Concerning the *n*C₁₇/Pr ratio, the data extend from 1.54 to 3.05. It is striking that, first the values are

6. Results

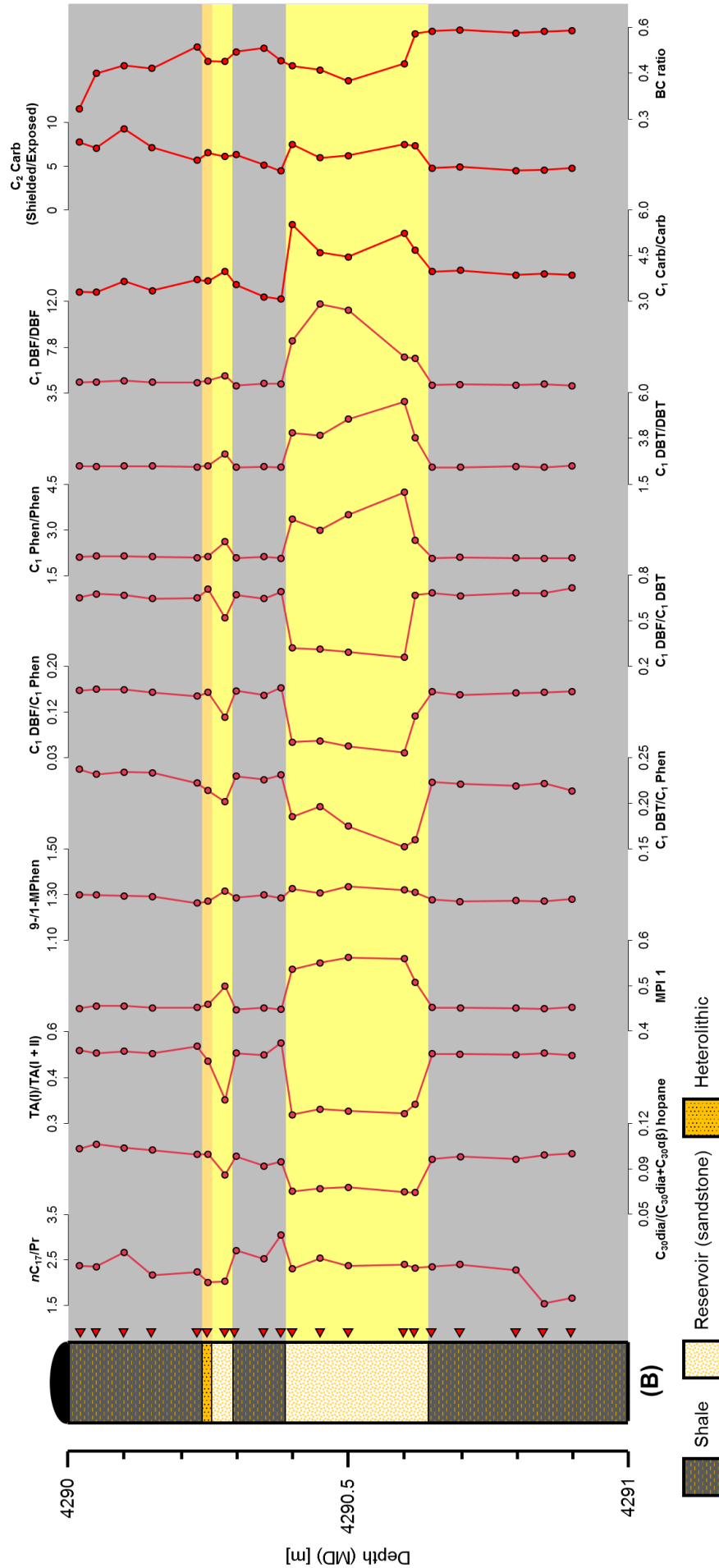
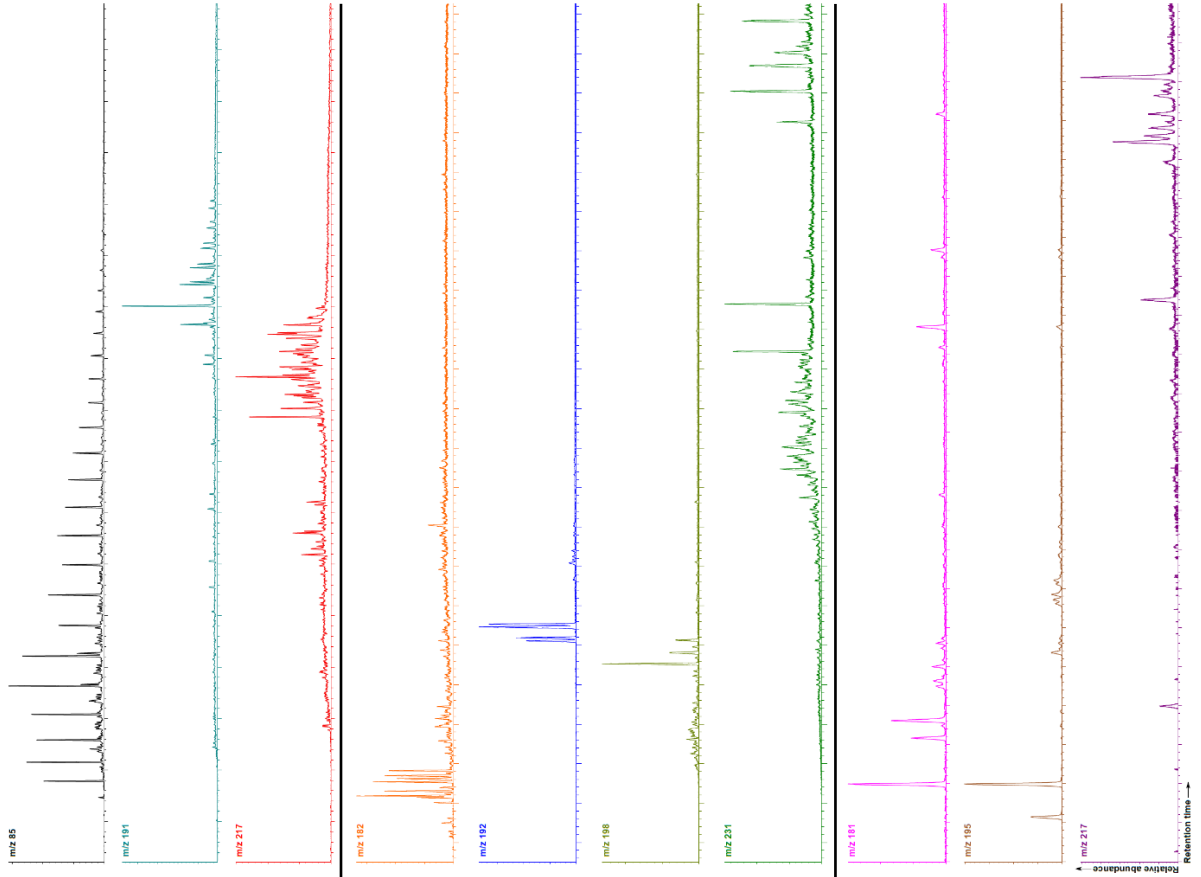


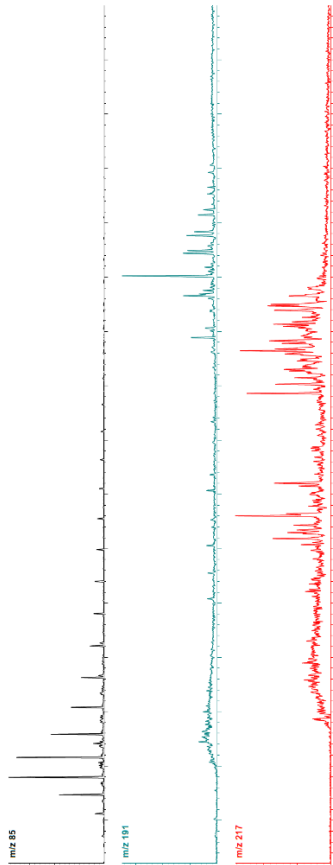
Fig. 34. Selected molecular geochemical depth profiles of expulsion scenario B, North Sea well 15/3-8, 4290-4291 m drilling depth. The depth is given as measured depth (MD) and comparable to the true vertical depth (TVD). One tick on the depth axis represents 0.1 m. Abbreviations: nC_{17}/Pr = *n*-Heptadecane/Pristane; $C_{30}dia/(C_{30}dia+C_{30}\alpha\beta)$ = C_{30} Diahopane/ C_{30} Hopane; $TA(I)/TA(I+II)$ = Short-/Long-Chain Triaromatic Steroid Ratio ($(C_{20}+C_{21})/(C_{20}+C_{21}+C_{26}+C_{27}+C_{28})$); MPI 1= Methylphenanthrene Index; 9-/1-MPhen= 9-Methylphenanthrene/1-Methylphenanthrene; $C_1 DBT/C_1 Phen$ = C_1 -alkylated Dibenzofurans/ C_1 -alkylated Phenanthrenes; $C_1 DBF/C_1 Phen$ = C_1 -alkylated Dibenzofurans/ C_1 -alkylated Phenanthrenes; $C_1 DBT/DBT$ = C_1 -alkylated Dibenzothiophenes/Dibenzothiophene; $C_1 DBF/DBF$ = C_1 -alkylated Dibenzofurans/Dibenzofuran; $C_1 Carb/Carb$ = C_1 -alkylated Carbazoles/Carbazole; $C_2 Carb (Shielded/Exposed)$ = Shielded/Exposed C_2 -alkylated Carbazoles (1,3-, 1,6-, 1,7, 1,4-, 1,5-Dimethylcarbazole)/(2,7-, 2,4-, 2,5-Dimethylcarbazole); BC ratio= Benzocarbazoles Ratio.

6. Results

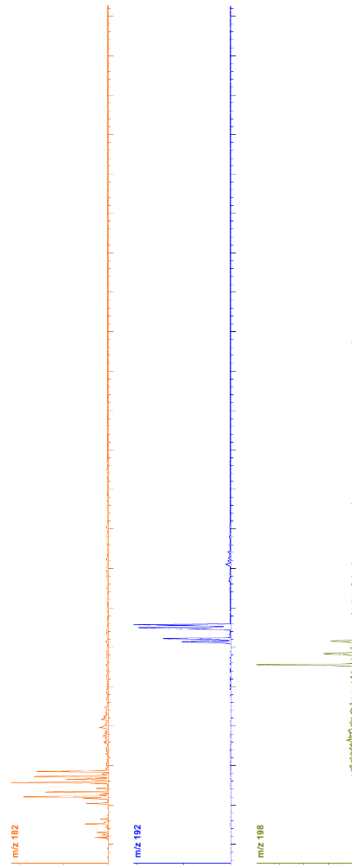
Reservoir



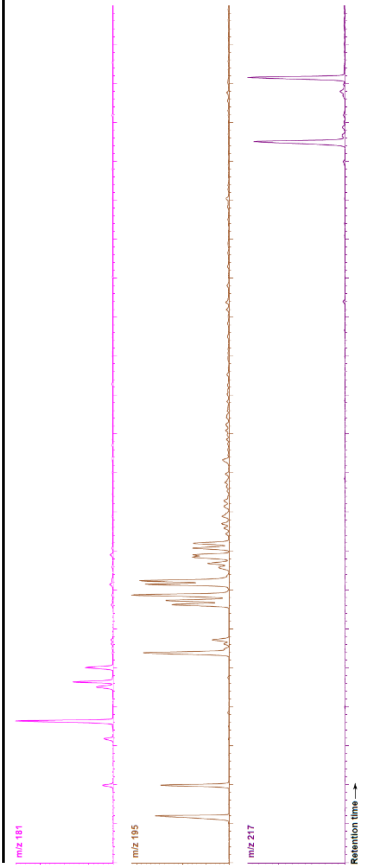
Aliphatics



Aromatics



Carbazoles



Shale

6. Results

Fig. 35. Exemplary ion chromatograms of a selected source (K012448) vs. a carrier bed sample (K012443) for expulsion scenario B. The ion chromatograms shown comprise alkanes (m/z 85), hopanes (m/z 191), steranes (m/z 217), methyl dibenzofurans (m/z 182), methylphenanthrenes (m/z 192), methyl dibenzothiophenes (m/z 198), triaromatic steroids (m/z 231), methylcarbazoles (m/z 181), C₂-alkylated carbazoles (m/z 195), and benzocarbazoles (m/z 217). See Fig. 33 for peak numbers. Peak identification can be found in Table 5.

generally lower than in scenario A and, second, the difference between sandstone and source rock intervals is much less pronounced than in profile 1. The tendentially highest values are reached in the small, intercalated source layer directly above the central reservoir unit. Moreover, the nC_{17}/Pr ratio in the upper small carrier horizon is slightly lower than in the reservoir unit in the center. With respect to the C₃₀ dia-hopane ratio, the values plot in the range of 0.07 to 0.10, which is on average slightly lower than in the previous section. Nevertheless, in both scenarios the C₃₀ diahopane ratio is lower in the reservoir than in the source units. Therefore, despite differences in the absolute values, the curves are shaped quite similar. Regarding the short- over long-chain triaromatic steroid ratio, the trendline closely resembles the curve of the C₃₀ diahopane ratio. In particular, the TA(I)/TA(I + II) values display a range from 0.28 to 0.51 and are highest in the source (0.47-0.51) and lowest in the reservoir units (0.28-0.33). Thus, similar to the C₃₀ diahopane ratio described before, the values are remarkably lower than in scenario A. Looking at the third investigated maturity parameter, the MPI 1, the data maximize at 0.56 and minimize at 0.45. Thereby, the MPI 1 values are constantly lower in the source (0.45-0.46) than in the sandstone units (0.51-0.56). Though, in contrast to the previously mentioned maturity indicators, the MPI 1 data are in the same range as in section A. Concerning the 9- to 1-methylphenanthrene ratio, which scatters in a quite narrow area between 1.26 and 1.33, slightly elevated values were determined in the reservoir (mean value: 1.32) than in the organic-rich, shaly intervals (average value: 1.28). These differences are, however, quite small and should not be overinterpreted. The next graph shows the C₁ dibenzothiophene/C₁ phenanthrene ratio, which varies in total between 0.15 and 0.24 and is thus in a similar range as in scenario A. In terms of the shape of curve, it can be said that, similar to scenario A, the highest values were determined in the source (0.21-0.24) and the lowest values in the reservoir intervals (0.15-0.20). This trend continues for the C₁ dibenzofurans against C₁ phenanthrenes ratio, which ranges from 0.04 to 0.16. Here, the data remain fairly constant at around 0.15 in the shale strata, and plot on average 0.08 units lower at around 0.07 in the intercalated carrier horizons. If plotting the sum of methylated dibenzofurans vs. the sum of the C₁-alkylated

6. Results

dibenzothiophenes, the values vary between 0.26 and 0.72, whereby the graph looks similar to the previous ratio. In addition, although the absolute values are slightly higher, there are also parallels to the trend shown before in expulsion scenario A (Fig. 32). Essentially, the highest C_1 DBF/ C_1 DBT values (0.65-0.72) were again calculated for the source rock intervals and the lowest ratios were determined in the reservoir units (0.26-0.67). With regard to the alkylated vs. non-alkylated ratios (C_1 Phen/Phen, C_1 DBT/DBT, C_1 DBF/DBF, C_1 Carb/Carb), all trends once more show a very similar pattern. In particular, in all four diagrams the reservoir units are clearly enriched in alkylated vs. non-alkylated components, which is in good agreement with the trends documented approximately 80 m above in scenario A. Looking at the data, the values extend from 2.07 to 4.23 for the C_1 Phen/Phen ratio, from 2.32 to 5.55 for the C_1 DBT/DBT ratio, from 4.17 to 11.74 for the C_1 DBF/DBF, and from 3.06 to 5.53 for the C_1 Carb/Carb ratio. Regarding differences in the distribution of nitrogen-shielded vs. nitrogen-exposed C_2 carbazoles, the results for expulsion scenario B fall in an area between 4.49 and 9.29. Thereby, it is clearly visible that especially the central reservoir unit is enriched in shielded C_2 carbazoles (5.96-7.52). Surprisingly, this tendency is not observable in the small sandstone horizon in the upper half. Here, the C_2 Carb (Shielded/Exposed) ratios of the reservoir and the surrounding shale units are roughly the same. Note, however, that the average value of the sandstone units (6.78) still exceeds that of the source beds (5.89). Finally, with regard to the distribution of the benzocarbazoles, the BC ratio of expulsion scenario B is in the magnitude of 0.33 to 0.54. It displays a great variability over the profile and is constantly higher in the lower (0.53-0.54) than in the upper and central shale units (0.33-0.50). Furthermore, the BC ratio of the reservoir units is on average (0.45) considerably lower than in the lowermost source unit (0.54) but in a similar range as in the two upper source beds (0.45).

In general, however, the distribution patterns of key compounds in the source vs. the reservoir rock (Fig. 35) look quite similar for expulsion scenario B. Nonetheless, again some important differences exist. In particular, reservoir samples display a different *n*-alkane distribution, exhibit a lower T_s/T_m ratio, contain lower proportions of diasteranes, are significantly depleted in carbazoles, and once more contain gammacerane, but yet in lower abundance than in scenario A, which could again indicate contribution from an external source.

6. Results

Yet, the molecular geochemical depth profiles shown above principally fit well with the expectations for this section. In particular, dibenzothiophenes and dibenzofurans seem to be preferentially retained in the source rock, not much differences between source and carrier beds were found for the 9-/1-methylphenanthrene ratio, and the reservoir strata tends to be enriched in nitrogen-shielded over nitrogen-exposed carbazoles. Surprisingly, however, as in profile 1 shown before, the maturity parameters again display contrary maturity signals for the reservoir petroleum. While the C_{30} diahopane and the $TA(I)/TA(I + II)$ trends again point to a lower thermal maturity of the reservoir petroleum relative to the source bitumen, the MPI 1, on the other hand, suggests that the thermal maturity of the reservoir extract is higher than that of the source bitumen. Another interesting observation is that the sandstone intervals tend to be enriched in alkylated vs. non-alkylated components (e.g. C_1 Phen/Phen, C_1 DBT/DBT), which was similarly observed in scenario A and could perhaps be associated with petroleum expulsion.

15/3-9 T2 Draupne section (expulsion scenario C)

Fig. 36 shows the most essential molecular geochemical trends of the highly alternating Draupne profile of well 15/3-9 T2. Corresponding ion chromatograms are presented in Fig. 37. The nC_{17}/Pr ratio of this section extends in total from 1.85 to 4.16. However, no clear differences between sandstone and source units were found. In fact, the trendline of the nC_{17}/Pr ratio is shaped highly irregular and no definite trend is visible over the profile. Concerning the molecular maturity proxies, the C_{30} diahopane ratio varies between 0.13 and 0.20, the triaromatic steroid ratio ($TA(I)/TA(I + II)$) ranges from 0.36 to 0.71, and the MPI 1 is in the order of 0.46 to 0.59. Similar to the previous scenarios, the source intervals of section C again show both higher $C_{30}dia/(C_{30}dia+C_{30}\alpha\beta)$ (mean value: 0.19) and $TA(I)/TA(I + II)$ values (average: 0.69) as the surrounding carrier beds (average values of 0.15 and 0.45, respectively). By contrast, the MPI 1 repeatedly exhibits an inverse pattern and was on average found to be slightly higher in the reservoir (0.54) than in the source units (0.48). If comparing the absolute numbers with the two previous sections from quadrant 15, the C_{30} diahopane ratios of scenario C are clearly higher than in expulsion scenario B, but only marginally greater than those in expulsion scenario A. The same is true for the short-against long-chain triaromatic steroid ratio. For this parameter, the values calculated for section C clearly exceed those determined in

6. Results

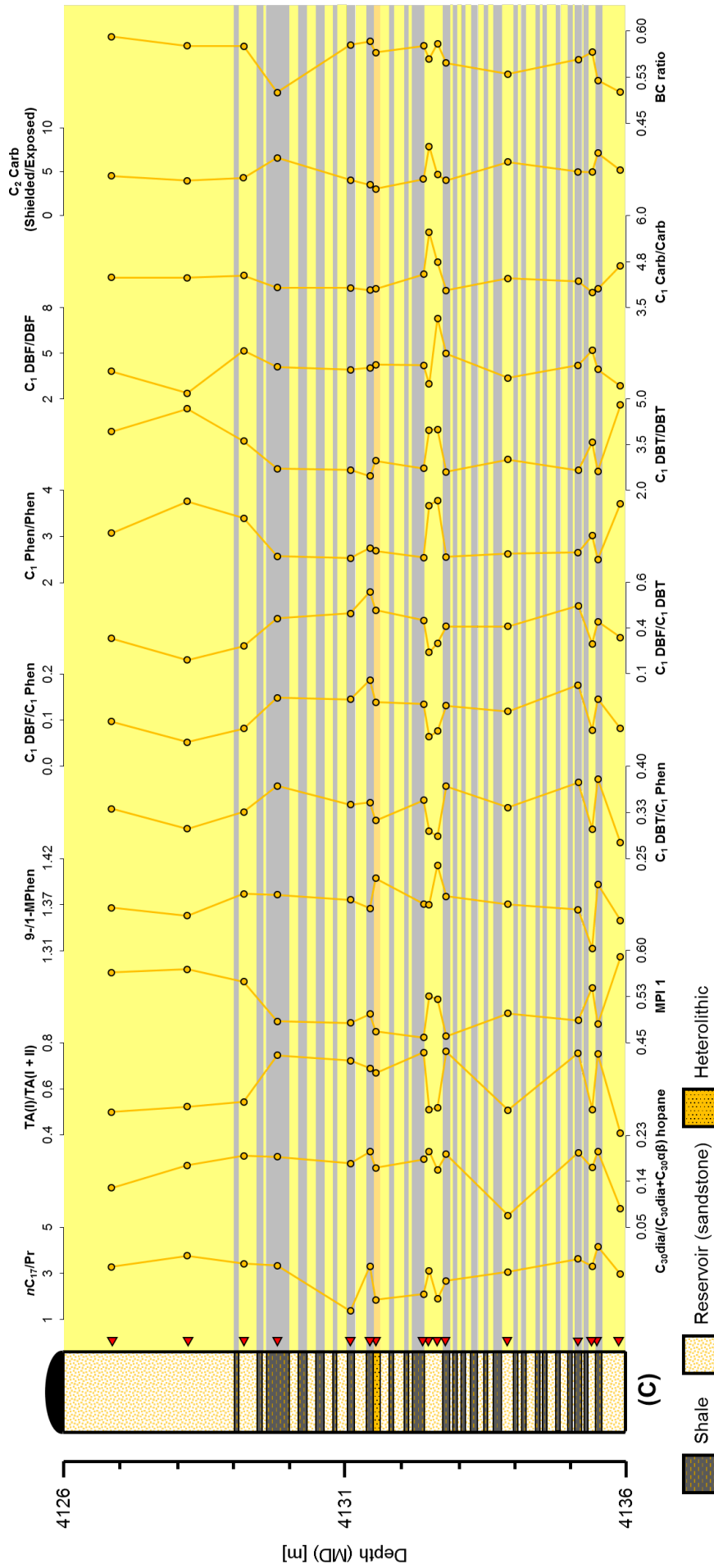
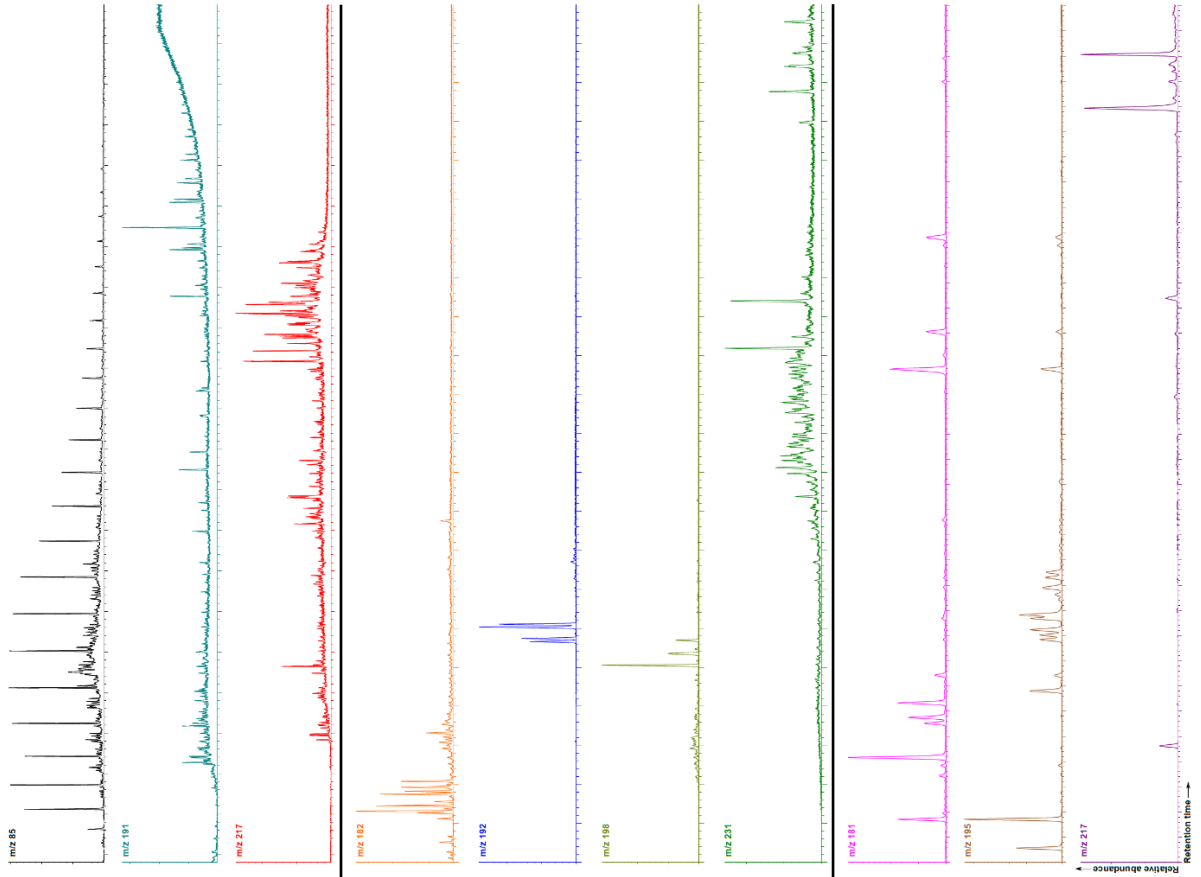


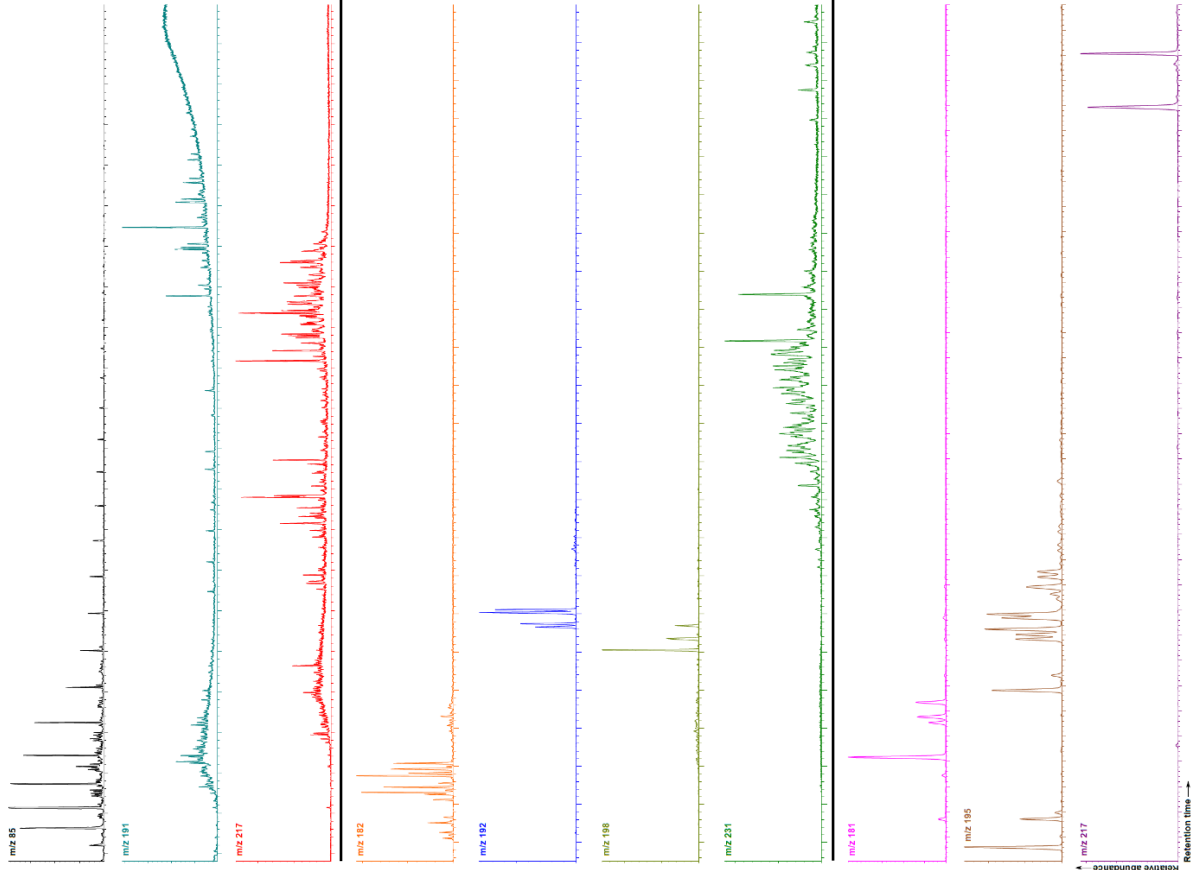
Fig. 36. Selected molecular geochemical depth profiles of expulsion scenario C, North Sea well 15/3-9 T2 (Draupne core), 4126-4136 m drilling depth. The depth is given as measured depth (MD) and comparable to the true vertical depth (TVD). One tick on the depth axis represents 1 m. Abbreviations: nC_{17}/Pr = *n*-Heptadecane/Pristane; $C_{30dia}/(C_{30dia}+C_{30q\beta})$ = C_{30} Diahopane/ C_{30} Diahopane+ C_{30} Hopane); $TA(I)/TA(I+II)$ = Short-/Long-Chain Triaromatic Steroid Ratio ($(C_{20}+C_{21})/(C_{20}+C_{21}+C_{26}+C_{27}+C_{28})$); MPI 1= Methylphenanthrene Index; 9-/1-MPhen= 9-Methylphenanthrene/1-Methylphenanthrene; $C_1 DBT/C_1 Phen$ = C-alkylated Dibenzofurans/C-1-alkylated Phenanthrenes; $C_1 DBF/C_1 Phen$ = C-alkylated Dibenzofurans/C-1-alkylated Phenanthrenes; $C_1 DBT/DBT$ = C-alkylated Dibenzofurans/Phenanthrene; $C_1 DBT/DBT$ = C-alkylated Dibenzofurans/Phenanthrene; $C_1 DBF/DBF$ = C-alkylated Dibenzofurans/Dibenzofuran; $C_1 Carb/Carb$ = C-alkylated Carbazoles/Carbazole; $C_2 Carb$ (Shielded/Exposed)= Shielded/Exposed C_2 -alkylated Carbazoles (1,3-, 1,6-, 1,7-, 1,4-, 1,5-Dimethylcarbazole)/(2,7-, 2,4-, 2,5-Dimethylcarbazole); BC ratio= Benzocarbazoles Ratio.

6. Results

Reservoir



Aliphatics



Shale

6. Results

Fig. 37. Exemplary ion chromatograms of a selected source (K011236) vs. a carrier bed sample (K011230) for expulsion scenario C. The ion chromatograms shown comprise alkanes (m/z 85), hopanes (m/z 191), steranes (m/z 217), methyl dibenzofurans (m/z 182), methylphenanthrenes (m/z 192), methyl dibenzothiophenes (m/z 198), triaromatic steroids (m/z 231), methylcarbazoles (m/z 181), C₂-alkylated carbazoles (m/z 195), and benzocarbazoles (m/z 217). See Fig. 33 for peak numbers. Peak identification can be found in Table 5.

section B, but are only slightly higher than those calculated for scenario A. With respect to the MPI 1, the values calculated for scenario C are very similar to those determined in the expulsion scenarios A and B. Nevertheless, the MPI 1 seems to be slightly higher in scenario C than in A and B. Regarding only the ratio between 9- and 1-methylphenanthrene, which amounts to 1.31-1.41 for section C, no consistent trend is observable over the profile. A more pronounced trend can be seen for the C₁ DBT/C₁ Phen ratio (0.28-0.38), which, equivalent to the two previous scenarios, maximizes in the source horizons and is lowest in the reservoir strata. The same tendency is observable for the C₁ DBF/C₁ Phen ratio, which climaxes at a value of 0.19 (source layer) and minimizes at 0.05 (sandstone reservoir). Moreover, an almost 1:1 trend is visible for the ratio of methyl dibenzofurans against methyl dibenzothiophenes. For this graph, the data range from 0.18 to 0.55 and average at 0.43 in the shale and 0.27 in the reservoir horizons, which implicates a difference of around 0.16 between source rock and sandstone units. With respect to the methylated vs. non-methylated plots, clear trends and nearly equivalently formed curves are visible for the C₁ Phen/Phen (2.37-3.33) and C₁ DBT/DBT (2.46-4.80) ratios. For these diagrams, the highest values were consistently calculated for the sandstone intervals, which fits well with the trends monitored in the expulsion scenarios A and B. Less pronounced trends are visible for the ratios of methylated dibenzofurans against dibenzofuran (2.38-7.29) and methylcarbazoles vs. carbazole (3.91-5.54). Although most values are still higher in the sandstone than in the shale intervals, the differences are generally much smaller. In addition, some data points from reservoir horizons display values considerably lower than those from corresponding shaly layers. In contrast to the alkylated vs. non-alkylated diagrams, the ratio of nitrogen-shielded against nitrogen-exposed dimethylcarbazoles exhibits a much less distinct trend than in the previous expulsion scenarios. In particular, the data for this ratio, which scatters between 3.01 to 7.85, are highly variable over the profile and no selective enrichment or depletion effects are recognizable. The last trend that is shown in Fig. 36 is again the benzocarbazoles ratio. For this section, it is in the magnitude of 0.50 to 0.59 and therefore similar to scenario A, but slightly higher than in section B. The data average at 0.55 in the source and

6. Results

0.56 in the reservoir units, suggesting only marginal differences between sandy and shaly intervals. Indeed, no clear trend for the BC ratio is observable over the profile.

If comparing the ion chromatograms for a selection of saturates, aromatics and carbazoles in a source vs. a reservoir sample (Fig. 37), it can be seen that the compound distribution patterns are in principal very similar. However, the reservoir samples are clearly enriched in *n*-alkanes, contain higher amounts of tricyclic terpanes and lower amounts of diasteranes, and are depleted in carbazoles.

Though, the trends for this section are in relatively good accordance with the expectations. In this respect, particularly noticeable are again the enrichment of dibenzothiophene and dibenzofuran over phenanthrene in the source rock units and the comparatively small differences between shales and sandstones in the graph of the 9-/1-methylphenanthrene ratio. It is, however, surprising that the trend for the nitrogen-shielded vs. nitrogen-exposed C₂ carbazoles is much less pronounced than in the two sections before, where the reservoir units frequently showed a predominance of nitrogen-shielded over non-shielded dimethylcarbazoles. It is also interesting that the maturity parameters again exhibit contrasting signals in the sandstone intervals, whereby the MPI 1 is opposing the C₃₀ diahopane and the TA(I)/TA(I + II) ratio.

15/3-9 T2 Hugin section (expulsion scenario D)

The next subsection concentrates on the most important molecular geochemical results of the coaly-deltaic Hugin Formation, which are summarized in Fig. 38. Exemplary ion chromatograms of a shale, coal, and reservoir sample are given in Fig. 39. First, regarding the *n*C₁₇/Pr ratio, the data reach values of 0.65 to 3.05 and maximize in the lowermost shale unit. Thereby, the *n*C₁₇/Pr ratios obtained in the sandstone intervals (1.48-2.45) tend on average to be higher than in the coals and most parts of the shales. With respect to the C₃₀ diahopane ratio, the data for the Hugin Formation plot between 0.23 and 0.69 and thus significantly higher than in all previous sections. A close examination reveals that the reservoir units generally exhibit much lower C₃₀dia/(C₃₀dia+C₃₀αβ) values (0.23-0.42) than the coals (0.39-0.61) and the shales (0.62-0.67). Looking at the short- vs. long-chain triaromatic steroid ratio, it is remarkable that triaromatic steroids occur in only very low abundances in both coals and

6. Results

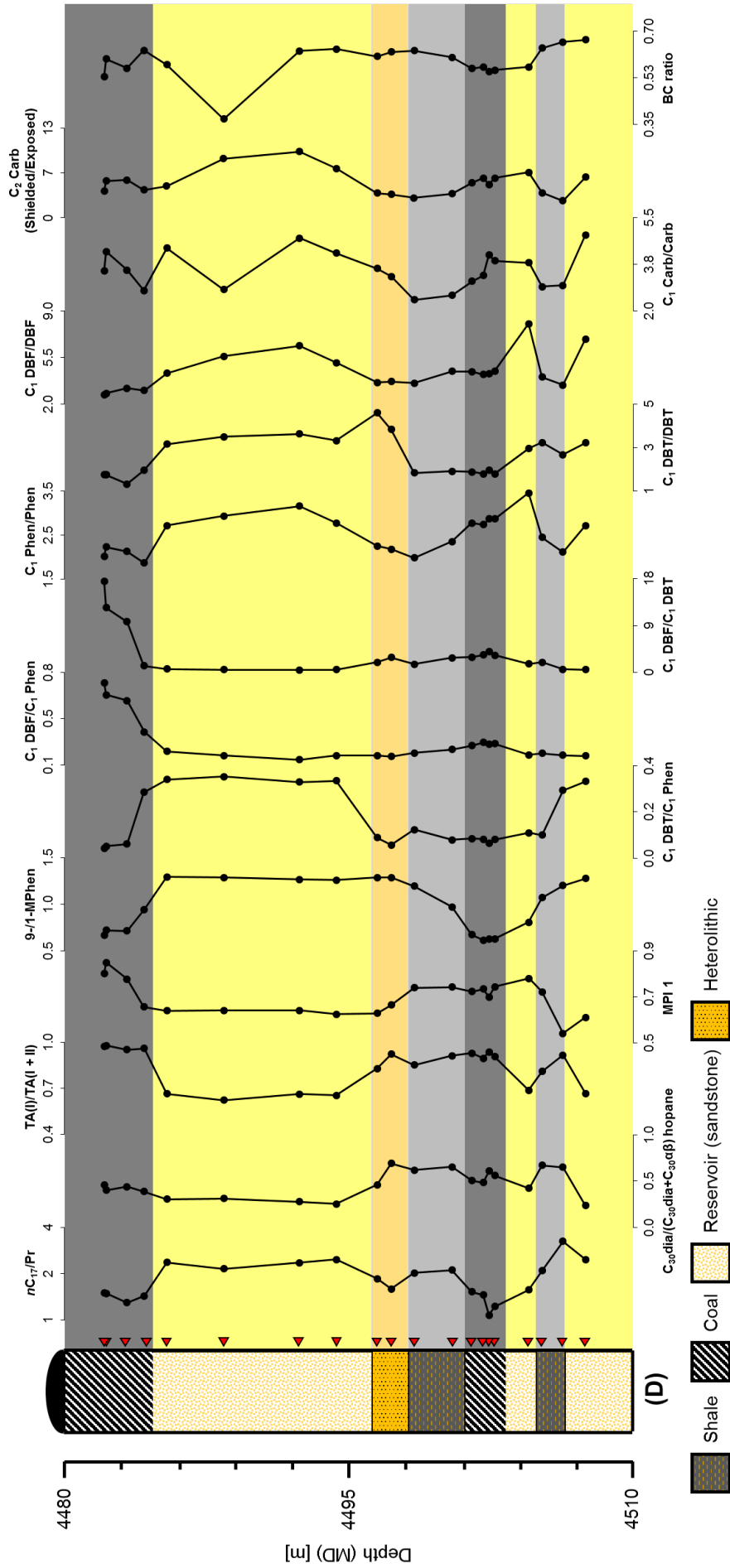
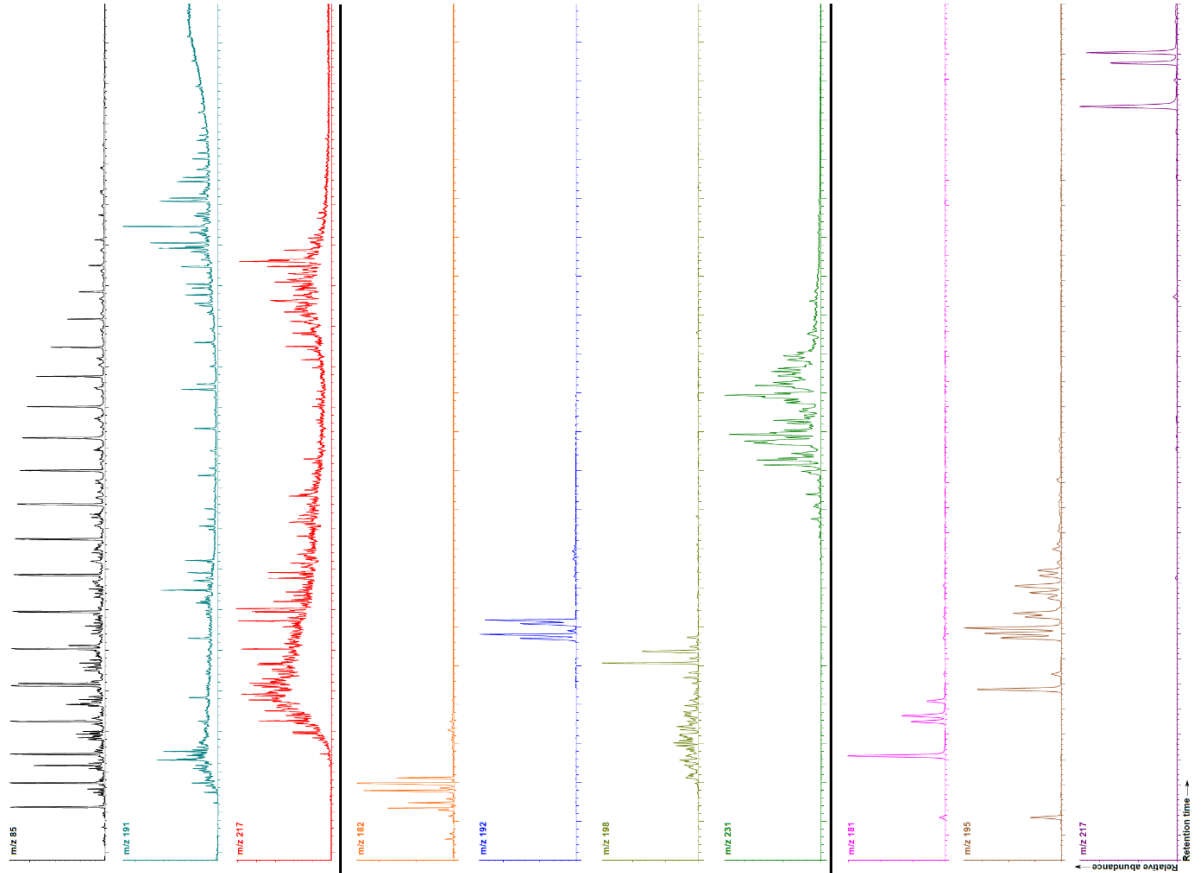


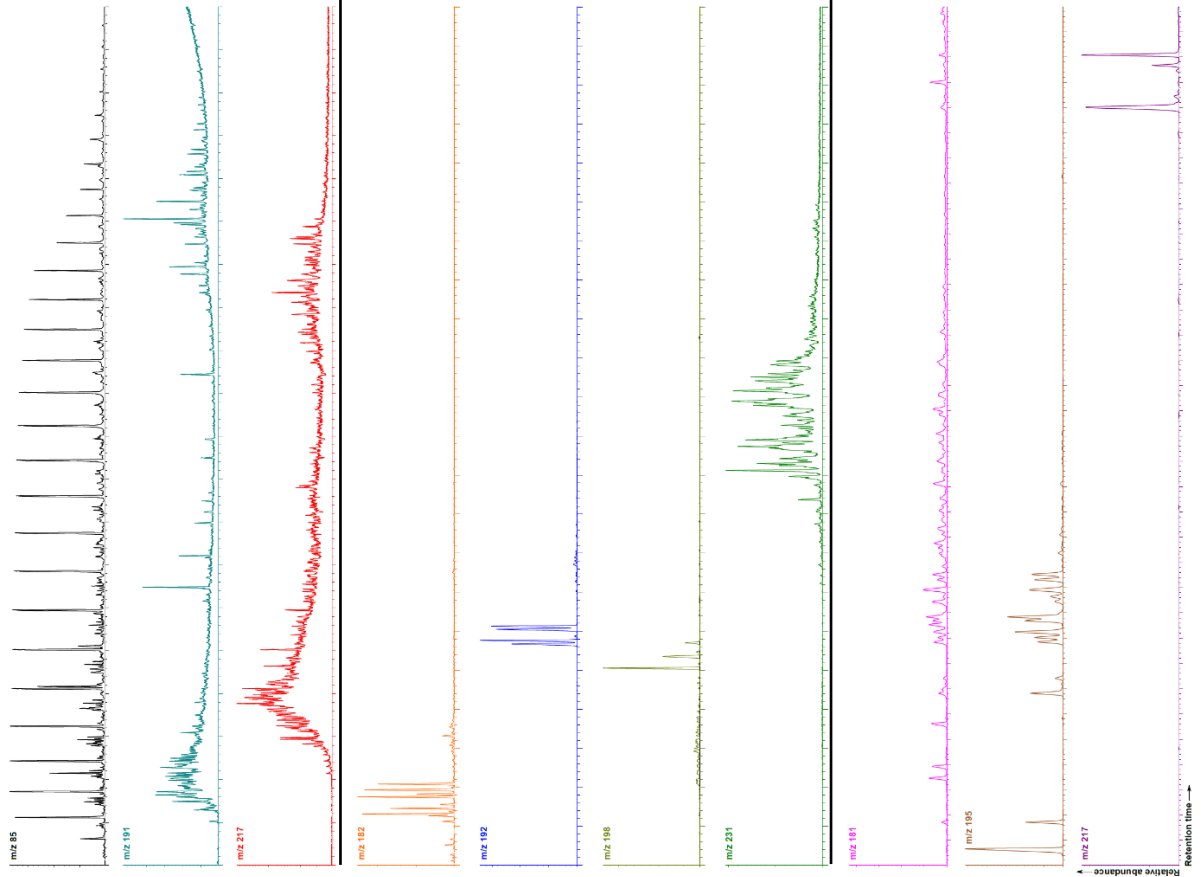
Fig. 38. Selected molecular geochemical depth profiles of expulsion scenario D, North Sea well 15/3-9 T2 (Hugin core), 4480-4510 m drilling depth. The depth is given as measured depth (MD) and comparable to the true vertical depth (TVD). One tick on the depth axis represents 3 m. Abbreviations: $nC_{17}/Pr = n$ -Heptadecane/Pristane; $C_{30}dia/(C_{30}dia+C_{30}q\beta) = C_{30}$ Diahopane/ C_{30} Diahopane+ C_{30} Hopane); $TA(I)/TA(I+II) =$ Short-/Long-Chain Triaromatic Steroid Ratio ($(C_{20}+C_{21})/(C_{20}+C_{21}+C_{26}+C_{27}+C_{28})$); MPI 1 = Methylphenanthrene Index; 9-/1-MPhen = 9-Methylphenanthrene/1-Methylphenanthrene; $C_1 DBT/C_1 Phen = C_1$ -alkylated Dibenzofurans/ C_1 -alkylated Phenanthrenes; $C_1 DBF/C_1 Phen = C_1$ -alkylated Dibenzofurans/ C_1 -alkylated Phenanthrenes; $C_1 DBT/DBT = C_1$ -alkylated Dibenzofurans/Dibenzothiophenes; $C_1 DBF/DBF = C_1$ -alkylated Dibenzofurans/Dibenzofuran; $C_1 Carb/Carb = C_1$ -alkylated Carbazoles/Carbazole; $C_2 Carb (Shielded/Exposed) =$ Shielded/Exposed C_2 -alkylated Carbazoles (1,3-, 1,6-, 1,7-, 1,4-, 1,5-Dimethylcarbazole)/(2,7-, 2,4-, 2,5-Dimethylcarbazole); BC ratio = Benzocarbazoles Ratio.

6. Results

Coal



Shale



6. Results

Reservoir

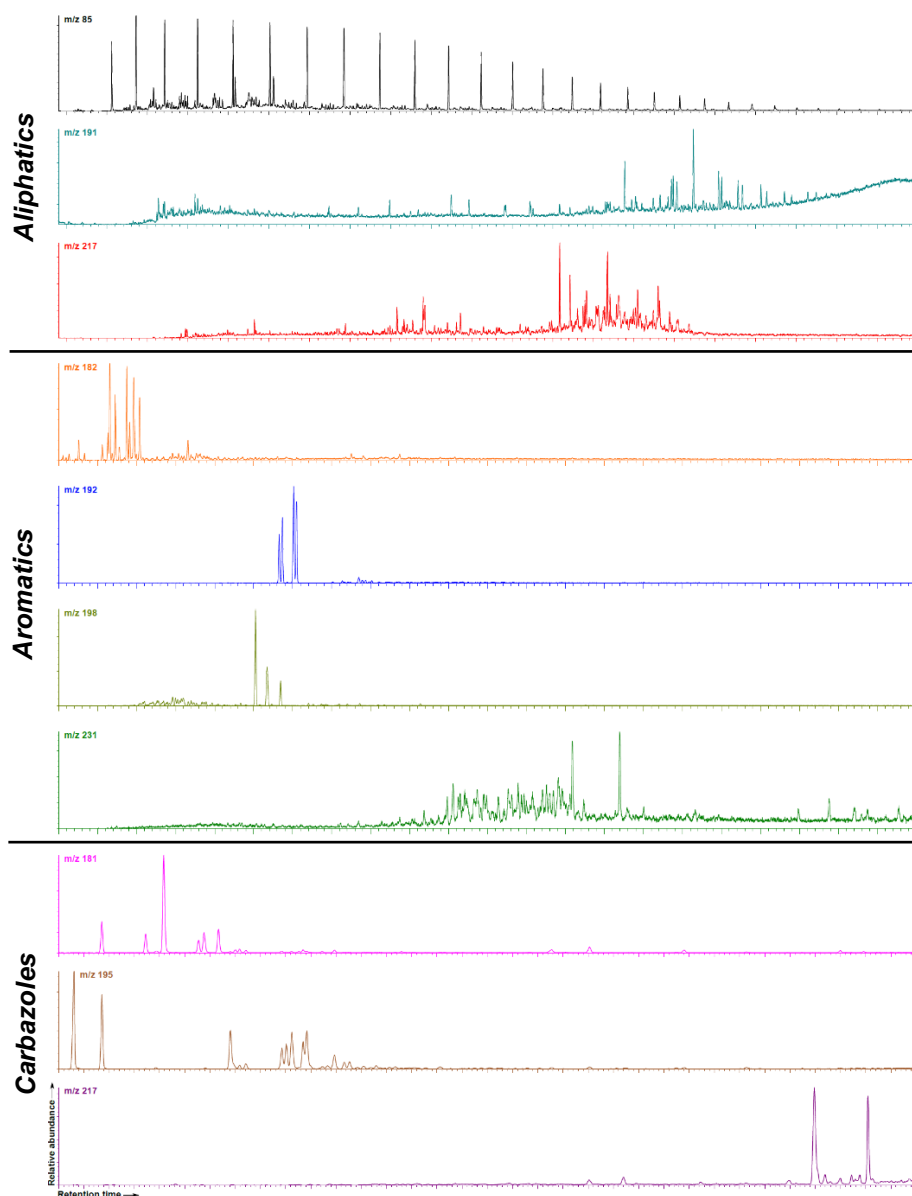


Fig. 39. Exemplary ion chromatograms of a selected shale (K011247), coal (K011240) and reservoir sample (K011245) for expulsion scenario D. The ion chromatograms shown comprise alkanes (m/z 85), hopanes (m/z 191), steranes (m/z 217), methyl dibenzofurans (m/z 182), methyl phenanthrenes (m/z 192), methyl dibenzothiophenes (m/z 198), triaromatic steroids (m/z 231), methylcarbazoles (m/z 181), C₂-alkylated carbazoles (m/z 195), and benzocarbazoles (m/z 217). See Fig. 33 for peak numbers. Peak identification can be found in Table 5.

shales, but are very abundant in the reservoir (see also Fig. 39). Altogether, the TA(I)/TA(I + II) ratio of expulsion scenario D ranges from 0.62 in the central sand-stone unit to 0.98 in the uppermost coal bed, whereby the values determined in the reservoir units are significantly lower than in the surrounding source rocks. Concerning the methylphenanthrene index, the data are, first, higher (0.54-0.81) than in the previous sections and, second, show an inverse pattern compared to the scenarios A, B, and C, where the MPI 1 is frequently higher in the reservoir than in the source intervals. Conversely, for the Hugin Formation, the average lowest MPI 1 values were

6. Results

determined in the sandstone horizons, which plot on average 0.06 units below those of the source rock samples. Compared to the MPI 1, the 9-/1-MPhen ratio, which ranges from 0.61 to 1.30, exhibits an opposite pattern. In particular, the highest values are attained in the carrier and heterolithic units, whereas the lowest ratios were calculated for the source rock strata, specifically for the coal beds. Note that there is a gradual increase of the 9-/1-MPhen ratio from the first shale layer in the lower half towards the overlying sandstone reservoir. A very interesting trend is visible for the ratio of methylated dibenzothiophenes against methylated phenanthrenes. In contrast to the previous profiles, the highest values were not identified in the source but rather in the carrier intervals. Thereby, the C₁ DBT/C₁ Phen ratio totally ranges from 0.04 to 0.35 with average values of 0.09, 0.15, and 0.30 for the coals, shales and sandstones, respectively. However, if replacing the C₁ dibenzothiophenes with methylated dibenzofurans (C₁ DBF/C₁ Phen) (0.14-0.72), the curve looks considerably different. While particularly the coals tend to be enriched in dibenzofurans, both sandstones and shales are, on the other hand, comparatively depleted in these oxygen-substituted aromatics. Very high ratios were calculated for the upper coal bed, pointing to a strong enrichment of dibenzofurans over phenanthrenes. An almost 1:1 mirror image trend is visible for the C₁ DBF/C₁ DBT ratio, which is in the magnitude of 0.42 to 17.48. Again, the highest values were determined in the coaly units, particularly in the upper coal bed, whereas the lowest values were ascertained in the reservoir and shale packages. The subsequent molecular geochemical depth profiles illustrated in Fig. 38 comprise the trends of alkylated vs. non-alkylated phenanthrenes, dibenzothiophenes, dibenzofurans, and carbazoles. Except for the C₁ Carb/Carb ratio, all other shown trends (C₁ Phen/Phen: 1.86-3.45, C₁ DBT/DBT: 1.30-4.60, C₁ DBF/DBF: 2.80-8.04) display a similar pattern: while the reservoir horizons are clearly enriched in methylated compounds, the source units, by contrast, appear to be largely depleted in higher homologues. This observation is in good accordance with the alkylated vs. non-alkylated trends described for the previous scenarios. A slightly different trend is yet visible for the ratio of methylated carbazoles against carbazole, which lies between 2.41 and 4.84. Although the general tendency, i.e. the enrichment of the alkylated molecules in the reservoir units, is principally maintained, the curve is much more variable than the previous trends, especially in the upper part of the section. Based on the mean values, which are 3.55, 2.71, and 4.11 for coals, shales, and reservoir intervals, respectively, it can be concluded that the shales are most strongly depleted

6. Results

in alkylated carbazoles. Concerning the ratio between nitrogen-shielded and nitrogen-exposed C₂-alkylated carbazoles, the data generally fall in the range of 2.45 to 9.56 and climax in the large reservoir unit in the center. In opposite, both coals and particularly shales exhibit reproducibly low values, indicating they are depleted in nitrogen-shielded dimethylcarbazoles. A minimum value is reached in the lowermost shale horizon. The last ratio that is shown in Fig. 38 is again the benzocarbazoles ratio, which ranges between 0.37 and 0.67. Interestingly, both the highest and the lowest value were determined in a reservoir sample, indicating a large variability. However, considering the lowest value of 0.37 as an outlier, the variability is much smaller (0.53-0.67). On average, the BC ratio is lowest in the coals (0.57), second highest in the reservoir (0.61, excluding the outlier), and highest in the shales (0.63). Therefore, the BC ratio of the Hugin Formation is in the main higher than in the previous scenarios. Interestingly, concerning the distribution of benzocarbazoles in general (Fig. 39), very high concentrations of benzo[b]carbazole were detected in shales and particularly coals of the Hugin Formation. This is in strong contrast to all other expulsion scenarios, where benzo[b]carbazole was present only in trace amounts. In addition, remarkably, only insignificant quantities benzo[b]carbazole were found in reservoir samples from the Hugin Formation.

Fig. 39 documents not only differences in the distribution of benzocarbazoles but also compares the distribution patterns of alkanes, hopanes, steranes, methyl dibenzofurans, methylphenanthrenes, methyl dibenzofurans, triaromatic steroids, methylcarbazoles and C₂-alkylated carbazoles between shale, coal and reservoir samples. Note that the degree of similarity is higher for shale vs. coal than for shale/coal vs. reservoir. Compared to the source rock samples, the molecular signature of the reservoir sample is fundamentally different. This is particularly evident in the relatively low amounts of pristane compared to nC₁₇, the higher abundance of triaromatic steroids, and the absence of benzo[b]carbazole.

Due to the strong compositional differences between source bitumen and reservoir extracts it is thus questionable whether the reservoir petroleum indeed originates from the surrounding shales and, therefore, allows for the investigation of expulsion-related fractionation effects. However, in agreement with most previous sections, the reservoir units seem to be enriched in alkylated vs. non-alkylated components and nitrogen-shielded over nitrogen-exposed C₂ carbazoles. Note also that, in contrast to the

6. Results

sections shown before, the maturity parameters are this time in good accordance with each other and clearly suggest that the maturity of the reservoir petroleum is lower than that of the source bitumen. Besides, particularly interesting in the Hugin section are the elevated BC ratios in the source rock samples.

24/9-1 Profile 1 (expulsion scenario E)

The most significant molecular geochemical depth trends of expulsion scenario E are illustrated in Fig. 40. Corresponding ion chromatograms of an exemplary shale sample and a sample from a heterolithic unit are presented in Fig. 41. Again, the first ratio that is shown is the nC_{17}/Pr ratio. For scenario G, it varies from 1.29 to 1.70 and is therefore tendentially lower than in the previous scenarios. The nC_{17}/Pr curve is strongly variable over the profile and exhibits no particular differences between pure source and heterolithic units. In contrast to the previous scenarios, due to the virtual absence of hopanes (Fig. 41), the $C_{29} \beta\beta/(\beta\beta+\alpha\alpha)$ sterane maturity parameter was used instead of the C_{30} diahopane ratio. The $C_{29} \beta\beta/(\beta\beta+\alpha\alpha)$ sterane ratio is, despite slight variations, fairly constant over the profile. Effectively, it ranges from 0.59 to 0.69, whereby no clear differences exist between shales and heterolithic carrier units. With regard to the ratio of short- over long-chain triaromatic steroids, the data fall in a very narrow area between 0.66 and 0.71. Although exceptions do exist, the values tend on average to be slightly higher in source (0.70) than in heterolithic samples (0.68). With regard to the MPI 1 and the subsequently shown ratio of 9- to 1-methyl-phenanthrene, not much variability is visible over the profile. In particular, the data vary from 0.60 to 0.62 for the methylphenanthrene index and from 1.32 to 1.41 for the 9-/1-MPhen ratio. A more variable pattern is observable for the ratio of methyl-ated dibenzothiophenes to methylated phenanthrenes. For this ratio, the calculated values extend from 0.02 to 0.16 and are on average lowest in the intercalated heterolithic layers (0.05 vs. 0.08). The subsequently shown C_1 DBF/ C_1 Phen ratio is, compared to the previous sections, very low and varies only between 0.03 and 0.04. In addition, it scatters much less variable than the previous ratio involving dibenzo-thiophenes. Though, no clear differences are visible between source and heterolithic units. If comparing the abundance of methylated dibenzofurans with that of methyl-di-benzothiophenes, values of 0.25 to 2.12 were determined for this section. Thereby, the heterolithic carrier beds seem to be slightly enriched in dibenzofurans, although

6. Results

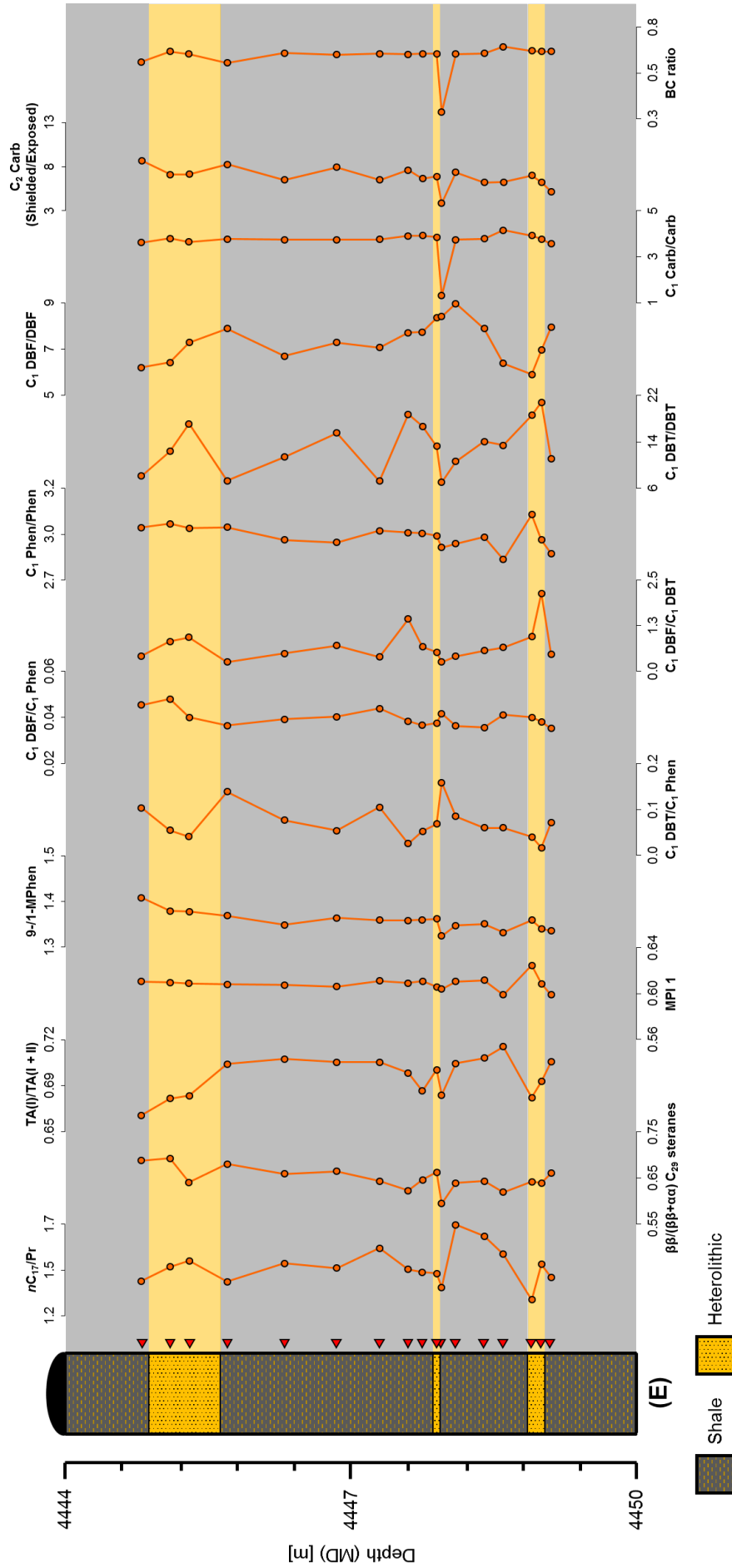
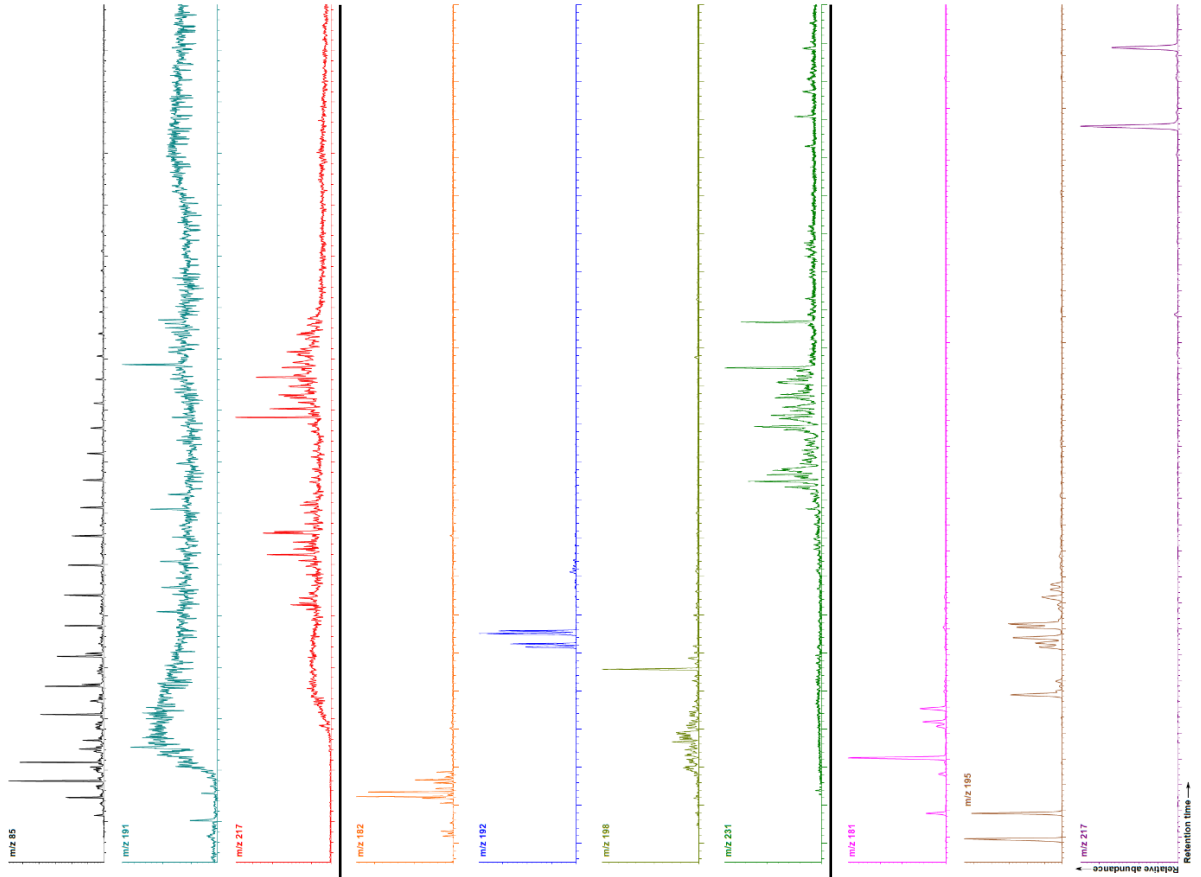


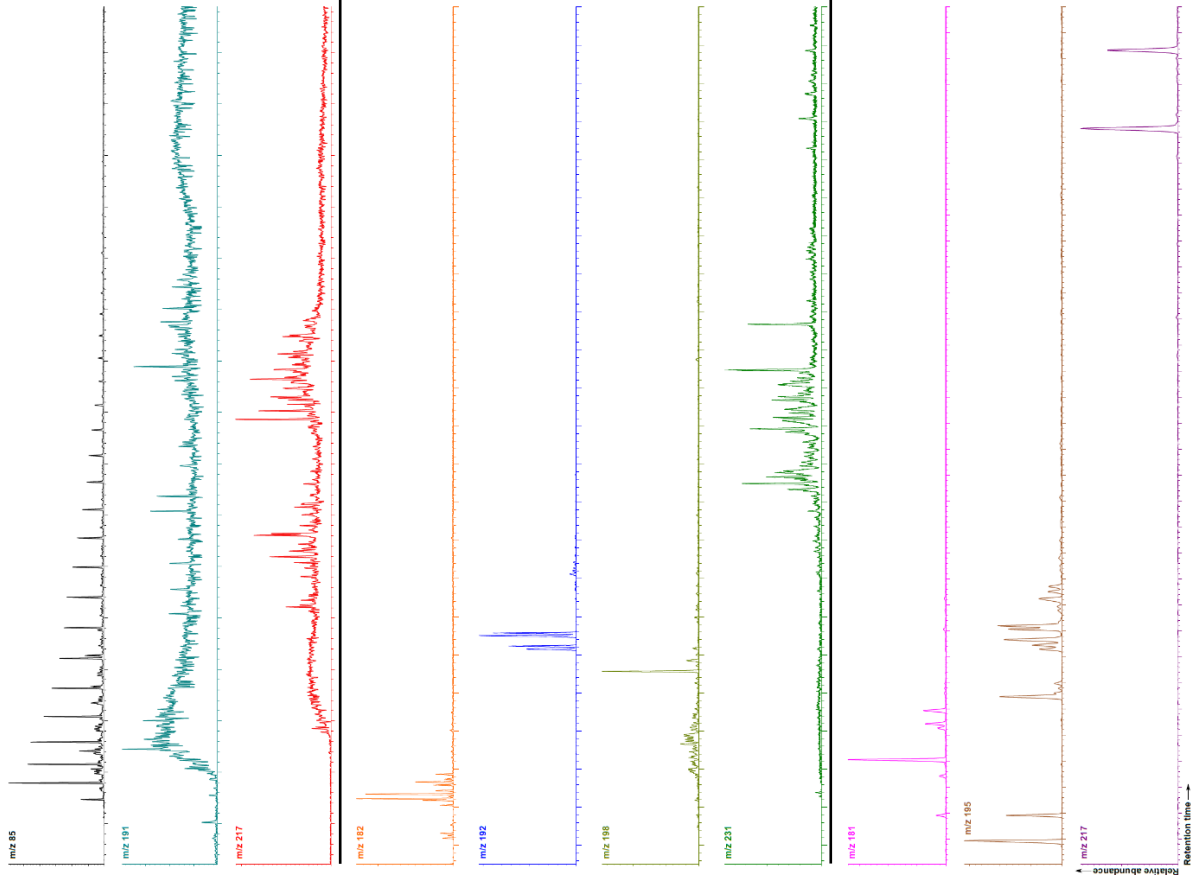
Fig. 40. Selected molecular geochemical depth profiles of expulsion scenario E, North Sea well 24/9-1, 4444-4450 m drilling depth. The depth is given as measured depth (MD) and comparable to the true vertical depth (TVD). One tick on the depth axis represents 0.6 m. Note that due to only trace quantities of hopanes, a sterane-based maturity indicator was used instead of the C_{30} Diahopane/ C_{30} Diahopane+ C_{30} Hopane) ratio. Abbreviations: nC_{17}/Pr = *n*-Heptadecane/Pristane; $\beta\beta/(\beta\beta+\alpha\alpha)$ C_{29} Steranes= $\beta\beta$ -configured/ $\beta\beta$ -configured+ $\alpha\alpha$ -configured) Stigmastane; $TA(I)/TA(I+II)$ = Short-/Long-Chain Triaromatic Steroid Ratio ($(C_{20}+C_{21})/(C_{20}+C_{21}+C_{28}+C_{27}+C_{29})$); $MPI\ 1$ = Methylphenanthrene Index; 9-/1-MPhen= 9-Methylphenanthrene/1-Methylphenanthrene; $C_1\ DBT/C_1\ Phen$ = C_1 -alkylated Dibenzofurans/ C_1 -alkylated Dibenzothiophenes/ C_1 -alkylated Phenanthrenes; $C_1\ DBF/C_1\ Phen$ = C_1 -alkylated Dibenzofurans/ C_1 -alkylated Phenanthrenes; $C_1\ DBT/DBT$ = C_1 -alkylated Dibenzothiophenes/Dibenzothiophenes; $C_1\ DBF/DBF$ = C_1 -alkylated Dibenzofurans/Dibenzofurans; $C_1\ Carb/Carb$ = C_1 -alkylated Carbazoles/Carbazole; $C_2\ Carb$ (Shielded/Exposed)= Shielded/Exposed C_2 -alkylated Carbazoles (1,3-, 1,6-, 1,7, 1,4-, 1,5-Dimethylcarbazole)/(2,7-, 2,4-, 2,5-Dimethylcarbazole); BC ratio= Benzocarbazoles Ratio.

6. Results

Heterolithic



Shale



6. Results

Fig. 41. Exemplary ion chromatograms of a selected source (K012456) vs. a carrier bed (heterolithic) sample (K012453) for expulsion scenario E. The ion chromatograms shown comprise alkanes (m/z 85), hopanes (m/z 191), steranes (m/z 217), methyl dibenzofurans (m/z 182), methylphenanthrenes (m/z 192), methyl dibenzothiophenes (m/z 198), triaromatic steroids (m/z 231), methylcarbazoles (m/z 181), C_2 -alkylated carbazoles (m/z 195), and benzocarbazoles (m/z 217). See Fig. 33 for peak numbers. Peak identification can be found in Table 5.

this trend is less pronounced in the lower half of the profile. The following four diagrams that are presented comprise the trends of methylated phenanthrenes, dibenzothiophenes, dibenzofurans and carbazoles against their non-alkylated counterparts. The data range from 2.81 to 3.06 for the C_1 Phen/Phen ratio, from 7.03 to 20.77 for the C_1 DBT/DBT ratio, from 5.89 to 8.96 for the C_1 DBF/DBF, and from 1.30 to 4.15 for the C_1 Carb/Carb ratio. While in the scenarios before the reservoir units tended to be enriched in methylated over non-methylated compounds, this tendency is much less clear for this section. Rather, the curves display either zigzag patterns, or remain fairly constant across the profile. Concerning the ratio of shielded vs. non-shielded C_2 carbazoles, the calculated values fall in an order of 3.83 to 8.69 with no clear differences between pure source and heterolithic strata. A strongly deviating value in the lower half of the profile can be considered as an outlier. With respect to the benzocarbazoles ratio, the data plot, excluding the same outlier in the lower part, always above 0.55 and average at 0.60 for the shale and 0.61 for the reservoir units, which is very similar. Indeed, if ignoring the outlier, not much variability is visible over the profile.

This is also evident in Fig. 41, which compares important ion chromatograms from a shale and a heterolithic sample. If looking at the m/z 217 mass trace that shows the distribution of benzocarbazoles, a very similar ratio is observable for source and heterolithic units. In general, based on the comparison of the ion chromatograms for the most important compounds (Fig. 41), no clear differences between shaly and heterolithic samples are ascertainable. Interestingly, however, if comparing the n -alkane signatures (m/z 85), the heterolithic sample seem to lack nC_{15} . Nevertheless, the most essential characteristic of this section is the virtual absence of hopanes (m/z 191 in the aliphatic fraction), which were found only in trace amounts, even after molecular sieving.

Except for the practical absence of hopanes and considering the fact that no real reservoir horizons are present, the trends are in quite good agreement with the expectations. Indeed, in view of the nearly homogenous source rock column, only

6. Results

marginal differences were expected between pure source rock and heterolithic carrier samples. Nevertheless, of particular interest are, like in the previous section, the comparatively high BC ratios.

24/9-1 Profile 2 (expulsion scenario F)

Molecular geochemical depth profiles of expulsion scenario F are illustrated in Fig. 42. Representative ion chromatograms of a source vs. a carrier bed sample can be found subsequently in Fig. 43. The nC_{17}/Pr ratio of this section varies between 1.33 and 1.67. No major differences exist between shale and reservoir samples, although, however, the nC_{17}/Pr ratio is on average slightly lower in the carrier (1.40) than in the shale unit (1.51). Analogous to the previous scenario, as hopanes are only marginally present in both reservoir and shale intervals (Fig. 43), a sterane-based maturity parameter ($C_{29} \beta\beta/(\beta\beta+\alpha\alpha)$) was chosen as a substitute for the C_{30} diahopane ratio. For section F, the $C_{29} \beta\beta/(\beta\beta+\alpha\alpha)$ sterane ratio ranges in total from 0.63 to 0.67 and averages at around 0.65, which is very similar to the values determined in scenario E. No significant differences between the carrier bed and the surrounding shales were observed. A slightly different trend is observable for the triaromatic steroid-based maturity parameter $TA(I)/TA(I + II)$. This ratio totally extends from 0.69 to 0.76, whereby minimum values are reached in the reservoir interval. In opposite, the $TA(I)/TA(I + II)$ ratio remains fairly constant at around 0.74 in the shale strata, which is slightly higher than in the previous section (0.70). With regard to the MPI 1, the data for scenario F fall in a very narrow range from 0.60 to 0.62 and thus remain very constant across the profile. Besides, these values are strongly comparable to the MPI 1 data of the previous section. Regarding only the ratio of 9- to 1-methylphenanthrene, which varies between 1.33 and 1.40, the values calculated in the carrier bed tend to exceed those of the shale samples. The numeric range of the 9-/1-MPhen ratio is thereby very similar to that of the previous expulsion scenario. The following three plots that are shown in Fig. 52 again include the ratios of methylated dibenzo-thiophenes vs. methylated phenanthrenes, methylated dibenzofurans against methylphenanthrenes, and methylated dibenzofurans vs. methylated dibenzothiophenes. The absolute values for these three ratios range from 0.21 to 0.37 for C_1 DBT/ C_1 Phen ratio, from 0.04 to 0.05 for the C_1 DBF/ C_1 Phen ratio, and from 0.25 to 0.76 for the C_1 DBF/ C_1 DBT ratio. With respect to the C_1 DBT/ C_1 Phen graph, the shale samples were found to be enriched in dibenzothiophenes relative to phenanthrenes. In

6. Results

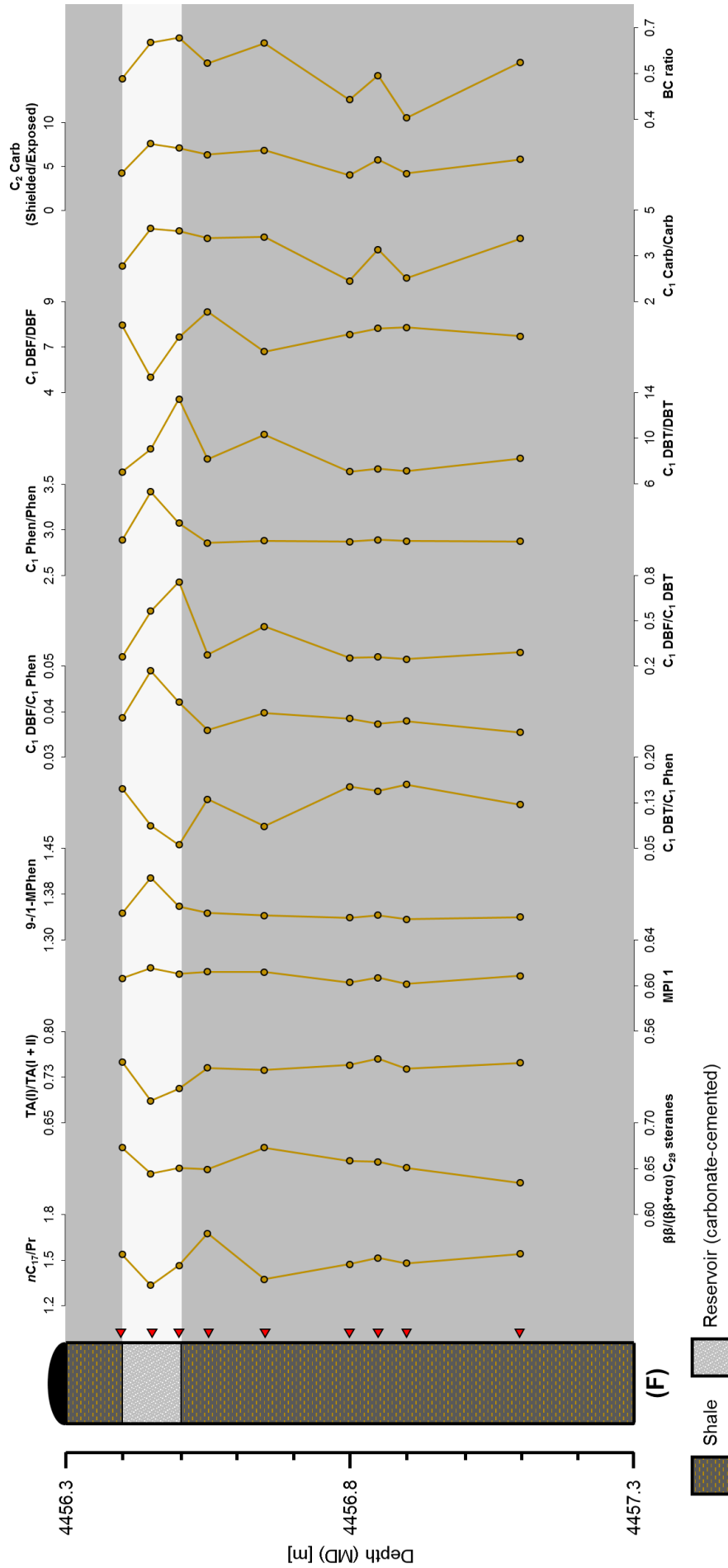
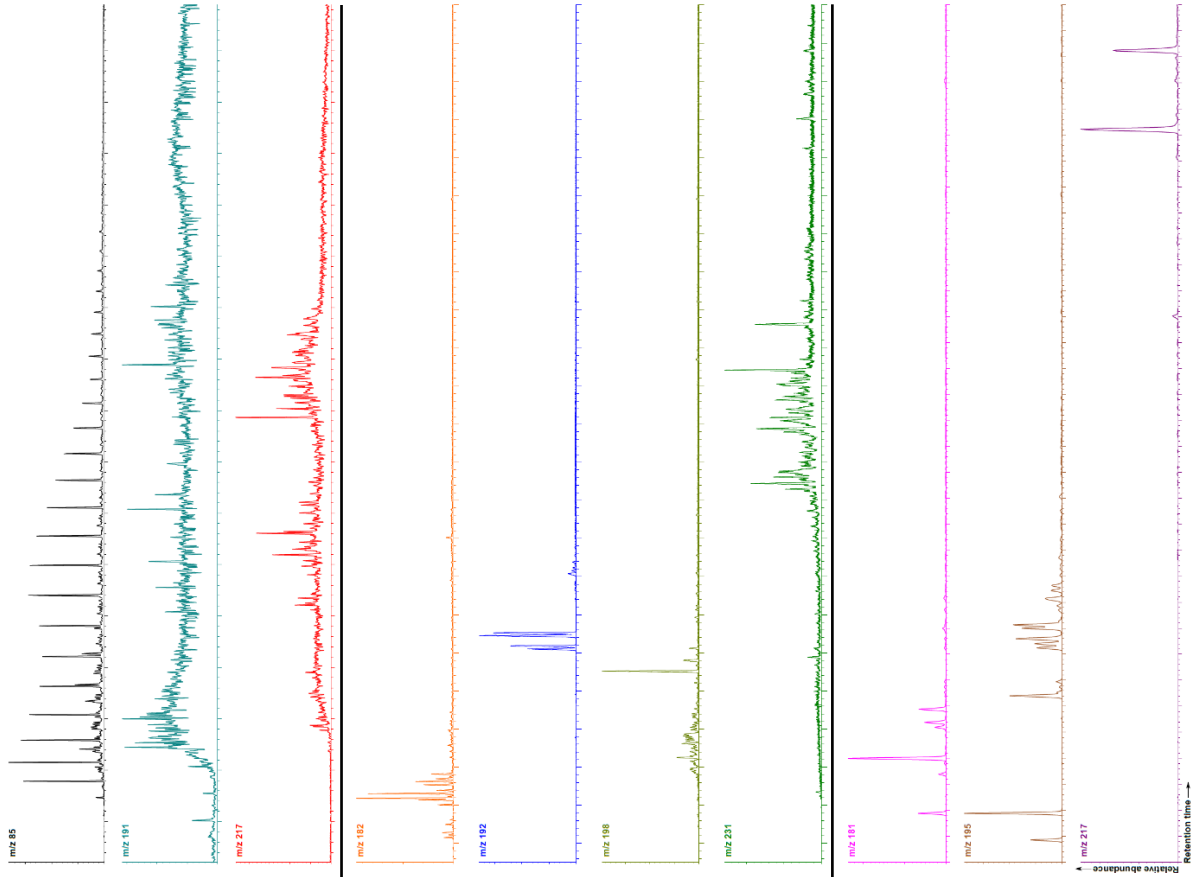


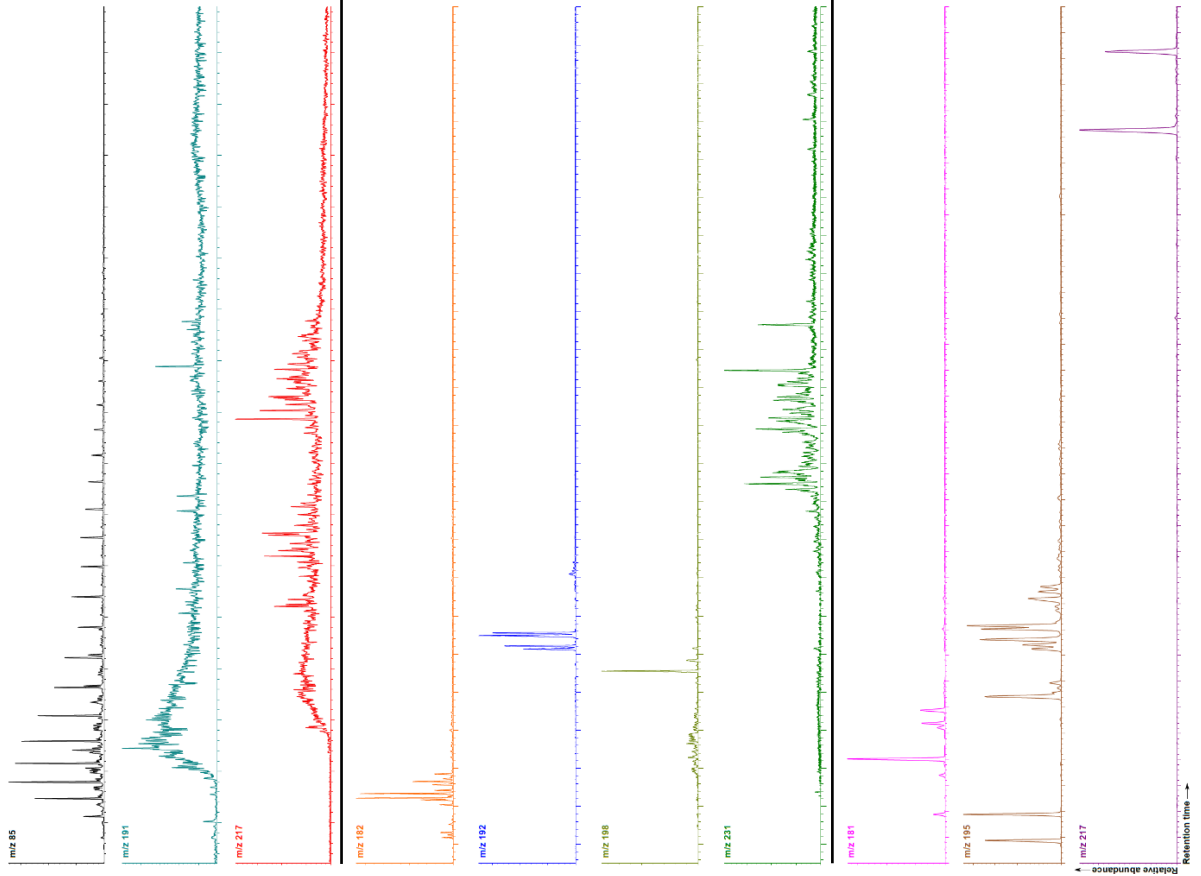
Fig. 42. Selected molecular geochemical depth profiles of expulsion scenario F, North Sea well 24/9-1, 4456.3-4457.3 m drilling depth. The depth is given as measured depth (MD) and comparable to the true vertical depth (TVD). One tick on the depth axis represents 0.1 m. Note that due to only trace quantities of hopanes, a sterane-based maturity indicator was used instead of the C_{30} Diahopane/ $(C_{30}$ Diahopane+ C_{30} Hopane) ratio. Abbreviations: nC_{17}/Pr = n -Heptadecane/Pristane; $\beta\beta/(\beta\beta+\alpha\alpha)$ C_{29} Steranes= $\beta\beta$ -configured/ $(\beta\beta$ -configured+ $\alpha\alpha$ -configured) Stigmastane; $TA(I)/TA(I+II)$ = Short-/Long-Chain Triaromatic Steroid Ratio ($(C_{20}+C_{21})/(C_{20}+C_{21}+C_{26}+C_{27}+C_{28})$); $MPI\ 1$ = Methylphenanthrene Index; $9/1-MPhen$ = 9-Methylphenanthrene/1-Methylphenanthrene; $C_1\ DBT/C_1\ Phen$ = C_1 -alkylated Dibenzofurans/ C_1 -alkylated Phenanthrenes; $C_1\ DBF/C_1\ Phen$ = C_1 -alkylated Dibenzofurans/ C_1 -alkylated Phenanthrenes; $C_1\ DBT/DBT$ = C_1 -alkylated Dibenzothiophenes/Dibenzothiophene; $C_1\ Phen/Phen$ = C_1 -alkylated Phenanthrenes/Phenanthrene; $C_1\ Carb/Carb$ = C_1 -alkylated Carbazoles/Carbazole; $C_2\ Carb$ (Shielded/Exposed)= Shielded/Exposed C_2 -alkylated Carbazoles (1,3-, 1,6-, 1,7, 1,4-, 1,5-Dimethylcarbazole)/(2,7-, 2,4-, 2,5-Dimethylcarbazole); BC ratio= Benzocarbazoles Ratio.

6. Results

Reservoir



Shale



6. Results

Fig. 43. Exemplary ion chromatograms of a selected source (K012472) vs. a carrier bed sample (K012469) for expulsion scenario F. The ion chromatograms shown comprise alkanes (m/z 85), hopanes (m/z 191), steranes (m/z 217), methyl dibenzofurans (m/z 182), methylphenanthrenes (m/z 192), methyl dibenzothiophenes (m/z 198), triaromatic steroids (m/z 231), methylcarbazoles (m/z 181), C₂-alkylated carbazoles (m/z 195), and benzocarbazoles (m/z 217). See Fig. 33 for peak numbers. Peak identification can be found in Table 5.

contrast, tendentially lower values in the carrier interval point to an enrichment of phenanthrenes. An inverse pattern is observable for the C₁ DBF/C₁ Phen, as well as the C₁ DBF/C₁ DBT ratio, which both maximize in the reservoir unit. In particular, the carrier bed seems to be enriched in dibenzofurans, whereas, on the other hand, the shaly parts of the section appear to be depleted in these oxygen-substituted aromatics. As in the scenarios before, the ensuing four diagrams that are displayed in Fig. 42 comprise the ratios of methylated phenanthrenes, dibenzothiophenes, dibenzofurans, and carbazoles against their non-methylated analogs. With respect to the phenanthrenes, the data extend from 2.86 to 3.41. The highest values of 3.07-3.41 were calculated in the reservoir unit. By contrast, the C₁ Phen/Phen ratio is, with an average value of 2.88, frequently lower in the source rock samples. Regarding the data for the dibenzothiophenes, values between 7.03 and 13.42 were calculated. Similar to the phenanthrenes before, the highest value was determined in the reservoir interval. However, compared to the phenanthrenes, the trendline for the C₁ dibenzothiophenes is overall more variable. Concerning the distribution pattern of methylated dibenzothiophenes in general (Fig. 43), it is in both shales and reservoir unit clearly dominated by the 4-isomer. This is equally the case in the previous expulsion scenario E. Conversely, when looking at the curve of methylated against non-methylated dibenzofurans an opposite trend is visible. For this graph, the data totally range from 4.83 to 8.44, whereby, remarkably, the lowest value was determined in the reservoir section. By contrast, the data are mostly higher in the shales and average at around 7.39. For the carbazoles, the corresponding C₁ Carb/Carb ratio reaches values of 2.16 to 3.89. As the C₁ Phen/Phen and the C₁ DBT/DBT ratio, the C₁ Carb/Carb ratio also tends to be higher in the reservoir unit than in the surrounding shales. A very similar trend was documented for the ratio of shielded against exposed C₂ carbazoles, which falls in an area between 4.01 and 7.60. Remarkably, the two highest values were calculated in the carrier interval. For the shales, the ratio is generally lower and averages at 5.33, which is 2.03 units lower than the mean value of the reservoir layer (7.36). The benzocarbazoles ratio is again the last trend that is shown in Fig. 42. For expulsion scenario F, the BC ratio is in the order of 0.35 to 0.62 and displays a large

6. Results

variability over the profile. Thereby, on average higher values were calculated for the carrier interval (0.61) than for the source strata (0.49).

Fig. 43 compares the molecular geochemical signatures of a source rock sample from the lower half of the profile vs. a sample from the reservoir unit. Although the patterns look essentially similar, two vital differences exist. First, the *n*-alkane signature of the reservoir unit is fundamentally different to that of the source rock. More specifically, the carrier bed shows a slightly bimodal *n*-alkane signature with significant proportions of long-chain *n*-alkanes between nC_{20} and nC_{30} , whereas the *n*-alkane distribution of the shale sample is unimodal and dominated by short-chain compounds. Second, C_2 -alkylated carbazoles occur in greater abundance in the shale than in the reservoir strata. No major differences exist in the distribution patterns of hopanes (almost absent), steranes, methyl dibenzofurans, methylated phenanthrenes, methyl dibenzothiophenes, triaromatic steroids, C_1 carbazoles and benzocarbazoles.

Except for the absence of hopanes, which was in both profiles from well 24/9-1 relatively unexpected, the trends principally fit well with the expectations for this section, as well as the trends observed in the Draupne profiles from quadrant 15. For example, dibenzothiophene seems to be more abundant in the source than in the carrier intervals and the ratio of shielded to exposed C_2 carbazoles is slightly higher in the carrier bed than in the surrounding source rock units. Moreover, as already observed in the sections before, the maturity parameters within the organic-rich shales appear to correlate well with the T_{max} values. However, although not that clear, the molecular maturity parameters again partially contrast in the reservoir units. While the steranes and the triaromatic steroids both point to a slightly lower thermal maturity of the carrier bed petroleum compared to the source rock bitumen, the MPI 1, by contrast, suggests equal or even marginally greater thermal maturity. Another remarkable finding is that, except for the C_1 DBF/DBF trend, the carrier bed again shows the tendency to be enriched in alkylated vs. non-alkylated compounds.

34/7-23 A (expulsion scenario G)

Fig. 44 summarizes the most important molecular geochemical depth profiles of expulsion scenario G and therefore the first section of quadrant 34 located in the northern part of the Viking Graben. Fig. 45 shows corresponding ion chromatograms for a selected shale vs. a reservoir sample. The first ratio that is shown is again the

6. Results

nC_{17}/Pr ratio, which for this expulsion scenario is in the magnitude of 0.69 to 1.99. Regarding the trendline, significantly higher nC_{17}/Pr values were calculated in the sandstone than in the shaly part of the section. In particular, an average difference of 0.82 was calculated between the basal, shaly part (0.99) and the reservoir unit at the top (1.81). Values calculated in the heterolithic middle section principally resemble those of the reservoir. With respect to the C_{30} diahopane ratio, a slight zigzag pattern is observable over the profile. In total, the values for this ratio range from 0.06 to 0.12 and are hence comparatively low. However, on average higher values were calculated for the sandstone unit (0.12) than for the black shale samples (0.09). The heterolithic part in the center exhibits an intermediate signal. Concerning the triaromatic steroid ratio, the data fluctuate between 0.05 and 0.25, whereby the lowest values were calculated in the source rock section in the lower half profile and the highest values were obtained in upper part of the heterolithic middle section and the sandstone reservoir at the top. Note that, interestingly, the $TA(I)/TA(I + II)$ ratio of the two uppermost heterolithic samples is higher than in the overlying reservoir. A similar shaped data curve is visible for the MPI 1, which totally ranges between 0.28 and 0.62. As for the triaromatic steroid ratio, the overall highest values were calculated in the sandstone reservoir at the top of the section, while, in contrast, the lowest values are reached in the organic-rich shales in the lower half of the profile. Except for one outlier, intermediate values were calculated in the heterolithic zone in the center. There is an average difference of 0.19 between the mean MPI 1 of the reservoir (0.60) and the shale interval (0.41). An inverse image is visible for the 9-/1-MPhen curve, which scatters between 1.30 and 1.68 and maximizes in the source rock strata. From here, the 9-/1-MPhen ratio gradually decreases towards the top of the section, where an average value of 1.33 was determined in the sandstone reservoir, which is around 0.26 lower than in the organic-rich shales (1.59). Values calculated for the heterolithic part principally correspond to those of the sandstone samples. Concerning the ratio of methylated dibenzothiophenes against methylated phenanthrenes, considerably higher values were found in the source than in the reservoir section of scenario G. In particular, the data totally extend from 0.29 to 0.85 and average at 0.74 in the shale package and 0.34 in the superimposing sandstone reservoir. The heterolithic unit, with a mean value of 0.44, again represents a

6. Results

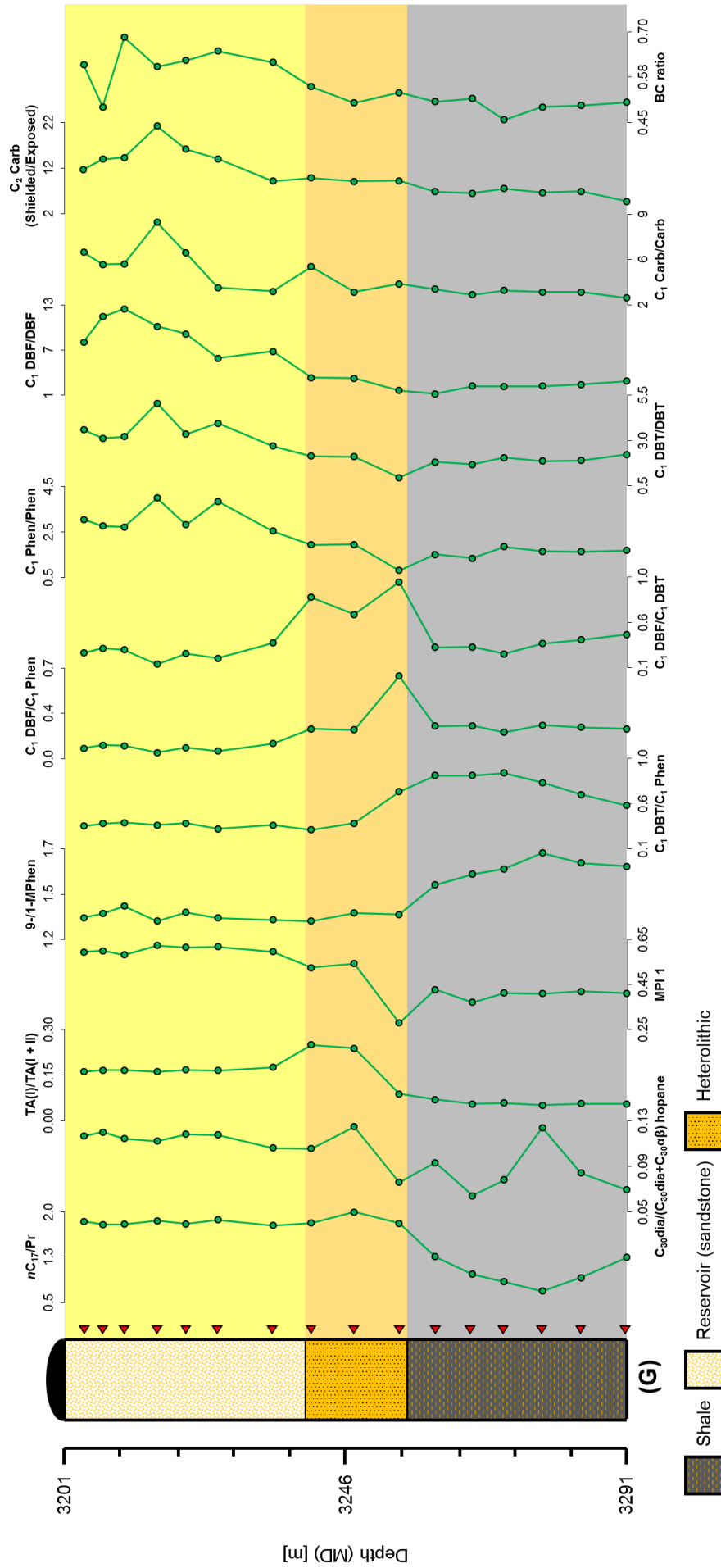
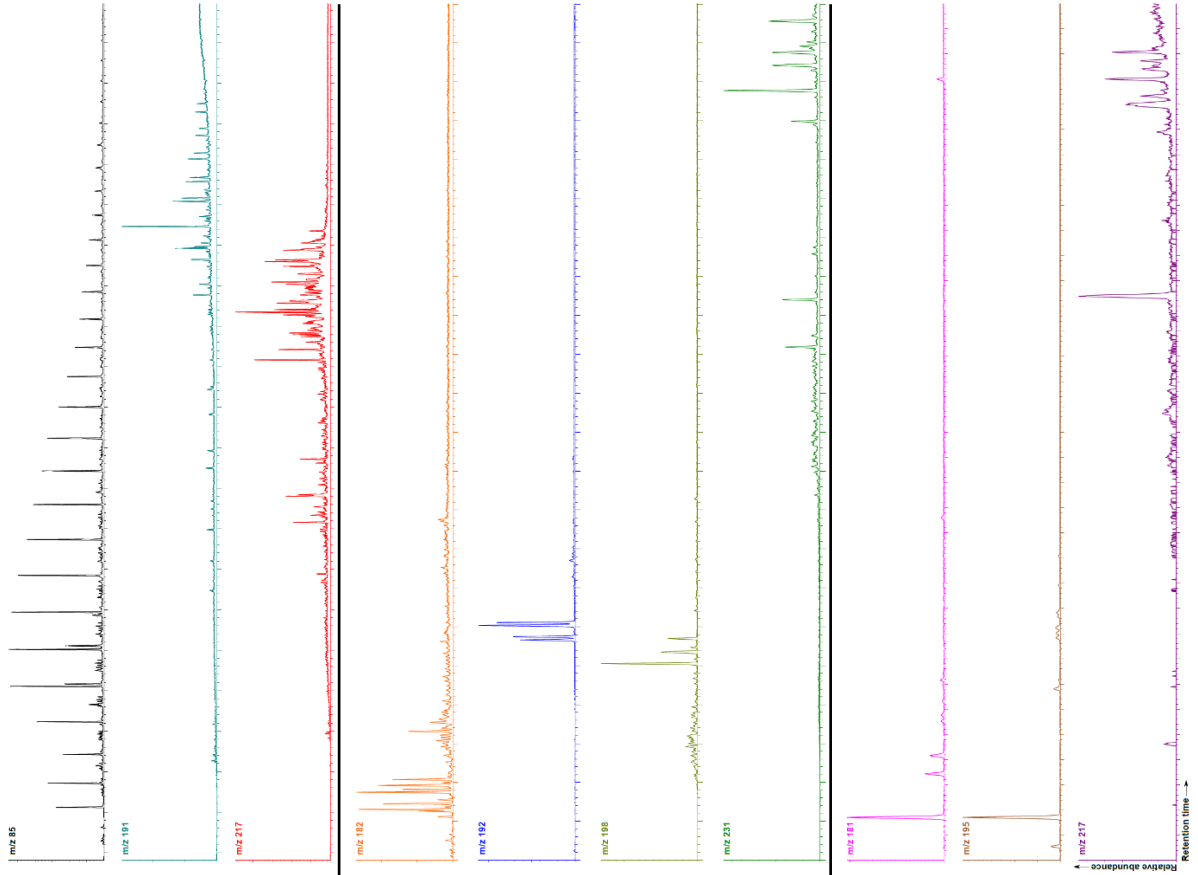


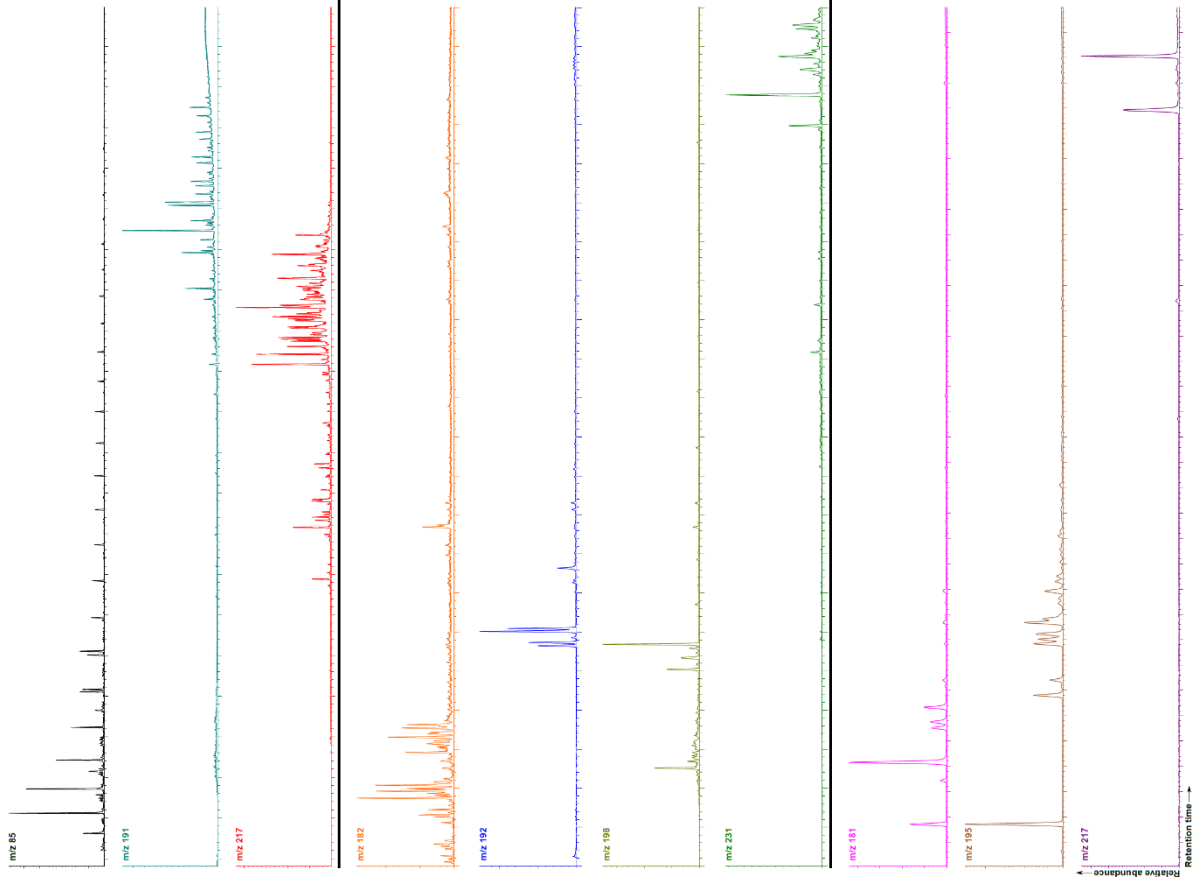
Fig. 44. Selected molecular geochemical depth profiles of expulsion scenario G, North Sea well 34/7-23 A, 3201-3291 m drilling depth. The depth is given as measured depth (MD), but corresponds to a true vertical depth (TVD) of only ~2619.5-2678 m. One tick on the depth axis represents 9 m. Abbreviations: nC_{17}/Pr = *n*-Heptadecane/Pristane; $C_{30}dia/(C_{30}dia+C_{30}q\beta)$ = C_{30} Diahopane/(C_{30} Diahopane+ C_{30} Hopane); $TA(I)/TA(I+II)$ = Short-/Long-Chain Triaromatic Steroid Ratio ($(C_{20}+C_{21})/(C_{20}+C_{21}+C_{26}+C_{27}+C_{28})$); MPI 1= Methylphenanthrene Index; 9-1-MPhen= 9-Methylphenanthrene/1-Methylphenanthrene; $C_1,DBT/C_1,Phen$ = C_1 -alkylated Dibenzofurans/ C_1 -alkylated Phenanthrenes; $C_1,DBF/C_1,Phen$ = C_1 -alkylated Dibenzofurans/Dibenzothiophenes/Phenanthrene; $C_1,Phen/Phen$ = C_1 -alkylated Phenanthrenes/Phenanthrene; $C_1,DBT/DBT$ = C_1 -alkylated Dibenzofurans/Dibenzothiophenes; $C_1,DBF/DBF$ = C_1 -alkylated Dibenzofurans/Dibenzofuran; $C_1,Carb/Carb$ = C_1 -alkylated Carbazoles/Carbazole; $C_2,Carb$ (Shielded/Exposed)= Shielded/Exposed C_2 -alkylated Carbazoles (1,3-, 1,6-, 1,7-, 1,4-, 1,5-Dimethylcarbazole)/(2,7-, 2,4-, 2,5-Dimethylcarbazole); BC ratio= Benzocarbazoles Ratio.

6. Results

Reservoir



Shale



6. Results

Fig. 45. Exemplary ion chromatograms of a selected source (K011224) vs. a carrier bed sample (K011216) for expulsion scenario G. The ion chromatograms shown comprise alkanes (m/z 85), hopanes (m/z 191), steranes (m/z 217), methyl dibenzofurans (m/z 182), methylphenanthrenes (m/z 192), methyl dibenzothiophenes (m/z 198), triaromatic steroids (m/z 231), methylcarbazoles (m/z 181), C₂-alkylated carbazoles (m/z 195), and benzocarbazoles (m/z 217). See Fig. 33 for peak numbers. Peak identification can be found in Table 5.

transition zone. Note that the two uppermost samples display data very close to the reservoir samples, whereas, by contrast, the lowermost heterolithic sample exhibits a signal that resembles that of the source rock lithology. Regarding the same ratio with methylated dibenzofurans, the values are in the order of 0.05 to 0.64. Excluding one outlier in the center, the data curve is very similar to that of the C₁ DBT/C₁ Phen ratio. Indeed, the values maximize in the source rock section at the bottom of the profile and become smallest in the sandstone section at the top. Remarkably, the heterolithic middle section this time rather bears resemblance to the source than to the sandstone unit. The differences between the source and reservoir unit are much smaller in the C₁ DBF/C₁ DBT ratio, which ranges from 0.14 to 0.95 and is reproducibly highest in the heterolithic part in the middle of the profile. However, although the absolute differences are smaller than for the previous ratios, the C₁ DBF/C₁ DBT ratio remains on average slightly higher in the source (0.33) than in the sandstone strata (0.25). Inverse trends can be observed for the following four ratios of C₁ Phen/Phen, C₁ DBT/DBT, C₁ DBF/DBF, and C₁ Carb/Carb, where the highest values were always calculated for the sandstone reservoir. With respect to the C₁ Phen/Phen ratio, the data plot between 0.80 and 3.98 and average at 1.60 in the source and 3.09 in the reservoir strata, indicating the reservoir is enriched in methylated relative to non-methylated phenanthrenes. An identical trend is evident for the C₁ DBT/DBT ratio, which is in the order of 0.94 to 5.06. Equivalent to the phenanthrenes, the reservoir is clearly enriched in methylated over non-methylated dibenzothiophenes. In addition, there is also a strong agreement with the C₁ DBF/DBF curve (1.18-12.46), which straightly increases from the source rock towards the sandstone section. Therefore, the data suggest, similar to the trends before, that the reservoir unit is significantly enriched in methylated dibenzofurans. The same is true for the ratio of methylated against non-methylated carbazoles, for which average values of 2.92 and 5.29 were calculated for the shale and the sandstone strata, respectively. The heterolithic section again represents a transition zone, whereby the uppermost sample principally resembles the reservoir and the two lowermost samples basically reflect the signature of the source rock. Concerning the ratio between shielded and exposed dimethylcarbazoles, the values

6. Results

calculated for expulsion scenario G range from 4.72 to 21.21. Thereby, analogous to the methylated vs. non-methylated trends shown before, tendentially higher values were observed for the sandstone than for the source rock samples. This is reflected by a slight increase of the curve from the source towards the reservoir section. Intermediate values were calculated for the heterolithic middle part. With respect to the last ratio shown in Fig. 44, the benzocarbazoles ratio, which varies between 0.46 and 0.65, continuously lower values were determined in the source than in the reservoir unit. Except for one outlier in the upper half of the reservoir, only values exceeding 0.60 were calculated for the sandstones. Note, however, that for the sandstone samples the error of the BC ratio is very high, due mainly to a very low abundance of benzocarbazoles that causes a large integration uncertainty (Fig. 45). In contrast, highly reliable data was obtained for the shale samples, in which benzocarbazoles are very abundant (Fig. 45) and the BC ratio is, with an average of 0.50, relatively constant.

Regarding explicitly the molecular geochemical signatures of a source rock vs. a reservoir sample (Fig. 45), a number of remarkable differences exist. Apart from a different *n*-alkane signature, which is for the reservoir sample clearly shifted towards longer chain lengths, the most conspicuous difference between the two samples is the S-R isomerization pattern of the C₃₁ to C₃₅αβ hopanes. While the configuration in the source rock sample is dominated by the R-isomer, the isomerization in the reservoir sample favors the S-isomer. Furthermore, source and reservoir samples display different Ts/Tm ratios. In particular, the Tm isomer is much more abundant in the source than in the reservoir unit, resulting in overall higher Ts/Tm ratios in the sandstone section. Concerning the distribution of aromatics, methyldibenzofurans are overall much less abundant in the reservoir than in the source rock sample, the reservoir section contains greater proportions of 3- and 2-methylphenanthrene compared to the black shale part, the methyldibenzothiophenes are dominated by the 1-isomer in the shaly and by the 4-isomer in the reservoir strata, and short-chain triaromatic steroids occur in higher abundance in the reservoir than in the shale package. Similar huge differences are visible in the distribution of carbazoles. While the reservoir is significantly depleted in methylcarbazoles, C₂-alkylated carbazoles, as well as benzocarbazoles, all of these compounds occur in greater quantities in the source rock sample. Moreover, ratios between compounds from all fractions can significantly deviate, as already indicated by the molecular geochemical depth profiles shown before in Fig. 44.

6. Results

As expected from the very low T_{\max} values, the molecular geochemical maturity indicators point for this section to a relatively low thermal maturity of the source rock bitumen. It is therefore remarkable that the reservoir unit exhibits a significantly higher maturity signal, which could indicate a different source. Hence, considering the low thermal maturity of the source rock, the strong compositional differences between source bitumen and reservoir petroleum were not completely unexpected. Note, however, that the reservoir unit is again enriched in alkylated vs. non-alkylated compounds and nitrogen-shielded over nitrogen-exposed C_2 carbazoles, which fits well with the reservoir trends documented in most previous sections. Besides, it is also interesting that the molecular maturity parameter in the reservoir are this time consistent and the source rock column appears to be enriched in dibenzothiophenes and dibenzofurans.

34/7-23 S (expulsion scenario H)

Fig. 46 and Fig. 47 show the most important molecular geochemical data of the penultimate expulsion scenario, section H. Again, Fig. 46 first illustrate the most essential depth plots, while Fig. 47 subsequently shows the corresponding ion chromatograms for a selected source vs. a reservoir sample. Regarding first the nC_{17}/Pr ratio, the data totally range from 0.65 to 1.54. Remarkably, the three highest values were calculated for the carrier bed, whereas, on the other hand, the nC_{17}/Pr ratio plots mostly below 1.00 in the shaly parts of the profile. Thus, the sandstone interval seems to be enriched in n -alkanes relative to isoprenoids compared to the surrounding shale packages. The next diagram that is shown comprises the C_{30} diahopane ratio. Similar to the source rock zone of scenario G, the C_{30} diahopane ratio of scenario H is correspondingly low and fluctuates between 0.06 and 0.09. Indeed, only insignificant quantities of C_{30} diahopane were detected in both shale and reservoir samples of this section (Fig. 47). Except for one outlier in the lower part of the sandstone interval, the C_{30} diahopane ratio indicates no major differences between source and reservoir strata. With respect to the ratio of short- vs. long-chain triaromatic steroids, expulsion scenario H exhibits very low values ranging from 0.05 to 0.07, which are in good agreement with those calculated for the source rock unit of the previous section. As evident from the ion chromatograms shown in Fig. 47, such

6. Results

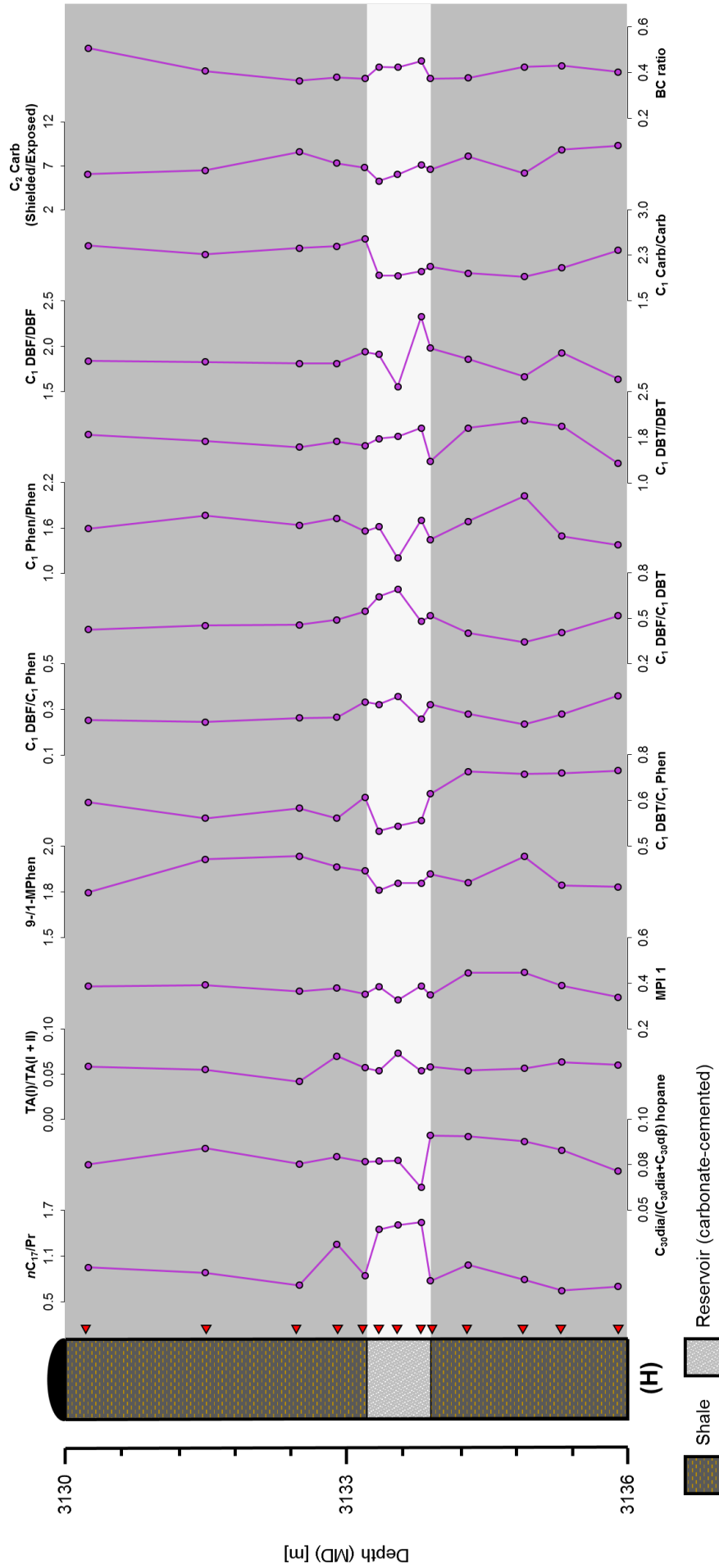
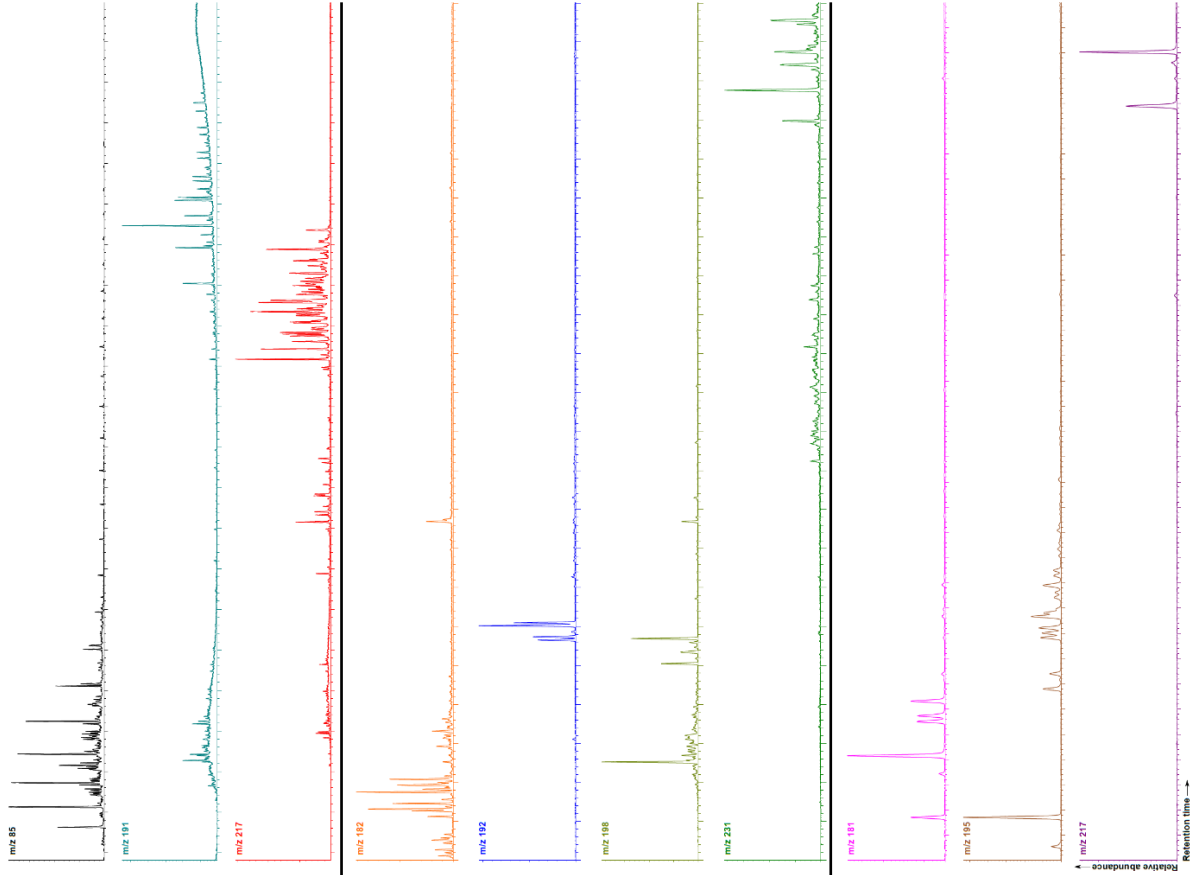


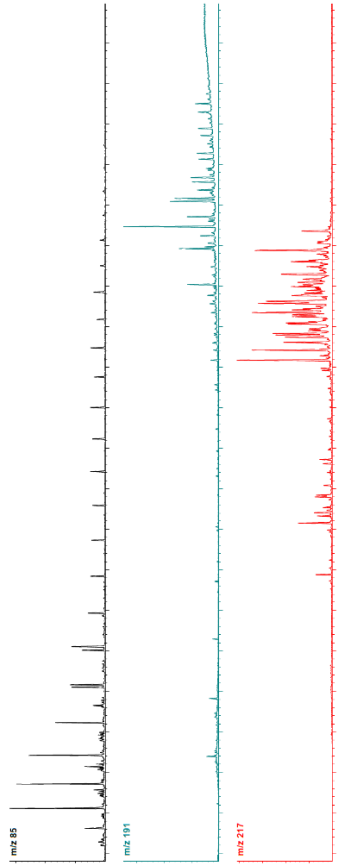
Fig. 46. Selected molecular geochemical depth profiles of expulsion scenario H, North Sea well 34/7-23 S, 3130-3136 m drilling depth. The depth is given as measured depth (MD), but corresponds to a true vertical depth (TVD) of only ~2652.6-2659.3 m. One tick on the depth axis represents 0.6 m. Abbreviations: nC_{17}/Pr = *n*-Heptadecane/Pristane; $C_{30dial}/(C_{30dial}+C_{30df})$ = C_{30} Diahopane/ C_{30} Diahopane+ C_{30} Hopane); $TA(I)/TA(I+II)$ = Short-/Long-Chain Triaromatic Steroid Ratio ($(C_{20}+C_{21})/(C_{20}+C_{21}+C_{26}+C_{27}+C_{28})$); $MPI1$ = Methylphenanthrene Index; $9-/1-MPhen$ = 9-Methylphenanthrene/1-Methylphenanthrene; $C_1 DBT/C_1 Phen$ = C₁-alkylated Dibenzofurans/C₁-alkylated Phenanthrenes; $C_1 DBF/C_1 Phen$ = C₁-alkylated Dibenzofurans/Phenanthrenes; $C_1 DBT/DBT$ = C₁-alkylated Dibenzofurans/Dibenzothiophenes; $C_1 DBF/DBT$ = C₁-alkylated Dibenzofurans/Dibenzothiophenes; $C_1 Phen/Phen$ = C₁-alkylated Phenanthrenes/Phenanthrene; $C_1 DBT/DBT$ = C₁-alkylated Dibenzofurans/Carbazole; $C_2 Carb$ (Shielded/Exposed) = Shielded/Exposed C₂-alkylated Carbazoles (1,3-, 1,6-, 1,7-, 1,4-, 1,5-Dimethylcarbazole)/(2,7-, 2,4-, 2,5-Dimethylcarbazole); BC ratio = Benzocarbazoles Ratio.

6. Results

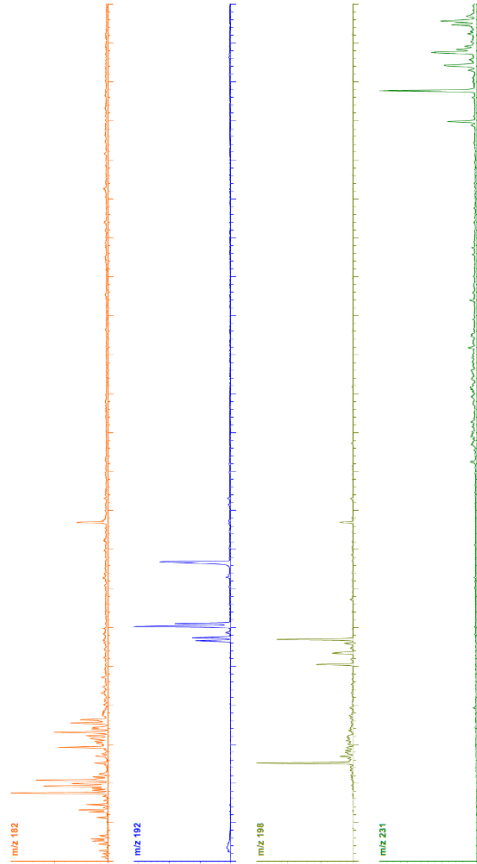
Reservoir



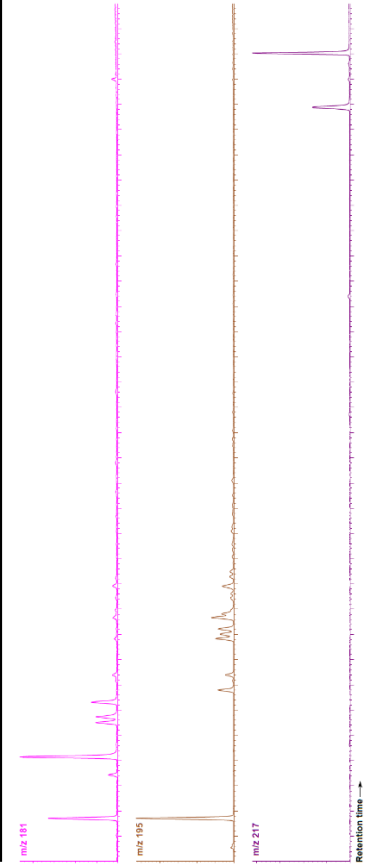
Aliphatics



Aromatics



Carbazoles



Shale

6. Results

Fig. 47. Exemplary ion chromatograms of a selected source (K011201) vs. a carrier bed sample (K011205) for expulsion scenario H. The ion chromatograms shown comprise alkanes (m/z 85), hopanes (m/z 191), steranes (m/z 217), methyl dibenzofurans (m/z 182), methylphenanthrenes (m/z 192), methyl dibenzothiophenes (m/z 198), triaromatic steroids (m/z 231), methylcarbazoles (m/z 181), C₂-alkylated carbazoles (m/z 195), and benzocarbazoles (m/z 217). Remnants of sulfur are visible in the m/z 192 ion chromatogram of the shale sample. See Fig. 33 for peak numbers. Peak identification can be found in Table 5.

low values indicate only marginal amounts of short-chain triaromatic steroids, which face large quantities of equivalent long-chain components. No significant differences in the TA(I)/TA(I + II) ratio exist between source rock and reservoir samples. The same applies for the MPI 1, which, for this section, varies between 0.33 and 0.45. Indeed, average values of 0.38 for the shale samples and 0.37 for the reservoir bed suggest negligible differences in the MPI 1 between source rock samples and carrier interval. If regarding only the ratio between the 9- and the 1-methylphenanthrene isomers, a slightly different trend is apparent. For this graph, which ranges in total from 1.75 to 1.94, the average lowest values (1.78) were identified in the carrier unit. By contrast, the source rock samples exhibit a mean signal of 1.85, which is slightly higher. Yet, the differences are very small, especially in comparison to the lower half of the profile. The following curve compares the relative amounts of methyl dibenzo-thiophenes and methylphenanthrenes (0.50-0.70). Similar to the expulsion scenarios before, frequently higher values were monitored in the source units than in the reservoir interval. Thereby, particularly high values were calculated for the lower shale unit. The severe decrease of the C₁ DBT/C₁ Phen ratio in the carrier bed clearly suggest the enrichment of methylated phenanthrenes and, conversely, depletion of methyl dibenzothiophenes. A less pronounced tendency is discernable for the ensuing C₁ DBF/C₁ Phen ratio, which for this expulsion scenario lies in a relatively small range between 0.23 and 0.36. Although the trendline slightly increases towards the carrier bed, the differences between the C₁ DBF/C₁ Phen ratio of the shales and the reservoir are very small. A similar but clearer trend is evident for the C₁ DBF/C₁ DBT ratio, which extends from 0.34 to 0.69. For this ratio, high values in the carrier bed indicate enrichment of methyl dibenzofurans relative to methylated dibenzothiophenes. Analogous to the previous figures, the following four trends display the ratios of methylated vs. non-methylated phenanthrenes (1.20-2.02), dibenzothiophenes (1.35-2.02), dibenzofurans (1.56-2.32), and carbazoles (1.89-2.52). Concerning the C₁ Phen/Phen ratio, the data maximize in the lower half of the profile, whereas it remains fairly constant in the rest of the section, including the reservoir horizon. This is in contrast to most previous expulsion scenarios, in which the reservoir units frequently showed a clear enrichment

6. Results

of methylated phenanthrenes. Likewise, there are no big differences in the C₁ DBT/DBT ratio of the shales compared to that of the reservoir unit. With respect to the following dibenzo-furan data curve, a zigzag pattern is recognizable within the reservoir interval. Thus, also no selective enrichment of either methylated dibenzofuran or dibenzofuran in the carrier bed is ascertainable. The subsequent C₁ Carb/Carb plot can roughly be divided into two parts: (1) an upper half with relatively high C₁ Carb/Carb values, and (2) a lower part including the reservoir unit that displays comparatively low C₁ Carb/Carb values. Thereby, interestingly, the data of the carrier bed closely resemble that of the lower black shale package. Therefore, as for the methylated vs. non-methylated diagrams described before, also no clear differences between source rock and reservoir samples were revealed for the C₁ Carb/Carb ratio. Furthermore, the same applies to the ratio of shielded vs. exposed dimethylcarbazoles, which plots between 5.22 and 9.28, but remains relatively constant over the profile. Slight differences between the carrier bed and the surrounding shales were, however, found for the benzocarbazoles ratio. For scenario H, the BC ratio reaches orders of 0.36 to 0.51 and is therefore quite variable, even over only around six meters of profile. Thereby, slightly higher BC ratios were calculated for the reservoir unit than for the shale samples, suggesting a somewhat higher abundance of benzo[a]- compared to benzo[c]carbazole in the carrier bed, which is indeed visible in Fig. 47.

However, Fig. 47 shows that the molecular geochemical signatures of the source and the reservoir unit are very similar, which is in strong contrast to scenario G (Fig. 45), where the signatures of the source and the reservoir section were fundamentally different.

Again, as already expected from the T_{max} data, the molecular geochemical maturity parameters of this section point to a very low thermal maturity of the source bitumen. Therefore, active petroleum generation and expulsion can principally be ruled out. Though, a very interesting observation is that the sandstone interval yet contains a hydrocarbon phase, whose composition is similar to that of the the adjacent source bitumen. Despite the low thermal maturity, this could point to an origin from the surrounding shales, which is supported by the intra-formational character of the reservoir unit that largely precludes filling by externally sourced petroleum. It is also quite interesting that the benzocarbazoles ratio is that low in most parts of the section and the reservoir units do not seem to be enriched in alkylated over non-alkylated

6. Results

compounds, which was observed in most previous sections. Note also that the molecular maturity parameters are in good accordance with each other, which, considering the trends in the previous profiles, is not something to be taken for granted.

34/10-36 (expulsion scenario I)

The most meaningful molecular geochemical depth profiles of expulsion scenario I are shown below in Fig. 48. Corresponding exemplary ion chromatograms of a source rock and a reservoir sample are subsequently illustrated in Fig. 49. Note that the reservoir sample is biodegraded, which may tremendously influence molecular geochemical parameters. Concerning the nC_{17}/Pr ratio, the data range from 0.56 to 1.09, whereby the highest value was calculated in the reservoir unit. If regarding only the source rock column, the data display a much smaller range and average at 0.66. Since alkanes are particularly susceptible to biodegradation (e.g. Peters et al. 2005b), it can be assumed that the nC_{17}/Pr ratio of the reservoir unit is heavily influenced by microorganisms and therefore does not reflect an original signal. Regarding the ensuing C_{30} diahopane ratio, the data are in the magnitude of 0.06 to 0.09, which is comparable to the values determined in source rock material from scenario G and H. The lowest value of 0.06 was calculated in the reservoir sample, which, however, is probably also significantly affected by biodegradation, as indicated by the “hump” in the corresponding hopane signature (m/z 191) (Fig. 49). The average value of the source rock material is 0.08. With respect to the short- against long-chain triaromatic steroid ratio, the data of scenario H altogether vary between 0.05 and 0.19, whereby the elevated value in the reservoir is likely also an artifact related to biodegradation. In general, short-chain triaromatic steroids occur only in low abundance (Fig. 49). For the source rock material, this results in an average $TA(I)/TA(I + II)$ ratio of 0.06, which is very similar to the $TA(I)/TA(I + II)$ data of source rock material from scenario G and H. An equivalently-shaped curve is observable for the MPI 1 (0.42-0.46), which is relatively constant in the source unit and then sharply increases to the maximum value in the small carrier interval. Similar to the previous trends, the MPI 1 value of the reservoir sample can be expected to be influenced by biodegradation. Regarding next the diagram of 9- to 1-methylphenanthrene, the data scatter between 1.21 and 1.37. In this plot, differences between source and reservoir

6. Results

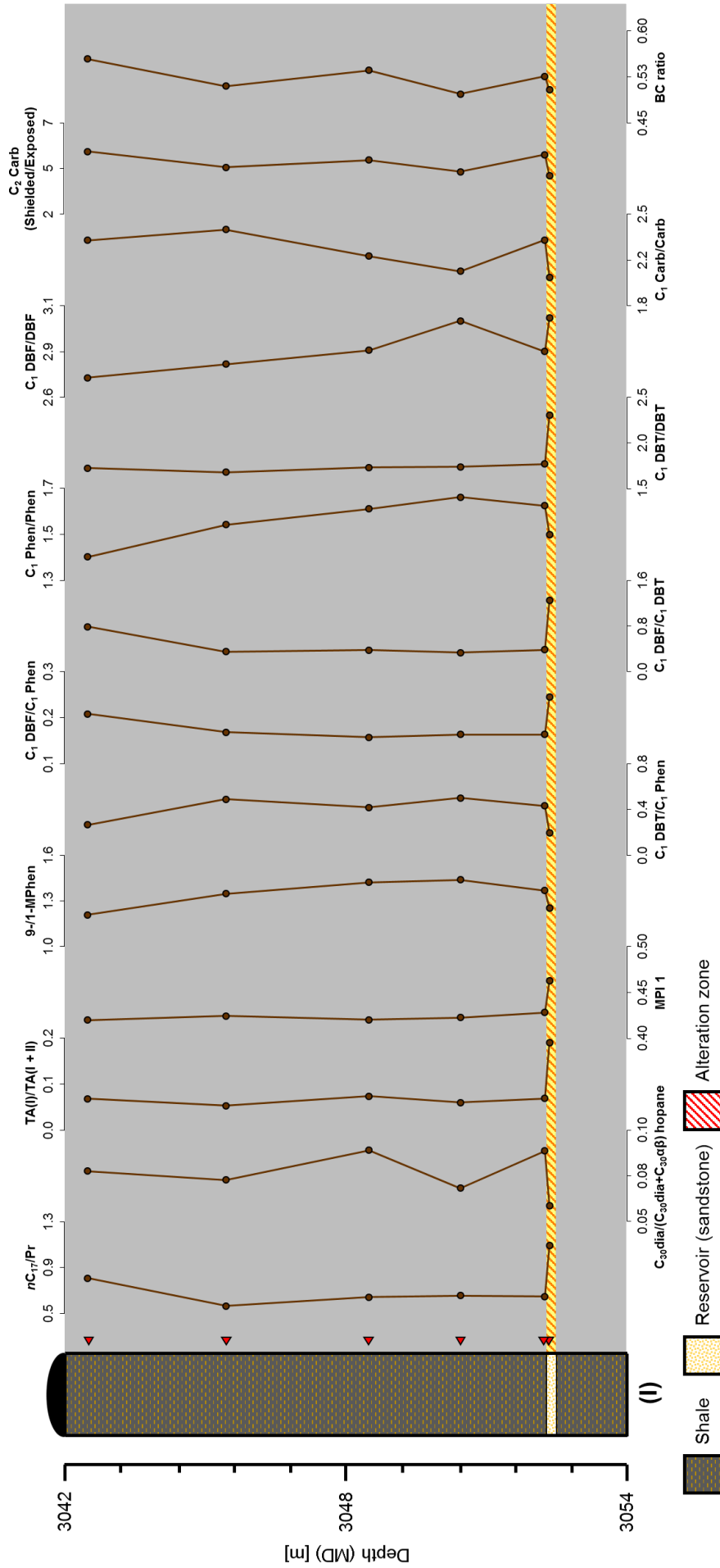
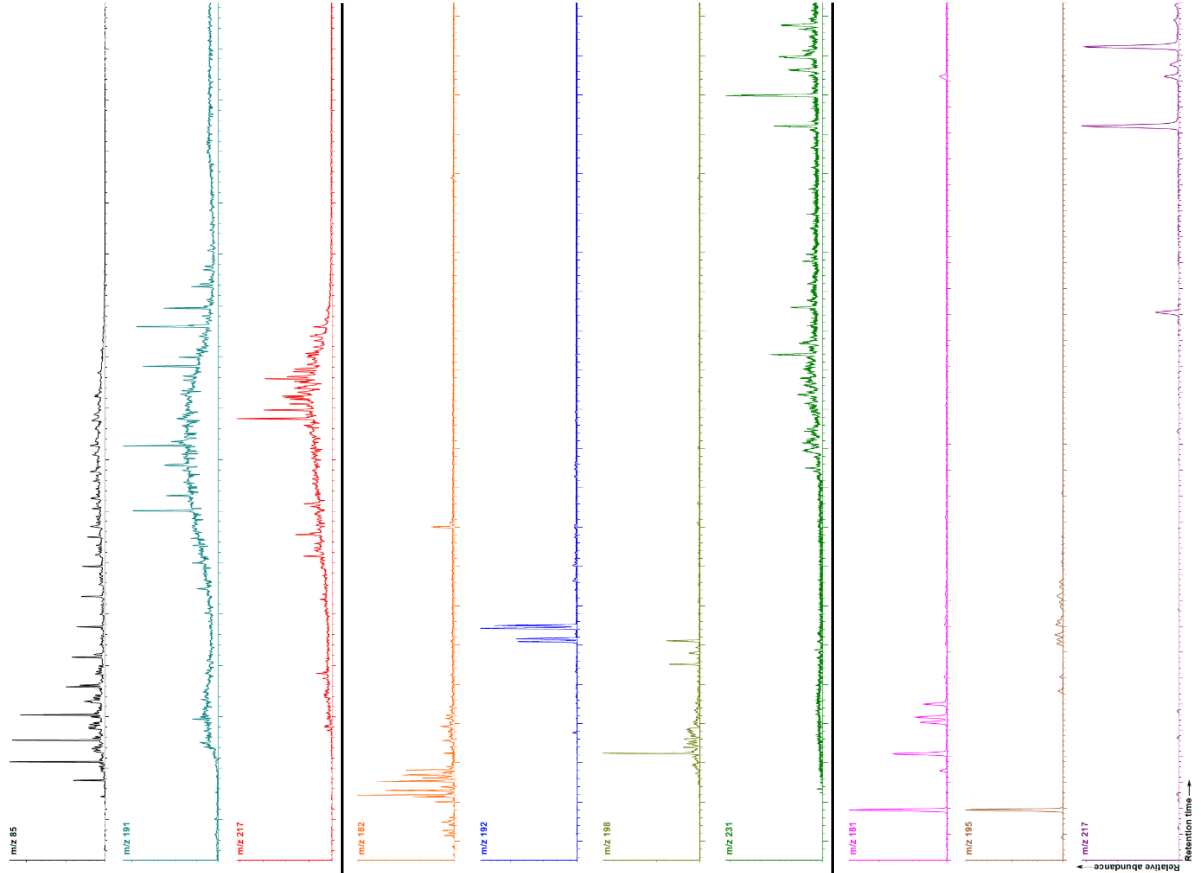


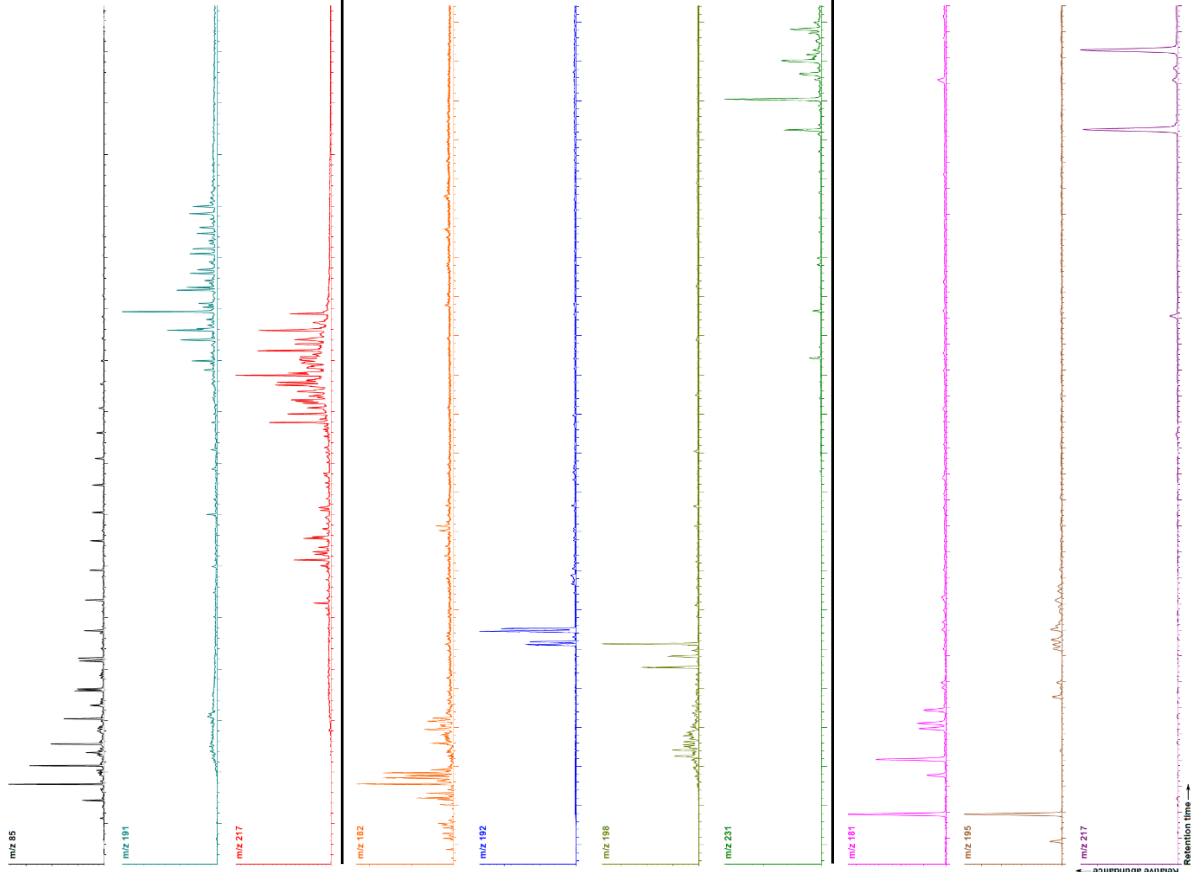
Fig. 48. Selected molecular geochemical depth profiles of expulsion scenario I, North Sea well 34/10-36, 3042-3054 m drilling depth. The depth is given as measured depth (MD) and comparable to the true vertical depth (TVD). One tick on the depth axis represents 1.2 m. Abbreviations: nC_{17}/Pr = *n*-Heptadecane/Pristane; $C_{30dia}/(C_{30dia}+C_{30df})$ = C_{30} Diahopane/ C_{30} Diahopane+ C_{30} Hopane); $TA(I)/TA(I+II)$ = Short-/Long-Chain Triaromatic Steroid Ratio ($(C_{20}+C_{21})/(C_{20}+C_{21}+C_{26}+C_{27}+C_{28})$); MPI 1= Methylphenanthrene Index; 9-/1-MPhen= 9-Methylphenanthrene/1-Methylphenanthrene; $C_1 DBT/C_1 Phen$ = C_1 -alkylated Dibenzofurans/ C_1 -alkylated Phenanthrenes; $C_1 DBF/C_1 Phen$ = C_1 -alkylated Dibenzofurans/ C_1 -alkylated Phenanthrenes; $C_1 DBT/DBT$ = C_1 -alkylated Dibenzofurans/ C_1 -alkylated Dibenzofurans; $C_1 DBF/DBF$ = C_1 -alkylated Dibenzofurans/ C_1 -alkylated Dibenzofurans; $C_1 Carb/Carb$ = C_1 -alkylated Carbazoles/Carbazole; $C_2 Carb$ (Shielded/Exposed)= Shielded/Exposed C_2 -alkylated Carbazoles (1,3-, 1,6-, 1,7, 1,4-, 1,5-Dimethylcarbazole)/(2,7-, 2,4-, 2,5-Dimethylcarbazole); BC ratio= Benzocarbazoles Ratio.

6. Results

Reservoir



Shale



6. Results

Fig. 49. Exemplary ion chromatograms of a selected source (K012480) vs. the only carrier bed sample (K012482) for expulsion scenario I. The ion chromatograms shown comprise alkanes (m/z 85), hopanes (m/z 191), steranes (m/z 217), methyl dibenzofurans (m/z 182), methylphenanthrenes (m/z 192), methyl dibenzothiophenes (m/z 198), triaromatic steroids (m/z 231), methylcarbazoles (m/z 181), C₂-alkylated carbazoles (m/z 195), and benzocarbazoles (m/z 217). See Fig. 33 for peak numbers. Peak identification can be found in Table 5.

unit are comparatively small, even considering biodegradation in the carrier bed. However, the 9-/1-MPhen ratio sharply decreases in the reservoir unit and is lower than the average value of the source package. Looking at the trend of methylated dibenzothiophenes against methylated phenanthrenes, the calculated values totally range between 0.20 and 0.50. Compared to the source package, which exhibits an average value of 0.42, the C₁ DBT/C₁ Phen ratio of the reservoir unit is somewhat lower. Within the source unit, the C₁ DBT/C₁ Phen ratio is subject to only minor variations. Regarding next the C₁ DBF/C₁ Phen ratio, the data plot between 0.16 and 0.24. Similar to the diagrams described before, relatively constant values were obtained in the source strata, whereas the reservoir unit displays a different signal. This time, the ratio considerably increases when reaching the sandstone horizon. Almost the same trend is visible for the subsequent C₁ DBF/C₁ DBT ratio (0.33-1.24). Correspondingly, the data remain pretty constant in the organic-rich shales, and then abruptly increases to the maximum value upon entering the sandstone unit. Concerning the subsequently shown ratio of methylphenanthrenes over phenanthrene, the data for scenario I vary from 1.40 to 1.66 and show an increasing tendency towards the reservoir unit. Yet, in contrast to most previous expulsion scenarios, the ratio suddenly decreases within the sandstone interval. Besides, it is slightly lower (1.50) than the average C₁ Phen/Phen ratio of the shale samples (1.57). With respect to the same ratio but with dibenzothiophenes (1.68-2.31), very constant data were obtained in the shale package, whereas a significantly higher value was calculated for the carrier bed. In contrast to the C₁ Phen/Phen and the C₁ DBT/DBT ratio, the trend for the equivalent ratio with dibenzofurans (2.71-3.03) is shaped more irregular. Although there is a clear increase within the sandstone unit, the value is not fundamentally different to those of the source rock column. Regarding the ratio of methylated carbazoles against carbazole, which falls in a magnitude of 2.02 to 2.38, a similar irregular trend as for the dibenzofurans is apparent. In particular, the difference between the C₁ Carb/Carb ratio of the source rock interval and that of the carrier bed is comparatively small. Nonetheless, the C₁ Carb/Carb ratio shows a clear drop to 2.02 upon reaching the reservoir and is additionally slightly lower than the average value of

6. Results

the source rock material (2.24). Zigzag trends are observable for the last two plots that are presented in Fig. 48, the ratio of shielded vs. exposed C₂-alkylated carbazoles and the benzocarbazoles ratio. For the former diagram, the data totally fluctuate between 4.10 and 5.43, average at 4.91 within the source unit, and minimize in the sandstone carrier horizon. A virtually 1:1 image is observable for the BC ratio, which scatters in a quite narrow range between 0.50 and 0.55. Similar to the previous trend, the difference between source and carrier interval is again very small. However, the BC ratio appears to decrease at the transition from the source column into the reservoir layer and is here marginally lower (0.50) than the mean BC ratio of the organic-rich shales (0.52).

Concerning differences in the ion chromatograms between source bitumen and reservoir extract (Fig. 49), the most obvious variance is, as already stated, clear evidence for biodegradation in the sandstone unit. This is particularly evident in the distribution pattern of hopanes, which is characterized by the presence of an unresolved complex mixture, but also in the *n*-alkane and sterane signatures. The aromatics appear, at first sight, not to be biodegraded but may perhaps also have undergone microbial alteration. Except for the evidence of biodegradation, differences between source and reservoir are comparatively small. However, the source rock sample contains lower quantities of 3- and 2-methylphenanthrene and displays a different methylthiophene distribution pattern, which is clearly dominated by the 1-isomer. The distributions of carbazoles are roughly comparable.

While biodegradation in the sandstone unit was unexpected, the trends mostly fit well with the expectations for this section. More specifically, a low thermal maturity was predictable from the T_{max} values and relatively constant trends were expected for the virtually homogenous source rock column. Because of the low thermal maturity, active petroleum generation and expulsion appear rather unlikely. However, as a hydrocarbon phase is present in the reservoir unit, which is unlikely to originate from an external source or to derive from drilling fluids, the adjacent organic-rich shales could also have expelled a kind of pre-mature petroleum phase into the small sandstone interval. Yet, it is important to point out that due to microbial alteration any molecular geochemical parameters in the carrier unit have to be regarded with caution.

6.2 Geochromatographic experiment

6. Results

After having shown and described the most important data obtained from the natural case histories, part two of the chapter now focuses on the results of the geochromatographic experiment. Essentially, two different approaches were followed: (1) the determination of the elution order, and (2) a mass balance approach using an internal quantification standard.

6.2.1 Compound elution

In total, the geochromatographic experiment lasted 65 days. It was run until only trace amounts of target compounds were left in the eluates. As already mentioned in the material and methods chapter (see 5.4), altogether 32 fractions of 0.8 to 8 ml were collected during this time period. The elution results are presented below in Fig. 50. Table 6 illustrates the compound concentrations over time.

The first fraction that was eluted after around two days contained significant quantities of 2-ethyl dibenzofuran (1.70 $\mu\text{g/ml}$), 9- (1.62 $\mu\text{g/ml}$) and 1-methylphenanthrene (2.24 $\mu\text{g/ml}$), and 4,6- (1.43 $\mu\text{g/ml}$) and 2,8-dimethyldibenzothiophene (1.88 $\mu\text{g/ml}$). Remarkably, carbazoles were not yet detected. In the further course of the

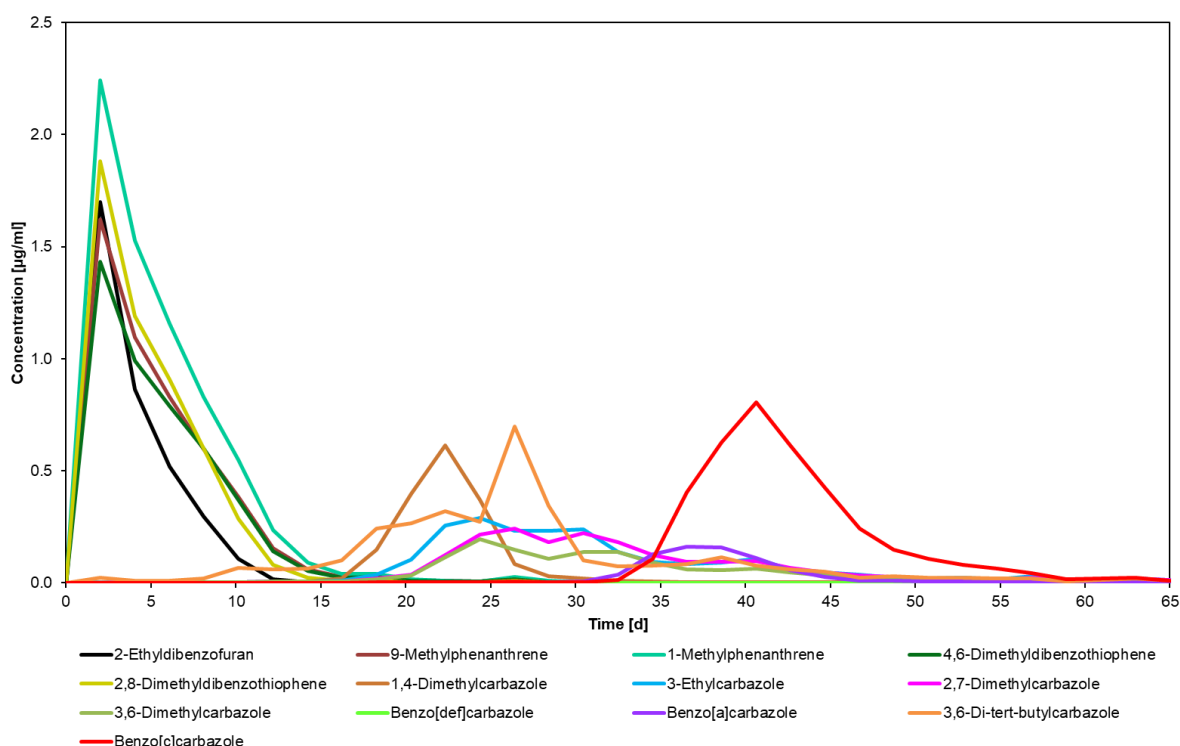


Fig. 50. Concentrations of tracer molecules in the fractions eluted over time. While the ethyldibenzofuran, the phenanthrenes, and the dibenzothiophenes passed the column rapidly, carbazoles were retarded, whereby the partially shielded 1,4-isomer migrated faster than the exposed isomers. Among the benzocarbazoles, benzo[a]- migrated slightly faster than benzo[c]carbazole.

6. Results

Table 6. Tracer concentrations over time

| Eluted Time [d] | 2- volume [ml] | 9- Methylphenanthrene [µg/ml] | 1- Methylphenanthrene [µg/ml] | 4,6- Dimethylidibenzo thiophene [µg/ml] | 2,8- Dimethylidibenzo thiophene [µg/ml] | 1,4- Dimethylcarbazole [µg/ml] | 3- Ethylcarbazole [µg/ml] | 2,7- Dimethylcarbazole [µg/ml] | 3,6- Dimethylcarbazole [µg/ml] | Benzo[def]carbazole [µg/ml] | Benzo[a]carbazole [µg/ml] | 3,6-Di-tert-butylcarbazole [µg/ml] | Benzo[c]carbazole [µg/ml] |
|-----------------|-------------------|----------------------------------|----------------------------------|--|--|-----------------------------------|------------------------------|-----------------------------------|-----------------------------------|-----------------------------|---------------------------|------------------------------------|---------------------------|
| 0 | 0.0 | 0.00 | 0.00 | 0.00 | 0.00 | 0.00 | 0.00 | 0.00 | 0.00 | 0.00 | 0.00 | 0.00 | 0.00 |
| 2 | 1.5 | 1.70 | 2.24 | 1.43 | 1.88 | 0.00 | 0.00 | 0.00 | 0.00 | 0.00 | 0.00 | 0.02 | 0.00 |
| 4 | 0.8 | 0.86 | 1.53 | 0.99 | 1.19 | 0.00 | 0.00 | 0.00 | 0.00 | 0.00 | 0.00 | 0.01 | 0.00 |
| 6 | 1.1 | 0.52 | 1.16 | 0.79 | 0.91 | 0.00 | 0.00 | 0.00 | 0.00 | 0.00 | 0.00 | 0.01 | 0.00 |
| 8 | 1.6 | 0.30 | 0.83 | 0.60 | 0.60 | 0.00 | 0.00 | 0.00 | 0.00 | 0.00 | 0.00 | 0.02 | 0.00 |
| 10 | 2.5 | 0.11 | 0.38 | 0.37 | 0.29 | 0.00 | 0.00 | 0.00 | 0.00 | 0.00 | 0.00 | 0.07 | 0.00 |
| 12 | 1.0 | 0.02 | 0.16 | 0.14 | 0.08 | 0.00 | 0.01 | 0.00 | 0.00 | 0.00 | 0.00 | 0.06 | 0.00 |
| 14 | 4.0 | 0.00 | 0.06 | 0.05 | 0.02 | 0.00 | 0.01 | 0.01 | 0.01 | 0.00 | 0.00 | 0.06 | 0.00 |
| 16 | 2.0 | 0.00 | 0.03 | 0.02 | 0.01 | 0.02 | 0.01 | 0.01 | 0.01 | 0.00 | 0.00 | 0.10 | 0.00 |
| 18 | 1.8 | 0.00 | 0.03 | 0.03 | 0.01 | 0.15 | 0.04 | 0.02 | 0.02 | 0.00 | 0.00 | 0.24 | 0.00 |
| 20 | 2.0 | 0.00 | 0.01 | 0.01 | 0.00 | 0.40 | 0.10 | 0.04 | 0.03 | 0.00 | 0.00 | 0.27 | 0.00 |
| 22 | 1.7 | 0.00 | 0.01 | 0.01 | 0.00 | 0.61 | 0.26 | 0.12 | 0.11 | 0.00 | 0.00 | 0.32 | 0.00 |
| 24 | 1.5 | 0.00 | 0.01 | 0.01 | 0.00 | 0.37 | 0.29 | 0.22 | 0.19 | 0.00 | 0.00 | 0.27 | 0.00 |
| 26 | 1.0 | 0.00 | 0.02 | 0.02 | 0.01 | 0.08 | 0.23 | 0.24 | 0.15 | 0.00 | 0.00 | 0.70 | 0.01 |
| 28 | 1.5 | 0.00 | 0.01 | 0.00 | 0.00 | 0.03 | 0.23 | 0.18 | 0.11 | 0.00 | 0.00 | 0.34 | 0.00 |
| 30 | 1.5 | 0.00 | 0.00 | 0.00 | 0.00 | 0.02 | 0.24 | 0.22 | 0.14 | 0.00 | 0.00 | 0.10 | 0.00 |
| 33 | 2.0 | 0.00 | 0.00 | 0.00 | 0.00 | 0.01 | 0.14 | 0.18 | 0.14 | 0.00 | 0.04 | 0.07 | 0.01 |
| 35 | 1.8 | 0.00 | 0.00 | 0.00 | 0.00 | 0.00 | 0.09 | 0.12 | 0.09 | 0.00 | 0.13 | 0.08 | 0.11 |
| 37 | 2.1 | 0.00 | 0.00 | 0.00 | 0.00 | 0.00 | 0.08 | 0.09 | 0.06 | 0.00 | 0.16 | 0.08 | 0.40 |
| 39 | 0.8 | 0.00 | 0.00 | 0.00 | 0.00 | 0.00 | 0.09 | 0.09 | 0.06 | 0.00 | 0.16 | 0.11 | 0.63 |
| 41 | 2.3 | 0.00 | 0.00 | 0.00 | 0.00 | 0.00 | 0.11 | 0.10 | 0.06 | 0.00 | 0.11 | 0.08 | 0.81 |
| 43 | 1.5 | 0.00 | 0.00 | 0.00 | 0.00 | 0.00 | 0.06 | 0.07 | 0.05 | 0.00 | 0.06 | 0.06 | 0.61 |
| 45 | 2.5 | 0.00 | 0.00 | 0.00 | 0.00 | 0.00 | 0.05 | 0.05 | 0.03 | 0.00 | 0.03 | 0.05 | 0.43 |
| 47 | 2.3 | 0.00 | 0.00 | 0.00 | 0.00 | 0.00 | 0.04 | 0.03 | 0.02 | 0.00 | 0.01 | 0.02 | 0.24 |
| 49 | 1.3 | 0.00 | 0.00 | 0.00 | 0.00 | 0.00 | 0.02 | 0.03 | 0.02 | 0.00 | 0.01 | 0.03 | 0.15 |
| 51 | 3.3 | 0.00 | 0.00 | 0.00 | 0.00 | 0.00 | 0.02 | 0.02 | 0.01 | 0.00 | 0.01 | 0.02 | 0.11 |
| 53 | 4.0 | 0.00 | 0.00 | 0.00 | 0.00 | 0.00 | 0.02 | 0.02 | 0.01 | 0.00 | 0.00 | 0.02 | 0.08 |
| 55 | 4.5 | 0.00 | 0.00 | 0.00 | 0.00 | 0.00 | 0.02 | 0.02 | 0.01 | 0.00 | 0.00 | 0.02 | 0.06 |
| 57 | 4.0 | 0.00 | 0.00 | 0.00 | 0.00 | 0.00 | 0.03 | 0.02 | 0.02 | 0.00 | 0.00 | 0.02 | 0.04 |
| 59 | 3.5 | 0.00 | 0.00 | 0.00 | 0.00 | 0.00 | 0.01 | 0.01 | 0.01 | 0.00 | 0.00 | 0.01 | 0.02 |
| 61 | 5.0 | 0.00 | 0.00 | 0.00 | 0.00 | 0.00 | 0.02 | 0.01 | 0.01 | 0.00 | 0.00 | 0.01 | 0.02 |
| 63 | 6.0 | 0.00 | 0.00 | 0.00 | 0.00 | 0.00 | 0.02 | 0.02 | 0.01 | 0.00 | 0.00 | 0.02 | 0.02 |
| 65 | 8.0 | 0.00 | 0.00 | 0.00 | 0.00 | 0.00 | 0.01 | 0.01 | 0.01 | 0.00 | 0.00 | 0.01 | 0.01 |

6. Results

experiment, the abundance of dibenzofuran, phenanthrenes, and dibenzothiophenes gradually decreased until virtual absence after 15 days. Carbazoles were practically not eluted until day 10, at which the first carbazole in the form of 3,6-di-tert-butylcarbazole was recovered in measurable concentrations. However, the vast majority of the carbazoles passed the column in the time span between day 15 and day 50 and therefore significantly later than the dibenzofuran, phenanthrenes, and dibenzothiophenes. After the 3,6-di-tert-butylcarbazole, the C₂ carbazoles were the next compounds that were identified in the eluates. Thereby, the partially shielded 1,4-isomer migrated slightly faster than the exposed 2,7- and 3,6-isomers, as well as the 3-ethylcarbazole, which eluted more or less simultaneously. Maximum concentrations for the 3,6-di-tert-butylcarbazole, the 1,4-, 2,7- and 3,6-dimethylcarbazole, and the 3-ethylcarbazole were measured after approximately 26, 22, 26, 24, and 24 days, respectively. The highest absolute concentration was determined for the 1,4-dimethylcarbazole, followed by the 3-ethylcarbazole and the 2,7- and 3,6-dimethylcarbazoles. Benzocarbazoles were not detected until around day 33. Among the benzocarbazoles, benzo[a]carbazole passed the column more rapidly than benzo[c]carbazole. However, compared to benzo[a]carbazole, benzo[c]carbazole was found in much higher concentrations in the collected fractions and eluted over a considerably longer time scale than benzo[a]carbazole. In particular, benzo[c]carbazole was present even after 50 days, whereas most benzo[a]carbazole eluted before day 45. Surprisingly, no traces of benzo[def]carbazole were recovered throughout the experiment.

6.2.2 Mass balance approach

Besides only regarding the elution pattern, a quantification using an internal standard (9-phenylcarbazole, 10 µg/ml) was conducted to determine the absolute amounts of compounds passing the column. In view of the fact that 2 ml of tracer solution with defined compound concentrations (Table 4) were added to the column, this principally enables a mass balance approach to provide insights into the absolute amounts of tracers retained by the source rock material. The results of the mass balance approach are shown in Fig. 51 and Table 7. Losses due to evaporation or photo-oxidation can be ruled out since the boiling points of the utilized components are comparatively high and the experiment was conducted under low light conditions and coated with aluminum foil.

6. Results

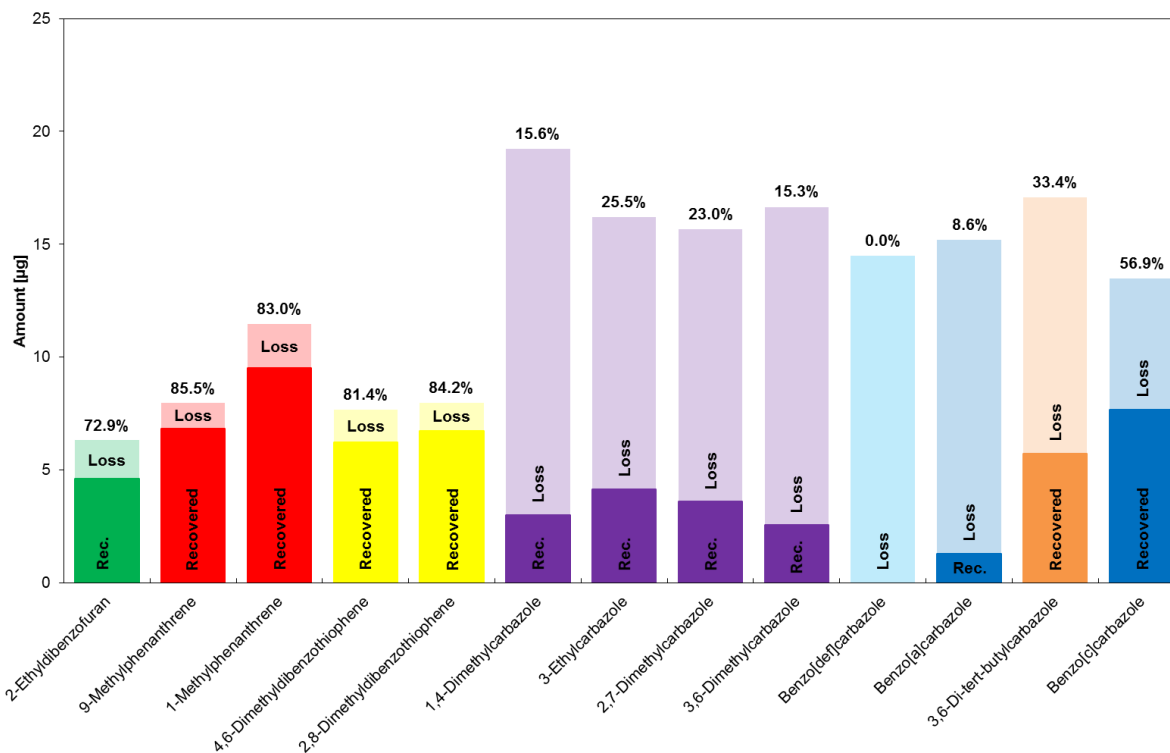


Fig. 51. Recovery rates of tracer molecules added to the source rock column. Note that the carbazoles were strongly retained by the source rock column compared to the ethyldibenzofuran, the phenanthrenes, and the dibenzothiophenes. Interestingly, comparatively large amounts of benzo[c]carbazole were recovered relative to benzo[a]carbazole and the C₂ carbazoles. Conversely, around 3/4 of the furan, and 4/5 of the phenanthrenes and dibenzothiophenes were recovered.

Regarding first the 2-ethyl dibenzofuran, a total quantity of 4.60 µg was recovered from the column. Compared to the initial amount of 6.31 µg, this represents a recovery rate of 72.9% and therefore around 3/4 of the original amount. With respect to the phenanthrenes, altogether 6.82 µg of 9- and 9.50 µg of 1-methylphenanthrene were found in the eluates. In relation to the originally used quantities of 7.98 µg and 11.45 µg, these values reflect recovery rates of 85.5% and 83.0% for the 9- and 1-isomer, respectively. Hence, overall comparatively greater amounts of 9- than 1-methylphenanthrene passed the column. However, still nearly 4/5 of the added phenanthrenes were successfully eluted. Concerning the dimethyldibenzothiophenes, absolute amounts of 6.24 µg and 6.72 µg were recovered for the 4,6- and the 2,8-isomer, respectively. In view of initial quantities of 7.67 µg and 7.98 µg, these data reflect recovery rates of 81.4% for the 4,6- and 84.2% for the 2,8-dimethyldibenzothiophene. Therefore, similar to the phenanthrenes, it was possible to recover approximately 4/5 of the originally added amounts. Note that the recovery rates of phenanthrenes and dibenzothiophenes are roughly similar, while that of the 2-ethyl dibenzofuran is slightly lower. Compared to the previous tracers, mostly only small amounts of the initially added carbazoles were found in the eluates. In

6. Results

Table 7. Mass balance results

| Component | Amount added [μg] | Amount recovered [μg] | Recovery rate [%] |
|------------------------------|--------------------------------|------------------------------------|-------------------|
| 2-Ethylidibenzofuran | 6.31 | 4.60 | 72.9 |
| 9-Methylphenanthrene | 7.98 | 6.82 | 85.5 |
| 1-Methylphenanthrene | 11.45 | 9.50 | 83.0 |
| 4,6-Dimethyldibenzothiophene | 7.67 | 6.24 | 81.4 |
| 2,8-Dimethyldibenzothiophene | 7.98 | 6.72 | 84.2 |
| 1,4-Dimethylcarbazole | 19.22 | 3.01 | 15.6 |
| 3-Ethylcarbazole | 16.20 | 4.13 | 25.5 |
| 2,7-Dimethylcarbazole | 15.65 | 3.60 | 23.0 |
| 3,6-Dimethylcarbazole | 16.65 | 2.55 | 15.3 |
| Benzo[def]carbazole | 14.47 | 0.00 | 0.0 |
| Benzo[a]carbazole | 15.19 | 1.30 | 8.6 |
| 3,6-Di-tert-butylcarbazole | 17.07 | 5.71 | 33.4 |
| Benzo[c]carbazole | 13.46 | 7.67 | 56.9 |

particular, only 3.01 μg of 19.22 μg 1,4-dimethylcarbazole, 4.13 μg of 16.20 μg 3-ethylcarbazole, 3.60 μg of 15.65 μg 2,7-dimethylcarbazole, 2.55 μg of 16.65 μg 3,6-dimethylcarbazole, 1.30 μg of 15.19 μg benzo[a]carbazole, and 5.71 μg of 17.07 μg 3,6-di-tert-butylcarbazole were recovered from the column. In addition, benzo[def]carbazole was completely absent (0.00 μg of 14.47 μg). By contrast, surprisingly, the experiment yielded significantly greater amounts of benzo[c]carbazole (7.67 μg of 13.46 μg) compared to the rest of the nitrogen aromatics. Based on the ratios of initial vs. recovered quantities, these values denote recovery rates of 15.6% for 1,4-dimethylcarbazole, 25.5% for 3-ethylcarbazole, 23.0% for 2,7-dimethylcarbazole, 15.3% for 3,6-dimethylcarbazole, 0.0% for benzo[def]carbazole, 8.6% for benzo[a]carbazole, 33.4% for 3,6-di-tert-butylcarbazole, and 56.9% for benzo[c]carbazole.

7. Discussion

The penultimate chapter of this work focusses on the discussion of the data and ultimately on the identification of compositional changes attributable to petroleum expulsion. Thereby, the geochromatographic retardation experiment provides important insights into fractionation effects in natural systems.

7.1 Bulk characterization

Before identifying expulsion-related fractionation effects, it is first necessary to classify the samples based on their bulk geochemical characteristics. Essentially, this allows to determine, (1) the real sample type (shale, coal, heterolithic, reservoir), and, (2) whether petroleum has already been generated and expelled. The determination of the true lithological character of a sample based on bulk parameters is required since subtle differences may not have been recognized during the sampling procedure. Therefore, it is crucial to distinguish between samples that could receive petroleum from adjacent source rock material (heterolithic, reservoir) and samples that are able to generate and expel petroleum (shaly source rocks, coaly source rocks). This is essential with respect to the identification of compositional changes attributable to petroleum expulsion. The coals are special in this context because they may, due to their porous structure, also be invaded by non-in situ petroleum.

Basically, the true sample character can be evaluated using a cross-plot of TOC vs. extract yield, which is shown in Fig. 52. The diagram reveals that the investigated sample material consists, as expected from the sampling procedure in the core storage, of four different types: shaly source rocks, coals, heterolithic samples, and pure reservoir (carrier bed) samples. While the reservoir samples are characterized by relatively high extract yields compared to TOC, the shales are marked by elevated amounts of organic carbon and extract yields mostly below 10.000 ppm. In comparison, the Hugin coals, which are not shown in Fig. 52 because of the very high TOC contents, yielded extract volumes in the range of 11.000 to 25.000 ppm. Samples that display a mixed character plot between the fields of reservoir rocks and organic-rich shales and are termed heterolithic. Summarized, the bulk data confirms that each expulsion scenario contains samples that could potentially generate and expel petroleum, as well as samples that could principally take up expelled petroleum.

7. Discussion

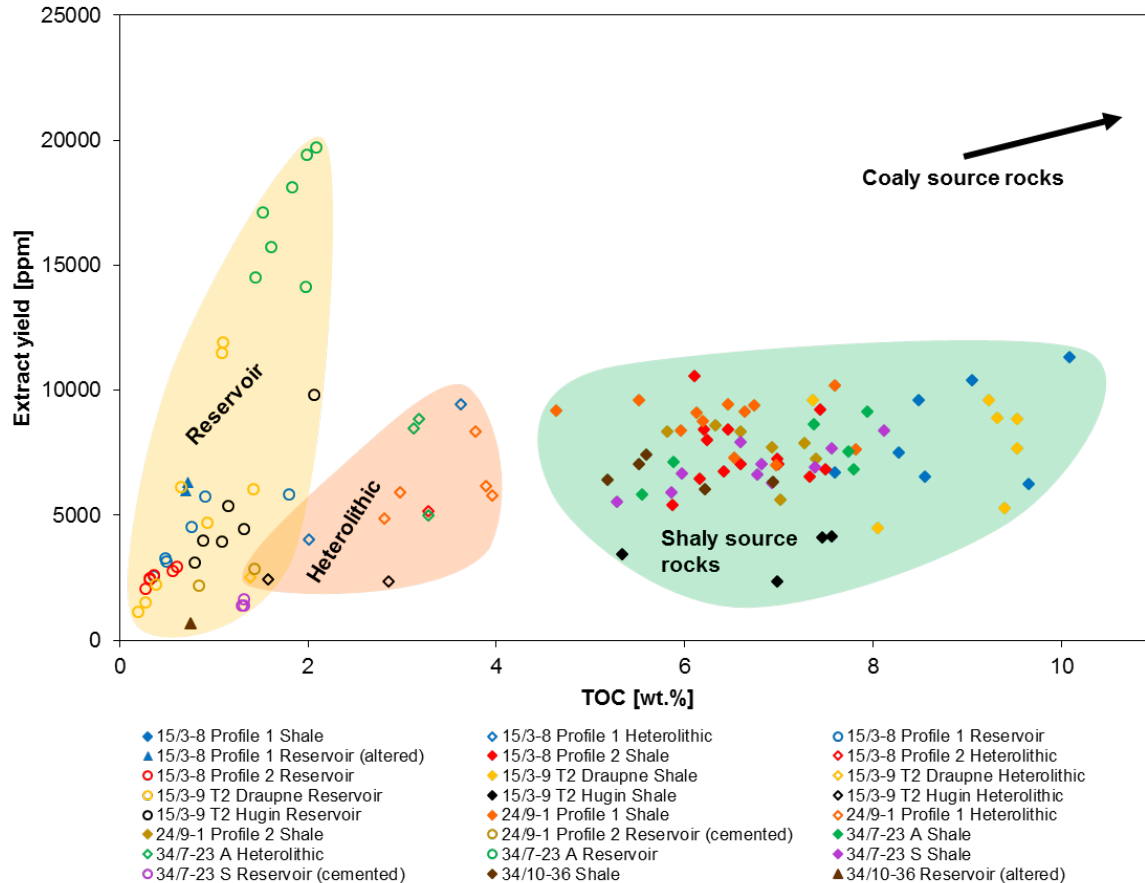


Fig. 52. Cross-plot of the total organic carbon (TOC) vs. the extract yield for the investigated expulsion scenarios. The diagram allows to group the sample material into four different categories: shaly source rocks, coaly source rocks, heterolithic samples, and reservoir samples. The Hugin coals are not shown due to very high TOC values.

Even without, to this point, precise knowledge on the thermal maturity of the sample material, a combination of bulk parameters additionally provides basic insights into whether the samples from the different expulsion scenarios could have already generated and expelled petroleum into the adjacent carrier units. For example, one approach is a diagram of the TOC against the production index for each sample, which is presented in Fig. 53. In essence, the bulk data indicate active petroleum generation and expulsion for source rock samples from well 15/3-8, the Draupne section of well 15/3-9 T2, and well 24/9-1. More specifically, the combination of high TOC and elevated PI values can be interpreted as an indication of active petroleum generation and expulsion into adjacent carrier rocks. Thereby, stronger retention of generated petroleum is indicated for source rock samples with very high PI and comparatively low to moderate TOC values. Conversely, the low TOC and high PI values determined for most reservoir samples clearly indicate the uptake of petroleum, possibly from the surrounding shales. For the first profile from well 15/3-8 (expulsion scenario A), this assumption is further corroborated by increasing extract

7. Discussion

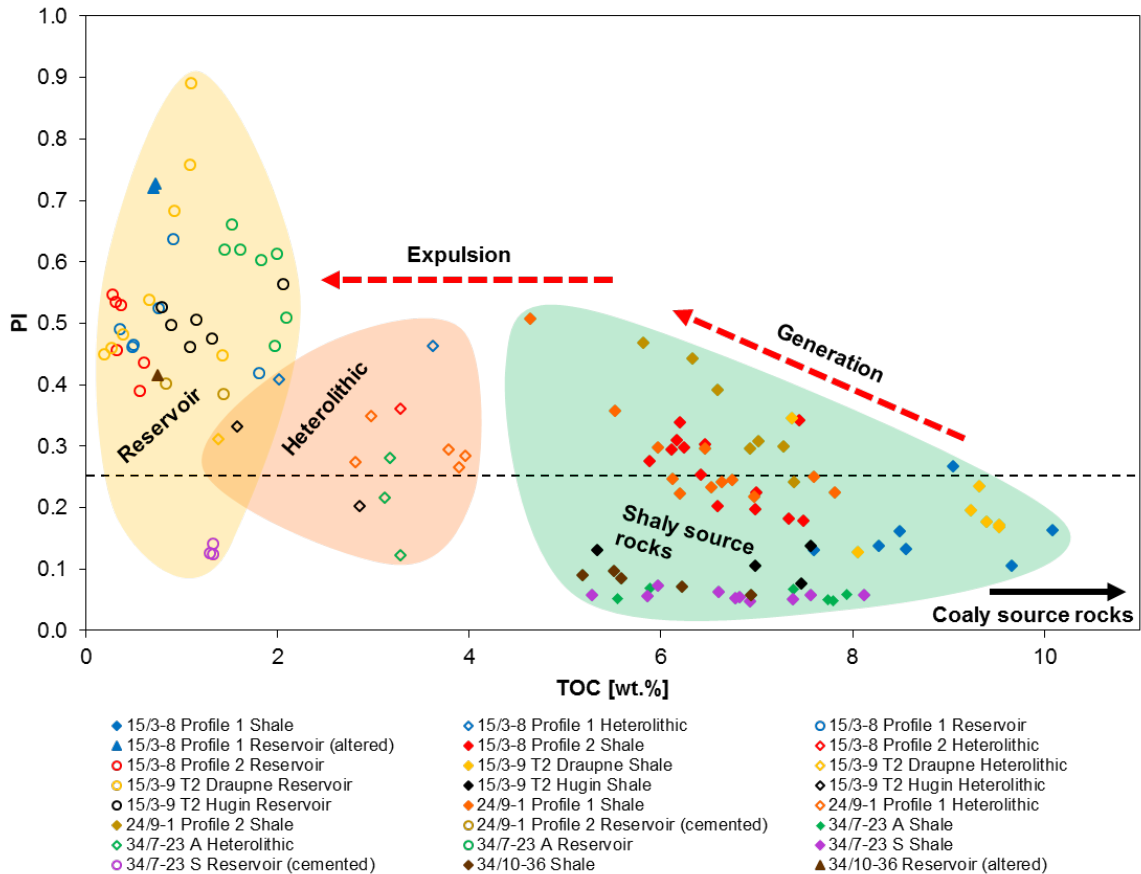


Fig. 53. Diagram showing the total organic carbon (TOC) against the production index (PI) for the examined sample material. Essentially, active petroleum generation and expulsion is indicated for source rock samples from well 15/3-8, the Draupne section of well 15/3-9 T2, and 24/9-1. By contrast, samples from the Hugin section of well 15/3-9 T2, 34/7-23 A, 34/7-23 S, and 34/10-36 do not seem to actively generate and expel petroleum into adjacent carrier units. Elevated TOC values combined with a production index of around 0.25 can be interpreted as an indication of active petroleum generation. The Hugin coals are not shown due to very high TOC values.

yields and, in part, Rock-Eval S_1 values towards the edges of the central shale unit (Fig. 23), which could reflect primary migration of generated petroleum towards the adjacent sandstone units. On the other hand, mostly low PI values were identified for source rock samples from the Hugin Formation, including the coals (not shown), well 34/7-23 A, 34/7-23 S, and 34/10-36, suggesting, despite sufficient organic richness and quality, if any, weak petroleum expulsion. Again, samples that exhibit characteristics of both source rock and reservoir constitute the heterolithic zone, which is located between the two major end member fields and could also have received petroleum from nearby source rock material.

Further information on the expulsion/retention characteristics of the source rock material can be derived from a diagram of the TOC against the Rock-Eval S_1 (Pepper and Corvi, 1995b; Ziegls et al., 2017). Such a diagram is given in Fig. 54. The Draupne (Kimmeridge Clay) Formation has previously been described as a good to

7. Discussion

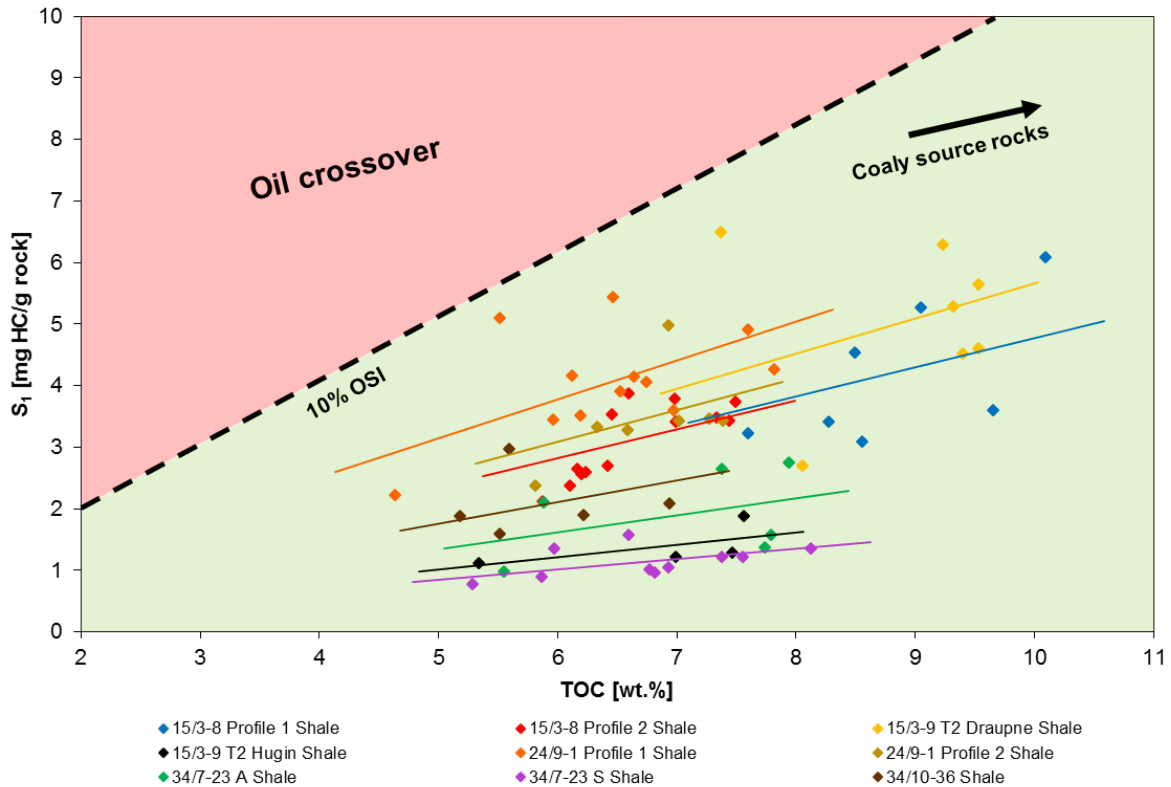


Fig. 54. Cross-plot of the total organic carbon (TOC) vs. the Rock-Eval S_1 (after Ziegls et al., 2017) for the investigated source rock material. S_1 /TOC gradients (calculated) are illustrated for each sample series. The “oil saturation index” (OSI) is incorporated after Jarvie (2012). The so-called “oil crossover effect” occurs above an oil saturation exceeding 100 mg/g TOC (10% OSI) and denotes potentially producible intervals. Note that all samples plot in the area below 10% OSI, indicating relatively efficient petroleum expulsion. The Hugin coals are not shown due to very high TOC values.

excellent expeller (e.g. Goff, 1983; Cooles et al., 1986). Basically, the shown S_1 /TOC gradients reflect the degree of oil saturation of the source rock samples and therefore allow conclusions about the retention capacity of the organic material. In this context, the so-called “oil crossover effect” (Jarvie, 2012) corresponds to an oil saturation exceeding 100 mg/g TOC (10% OSI) and thus indicates potentially producible intervals. In general, however, S_1 /TOC gradients and hence OSI values tend to decrease with increasing thermal maturity due to petroleum generation and expulsion (Ziegls et al., 2017). Thereby, Ziegls et al. (2017) mentioned that steeper S_1 /TOC gradients may be related to higher retention capacities. In the case of the investigated source rock material from the Draupne and the Hugin Formation, all samples plot clearly below the “oil crossover” threshold of 10% OSI. In particular, the overall steepest S_1 /TOC gradients were revealed for samples from well 15/3-8, the Draupne section of well 15/3-9 T2, and well 24/9-1, which can be interpreted as another indication for active petroleum generation and expulsion. On the other hand, relatively shallow S_1 /TOC gradients were identified for samples from the Hugin Formation, including the coals (not shown), well 34/7-23 A, well 34/7-23 S, and well 34/10-36,

7. Discussion

which is in good agreement with the hypothesis that there is no or only weak petroleum expulsion. Concerning the Hugin coals, the combination of very high TOC, but only low to moderate S_1 values could be explained by a high expulsion threshold (Jarvie, 2012). The observable differences in the S_1 /TOC gradients between the different expulsion scenarios may be interpreted either with different levels of thermal maturity or, alternatively, varying retention capacities of the organic material. More data, particularly molecular geochemical maturity indicators (see below), are required for a clearer picture. Yet, note that the S_1 /TOC gradients determined for samples from well 15/3-8, the Draupne scenario of well 15/3-9 T2, and well 24/9-1, which, based on the bulk data, seem to actively generate and expel petroleum, are pretty similar, supporting the theory that the Draupne Formation is an excellent expeller, independent of the respective location in the Viking Graben.

Further insights into the expulsion/retention characteristics of the sample material on the basis of bulk geochemical parameters are provided by a diagram of the Rock-Eval parameters S_2 vs. S_1 (Fig. 55), which principally compares the proportions of retained petroleum (S_1) and labile kerogen (S_2) present in the sample material (Han et al., 2015; Ziegls et al., 2017). In this context, labile carbon is supposed to represent the major sorption surface instead of TOC (Han et al., 2015). It has been suggested that the S_1/S_2 gradients are largely controlled by the thermal maturity, whereby proceeding maturation first leads to increasing S_1/S_2 gradients, followed by declining gradients at post-oil window maturity (e.g. Ziegls et al., 2017). Thereby, interferences may be attributed to variations of the organofacies, suggesting the depositional conditions exert a strong influence on the expulsion/retention characteristics of source rock samples (Pepper and Corvi, 1995b; Ziegls et al., 2017). With respect to the investigated Draupne and Hugin samples, the steepest S_1/S_2 gradients were identified for samples from well 24/9-1, followed by organic-rich shales from the second profile of well 15/3-8 and samples from the Draupne section of well 15/3-9 T2. For samples from these scenarios, this observation is another hint towards active petroleum generation and expulsion. Surprisingly, however, a considerably shallower S_1/S_2 gradient is visible for samples from the first than from the second profile of well 15/3-8. Since both sections are only about 80 m apart from each other and maturity differences are therefore rather unlikely, this could point to variations of the organic facies and hence differences in the retention capacities of the organic material. In this respect, steeper S_1/S_2 gradients may be related to greater retention

7. Discussion

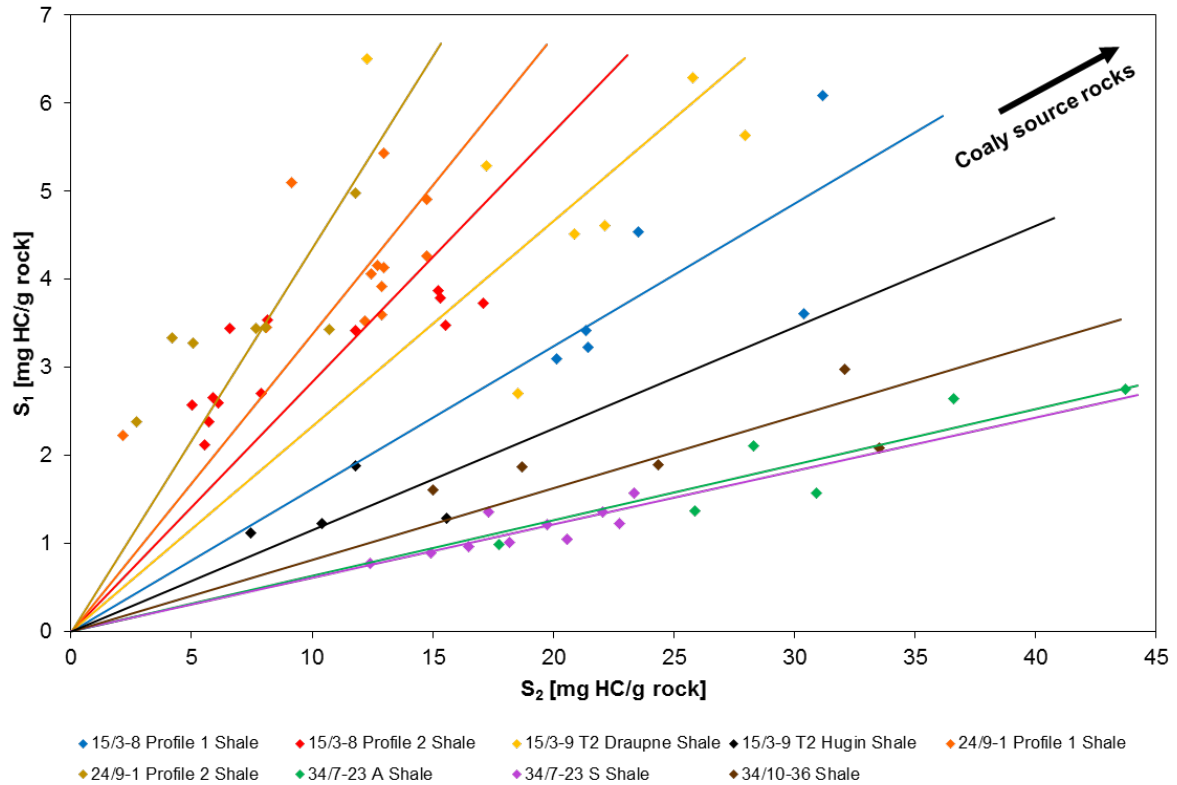


Fig. 55. Diagram showing the Rock-Eval S_2 against the Rock-Eval S_1 for the investigated source rock samples. S_1/S_2 gradients (calculated) are illustrated for each sample series. The overall steepest gradients were identified for samples from well 24/9-1, 15/3-8, and the Draupne section of well 15/3-9 T2, pointing to active petroleum generation and expulsion. Note that there are considerable differences in the shape of the S_1/S_2 gradient within scenarios from the same wells (15/3-8, 24/9-1), which are not explainable by differences in the thermal maturity, but rather by different retention capacities of the organic material. Thereby, higher proportions of land plant material may possibly cause steeper gradients and thus stronger retention (Ziegs et al., 2017). The Hugin coals are not shown due to very high TOC values.

potentials of the organic matter and thus potentially to a more terrigenous organic facies. For the black shales from well 15/3-8, this indicates a more terrestrial facies type and hence a lower generation and higher retention potential for expulsion scenario B than for scenario A. Slightly different S_1/S_2 gradients are also recognizable for the two expulsion sections from well 24/9-1, which are only around 6 m away from each other. Again, since maturity differences are unlikely, variations of the organic facies and hence different retention capacities of the organic matter are strongly suggested. In particular, the second profile of well 24/9-1 (expulsion scenario F) seems to comprise a more terrigenously influenced organic facies, which causes a higher retention capacity. Conversely, once again relatively shallow gradients were determined for source rock samples from the Hugin Formation, including the coals (not shown), well 34/7-23 A, 34/7-23 S, and 34/10-36. In accordance with the previous data, this points to no or only weak petroleum expulsion.

A further characterization of the expulsion/retention characteristics of the sample

7. Discussion

material could be achieved by means of additional Rock-Eval measurements on corresponding solvent-extracted source rock material. In fact, it has been evidenced that parts of the Rock-Eval S₂ peak actually represent an invaporizable proportion of the S₁ peak (e.g. Han et al., 2015; Sanei et al., 2015; Ziegs et al., 2017), which may have profound impact on the expulsion/retention characteristics of the source rock material. For example, without considering, this effect could lead to a severe underestimation of the petroleum generation potential (e.g. Han et al., 2015; Ziegs et al., 2017).

7.2 Palaeofacies characterization

Leythaeuser et al. (1984a) mentioned that the two most important criteria for the investigation of petroleum expulsion in natural systems consisting of source rock-reservoir couplets are knowledge about the organic facies and the thermal maturity of the sample material. In particular, it was stated that molecular redistribution effects associated with primary migration can only be investigated if facies and maturity influences can largely be neglected. In this subsection, it is attempted to characterize the organic facies of the sample material as one important prerequisite for the identification of expulsion-related compositional changes.

7.2.1 Type of organic material

Source type and quality, and to a limited extent thermal maturity can be estimated using a pseudo-Van Krevelen diagram (Fig. 56). In principle, application is better for immature sediments since significant amounts of oxygen might be lost during diagenesis, mostly as CO₂, and the hydrogen index typically decreases with maturity. Fig. 56 shows a pseudo-Van Krevelen diagram for the source rock material from the investigated North Sea wells. All samples plot in a relatively narrow area in the lower left half of the diagram. The samples are overall characterized by low OI and a wide range of HI values. While the highest HI values were calculated for organic-rich shales from quadrant 34, the HI data are lowest in samples from the second profile of well 24/9-1 (expulsion scenario F). Note again that coals from the Hugin Formation exhibit unusually high HI values. Nevertheless, these values are in good agreement with those determined by Isaksen et al. (1998).

In general, however, since deeply buried source rock samples like those investigated in this work have definitely undergone diagenesis and to some extent catagenesis, a

7. Discussion

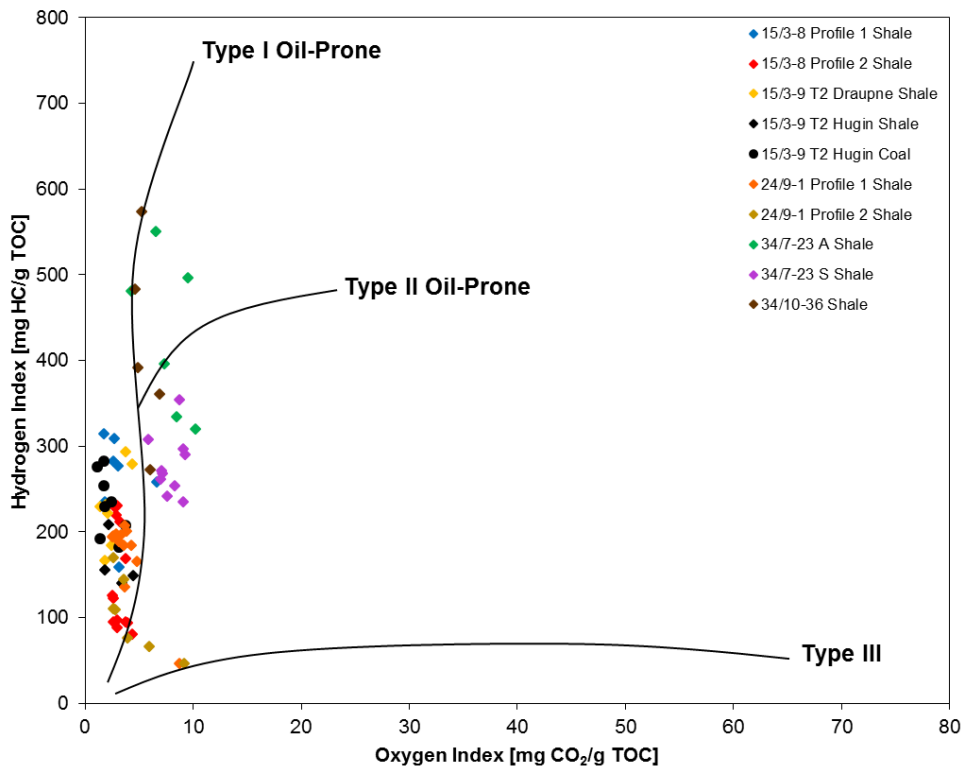


Fig. 56. Cross-plot of oxygen index (OI) vs. hydrogen index (HI) (pseudo-Van Krevelen diagram). Essentially, pseudo-Van Krevelen diagrams serve to determine source type and quality of sample material. In addition, the diagram principally allows to draw conclusions about the thermal maturity.

pseudo-Van Krevelen diagram is this time not suitable to characterize the organic facies of the source rock material. For that reason, a cross-plot of the T_{max} against the hydrogen index (Fig. 57) is principally better applicable. Similar to a pseudo-Van Krevelen diagram, this plot allows conclusions about the type, quality and thermal maturity of organic material, even for samples within the oil window. The type curves for type I, II, and III kerogens are based on the transformation ratio (TR), which corresponds to the magnitude of conversion of original organic material into hydrocarbons and can be calculated from standard Rock-Eval pyrolysis measurements according to the following equation (after Banerjee et al., 1998; as pointed out by Berner in a personal communication, 2018):

$$TR = \frac{a * C e^{[b*(T_{max}-435)]}}{a * C e^{[b*(T_{max}-435)]} + 1} \quad (23)$$

In this equation, a , b and C represent kerogen-specific constants, which relate the transformation ratio to the Rock-Eval T_{max} (Banerjee et al., 1998). Table 8 shows the values published by Banerjee et al. (1998) for each kerogen type. The constants of Banerjee et al. (1998) were chosen because they work quite well as a substitute for

7. Discussion

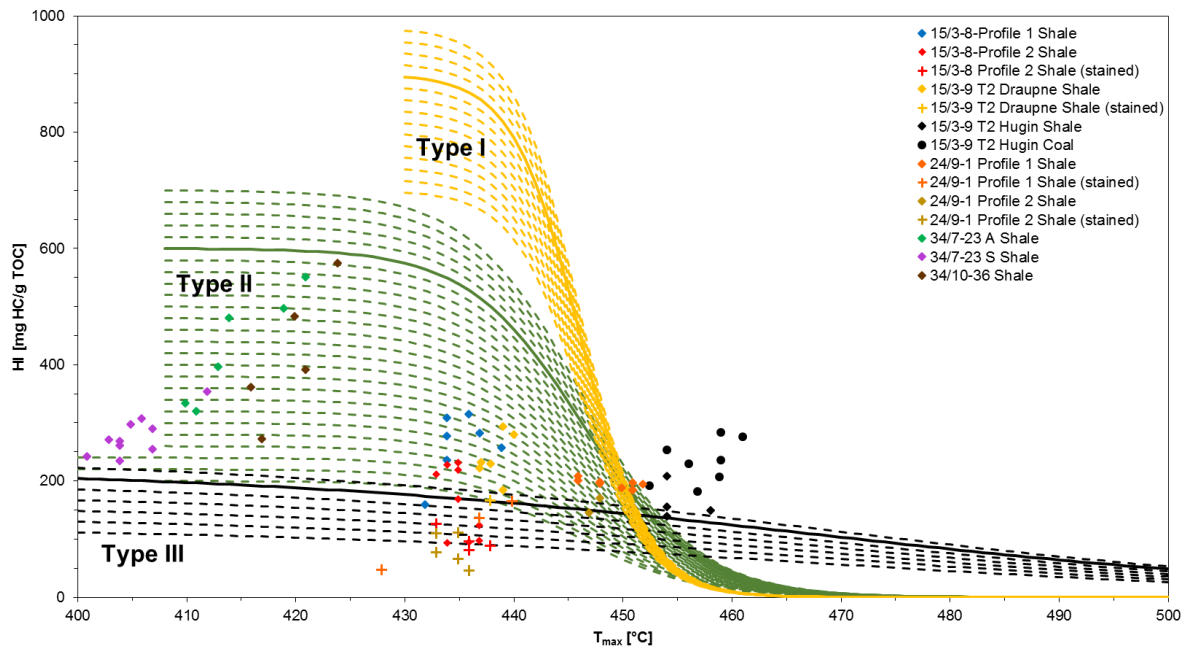


Fig. 57. Diagram of the T_{max} vs. the hydrogen index (HI) for the investigated source rock samples (type curves calculated after Banerjee et al., 1998; design after Berner, personal communication, 2018). Rock-Eval pyrolysis was performed on unextracted (whole rock) material. Similar to a pseudo-Van Krevelen plot, this type of diagram allows conclusions about type, quality, and thermal maturity of organic matter. In addition, based on transformation ratio paths for type I, II, and III kerogens (Banerjee et al., 1998), it enables to calculate the HI of a sample prior to the catagenesis kerogen maturation stage, which is required to determine the original type of organic material at the time of deposition (not done in this work). Samples with a production index (PI) ≥ 0.3 are labeled as "stained".

kinetic modelling and allow a reliable back calculation of bulk parameters within the oil window (Berner, personal communication, 2018). As can be seen from the diagram, the majority of the investigated source rock material plots in the field of a marine type II kerogen. More precisely, this applies to all samples from quadrant 34 and about half of the samples from quadrant 15 and 24. Exceptions are one sample from expulsion scenario A (15/3-8, profile 1), approximately half of the samples from expulsion scenario B (15/3-8, profile 2), two samples from section E (24/9-1, profile 1), most samples from expulsion scenario F (24/9-1, profile 2), and coals and shales of the Hugin Formation. While the former mentioned are shifted towards the area of a type III kerogen, samples from the Hugin Formation plot outside the defined zones, due primarily to the combination of high HI and elevated T_{max} values. Note, however, that Isaksen et al. (1998) stated that for samples containing large proportions of terrigenous organic material, such as the Hugin coals, the HI represents an alteration rather than a petroleum generation indicator and has thus to be regarded with caution.

Similarly, Leythaeuser et al. (1984a) mentioned that facies characterization solely on

7. Discussion

Table 8. Transformation ratio constants (after Banerjee et al., 1998)

| Kerogen type | <i>a</i> | <i>b</i> | <i>c</i> |
|--------------|-----------|----------|----------|
| Type I | 0.0000308 | 0.325500 | 882 |
| Type II | 0.0001910 | 0.192500 | 602 |
| Type III | 0.0011900 | 0.038100 | 250 |

the basis of Rock-Eval parameters may be problematic. Therefore, these authors strongly recommended to additionally regard biomarker molecules and, in this respect, particularly steranes, which derive from eukaryotic organisms and are widely believed to be largely unaffected by fractionation processes during petroleum migration (e.g. Cornford et al., 1983; Leythaeuser et al., 1984a; Lewan et al., 1986; Larter et al., 2000; Han et al., 2017). Theoretically, the distribution of C₂₇ to C₂₉ steranes enables to distinguish between different organic facies types and hence to get an idea about the degree of similarity of sample material (e.g. Huang and Meinschein, 1979, Leythaeuser et al., 1984a, Han et al., 2017). Thereby, C₂₇ steranes are supposed to derive mainly from marine algae, whereas land plants are the most common source of C₂₉ steranes. By contrast, the sources of C₂₈ steranes can be much more variable. Though, a major source of C₂₈ steranes are *Haptophyceae* (Volkman et al., 1998), i.e. coccolithophorids, which are ubiquitous in marine environments and represent major primary producing organisms. Fig. 58 shows a ternary diagram of the C₂₇ to C₂₉ 5 α ,14 β ,17 β (H)-steranes (20S+20R) for the source rock material examined in this work. Essentially, three data clusters are visible. The first cluster (green-colored) is characterized by around 33 to 42% C₂₇, 25 to 33% C₂₈, and 30 to 40% C₂₉ steranes. It contains all samples from the Draupne Formation and one shale sample from the Hugin Formation, which can be considered as an outlier. According to the classification scheme proposed by Huang and Meinschein (1979) (also shown in Fig. 58, lower left corner), this area refers to organic material deposited in a marine-brackish environment, which is in good agreement with the generally accepted depositional conditions of the Draupne Formation (see 4.4.3). Compared to the first cluster, the two remaining zones are marked by elevated quantities of C₂₉ steranes and contain exclusively source rock samples from the Hugin Formation. Thereby, the highest abundances of C₂₉ compounds (~57-69%) were found in the coals, which additionally contain the lowest proportions of C₂₇ steranes (~10-21%). C₂₈ steranes occur in low to moderate amounts (~17-23%) and are generally less abundant than in samples from the Draupne Formation. The third data cluster (light gray) is situated between both fields

7. Discussion

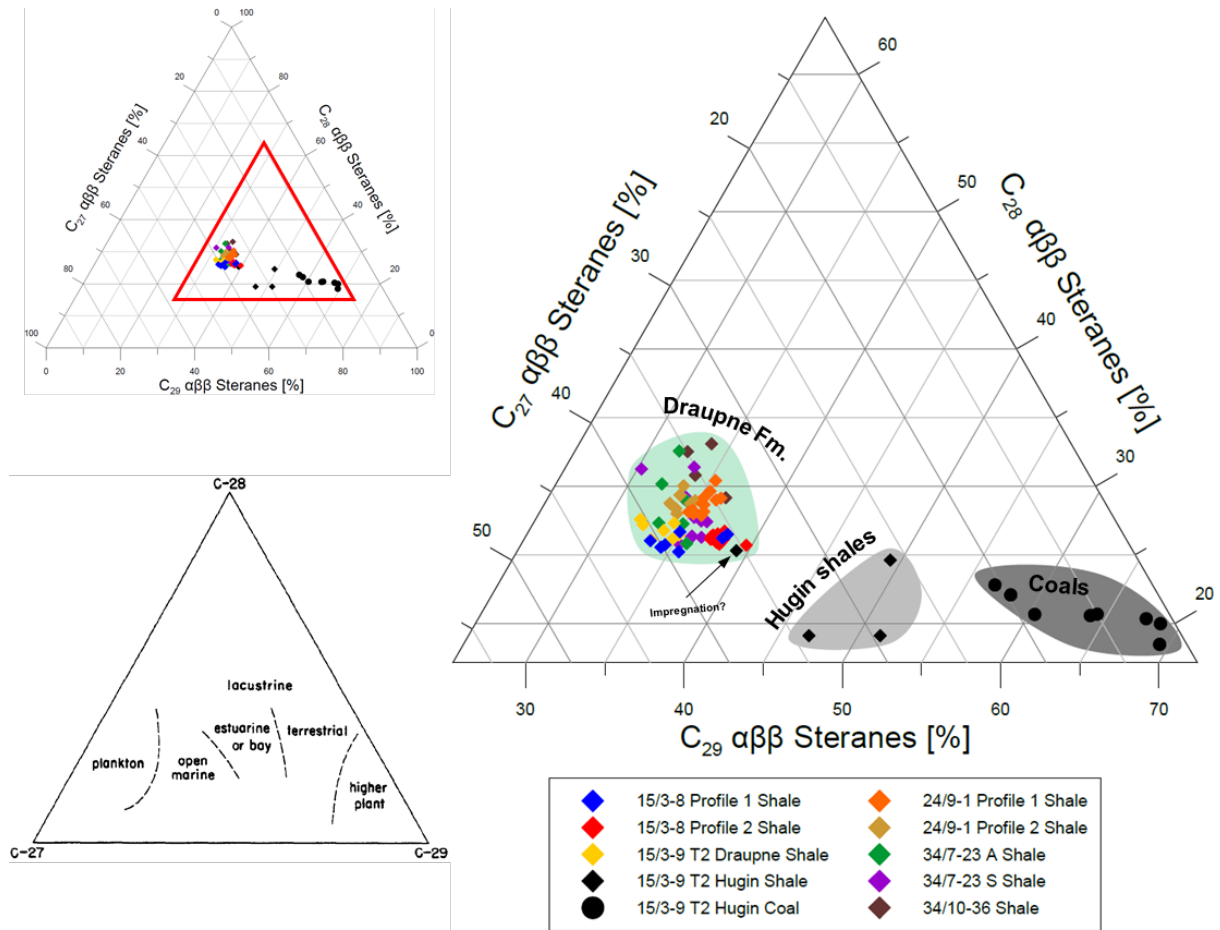


Fig. 58. Ternary diagram showing the relative distributions of C_{27} to C_{29} $5\alpha,14\beta,17\beta(H)$ -steranes (20S+20R) in the source rock material (original diagram in the lower left corner from Huang and Meinschein, 1979). In total, three different facies types are identifiable. While coals of the Hugin Formation contain the highest amounts of C_{29} steranes, C_{29} components are much less abundant in samples from the Draupne Formation, which are instead characterized by greater proportions of C_{27} and C_{28} steranes. Hugin shales plot between both fields. Note that, despite variations in the Rock-Eval parameters, the distribution of steranes indicate very similar types of organic material, hence allowing for the investigation petroleum expulsion. Note also that a shale sample from the Hugin Formation (K011253, 4506.3 m MD) plots in the Draupne zone, which could be due to impregnation.

and comprises the shales of the Hugin Formation. It is marked by approximately 26 to 43% C_{27} , 16 to 25% C_{28} , and 41 to 52% C_{29} steranes. The location of this data field thus indicates that, first, C_{29} steranes occur in greater quantities than in the Draupne Formation, but are less abundant than in the coals, second, the content of C_{28} steranes is similar to that of the coals, but lower compared to the Draupne Formation and, third, the amounts of C_{27} steranes in shales of the Hugin and the Draupne Formation are comparable, suggesting a considerable marine influence, which is also indicated by the Rock-Eval data. Hence, according to the classification scheme of Huang and Meinschein (1979), samples from the Hugin Formation are severely influenced by terrigenous organic material. As expected, particularly the coals appear to be mainly composed of land plant material. On the other hand, the elevated amounts of C_{27} steranes in shales of the Hugin Formation indicate a significant proportion of marine

7. Discussion

organic matter, which principally fit well with the salt marsh environment described by Folkestad and Satur (2008) (see 4.4.3).

Concerning the geochromatographic experiment, this means that the source rock column consisting of powdered material from both expulsion scenarios of well 15/3-8 contains a mixed type II/III kerogen, which is composed of different proportions of marine and terrestrial organic matter.

In summary, the sterane data indicate that, regardless of slight variations in the Rock-Eval data, the facies types within individual expulsion sections are comparable. Therefore, with respect to the criterion of a similar organic facies, the investigated source rock material is principally suitable for the investigation of petroleum expulsion.

7.2.2 Depositional conditions

After having determined the principal types of organic material, the next subsection addresses the depositional conditions of the examined source rock samples and thus attempts to provide further insights into the comparability of samples from individual scenarios and their applicability for the investigation of petroleum expulsion. Basically, the reconstruction of the depositional conditions includes the evaluation of the depositional setting and the redox milieu, which may vary from oxidizing to reducing.

A possibility to evaluate the environmental setting is a plot of pristane/phytane vs. dibenzothiophene/phenanthrene (Hughes et al., 1995). Fig. 59 shows such a dia-gram for the investigated sample material. Note that most samples from the Draupne Formation plot in the transition zone between the categories 2 and 3, pointing to a marine-brackish environment. By contrast, shales and particularly coals of the Hugin Formation are shifted towards higher pristane/phytane ratios, suggesting a considerable terrigenous influence. Indeed, the differences between the samples are too irregular to be solely caused by maturity differences, which may also impact the Pr/Ph ratio (e.g. Peters et al. 2005a, b and references therein). Therefore, since samples from the Draupne Formation plot again very close to each other, similar depositional environments can be deduced, most likely shallow marine, coastal-

7. Discussion

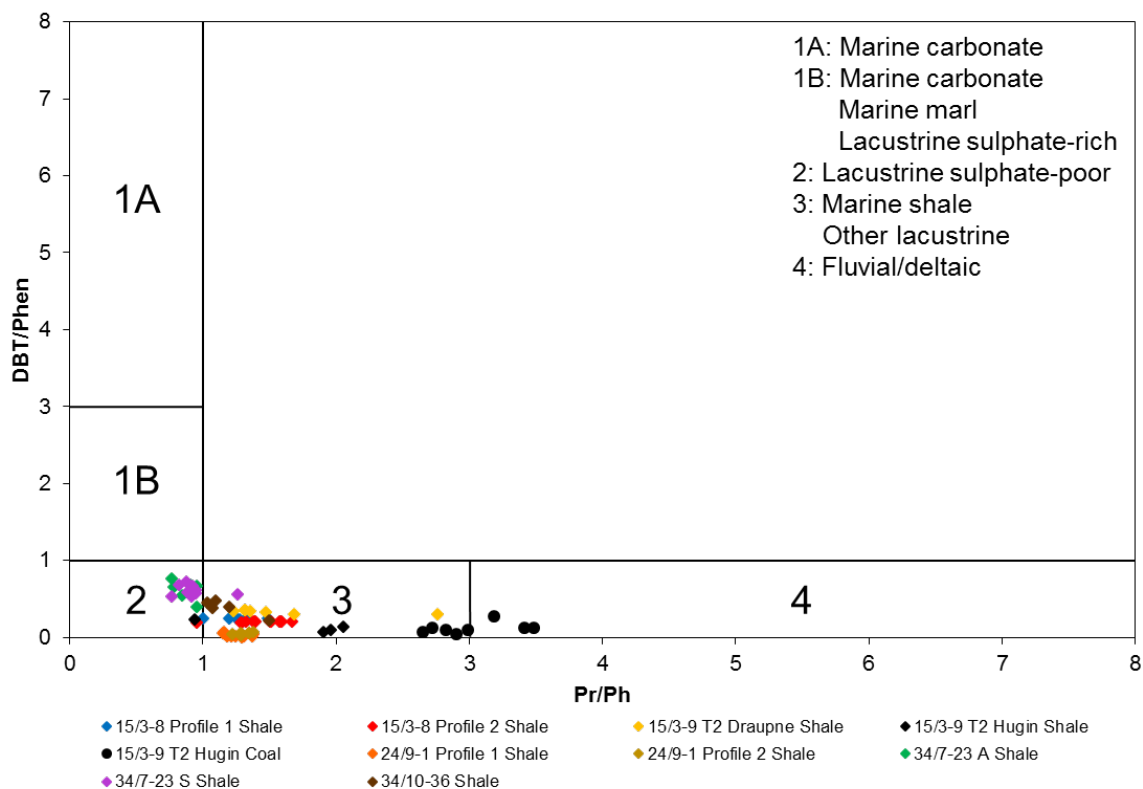


Fig. 59. Diagram of pristane/phytane (Pr/Ph) against dibenzothiophene/phenanthrene (DBT/Phen) (after Hughes et al., 1995). Essentially, the cross-plot enables to distinguish between different depositional environments and therefore allows a facies classification. Most samples from the Draupne Formation plot between field 2 and 3, pointing to a marine-brackish environment. Coals and shales of the Hugin Formation are shifted towards higher pr/ph ratios, indicating a considerable terrigenous influence.

related subbasins. The two data clusters including Hugin coals and shales indicate deposition in different environments. Interestingly, the pattern is similar to the distribution of steranes shown before (Fig. 58). While the location of the coals in the diagram suggest a strong terrestrial influence, for example, deposition in a coastal swamp environment, the shales plot in a region near the Draupne shales, indicating deposition in a marine influenced environment, e.g. salt marshes. Therefore, the results are principally in good agreement with the facies analysis of Folkestad and Satur (2008). Note, however, that two outliers exist, one shale sample from the Hugin Formation that plots in the Draupne cluster (K011253, 4506.3 m MD), and one sample from the Draupne profile of well 15/3-9 T2, which is located close to the Hugin coals (K011232, 4131.1 m MD). Similar to the sterane data, the pristane/ phytane vs. dibenzothiophene/phenanthrene plot indicates that samples from individual expulsion scenarios were deposited in comparable depositional environments and are thus suitable for the investigation of petroleum expulsion. The outliers were not excluded from further analysis but must, however, be regarded with caution.

Palaeoredox conditions can be evaluated using a combination of bulk and molecular

7. Discussion

geochemical proxies. One approach is a cross-plot of TOC against TS (Fig. 60), which therefore bases on the results of the elemental analysis. As shown in Fig. 60, most samples, including the shales of the Hugin Formation, are characterized by TOC values between 5 and 10 wt.% and TS contents in the range of 1 to 13 wt.%. Hence, they contain relatively high amounts of sulfur compared to TOC, pointing to a deposition in oxygen-depleted, reducing environments. As in a marine depositional environment reactive iron can be expected to have been abundant, it is likely that most sulfur within the Draupne samples is bound in pyrite, which was similarly mentioned, for example, by Kubala et al. (2003). The same can be assumed for shales from the Hugin Formation, which appear to have been deposited in a marine transitional environment. By contrast, the Hugin coals contain on average significantly lower amounts of sulfur and much greater amounts of organic carbon, causing them to plot in the lacustrine region, suggesting a largely oxidizing depositional milieu, which is another argument for a coastal swamp environment.

A possibility to estimate the redox potential using molecular geochemical indicators is, for example, a diagram of phytane/ nC_{18} (Ph/nC_{18}) against pristane/ nC_{17} (Pr/nC_{17})

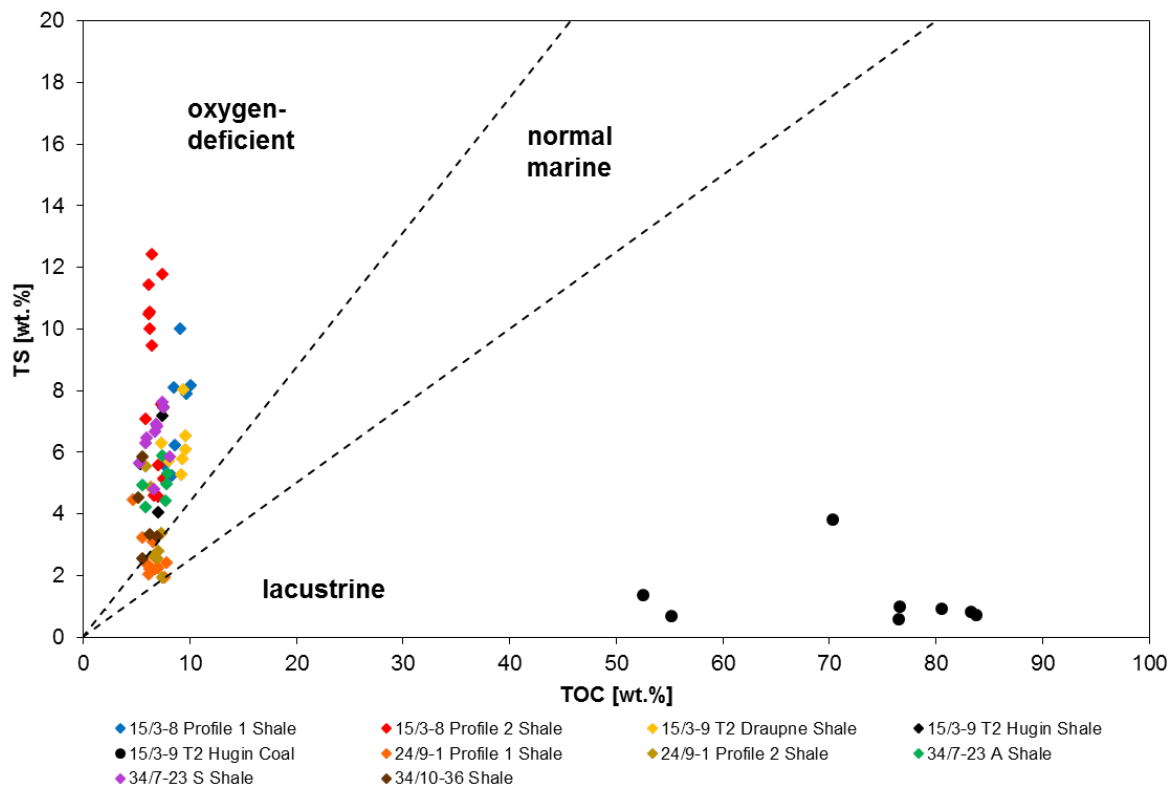


Fig. 60. Cross-plot of total organic carbon (TOC) vs. total sulfur (TS) (Berner, personal communication, 2018). The diagram allows to draw conclusions about the depositional environment and redox milieu. Note that, according to the data obtained from the elemental analysis, the majority of samples from the Draupne Formation and shales of the Hugin Formation were deposited under predominantly oxygen-depleted, reducing conditions. By contrast, the Hugin coals appear to have been deposited under largely oxidizing conditions.

7. Discussion

(Fig. 61) (Shanmugam, 1985). In addition, it also allows for a simple facies characterization. Assuming that phytane is preferentially preserved under anoxic, reducing conditions (Didyk et al., 1978), higher phytane/ nC_{18} ratios may be interpreted with stronger reducing conditions. However, the relationship between pristane, phytane and the redox milieu has been called into question by many authors, meaning pristane/phytane data must generally be regarded with caution. For example, it has been shown that thermal maturation can increase the pristane/phytane ratio and there may be different sources for pristane and phytane except for the phytol side chain of chlorophyll (e.g. Peters et al., 2005b and references therein). Nevertheless, the data shown in Fig. 61 are in good agreement with the sterane and the bulk geochemical results presented before. As shown in the diagram, the samples display a wide range of Pr/nC_{17} and Ph/nC_{18} values. Since biodegradation can be ruled out for the source rock samples, organic facies, redox milieu and thermal maturity can be considered as the principal factors responsible for the distribution pattern. Most samples, especially those from the Draupne Formation, plot

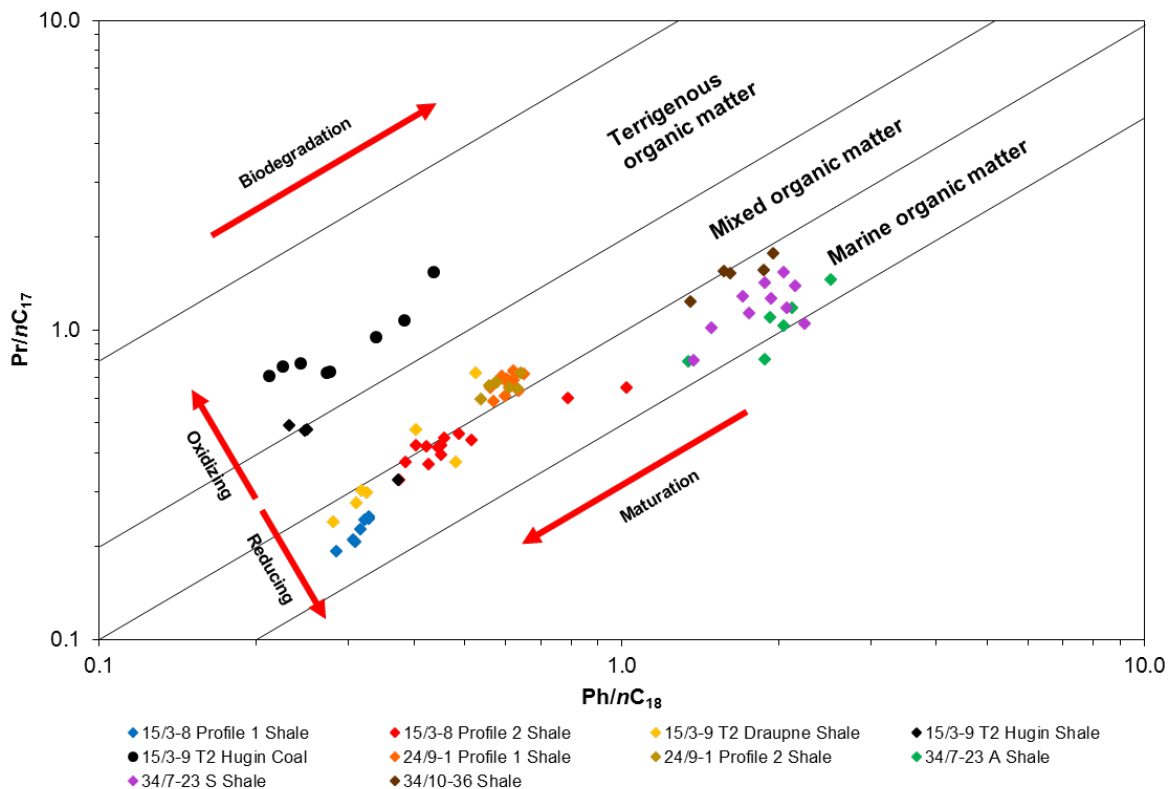


Fig. 61. Logarithmic diagram of phytane/ nC_{18} (Ph/nC_{18}) against pristane/ nC_{17} (Pr/nC_{17}) (after Shanmugam, 1985). Essentially, the cross-plot enables, (1) to reconstruct the redox milieu in which a sample has been deposited, and (2) to distinguish between different organic matter types. Thereby, thermal maturation tends to shift samples towards the lower left corner, while biodegradation does the opposite. Note that samples from individual expulsion scenarios mostly plot close to each other, suggesting similar organic facies. Note also that samples from the Hugin Formation plot above those of the Draupne Formation, which is due likely to large proportions of terrigenous organic matter and a partly oxidizing redox milieu. Samples from the Draupne Formation display a marine signal and were probably deposited under mostly reducing conditions.

7. Discussion

in the zone of marine to mixed organic matter, which is in good accordance with the bulk and sterane data. However, both the Pr/nC_{17} and the Ph/nC_{18} ratios display a great variability, indicating that thermal maturation, which shifts the data towards lower values, as well as small differences in the composition of the organic material exert a strong influence. Samples from the Hugin Formation plot mostly in the terrigenous sector and therefore in a different region as material from the Draupne Formation. Again, this is in good agreement with the trends shown before.

Summarized, concerning the redox conditions, the data indicate that samples from the Draupne Formation were deposited in a reducing milieu, while coals and shales of the Hugin Formation were deposited in a more oxygenated environment. Note that, similar to the plots presented before, samples from individual expulsion scenarios plot once again very close to each other, suggesting a high degree of similarity, which is essential for the investigation of petroleum expulsion.

7.3 Maturity assessment

According to Leythaeuser et al. (1984a), the second criterion for the investigation of petroleum expulsion in natural systems is precise information on the thermal maturity of the sample material. In particular, the maturity of the examined source rock samples needs, on one hand, to be within the oil window, and, on the other hand, to be similar within individual expulsion scenarios. Therefore, the following subsection aims to characterize the thermal maturity of the samples in order to assess their suitability for the investigation of petroleum expulsion. Similar to the evaluation of the organic facies, the thermal maturity of samples can be inferred using a combination of bulk and molecular geochemical indicators. The most essential bulk parameter is the T_{max} value obtained from the Rock-Eval pyrolysis, which can be converted into a vitrinite reflectance using, for example, equation 18 (from Jarvie et al., 2007 and reference therein). As mentioned in section 3.6.1, this equation was chosen because it is supposed to be well applicable for a lot of type II and III kerogens (Peters et al., 2005a) and therefore for the sample material investigated in this work. Note again that caution must be taken when applying this equation to immature (T_{max} below 420 °C) and highly mature (T_{max} above 500 °C) source rock material (Peters et al., 2005a) and thus to samples from quadrant 34, which repeatedly display T_{max} values below 420 °C.

7. Discussion

A famous molecular maturity indicator is the MPI 1 (equation 8), which bases on the distribution of methyl groups around a phenanthrene molecule, whereby, with increasing maturity, there is a preference of the more stable 2- and 3- over the less stable 1- and 9-positions. Keep in mind, however, that the MPI 1 tends to decrease at very high stages of thermal maturity, meaning several different maturity indicators are necessary for a clear picture (e.g. Peters et al., 2005b). Fig. 62 shows a diagram of the T_{\max} vs. the MPI 1 in order to estimate the thermal maturity of the investigated source rock samples. Corresponding T_{\max} -based vitrinite reflectance values are given at the top. Samples with a production index exceeding 0.3 are labeled as “stained” and may carry either large proportions of in situ bitumen, due, for example, to active petroleum generation, or, alternatively, external petroleum and, since this may impact the Rock-Eval results, must therefore be regarded with caution. Consequently, these samples were excluded from the maturity calibration. Note that there is a good correlation between the T_{\max} and the MPI 1, i.e. the samples with the highest T_{\max} values tend to exhibit the greatest MPI 1 values, and vice versa. According to the data shown, source rock samples from quadrant 34 are immature, whereas those

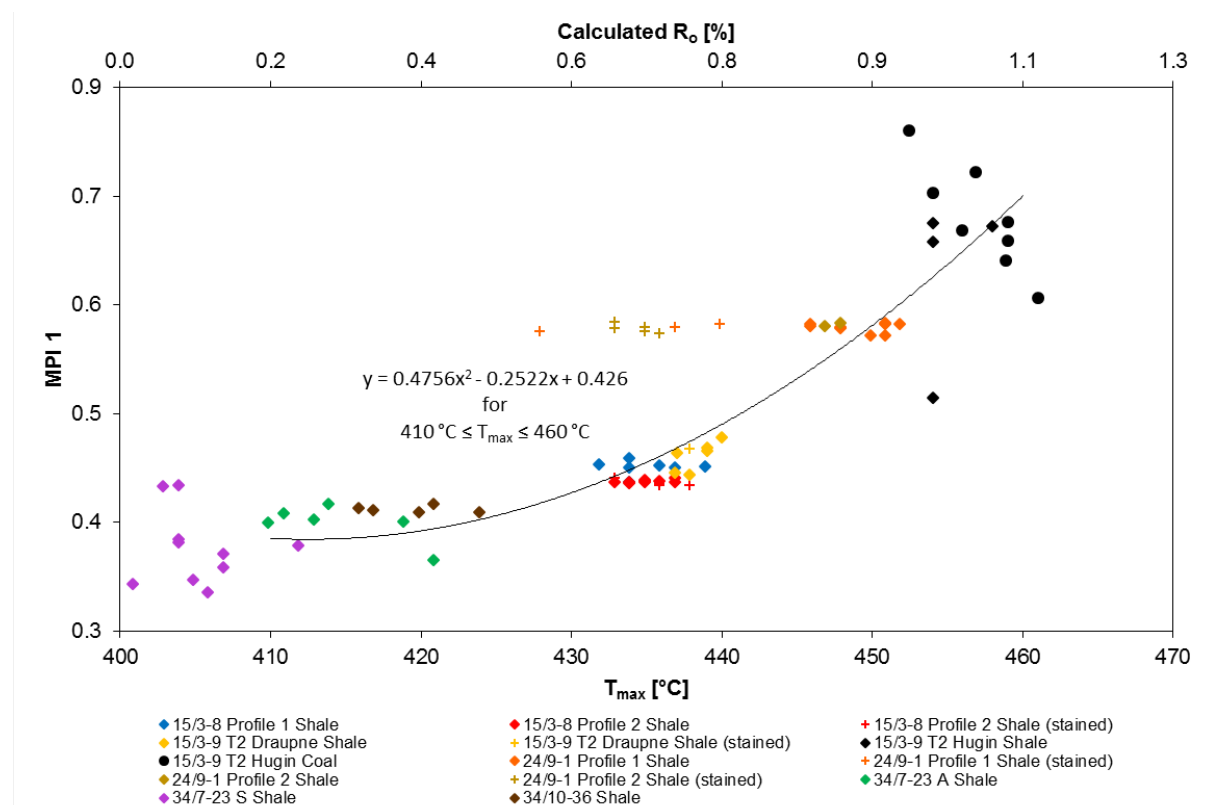


Fig. 62. T_{\max} -MPI 1 maturity correlation. Vitrinite reflection (R_o) calculated after equation 18 (from Jarvie et al., 2007 and reference therein). Note that there is a good correlation between the T_{\max} and the MPI 1, indicating thermal maturity exerts a strong influence. The data suggest that coals and shales of the Hugin Formation are most mature, while samples from quadrant 34 can be considered as immature. Samples from quadrant 15 and 24 are likely within the oil window. Samples with a production index (PI) ≥ 0.3 are labeled as “stained” and excluded from the maturity calibration. R_o values below 0.2 are shown only for completeness.

7. Discussion

from quadrant 15 and 24 are within the oil window. In particular, the highest levels of thermal maturity (0.9-1.1% R_o , T_{max} -based) were determined for coals and shales of the Hugin Formation, whereas the lowest thermal maturities were calculated for samples from well 34/7-23 A, 34/7-23 S, and 34/10-36. Organic-rich shales from well 15/3-8 and the Draupne section of well 15/3-9 T2 display maturities within the early oil window (0.6-0.8% R_o , T_{max} -based). Compared to source rock material from these sections, samples from well 24/9-1 exhibit slightly greater T_{max} and MPI 1 values, indicating a marginally higher thermal maturity.

Another excellent molecular maturity parameter is the C_{30} diahopane ratio, which has been shown to increase with increasing thermal stress due to rearrangement of the $C_{30}\alpha\beta$ hopane (e.g. Isaksen, 2004). A cross-plot of the T_{max} vs. the C_{30} diahopane ratio for the investigated source rock samples is presented in Fig. 63. Note that samples from well 24/9-1 are missing due to only low amounts of hopanes present. This special feature could be related to a combination of elevated thermal maturity and depositional environment, in which primary production appears to have been

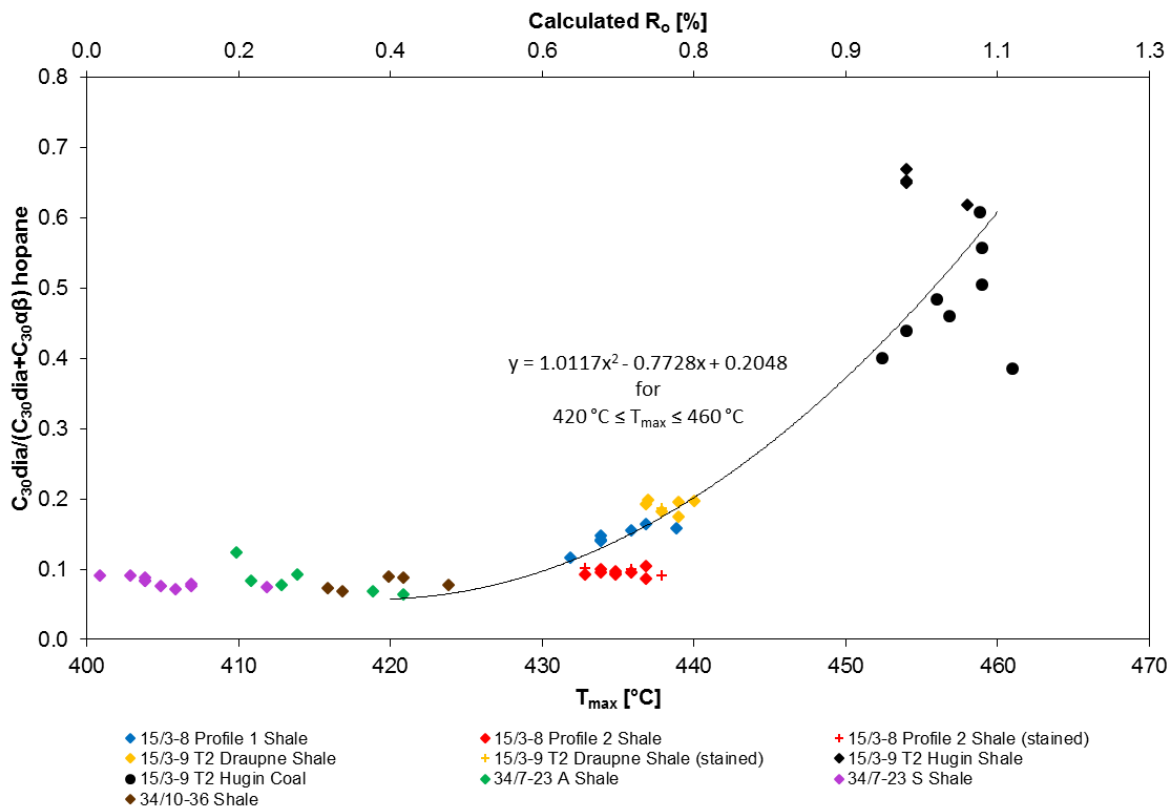


Fig. 63. T_{max} - C_{30} diahopane ratio maturity correlation. Vitrinite reflection (R_o) calculated after equation 18 (from Jarvie et al., 2007 and reference therein). Note that the C_{30} diahopane ratio steeply increases with increasing thermal maturity above a T_{max} of ~420 °C. Similar to the MPI 1 data, the C_{30} diahopane ratio suggests that samples from the Hugin Formation are most mature, while organic-rich shales from quadrant 34 experienced the lowest levels of thermal stress. Samples from well 24/9-1 are not shown due to only low amounts of hopanes present. Samples with a production index (PI) ≥ 0.3 are labeled as "stained" and excluded from the maturity calibration. R_o values below 0.2 are shown only for completeness.

7. Discussion

mainly carried out by eukaryotic, sterane-producing organisms, consequently leading to very low amounts of bacterial organic matter and thus hopanes in the sediment. Progressing burial and thermal maturation then further decreased the already low quantities of hopanes. By contrast, coals and shales of the Hugin Formation, which seem to be thermally more mature but contain hopanes, likely experienced much greater input of bacterial organic matter. Indeed, coals are known to undergo partly intense bacterial reworking during deposition (e.g. Petersen et al., 1996; Mann et al., 1998). Essentially, with regard to the C₃₀ diahopane ratio, similar tendencies as observed before for the MPI 1 are discernable. In general, samples from the Hugin Formation appear to have experienced the highest level of thermal stress, while shales from quadrant 34 are apparently least mature. Organic-rich shales from well 15/3-8 and the Draupne section of well 15/3-9 T2 plot between both fields, suggesting early oil window maturity.

The thermal maturity can also be assessed using steranes, for example via the ratio of $14\beta,17\beta/(14\beta,17\beta+14\alpha,17\alpha)$ for the C₂₉ steranes (Fig. 64). Assuming the proportion of $\beta\beta$ steranes increases with increasing maturity by reasons of thermal stability up to a vitrinite reflectance of around 0.9% (Killops and Killops, 2005; Peters et al., 2005b), the highest values are expected for samples from the Hugin Formation and well 24/9-1, which hitherto exhibit the highest maturity signals. This is, however, only partly the case, since the values calculated for the Hugin Formation are mostly lower or similar to those determined for samples from well 15/3-8 and the Draupne section of well 15/3-9 T2. Nevertheless, the highest $\beta\beta/(\beta\beta+\alpha\alpha)$ ratios were indeed calculated for samples from well 24/9-1, supporting the hypothesis that the thermal maturity is higher than in expulsion scenario A (15/3-8, profile 1), B (15/3-8, profile 2) and C (15/3-9 T2, Draupne section). The comparatively low values for samples from the Hugin Formation can be interpreted either as a facies effect or may, alternatively, be related to the progressive thermal decomposition of steranes above a maturity of around 0.9% R_o, which can be inferred from the T_{max} data. Another possible explanation could be thermally-induced back rearrangement of $\beta\beta$ - to $\alpha\alpha$ -steranes at advanced levels of thermal maturity (Schwark, personal communication, 2018).

For a final conclusion about the thermal maturity, another ratio, the ratio of short-against long-chain triaromatic steroids (TA(I)/TA(I + II)) was examined for all samples. It is supposed to increase with increasing maturity due to irreparable side-

7. Discussion

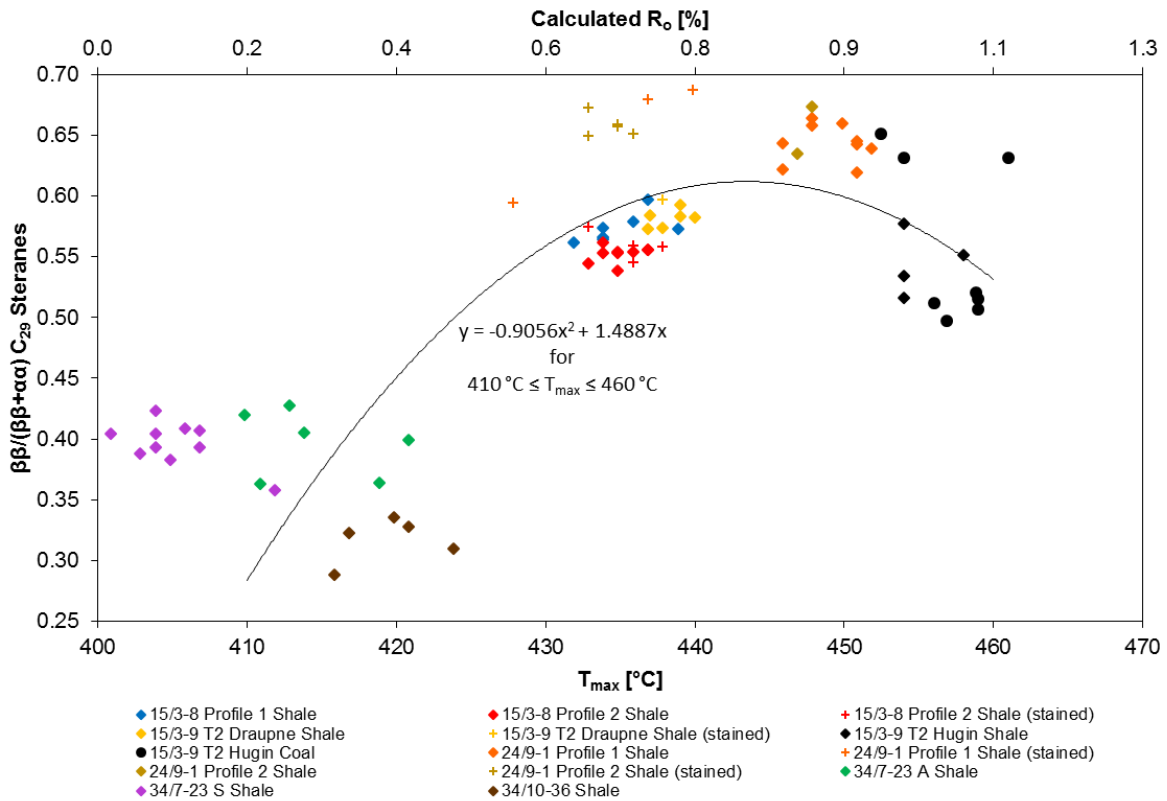


Fig. 64. T_{\max} - $\beta\beta/(\beta\beta+\alpha\alpha)$ C_{29} steranes maturity correlation. Vitrinite reflection (R_o) calculated after equation 18 (from Jarvie et al., 2007 and reference therein). Note that there is an increase of the $\beta\beta/(\beta\beta+\alpha\alpha)$ C_{29} steranes ratio with increasing thermal maturity up to vitrinite reflectance of around 0.8. Again, samples from quadrant 34 were found to be immature, while organic-rich shales from quadrant 15 and 24 are likely within the oil window. The comparatively low sterane ratios in most samples from the Hugin Formation may be explained either by facies, the thermal decomposition of steranes at advanced stages of thermal maturity, or by thermally-induced back rearrangement of $\beta\beta$ - to $\alpha\alpha$ -steranes. Samples with a production index (PI) ≥ 0.3 are labeled as “stained” and excluded from the maturity calibration. R_o values below 0.2 are shown only for completeness.

chain cleavage of long-chain triaromatic steroids (e.g. Peters et al., 2005b). A corresponding cross-plot of the T_{\max} against the TA(I)/TA(I + II) ratio is shown in Fig. 65. The lowest thermal maturity is again indicated for samples from the expulsion scenarios G, H, and I from quadrant 34, which contain the greatest proportions of long-chain triaromatic steroids. By contrast, coals and shales of the Hugin Formation exhibit the highest maturity signal among the shown samples, followed by source rock material from well 24/9-1, which is in good accordance with the previous trends. Samples from well 15/3-8 and the Draupne profile of well 15/3-9 T2 display marginally lower TA(I)/TA(I + II) ratios than organic-rich shales from well 24/9-1, suggesting slightly lower thermal maturity.

In summary, source rock material from quadrant 34 can be considered as immature, whereas organic-rich shales from quadrant 15 and 24 display oil window maturities. More specifically, among the mature samples, material from well 15/3-8 and the Draupne section of well 15/3-9 T2 was found to be in the early oil window, while

7. Discussion

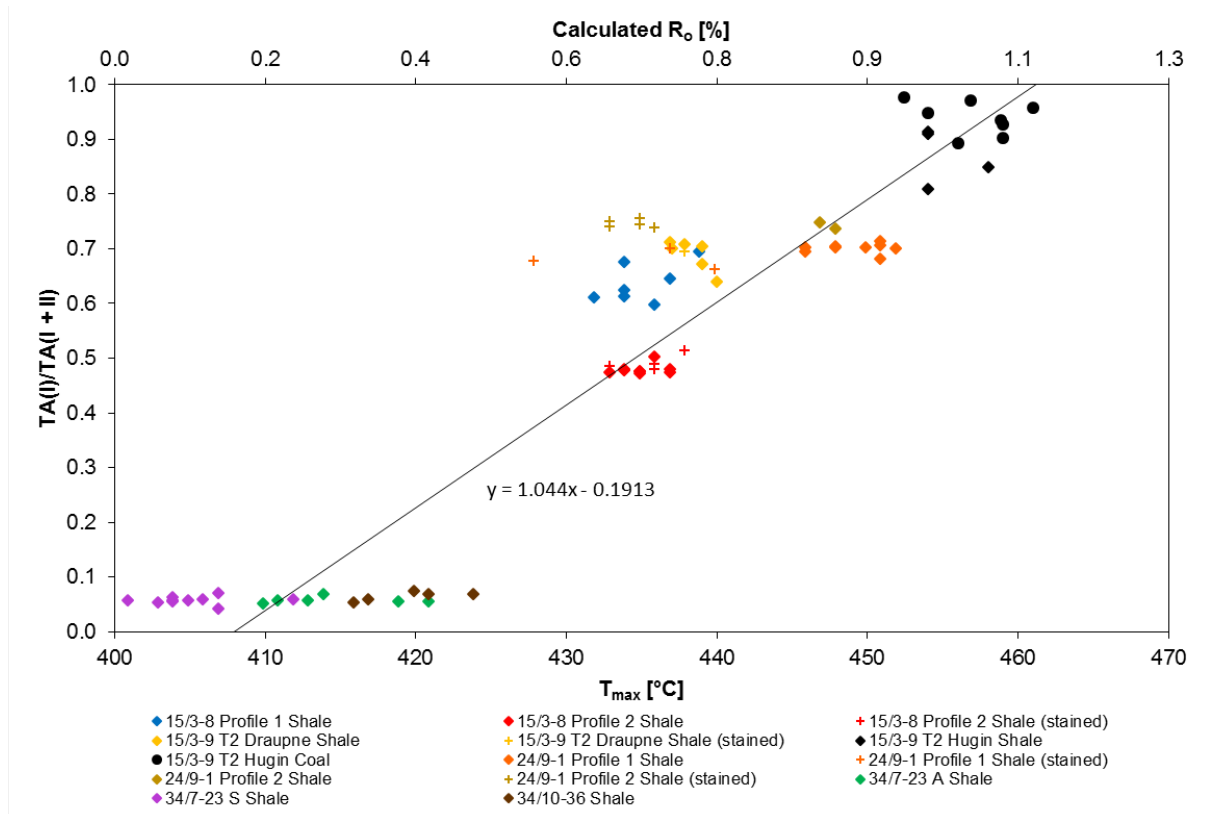


Fig. 65. T_{max} - $TA(I)/TA(I + II)$ maturity correlation. Vitrinite reflection (R_o) calculated after equation 18 (from Jarvie et al., 2007 and reference therein). Essentially, the ratio of short- to long-chain triaromatic steroids tends to increase with maturity, whereby the highest values were calculated for coals and shales of the Hugin Formation, followed by samples from well 24/9-1. Conversely, both T_{max} and $TA(I)/TA(I + II)$ data are lowest in shales from quadrant 34, indicating the lowest thermal maturity. Samples with a production index (PI) ≥ 0.3 are labeled as "stained" and excluded from the maturity calibration. R_o values below 0.2 are shown only for completeness.

samples from well 24/9-1 are slightly more mature and have probably reached peak oil generation. The highest levels of thermal maturity (late oil window) were determined for coals and shales of the Hugin Formation. Maturity differences within individual expulsion scenarios could not be detected. As a consequence, petroleum expulsion can be expected to have occurred in scenarios A (15/3-8, profile 1), B (15/3-8, profile 2), C (15/3-9 T2, Draupne section), D (15/3-9 T2, Hugin section), E (24/9-1, profile 1), and F (24/9-1, profile 2). By contrast, the data strongly suggest that source rock samples from the sections G (34/7-23 A), H (34/7-23 S), and I (34/10-36) are too immature to investigate petroleum expulsion. Note, however, that the maturity data also indicate that samples from well 34/10-36 are marginally more mature than material from well 34/7-23 A and its sidetrack 34/7-23 S, due primarily to slightly elevated T_{max} values and the maturity-dependent 22S/22R isomerization pattern of the C_{31} - C_{35} $17\alpha,21\beta(H)$ -homohopanes (see Fig. 45, 47, 49). In particular, the GC-MS data show that equilibrium is reached in samples from well 34/10-36, but not in samples from well 34/7-23 A and 34/7-23 S, which can therefore be regarded as least mature. This fact

7. Discussion

is very well expressed in a cross-plot showing the $22S/(22S+22R)$ C_{32} hopane ratio against the ratio of $20S/(20S+20R)$ C_{29} steranes, which is also controlled by the thermal maturity (Fig. 66). Essentially, both ratios increase with increasing thermal stress until equilibria are reached within the oil window. The diagram strongly suggests that source rock material from well 34/7-23 A is least mature, closely followed by organic-rich shales from well 34/7-23 S. Samples from well 34/10-36 are slightly more mature, but have probably also not yet reached the oil window. On the other hand, isomerization equilibria for both ratios are attained in samples from quadrant 15 and 24 (steranes only, not shown in Fig. 66), supporting the hypothesis of active petroleum generation and expulsion.

Based on the maturity data, the source rock column used for the geochromatographic experiment consisting of material from well 15/3-8 is most likely early oil window-mature.

7.4 Oil-source rock correlation

To identify expulsion-related compositional differences between source bitumen and reservoir petroleum, it is necessary clarify the origin of the investigated carrier bed

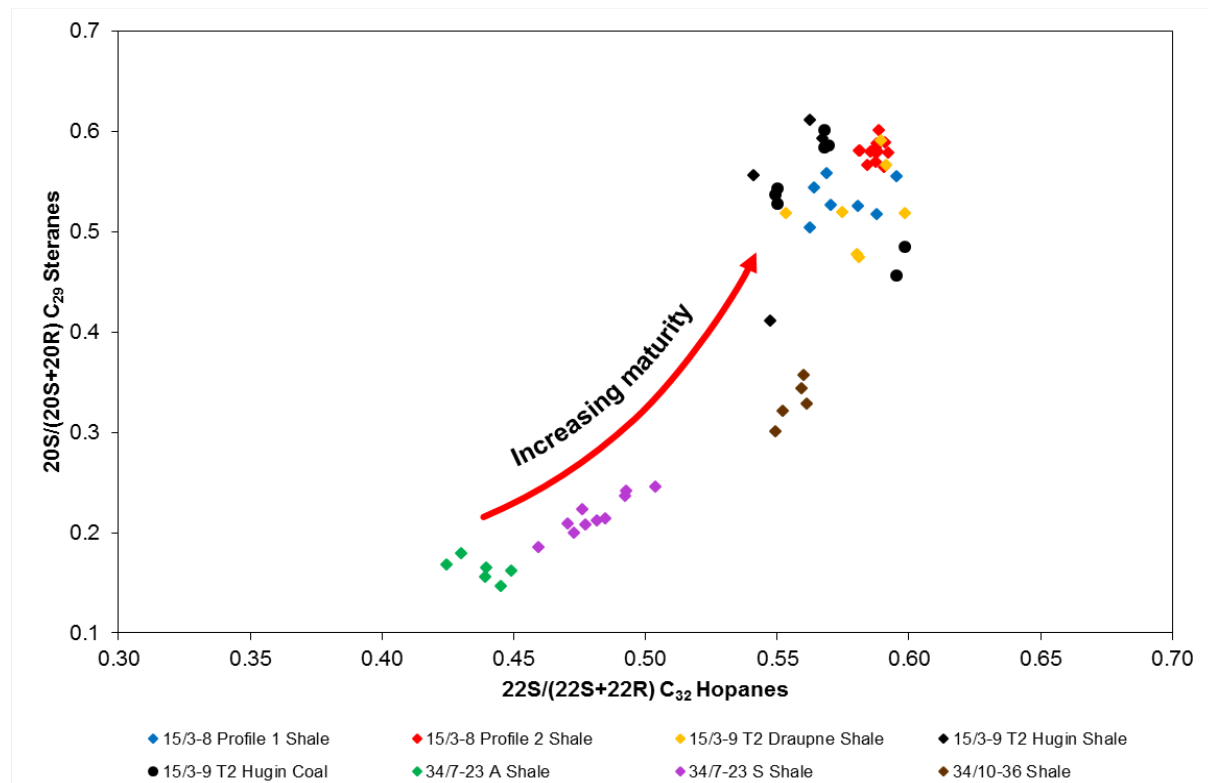


Fig. 66. Cross-plot of the $22S/(22S+22R)$ $C_{32}\alpha\beta$ hopanes ratio vs. the ratio of $20S/(20S+20R)$ $C_{29}\alpha\alpha\alpha$ steranes. Note that both ratios increase with increasing thermal maturity. Organic-rich shales from quadrant 34 can be considered as immature. Samples from well 24/9-1 are not shown due to the low abundance of hopanes. Since no striking differences between "stained" and "non-stained" samples were identified, they were, for this plot, no longer differentiated.

7. Discussion

extracts. In particular, to avoid interpretation errors due, for example, to contamination or secondary migration, it is essential that the reservoir oils are at least to a large extent sourced from the surrounding shales. Therefore, compounds are required that are supposed to do not undergo fractionation during primary migration, i.e. saturates like steranes and hopanes, but also several aromatics, e.g. individual phenanthrene and dibenzothiophene isomers (see 3.4.4).

Fig. 67 shows again a ternary diagram of C_{27} to C_{29} $5\alpha,14\beta,17\beta(H)$ -steranes ($20S+20R$), but this time with the associated reservoir extracts included. Although there is some more variability, the same data clusters as observed before in Fig. 58 are visible. Essentially, source rock samples and reservoir extracts from the Draupne Formation contain greater quantities of C_{27} and C_{28} steranes than coals and shales of the Hugin Formation. Remarkably, the carrier fluids from the Hugin Formation plot

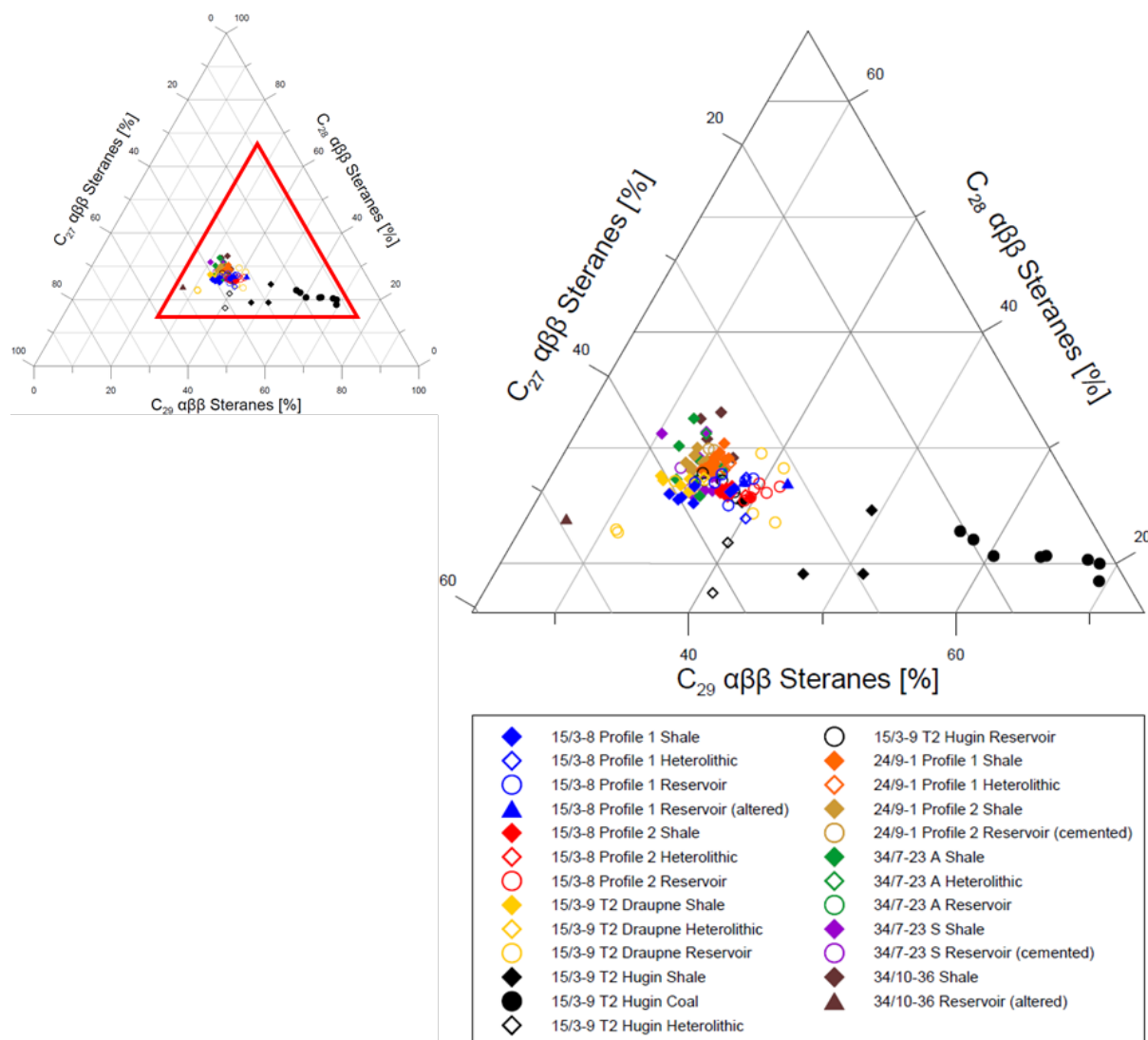


Fig. 67. Ternary diagram showing the relative distributions of C_{27} to C_{29} $5\alpha,14\beta,17\beta(H)$ -steranes ($20S+20R$) in the source rock material and the associated reservoir extracts. Note that all oils, including those from the Hugin Formation, plot in the Draupne cluster, strongly pointing to an origin from the Draupne Formation.

7. Discussion

entirely in the Draupne cluster, suggesting they are in the main Draupne-sourced. Note that the sterane signature of some Draupne oils, especially those from expulsion scenario B (15/3-8, profile 2) and the Draupne section of well 15/3-9 T2 (expulsion scenario C), does not completely resemble that of the related source rocks, which could indicate contribution of Draupne oils from slightly different organic facies. However, based on the sterane data, it is likely that all investigated reservoir extracts mainly originate from the Draupne Formation, which, for the Draupne scenarios, principally enables the investigation of petroleum expulsion.

Two excellent oil-source rock correlation parameters are the ratio of $C_{27}\beta\alpha$ (20S+20R) diasteranes against the sum of $C_{29}\alpha\alpha$ (20S+20R) and $C_{29}\alpha\beta$ (20S+20R) steranes (C_{27} Dia/ C_{29} Reg ratio), and the steranes/hopanes ratio, which is in this work defined as the ratio of C_{27} to $C_{29}\alpha\beta$ steranes (20S+20R) divided through the sum of C_{30} to $C_{35}\alpha\beta$ hopanes (22S+22R). Basically, variations in these parameters between source bitumen and reservoir petroleum may reveal contribution of different,

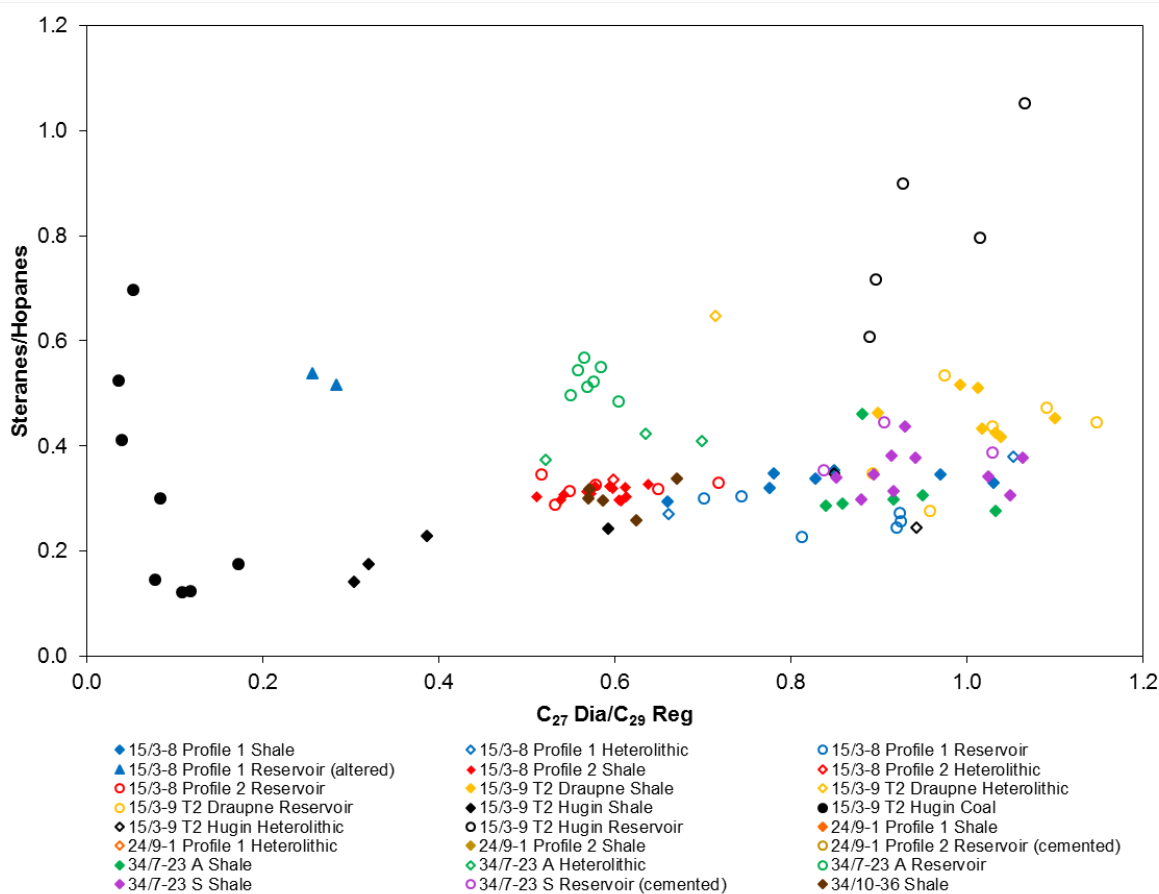


Fig. 68. Cross-plot of the C_{27} diasteranes/ C_{29} regular steranes ratio against the steranes/hopanes ratios for the investigated expulsion scenarios. The C_{27} Dia/ C_{29} Reg parameter is defined as the ratio between the $C_{27}\beta\alpha$ (20S+20R) diasteranes divided through the sum of $C_{29}\alpha\alpha$ (20S+20R) and $C_{29}\alpha\beta$ (20S+20R) steranes. The steranes/hopanes ratio describes the sum of C_{27} to $C_{29}\alpha\beta$ (20S+20R) steranes vs. the sum of C_{30} to $C_{35}\alpha\beta$ (22S+22R) hopanes. Samples from well 24/9-1 are not shown due to the low abundance of hopanes. Four outliers (reservoir; 15/3-9 T2 Draupne, 15/3-9 T2 Hugin, 34/10-36) are excluded, too.

7. Discussion

external sources to the reservoir. Fig. 68 shows a cross-plot of the C_{27} Dia/ C_{29} Reg ratio against the steranes/hopanes ratios for the investigated expulsion scenarios. Very similar values for both parameters were, even with some scattering, calculated for oils and source bitumens from well 15/3-8, suggesting the reservoir units are mainly sourced by the surrounding shales, which, as indicated by the maturity data (see 7.3), are in the active stage of petroleum generation and expulsion. Note, however, that the occurrence of gammacerane in reservoir extracts from both sections (Fig. 33, 35) indicate marginal contribution of a different, probably yet undrilled Draupne source, since gammacerane was not detected in the corresponding source rock material. Quite similar C_{27} Dia/ C_{29} Reg and steranes/hopanes ratios were also determined for source and reservoir samples from the Draupne profile of well 15/3-9 T2 (expulsion scenario C). Together with the sterane data shown in Fig. 67 and thermal maturity within the oil window (see 7.3), this also indicates that the reservoir petroleum largely derives from the surrounding shales. In contrast to well 15/3-8, gammacerane was neither present in source nor in reservoir samples from well 15/3-9 T2. Concerning the Hugin section, considerably greater C_{27} Dia/ C_{29} Reg and steranes/hopanes ratios were determined in the reservoir units than in the corresponding source rock material. As a consequence, this points to a different origin, most likely the Draupne Formation, as suggested by the distribution of steranes (Fig. 67). With regard to the expulsion scenarios E and F from quadrant 24, the steranes/hopanes ratios are, because hopanes are almost absent (Fig. 31, 33), zero for all samples and therefore not shown in Fig. 68. Nevertheless, as this is the case for both source and heterolithic/reservoir units, this indicates that the latter are charged by the surrounding, oil window-mature black shales. With respect to well 34/7-23 A, substantially lower C_{27} Dia/ C_{29} Reg and overall greater steranes/hopanes ratios were identified in the reservoir than in the source package. This clearly hints to a different origin, which is supported by the low thermal maturity of the source rock material (see 7.3). In fact, the source rock column was found to be too immature to have sourced the thick overlying reservoir. Therefore, a different origin is likely, potentially mature parts of the Draupne Formation, as suggested by the distribution of C_{27} to $C_{29}\alpha\beta\beta$ steranes (Fig. 67), in which reservoir extracts from well 34/7-23 A plot right within the Draupne cluster. For expulsion scenario H (well 34/7-23 S), both the C_{27} Dia/ C_{29} Reg, as well as the steranes/hopanes ratios of the carbonate-cemented reservoir are very similar to the adjacent source rock units. Although the section is immature and petroleum generation and expulsion can principally be

7. Discussion

excluded, the high degree of similarity strongly indicates an origin from the surrounding shales. Perhaps, the reservoir extracts from well 34/7-23 S could represent an early, pre-mature bitumen phase released upon burial-induced compaction of the surrounding black shales. Petroleum expulsion associated with catagenesis is, however, not examinable. Regarding the last expulsion scenario (well 34/10-36), GC-MS analysis provided, as already mentioned, clear evidence that the reservoir sample is biodegraded, indicating the molecular geochemical data are biased and may thus not necessarily point towards a different source. However, the maturity data of the source rock material (see 7.3) also indicate that the section is too immature to have generated and expelled large quantities of oil.

Apart from biomarkers, the distribution of selected aromatics within source vs. reservoir samples may also provide evidence for a genetic relationship between oils and source bitumens. One class of such aromatic compounds are methylphenanthrenes, which are relatively resistant to evaporation and not believed to be heavily fractionated upon primary migration (Leythaeuser et al., 1988b). A ternary diagram illustrating the distribution of the different methylphenanthrene isomers in the sample material is shown in Fig. 69. Basically, three data clusters are visible, which are principally separated by the respective abundances of 9-methylphenanthrene. While shales from well 34/7-23 A and 34/7-23 S contain the highest proportions of 9-methylphenanthrene, coals and shales of the Hugin Formation are comparatively depleted in 9-methylphenanthrene, but enriched in 2+3-methylphenanthrene. Organic-rich shales from quadrant 15 and 24, as well as from well 34/10-36 plot between both fields and exhibit intermediate proportions of 9- and 2+3-methylphenanthrene. Compared to source rock samples from well 34/7-23 A and 34/7-23 S, both other data clusters show slightly elevated proportions of 1-methylphenanthrene, particularly the Hugin coals, which could reflect a facies effect. Furthermore, when looking at the pattern, it is noteworthy that the distribution of methylphenanthrenes seems to be fundamentally controlled by the thermal maturity. In particular, with increasing maturity there is an increase in the relative proportions of 2- and 3-methylphenanthrene, which forms the basis for the methylphenanthrene index (equation 8). Note in this context that coals and shales of the Hugin Formation contain the greatest proportions of 2- and 3-methylphenanthrene, followed by samples from well 24/9-1, which is good accordance with the maturity data presented

7. Discussion

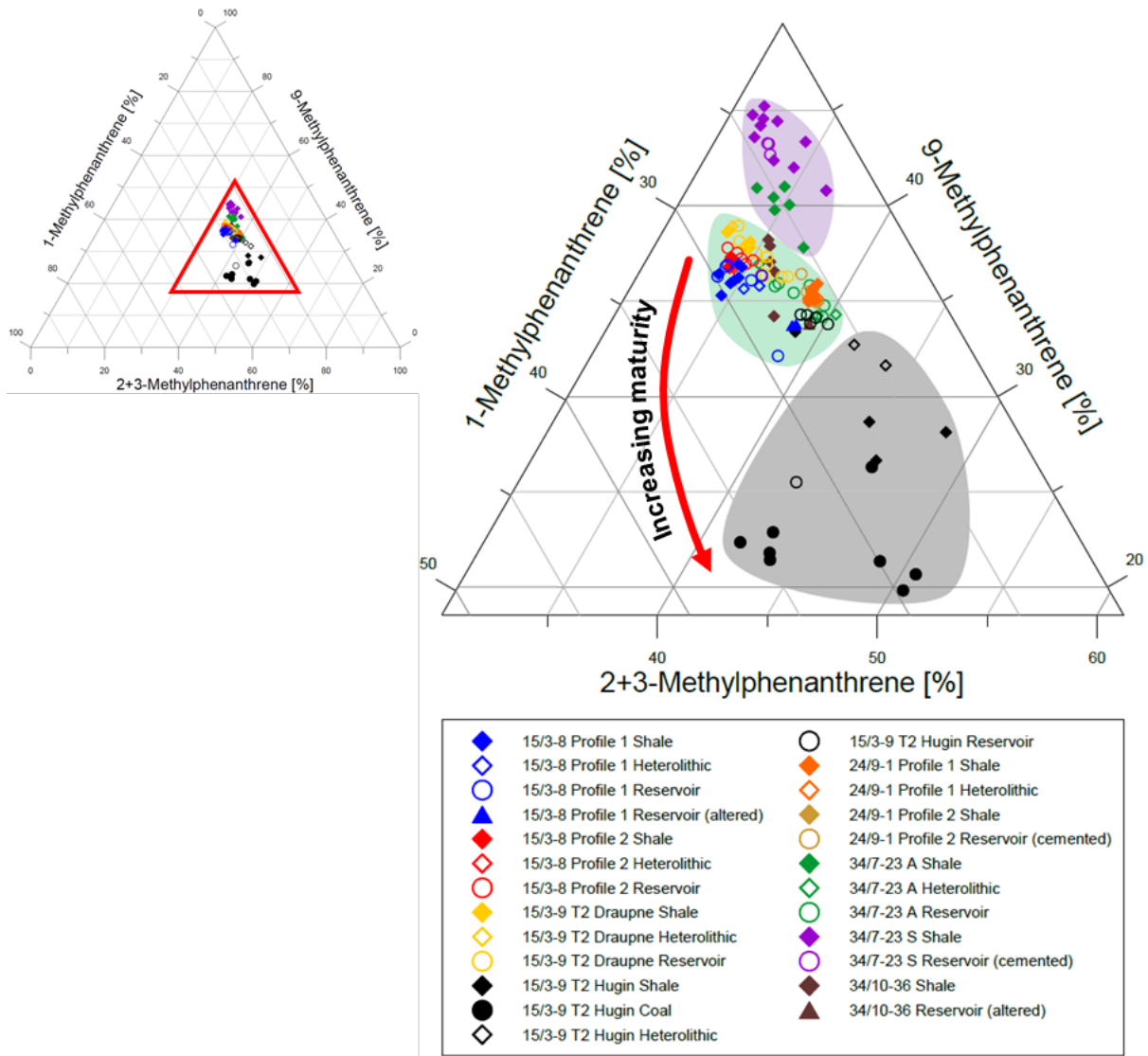


Fig. 69. Ternary diagram showing the relative distributions of methylphenanthrenes in the source rock material and the associated reservoir extracts. Note that with increasing thermal maturity there is an increase in the relative amounts of 2- and 3-methylphenanthrene. Except for oils from the Hugin section and well 34/7-23 A, most reservoir extracts plot close to the corresponding source rock material, indicating genetic relationship.

above (see 7.3). Since methylphenanthrenes are not expected to be heavily fractionated upon expulsion (Leythaeuser et al., 1988b), their distribution in reservoir oils may provide insights into the origin of the oils. Except for one outlying carrier sample from the Hugin Formation and oils from well 34/7-23 A, all reservoir extracts, including those from the immature section from well 34/7-23 S (expulsion scenario H), plot close to the corresponding source rock material. For expulsion scenario A (15/3-8, profile 1), B (15/3-8, profile 2), C (15/3-9 T2, Draupne section), E (24/9-1, profile 1), F (24/9-1, profile 2), H (34/7-23 S), and I (34/10-36), this strongly suggests, at least to a large extent, an origin from the associated source rock samples. By contrast, for expulsion scenario D (15/3-9 T2, Hugin section) and G (34/7-23 A), the distribution of methylphenanthrenes in the reservoir points to a different origin, most probably the

7. Discussion

Draupne Formation. This is in good accordance with the distribution of steranes (Fig. 67), as well as the C_{27} Dia/ C_{29} Reg and steranes/hopanes ratios (Fig. 68).

In addition to methylphenanthrenes, methyl dibenzothiophenes represent another group of aromatics that are principally suitable for the correlation of oils and source rocks. Similar to methylphenanthrenes, there is so far no clear evidence that petroleum expulsion is associated with a fractionation of methyl dibenzothiophenes. Among others, Radke (1988) proposed that their distribution may be related to the thermal maturity. Essentially, the author suggested a lower thermal stability of 1- over 4-methyl dibenzothiophene and put forward the idea of the methyl dibenzothiophene ratio as potential maturity indicator (equation 9). Fig. 70 shows a ternary diagram illustrating the distribution of methyl dibenzothiophenes in the examined sample material from the North Sea. Consider that the distribution pattern is substantially different to that of the methylphenanthrenes shown previously (Fig. 69). First, the data are generally much wider spread and, second, four instead of three data clusters are visible. The first cluster is located in the lower right corner of the diagram and characterized by elevated proportions of 1-methyl dibenzothiophene. It comprises all samples from quadrant 34, except for reservoir and some heterolithic samples from well 34/7-23 A, which contain significantly greater proportions of 4-methyl dibenzothiophene and, therefore, plot in a different cluster, together with many samples from quadrant 15. This is another evidence for a different source, most likely deeper, oil window-mature parts of the Draupne Formation. Note in this context that reservoir extracts from well 34/7-23 S, remarkably, display a composition very similar to that of the source rock samples, indicating a genetic relationship. Since there is no evidence for biodegradation and a water-based mud was used for drilling, a primary signal can be deduced. Data clusters two and three are located in the central left half of the diagram. Thereby, coals, shales and partially oils from the Hugin Formation constitute data cluster three and are characterized by slightly lower amounts of 1-methyl dibenzothiophene than source rock and reservoir samples from well 15/3-8 and the Draupne scenario of well 15/3-9 T2, which form data cluster two. Differences in the relative amount of 2+3-methyl dibenzothiophene are generally small and vary only in the magnitude of around 20%. However, coals from the Hugin Formation are marginally enriched in these compounds, which could reflect a facies effect. Shales and oils from the Hugin Formation, as well as Draupne samples from well 15/3-8 and

7. Discussion

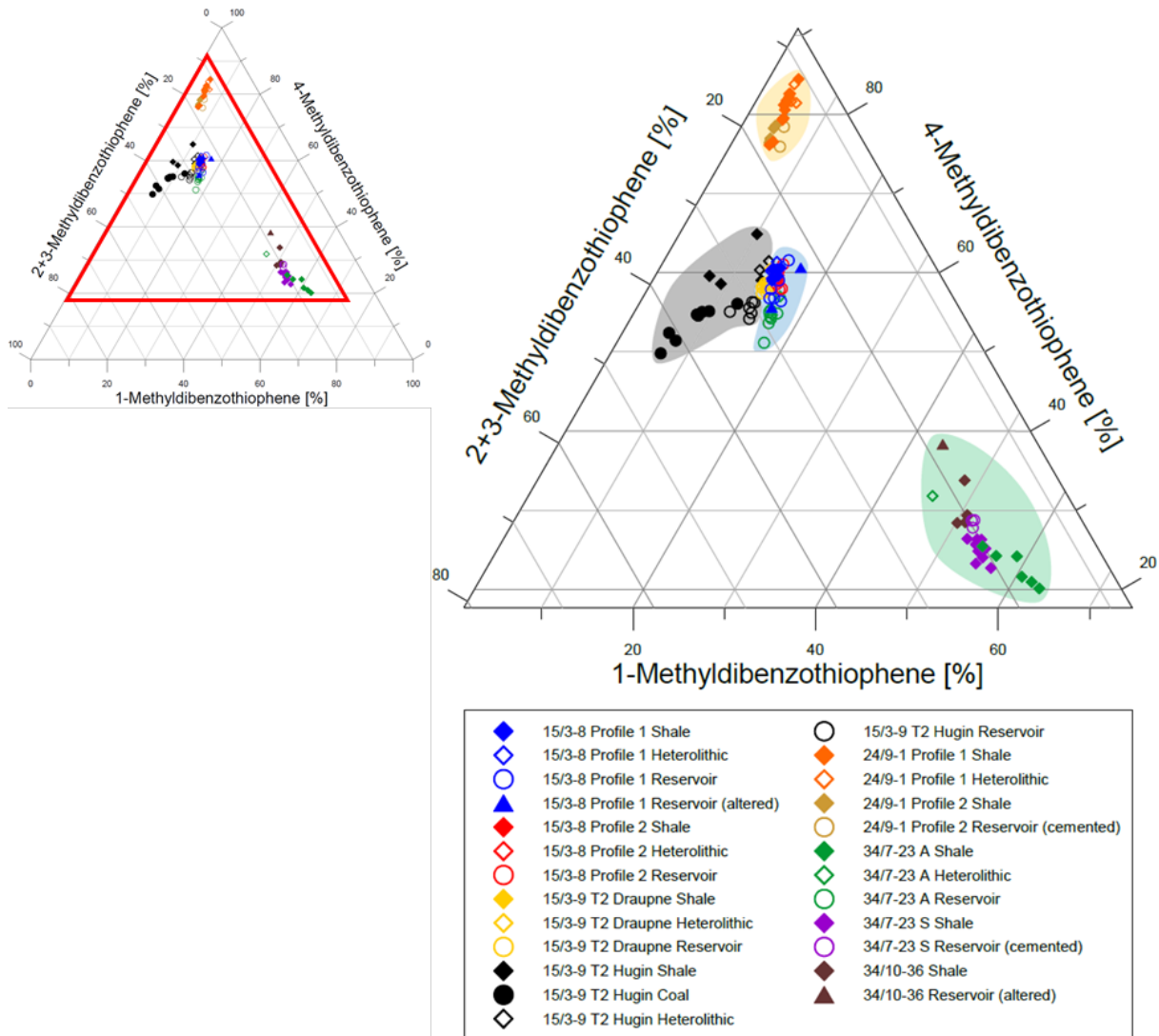


Fig. 70. Ternary diagram showing the relative distributions of methyl dibenzothiophenes in the sample material. In principal, the diagram enables the correlation of reservoir extracts and source rock samples. The distribution strongly suggests a genetic relationship between oils and shales from well 15/3-8, the Draupne section of well 15/3-9 T2, well 24/9-1, well 34/7-23 S, and, despite microbial alteration, well 34/10-36. By contrast, oils from well 34/7-23 A plot far away from the corresponding source rock material, suggesting a mature Draupne source. Oils from the Hugin Formation cannot be clearly allocated based on the distribution of methyl dibenzothiophenes, but other data suggest that they originate from the Draupne Formation. Note that the distribution of methyl dibenzothiophenes is also, but not fundamentally controlled by the thermal maturity.

15/3-9 T2 contain comparable quantities of 2+3-methyl dibenzothiophene. The lowest absolute abundances of 2+3-methyl dibenzothiophene were detected in shales and oils from well 24/9-1, closely followed by samples from quadrant 34. The former constitute the fourth and topmost data cluster, and are not only characterized by the lowest amounts of 2+3-methyl dibenzothiophene, but also by the highest relative abundances of 4-methyl dibenzothiophene. This is irrespective of the lithology, indicating petroleum extracted from carrier units of well 24/9-1 originates from the surrounding shales. This is strongly supported by the distribution of steranes and methylphenanthrenes, as well as the low abundance of hopanes in both source and carrier bed samples. The relative

7. Discussion

proportions of 1-methyldibenzothiophene are comparable to those of samples from the Hugin Formation. Regarding the distribution pattern of methyldibenzothiophenes in general, the data indeed suggest that there is an increase in the amount of 4-methyldibenzothiophene with increasing thermal maturity. However, in contrast to the methylphenanthrenes, the distribution pattern of methyldibenzothiophenes does not seem to be primarily controlled by the thermal maturity, as samples from well 24/9-1, which were not found to be most mature (see 7.3), display the greatest proportions of 4-methyldibenzothiophene. In fact, both bulk and molecular geochemical data indicate that source material from the Hugin Formation experienced the highest level of thermal stress. Therefore, it appears that, in addition to thermal maturity, facies has a strong impact on the distribution pattern of methyldibenzothiophenes. Note that, similar to the distribution of methylphenanthrenes, reservoir extracts from individual expulsion scenarios, except for section G, generally plot extremely close to the corresponding source material. This time, this is also true for oils from the Hugin Formation, which exhibit a similar methyldibenzo-thiophene signature as the adjacent coals and shales. In principal, this would point to an in situ origin, but, however, other organic geochemical data, i.e. the distribution of steranes, the steranes/hopanes ratio, and the maturity signal of the oils are considerably different and rather indicate a Draupne than a Hugin source. In support, Draupne shales and oils plot right next to them in the ternary diagram of the methyldibenzothiophenes (Fig. 70). The absence of benzo[b]carbazole in reservoir extracts from the Hugin Formation is another argument for this theory. Since benzo[b]carbazole was detected in high concentrations in both coals and shales of the Hugin Formation (Fig. 39), it would be expected to be found in any Hugin-sourced oils. As this is not the case, it seems very likely that the petroleum extracted from the reservoir units of the Hugin section is in the main Draupne-sourced. These findings are in good agreement with Isaksen et al. (1998), who proposed that Hugin coals expelled petroleum predominantly as a volatile gas/condensate phase.

Another approach to correlate reservoir oils with source rock extracts is to compare their respective maturity signals. Thereby, the best strategy is to use again compounds that are not believed to be heavily fractionated during petroleum expulsion, i.e. aliphatic biomarkers like steranes and hopanes. One variant is to apply a binary diagram of $\beta\beta/(\beta\beta+\alpha\alpha)$ C₂₉ steranes against the C₃₀ diahopane ratio, which is principally applicable within the oil window and thus allows for a correlation of oil window-mature source rocks and reservoir extracts. Fig. 71 shows such a diagram for the investigated

7. Discussion

samples, except for those from well 24/9-1, which, due likely to the combination of elevated thermal maturity and very low amounts of bacterial biomass, contain only trace quantities of hopanes. Basically, with increasing maturity, an increase in both the C_{30} diahopane ratio, as well as the $\beta\beta/(\beta\beta+\alpha\alpha)$ C_{29} sterane ratio is expected. This can indeed be observed in the diagram. While coals and shales of the Hugin Formation display the highest C_{30} diahopane ratios, indicating the highest thermal maturity, samples from quadrant 34, by contrast, exhibit the lowest maturity signal, suggesting they are immature. Samples from well 15/3-8 and the Draupne section of well 15/3-9 T2 show relatively high $\beta\beta/(\beta\beta+\alpha\alpha)$ C_{29} sterane ratios and comparatively low C_{30} diahopane ratios, implying they are less mature than source rocks from the Hugin Formation, but more mature than samples from

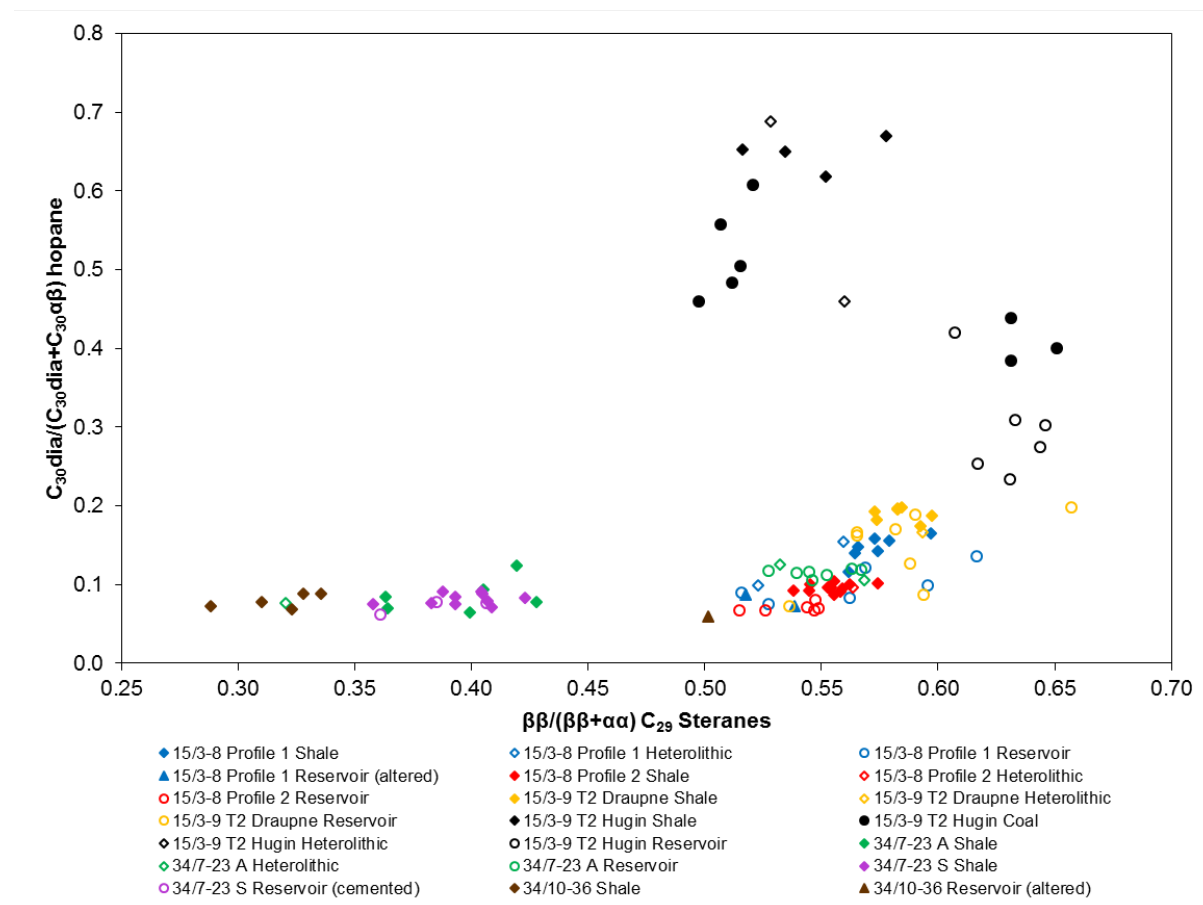


Fig. 71. Cross-plot showing the $\beta\beta/(\beta\beta+\alpha\alpha)$ C_{29} sterane ratio against the C_{30} diahopane ratio for the investigated sample material. Samples from well 24/9-1 are missing due to the low abundance of hopanes in both source rock and carrier bed extracts. As steranes and hopanes are widely not believed to be fractionated upon expulsion, the shown ratios are principally suitable to compare the maturities of oil and source rock samples and therefore enable correlation. Note that the maturity of most oils fits well with the maturity signal of the associated source rock material. However, oils from well 15/3-8 and the Draupne section of well 15/3-9 T2 show a tendency towards lower maturities and could therefore represent early expulsion products. Consider also that reservoir extracts from well 34/7-23 A and the Hugin Formation do mostly not resemble the signal of the corresponding source rock material, indicating different sources.

7. Discussion

quadrant 34. As already mentioned in section 7.3, the reduced $\beta\beta/(\beta\beta+\alpha\alpha)$ C₂₉ sterane ratios of samples from the Hugin Formation may be due to thermal degradation, facies, or back rearrangement reactions. In general, it is conspicuous that most reservoir samples plot very close to the associated source rock material, indicating a similar maturity and therefore, in principle, genetic relationship. Exceptions are reservoir extracts from well 34/7-23 A, 34/10-36, and the Hugin Formation, which exhibit different maturity signals. While for the reservoir sample from well 34/10-36 this may be due to microbial alteration, the maturity signal of oils from well 34/7-23 A and the Hugin Formation points to a different source, which is supported by other geochemical data (see above). On closer inspection of the plot, it is, however, also noticeable that reservoir extracts from well 15/3-8 and the Draupne section of well 15/3-9 T2 seem, despite the high degree of similarity, to be marginally less mature than the corresponding source extracts. Due to the early oil window maturity of the corresponding source rock material, it is proposed that these reservoir extracts represent relatively early expulsion products from the surrounding shales. However, as traces of gammacerane were detected in reservoir, but not in source rock samples from well 15/3-8 (Fig. 33, 35), lateral transport of petroleum from another, slightly less mature source can, for expulsion scenario A and B, not fully be excluded. Nevertheless, because the molecular signals of source and reservoir samples from well 15/3-8 are otherwise extremely similar, it is likely that the majority of the extracted reservoir petroleum derives directly from the surrounding, mature Draupne shales. Additional support for this hypothesis comes from the fact that all samples from quadrant 15 originate from places right within the Draupne Formation, which means additional, partly massive source rock units that are not part of the investigated expulsion scenarios are present above and below. Maturity estimation of the reservoir petroleum is, however, generally difficult, primarily because many different factors, e.g. expulsion, secondary migration, and contamination may impact its molecular composition. This is especially evident in the partially contradictory maturity profiles shown in section 6.1.2. For example, looking at the maturity-related depth profiles of expulsion scenarios A (15/3-8, profile 1) (Fig. 32), B (15/3-8, profile 2) (Fig. 34), and C (15/3-9 T2, Draupne section) (Fig. 36), the C₃₀ dihopane ratio and the triaromatic steroid ratio TA(I)/TA(I + II) are contrary to the MPI 1. More specifically, the former indicate lower maturity of the reservoir petroleum compared to the source bitumen, whereas the MPI 1 points to a higher maturity. It is postulated that, among these ratios,

7. Discussion

the C₃₀ diahopane ratio is most reliable, since biomarkers are widely assumed to be least sensitive to fractionation processes upon primary migration. By contrast, both the TA(I)/TA(I + II) ratio, as well as the MPI 1 (equation 8) comprise components of different molecular weight and structure and may thus possibly be influenced by expulsion fractionation.

In summary, the oil-source rock correlation has shown that, except for reservoir extracts from well 34/7-23 A and the Hugin Formation, most analyzed reservoir fluids originate to a large extent directly from surrounding organic-rich shales, thus enabling the identification of compositional differences related to petroleum expulsion. However, concerning expulsion scenario A and B from well 15/3-8, traces of gamma-cerane were detected in reservoir, but not in source rock samples, which could reflect marginal contribution of a different, perhaps yet undrilled Draupne facies. None-theless, since the molecular compositions of carrier bed and source extracts are very similar, this potential contribution is likely very low and therefore not believed to significantly bias interpretations. On the other hand, with respect to reservoir extracts from the Hugin Formation and well 34/7-23 A, the molecular signatures were found to be fundamentally different compared to those of the associated source bitumens, which strongly indicates different sources, most likely the Draupne Formation, as suggested by the distribution pattern of steranes (Fig. 67), methylphenanthrenes (Fig. 69), and methyldibenzothiophenes (Fig. 70). In this context, note also that both coals and shales of the Hugin Formation seem to exhibit an original molecular geochemical signature and therefore do not appear to be invaded by external petroleum. Interestingly, reservoir samples from well 34/7-23 S display a composition very similar to the surrounding, immature shales, strongly indicating a genetic relationship. For example, the extracted reservoir petroleum could represent a very early, perhaps compressionally released bitumen phase derived from the surrounding shales. Due to the low thermal maturity of the adjacent source packages, petroleum expulsion related to catagenesis is, however, rather unlikely. Therefore, this expulsion scenario is not suitable to investigate catagenetic fractionation effects related to primary migration. The same is true for well 34/10-36. Although sterane and hopane data suggest that the source material is slightly more mature than in well 34/7-23 A and 34/7-23 S (Fig. 66), the section is still too immature for effective petroleum expulsion. The carrier bed extract from well 34/10-36 is, because of secondary alteration, practically unusable,

7. Discussion

but could perhaps also represent an early, compression-related product from the surrounding shales.

Based on both the maturity assessment and the oil-source rock correlation, the most promising sections for the investigation of expulsion-related compositional differences are the sections from well 15/3-8 (expulsion scenario A, B), the Draupne section of well 15/3-9 T2 (expulsion scenario C), and the profiles from well 24/9-1 (expulsion scenario E, F). For that reason, samples from quadrant 34 and the Hugin Formation will in the following no longer be considered.

7.5 Implications from the geochromatographic experiment

The geochromatographic experiment has important implications concerning expulsion fractionation effects in natural systems. Although it is only partially comparable to nature due to the lack of pressure, temperature, and an intact rock matrix, this was, however, to the knowledge of the author, the first time that a geochromatographic experiment comprised pure, oil window-mature source rock material. Therefore, the elution pattern of the involved tracer compounds provides vital insights into their expulsion/retention characteristics, which may be transferred to natural systems.

First, based on the mass balance approach (Fig. 51), it is concluded that phenanthrenes, dibenzothiophenes, and furans are preferentially expelled from the source rock compared to carbazoles, from which generally only low amounts were recovered from the column. Indeed, while more than 70% of the furan, the phenanthrenes, and the dibenzothiophenes were successfully eluted, only around 15-25% of the C₂ carbazoles and 8.6% of the benzo[a]carbazole effectively passed the column, indicating strong molecular retention, due likely to interaction with clay minerals and/or organic material. Only benzo[c]carbazole was eluted in greater quantities (56.9%), but still not in the same order of magnitude as the furan, the phenanthrenes, and the dibenzothiophenes. The higher recovery rate of the highly alkylated 3,6-di-tert-butylcarbazole compared to the C₂ carbazoles thereby suggests that the expulsion efficiency of carbazoles increases with the degree of alkylation, which principally results in a reduction of the compound polarity.

Fractionation between phenanthrenes, dibenzothiophenes and carbazoles can be

7. Discussion

investigated using a ternary diagram of the involved C₂ carbazoles (1,4-dimethylcarbazole, 3-ethylcarbazole, 2,7-dimethylcarbazole, 3,6-dimethylcarbazole), the two dimethyldibenzothiophene isomers (4,6-dimethyldibenzothiophene, 2,8-dimethyldibenzothiophene), and the methylphenanthrenes (9-methylphenanthrene, 1-methylphenanthrene) (Fig. 72). The composition of the tracer stock solution is shown as a red dot. Only the first 20 fractions are included because later eluates did not contain significant quantities of phenanthrenes and dibenzothiophenes. Essentially, it was found that phenanthrenes were preferentially released compared to dibenzothiophenes and carbazoles, and dibenzothiophenes migrated overall faster than C₂ carbazoles. With respect to primary migration in natural systems, this indicates a preferential expulsion of phenanthrenes over dibenzothiophenes and carbazoles, which is probably polarity-controlled. Furthermore, the diagram strongly implicates that dibenzothiophenes are more easily released than carbazoles, for which the experiment suggests strong retention in the source rock. In addition, as

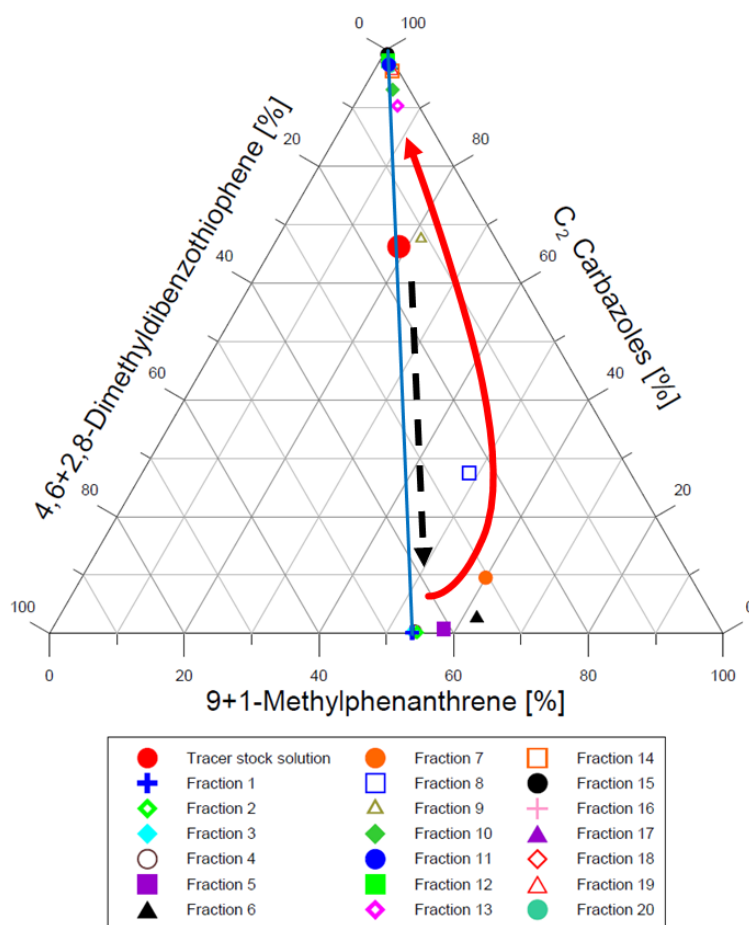


Fig. 72. Ternary diagram showing the relative distributions of C₂ carbazoles, dimethyldibenzothiophenes, and methylphenanthrenes in the eluates from the geochromatographic experiment. Basically, the data indicate a preferential release of methylphenanthrenes compared to dimethyldibenzothiophenes and C₂ carbazoles. Furthermore, there is evidence that the dimethyldibenzothiophenes migrate faster than the C₂ carbazoles. The involved C₂ carbazoles comprise 1,4-dimethylcarbazole, 3-ethylcarbazole, 2,7-dimethylcarbazole, and 3,6-dimethylcarbazole.

7. Discussion

indicated by the mass balance approach, carbazoles are likely expelled in much lower quantities compared to phenanthrenes and dibenzothiophenes, thus leading to an enrichment of phenanthrenes and dibenzothiophenes over carbazoles in reservoir units.

A similar pattern is observable when replacing the methylphenanthrenes by the 2-ethylidibenzofuran. A corresponding diagram is presented in Fig. 73. Again, it was demonstrated that carbazoles elute very late compared to their and oxygen- and sulfur-substituted counterparts and therefore seem to be preferentially retained by the source rock column. In contrast, both the dibenzothiophenes, as well as the furan appear to migrate relatively fast and pass the column efficiently. If comparing the retention characteristics of the furan and the dibenzothiophenes, the data indicate that the latter are more effectively released than the furan, suggesting a preferential expulsion of dibenzothiophenes over furans in natural systems.

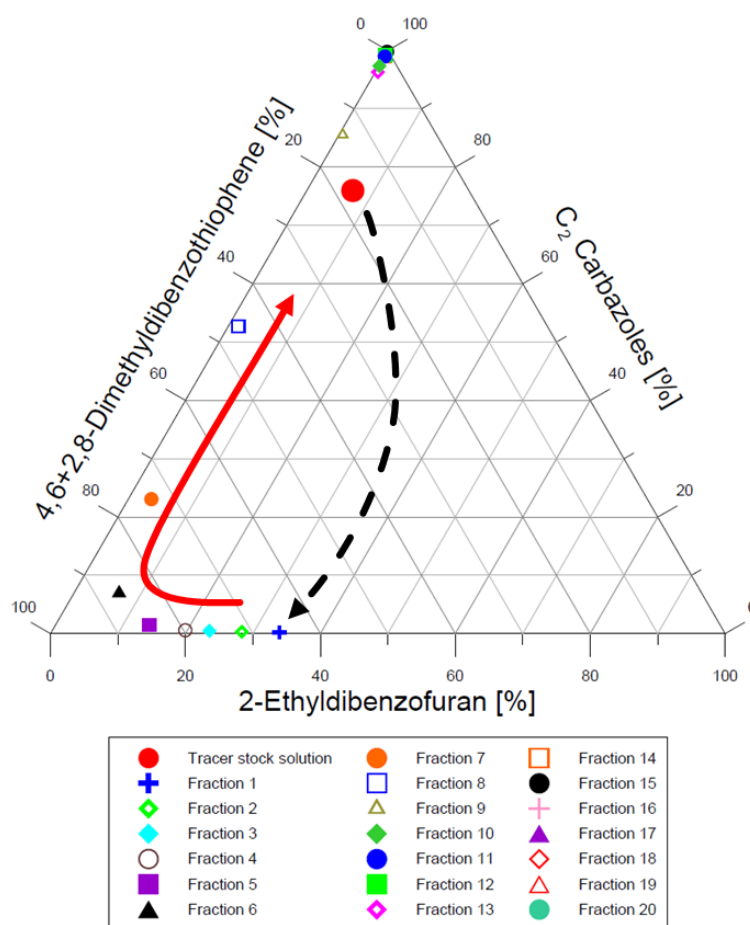


Fig. 73. Ternary diagram showing the relative distributions of C₂ carbazoles, dimethylidibenzothiophenes, and 2-ethylidibenzofuran in the eluates from the geochromatographic experiment. Note that the dimethylidibenzothiophenes appear to be preferentially released compared to the 2-ethylidibenzofuran and the C₂ carbazoles, which elute last. The involved C₂ carbazoles comprise 1,4-dimethylcarbazole, 3-ethylcarbazole, 2,7-dimethylcarbazole, and 3,6-dimethylcarbazole.

7. Discussion

Among the C₂ carbazoles, the partially nitrogen-shielded 1,4-isomer was shown to migrate slightly faster than the nitrogen-exposed equivalents, as well as the 3-ethylcarbazole (Fig. 50). Concerning natural systems, this points to a preferential expulsion of shielded over exposed C₂ carbazoles and hence higher shielded/ exposed ratios in reservoir than in source rock units. Furthermore, the mass balance approach suggests that C₂ carbazoles are expelled in approximately equal proportions (Fig. 51).

Regarding the benzocarbazoles, it was found that benzo[a]carbazole passed the column slightly faster than benzo[c]carbazole, although in significantly lower absolute quantities. Fig. 74 illustrates the evolution of the BC ratio over time. Essentially, the experiment has shown that the BC ratio was, compared to the tracer stock solution, first very high and then gradually decreased towards the end of the experiment where it remained constantly low. With respect to natural systems, the shape of this curve strongly suggests a preferential migration of benzo[a]- relative to benzo[c]carbazole. Yet, the low total quantities recovered from the column indicate that the majority of the generated benzo[a]carbazole remains in the source rock. Based on the data obtained from the experiment, it can be deduced that greater amounts of benzo[c]- than benzo[a]carbazole are expelled from a natural source rock. However, since

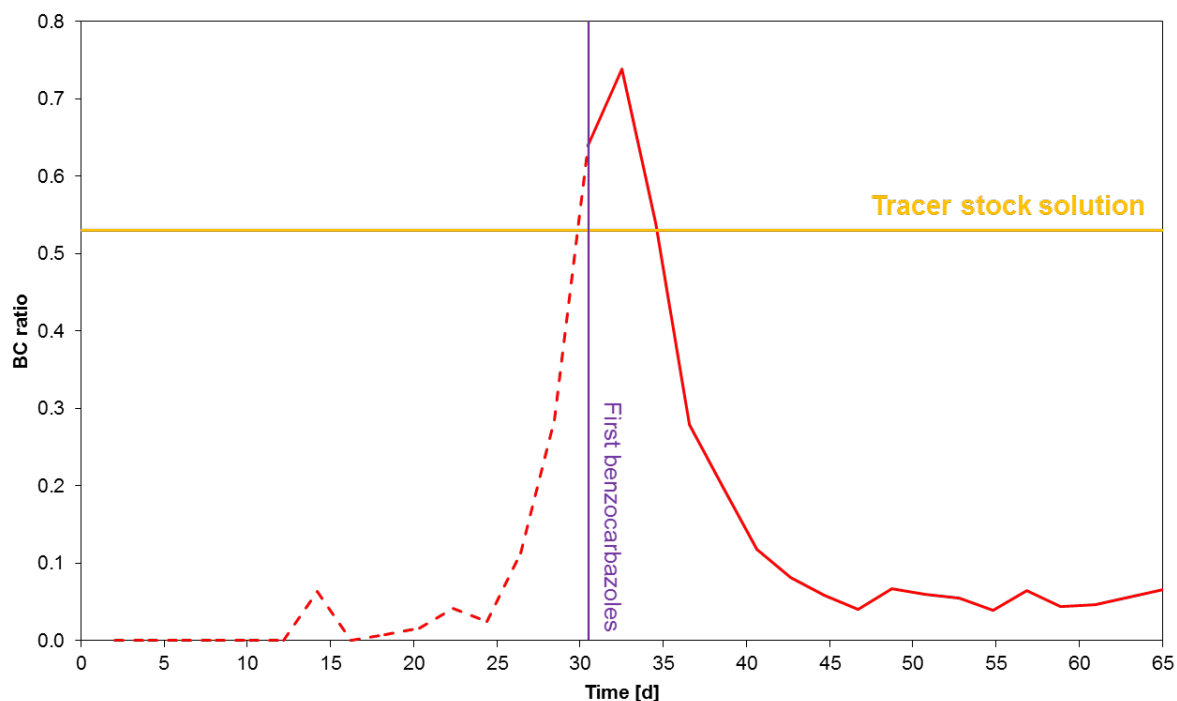


Fig. 74. Geochromatographic experiment: evolution of the benzocarbazoles ratio (BC ratio) over time. The first benzocarbazoles were eluted after around 30 days. Note that the BC ratio was first very high and then continuously decreased towards the end of the experiment. Benzo[a]carbazole passed the source rock column slightly before benzo[c]carbazole.

7. Discussion

benzo[a]carbazole left the source rock column before benzo[c]carbazole, it is proposed that the BC ratio of the initial oil expelled into a natural reservoir is very high. As time goes by, a continuous decline is expected, due primarily to the expulsion of greater quantities of benzo[c]carbazole.

In contrast to the BC ratio, no significant differences between the tracer stock solution and the eluted fractions were found for the ratio between 9- and 1-methylphenanthrene (Fig. 75). Nevertheless, slightly elevated ratios at the very beginning of the experiment may be interpreted by a marginally faster migration of 9- over 1-methylphenanthrene, which could be related to the molecular structure. Progressing time led to a decrease towards the initial value of the stock solution. Most methylphenanthrenes were eluted before day 20, indicating relatively weak interaction with the source rock column. The recovery rates for both compounds were found to be very similar (Fig. 51), but with a slight preference of the 9-isomer. It is, however, questionable in how far these comparatively small differences are transferable to and actually observable in natural systems.

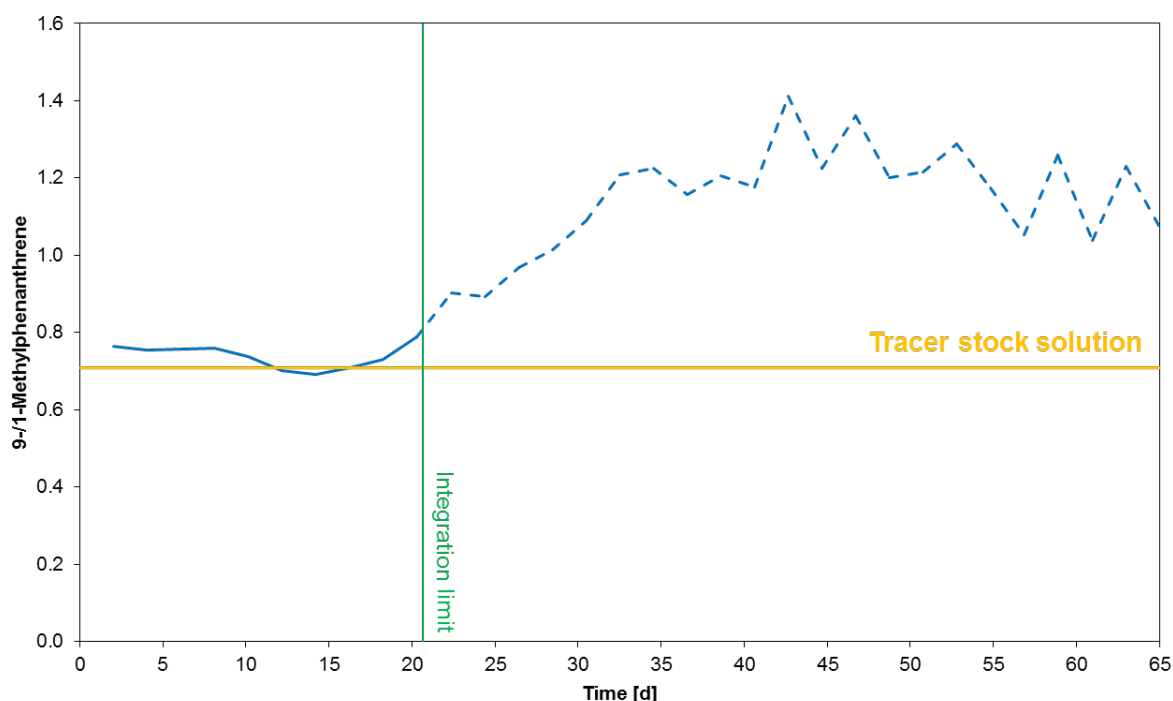


Fig. 75. Geochromatographic experiment: evolution of the 9-/1-methylphenanthrene ratio over time. Note that only small differences in the 9-/1-methylphenanthrene ratio between the tracer stock solution and the eluates were observed, indicating weak fractionation. If any, slightly higher 9-/1-methylphenanthrene ratios at the very beginning of the experiment could indicate marginally faster migration of 9- over 1-methylphenanthrene. Only trace quantities of methylphenanthrenes were present after day 22.

7.6 Identifying fractionation effects in the natural case scenarios

As expulsion scenario D (15/3-9 T2, Hugin section), G (34/7-23 A), H (34/7-23 S), and I (34/10-36) turned out to be not suitable for the investigation of petroleum expulsion, the following section concentrates on the expulsion scenarios A (15/3-8, profile 1), B (15/3-8, profile 2), C (15/3-9 T2 Draupne section), E (24/9-1, profile 1), and F (24/9-1, profile 2), where active expulsion can be expected based on the maturity data. Moreover, the oil-source rock correlation strongly suggests genetic relationship between source bitumen and corresponding reservoir petroleum. In conformity with the geochromatographic experiment, the investigation of fractionation effects in the natural scenarios predominantly focused on phenanthrenes, dibenzothiophenes, dibenzofurans, as well as carbazoles. As not considered in the geochromatographic experiment, the aliphatic fraction played a rather subordinate role. It is, however, strongly recommended to examine the migration behavior of aliphatic components, particularly biomarkers, in similar retardation experiments in the future.

Ternary component systems involving phenanthrenes, dibenzothiophenes, dibenzofurans, and carbazoles are a good approach to investigate expulsion fractionation effects of these compounds between source and adjacent reservoir rocks. Due to a higher resistivity to evaporation and therefore a greater result reliability, the triangular diagrams shown in the following comprise, yet, only the respective methylated (C_1) analogs. Thereby, the C_1 phenanthrenes involve 3-, 2-, 9-, and 1-methylphenanthrene, the C_1 dibenzothiophenes include 4-, 2-, 3-, and 1-methyldibenzothiophene, the C_1 dibenzofurans comprise 4-, 2-, 3-, and 1-methyldibenzofuran, and the C_1 carbazoles encompass 1-, 3-, 2-, and 4-methylcarbazole, respectively. Nevertheless, note that supplementary plots including exclusively the non-methylated counterparts (not shown) produced the same results, pointing to a high degree of reliability.

7.6.1 System C_1 phenanthrenes- C_1 dibenzofurans- C_1 dibenzothiophenes

Since the retention behaviour of phenanthrenes, dibenzofurans, and dibenzothiophenes was a major part of the geochromatographic retardation experiment, the first component system that was examined for expulsion effects was the ternary system C_1 phenanthrenes- C_1 dibenzofurans- C_1 dibenzothiophenes. A corresponding diagram showing the relative distributions of methylated phenanthrenes, dibenzofurans, and

7. Discussion

dibenzothiophenes in source and reservoir samples from the sections comprising actively generating and expelling source rock material can be found in Fig. 76. Note the strong enrichment of phenanthrenes over dibenzothiophenes and especially dibenzofurans in the carrier beds compared to the associated source rock samples. It is postulated that this is due primarily to expulsion fractionation with a clear preference of the less polar phenanthrenes over dibenzothiophenes and dibenzofurans, which appear to be stronger retained by the source rock. Among the latter, dibenzofurans seem to be most strongly retained, probably because of a higher polarity and therefore greater interaction with minerals and/or organic material in the source rock compared to the dibenzothiophenes. The heterolithic samples

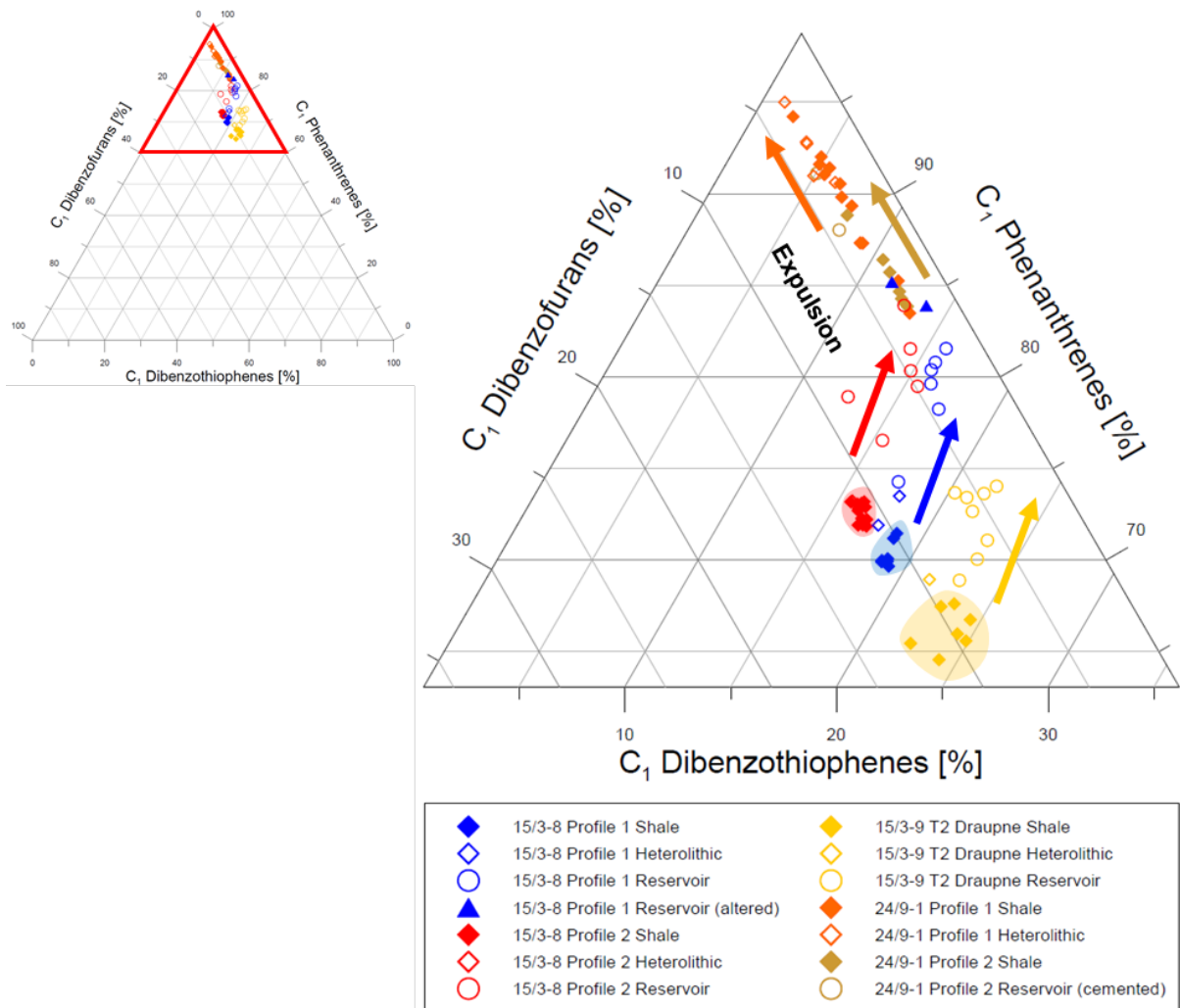


Fig. 76. Ternary system C₁ phenanthrenes-C₁ dibenzofurans-C₁ dibenzothiophenes for the samples from the natural expulsion sequences comprising actively generating and expelling source rock material. Note the clear enrichment of phenanthrenes over dibenzothiophenes and dibenzofurans in reservoir compared to source rock samples. In addition, dibenzofurans appear to be preferentially retained by the source rock compared to dibenzothiophenes. Biodegradation seems to shift the data towards higher phenanthrene contents, as indicated by the two altered samples from expulsion scenario A (well 15/3-8, profile 1).

7. Discussion

were found to display mostly an intermediate signal and have thus likely also received some petroleum from the surrounding shales.

The results are in very good agreement with both the data obtained from the geochromatographic experiment, as well as the kerogen solubility parameters calculated by Ritter (2003). Indeed, like in the natural scenarios, the geochromatographic experiment demonstrated a preferential release of phenanthrenes compared to dibenzothiophenes, dibenzofurans, and carbazoles. In support, Ritter (2003) calculated greater polymer solubility parameters for dibenzothiophene than for phenanthrene and methylphenanthrenes, suggesting a stronger interaction with the kerogen network and hence a preferential expulsion of phenanthrenes into the reservoir. This is corroborated by the shapes of the corresponding molecular geochemical depth profiles shown in chapter 6, where the source rock intervals frequently show higher C_1 DBT/ C_1 Phn and C_1 DBF/ C_1 Phn ratios as the adjacent carrier beds, indicating phenanthrenes are more readily expelled.

Interestingly, the ternary diagram additionally suggests that biodegradation shifts the data towards higher phenanthrene contents, as indicated by the two microbially altered reservoir samples from expulsion scenario A (15/3-8, profile 1). Conversely, this means that dibenzofurans and dibenzothiophenes are, compared to phenanthrenes, preferentially degraded by microorganisms.

7.6.2 System C_1 phenanthrenes- C_1 carbazoles- C_1 dibenzothiophenes

The second ternary component system that was regarded compared the relative proportions of C_1 phenanthrenes, C_1 carbazoles and C_1 dibenzothiophenes in source rock and carrier bed extracts from the relevant expulsion scenarios. A corresponding triangular diagram is presented in Fig. 77. Essentially, similar to the previously examined system that included dibenzofurans instead of carbazoles, a clear enrichment of phenanthrenes over dibenzothiophenes and carbazoles was identified in the reservoir. Therefore, it is concluded that phenanthrenes are more easily expelled than dibenzothiophenes and carbazoles. If comparing the relative proportions of C_1 carbazoles and C_1 dibenzothiophenes, it seems that the reservoir rocks are slightly more enriched in dibenzothiophenes than in carbazoles, which could indicate that carbazoles are even stronger retained than dibenzothiophenes, due probably to a stronger interaction with minerals, particularly clays, and/or organic material. This is

7. Discussion

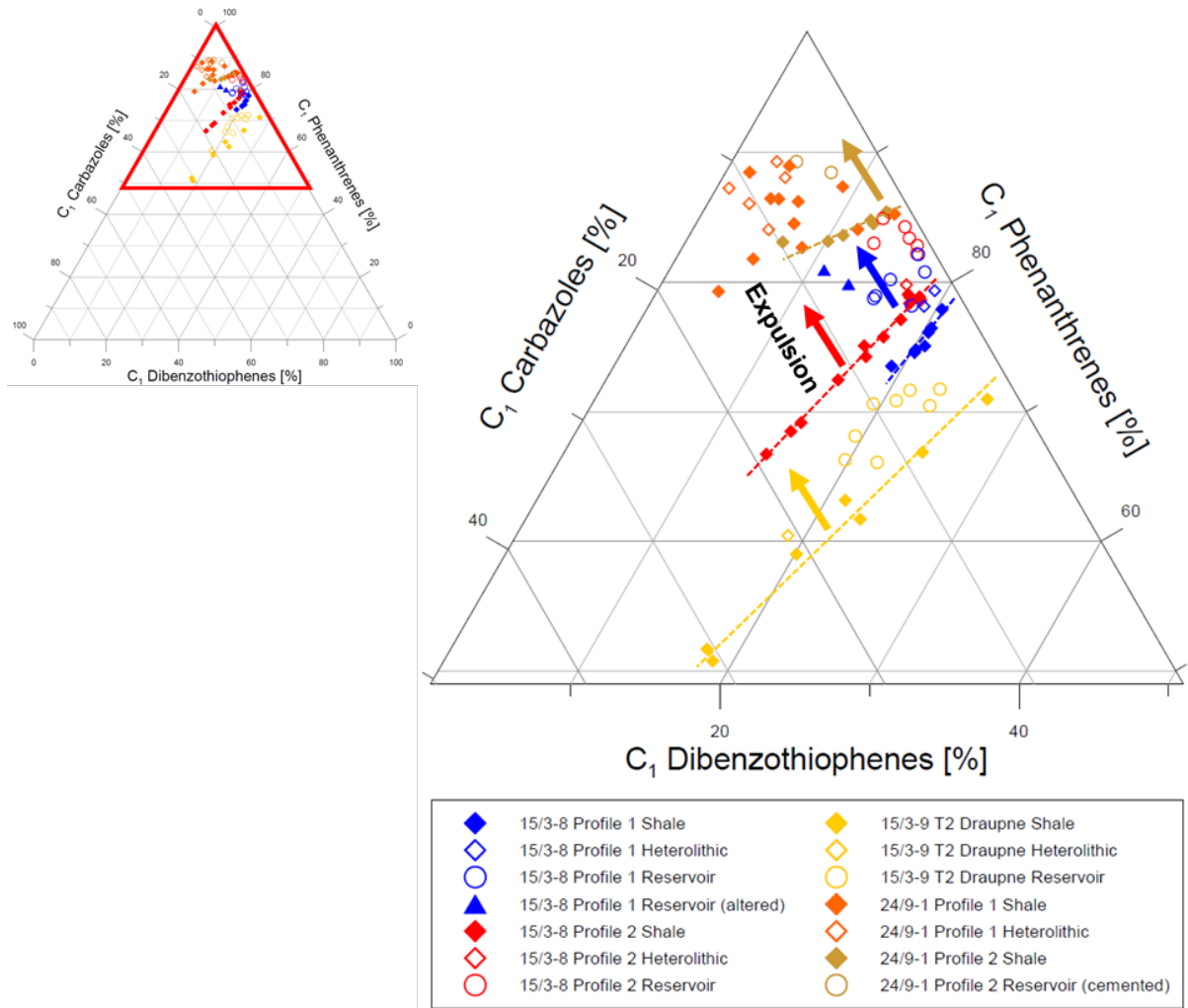


Fig. 77. Ternary system C₁ phenanthrenes-C₁ carbazoles-C₁ dibenzothiophenes for the samples from the natural expulsion sequences comprising actively generating and expelling source rock material. There is a clear tendency of phenanthrene enrichment over carbazoles and dibenzothiophenes in the reservoir, strongly pointing to a preferential expulsion of phenanthrenes. Furthermore, dibenzothiophenes seem to be preferentially released compared to carbazoles.

supported by the results of the geochromatographic experiment, in which carbazoles eluted later and in substantially lower absolute quantities than phenanthrenes and dibenzothiophenes. Again, heterolithic samples tend to exhibit intermediate signals.

Similar to the previous component system, biodegradation seems to increase the content of phenanthrenes relative to carbazoles and dibenzothiophenes, indicating a higher resistance to microbial alteration. Note also the partially large variations in the content of C₁ carbazoles within source rock samples, particularly from quadrant 15, indicating the proportion of C₁ carbazoles in a source rock sample is also related to depositional factors, perhaps fluctuations of the organic matter input.

7.6.3. System C₁ carbazoles-C₁ dibenzofurans-C₁ dibenzothiophenes

The next component system that was investigated for expulsion-related fractionation

7. Discussion

effects comprised C₁ carbazoles, C₁ dibenzofurans, and C₁ dibenzothiophenes (Fig. 78). Interestingly, much less clear trends as in the systems before are visible. While on one hand the geochromatographic experiment clearly points to an enrichment of dibenzothiophenes and dibenzofurans over carbazoles in the reservoir this is, however, only in part observable in the natural expulsion scenarios. Yet, despite some variation, C₁ dibenzothiophenes indeed appear to be enriched in most reservoir extracts, which could be interpreted by a preferential expulsion of dibenzothiophenes relative to carbazoles and dibenzofurans. A similar tendency was observed in the geochromatographic experiment, in which the dibenzothiophene isomers passed the source rock column more efficiently than the dibenzofuran and the carbazoles. Further evidence for a preferential expulsion of dibenzothiophenes relative to dibenzofurans derives from the molecular geochemical depth profiles presented in

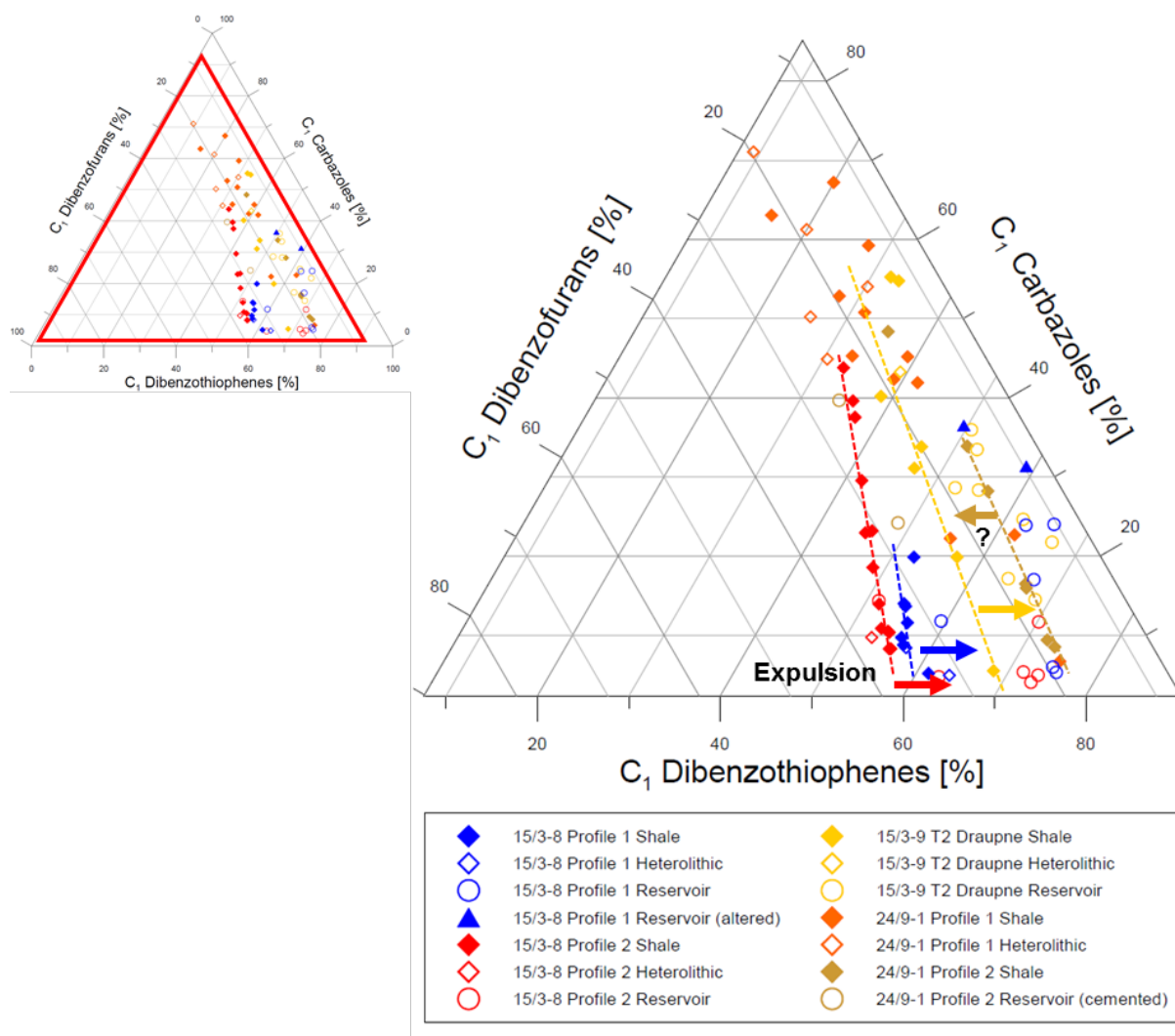


Fig. 78. Ternary system C₁ carbazoles-C₁ dibenzofurans-C₁ dibenzothiophenes for the samples from the natural expulsion sequences comprising actively generating and expelling source rock material. Note the general tendency of dibenzothiophenes enrichment in the reservoir samples, which indicates a preferential expulsion of dibenzothiophenes over dibenzofurans and carbazoles into the reservoir. However, this trend is not observable in samples from quadrant 24, suggesting that other, perhaps depositional-related factors may play a role.

7. Discussion

chapter 6. In the majority of the relevant expulsion sections, C₁ dibenzothiophenes are, compared to C₁ dibenzofurans, depleted in the source rock compared to reservoir unit, indicating they are preferentially released into the carrier bed. This tendency was, however, not observed in expulsion scenario E and F from quadrant 24, which may be an artifact of elevated thermal maturity or, as maturity effects within individual expulsion scenarios can be ruled out, indicate the contribution of other, perhaps depositional-related factors.

7.6.4 Distribution of methylated dibenzofurans

The close similarity between source bitumens and reservoir extracts in their distributions of methylphenanthrene and methyl dibenzothiophene isomers revealed during the oil-source rock correlation (see 7.4) strongly suggests that both methylated phenanthrenes, as well as methylated dibenzothiophenes are not significantly redistributed during petroleum expulsion and can therefore well be applied for oil-source rock correlations. Although the results of the retardation experiment point to a weaker retention of the 9- over the 1-methylphenanthrene isomer this effect was, however, not witnessed in the natural scenarios. Therefore, the results are so far in good agreement with the findings of Leythaeuser et al. (1988b), who also did not recognize expulsion-related fractionation effects among individual methylphenanthrene isomers.

Equivalent to Fig. 69 and Fig. 70, Fig. 79 illustrates the relative distributions of methyl dibenzofuran isomers in source vs. carrier rocks of the relevant expulsion scenarios. As shown in the diagram, all samples, including the reservoir extracts, plot in a relatively narrow area in the center of the diagram. This indicates that differences between source and reservoir rocks are generally small, which further strengthens the assumption of a genetic relationship between source bitumen and reservoir petroleum. However, a closer examination reveals that the reservoir samples, particularly those from quadrant 15, are commonly enriched in 2- and 3-methyl dibenzofuran compared to the associated source rock material, which may be explained by a preferential expulsion of the 2- and 3- over the 1- and 4-isomer. As both the 2- and the 3-isomer can be considered as “oxygen-exposed” compounds, this effect seems to be related to the molecular structure, which appears to impede interaction with the surrounding environment. Nevertheless, the trend is less clear for samples from the first profile of well 24/9-1, underscoring the necessity of further

7. Discussion

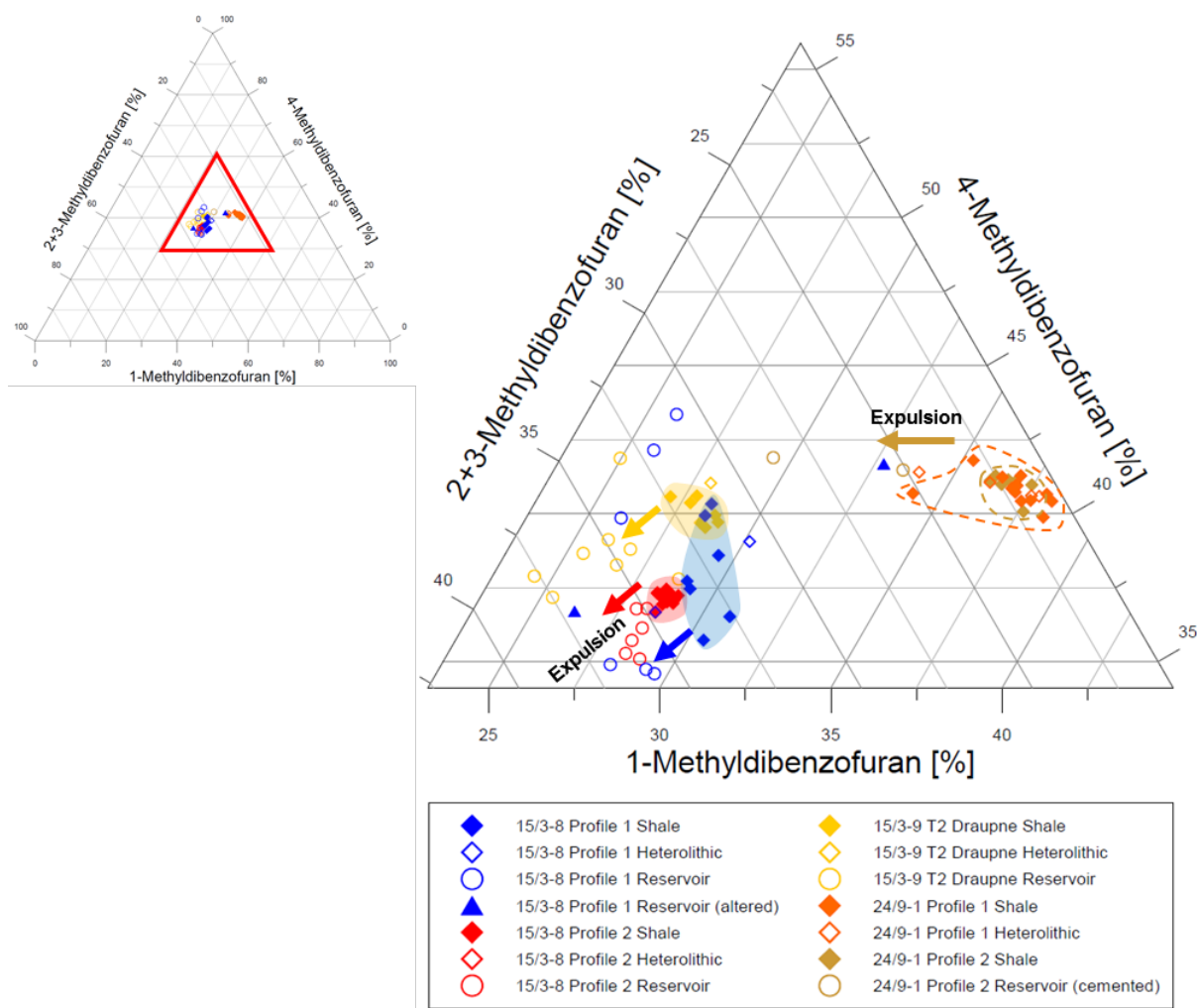


Fig. 79. Ternary system showing the relative distributions of methyl dibenzofurans in the samples from the natural expulsion sequences comprising actively generating and expelling source rock material. Note that 2- and 3-methyl dibenzofuran are usually enriched in the reservoir compared to the source rock units. This could be interpreted by a preferential expulsion of 2- and 3- over 1- and 4-methyl dibenzofuran, which may be due to the molecular structure.

examinations. The apparent expulsion-dependency of the methyl dibenzofuran distribution principally contrasts the observations made for the methylphenanthrene and methyl dibenzothiophene isomers, where no fractionation effects between source and reservoir rocks were documented. For the future, it is strongly recommended to conduct a geochromatographic experiment comprising different methyl dibenzofuran isomers.

7.6.5 Distribution of methylated carbazoles

The distribution of C₁-alkylated carbazoles in crude oils and source bitumens has, due to molecular shielding effects of the nitrogen functionality, often been discussed in the context of fractionation effects related to petroleum migration (e.g. Li et al. 1995; Clegg et al. 1997, 1998a; Horsfield et al., 1998). However, there is so far no clear evidence for a selective retention of certain isomers during primary or secondary migration.

7. Discussion

Instead, the distribution has been proposed to be influenced by the thermal maturity (Clegg et al., 1997, 1998b) and the depositional conditions of the source rock (Bakr and Wilkes, 2002). Nevertheless, methylated carbazoles seem to have application potential to reconstruct lateral migration in petroleum systems comprising high-sulfur crudes and carbonate source rocks (Horsfield et al., 1998).

Fig. 80 shows a triangular diagram (after Li et al., 1995) illustrating the distribution of methylcarbazoles in source and reservoir units of the natural scenarios that are supposed to record active petroleum expulsion. Essentially, the data are in good agreement with, for example, Clegg et al. (1998a) and Horsfield et al. (1998), who did not observe expulsion-related fractionation effects among C₁ carbazoles. On the other hand, this is contrary to the findings of Li et al. (1995), who described a preferential expulsion of nitrogen-shielded vs. nitrogen-exposed compounds.

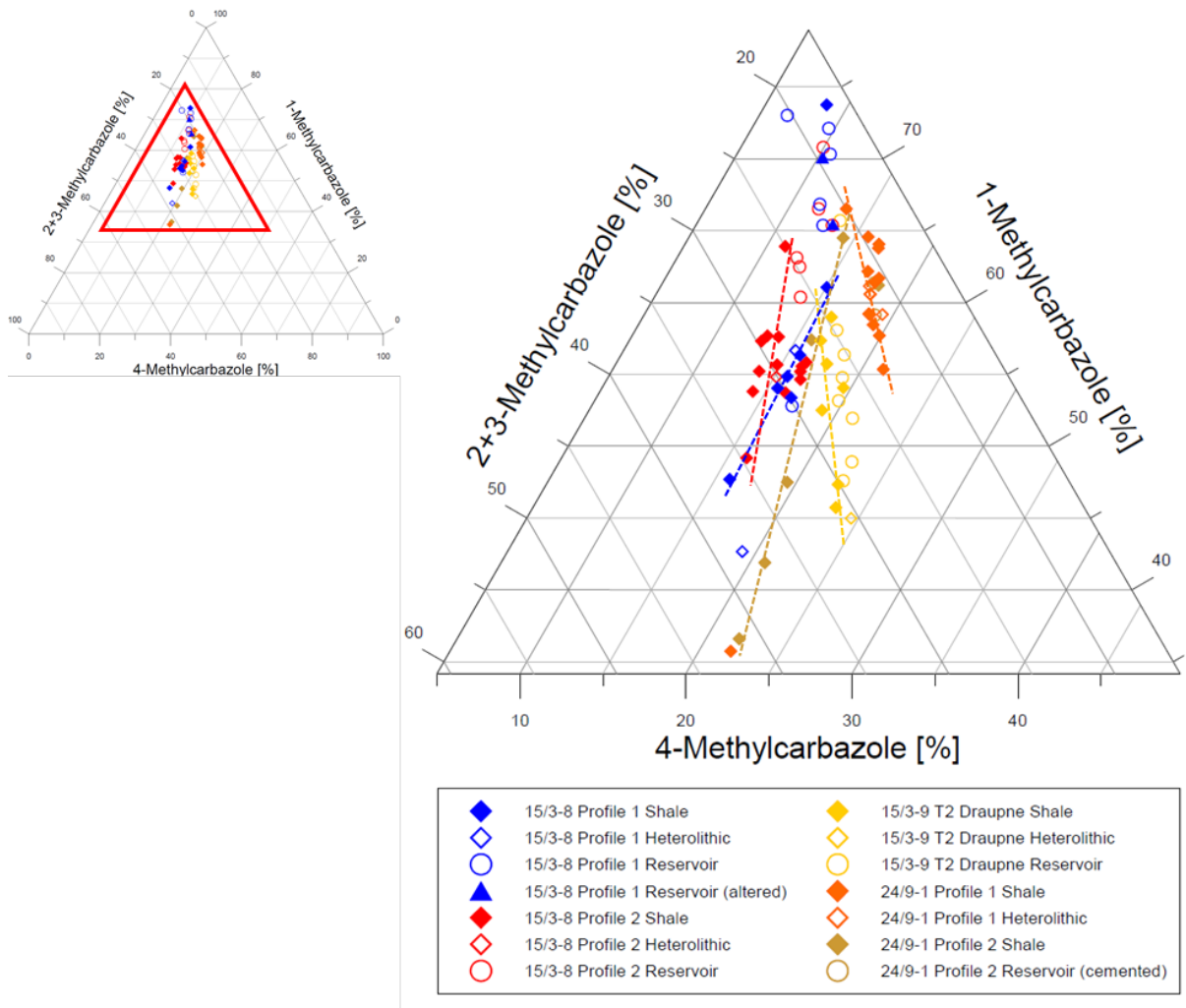


Fig. 80. Ternary system showing the relative distributions of methylcarbazoles in the samples from the natural expulsion sequences comprising actively generating and expelling source rock material (after Li et al., 1995). No clear evidence for selective retention of certain isomers was found. Rather, the distribution is highly variable, even within individual scenarios. As maturity effects can largely be excluded, this indicates that other, maybe depositional-related factors play a role.

7. Discussion

Therefore, similar to the distributions of methylphenanthrenes and methyl dibenzothiophenes discussed before, the distribution of methylated carbazoles in source rock and crude oils does, according to the results of this work, not seem to be influenced by petroleum expulsion and hence selective retention of certain isomers. Nonetheless, the partially high variability within individual expulsion scenarios, for which maturity differences can be excluded (see 7.3), additionally suggests that the distribution of methylcarbazoles is considerably influenced by depositional-related factors, perhaps small-scale variations of the organic facies. Similar tendencies were already observed before in the triangular diagrams comprising the C₁ carbazoles as a whole.

7.6.6 Nitrogen-shielded vs. nitrogen-exposed C₂ carbazoles

Like the distribution of methylcarbazoles, the distribution pattern of C₂-alkylated carbazoles has also been suggested to be influenced by fractionation processes during petroleum migration (e.g. Larter and Aplin, 1995; Li et al., 1995; Stoddart et al., 1995). Similarly, nitrogen-shielded isomers have been proposed to migrate faster and to be less retained than nitrogen-exposed isomers, which are more prone to molecular interaction with reactive surfaces and/or pore water, primarily by means of hydrogen bonding (Li et al., 1995). However, whether C₂-alkylated carbazoles are indeed fractionated during primary and secondary migration remains a matter of debate. For example, in contrast to Li et al. (1995), Clegg et al. (1998a) did not find evidence for a preferential migration of nitrogen-shielded over nitrogen-exposed C₂ carbazoles. Likewise, Bakr and Wilkes (2002) noted only minor variability in the distribution of C₂-alkylated carbazoles, leading them to the conclusion that alkyl-carbazoles are not suitable for petroleum exploration purposes. By contrast, the case study of Stoddart et al. (1995), who detailedly investigated the geochemistry of the Eldfisk Field in the Norwegian North Sea, largely supports the findings of Li et al. (1995). Correspondingly, variations in the distribution of pyrrolic nitrogen compounds were mainly attributed to petroleum migration.

Fig. 81 presents a triangular diagram (after Clegg et al., 1998b) comparing the relative distributions of selected fully nitrogen-shielded (1,8-dimethylcarbazole), partially nitrogen-shielded (1,3-dimethylcarbazole), and nitrogen-exposed (2,7-dimethylcarbazole) C₂ carbazoles in samples from the investigated natural scenarios comprising actively generating and expelling source rock material. Note that there is

7. Discussion

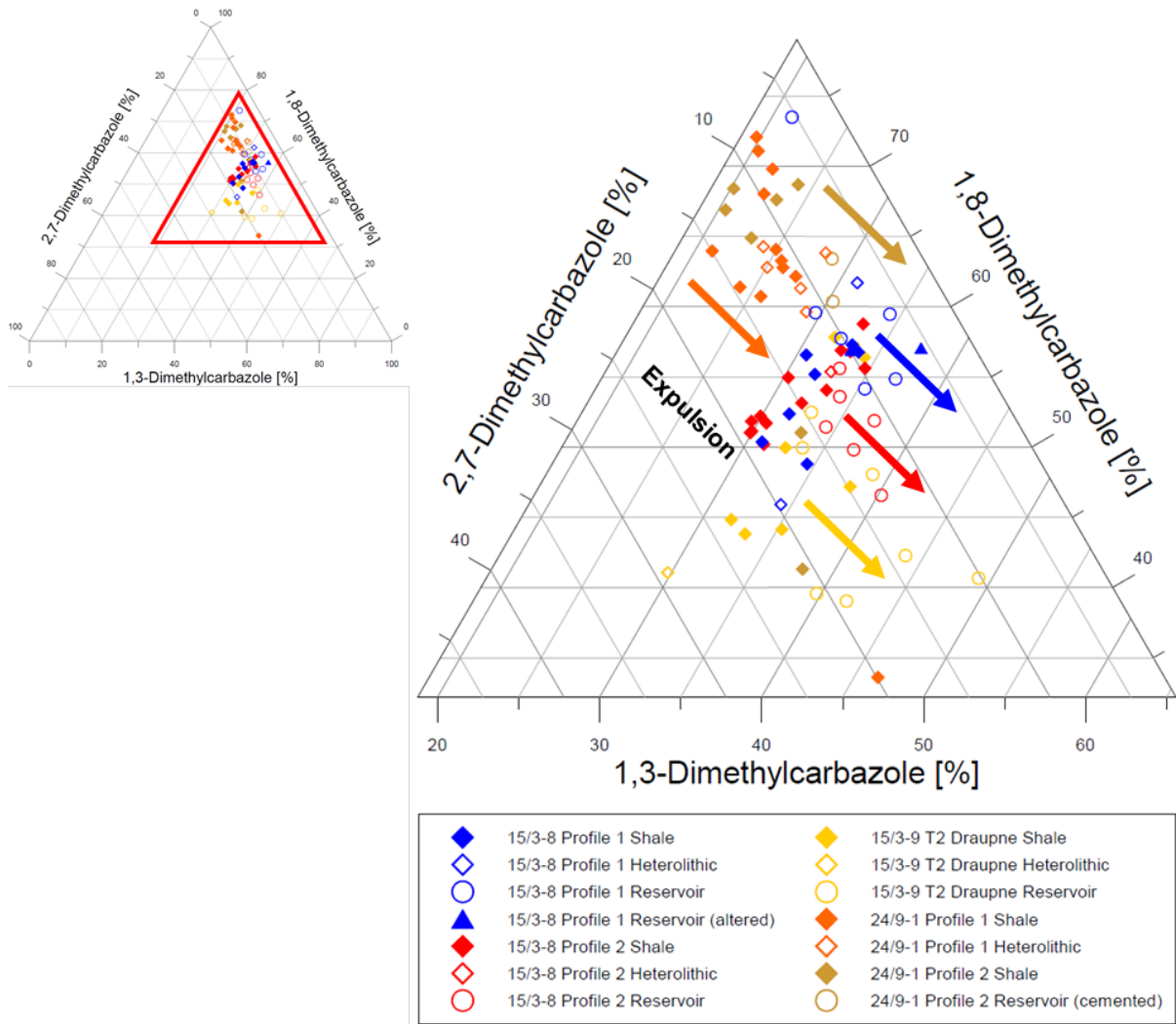


Fig. 81. Ternary system 1,8-dimethylcarbazole-2,7-dimethylcarbazole-1,3-dimethylcarbazole for the samples from the natural expulsion sequences comprising actively generating and expelling source rock material (after Clegg et al., 1998b). Note that the reservoir extracts are mostly enriched in 1,8- and especially 1,3-dimethylcarbazole compared to the associated source rock units, which may be interpreted by a preferential expulsion of nitrogen-shielded (1,8-, 1,3-dimethylcarbazole) over nitrogen-exposed (2,7-dimethylcarbazole) C_2 carbazoles. Surprisingly, the partially shielded 1,3-isomer seems to be easier expelled than the fully shielded 1,8-isomer, which may indicate that the molecular structure plays a key role, too.

a tendency of an enrichment of the 1,8- and particularly the 1,3-dimethylcarbazole isomers in the carrier beds compared to the source rock units. This strongly supports the theory of a preferential expulsion/migration of nitrogen-shielded over nitrogen-exposed C_2 carbazoles. In addition, the data are in very good agreement with the trends observed in the geochromatographic experiment, in which the partially nitrogen-shielded 1,4-isomer passed the source rock column before the corresponding nitrogen-exposed isomers. Moreover, a preferential expulsion of shielded vs. non-shielded compounds is also indicated by the C_2 carbazoles (Shielded/Exposed) curves shown in chapter 6. Essentially, for the relevant profiles, the curves usually maximize in the reservoir units, indicating a preferential release of shielded over exposed dimethylcarbazoles. It is, however, surprising why particularly the partially nitrogen-

7. Discussion

shielded 1,3-isomer is so much enriched in the reservoir. Although the fully shielded 1,8-isomer is also slightly enriched, one might actually expect the opposite, i.e. a stronger enrichment of the fully over the partially shielded isomer. This is, however, not or only partly the case, suggesting that other factors apart from the interaction of the nitrogen functionality with the surrounding environment may play a role, perhaps the molecular structure and associated molecular sieving effects.

7.6.7 Higher vs. lower alkylated compounds and implications for the MPI 1

Li et al. (1995) reported a preferential expulsion/migration of C₃ over C₂ carbazoles and therefore an enrichment of higher vs. lower alkylated carbazoles in the reservoir relative to the source rock. It was speculated that this observation might be related to a stronger molecular interaction of lower alkylated homologues with, for example, mineral surfaces, kerogen, and/or bitumen. Correspondingly, Stoddart et al. (1995) described an enrichment of higher compared to lower alkylated carbazoles in Eldfisk Bravo vs. Eldfisk Alpha drill-stem test oils, which was attributed to a longer migration distance. A preferential migration of C₃ over C₂ carbazoles was, however, called into question by Clegg et al. (1998a), who did not observe such effects in a series of Tithonian source rocks and related crude oils. Nevertheless, in accordance with Li et al. (1995), the results of this study also strongly point to a preferential expulsion of more alkylated relative to less alkylated carbazoles. This is very well expressed in the C₁ Carb/Carb depth profiles shown in chapter 6, which commonly maximize in the carrier beds and thus indicate an enrichment of methylcarbazoles over carbazole in the reservoir units. In addition, remarkably, this does not only seem to be the case for carbazoles, but also for phenanthrenes (C₁ Phen/Phen), dibenzothiophenes (C₁ DBT/DBT), and dibenzofurans (C₁ DBF/DBF), whose curves look mostly quite similar. Hence, the data obtained in this work indicate that the reservoir beds are enriched in alkylated vs. non-alkylated compounds, which seem to remain in the source rock. Since contribution of petroleum from other sources to the investigated intra-Draupne carrier beds can largely be ruled out, these trends are probably directly attributable to petroleum expulsion. It therefore indeed seems that the molecular interaction of a compound with the surrounding environment weakens with increasing degree of alkylation. The exact reasons for this phenomenon remain, however, open to discussion. Yet, in agreement with the findings of Li et al. (1995), it appears likely that non-alkylated compounds interact stronger with minerals and organic material, which

7. Discussion

ultimately causes stronger retardation. Also, the solubility in pore water can be expected to decrease with increasing number of carbon atoms (e.g. Tissot and Welte, 1984), which, as primary migration via molecular solution in pore water seems rather unlikely (see 3.1.3), could be particularly relevant for secondary migration processes and therefore reservoir filling dynamics.

Support for the theory of a preferential expulsion of alkylated vs. non-alkylated compounds comes from the results of the geochromatographic retardation experiment, which also indicate a preferential migration of more compared to less alkylated compounds, due primarily to the earlier elution and higher recovery rate of the highly alkylated 3,6-di-tert-butylcarbazole compared to the less alkylated C₂ carbazoles (see 6.2). Note that the findings are in good accordance with the kerogen solubility parameters determined by Ritter (2003) (Fig. 8), which indicate that methylphenanthrenes are less sensitive to kerogen absorption than phenanthrene. This underpins the theory of a preferential release of methylated over non-methylated compounds. Further evidence derives from supplementary diagrams (not shown) of C₂- against C₁-alkylated phenanthrenes, dibenzothiophenes, and carbazoles, which produced the same trends.

A preferential expulsion/migration of higher vs. lower alkylated compounds has important implications for organic geochemical maturity and migration indicators that are based on ratios between alkylated and non-alkylated compounds of the same class. A good example is the methylphenanthrene index (equation 8), which is defined as the ratio between the thermally more stable 2- and 3-isomers relative to the sum of phenanthrene and the thermally less stable 9- and 1-isomers (e.g. Radke, 1988). As the data of this work clearly indicate a preferential expulsion of methylated phenanthrenes over phenanthrene, a discrepancy in the MPI 1 between source and carrier units is expected, which is indeed observable in the sample material. This is very well expressed in a cross-plot of the MPI 1 against the $\beta\beta/(\beta\beta+\alpha\alpha)$ C₂₉ sterane ratio for the relevant expulsion scenarios (Fig. 82). While there is a relatively good correlation between both maturity parameters for the source rock samples, the MPI 1 values of the carrier beds are mostly conspicuously higher than those of the source rock material. On the other hand, however, source and reservoir samples exhibit very similar $\beta\beta/(\beta\beta+\alpha\alpha)$ C₂₉ sterane ratios, which is in strong contrast to the elevated

7. Discussion

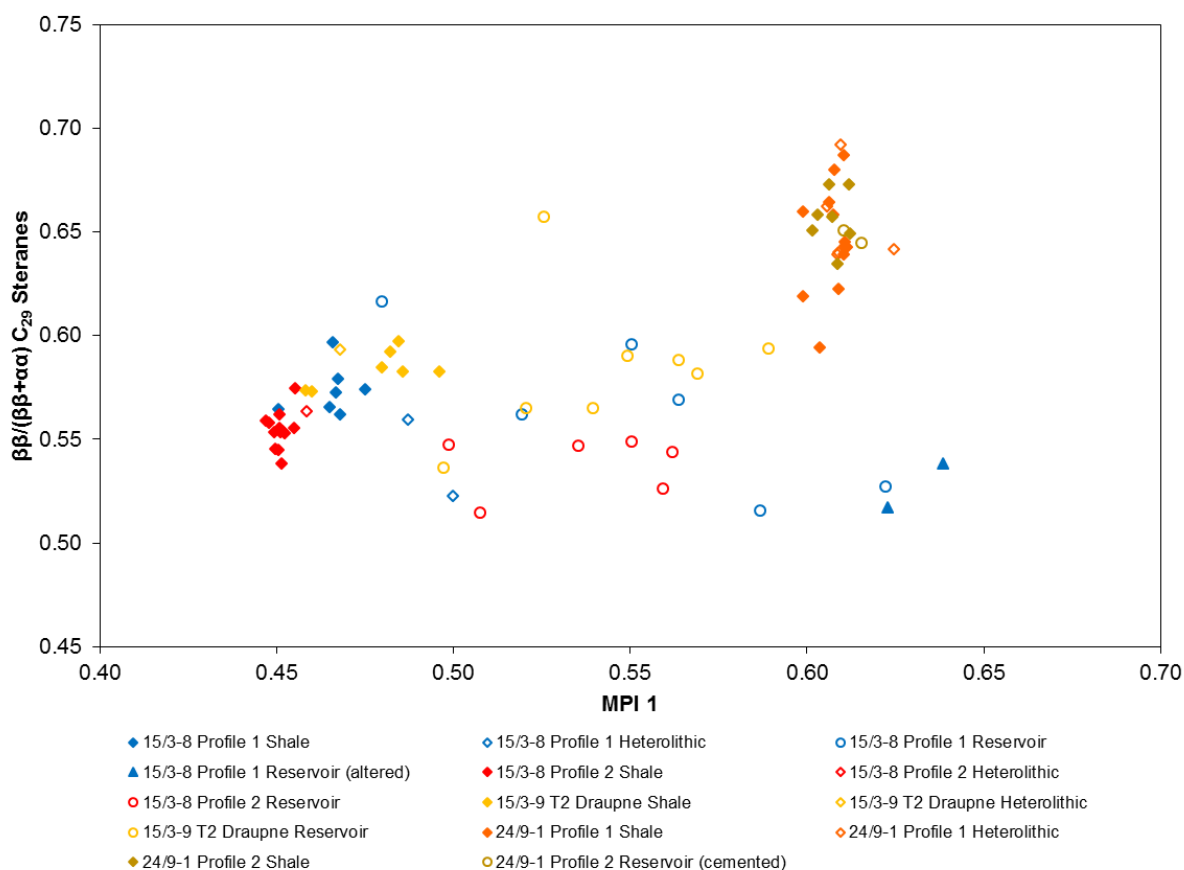


Fig. 82. Cross-plot of the methylphenanthrene index (MPI 1) vs. the $\beta\beta/(\beta\beta+\alpha\alpha)$ C₂₉ sterane ratio for the samples from the natural expulsion scenarios comprising actively generating and expelling source rock material. Note the strong discrepancy between both parameters for most reservoir samples from quadrant 15. While there is a good correlation for the organic-rich shales, the MPI 1 values of the reservoir units are usually higher than those of the source rock samples. Since no evidence for a major contribution from other sources was found, it is suggested that this effect is related to the preferential expulsion of C₁ phenanthrenes over phenanthrene, which leads, considering the equation of the MPI 1, to higher MPI 1 values in the reservoir.

MPI 1 values in the majority of the investigated reservoir units. Interestingly, this tendency is less pronounced for samples from well 24/9-1, which could be related to the heterolithic character of most carrier intervals and hence the absence of real reservoir horizons. Rather, the bulk data suggest that the heterolithic samples can be expected to have a remaining source potential. Moreover, with regard to the second profile of well 24/9-1 (expulsion scenario F), carbonate cementation of the reservoir interval could have largely prevented the uptake of petroleum from the surrounding shales, consequently leading to less distinct trends. In fact, however, the MPI 1 suggests for most reservoir extracts a higher maturity compared to the associated source rock bitumen, which is in strong contrast to other molecular maturity indicators, e.g. the C₃₀ dihopane ratio, that point to a similar or even slightly lower thermal maturity. It is proposed that this paradox is due to the influence of petroleum expulsion, which selectively enriches the reservoir with alkylated vs. non-alkylated compounds. Therefore, the results of this work are in this point contrary to the findings of

7. Discussion

Leythaeuser et al. (1988b), who did not describe an expulsion influence on the MPI 1. Though, on the other hand, there is no evidence for a fractionation of individual methylphenanthrene isomers, which is in good accordance with the data of these researchers.

As a consequence, concerning maturity estimations of crude oils and oil-source rock correlations, it is, based on the findings of this work, strongly recommended to compare only equally alkylated compounds. With respect to the MPI 1, this means to exclude phenanthrene from the equation. Corresponding diagrams showing, (A) only the samples from the sections involving actively generating and expelling source rock material, and (B) all samples are presented in Fig. 83. Although there is still a slight tendency of an enrichment of the 2- and 3-methylphenanthrene isomers in the reservoir units, the differences are, however, much smaller. This becomes especially clear when adding the samples from the other sections where the data are wider spread. Essentially, if including all samples, the diagram enables to group the sample material into five different clusters, which comprise, (1) source rock samples from well 34/7-23 A, 34/7-23 S, as well as carrier bed extracts from well 34/7-23 S, (2) most source rock and reservoir extracts from well 15/3-8 and the Draupne section of well 15/3-9 T2, (3) reservoir samples from well 34/7-23 A, (4) source and carrier bed extracts from well 24/9-1, and (5) coals and shales of the Hugin Formation. Reservoir extracts from the Hugin Formation tend to plot close to samples from well 24/9-1 and therefore considerably away from the surrounding Hugin source strata. Similarly, reservoir extracts from well 34/7-23 A plot apart from the corresponding source rock material and constitute an individual data cluster in the upper part of the diagram. Note the large variability in the ratio between 2+3- and 9+1-methylphenanthrene for source rock samples from the Hugin Formation, indicating the ratio between these isomers is not only influenced by the thermal maturity, but probably also by the organic facies of the source rock. Therefore, for maturity estimations of source rock samples, it is recommended to apply the original MPI 1 (which appears to work quite well for source rock samples) instead of the $(2+3\text{-methylphenanthrene})/(1+9\text{-methylphenanthrene})$ ratio, which seems to be heavily influenced by facies effects. This is supported by a diagram showing the T_{\max} against the $(2+3\text{-methylphenanthrene})/(1+9\text{-methylphenanthrene})$ ratio (Fig. 84). While the MPI 1 and the T_{\max} display a relatively good correlation (Fig. 62), this is not the case for the T_{\max} vs. the ratio between 2+3- and 9+1-methylphenanthrene, which therefore appears

7. Discussion

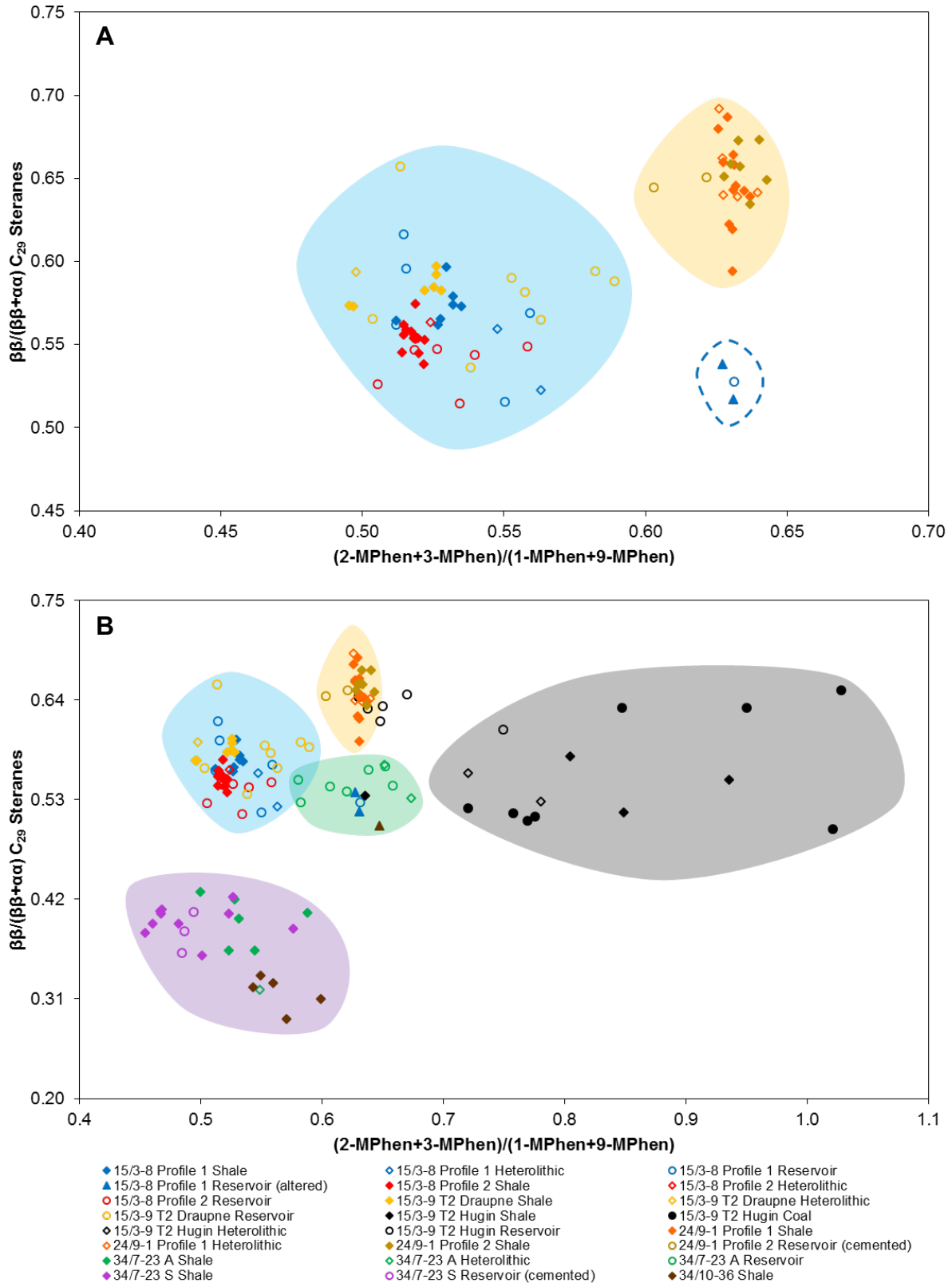


Fig. 83. Cross-plots of $(2+3\text{-methylphenanthrene})/(1+9\text{-methylphenanthrene})$ vs. the $\beta\beta/(\beta\beta+\alpha\alpha) C_{29}$ sterane ratio for the sample material from the natural expulsion scenarios. A: Samples from the profiles comprising actively generating and expelling source rock material. B: Samples from all profiles. Note that this time the reservoir extracts plot substantially closer to the source rock samples than in the previous figure showing the same diagram but with the methylphenanthrene index (MPI 1) instead of the ratio between 2+3- and 9+1-methylphenanthrene. Note also that, if including all samples, the diagram very well allows to group the sample material into different clusters. The diagram further corroborates the hypothesis that the reservoir extracts from well 34/7-23 A and the Hugin Formation originate from external sources.

7. Discussion

appears unsuitable for maturity estimations. However, since expulsion influences on the distribution of individual methylphenanthrenes seem, according to the data of this work, to be negligible, the (2+3-methylphenanthrene)/(1+9-methylphenanthrene) ratio is suggested to have an application potential for the correlation of oils and source rocks. Indeed, the cross-plot against the $\beta\beta/(\beta\beta+\alpha\alpha)$ C₂₉ sterane ratio (Fig. 83) further supports the theory that the reservoir fluids extracted from the carrier intervals of the Hugin Formation and the sandstone package of well 34/7-23 A originate from external sources and therefore cannot be used to investigate molecular redistribution effects related to petroleum expulsion. Another remarkable observation is that microbial degradation appears to shift the data towards higher (2+3-methylphenanthrene)/(1+9-methylphenanthrene) ratios, as indicated by the two altered samples from the first profile of well 15/3-8, as well as the degraded sample from well 34/10-36. Hence, the data suggest that 1- and 9-methylphenanthrene are preferentially degraded by microorganisms compared to 2- and 3-methylphenanthrene.

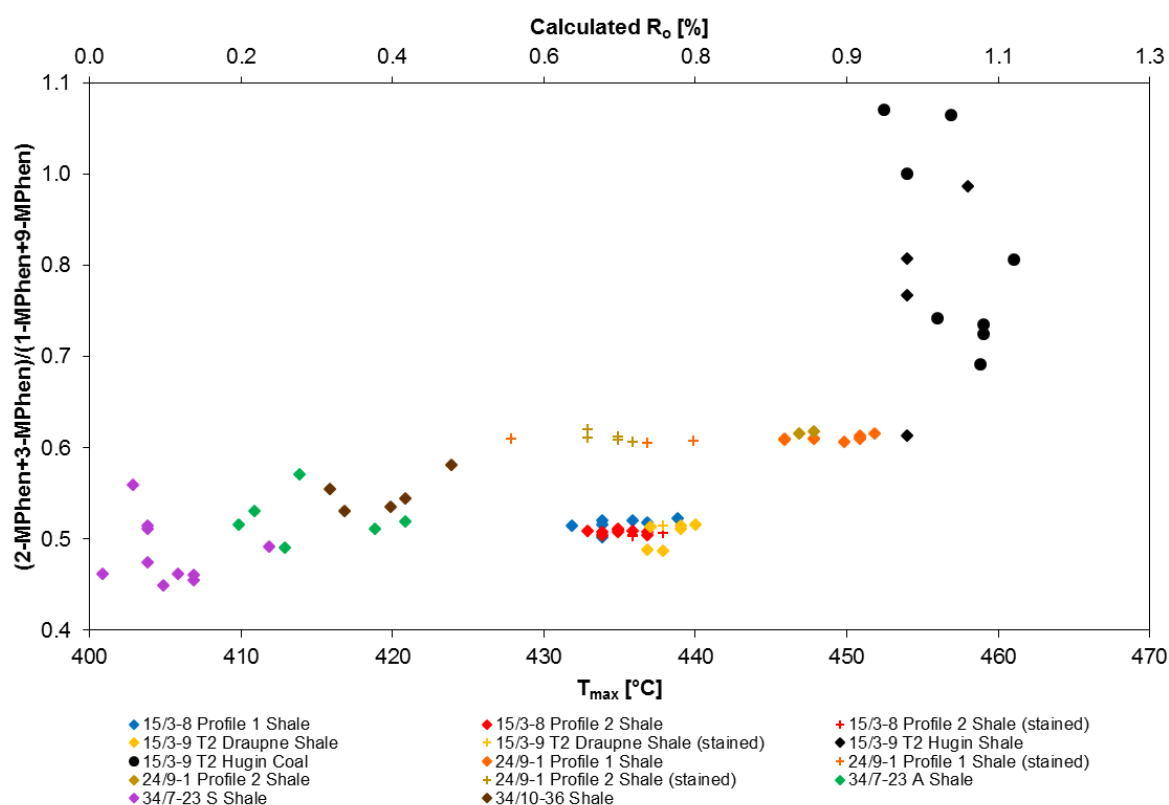


Fig. 84. Cross-plot of the T_{max} vs. the (2+3-methylphenanthrene)/(1+9-methylphenanthrene) ratio for the investigated source rock samples. Vitrinite reflection (R_o) calculated after equation 18 (from Jarvie et al., 2007 and reference therein). Note the large, probably facies-related variability of the (2+3-methylphenanthrene)/(1+9-methylphenanthrene) ratio, which therefore does not seem to be suitable for maturity estimations. Samples with a production index (PI) ≥ 0.3 are labeled as "stained". R_o values below 0.2 are shown only for completeness.

Summarized, the results of this study point to a preferential expulsion/migration of higher vs. lower alkylated compounds, which could have profound impact on organic

geochemical maturity and migration parameters. Further investigations including laboratory experiments and additional natural case studies are necessary to verify this theory.

7.6.8 Fractionation effects among aliphatics

Although the work focused predominantly on aromatic compounds and saturates were not extensively regarded, careful analysis of the data indicates no compositional fractionation among aliphatic biomarkers, i.e. steranes and hopanes, suggesting these molecules are not redistributed during petroleum expulsion, which principally supports the findings of Leythaeuser et al. (1984a) and Han et al. (2017).

The first aliphatic compounds that were investigated for potential fractionation effects were hopanes. More specifically, it was examined whether redistribution occurs as a result of the molecular structure (22S vs. 22R isomerization) or the molecular chain length (C_{31} vs. C_{32} homohopanes). A corresponding diagram showing the ratio between the C_{31} and C_{32} (22S+22R) homohopanes against the 22S/(22S+22R) ratio of the C_{32} hopanes, which is frequently applied for maturity estimations (e.g. Peters et al., 2005b), is illustrated in Fig. 85. Essentially, both organic-rich shales and reservoir units of the natural sections comprising actively generating and expelling source rock material exhibit very similar hopane signatures, suggesting hopanes do not undergo fractionation during primary migration, neither because of the number of carbon atoms nor the structural configuration. This is in good agreement with the Barnett Shale data recently published by Han et al. (2017), but contrary to the experimental results of Zhusheng et al. (1988), who passed a natural crude oil through an alumina column. While Han et al. (2017) did not observe expulsion-related fractionation effects among hopanes, Zhusheng et al. (1988), by contrast, reported inter alia a preferential migration of 22S over 22R $\alpha\beta$ hopanes. Note, however, that Han et al. (2017) mentioned that potential fractionation effects between S and R isomers for both steranes and hopanes may be masked and overprinted by the thermal maturity, as thermal equilibration occurs relatively early with proceeding maturation. It is likely that this also applies to the oil window-mature source rock-carrier bed sequences studied here. In particular, the 22S/(22S+22R) isomerization ratio has already reached the thermal equilibrium in almost all samples from both

7. Discussion

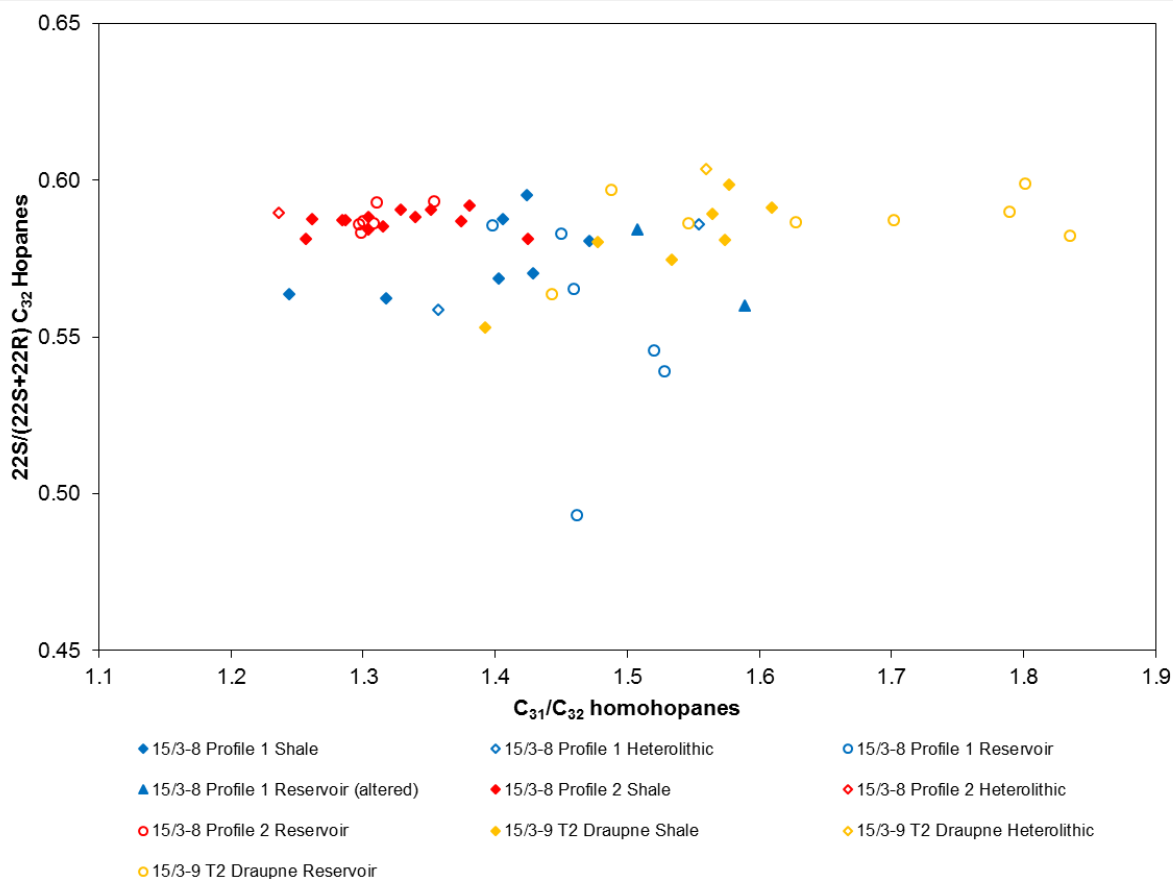


Fig. 85. Cross-plot of the ratio between the C₃₁ and C₃₂ homohopanes vs. the 22S/(22S+22R) C₃₂ hopanes ratio for the samples from the natural expulsion sequences comprising actively generating and expelling source rock material. Samples from well 24/9-1 are not shown due to the low abundance of hopanes. No preferential expulsion of either S or R isomers nor according to the molecular chain length was revealed, indicating hopanes are not fractionated upon primary migration and therefore very suitable for maturity estimations and/or oil-source rock correlations. Note, however, that the opportunity exists that potential fractionation effects between S and R isomers are masked by the thermal state of the sample material, as the ratio between the S and the R isomer has already reached equilibrium in both source and reservoir units.

source and reservoir units, indicating any potential fractionation effects are overprinted by maturation. Remarkably, some reservoir extracts from the Draupne section of well 15/3-9 T2 are enriched in C₃₁ over C₃₂ homohopanes, which could potentially indicate fractionation. Yet, this phenomenon was not observed in any other of the relevant expulsion scenarios, thus supporting the assumption that hopanes are not probably redistributed as a consequence of differences in the molecular chain length. A geochromatographic experiment like that conducted in this work including different hopanes could provide further insights. Nevertheless, based on the data obtained in this work, it appears that hopanes are not redistributed upon primary migration and are therefore very useful for maturity estimations of source rocks and crude oils, oil-source rock correlations, as well as palaeofacies characterizations.

7. Discussion

Similar to hopanes, steranes have previously also been proposed to be partially influenced by geochromatographic separation processes during petroleum migration (e.g. Seifert and Moldowan, 1978, 1981; Carlson and Chamberlain, 1986; Zhusheng et al., 1988). For example, Zhusheng et al. (1988) did not only observe redistribution effects among hopanes, but also recognized a faster migration of dia over regular, $\beta\beta$ over $\alpha\alpha$, and $\alpha\alpha$ 20S over $\alpha\alpha$ 20R steranes. Once again, this contrasts with the results of Han et al. (2017), who did not witness such effects in the investigated Barnett Shale sequence. Basically, these researchers found no evidence for fractionation for the ratio between 20S and (20S+20R) for the C_{27} steranes, the S/R isomerization ratios of diasteranes, and the ratios of diasteranes against regular steranes. Like for the hopanes, the sterane data of this work are largely in good agreement with the findings of Han et al. (2017), i.e. steranes were not found to be redistributed during petroleum expulsion. In this context, the first ratios that were compared and examined for potential fractionation effects were the $20S/(20S+20R)$ and the $\beta\beta/(\beta\beta+\alpha\alpha)$ ratio for the C_{29} steranes (Fig. 86). Essentially, no substantial differences were revealed for source rock vs. carrier bed samples from the actively generating and expelling intra-Draupne sequences studied in this work. Rather, both the $20S/(20S+20R)$, as well as the $\beta\beta/(\beta\beta+\alpha\alpha)$ C_{29} sterane ratios of the reservoir petroleum are very similar to those of the corresponding source bitumen, indicating steranes are not fractionated due to differences in the molecular structure. However, similar to the $22S/(22S+22R)$ ratio of the C_{32} hopanes, the $20S/(20S+20R)$ C_{29} steranes ratio is also close to thermal equilibrium in most samples, which may potentially mask fractionation effects related to petroleum expulsion. An additional geochromatographic experiment involving different steranes could provide further information.

The next ratio that was investigated for molecular fractionation effects was the ratio between C_{27} diasteranes against C_{29} regular steranes, which could reveal fractionation effects due either to the structural configuration and/or the number of carbon atoms. In Fig. 87, it is compared with the $\beta\beta/(\beta\beta+\alpha\alpha)$ C_{29} steranes ratio, which turned out to be largely unaffected by fractionation processes and rather appears to depend primarily on the thermal maturity of the sample material. A closer look at the diagram reveals a very good correlation between both parameters, indicating the C_{27} Dia/ C_{29} Reg steranes ratio increases with proceeding thermal maturation. This is in good accordance with the generally accepted theory that the proportion of diasteranes

7. Discussion

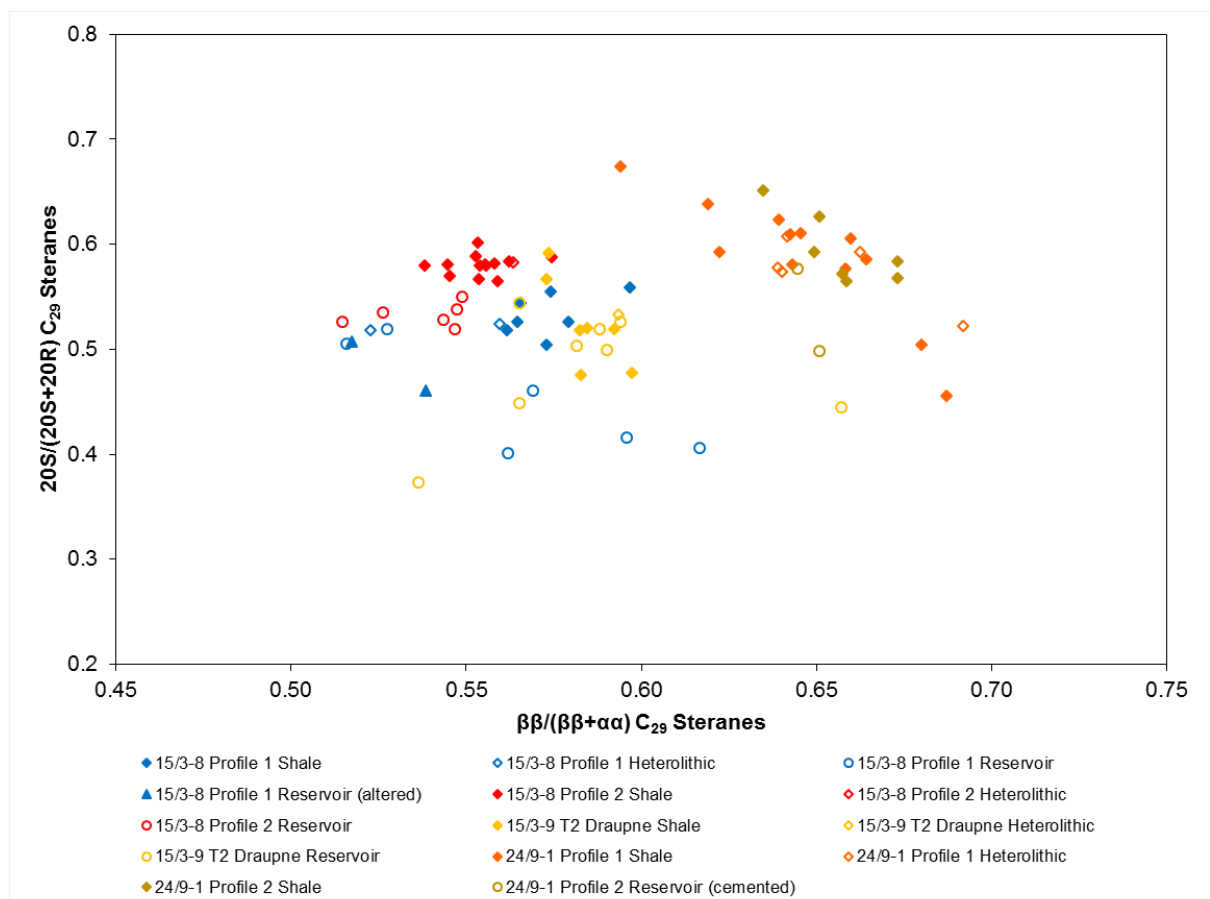


Fig. 86. Cross-plot of the $\beta\beta/(\beta\beta+\alpha\alpha)$ C_{29} sterane ratio vs. the ratio of $20S/(20S+20R)$ C_{29} steranes for the samples from the natural expulsion profiles comprising actively generating and expelling source rock material. Note that no preferential migration of certain isomers is visible, indicating the distribution of C_{29} steranes is not affected by expulsion fractionation. However, the mostly lower $20S/(20S+20R)$ ratios of the reservoir compared to the source rock samples from quadrant 15 suggest a slightly lower thermal maturity of the reservoir petroleum, which may be related to the relatively early stage of expulsion. Nonetheless, similar to the hopanes, the opportunity exists that potential fractionation effects between S and R isomers are masked by the maturity of the sample material, as the ratio between the 20S and the 20R isomer is mostly close to thermal equilibrium in both source and reservoir units.

compared to steranes increases with increasing thermal maturity (eg. Peters et al., 2005a). However, there are differences in the C_{27} Dia/ C_{29} Reg ratio between source rock material from the first and the second profile from well 15/3-8, as well as well 24/9-1, which could be related to differences in the clay mineral content, as diasterane formation is favored by clay mineral catalysis (e.g. Peters et al., 2005a). Besides, the substantially lower C_{27} Dia/ C_{29} Reg sterane ratios within the small, carbonate-cemented reservoir layer in the second profile of well 24/9-1 could similarly relate to the presence and therefore catalytic influence of clay minerals. What is important is that, except for the reservoir extracts from the second profile of well 24/9-1 and a few outliers from quadrant 15, most reservoir samples plot right next to the associated source rock material, suggesting diasteranes and steranes are not fractionated upon primary migration. Furthermore, since the reservoir units are not

7. Discussion

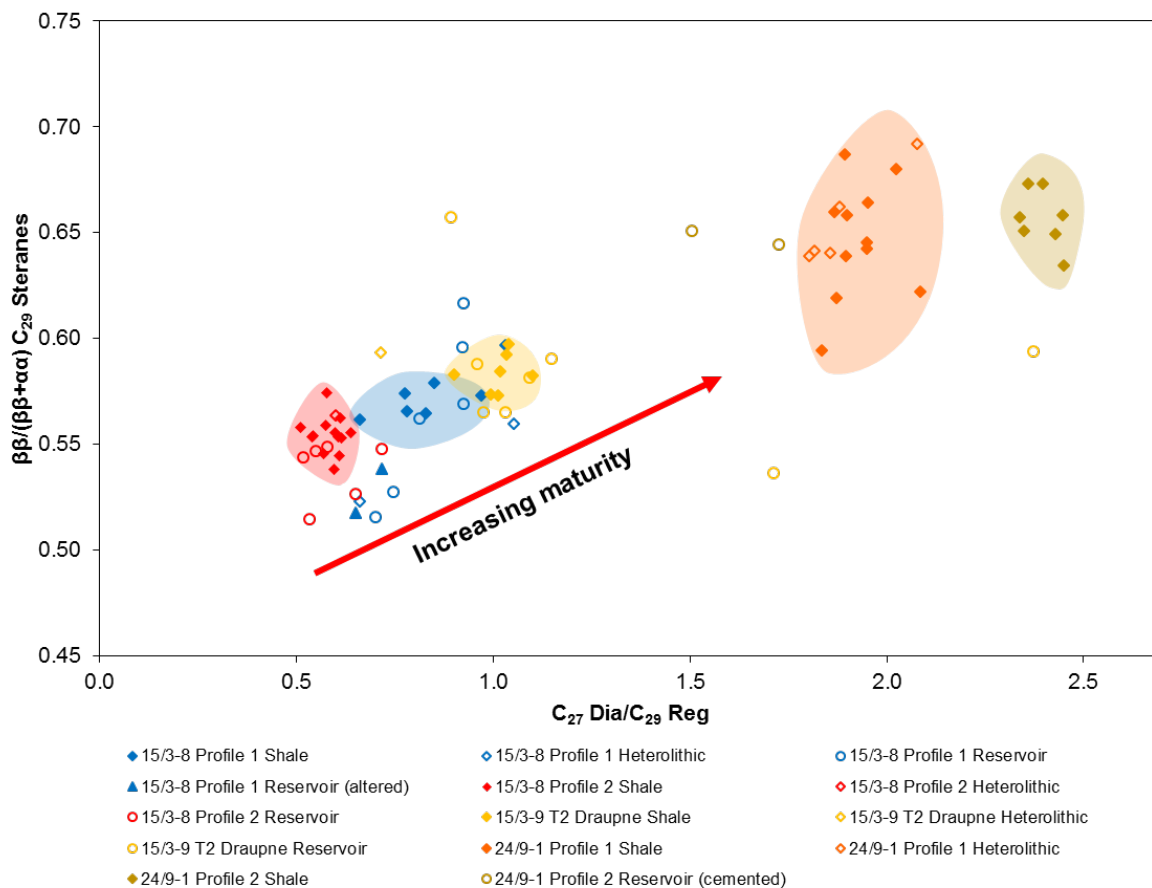


Fig. 87. Cross-plot of the ratio between C_{27} diasteranes and C_{29} regular steranes vs. the $\beta/(\beta+\alpha)$ C_{29} sterane ratio for the samples from the natural expulsion sequences comprising actively generating and expelling source rock material. Note that there is a good correlation between both parameters, even for the reservoir samples, which is probably related to the thermal maturity. Remarkably, no fractionation between dia- and regular steranes was observed, indicating dia- and regular steranes are not fractionated upon primary migration. Deviations between the first and the second profile from well 24/9-1 may perhaps owe to differences in the clay mineral content. One outlier (shale; 24/9-1, profile 1) is excluded from the diagram.

selectively enriched in C_{27} over C_{29} compounds, the data indicate that the molecular chain length plays a rather subordinate role with respect to the expulsion of aliphatic biomarkers. This is largely supported by an additional cross-plot of the $\beta/(\beta+\alpha)$ C_{29} steranes ratio against the ratio between C_{27} and $C_{29}\alpha\beta\beta$ steranes (Fig. 88). Indeed, similar to the ratio between C_{27} diasteranes and C_{29} regular steranes shown before, no selective enrichment of C_{27} over C_{29} compounds was observed in the reservoir, thus corroborating the hypothesis that the number of carbon atoms does not exert a major control on the expulsion behavior of steranes. Concerning the distribution of paraffins, fractionation between n -alkanes of different chain length, and between n - and iso -alkanes could not unambiguously be identified in this work. Though, the very bell-shaped curves of both nC_{17}/Pr (Fig. 32) and nC_{18}/Ph (not shown) within the central source rock unit in expulsion scenario A (15/3-8, profile 1) may be interpreted as an indication of a preferential migration of n - over iso -alkanes

7. Discussion

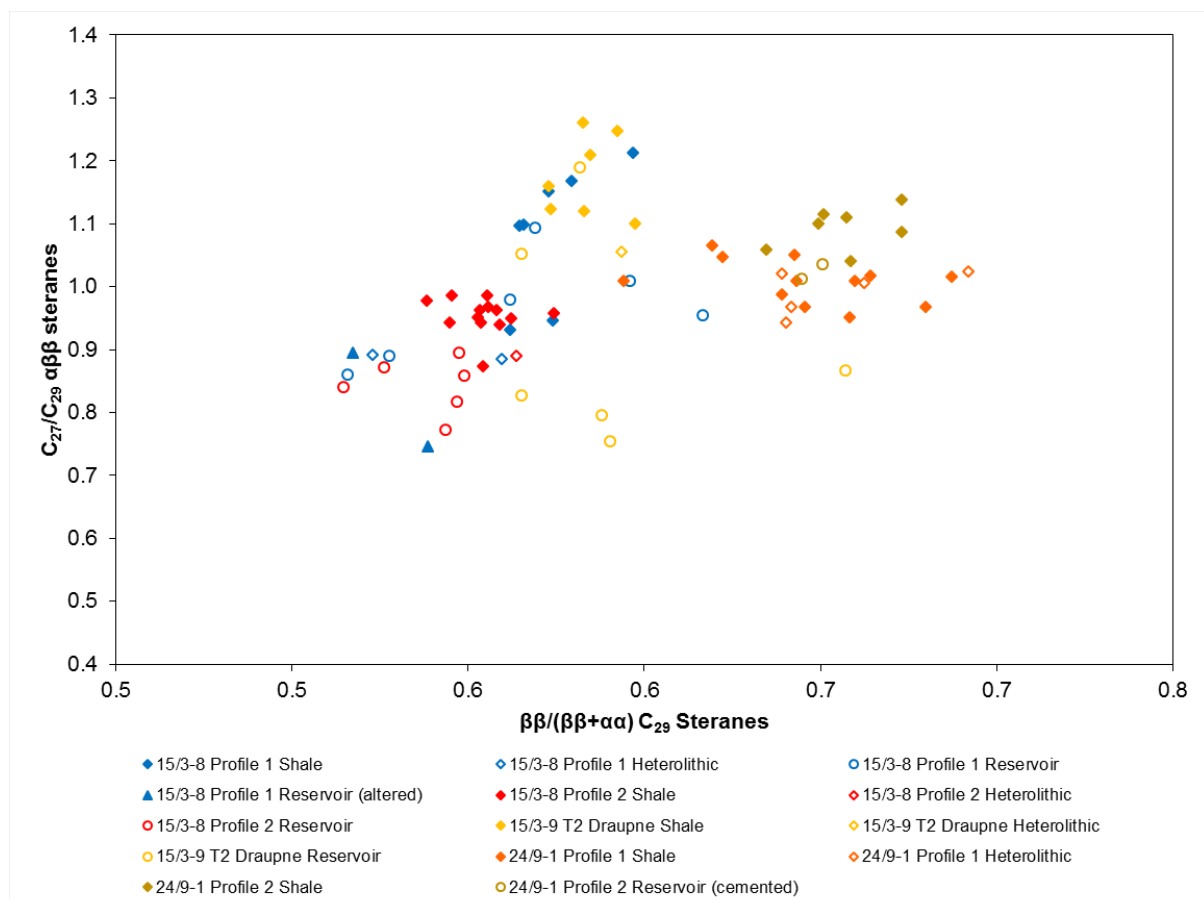


Fig. 88. Cross-plot of the $\beta/(\beta+\alpha)$ C_{29} sterane ratio vs. the ratio between the C_{27} and the $C_{29}\alpha\beta$ steranes for the samples from the natural expulsion sequences comprising actively generating and expelling source rock material. Despite some variation, only marginal differences exist between source bitumens and reservoir extracts, indicating steranes are not redistributed because of differences in the number of carbon atoms and are therefore largely unaffected by expulsion fractionation. Two outliers (reservoir; 15/3-9 T2 Draupne) are excluded.

towards the shale edges. Surprisingly, however, this effect was, in this form, not observed in any other expulsion scenario, even not in scenario B (15/3-8, profile 2) from the same well (Fig. 34). Yet, on the other hand, against expectations, very low nC_{17}/Pr (and nC_{18}/Ph) values were observed in the adjacent reservoir units, which may, for example, indicate evaporative losses of n -alkanes due core storage conditions, preferential, intra-formational secondary migration of short-chain n -alkanes over isoprenoids, or contamination of the n -alkane fraction by drilling fluids. This issue could be addressed in subsequent examinations. However, increasing nC_{17}/Pr ratios towards the reservoir in expulsion scenario F (Fig. 42) and in the small, intercalated reservoir bed in the center of expulsion scenario B (Fig. 34), could yet also be interpreted as an indication of a faster migration of n - over *iso*-alkanes.

Based on the observations made in this study, it is proposed that primary migration effects within source rock units are best visible through high-resolution investigation of source rock intervals completely enclosed by reservoir strata, as is the case in

7. Discussion

expulsion scenario A (15/3-8, profile 1). Thereby, the more terrigenous the organic facies, the stronger the retention of generated petroleum compounds and the less clear the molecular trends related to primary migration. As the bulk characterization (see 7.1) revealed a slightly more terrigenous character and therefore stronger retention potential for source rock material from the second than from the first profile from well 15/3-8, this could, in combination with the early oil window maturity, be a reason for the often less distinct trends. Concerning expulsion scenario C (15/3-9 T2, Draupne section), it is proposed that due to the relatively low sample resolution only gross compositional differences between source and reservoir units are identifiable. Supplementary preliminary quantification results of aliphatics, including *n*-alkanes, *iso*-alkanes, as well as biomarkers like steranes and hopanes in source and reservoir units on the basis of the added internal quantification standard (not shown in this work) suggest enrichment in the reservoir compared to the source rock, pointing to a relatively efficient expulsion. The opposite was observed for the aromatic and the carbazole fraction, which were found to be depleted in the reservoir compared to the source rock, indicating, in contrast to the saturate fraction, preferential retention in the source rock. These findings fit very well with the general assumption of a preferential expulsion of low polar saturates over aromatic hydrocarbons and heteroatomic compounds, which leads to an enrichment of saturates over aromatics and heteroatomic compounds in crude oils.

Summarized, regarding the aliphatic fraction, the data of this work suggest that biomarker molecules like steranes and hopanes are not sensitive to fractionation upon primary migration and are therefore highly reliable with regard to oil-source rock correlations, maturity estimations and palaeofacies characterizations. Conversely, no clear evidence for or against a fractionation of *n*- and *iso*-alkanes was found, perhaps in part due to the use of paraffin-containing drilling muds in some of the natural sections that are likely in the stage of active petroleum expulsion, as mentioned in chapter 5. Yet, the very bell-shaped trendlines of the nC_{17}/Pr and the nC_{18}/Ph (not shown) ratio within the central source unit of expulsion scenario A (15/3-8, profile 1) could be interpreted as indications of a preferential retention of *iso*- over *n*-alkanes. Further investigations including additional geochromatographic retardation experiments involving *n*-alkanes and isoprenoids, as well as high resolution sampling of other, oil window-mature and well-defined source rock intervals are necessary for a clearer picture.

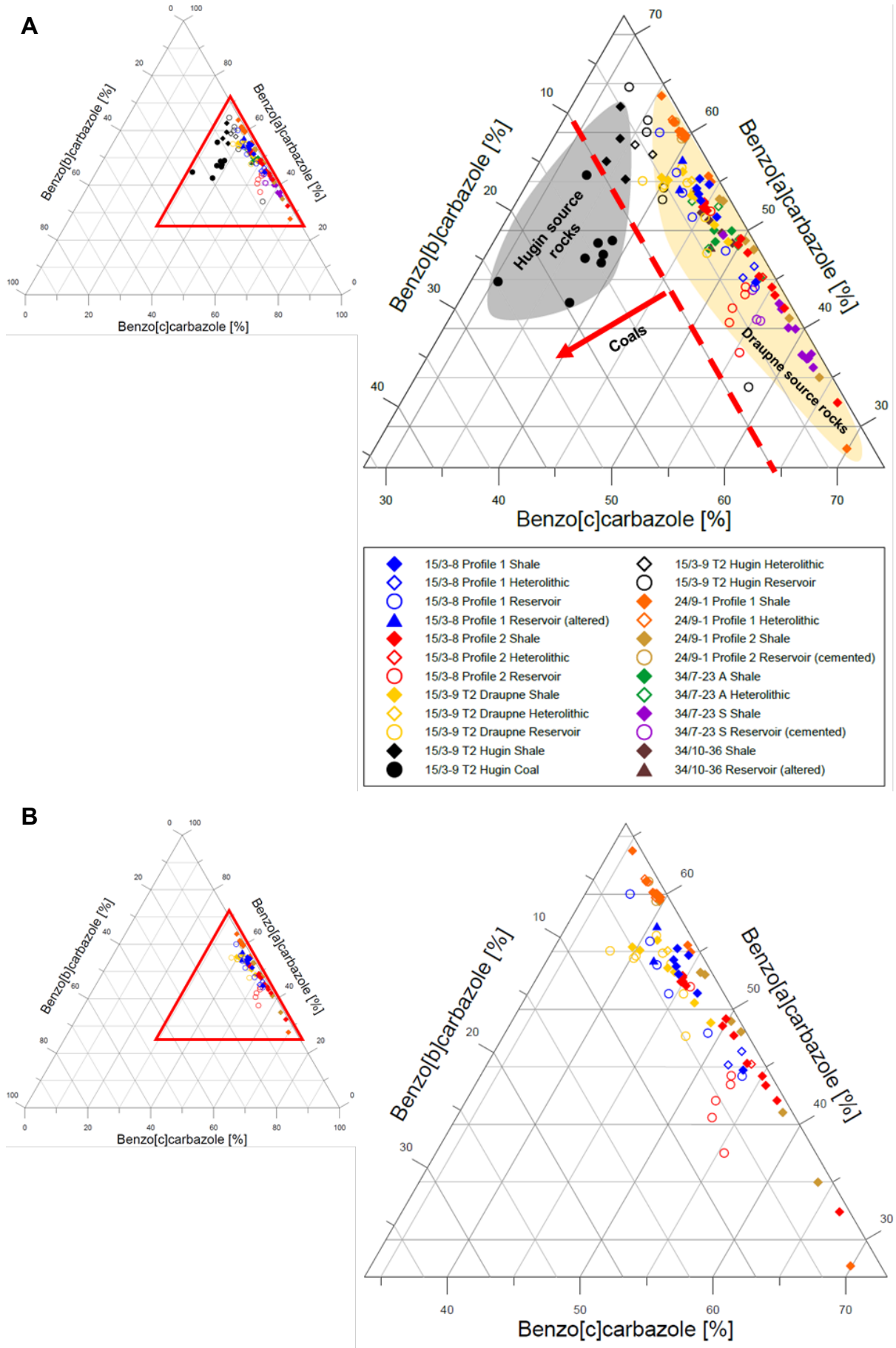
7.7 Influences on the benzocarbazoles ratio

A major task of this work was also to investigate potential influences on the benzocarbazoles ratio (Larter et al., 1996), especially possible fractionation effects due to petroleum expulsion. As mentioned in chapter 3, the benzocarbazoles ratio, i.e. the relationship between benzo[a]- and benzo[c]carbazole, has been proposed as an organic geochemical parameter to calculate the migration distance of crude oils in a sedimentary basin (Larter et al., 1996). However, the factors influencing the BC ratio remain, even after years of research, strongly debated. For example, it has been suggested that the BC ratio of natural crudes does not only depend on the migration distance and therefore adsorption/desorption effects, but is also considerably influenced by thermal maturity (Clegg et al., 1997, 1998a, b; Horsfield et al., 1998) and the organic facies (Bakr and Wilkes, 2002) of the source rock. If or to what extent the BC ratio is influenced by petroleum expulsion is unknown. This work attempted to provide further insights. However, the benzocarbazoles data obtained from both the geochromatographic experiment, as well as the natural expulsion profiles are, complex and difficult to interpret.

Regarding the geochromatographic experiment, benzo[a]carbazole was found to migrate slightly faster than benzo[c]carbazole, but though was recovered in substantially lower total quantities. With respect to natural systems, this observation implies that the first oil expelled from a source into an adjacent carrier rock has a very high BC ratio, which then decreases over time. Though, the trends observed in the natural case scenarios are mostly not consistent, even not in the sections comprising early oil window-mature source rocks, indicating the BC ratio is a very complex parameter that depends on more than just one factor. This is in good accordance with the conclusions drawn by Clegg et al. (1997). Therefore, any BC ratio-based calculations of crude oil migration distances should be conducted with caution and verified by other data. No clear evidence for fractionation during expulsion under natural conditions was found.

While the geochromatographic experiment clearly suggests a preferential migration of the [a]- over the [c]-isomer, this effect is not recognizable in the natural scenarios. This is well expressed by a triangular diagram showing the relative distributions of benzo[a]-, benzo[b]-, and benzo[c]carbazole in, (A) the whole sample material (except for reservoir extracts from well 34/7-23 A due to extremely low abundances

7. Discussion



7. Discussion

Fig. 89. Ternary diagram showing the relative distributions of benzocarbazoles in the sample material. A: Distribution in all samples. Reservoir extracts from well 34/7-23 A are not shown due to extremely low concentrations of benzo[b]carbazole. B: Distribution in the samples from the expulsion scenarios comprising actively generating and expelling source rock material. There is no clear evidence for a fractionation of benzocarbazoles during petroleum expulsion. Instead, the data are highly variable, indicating the ratio is influenced by various factors. Note also the high concentrations of benzo[b]carbazole in coals and shales of the Hugin Formation, which is proposed to represent an excellent oil-source rock correlation parameter.

of benzo[b]carbazole), and (B) only the samples that are likely influenced by petroleum expulsion (Fig. 89). As can be seen from the ternary system, there is a very large variability, especially in the ratio between benzo[a]- and benzo[c]-carbazole, even within individual expulsion scenarios. Benzo[b]carbazole, which has previously been considered as an indicator of terrigenous input (e.g. Bakr and Wilkes, 2002), is close to the detection limit in most samples, thus substantiating the predominantly marine character of the Draupne samples. Only the substantially terrigenously-influenced source rock samples from the Hugin Formation, especially the coals, were found to contain elevated quantities of benzo[b]carbazole, which strongly supports the assumption that the amount of benzo[b]carbazole present in a source rock sample correlates with the degree of terrestrial contribution. It is

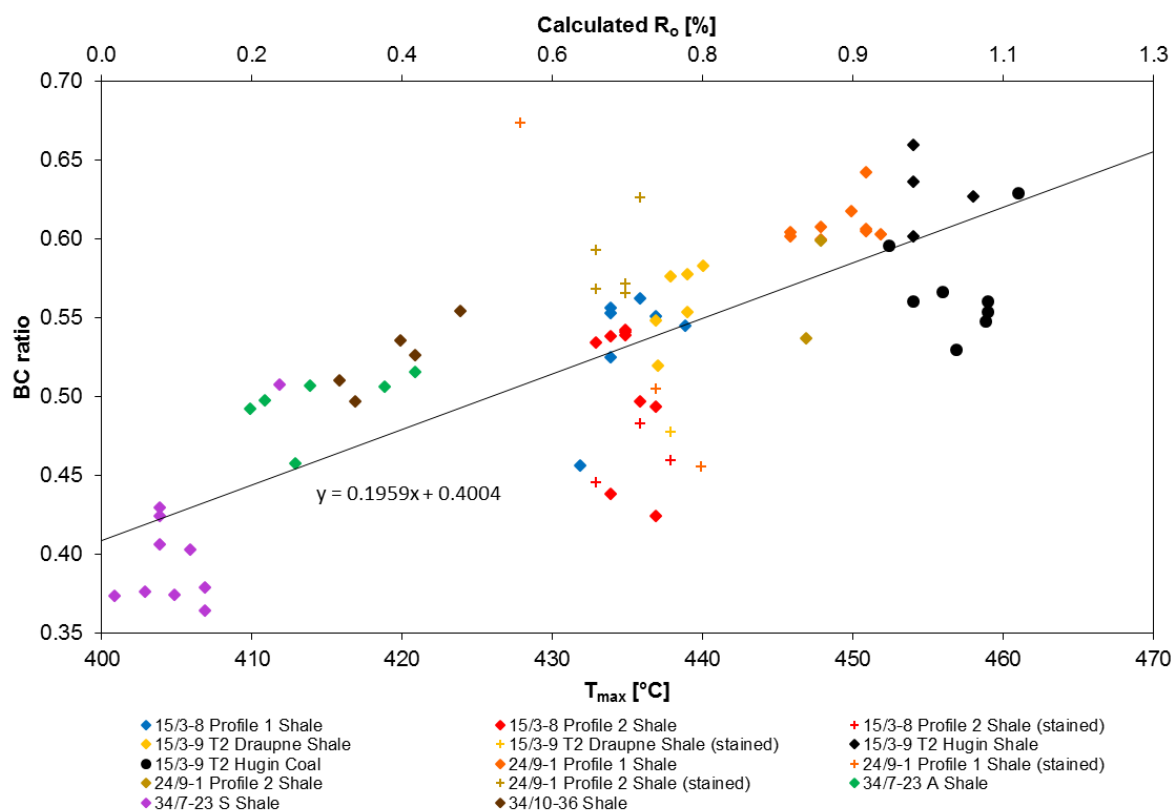


Fig. 90. T_{max} -BC ratio maturity correlation for the investigated source rock samples. Vitrinite reflection (R_o) calculated after equation 18 (from Jarvie et al., 2007 and reference therein). Note that there is a fairly good correlation between the BC ratio and the thermal maturity across the study area, indicating the BC ratio is at least partially influenced by the thermal maturity. However, the large variability, even at the immature stage, indicates contribution of other, potentially depositional-related factors. Samples with a production index (PI) ≥ 0.3 are labeled as "stained" and are excluded from the calibration. R_o values below 0.2 are shown only for completeness.

7. Discussion

therefore proposed that benzo[b]carbazole represents an excellent oil-source rock correlation parameter, which would be expected to be seen in mainly terrestrially (e.g. humic coal) derived oils. Although no direct evidence for a fractionation of benzocarbazoles during petroleum expulsion was found, the data suggest, however, that the BC ratio is at least partially controlled by the thermal maturity of the source rock, which is in good agreement with the findings of Clegg et al. (1997, 1998a, b) and Horsfield et al. (1998). A maturity dependency becomes evident in cross-plots of the BC ratio against the Rock-Eval T_{max} (Fig. 90) and the triaromatic steroid ratio TA(I)/TA(I + II) (Fig. 91), which both turned out to be very maturity-sensitive over the study area (see 7.3). Despite some variability that underpins the complexity of the BC ratio, it seems, however, to increase with increasing thermal maturity. Yet, the high degree of variability, even at the immature stage (i.e. in source rock samples from quadrant 34) strongly suggests that other, maybe depositional-related factors play a role. Indeed, the biological precursor molecules and formation mechanisms of carbazoles and benzocarbazoles are still poorly understood (Clegg et al., 1997; Bennett et al., 2004). For instance, it has been postulated that carbazoles may originate from algae, bacteria, as well as archaea, whereas benzocarbazoles, as

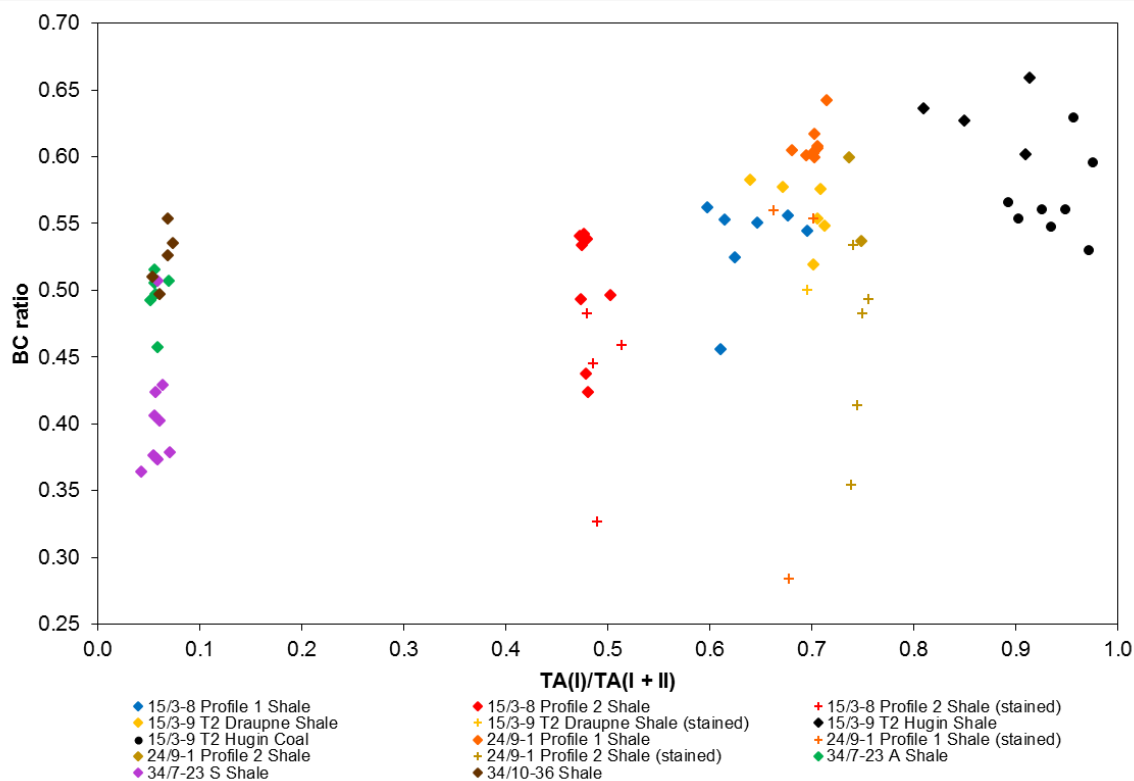


Fig. 91. TA(I)/TA(I + II)-BC ratio maturity correlation for the investigated source rock samples. Note that the BC ratio tends to increase with increasing TA(I)/TA(I + II) ratio (thermal maturity). However, there is a large degree of variability, even at the immature stage, which underscores the complexity of the BC ratio. Other, probably depositional-related factors appear to play a key role. Samples with a production index (PI) ≥ 0.3 are labeled as "stained".

7. Discussion

absent in hydropyrolysates of these organisms, could potentially be formed during diagenesis (Bennett et al., 2004). Yet, a possible origin of benzocarbazoles from organisms was, due to the limited data set, not generally excluded. Earlier, Snyder (1965) already invoked a potential origin of carbazoles from alkaloids present for example in land plants. The distribution of benzocarbazoles in the source rock samples studied here principally support the theory that benzocarbazoles are sensitive to changes in the depositional conditions (Bennett et al., 2004). Further research is necessary to understand the principal factors controlling the distribution of benzocarbazoles in both source rocks and crude oils. Although the BC ratio appears to be principally suitable for the reconstruction of secondary migration (e.g. Larter et al., 1996; Terken and Frewin, 2000), caution must, however, be taken since it is still not clear what exactly controls the distribution of benzocarbazoles in the geosphere.

8. Conclusions and further research

A comprehensive organic geochemical study on molecular fractionation effects associated with petroleum expulsion has been conducted in purpose to contribute to a better understanding of molecular redistribution effects upon primary petroleum migration. Therefore, nine different natural petroleum expulsion scenarios from six exploration wells (15/3-8, 15/3-9 T2, 24/9-1, 34/7-23 A, 34/7-23 S, 34/10-36) located in the Norwegian North Sea have been investigated with bulk and molecular geochemical methods to characterize the organic facies, the thermal maturity, and the selective retention of organic compounds, particularly aromatic maturation and migration tracers, in source rock vs. adjacent reservoir units. In addition, a geochromatographic retardation experiment involving oil window-mature Draupne source rock material, a tracer stock solution, and a synthetic oil was conducted to investigate the effects of geochromatography on selected organic compounds. Sampling of the natural expulsion scenarios mainly concentrated on the Upper Jurassic Draupne (Kimmeridge Clay) Formation, which represents the principal source rock for oil and gas in the North Sea region, but also on the Middle Jurassic, coaly-deltaic Hugin Formation that is rich in source units as well. The results show that organic-rich shales from quadrant 34 can be considered as immature to low mature based on bulk and molecular geochemical data, whereas source rock samples from quadrant 15 and 24 display maturities within the oil window, pointing to active petroleum generation and expulsion. A series of ternary discrimination diagrams strongly suggest a genetic relationship between oils and source bitumens in well 15/3-8, 24/9-1, 34/7-23 S, and the Draupne section of well 15/3-9 T2, indicating, for the oil window-mature sections, that compositional differences between reservoir extracts and source bitumens are indeed mainly controlled by petroleum expulsion. This is strongly supported by the intra-formational character of the sampled reservoir beds, which largely precludes lateral migration and contribution of oils from different sources. On the other hand, the molecular signature of petroleum extracted from reservoir units of well 34/7-23 A and the Hugin scenario of well 15/3-9 T2 clearly points to an external origin, most likely mature parts of the Draupne Formation. Concerning the organic facies, it was shown that the source rock material of most expulsion scenarios contains a mixed type II/III kerogen typical of marine environments. This is in good agreement with the generally assumed depositional conditions of the Draupne Formation. Higher proportions of land plant material have only been evidenced for samples from the

8. Conclusions and further research

Hugin Formation, particularly for the coals, which indicates deposition in a coastal swamp environment. By contrast, the geochemical signature of the corresponding shales suggests a considerable marine influence, pointing to a deposition in a transitional environment. Except for the Hugin section, facies variations within individual expulsion scenarios appear to be relatively small, which is important for the investigation of petroleum expulsion.

Based on the maturity data, the oil-source rock correlation, and the palaeofacies characterization, five out of nine natural scenarios were identified to be suitable for the investigation of petroleum expulsion: both sections from well 15/3-8, the Draupne scenario of well 15/3-9 T2, and both profiles from well 24/9-1. The trends documented in this study imply that molecular fractionation during primary migration is essentially controlled by the polarity and the molecular shape of the expelled components. In particular, the data indicate a stronger retention of heteroatom-bearing aromatics (e.g. carbazoles, dibenzofurans, dibenzothiophenes) compared to phenanthrenes, a preferential expulsion of alkylated vs. non-alkylated aromatics, and a preferential migration of nitrogen-shielded over nitrogen-exposed C₂ carbazoles. Moreover, the results generally support the theory of a preferential release of saturates relative to aromatic hydrocarbons and heteroatomic compounds. Also, trends have been observed that could perhaps relate to a preferential migration of *n*-alkanes over isoprenoids. With respect to well-established organic geochemical maturity and migration parameters, the data obtained in this work suggest that petroleum expulsion exerts an influence on the methylphenanthrene index (MPI 1), as the reservoir intervals appear to become progressively enriched in alkylated phenanthrenes compared to the source rock units, leading to higher MPI 1 values in the reservoir. However, remarkably, the MPI 1 yet seems to be a fairly good maturity indicator for source rocks, as evidenced by an excellent correlation between the thermal maturity and the MPI 1 for most source rock samples. On the other hand, no evidence for a fractionation among C₁ phenanthrenes was found, indicating that individual methylphenanthrene isomers are not redistributed during primary migration. The same was observed for methylated dibenzothiophenes and methylated carbazoles. In contrast, regarding the C₁ dibenzofurans, most reservoir units were found to be slightly enriched in the 2- and 3-isomer, which could relate to a preferential release of the 2- and 3- over the 1- and 4-isomer. Similar to the methylphenanthrenes, the C₁ dibenzothiophenes, the C₁ dibenzofurans, as well as the C₁ carbazoles seem to be preferentially expelled from the

8. Conclusions and further research

source rock compared to their non-methylated counterparts. Regarding the aliphatic fraction, no evidence for a fractionation of sterane or hopane biomarkers was found in this study, indicating these compounds are highly reliable as maturity and/or oil-source correlation parameters.

The data obtained from the geochromatographic experiment are principally in good agreement with the trends observed in the natural systems. In particular, the experiment demonstrated a preferential release of phenanthrenes over dibenzofuran, dibenzothiophenes, and carbazoles, a slightly faster migration of nitrogen-shielded compared to nitrogen-exposed C₂ carbazoles, and a significantly greater retention of carbazoles relative to phenanthrenes, dibenzothiophenes, and dibenzofurans. Concerning benzocarbazoles, the experiment suggests that benzo[a]carbazole migrates slightly faster than benzo[c]carbazole, but is released in significantly lower absolute quantities. With respect to natural systems, this observation indicates that the first oil expelled into a secondary migration system has a relatively high BC ratio, which decreases over time. Yet, no clear trends in the BC ratio are observable in the natural expulsion scenarios, suggesting the BC ratio is a very complex parameter that needs to be applied with caution. Though, the data suggest that the BC ratio at least partially depends on the thermal maturity of the source rock, as indicated by a relatively good correlation between the BC ratio and the T_{max} and triaromatic steroid ratio TA(I)/TA(I + II) across the study area. Based on the observations documented here, the following expulsion sequence is proposed: asphaltenes < aromatics < isoprenoids < *n*-alkanes. Within the aromatic fraction, less polar compounds (e.g. phenanthrenes) seem to be more easily expelled than heteroatom-substituted compounds with carbazoles being stronger retained than dibenzofurans and dibenzothiophenes. With respect to the Hugin case scenario, this work was able to show that both coals and shales of the Hugin Formation do not or only marginally contribute to the oil extracted from the surrounding reservoir intervals, which displays a markedly different molecular composition, as well as a lower thermal maturity. For example, benzo[b]carbazole, which is strongly enriched in source units of the Hugin Formation and would be expected to be seen in any related oils, is mostly below the detection limit in corresponding Hugin reservoir extracts. Therefore, in accordance with previous research, it seems that organic-rich rocks of the Hugin Formation have expelled hydrocarbons predominantly via a volatile gas/condensate phase. Benzo[b]-carbazole is proposed to represent an excellent oil-source rock correlation parameter.

8. Conclusions and further research

For the future, it is strongly recommended to extend the geochromatographic experiment conducted in this work using, for example, different or mixed source rock material, additional organic compounds, particularly biomarkers, *n*-alkanes, and *iso*-alkanes, and/or modified experimental conditions. In addition, it would be interesting to pass a natural crude oil through the column. Furthermore, different experimental approaches could, for instance, include some of the major techniques developed to simulate primary migration on a laboratory scale, e.g. closed system hydrous pyrolysis and “Expulsinator” experiments. Also, a diffusion experiment could be conducted comprising, for example, a filter-separated, two-part steel cell loaded with pre-extracted source rock powder, from which one half is spiked with a defined amount of tracer molecules (e.g. phenanthrenes, carbazoles, dibenzothiophenes). Subsequent heating could then cause compound mobilization and ultimately diffusion through the filter into the second, untreated half of the steel cell. Solvent extraction of both halves after a defined time interval would then allow to calculate diffusion rates and to investigate potential diffusion-related molecular redistribution effects during primary migration. Additional work on natural expulsion scenarios should include measured vitrinite reflectance data to verify the thermal maturities assessed here from bulk and molecular geochemical proxies. In addition, it is strongly recommended to perform complementary Rock-Eval measurements on solvent-extracted source rock samples since recent studies have revealed striking differences between whole rock and solvent-extracted Rock-Eval analyses with significant implications regarding petroleum expulsion characteristics. Any sampling of new expulsion scenarios should focus on well-defined, oil window-mature source rock units completely surrounded by reservoir intervals, as potential expulsion-related trends are here expected to be most pronounced. Besides, as a kind of pre-mature oil phase was found in the small reservoir unit of the thermally immature section from well 34/7-23 S, it would also be interesting to further investigate its composition and origin. Subsequent studies should also address the applicability of benzo[b]carbazole as oil-source rock correlation parameter.

References

- Bailey, N.J.L., Jobson, A.M., Rogers, M.A., 1973. Bacterial degradation of crude oil: comparison of field and experimental data. *Chemical Geology* 11, pp. 203-221.
- Bakr, M.M.Y., Wilkes, H., 2002. The influence of facies and depositional environment on the occurrence and distribution of carbazoles and benzocarbazoles in crude oils: a case study from the Gulf of Suez, Egypt. *Organic Geochemistry* 33, pp. 561-580.
- Banerjee, A., Sinha, A.K., Jain, A.K., Thomas, N.J., Misra, K.N., Chandra, K., 1998. A mathematical representation of Rock-Eval hydrogen index vs T_{max} profiles. *Organic Geochemistry* 28, pp. 43-55.
- Behar, F., Vandenbroucke, M., 1987. Chemical modelling of kerogens. *Organic Geochemistry* 11, pp. 15-24.
- Behar, F., Kressmann, S., Rudkiewicz, J.L., Vandenbroucke, M., 1992. Experimental simulation in a confined system and kinetic modelling of kerogen and oil cracking. *Organic Geochemistry* 19, pp. 173-189.
- Behar, F., Lorant, F., Lewan, M., 2008. Role of NSO compounds during primary cracking of a Type II kerogen and a Type III lignite. *Organic Geochemistry* 39, pp. 1-22.
- Behar, F., Roy, S., Jarvie, D., 2010. Artificial maturation of a Type I kerogen in closed system: Mass balance and kinetic modelling. *Organic Geochemistry* 41, pp. 1235-1247.
- Bennett, B., Larter, S.R., 1997. Partition behaviour of alkylphenols in crude oil/brine systems under subsurface conditions. *Geochimica et Cosmochimica Acta* 61, pp. 4393-4402.
- Bennett, B., Chen, M., Brincat, D., Gelin, F.J.P., Larter, S.R., 2002. Fractionation of benzocarbazoles between source rocks and petroleum. *Organic Geochemistry* 33, pp. 545-559.
- Bennett, B., Lager, A., Russell, C.A., Love, G.D., Larter, S.R., 2004. Hydrolysis of algae, bacteria, archaea and lake sediments; insights into the origin of nitrogen compounds in petroleum. *Organic Geochemistry* 35, pp. 1427-1439.
- Berg, R.R., Gangi, A.F., 1999. Primary Migration by Oil-Generation Microfracturing in Low-Permeability Source Rocks: Application to the Austin Chalk, Texas. *American Association of Petroleum Geologists Bulletin* 83, pp. 727-756.
- Bernard, S., Horsfield, B., Schulz, H.-M., Wirth, R., Schreiber, A., Sherwood, N., 2012a. Geochemical evolution of organic-rich shales with increasing maturity: A STXM and TEM study of the Posidonia Shale (Lower Toarcian, northern Germany). *Marine and Petroleum Geology* 31, pp. 70-89.
- Bernard, S., Wirth, R., Schreiber, A., Schulz, H.-J., Horsfield, B., 2012b. Formation of nanoporous pyrobitumen residues during maturation of the Barnett Shale (Fort Worth Basin). *International Journal of Coal Geology* 103, pp. 3-11.
- Bjørlykke, K., Høeg, K., 1997. Effects of burial diagenesis on stresses, compaction and fluid flow in sedimentary basins. *Marine and Petroleum Geology* 14, pp. 267-276.
- Bjørlykke, K., 2015a. Compaction of Sedimentary Rocks: Shales, Sandstones and Carbonates. In: Bjørlykke, K. (Ed.), *Petroleum Geoscience: From Sedimentary Environments to Rock Physics*. Springer, Berlin, pp. 351-360.
- Bjørlykke, K., 2015b. Source Rocks and Petroleum Geochemistry. In: Bjørlykke, K. (Ed.), *Petroleum Geoscience: From Sedimentary Environments to Rock Physics*. Springer, Berlin, pp. 361-372.
- Blakemore, J.E., Barker, J.R., Corcoran, W.H., 1973. Pyrolysis of *n*-Butane and the Effect of Trace Quantities of Oxygen. *Industrial & Engineering Chemistry Fundamentals* 12, pp. 147-155.
- Bonilla, J.V., Engel, M.H., 1986. Chemical and isotopic redistribution of hydrocarbons during migration: Laboratory simulation experiments. *Organic Geochemistry* 10, pp. 181-190.
- Bonilla, J.V., Engel, M.H., 1988. Chemical alteration of crude oils during simulated migration through quartz and clay minerals. *Organic Geochemistry* 13, pp. 503-512.
- Bordenave, M.L., 1993. The Sedimentation of Organic Matter. In: Bordenave, M.L. (Ed.), *Applied Petroleum Geochemistry*. Éditions Technip, Paris, pp. 15-76.
- Brothers, L., Engel, M.H., Krooss, B.M., 1991. The effects of fluid flow through porous media on the distribution of organic compounds in a synthetic crude oil. *Organic Geochemistry* 17, pp. 11-24.
- Burnham, A.K., Braun, R.L., 1990. Development of a detailed model of petroleum formation, destruction, and expulsion from lacustrine and marine source rocks. *Organic Geochemistry* 16, pp. 27-39.
- Burst, J.F., 1969. Diagenesis of Gulf Coast Clayey Sediments and Its Possible Relation to Petroleum Migration. *American Association of Petroleum Geologists Bulletin* 53, pp. 73-93.
- Carlson, R.M.K., Chamberlain, D.E., 1986. Steroid biomarker-clay mineral adsorption free energies: Implications to petroleum migration indices. *Organic Geochemistry* 10, pp. 163-180.
- Charlesworth, J.M., 1986. Interaction of clay minerals with organic nitrogen compounds released by kerogen pyrolysis. *Geochimica et Cosmochimica Acta* 50, pp. 1431-1435.

References

- Christiansson, P., Faleide, J.I., Berge, A.M., 2000. Crustal structure in the northern North Sea: an integrated geophysical study. In: Nøttvedt, A. (Ed.), Dynamics of the Norwegian Margin. Geological Society Special Publication 167, The Geological Society, London, pp. 15-40.
- Clegg, H., Wilkes, H., Horsfield, B., 1997. Carbazole distributions in carbonate and clastic source rocks. *Geochimica et Cosmochimica Acta* 61, pp. 5335-5345.
- Clegg, H., Wilkes, H., Oldenburg, T., Santamaría-Orozco, D., Horsfield, B., 1998a. Influence of maturity on carbazole and benzocarbazole distributions in crude oils and source rocks from the Sonda de Campeche, Gulf of Mexico. *Organic Geochemistry* 29, pp. 183-194.
- Clegg, H., Horsfield, B., Wilkes, H., Sinninghe-Damsté, J., Koopmans, M.P., 1998b. Effect of artificial maturation on carbazole distributions, as revealed by the hydrous pyrolysis of an organic-sulphur-rich source rock (Ghareb Formation, Jordan). *Organic Geochemistry* 29, pp. 1953-1960.
- Colten-Bradley, V.A., 1987. Role of Pressure in Smectite Dehydration—Effects on Geopressure and Smectite-to-Illite Transformation. *American Association of Petroleum Geologists Bulletin* 71, pp. 1414-1427.
- Cooles, G.P., Mackenzie, A.S., Quigley, T.M., 1986. Calculation of petroleum masses generated and expelled from source rocks. *Organic Geochemistry* 10, pp. 235-245.
- Cooper, B.S., Barnard, P.C., Telnaes, N., 1995. The Kimmeridge Clay Formation of The North Sea. In: Katz, B.J. (Ed.), *Petroleum Source Rocks*. Springer, Berlin, pp. 89-110.
- Cornford, C., Morrow, J.A., Turrington, A., Miles, J.A., Brooks, J., 1983. Some Geological Controls on Oil Composition in the U.K. North Sea. In: Brooks, J. (Ed.), *Petroleum Geochemistry and Exploration of Europe*. Geological Society Special Publication 12, Blackwell Scientific Publications, Oxford, pp. 175-194.
- Coward, M.P., Dewey, J., Mange, M.A., Hempton, M., Holroyd, J., 2003. Tectonic evolution. In: Evans, D., Graham, C., Armour, A., Bathurst, P. (Eds.), *The Millennium Atlas: petroleum geology of the central and northern North Sea*. The Geological Society of London, London, pp. 26-65.
- Delvaux, D., Martin, H., Leplat, P., Paulet, J., 1990. Geochemical characterization of sedimentary organic matter by means of pyrolysis kinetic parameters. *Organic Geochemistry* 16, pp. 175-187.
- Demaison, G.J., Moore, G.T., 1980. Anoxic Environments and Oil Source Bed Genesis. *American Association of Petroleum Geologists Bulletin* 64, pp. 1179-1209.
- Didyk, B.M., Simoneit, B.R.T., Brassell, S.C., Eglinton, G., 1978. Organic geochemical indicators of palaeoenvironmental conditions of sedimentation. *Nature* 272, pp. 216-222.
- Dow, W.G., 1974. Application of Oil-Correlation and Source-Rock Data to Exploration in Williston Basin. *American Association of Petroleum Geologists Bulletin* 58, pp. 1253-1264.
- du Rouchet, J., 1981. Stress Fields, A Key to Oil Migration. *American Association of Petroleum Geologists Bulletin* 65, pp. 74-85.
- Durand, B., 1988. Understanding of HC migration in sedimentary basins (present state of knowledge). *Organic Geochemistry* 13, pp. 445-459.
- Eltantawy, I.M., Arnold, P.W., 1972. Adsorption of *n*-Alkanes by Wyoming Montmorillonite. *Nature Physical Science* 237, pp. 123-125.
- England, W.A., Mackenzie, A.S., Mann, D.M., Quigley, T.M., 1987. The movement and entrapment of petroleum fluids in the subsurface. *Journal of the Geological Society* 144, pp. 327-347.
- Erdmann, M., Horsfield, B., 2006. Enhanced late gas generation potential of petroleum source rocks via recombination reactions: Evidence from the Norwegian North Sea. *Geochimica et Cosmochimica Acta* 70, pp. 3943-3956.
- Eseme, E., Littke, R., Krooss, B.M., Schwarzbauer, J., 2006. Experimental investigation of the compositional variation of acyclic paraffins during expulsion from source rocks. *Journal of Geochemical Exploration* 89, pp. 100-103.
- Eseme, E., Littke, R., Krooss, B.M., Schwarzbauer, J., 2007. Experimental investigation of the compositional variation of petroleum during primary migration. *Organic Geochemistry* 38, pp. 1373-1397.
- Eseme, E., Krooss, B.M., Littke, R., 2012. Evolution of petrophysical properties of oil shales during high-temperature compaction tests: Implications for petroleum expulsion. *Marine and Petroleum Geology* 31, pp. 110-124.
- Espitalié, J., Laporte, J.L., Madec, M., Marquis, F., Leplat, P., Paulet, J., Boutefeu, A., 1977. Méthode rapide de caractérisation des roches mères, de leur potentiel pétrolier et de leur degré d'évolution. *Oil & Gas Science and Technology* 32, pp. 23-42.
- Espitalié, J., Madec, M., Tissot, B., 1980. Role of Mineral Matrix in Kerogen Pyrolysis: Influence on Petroleum Generation and Migration. *American Association of Petroleum Geologists Bulletin* 64, pp. 59-66.

References

- Faleide, J.I., Bjørlykke, K., Gabrielsen, R.H., 2015. Geology of the Norwegian Continental Shelf. In: Bjørlykke, K. (Ed.), *Petroleum Geoscience: From Sedimentary Environments to Rock Physics*. Springer, Berlin, pp. 603-637.
- Fleet, A.J., Scott, A.C., 1994. Coal and coal-bearing strata as oil-prone source rocks: an overview. In: Scott, A.C., Fleet, A.J. (Eds.), *Coal and Coal-bearing Strata as Oil-prone Source Rocks? Geological Society Special Publication 77*, The Geological Society, London, pp. 1-8.
- Folkestad, A., Satur, N., 2008. Regressive and transgressive cycles in a rift-basin: Depositional model and sedimentary partitioning of the Middle Jurassic Hugin Formation, Southern Viking Graben, North Sea. *Sedimentary Geology* 207, pp. 1-21.
- Fraser, S., Robinson, A., Johnson, H., Underhill, J., Kadolsky, D., Connell, R., Johannessen, P., Ravnås, R., 2003. Upper Jurassic. In: Evans, D., Graham, C., Armour, A., Bathurst, P. (Eds.), *The Millennium Atlas: petroleum geology of the central and northern North Sea*. The Geological Society of London, London, pp. 372-439.
- Freed, R.L., Peacor, D.R., 1989. Variability in temperature of the smectite/illite reaction in Gulf Coast sediments. *Clay Minerals* 24, pp. 171-180.
- Galimberti, R., Ghiselli, C., Chiaramonte, M.A., 2000. Acidic polar compounds in petroleum: a new analytical methodology and applications as molecular migration indices. *Organic Geochemistry* 31, pp. 1375-1386.
- Gallois, R.W., 1976. Coccolith blooms in the Kimmeridge Clay and origin of North Sea Oil. *Nature* 259, pp. 473-475.
- Glennie, K., Higham, J., Stemmerik, L., 2003. Permian. In: Evans, D., Graham, C., Armour, A., Bathurst, P. (Eds.), *The Millennium Atlas: petroleum geology of the central and northern North Sea*. The Geological Society of London, London, pp. 211-258.
- Goff, J.C., 1983. Hydrocarbon generation and migration from Jurassic source rocks in the E Shetland Basin and Viking Graben of the northern North Sea. *Journal of the Geological Society* 140, pp. 445-474.
- Golonka, J., 2007. Late Triassic and Early Jurassic palaeogeography of the world. *Palaeogeography, Palaeoclimatology, Palaeoecology* 244, pp. 297-307.
- Green, T.K., Kovac, J., Larsen, J.W., 1984. A rapid and convenient method for measuring the swelling of coals by solvents. *Fuel* 63, pp. 935-938.
- Greibrokk, T., Lundanes, E., Norli, H.R., Dyrstad, K., Olsen, S.D., 1994. Experimental simulation of oil migration — Distribution effects on organic compound groups and on metal/metal ratios. *Chemical Geology* 116, pp. 281-299.
- Grice, K., de Mesmay, R., Glucina, A., Wang, S., 2008. An improved and rapid 5A molecular sieve method for gas chromatography isotope ratio mass spectrometry of *n*-alkanes (C₈–C₃₀₊). *Organic Geochemistry* 39, pp. 284-288.
- Grunau, H.R., 1987. A worldwide look at the cap-rock problem. *Journal of Petroleum Geology* 10, pp. 245-265.
- Guo, X., He, S., Liu, K., Zheng, L., 2011. Quantitative estimation of overpressure caused by oil generation in petroliferous basins. *Organic Geochemistry* 42, pp. 1343-1350.
- Han, Y., Mahlstedt, N., Horsfield, B., 2015. The Barnett Shale: Compositional fractionation associated with intraformational petroleum migration, retention, and expulsion. *American Association of Petroleum Geologists Bulletin* 99, pp. 2173-2202.
- Han, Y., Horsfield, B., Curry, D.J., 2017. Control of facies, maturation and primary migration on biomarkers in the Barnett Shale sequence in the Marathon 1 Mesquite well, Texas. *Marine and Petroleum Geology* 85, pp. 106-116.
- Harvey, H.R., 2006. Sources and Cycling of Organic Matter in the Marine Water Column. In: Volkman, J.K. (Ed.), *Marine Organic Matter: Biomarkers, Isotopes and DNA*. Springer, Berlin, pp. 1-25.
- Harwood, R.J., 1977. Oil and Gas Generation by Laboratory Pyrolysis of Kerogen. *American Association of Petroleum Geochemists Bulletin* 61, pp. 2082-2102.
- Hedberg, H.D., 1974. Relation of Methane Generation to Undercompacted Shales, Shale Diapirs, and Mud Volcanoes. *American Association of Petroleum Geologists Bulletin* 58, pp. 661-673.
- Hoering, T.C., 1984. Thermal reactions of kerogen with added water, heavy water and pure organic substances. *Organic Geochemistry* 5, pp. 267-278.
- Horsfield, B., Disko, U., Leistner, F., 1989. The micro-scale simulation of maturation: outline of a new technique and its potential applications. *Geologische Rundschau* 78, pp. 361-374.
- Horsfield, B., Curry, D.J., Bohacs, K., Littke, R., Rullkötter, J., Schenk, H.J., Radke, M., Schaefer, R.G., Carroll, A.R., Isaksen, G., Witte, E.G., 1994. Organic geochemistry of freshwater and alkaline lacustrine sediments in the Green River Formation of the Washakie Basin, Wyoming, U.S.A.. *Organic Geochemistry* 22, pp. 415-440.

References

- Horsfield, B., Clegg, H., Wilkes, H., Santamaría-Orozco, D., 1998. Effect of maturity on carbazole distributions in petroleum systems: new insights from the Sonda de Campeche, Mexico, and Hils Syncline, Germany. *Naturwissenschaften* 85, pp. 233-237.
- Huang, H., Bowler, B.F.J., Zhang, Z., Oldenburg, T.B.P., Larter, S.R., 2003. Influence of biodegradation on carbazole and benzocarbazole distributions in oil columns from the Liaohe basin, NE China. *Organic Geochemistry* 34, pp. 951-969.
- Huang, W.-Y., Meinschein, W.G., 1979. Sterols as ecological indicators. *Geochimica et Cosmochimica Acta* 43, pp. 739-745.
- Hughes, W.B., Holba, A.G., Dzou, L.I.P., 1995. The ratios of dibenzothiophene to phenanthrene and pristane to phytane as indicators of depositional environment and lithology of petroleum source rocks. *Geochimica et Cosmochimica Acta* 59, pp. 3581-3598.
- Husmo, T., Hamar, G., Høiland, O., Johannessen, E.P., Rømuld, A., Spencer, A., Titterton, R., 2003. Lower and Middle Jurassic. In: Evans, D., Graham, C., Armour, A., Bathurst, P. (Eds.), *The Millennium Atlas: petroleum geology of the central and northern North Sea*. The Geological Society of London, London, pp. 314-371.
- Ingram, L.L., Ellis, J., Crisp, P.T., Cook, A.C., 1983. Comparative study of oil shales and shale oils from the Mahogany zone, Green River Formation (U.S.A.) and Kerosene Creek seam, Rundle Formation (Australia). *Chemical Geology* 38, pp. 185-212.
- Isaksen, G.H., Curry, D.J., Yeakel, J.D., Jenssen, A.I., 1998. Controls on the oil and gas potential of humic coals. *Organic Geochemistry* 29, pp. 23-44.
- Isaksen, G.H., Ledje, K.H., 2001. Source rock quality and hydrocarbon migration pathways within the greater Utsira High area, Viking Graben, Norwegian North Sea. *American Association of Petroleum Geologists Bulletin* 85, pp. 861-883.
- Isaksen, G.H., Patience, R., van Graas, G., Jenssen, A.I., 2002. Hydrocarbon system analysis in a rift basin with mixed marine and nonmarine source rocks: The South Viking Graben, North Sea. *C*, pp. 557-591.
- Isaksen, G.H., 2004. Central North Sea hydrocarbon systems: Generation, migration, entrapment, and thermal degradation of oil and gas. *American Association of Petroleum Geologists Bulletin* 88, pp. 1545-1572.
- Japsen, P., Chalmers, J.A., 2000. Neogene uplift and tectonics around the North Atlantic: overview. *Global and Planetary Change* 24, pp. 165-173.
- Jarvie, D.M., Hill, R.J., Ruble, T.E., Pollastro, R.M., 2007. Unconventional shale-gas systems: The Mississippian Barnett Shale of north-central Texas as one model for thermogenic shale-gas assessment. *American Association of Petroleum Geologists Bulletin* 91, pp. 475-499.
- Jarvie, D.M., 2012. Shale Resource Systems for Oil and Gas: Part 2—Shale-oil Resource Systems. In: Breyer, J.A. (Ed.), *Shale reservoirs—Giant resources for the 21st century*. American Association of Petroleum Geologists Memoir 97, The American Association of Petroleum Geologists, pp. 89-119.
- Kelemen, S.R., Walters, C.C., Ertas, D., Kwiatek, L.M., Curry, D.J., 2006a. Petroleum Expulsion Part 2. Organic Matter Type and Maturity Effects on Kerogen Swelling by Solvents and Thermodynamic Parameters for Kerogen from Regular Solution Theory. *Energy & Fuels* 20, pp. 301-308.
- Kelemen, S.R., Walters, C.C., Ertas, D., Freund, H., Curry, D.J., 2006b. Petroleum Expulsion Part 3. A Model of Chemically Driven Fractionation during Expulsion of Petroleum from Kerogen. *Energy and Fuels* 20, pp. 309-319.
- Keym, M., Dieckmann, V., Horsfield, B., Erdmann, M., Galimberti, R., Kua, L.-C., Leith, L., Podlaha, O., 2006. Source rock heterogeneity of the Upper Jurassic Draupne Formation, North Viking Graben, and its relevance to petroleum generation studies. *Organic Geochemistry* 37, pp. 220-243.
- Killops, S., Killops, V., 2005. *Introduction to Organic Geochemistry*, Second Edition. Blackwell Publishing, Malden.
- Koopmans, M.P., Larter, S.R., Zhang, C., Mei, B., Wu, T., Chen, Y., 2002. Biodegradation and mixing of crude oils in Eocene Es3 reservoirs of the Liaohe basin, northeastern China. *American Association of Petroleum Geologists Bulletin* 86, pp. 1833-1843.
- Krooss, B.M., Brothers, L., Engel, M.H., 1991. Geochromatography in petroleum migration: a review. In: England, W.A., Fleet, A.J. (Eds.), *Petroleum Migration*. Geological Society Special Publication 59, The Geological Society, London, pp. 149-163.
- Kubala, M., Bastow, M., Thompson, S., Scotchman, I., Oygard, K., 2003. Geothermal regime, petroleum generation and migration. In: Evans, D., Graham, C., Armour, A., Bathurst, P. (Eds.), *The Millennium Atlas: petroleum geology of the central and northern North Sea*. The Geological Society of London, London, pp. 663-733.
- Lafargue, E., Barker, C., 1988. Effect of Water Washing on Crude Oil Compositions. *American Association of Petroleum Geologists Bulletin* 72, pp. 263-276.

References

- Lafargue, E., Espitalie, J., Jacobsen, T., Eggen, S., 1990. Experimental simulation of hydrocarbon expulsion. *Organic Geochemistry* 16, pp. 121-131.
- Lafargue, E., Espitalie, J., Broks, T.M., Nyland, B., 1994. Experimental simulation of primary migration. *Organic Geochemistry* 22, pp. 575-586.
- Larsen, J.W., Li, S., 1994. Solvent Swelling Studies of Green River Kerogen. *Energy & Fuels* 8, pp. 932-936.
- Larsen, J.W., Li, S., 1997a. An initial comparison of the interactions of Type I and III kerogens with organic liquids. *Organic Geochemistry* 26, pp. 305-309.
- Larsen, J.W., Li, S., 1997b. Changes in the Macromolecular Structure of a Type I Kerogen during Maturation. *Energy & Fuels* 11, pp. 897-901.
- Larter, S.R., Horsfield, B., 1993. Determination of Structural Components of Kerogens by the Use of Analytical Pyrolysis Methods. In: Engel, M.H., Macko, S.A. (Eds.), *Organic Geochemistry: Principles and Applications*. Plenum Press, New York, pp. 271-287.
- Larter, S.R., Aplin, A.C., 1995. Reservoir geochemistry: methods, applications and opportunities. In: Cubitt, J.M., England, W.A. (Eds.), *The Geochemistry of Reservoirs*. Geological Society Special Publication 86, The Geological Society, London, pp. 5-32.
- Larter, S.R., Bowler, B.F.J., Li, M., Chen, M., Brincat, D., Bennett, B., Noke, K., Donohoe, P., Simmons, D., Kohnen, M., Allan, J., Telnaes, N., Horstad, I., 1996. Molecular indicators of secondary oil migration distances. *Nature* 383, pp. 593-597.
- Larter, S., Bowler, B., Clarke, E., Wilson, C., Moffatt, B., Bennett, B., Yardley, G., Carruthers, D., 2000. An experimental investigation of geochromatography during secondary migration of petroleum performed under subsurface conditions with a real rock. *Geochemical Transactions* 9, pp. 1-7.
- Lewan, M.D., Winters, J.C., McDonald, J.H., 1979. Generation of Oil-Like Pyrolyzates from Organic-Rich Shales. *Science* 203, pp. 897-899.
- Lewan, M.D., 1983. Effects of thermal maturation on stable organic carbon isotopes as determined by hydrous pyrolysis of Woodford Shale. *Geochimica et Cosmochimica Acta* 47, pp. 1471-1479.
- Lewan, M.D., Bjorøy, M., Dolcater, D.L., 1986. Effects of thermal maturation on steroid hydrocarbons as determined by hydrous pyrolysis of Phosphoria Retort Shale. *Geochimica et Cosmochimica Acta* 50, pp. 1977-1987.
- Lewan, M.D., 1993. Laboratory Simulation of Petroleum Formation: Hydrous Pyrolysis. In: Engel, M.H., Macko, S.A. (Eds.), *Organic Geochemistry: Principles and Applications*. Plenum Press, New York, pp. 419-442.
- Lewan, M.D., 1997. Experiments on the role of water in petroleum formation. *Geochimica et Cosmochimica Acta* 61, pp. 3691-3723.
- Lewan, M.D., Ruble, T.E., 2002. Comparison of petroleum generation kinetics by isothermal hydrous and nonisothermal open-system pyrolysis. *Organic Geochemistry* 33, pp. 1457-1475.
- Lewan, M.D., Kotarba, M.J., Curtis, J.B., Węclaw, D., Kosakowski, P., 2006. Oil-generation kinetics for organic facies with Type-II and -IIS kerogen in the Menilite Shales of the Polish Carpathians. *Geochimica et Cosmochimica Acta* 70, pp. 3351-3368.
- Leythaeuser, D., Mackenzie, A., Schaefer, R.G., Bjorøy, M., 1984a. A Novel Approach for Recognition and Quantification of Hydrocarbon Migration Effects in Shale-Sandstone Sequences. *American Association of Petroleum Geologists Bulletin* 68, pp. 196-219.
- Leythaeuser, D., Radke, M., Schaefer, R.G., 1984b. Efficiency of petroleum expulsion from shale source rocks. *Nature* 311, pp. 745-748.
- Leythaeuser, D., Schaefer, R.G., 1984. Effects of hydrocarbon expulsion from shale source rocks of high maturity in Upper Carboniferous strata of the Ruhr area, Federal Republic of Germany. *Organic Geochemistry* 6, pp. 671-681.
- Leythaeuser, D., Schaefer, R.G., Radke, M., 1988a. Geochemical effects of primary migration of petroleum in Kimmeridge source rocks from Brae field area, North Sea. I: Gross composition of C₁₅₊-soluble organic matter and molecular composition of C₁₅₊-saturated hydrocarbons. *Geochimica et Cosmochimica Acta* 52, pp. 701-713.
- Leythaeuser, D., Radke, M., Willsch, H., 1988b. Geochemical effects of primary migration of petroleum in Kimmeridge source rocks from Brae field area, North Sea. II: Molecular composition of alkylated naphthalenes, phenanthrenes, benzo- and dibenzothiophenes. *Geochimica et Cosmochimica Acta* 52, pp. 2879-2891.
- Leythaeuser, D., Littke, R., Radke, M., Schaefer, R.G., 1988c. Geochemical effects of petroleum migration and expulsion from Toarcian source rocks in the Hils syncline area, NW-Germany. *Organic Geochemistry* 13, pp. 489-502.
- Leythaeuser, D., Schwark, L., Keuser, C., 2000. Geological conditions and geochemical effects of secondary petroleum migration and accumulation. *Marine and Petroleum Geology* 17, pp. 857-859.

References

- Li, M., Larter, S.R., Frolov, Y.B., Bjoroy, M., 1994. Adsorptive Interaction Between Nitrogen Compounds and Organic and/or Mineral Phases in Subsurface Rocks Models for Compositional Fractionation of Pyrrolic Nitrogen Compounds in Petroleum During Petroleum Migration. *Journal of High Resolution Chromatography* 17, pp. 230-236.
- Li, M., Larter, S.R., Stoddart, D., Bjorøy, M., 1995. Fractionation of pyrrolic nitrogen compounds in petroleum during migration: derivation of migration-related geochemical parameters. In: Cubitt, J.M., England, W.A. (Eds.), *The Geochemistry of Reservoirs*. Geological Society Special Publication 86, The Geological Society, London, pp. 103-123.
- Li, M., Yao, H., Stasiuk, L.D., Fowler, M.G., Larter, S.R., 1997. Effect of maturity and petroleum expulsion on pyrrolic nitrogen compound yields and distributions in Duvernay Formation petroleum source rocks in central Alberta, Canada. *Organic Geochemistry* 26, pp. 731-744.
- Li, M., Yao, H., Fowler, M.G., Stasiuk, L.D., 1998. Geochemical constraints on models for secondary petroleum migration along the Upper Devonian Rimbey-Meadowbrook reef trend in central Alberta, Canada. *Organic Geochemistry* 29, pp. 163-182.
- Liao, Y., Geng, A., Xiong, Y., Liu, D., Lu, J., Liu, J., Zhang, H., Geng, X., 2004. The influence of hydrocarbon expulsion on carbon isotopic compositions of individual *n*-alkanes in pyrolyzates of selected terrestrial kerogens. *Organic Geochemistry* 35, pp. 1479-1488.
- Littke, R., Baker, D.R., Leythaeuser, D., 1988. Microscopic and sedimentologic evidence for the generation and migration of hydrocarbons in Toarcian source rocks of different maturities. *Organic Geochemistry* 13, pp. 549-559.
- Mackenzie, A.S., Leythaeuser, D., Schaefer, R.G., Bjorøy, M., 1983. Expulsion of petroleum hydrocarbons from shale source rocks. *Nature* 301, pp. 506-509.
- Mackenzie, A.S., Leythaeuser, D., Muller, P., Quigley, T.M., Radke, M., 1988. The movement of hydrocarbons in shales. *Nature* 331, pp. 63-65.
- Mann, U., Hantschel, T., Schaefer, R.G., Krooss, B., Leythaeuser, D., Littke, R., Sachsenhofer, R.F., 1997. Petroleum Migration: Mechanisms, Pathways, Efficiencies and Numerical Simulations. In: Welte, D.H., Horsfield, B., Baker, D.R. (Eds.), *Petroleum and Basin Evolution: Insights from Petroleum Geochemistry, Geology and Basin Modeling*. Springer, Berlin, pp. 403-520.
- Mann, U., Korkmaz, S., Boreham, C.J., Hertle, M., Radke, M., Wilkes, H., 1998. Regional geology, depositional environment and maturity of organic matter of Early to Middle Jurassic coals, coaly shales, shales and claystones from the Eastern Pontides, NE Turkey. *International Journal of Coal Geology* 37, pp. 257-286.
- Marzoli, A., Renne, P.R., Piccirillo, E.M., Ernesto, M., Bellieni, G., De Min, A., 1999. Extensive 200-Million-Year-Old Continental Flood Basalts of the Central Atlantic Magmatic Province. *Science* 284, pp. 616-618.
- Maxwell, J.C., 1964. Influence of depth, temperature, and geologic age on porosity of quartzose sandstone. *American Association of Petroleum Geologists Bulletin* 48, pp. 697-709.
- Moldowan, J.M., Sundararaman, P., Schoell, M., 1986. Sensitivity of biomarker properties to depositional environment and/or source input in the Lower Toarcian of SW-Germany. *Organic Geochemistry* 10, pp. 915-926.
- Monthioux, M., Landais, P., Monin, J.-C., 1985. Comparison between natural and artificial maturation series of humic coals from the Mahakam delta, Indonesia. *Organic Geochemistry* 8, pp. 275-292.
- Oldenburg, T.B.P., Wilkes, H., Horsfield, B., van Duin, A.C.T., Stoddart, D., Wilhelms, A., 2002. Xanthenes—novel aromatic oxygen-containing compounds in crude oils. *Organic Geochemistry* 33, pp. 595-609.
- Orr, W.L., 1986. Kerogen/asphaltene/sulfur relationships in sulfur-rich Monterey oils. *Organic Geochemistry* 10, pp. 499-516.
- Oschmann, W., 1988. Kimmeridge Clay sedimentation — A new cyclic model. *Palaeogeography, Palaeoclimatology, Palaeoecology* 65, pp. 217-251.
- Ozkaya, I., 1988. A simple analysis of primary oil migration through oil-propagated fractures. *Marine and Petroleum Geology* 5, pp. 170-174.
- Pepper, A.S., Corvi, P.J., 1995a. Simple kinetic models of petroleum formation. Part I: oil and gas generation from kerogen. *Marine and Petroleum Geology* 12, pp. 291-319.
- Pepper, A.S., Corvi, P.J., 1995b. Simple kinetic models of petroleum formation. Part III: Modelling an open system. *Marine and Petroleum Geology* 12, pp. 417-452.
- Peters, K.E., Walters, C.C., Moldowan, J.M., 2005a. *The Biomarker Guide: Volume 1, Biomarkers and Isotopes in the Environment and Human History*, Second Edition. Cambridge University Press, Cambridge.
- Peters, K.E., Walters, C.C., Moldowan, J.M., 2005b. *The Biomarker Guide: Volume 2, Biomarkers and Isotopes in Petroleum Exploration and Earth History*, Second Edition. Cambridge University Press, Cambridge.

References

- Petersen, H.I., Rosenberg, P., Andsbjerg, J., 1996. Organic Geochemistry in Relation to the Depositional Environments of Middle Jurassic Coal Seams, Danish Central Graben, and Implications for Hydrocarbon Generative Potential. *American Association of Petroleum Geologists Bulletin* 80, pp. 47-62.
- Petersen, H.I., Andsbjerg, J., Bojesen-Koefoed, J.A., Nytoft, H.P., 2000. Coal-generated oil: source rock evaluation and petroleum geochemistry of the Lulita oilfield, Danish North Sea. *Journal of Petroleum Geology* 23, pp. 55-90.
- Powers, M.C., 1967. Fluid-release mechanisms in compacting marine mudrocks and their importance in oil exploration. *American Association of Petroleum Geologists Bulletin* 51, pp. 1240-1254.
- Price, L.C., Clayton, J.L., 1992. Extraction of whole versus ground source rocks: Fundamental petroleum geochemical implications including oil-source rock correlation. *Geochimica et Cosmochimica Acta* 56, pp. 1213-1222.
- Quigley, T.M., Mackenzie, A.S., 1988. The temperatures of oil and gas formation in the sub-surface. *Nature* 333, pp. 549-552.
- Radke, M., 1988. Application of aromatic compounds as maturity indicators in source rocks and crude oils. *Marine and Petroleum Geology* 5, pp. 224-236.
- Ramanampisoa, L., Disnar, J.R., 1994. Primary control of paleoproduction on organic matter preservation and accumulation in the Kimmeridge rocks of Yorkshire (UK). *Organic Geochemistry* 21, pp. 1153-1167.
- Riolo, J., Hussler, G., Albrecht, P., Connan, J., 1986. Distribution of aromatic steroids in geological samples: Their evaluation as geochemical parameters. *Organic Geochemistry* 10, pp. 981-990.
- Ritter, U., 2003. Solubility of petroleum compounds in kerogen: implications for petroleum expulsion. *Organic Geochemistry* 34, pp. 319-326.
- Ritter, U., Grøver, A., 2005. Adsorption of petroleum compounds in vitrinite: implications for petroleum expulsion from coal. *International Journal of Coal Geology* 62, pp. 183-191.
- Robison, C.R., 1997. Hydrocarbon source rock variability within the Austin Chalk and Eagle Ford Shale (Upper Cretaceous), East Texas, U.S.A.. *International Journal of Coal Geology* 34, pp. 287-305.
- Röhl, H.-J., Schmid-Röhl, A., Oschmann, W., Frimmel, A., Schwark, L., 2001. The Posidonia Shale (Lower Toarcian) of SW-Germany: an oxygen-depleted ecosystem controlled by sea level and palaeoclimate. *Palaeogeography, Palaeoclimatology, Palaeoecology* 165, pp. 27-52.
- Rullkötter, J., 1993. The Thermal Alteration of Kerogen and the Formation of Oil. In: Engel, M.H., Macko, S.A. (Eds.), *Organic Geochemistry: Principles and Applications*. Springer, New York, pp. 377-396.
- Sagert, N.H., Laidler, K.J., 1963a. Kinetics and mechanisms of the pyrolysis of *n*-butane part I. The uninhibited decomposition. *Canadian Journal of Chemistry* 41, pp. 838-847.
- Sagert, N.H., Laidler, K.J., 1963b. Kinetics and mechanisms of the pyrolysis of *n*-butane part II. The reaction inhibited by nitric oxide. *Canadian Journal of Chemistry* 41, pp. 848-857.
- Sajgo, C., Maxwell, J.R., Mackenzie, A.S., 1983. Evaluation of fractionation effects during the early stages of primary migration. *Organic Geochemistry* 5, pp. 65-73.
- Sandvik, E.I., Mercer, J.N., 1990. Primary migration by bulk hydrocarbon flow. *Organic Geochemistry* 16, pp. 83-89.
- Sandvik, E.I., Young, W.A., Curry, D.J., 1992. Expulsion from hydrocarbon sources: the role of organic absorption. *Organic Geochemistry* 19, pp. 77-87.
- Sanei, H., Wood, J.M., Ardakani, O.H., Clarkson, C.R., Jiang, C., 2015. Characterization of organic matter fractions in an unconventional tight gas siltstone reservoir. *International Journal of Coal Geology* 150-151, pp. 296-305.
- Schaefer, R.G., Schenk, H.J., Hardelauf, H., Harms, R., 1990. Determination of gross kinetic parameters for petroleum formation from Jurassic source rocks of different maturity levels by means of laboratory experiments. *Organic Geochemistry* 16, pp. 115-120.
- Schlömer, S., Krooss, B.M., 1997. Experimental characterisation of the hydrocarbon sealing efficiency of cap rocks. *Marine and Petroleum Geology* 14, pp. 565-580.
- Schwark, L., Vliex, M., Schaeffer, P., 1998. Geochemical characterization of Malm Zeta laminated carbonates from the Franconian Alb, SW-Germany (II). *Organic Geochemistry* 29, pp. 1921-1952.
- Seewald, J.S., 1994. Evidence for metastable equilibrium between hydrocarbons under hydrothermal conditions. *Nature* 370, pp. 285-287.
- Seifert, W.K., Moldowan, J.M., 1978. Applications of steranes, terpanes and monoaromatics to the maturation, migration and source of crude oils. *Geochimica et Cosmochimica Acta* 42, pp. 77-95.
- Seifert, W.K., Moldowan, J.M., 1981. Paleoreconstruction by biological markers. *Geochimica et Cosmochimica Acta* 45, pp. 783-794.

References

- Selley, R.C., 1998. *Elements of Petroleum Geology*, Second Edition. Academic Press, San Diego.
- Shanmugam, G., 1985. Significance of Coniferous Rain Forests and Related Organic Matter in Generating Commercial Quantities of Oil, Gippsland Basin, Australia. *American Association of Petroleum Geologists Bulletin* 69, pp. 1241-1254.
- Sinninghe Damsté, J.S., Kohnen, M.E., de Leeuw, J.W., 1990. Thiophenic biomarkers for palaeoenvironmental assessment and molecular stratigraphy. *Nature* 345, pp. 609-611.
- Smirnov, M.B., Frolov, E.B., 1997. A study of petroleum alkylcarbazoles using ^1H NMR spectroscopy. *Organic Geochemistry* 26, pp. 33-42.
- Snyder, L.R., 1965. Distribution of Benzcarbazole Isomers in Petroleum as Evidence for their Biogenic Origin. *Nature* 205, p. 277.
- Stainforth, J.G., 2009. Practical kinetic modeling of petroleum generation and expulsion. *Marine and Petroleum Geology* 26, pp. 552-572.
- Stainforth, J.G., Reinders, J.E.A., 1990. Primary migration of hydrocarbons by diffusion through organic matter networks, and its effect on oil and gas generation. *Organic Geochemistry* 16, pp. 61-74.
- Stalker, L., Farrimond, P., Larter, S.R., 1994. Water as an oxygen source for the production of oxygenated compounds (including CO_2 precursors) during kerogen maturation. *Organic Geochemistry* 22, pp. 477-486.
- Stockhausen, M., 2015. Experimental simulation of hydrocarbon expulsion. PhD Thesis, Christian-Albrechts-Universität zu Kiel.
- Stoddart, D.P., Hall, P.B., Larter, S.R., Brasher, J., Li, M., Bjorøy, M., 1995. The reservoir geochemistry of the Eldfisk Field, Norwegian North Sea. In: Cubitt, J.M., England, W.A. (Eds.), *The Geochemistry of Reservoirs*. Geological Society Special Publication 86, The Geological Society, London, pp. 257-279.
- Tannenbaum, E., Huizinga, B.J., Kaplan, I.R., 1986. Role of Minerals in Thermal Alteration of Organic Matter—II: A Material Balance. *American Association of Petroleum Geologists Bulletin* 70, pp. 1156-1165.
- Taylor, P., Larter, S., Jones, M., Dale, J., Horstad, I., 1997. The effect of oil-water-rock partitioning on the occurrence of alkylphenols in petroleum systems. *Geochimica et Cosmochimica Acta* 61, pp. 1899-1910.
- Terken, J.M.J., Frewin, N.L., 2000. The Dhahaban Petroleum System of Oman. *American Association of Petroleum Geologists Bulletin* 84, pp. 523-544.
- Thomas, M.M., Clouse, J.A., 1990a. Primary migration by diffusion through kerogen: I. Model experiments with organic-coated rocks. *Geochimica et Cosmochimica Acta* 54, pp. 2775-2779.
- Thomas, M.M., Clouse, J.A., 1990b. Primary Migration by diffusion through kerogen: II. Hydrocarbon diffusivities in kerogen. *Geochimica et Cosmochimica Acta* 54, pp. 2781-2792.
- Thomas, M.M., Clouse, J.A., 1990c. Primary migration by diffusion through kerogen: III. Calculation of geologic fluxes. *Geochimica et Cosmochimica Acta* 54, pp. 2793-2797.
- Tissot, B.P., Welte, D.H., 1984. *Petroleum Formation and Occurrence*, Second Revised and Enlarged Edition. Springer, Berlin.
- Tourtletot, H.A., 1979. Black shale—its deposition and diagenesis. *Clays and Clay Minerals* 27, pp. 313-321.
- Trinidad, L.A.F., Brassell, S.C., Neto, E.V.S., 1992. Petroleum Migration and Mixing in the Potiguar Basin, Brazil. *The American Association of Petroleum Geologists Bulletin* 76, pp. 1903-1924.
- Tyson, R.V., Wilson, R.C.L., Downie, C., 1979. A stratified water column environmental model for the type Kimmeridge Clay. *Nature* 277, pp. 377-380.
- Ungerer, P., 1990. State of the art of research in kinetic modelling of oil formation and expulsion. *Organic Geochemistry* 16, pp. 1-25.
- Vandenbroucke, M., 1993. Migration of Hydrocarbons. In: Bordenave, M.L. (Ed.), *Applied Petroleum Geochemistry*. Éditions Technip, Paris, pp. 123-148.
- Vandenbroucke, M., Bordenave, M.L., Durand, B., 1993. Transformation of Organic Matter with Increasing Burial of Sediments and the Formation of Petroleum in Source Rocks. In: Bordenave, M.L. (Ed.), *Applied Petroleum Geochemistry*. Éditions Technip, Paris, pp. 101-122.
- Vandenbroucke, M., Largeau, C., 2007. Kerogen origin, evolution and structure. *Organic Geochemistry* 38, pp. 719-833.
- Volkman, J.K., Barrett, S.M., Blackburn, S.I., Mansour, M.P., Sikes, E.L., Gelin, F., 1998. Microalgal biomarkers: A review of recent research developments. *Organic Geochemistry* 29, pp. 1163-1179.
- Wei, Z., Zou, Y.-R., Cai, Y., Wang, L., Luo, X., Peng, P., 2012. Kinetics of oil group-type generation and expulsion: An integrated application to Dongying Depression, Bohai Bay Basin, China. *Organic Geochemistry* 52, pp. 1-12.

References

- White, R.S., 1988. A hot-spot model for early Tertiary volcanism in the N Atlantic. In Morton, A.C., Parson, L.M. (Eds.), *Early Tertiary Volcanism and the Opening of the NE Atlantic*. Geological Society Special Publication 39, Blackwell Scientific Publications, Oxford, pp. 3-13.
- Wilkins, R.W.T., George, S.C. (2002). Coal as source rock for oil: a review. *International Journal of Coal Geology* 50, pp. 317-361.
- Williams, P.F.V., 1986. Petroleum geochemistry of the Kimmeridge Clay of onshore southern and eastern England. *Marine and Petroleum Geology* 3, pp. 258-281.
- Yamamoto, M., 1992. Fractionation of azaarenes during oil migration. *Organic Geochemistry* 19, pp. 389-402.
- Yang, Y., Arouri, K., 2016. A Simple Geotracer Compositional Correlation Analysis Reveals Oil Charge and Migration Pathways. *Scientific Reports* 6, pp. 1-13.
- Young, A., McIver, R.D., 1977. Distribution of Hydrocarbons Between Oils and Associated Fine-Grained Sedimentary Rocks—Physical Chemistry Applied to Petroleum Geochemistry, II. *American Association of Petroleum Geologists Bulletin* 61, pp. 1407-1436.
- Zanella, E., Coward, M.P., McGrandle, A., 2003. Crustal structure. In: Evans, D., Graham, C., Armour, A., Bathurst, P. (Eds.), *The Millenium Atlas: petroleum geology of the central and northern North Sea*. The Geological Society of London, London, pp. 66-86.
- Zhang, C., Li, S., Yang, J., Yang, S., Wang, J., 2004. Petroleum migration and mixing in the Pearl River Mouth Basin, South China Sea. *Marine and Petroleum Geology* 21, pp. 215-224.
- Zhang, L., Li, M., Wang, Y., Yin, Q.-Z., Zhang, W., 2013. A novel molecular index for secondary oil migration distance. *Scientific Reports* 3, pp. 1-8.
- Zhang, S.C., Hanson, A.D., Moldowan, J.M., Graham, S.A., Liang, D.G., Chang, E., Fago, F., 2000. Paleozoic oil–source rock correlations in the Tarim basin, NW China. *Organic Geochemistry* 31, pp. 273-286.
- Zhusheng, J., Philp, R.P., Lewis, C.A., 1988. Fractionation of biological markers in crude oils during migration and the effects on correlation and maturation parameters. *Organic Geochemistry* 13, pp. 561-571.
- Ziegs, V., Horsfield, B., Skeie, J.E., Rinna, J., 2017. Petroleum retention in the Mandal Formation, Central Graben, Norway. *Marine and Petroleum Geology* 83, pp. 195-214.

Internet sources

Norwegian Petroleum Directorate (NPD):

- (1) www.npd.no/en/
- (2) <http://factpages.npd.no/factpages/Default.aspx?culture=en>
- (3) http://gis.npd.no/factmaps/html_21/
- (4) www.npd.no/Global/Norsk/4-Kart/Sokkelkart2016/Kontinentalsokkelkart_2016.pdf, processing request: 15.05.2017

Appendix: (1) Data

| Sample ID | TOC [wt.%] | TN [wt.%] | TC [wt.%] | TS [wt.%] | TIC [wt.%] | Carbonate [wt.%] | S ₁ [mg HC/g rock] | S ₂ [mg HC/g rock] | S ₃ [mg CO ₂ /g rock] | HI [mg HC/g TOC] | OI [mg CO ₂ /g TOC] | T _{max} [°C] | PI | Material used for extraction [g] | Extract yield [mg/g TOC] | Extract yield [ppm] |
|-----------|------------|-----------|-----------|-----------|------------|------------------|-------------------------------|-------------------------------|---|------------------|--------------------------------|-----------------------|------|----------------------------------|--------------------------|---------------------|
| K011188 | 0.76 | 0.05 | 1.26 | 0.47 | 0.50 | 4.17 | 2.18 | 1.98 | 0.08 | 262 | 11 | 438 | 0.52 | 25.11 | 598 | 4528 |
| K011189 | 1.80 | 0.07 | 1.85 | 0.83 | 0.05 | 0.42 | 3.11 | 4.31 | 0.06 | 239 | 3 | 439 | 0.42 | 25.13 | 324 | 5830 |
| K011190 | 2.01 | 0.09 | 2.19 | 2.20 | 0.17 | 1.45 | 1.99 | 2.87 | 0.12 | 142 | 6 | 437 | 0.41 | 20.12 | 200 | 4026 |
| K012302 | 8.55 | 0.26 | 8.56 | 6.23 | 0.01 | 0.05 | 3.10 | 20.14 | 0.16 | 236 | 2 | 434 | 0.13 | 4.98 | 77 | 6566 |
| K011191 | 8.28 | 0.26 | 8.54 | 5.23 | 0.26 | 2.18 | 3.42 | 21.35 | 0.55 | 258 | 7 | 439 | 0.14 | 4.95 | 91 | 7515 |
| K011192 | 7.60 | 0.24 | 7.76 | 5.60 | 0.16 | 1.31 | 3.22 | 21.47 | 0.20 | 282 | 3 | 437 | 0.13 | 4.95 | 88 | 6707 |
| K011193 | 9.66 | 0.27 | 9.84 | 7.91 | 0.18 | 1.50 | 3.60 | 30.42 | 0.17 | 315 | 2 | 436 | 0.11 | 5.02 | 65 | 6275 |
| K011194 | 8.49 | 0.24 | 8.63 | 8.09 | 0.14 | 1.17 | 4.54 | 23.55 | 0.26 | 277 | 3 | 434 | 0.16 | 4.98 | 113 | 9598 |
| K011195 | 10.09 | 0.29 | 10.36 | 8.16 | 0.27 | 2.27 | 6.09 | 31.18 | 0.28 | 309 | 3 | 434 | 0.16 | 4.96 | 112 | 11310 |
| K011196 | 0.49 | 0.03 | 0.50 | 0.42 | 0.01 | 0.10 | 1.34 | 1.56 | 0.13 | 321 | 26 | 433 | 0.46 | 25.09 | 672 | 3280 |
| K012303 | 0.36 | 0.01 | 0.75 | 0.22 | 0.40 | 3.30 | 0.92 | 0.96 | 0.07 | 268 | 20 | 429 | 0.49 | 5.09 | 714 | 2554 |
| K011197 | 0.49 | 0.03 | 0.44 | 0.61 | 0.00 | 0.00 | 1.36 | 1.57 | 0.06 | 318 | 13 | 434 | 0.47 | 25.15 | 638 | 3145 |
| K012304 | 9.05 | 0.27 | 9.06 | 10.02 | 0.02 | 0.13 | 5.27 | 14.41 | 0.28 | 159 | 3 | 432 | 0.27 | 5.10 | 115 | 10392 |
| K012305 | 3.62 | 0.13 | 3.71 | 3.93 | 0.09 | 0.75 | 4.28 | 4.97 | 0.18 | 137 | 5 | 433 | 0.46 | 5.01 | 260 | 9421 |
| K012430 | 0.91 | 0.05 | 1.00 | 0.63 | 0.08 | 0.70 | 2.88 | 1.65 | 0.07 | 180 | 7 | 436 | 0.64 | 5.02 | 629 | 5737 |
| K012306 | 0.73 | 0.02 | 0.73 | 0.33 | 0.01 | 0.06 | 3.94 | 1.48 | 0.04 | 204 | 6 | 435 | 0.73 | 5.14 | 872 | 6323 |
| K011198 | 0.70 | 0.03 | 0.71 | 0.27 | 0.01 | 0.05 | 4.17 | 1.62 | 0.10 | 231 | 15 | 433 | 0.72 | 25.17 | 851 | 5963 |
| K012431 | 6.20 | 0.18 | 6.19 | 10.01 | 0.00 | 0.00 | 2.57 | 5.02 | 0.27 | 81 | 4 | 436 | 0.34 | 5.10 | 136 | 8431 |
| K012432 | 6.24 | 0.17 | 6.29 | 10.57 | 0.06 | 0.47 | 2.60 | 6.11 | 0.18 | 98 | 3 | 437 | 0.30 | 5.03 | 128 | 8012 |
| K012433 | 6.46 | 0.17 | 6.50 | 12.43 | 0.04 | 0.35 | 3.54 | 8.14 | 0.16 | 126 | 2 | 433 | 0.30 | 5.08 | 130 | 8425 |
| K012434 | 6.11 | 0.17 | 6.24 | 11.44 | 0.14 | 1.15 | 2.38 | 5.72 | 0.24 | 94 | 4 | 434 | 0.29 | 5.10 | 173 | 10588 |
| K012435 | 5.88 | 0.18 | 5.97 | 7.09 | 0.09 | 0.75 | 2.12 | 5.56 | 0.15 | 95 | 3 | 436 | 0.28 | 5.10 | 92 | 5431 |
| K012436 | 3.28 | 0.12 | 3.25 | 4.50 | 0.00 | 0.00 | 1.53 | 2.69 | 0.27 | 82 | 8 | 433 | 0.36 | 5.09 | 158 | 5187 |
| K012437 | 0.60 | 0.04 | 0.62 | 1.72 | 0.01 | 0.12 | 1.07 | 1.39 | 0.08 | 230 | 13 | 435 | 0.44 | 5.86 | 485 | 2935 |
| K012438 | 6.16 | 0.19 | 6.07 | 10.48 | 0.00 | 0.00 | 2.65 | 5.89 | 0.23 | 96 | 4 | 436 | 0.31 | 5.01 | 105 | 6447 |
| K012439 | 6.42 | 0.20 | 6.47 | 9.46 | 0.05 | 0.39 | 2.70 | 7.90 | 0.17 | 123 | 3 | 437 | 0.25 | 5.03 | 105 | 6759 |
| K012440 | 7.44 | 0.21 | 7.51 | 11.80 | 0.07 | 0.57 | 3.44 | 6.60 | 0.22 | 89 | 3 | 438 | 0.34 | 4.99 | 124 | 9238 |
| K012441 | 0.32 | 0.03 | 0.32 | 0.46 | 0.00 | 0.00 | 0.92 | 1.10 | 0.06 | 342 | 20 | 431 | 0.46 | 5.80 | 768 | 2466 |
| K012442 | 0.31 | 0.04 | 0.32 | 0.37 | 0.00 | 0.02 | 1.17 | 1.02 | 0.04 | 325 | 13 | 433 | 0.54 | 5.87 | 783 | 2453 |
| K012443 | 0.28 | 0.04 | 0.28 | 0.33 | 0.01 | 0.06 | 1.01 | 0.84 | 0.08 | 303 | 27 | 429 | 0.55 | 6.38 | 753 | 2085 |
| K012444 | 0.36 | 0.04 | 0.36 | 0.28 | 0.01 | 0.04 | 1.14 | 1.01 | 0.09 | 280 | 24 | 428 | 0.53 | 6.35 | 723 | 2598 |
| K012445 | 0.56 | 0.05 | 0.65 | 1.11 | 0.08 | 0.68 | 1.09 | 1.70 | 0.07 | 302 | 12 | 438 | 0.39 | 6.00 | 490 | 2767 |
| K012446 | 6.99 | 0.24 | 7.37 | 4.57 | 0.38 | 3.18 | 3.79 | 15.32 | 0.20 | 219 | 3 | 435 | 0.20 | 5.22 | 104 | 7280 |
| K012447 | 6.99 | 0.20 | 7.07 | 5.58 | 0.08 | 0.64 | 3.42 | 11.78 | 0.26 | 169 | 4 | 435 | 0.22 | 5.11 | 101 | 7045 |
| K012448 | 7.33 | 0.20 | 7.37 | 7.56 | 0.04 | 0.32 | 3.48 | 15.55 | 0.23 | 212 | 3 | 433 | 0.18 | 5.14 | 89 | 6556 |
| K012449 | 7.49 | 0.20 | 7.15 | 5.13 | 0.00 | 0.00 | 3.73 | 17.10 | 0.21 | 228 | 3 | 434 | 0.18 | 5.06 | 91 | 6838 |
| K012450 | 6.59 | 0.18 | 6.68 | 4.61 | 0.08 | 0.68 | 3.87 | 15.24 | 0.19 | 231 | 3 | 435 | 0.20 | 5.00 | 107 | 7040 |
| K011228 | 1.09 | 0.05 | 1.25 | 0.57 | 0.16 | 1.34 | 8.74 | 2.79 | 0.13 | 256 | 11 | 429 | 0.76 | 25.00 | 1054 | 11488 |
| K011229 | 0.65 | 0.05 | 0.70 | 0.38 | 0.05 | 0.41 | 2.52 | 2.16 | 0.14 | 331 | 21 | 429 | 0.54 | 25.05 | 938 | 6144 |
| K011230 | 1.42 | 0.05 | 1.49 | 0.44 | 0.07 | 0.57 | 3.05 | 3.76 | 0.14 | 265 | 10 | 445 | 0.45 | 20.05 | 426 | 6040 |
| K011231 | 7.37 | 0.23 | 7.64 | 6.30 | 0.27 | 2.27 | 6.50 | 12.28 | 0.13 | 167 | 2 | 438 | 0.35 | 5.02 | 131 | 9622 |

(continued on next page)

Appendix

Bulk data (continued)

| Sample ID | TOC [wt.%] | TN [wt.%] | TC [wt.%] | TS [wt.%] | TIC [wt.%] | Carbonate [wt.%] | S ₁ [mg HC/g rock] | S ₂ [mg HC/g rock] | S ₃ [mg CO ₂ /g rock] | HI [mg HC/g TOC] | OI [mg CO ₂ /g TOC] | T _{max} [°C] | PI | Material used for extraction [g] | Extract yield [mg/g TOC] | Extract yield [ppm] |
|-----------|------------|-----------|-----------|-----------|------------|------------------|-------------------------------|-------------------------------|---|------------------|--------------------------------|-----------------------|------|----------------------------------|--------------------------|---------------------|
| K011232 | 9.53 | 0.26 | 10.05 | 6.55 | 0.51 | 4.29 | 5.64 | 27.96 | 0.36 | 293 | 4 | 439 | 0.17 | 4.96 | 93 | 8871 |
| K011233 | 9.23 | 0.26 | 10.20 | 5.27 | 0.97 | 8.07 | 6.29 | 25.79 | 0.40 | 279 | 4 | 440 | 0.20 | 5.08 | 104 | 9626 |
| K012421 | 1.38 | 0.05 | 2.99 | 0.49 | 1.61 | 13.38 | 1.60 | 3.52 | 0.05 | 255 | 3 | 447 | 0.31 | 5.24 | 184 | 2538 |
| K012422 | 8.05 | 0.29 | 8.09 | 5.72 | 0.04 | 0.35 | 2.71 | 18.53 | 0.11 | 230 | 1 | 438 | 0.13 | 4.96 | 56 | 4496 |
| K011234 | 0.19 | 0.02 | 0.24 | 1.86 | 0.05 | 0.41 | 0.49 | 0.60 | 0.11 | 309 | 57 | 425 | 0.45 | 25.07 | 582 | 1129 |
| K012423 | 0.38 | 0.04 | 0.96 | 0.85 | 0.58 | 4.81 | 1.21 | 1.30 | 0.09 | 340 | 23 | 433 | 0.48 | 4.92 | 579 | 2215 |
| K012424 | 9.40 | 0.34 | 9.29 | 8.03 | 0.00 | 0.00 | 4.52 | 20.89 | 0.19 | 222 | 2 | 437 | 0.18 | 5.15 | 56 | 5301 |
| K011235 | 0.93 | 0.05 | 0.92 | 0.64 | 0.00 | 0.00 | 3.63 | 1.69 | 0.12 | 183 | 13 | 438 | 0.68 | 25.11 | 506 | 4687 |
| K011236 | 9.32 | 0.36 | 9.32 | 5.79 | 0.00 | 0.02 | 5.29 | 17.24 | 0.23 | 185 | 2 | 439 | 0.23 | 4.99 | 95 | 8878 |
| K011237 | 0.27 | 0.03 | 0.33 | 0.24 | 0.06 | 0.53 | 0.75 | 0.88 | 0.08 | 327 | 30 | 433 | 0.46 | 25.37 | 570 | 1533 |
| K011238 | 9.53 | 0.33 | 9.55 | 6.10 | 0.01 | 0.12 | 4.61 | 22.15 | 0.18 | 232 | 2 | 437 | 0.17 | 5.06 | 80 | 7668 |
| K011239 | 1.10 | 0.02 | 1.22 | 0.47 | 0.12 | 1.03 | 12.17 | 1.50 | 0.09 | 136 | 8 | 431 | 0.89 | 20.05 | 1083 | 11900 |
| K012425 | 83.79 | 1.85 | 83.23 | 0.71 | 0.00 | 0.00 | 12.86 | 153.04 | 2.64 | 183 | 3 | 457 | 0.08 | 2.01 | 14 | 11990 |
| K011240 | 83.23 | 1.78 | 83.76 | 0.83 | 0.52 | 4.36 | 13.54 | 159.88 | 1.13 | 192 | 1 | 452 | 0.08 | 2.03 | 14 | 11330 |
| K011241 | 76.45 | 1.69 | 76.19 | 0.59 | 0.00 | 0.00 | 15.39 | 194.31 | 1.35 | 254 | 2 | 454 | 0.07 | 1.99 | 22 | 16482 |
| K011242 | 80.50 | 1.83 | 80.32 | 0.92 | 0.00 | 0.00 | 13.64 | 222.18 | 0.92 | 276 | 1 | 461 | 0.06 | 2.02 | 16 | 12624 |
| K011243 | 1.31 | 0.01 | 1.24 | 0.57 | 0.00 | 0.00 | 2.34 | 2.58 | 0.06 | 196 | 5 | 448 | 0.48 | 20.00 | 338 | 4445 |
| K011244 | 1.15 | 0.04 | 1.13 | 0.38 | 0.00 | 0.00 | 2.82 | 2.75 | 0.07 | 240 | 6 | 445 | 0.51 | 20.00 | 470 | 5395 |
| K011245 | 0.88 | 0.03 | 1.53 | 0.11 | 0.65 | 5.41 | 2.18 | 2.20 | 0.09 | 249 | 10 | 441 | 0.50 | 25.08 | 454 | 4011 |
| K011246 | 1.09 | 0.03 | 1.10 | 0.07 | 0.01 | 0.11 | 2.17 | 2.53 | 0.18 | 232 | 17 | 445 | 0.46 | 20.16 | 362 | 3943 |
| K012426 | 1.57 | 0.05 | 1.71 | 0.75 | 0.14 | 1.17 | 1.09 | 2.19 | 0.50 | 139 | 32 | 454 | 0.33 | 5.11 | 156 | 2446 |
| K012427 | 2.85 | 0.10 | 2.92 | 1.24 | 0.07 | 0.58 | 1.01 | 3.96 | 0.25 | 139 | 9 | 457 | 0.20 | 5.43 | 83 | 2376 |
| K011247 | 6.99 | 0.20 | 6.99 | 4.06 | 0.00 | 0.01 | 1.22 | 10.42 | 0.31 | 149 | 4 | 458 | 0.10 | 5.04 | 34 | 2361 |
| K011248 | 7.56 | 0.22 | 7.75 | 7.45 | 0.19 | 1.54 | 1.88 | 11.80 | 0.14 | 156 | 2 | 454 | 0.14 | 5.04 | 55 | 4147 |
| K011249 | 70.29 | 1.60 | 70.17 | 3.81 | 0.00 | 0.00 | 17.50 | 199.07 | 1.20 | 283 | 2 | 459 | 0.08 | 1.99 | 25 | 17286 |
| K011250 | 76.59 | 1.46 | 75.89 | 0.99 | 0.00 | 0.00 | 18.22 | 175.92 | 1.41 | 230 | 2 | 456 | 0.09 | 2.01 | 32 | 24677 |
| K012428 | 55.16 | 1.10 | 54.33 | 0.69 | 1.00 | 8.33 | 10.96 | 114.34 | 2.05 | 207 | 4 | 459 | 0.09 | 2.09 | 38 | 20909 |
| K011251 | 52.51 | 0.96 | 52.76 | 1.35 | 0.25 | 2.08 | 13.36 | 123.81 | 1.26 | 236 | 2 | 459 | 0.10 | 1.98 | 41 | 21667 |
| K012429 | 0.79 | 0.03 | 2.05 | 0.45 | 1.26 | 10.46 | 1.63 | 1.47 | 0.11 | 185 | 14 | 451 | 0.53 | 5.10 | 394 | 3118 |
| K011252 | 5.34 | 0.17 | 5.45 | 5.61 | 0.11 | 0.90 | 1.12 | 7.47 | 0.18 | 140 | 3 | 454 | 0.13 | 5.02 | 65 | 3466 |
| K011253 | 7.46 | 0.21 | 7.45 | 7.19 | 0.00 | 0.00 | 1.28 | 15.59 | 0.16 | 209 | 2 | 454 | 0.08 | 4.97 | 55 | 4125 |
| K011254 | 2.06 | 0.03 | 2.93 | 0.42 | 0.87 | 7.24 | 5.90 | 4.56 | 0.11 | 221 | 5 | 444 | 0.56 | 20.03 | 477 | 9835 |
| K012451 | 5.52 | 0.26 | 5.45 | 3.24 | 0.00 | 0.00 | 5.09 | 9.13 | 0.26 | 166 | 5 | 440 | 0.36 | 5.00 | 174 | 9600 |
| K012452 | 2.97 | 0.10 | 10.62 | 2.04 | 7.64 | 63.67 | 3.08 | 5.75 | 0.43 | 193 | 15 | 444 | 0.35 | 5.67 | 199 | 5926 |
| K012453 | 3.96 | 0.15 | 9.02 | 3.00 | 5.07 | 42.21 | 2.99 | 7.56 | 0.16 | 191 | 4 | 447 | 0.28 | 5.53 | 147 | 5805 |
| K012454 | 5.96 | 0.29 | 5.86 | 3.09 | 0.00 | 0.00 | 3.45 | 8.10 | 0.22 | 136 | 4 | 437 | 0.30 | 5.25 | 141 | 8400 |
| K012455 | 6.52 | 0.32 | 6.66 | 3.09 | 0.14 | 1.15 | 3.91 | 12.90 | 0.19 | 198 | 3 | 448 | 0.23 | 5.00 | 112 | 7320 |
| K012456 | 6.64 | 0.27 | 7.06 | 2.63 | 0.42 | 3.51 | 4.14 | 12.96 | 0.17 | 195 | 3 | 448 | 0.24 | 5.24 | 138 | 9141 |
| K012457 | 6.46 | 0.31 | 6.81 | 2.22 | 0.35 | 2.88 | 5.44 | 12.96 | 0.25 | 201 | 4 | 446 | 0.30 | 5.24 | 146 | 9427 |
| K012458 | 6.12 | 0.27 | 6.36 | 2.05 | 0.24 | 2.01 | 4.16 | 12.73 | 0.22 | 208 | 4 | 446 | 0.25 | 5.07 | 149 | 9112 |
| K012459 | 6.19 | 0.30 | 6.27 | 2.22 | 0.08 | 0.68 | 3.52 | 12.21 | 0.21 | 197 | 3 | 451 | 0.22 | 5.06 | 142 | 8775 |

(continued on next page)

Appendix

Bulk data (continued)

| Sample ID | TOC [wt.%] | TN [wt.%] | TC [wt.%] | TS [wt.%] | TIC [wt.%] | Carbonate [wt.%] | S ₁ [mg HC/g rock] | S ₂ [mg HC/g rock] | S ₃ [mg CO ₂ /g rock] | HI [mg HC/g TOC] | OI [mg CO ₂ /g TOC] | T _{max} [°C] | PI | Material used for extraction [g] | Extract yield [mg/g TOC] | Extract yield [ppm] |
|-----------|------------|-----------|-----------|-----------|------------|------------------|-------------------------------|-------------------------------|---|------------------|--------------------------------|-----------------------|------|----------------------------------|--------------------------|---------------------|
| K012460 | 3.89 | 0.18 | 5.24 | 5.53 | 1.35 | 11.24 | 2.40 | 6.62 | 0.19 | 170 | 5 | 448 | 0.27 | 5.47 | 158 | 6161 |
| K012461 | 4.64 | 0.22 | 4.62 | 4.46 | 0.00 | 0.00 | 2.22 | 2.16 | 0.41 | 47 | 9 | 428 | 0.51 | 5.00 | 198 | 9180 |
| K012462 | 7.59 | 0.35 | 7.61 | 1.94 | 0.01 | 0.10 | 4.91 | 14.74 | 0.19 | 194 | 3 | 452 | 0.25 | 5.25 | 134 | 10210 |
| K012463 | 6.74 | 0.30 | 7.00 | 2.22 | 0.25 | 2.11 | 4.06 | 12.47 | 0.29 | 185 | 4 | 451 | 0.25 | 4.93 | 140 | 9412 |
| K012464 | 6.98 | 0.33 | 7.26 | 2.23 | 0.29 | 2.40 | 3.60 | 12.89 | 0.25 | 185 | 4 | 451 | 0.22 | 5.02 | 101 | 7012 |
| K012465 | 3.78 | 0.15 | 5.46 | 1.71 | 1.68 | 13.95 | 3.26 | 7.82 | 0.14 | 207 | 4 | 449 | 0.29 | 5.12 | 221 | 8340 |
| K012466 | 2.81 | 0.11 | 9.97 | 2.25 | 7.16 | 59.63 | 1.81 | 4.79 | 0.21 | 170 | 7 | 447 | 0.27 | 5.08 | 174 | 4882 |
| K012467 | 7.81 | 0.36 | 8.46 | 2.43 | 0.65 | 5.37 | 4.26 | 14.75 | 0.24 | 189 | 3 | 450 | 0.22 | 4.96 | 98 | 7621 |
| K012468 | 6.59 | 0.29 | 6.65 | 2.66 | 0.06 | 0.53 | 3.27 | 5.07 | 0.26 | 77 | 4 | 433 | 0.39 | 5.00 | 127 | 8360 |
| K012469 | 0.84 | 0.04 | 8.68 | 1.28 | 7.85 | 65.35 | 0.85 | 1.26 | 0.20 | 150 | 23 | 444 | 0.40 | 5.08 | 261 | 2185 |
| K012470 | 1.43 | 0.06 | 10.84 | 1.43 | 9.41 | 78.39 | 1.56 | 2.49 | 0.24 | 174 | 17 | 446 | 0.39 | 5.10 | 200 | 2863 |
| K012471 | 7.01 | 0.32 | 7.11 | 2.80 | 0.10 | 0.81 | 3.44 | 7.69 | 0.19 | 170 | 3 | 433 | 0.31 | 5.00 | 80 | 5620 |
| K012472 | 6.93 | 0.31 | 6.81 | 2.55 | 0.00 | 0.00 | 4.98 | 11.82 | 0.18 | 171 | 3 | 448 | 0.30 | 5.04 | 112 | 7738 |
| K012473 | 6.33 | 0.27 | 6.46 | 4.87 | 0.13 | 1.12 | 3.33 | 4.18 | 0.38 | 66 | 6 | 435 | 0.44 | 5.00 | 136 | 8620 |
| K012474 | 7.28 | 0.32 | 7.15 | 3.37 | 0.00 | 0.00 | 3.46 | 8.07 | 0.19 | 111 | 3 | 435 | 0.30 | 5.01 | 109 | 7904 |
| K012475 | 5.82 | 0.26 | 5.90 | 5.55 | 0.08 | 0.70 | 2.38 | 10.72 | 0.53 | 46 | 9 | 436 | 0.47 | 5.01 | 144 | 8363 |
| K012476 | 7.39 | 0.34 | 7.29 | 1.96 | 0.00 | 0.00 | 3.43 | 10.72 | 0.26 | 145 | 4 | 447 | 0.24 | 5.00 | 99 | 7280 |
| K011212 | 1.60 | 0.01 | 1.88 | 0.70 | 0.27 | 2.27 | 8.82 | 5.41 | 0.19 | 337 | 12 | 419 | 0.62 | 20.14 | 980 | 15720 |
| K011213 | 2.08 | 0.02 | 2.28 | 1.13 | 0.19 | 1.60 | 12.17 | 11.69 | 0.29 | 561 | 14 | 415 | 0.51 | 19.98 | 945 | 19705 |
| K011214 | 1.99 | 0.02 | 2.07 | 0.93 | 0.08 | 0.70 | 10.22 | 6.44 | 0.14 | 324 | 7 | 302 | 0.61 | 20.06 | 977 | 19417 |
| K011215 | 1.52 | 0.03 | 1.92 | 1.03 | 0.40 | 3.36 | 9.28 | 4.77 | 0.10 | 314 | 7 | 297 | 0.66 | 20.06 | 1125 | 17104 |
| K011216 | 1.83 | 0.02 | 1.89 | 0.59 | 0.07 | 0.55 | 9.72 | 6.40 | 0.35 | 350 | 19 | 414 | 0.60 | 20.01 | 991 | 18106 |
| K011217 | 1.44 | 0.02 | 1.81 | 0.73 | 0.37 | 3.06 | 7.59 | 4.67 | 0.15 | 324 | 10 | 420 | 0.62 | 20.12 | 1009 | 14528 |
| K011218 | 1.97 | 0.02 | 2.03 | 0.92 | 0.06 | 0.50 | 6.26 | 7.25 | 0.21 | 367 | 11 | 420 | 0.46 | 20.01 | 716 | 14133 |
| K011219 | 3.12 | 0.08 | 3.39 | 2.08 | 0.28 | 2.29 | 3.75 | 13.57 | 0.16 | 435 | 5 | 418 | 0.22 | 4.96 | 272 | 8488 |
| K011220 | 3.17 | 0.09 | 3.21 | 4.53 | 0.04 | 0.33 | 2.70 | 6.89 | 0.32 | 217 | 10 | 405 | 0.28 | 5.05 | 279 | 8871 |
| K011221 | 3.28 | 0.10 | 3.79 | 6.18 | 0.51 | 4.27 | 0.97 | 6.93 | 0.47 | 211 | 14 | 409 | 0.12 | 4.97 | 153 | 5010 |
| K011222 | 5.89 | 0.17 | 6.22 | 4.22 | 0.34 | 2.79 | 2.11 | 28.32 | 0.25 | 481 | 4 | 414 | 0.07 | 5.05 | 121 | 7129 |
| K011223 | 7.94 | 0.22 | 8.08 | 5.33 | 0.14 | 1.16 | 2.75 | 43.73 | 0.52 | 551 | 7 | 421 | 0.06 | 5.00 | 115 | 9160 |
| K011224 | 7.79 | 0.22 | 7.84 | 4.97 | 0.05 | 0.38 | 1.57 | 30.92 | 0.57 | 397 | 7 | 413 | 0.05 | 4.94 | 88 | 6862 |
| K011225 | 7.74 | 0.24 | 7.76 | 4.43 | 0.02 | 0.15 | 1.37 | 25.87 | 0.66 | 334 | 9 | 410 | 0.05 | 4.98 | 98 | 7570 |
| K011226 | 5.55 | 0.16 | 5.52 | 4.94 | 0.00 | 0.00 | 0.99 | 17.76 | 0.57 | 320 | 10 | 411 | 0.05 | 5.02 | 105 | 5817 |
| K011227 | 7.38 | 0.22 | 7.98 | 5.89 | 0.60 | 5.03 | 2.64 | 36.63 | 0.70 | 497 | 9 | 419 | 0.07 | 5.03 | 117 | 8648 |
| K011199 | 6.60 | 0.20 | 6.52 | 4.79 | 0.00 | 0.00 | 1.57 | 23.36 | 0.58 | 354 | 9 | 412 | 0.06 | 5.00 | 120 | 7920 |
| K011200 | 5.28 | 0.14 | 5.10 | 5.65 | 0.00 | 0.00 | 0.77 | 12.43 | 0.48 | 235 | 9 | 404 | 0.06 | 5.00 | 105 | 5540 |
| K011201 | 5.86 | 0.15 | 5.74 | 6.32 | 0.00 | 0.00 | 0.89 | 14.93 | 0.49 | 255 | 8 | 407 | 0.06 | 5.03 | 101 | 5924 |
| K011202 | 5.97 | 0.16 | 5.96 | 6.46 | 0.00 | 0.00 | 1.35 | 17.31 | 0.55 | 290 | 9 | 407 | 0.07 | 4.96 | 112 | 6694 |
| K011203 | 6.93 | 0.17 | 6.80 | 6.86 | 0.00 | 0.00 | 1.04 | 20.58 | 0.63 | 297 | 9 | 405 | 0.05 | 4.99 | 91 | 6313 |
| K011204 | 1.29 | 0.03 | 10.31 | 0.69 | 9.01 | 75.08 | 0.62 | 4.35 | 0.31 | 336 | 24 | 421 | 0.13 | 25.24 | 108 | 1395 |
| K011205 | 1.32 | 0.03 | 10.35 | 0.82 | 9.03 | 75.18 | 0.68 | 4.10 | 0.28 | 311 | 21 | 419 | 0.14 | 25.11 | 123 | 1629 |
| K011206 | 1.32 | 0.04 | 10.35 | 0.90 | 9.03 | 75.24 | 0.58 | 4.04 | 0.35 | 306 | 27 | 417 | 0.12 | 25.02 | 105 | 1391 |

(continued on next page)

Appendix

Bulk data (continued)

| Sample ID | TOC [wt.%] | TN [wt.%] | TC [wt.%] | TS [wt.%] | TIC [wt.%] | Carbonate [wt.%] | S ₁ [mg HC/g rock] | S ₂ [mg HC/g rock] | S ₃ [mg CO ₂ /g rock] | HI [mg HC/g TOC] | OI [mg TOC] | T _{max} [°C] | PI | Material used for extraction [g] | Extract yield [mg/g TOC] | Extract yield [ppm] |
|-----------|------------|-----------|-----------|-----------|------------|------------------|-------------------------------|-------------------------------|---|------------------|-------------|-----------------------|------|----------------------------------|--------------------------|---------------------|
| K011207 | 6.82 | 0.18 | 6.56 | 6.91 | 0.00 | 0.00 | 0.96 | 16.52 | 0.52 | 242 | 8 | 401 | 0.05 | 5.01 | 104 | 7066 |
| K011208 | 8.12 | 0.20 | 8.00 | 5.84 | 0.00 | 0.00 | 1.36 | 22.05 | 0.58 | 272 | 7 | 403 | 0.06 | 4.99 | 103 | 8397 |
| K011209 | 7.56 | 0.18 | 7.39 | 7.46 | 0.00 | 0.00 | 1.22 | 19.74 | 0.53 | 261 | 7 | 404 | 0.06 | 4.96 | 101 | 7661 |
| K011210 | 6.77 | 0.16 | 6.71 | 6.67 | 0.00 | 0.00 | 1.01 | 18.21 | 0.49 | 269 | 7 | 404 | 0.05 | 4.96 | 98 | 6653 |
| K011211 | 7.38 | 0.18 | 7.23 | 7.62 | 0.00 | 0.00 | 1.23 | 22.73 | 0.43 | 308 | 6 | 406 | 0.05 | 4.98 | 94 | 6908 |
| K012477 | 5.59 | 0.16 | 5.86 | 2.56 | 0.27 | 2.29 | 2.97 | 32.10 | 0.29 | 574 | 5 | 424 | 0.08 | 5.04 | 133 | 7440 |
| K012478 | 5.18 | 0.16 | 5.20 | 4.54 | 0.02 | 0.17 | 1.87 | 18.73 | 0.36 | 361 | 7 | 416 | 0.09 | 5.06 | 124 | 6403 |
| K012479 | 6.94 | 0.22 | 7.08 | 3.26 | 0.14 | 1.19 | 2.09 | 33.53 | 0.32 | 483 | 5 | 420 | 0.06 | 5.00 | 92 | 6360 |
| K012480 | 5.51 | 0.17 | 5.44 | 5.85 | 0.00 | 0.00 | 1.60 | 15.03 | 0.33 | 273 | 6 | 417 | 0.10 | 5.01 | 128 | 7066 |
| K012481 | 6.21 | 0.18 | 6.20 | 3.32 | 0.00 | 0.00 | 1.89 | 24.35 | 0.31 | 392 | 5 | 421 | 0.07 | 5.02 | 97 | 6036 |
| K012482 | 0.75 | 0.03 | 4.84 | 0.46 | 4.09 | 34.05 | 0.26 | 0.37 | 0.15 | 49 | 20 | 425 | 0.42 | 5.29 | 93 | 699 |

Appendix

Molecular geochemical data (l): Saturates

| Sample ID | Pr/Ph | nC ₁₇ /Pr | Pr/nC ₁₇ | Ph/nC ₁₈ | C ₃₀ dia/(C ₃₀ dia+C ₃₀ αβ) Hopanes | ββ/(ββ+αα) Steranes | 20S/(20S+20R) Steranes | C ₂₉ ααα Hopanes | 22S/(22S+22R) Hopanes | Steranes/Hopanes | C ₂₇ Dia/C ₂₃ Reg Steranes | C ₃₁ /C ₃₂ Homohopanes | C ₂₇ /C ₂₉ αββ Steranes |
|-----------|-------|----------------------|---------------------|---------------------|---|------------------------|---------------------------|--------------------------------|--------------------------|------------------|---|---|--|
| K011188 | 0.82 | 2.93 | 0.34 | 0.43 | 0.12 | 0.57 | 0.46 | 0.49 | 0.27 | 0.92 | 1.46 | 0.92 | |
| K011189 | 1.01 | 3.09 | 0.32 | 0.40 | 0.14 | 0.62 | 0.41 | 0.57 | 0.26 | 0.92 | 1.46 | 0.92 | |
| K011190 | 1.37 | 2.83 | 0.35 | 0.38 | 0.15 | 0.56 | 0.52 | 0.56 | 0.38 | 1.05 | 1.36 | 1.05 | |
| K012302 | 1.00 | 4.75 | 0.21 | 0.31 | 0.14 | 0.57 | 0.56 | 0.60 | 0.32 | 0.78 | 1.42 | 0.78 | |
| K011191 | 1.27 | 4.11 | 0.24 | 0.32 | 0.16 | 0.60 | 0.50 | 0.56 | 0.35 | 0.97 | 1.32 | 0.97 | |
| K011192 | 1.25 | 4.07 | 0.25 | 0.33 | 0.16 | 0.60 | 0.56 | 0.57 | 0.33 | 1.03 | 1.40 | 1.03 | |
| K011193 | 1.19 | 4.00 | 0.25 | 0.33 | 0.16 | 0.58 | 0.53 | 0.57 | 0.35 | 0.85 | 1.43 | 0.85 | |
| K011194 | 1.31 | 4.39 | 0.23 | 0.32 | 0.15 | 0.57 | 0.54 | 0.56 | 0.35 | 0.78 | 1.24 | 0.78 | |
| K011195 | 1.34 | 5.18 | 0.19 | 0.28 | 0.14 | 0.56 | 0.53 | 0.58 | 0.34 | 0.83 | 1.47 | 0.83 | |
| K011196 | 0.92 | 3.21 | 0.31 | 0.41 | 0.08 | 0.56 | 0.40 | 0.54 | 0.23 | 0.81 | 1.53 | 0.81 | |
| K012303 | 0.75 | 3.31 | 0.30 | 0.44 | 0.09 | 0.52 | 0.51 | 0.59 | 0.30 | 0.70 | 1.40 | 0.70 | |
| K011197 | 0.86 | 3.26 | 0.31 | 0.42 | 0.10 | 0.60 | 0.42 | 0.55 | 0.24 | 0.92 | 1.52 | 0.92 | |
| K012304 | 1.49 | 4.84 | 0.21 | 0.31 | 0.12 | 0.56 | 0.52 | 0.59 | 0.30 | 0.66 | 1.41 | 0.66 | |
| K012305 | 0.94 | 4.09 | 0.24 | 0.44 | 0.10 | 0.52 | 0.52 | 0.59 | 0.27 | 0.66 | 1.55 | 0.66 | |
| K012430 | 0.72 | 2.66 | 0.38 | 0.50 | 0.08 | 0.53 | 0.52 | 0.58 | 0.30 | 0.74 | 1.45 | 0.74 | |
| K012306 | 0.55 | 2.52 | 0.40 | 0.78 | 0.09 | 0.52 | 0.51 | 0.58 | 0.28 | 0.65 | 1.51 | 0.65 | |
| K011198 | 0.51 | 2.53 | 0.39 | 0.81 | 0.07 | 0.54 | 0.46 | 0.56 | 0.26 | 0.72 | 1.59 | 0.72 | |
| K012431 | 1.67 | 2.37 | 0.42 | 0.42 | 0.10 | 0.55 | 0.57 | 0.59 | 0.31 | 0.57 | 1.29 | 0.57 | |
| K012432 | 1.51 | 2.35 | 0.43 | 0.40 | 0.10 | 0.56 | 0.58 | 0.58 | 0.33 | 0.64 | 1.26 | 0.64 | |
| K012433 | 1.59 | 2.67 | 0.37 | 0.39 | 0.10 | 0.57 | 0.59 | 0.59 | 0.32 | 0.58 | 1.26 | 0.58 | |
| K012434 | 1.38 | 2.17 | 0.46 | 0.49 | 0.10 | 0.56 | 0.58 | 0.59 | 0.32 | 0.61 | 1.28 | 0.61 | |
| K012435 | 1.38 | 2.24 | 0.45 | 0.46 | 0.10 | 0.55 | 0.58 | 0.59 | 0.31 | 0.54 | 1.30 | 0.54 | |
| K012436 | 1.37 | 2.01 | 0.50 | 0.46 | 0.10 | 0.56 | 0.58 | 0.59 | 0.34 | 0.60 | 1.24 | 0.60 | |
| K012437 | 1.16 | 2.03 | 0.49 | 0.56 | 0.08 | 0.55 | 0.54 | 0.58 | 0.33 | 0.72 | 1.30 | 0.72 | |
| K012438 | 1.39 | 2.71 | 0.37 | 0.43 | 0.09 | 0.56 | 0.57 | 0.59 | 0.31 | 0.57 | 1.35 | 0.57 | |
| K012439 | 1.32 | 2.52 | 0.40 | 0.45 | 0.09 | 0.56 | 0.58 | 0.59 | 0.32 | 0.60 | 1.37 | 0.60 | |
| K012440 | 1.58 | 3.05 | 0.33 | 0.38 | 0.09 | 0.56 | 0.58 | 0.58 | 0.30 | 0.51 | 1.42 | 0.51 | |
| K012441 | 1.14 | 2.31 | 0.43 | 0.49 | 0.07 | 0.55 | 0.52 | 0.59 | 0.31 | 0.55 | 1.30 | 0.55 | |
| K012442 | 1.18 | 2.53 | 0.39 | 0.48 | 0.07 | 0.55 | 0.55 | 0.59 | 0.33 | 0.58 | 1.30 | 0.58 | |
| K012443 | 1.05 | 2.37 | 0.42 | 0.47 | 0.07 | 0.54 | 0.53 | 0.59 | 0.35 | 0.52 | 1.35 | 0.52 | |
| K012444 | 0.97 | 2.40 | 0.42 | 0.49 | 0.07 | 0.53 | 0.54 | 0.59 | 0.32 | 0.65 | 1.31 | 0.65 | |
| K012445 | 1.21 | 2.32 | 0.43 | 0.52 | 0.07 | 0.51 | 0.53 | 0.59 | 0.29 | 0.53 | 1.31 | 0.53 | |
| K012446 | 1.51 | 2.35 | 0.42 | 0.45 | 0.09 | 0.54 | 0.58 | 0.59 | 0.32 | 0.59 | 1.38 | 0.59 | |
| K012447 | 1.58 | 2.40 | 0.42 | 0.44 | 0.09 | 0.55 | 0.57 | 0.58 | 0.30 | 0.54 | 1.30 | 0.54 | |
| K012448 | 1.28 | 2.27 | 0.44 | 0.51 | 0.09 | 0.54 | 0.58 | 0.59 | 0.30 | 0.61 | 1.31 | 0.61 | |
| K012449 | 0.95 | 1.54 | 0.65 | 1.02 | 0.10 | 0.55 | 0.60 | 0.59 | 0.30 | 0.61 | 1.34 | 0.61 | |
| K012450 | 1.29 | 1.66 | 0.60 | 0.79 | 0.10 | 0.55 | 0.59 | 0.59 | 0.30 | 0.61 | 1.33 | 0.61 | |
| K011228 | 1.01 | 3.28 | 0.30 | 0.34 | 0.13 | 0.59 | 0.52 | 0.59 | 0.28 | 0.96 | 1.79 | 0.96 | |
| K011229 | 0.89 | 3.75 | 0.27 | 0.30 | 0.17 | 0.58 | 0.50 | 0.59 | 0.47 | 1.09 | 1.70 | 1.09 | |
| K011230 | 0.89 | 3.42 | 0.29 | 0.33 | 0.19 | 0.59 | 0.50 | 0.60 | 0.45 | 1.15 | 1.49 | 1.15 | |
| K011231 | 1.47 | 3.34 | 0.30 | 0.33 | 0.19 | 0.60 | 0.48 | 0.58 | 0.42 | 1.04 | 1.48 | 1.04 | |

(continued on next page)

Appendix

Molecular geochemical data (I): Saturates (continued)

| Sample ID | Pr/Ph | n C ₁₇ /Pr | Pr/n C ₁₇ | Ph/n C ₁₈ | C ₃₀ dia/(C ₃₀ dia+C ₃₀ αβ) Hopanes | ββ/(ββ+αα) Steranes | C ₂₉ αα 20S/(20S+20R) Steranes | 22S/(22S+22R) C ₃₂ Hopanes | Steranes/Hopanes | C ₂₇ Dia/C ₂₃ Reg Steranes | C ₃₁ /C ₃₂ Homohopanes | C ₂₇ /C ₂₉ αββ Steranes |
|-----------|-------|-----------------------|----------------------|----------------------|---|------------------------|--|--|------------------|---|---|--|
| K011232 | 2.76 | 1.37 | 0.73 | 0.53 | 0.17 | 0.59 | 0.52 | 0.55 | 0.43 | 1.03 | 1.39 | 1.03 |
| K011233 | 1.31 | 3.31 | 0.30 | 0.32 | 0.20 | 0.58 | 0.52 | 0.60 | 0.45 | 1.10 | 1.58 | 1.10 |
| K012421 | 1.37 | 1.85 | 0.54 | 0.61 | 0.17 | 0.59 | 0.53 | 0.60 | 0.65 | 0.71 | 1.56 | 0.71 |
| K012422 | 1.69 | 2.10 | 0.48 | 0.40 | 0.18 | 0.57 | 0.59 | 0.59 | 0.52 | 0.99 | 1.56 | 0.99 |
| K011234 | 0.66 | 3.12 | 0.32 | 0.39 | 0.20 | 0.66 | 0.44 | 0.56 | 0.35 | 0.89 | 1.44 | 0.89 |
| K012423 | 1.27 | 1.89 | 0.53 | 0.53 | 0.16 | 0.57 | 0.54 | 0.59 | 0.53 | 0.98 | 1.63 | 0.98 |
| K012424 | 1.23 | 2.67 | 0.37 | 0.48 | 0.19 | 0.57 | 0.57 | 0.59 | 0.51 | 1.01 | 1.61 | 1.01 |
| K011235 | 0.77 | 3.05 | 0.33 | 0.41 | 0.07 | 0.54 | 0.37 | 0.58 | 0.21 | 1.71 | 1.84 | 1.71 |
| K011236 | 1.32 | 3.63 | 0.28 | 0.31 | 0.20 | 0.58 | 0.48 | 0.58 | 0.46 | 0.90 | 1.57 | 0.90 |
| K011237 | 0.95 | 3.30 | 0.30 | 0.31 | 0.17 | 0.57 | 0.45 | 0.59 | 0.44 | 1.03 | 1.55 | 1.03 |
| K011238 | 1.35 | 4.16 | 0.24 | 0.28 | 0.20 | 0.58 | 0.52 | 0.57 | 0.43 | 1.02 | 1.53 | 1.02 |
| K011239 | 0.72 | 2.97 | 0.34 | 0.48 | 0.09 | 0.59 | 0.53 | 0.60 | 0.20 | 2.37 | 1.80 | 2.37 |
| K012425 | 2.91 | 1.38 | 0.72 | 0.27 | 0.46 | 0.50 | 0.46 | 0.60 | 0.18 | 0.17 | 1.55 | 0.17 |
| K011240 | 2.65 | 1.36 | 0.73 | 0.28 | 0.40 | 0.65 | 0.59 | 0.57 | 0.12 | 0.11 | 1.62 | 0.11 |
| K011241 | 2.83 | 1.06 | 0.95 | 0.34 | 0.44 | 0.63 | 0.58 | 0.57 | 0.15 | 0.08 | 1.47 | 0.08 |
| K011242 | 3.18 | 1.28 | 0.78 | 0.24 | 0.39 | 0.63 | 0.60 | 0.57 | 0.12 | 0.12 | 1.57 | 0.12 |
| K011243 | 0.83 | 2.36 | 0.42 | 0.54 | 0.30 | 0.65 | 0.40 | 0.55 | 0.90 | 0.93 | 1.46 | 0.93 |
| K011244 | 0.79 | 2.15 | 0.46 | 0.61 | 0.31 | 0.63 | 0.50 | 0.58 | 1.05 | 1.07 | 1.62 | 1.07 |
| K011245 | 0.85 | 2.35 | 0.43 | 0.52 | 0.27 | 0.64 | 0.49 | 0.54 | 0.80 | 1.02 | 1.32 | 1.02 |
| K011246 | 1.01 | 2.45 | 0.41 | 0.46 | 0.25 | 0.62 | 0.43 | 0.56 | 0.72 | 0.90 | 1.46 | 0.90 |
| K012426 | 2.35 | 1.83 | 0.55 | 0.33 | 0.46 | 0.56 | 0.53 | 0.61 | 0.35 | 0.85 | 1.49 | 0.85 |
| K012427 | 2.71 | 1.51 | 0.66 | 0.27 | 0.69 | 0.53 | 0.55 | 0.59 | 0.25 | 0.94 | 1.15 | 0.94 |
| K011247 | 2.05 | 2.02 | 0.49 | 0.23 | 0.62 | 0.55 | 0.56 | 0.54 | 0.18 | 0.32 | 1.30 | 0.32 |
| K011248 | 1.96 | 2.12 | 0.47 | 0.25 | 0.65 | 0.52 | 0.59 | 0.57 | 0.23 | 0.39 | 1.24 | 0.39 |
| K011249 | 3.41 | 1.41 | 0.71 | 0.21 | 0.51 | 0.52 | 0.54 | 0.55 | 0.30 | 0.08 | 1.36 | 0.08 |
| K011250 | 3.49 | 1.31 | 0.76 | 0.22 | 0.48 | 0.51 | 0.54 | 0.55 | 0.41 | 0.04 | 1.36 | 0.04 |
| K012428 | 2.99 | 0.65 | 1.53 | 0.44 | 0.61 | 0.52 | 0.49 | 0.60 | 0.70 | 0.05 | 1.20 | 0.05 |
| K011251 | 2.72 | 0.93 | 1.07 | 0.38 | 0.56 | 0.51 | 0.53 | 0.55 | 0.52 | 0.04 | 1.19 | 0.04 |
| K012429 | 1.22 | 1.48 | 0.68 | 0.61 | 0.42 | 0.61 | 0.59 | 0.60 | 2.21 | 1.16 | 1.70 | 1.16 |
| K011252 | 1.91 | 2.09 | 0.48 | 0.25 | 0.67 | 0.58 | 0.41 | 0.55 | 0.14 | 0.30 | 1.17 | 0.30 |
| K011253 | 0.94 | 3.05 | 0.33 | 0.37 | 0.65 | 0.53 | 0.61 | 0.56 | 0.24 | 0.59 | 1.22 | 0.59 |
| K011254 | 0.83 | 2.45 | 0.41 | 0.52 | 0.23 | 0.63 | 0.47 | 0.57 | 0.61 | 0.89 | 1.38 | 0.89 |
| K012451 | 1.16 | 1.39 | 0.72 | 0.65 | - | 0.69 | 0.46 | - | - | 1.89 | - | 1.89 |
| K012452 | 1.29 | 1.47 | 0.68 | 0.62 | - | 0.69 | 0.52 | - | - | 2.08 | - | 2.08 |
| K012453 | 1.18 | 1.50 | 0.67 | 0.59 | - | 0.64 | 0.57 | - | - | 1.86 | - | 1.86 |
| K012454 | 1.15 | 1.39 | 0.72 | 0.63 | - | 0.68 | 0.50 | - | - | 2.02 | - | 2.02 |
| K012455 | 1.31 | 1.49 | 0.67 | 0.61 | - | 0.66 | 0.58 | - | - | 1.90 | - | 1.90 |
| K012456 | 1.18 | 1.46 | 0.69 | 0.61 | - | 0.66 | 0.59 | - | - | 1.95 | - | 1.95 |
| K012457 | 1.38 | 1.57 | 0.64 | 0.63 | - | 0.64 | 0.58 | - | - | 3.91 | - | 3.91 |
| K012458 | 1.29 | 1.45 | 0.69 | 0.62 | - | 0.62 | 0.59 | - | - | 2.08 | - | 2.08 |
| K012459 | 1.22 | 1.44 | 0.70 | 0.60 | - | 0.65 | 0.61 | - | - | 1.95 | - | 1.95 |

(continued on next page)

Appendix

Molecular geochemical data (I): Saturates (continued)

| Sample ID | Pr/Ph | nC ₁₇ /Pr | Pr/nC ₁₇ | Ph/nC ₁₈ | C ₃₀ dia/(C ₃₀ dia+C ₃₀ αβ) Hopanes | ββ/(ββ+αα) Steranes | C ₂₉ αα 20S/(20S+20R) Steranes | 22S/(22S+22R) Hopanes | C ₃₂ Steranes/Hopanes | C ₂₇ Dia/C ₂₃ Reg Steranes | C ₃₁ /C ₃₂ Homohopanes | C ₂₇ /C ₂₉ αββ Steranes |
|-----------|-------|----------------------|---------------------|---------------------|---|------------------------|--|--------------------------|-------------------------------------|---|---|--|
| K012460 | 1.29 | 1.43 | 0.70 | 0.62 | - | 0.66 | 0.59 | - | - | 1.88 | - | 1.88 |
| K012461 | 1.16 | 1.36 | 0.74 | 0.62 | - | 0.59 | 0.67 | - | - | 1.84 | - | 1.84 |
| K012462 | 1.30 | 1.70 | 0.59 | 0.57 | - | 0.64 | 0.62 | - | - | 1.90 | - | 1.90 |
| K012463 | 1.24 | 1.63 | 0.61 | 0.60 | - | 0.64 | 0.61 | - | - | 1.95 | - | 1.95 |
| K012464 | 1.37 | 1.54 | 0.65 | 0.56 | - | 0.62 | 0.64 | - | - | 1.87 | - | 1.87 |
| K012465 | 1.21 | 1.29 | 0.78 | 0.65 | - | 0.64 | 0.61 | - | - | 1.82 | - | 1.82 |
| K012466 | 1.23 | 1.48 | 0.68 | 0.62 | - | 0.64 | 0.58 | - | - | 1.80 | - | 1.80 |
| K012467 | 1.30 | 1.41 | 0.71 | 0.59 | - | 0.66 | 0.61 | - | - | 1.87 | - | 1.87 |
| K012468 | 1.35 | 1.54 | 0.65 | 0.61 | - | 0.67 | 0.57 | - | - | 2.40 | - | 2.40 |
| K012469 | 1.18 | 1.33 | 0.75 | 0.70 | - | 0.64 | 0.58 | - | - | 1.73 | - | 1.73 |
| K012470 | 1.28 | 1.46 | 0.68 | 0.64 | - | 0.65 | 0.50 | - | - | 1.50 | - | 1.50 |
| K012471 | 1.29 | 1.67 | 0.60 | 0.54 | - | 0.65 | 0.59 | - | - | 2.43 | - | 2.43 |
| K012472 | 1.29 | 1.37 | 0.73 | 0.64 | - | 0.67 | 0.58 | - | - | 2.36 | - | 2.36 |
| K012473 | 1.28 | 1.47 | 0.68 | 0.58 | - | 0.66 | 0.57 | - | - | 2.45 | - | 2.45 |
| K012474 | 1.35 | 1.51 | 0.66 | 0.56 | - | 0.66 | 0.57 | - | - | 2.34 | - | 2.34 |
| K012475 | 1.38 | 1.48 | 0.68 | 0.57 | - | 0.65 | 0.63 | - | - | 2.35 | - | 2.35 |
| K012476 | 1.22 | 1.54 | 0.65 | 0.63 | - | 0.63 | 0.65 | - | - | 2.45 | - | 2.45 |
| K011212 | 0.80 | 1.84 | 0.54 | 0.59 | 0.12 | 0.54 | 0.49 | 0.55 | 0.50 | 0.55 | 1.54 | 0.55 |
| K011213 | 0.87 | 1.79 | 0.56 | 0.59 | 0.12 | 0.56 | 0.47 | 0.55 | 0.48 | 0.60 | 1.51 | 0.60 |
| K011214 | 0.89 | 1.79 | 0.56 | 0.60 | 0.11 | 0.54 | 0.47 | 0.54 | 0.52 | 0.58 | 1.54 | 0.58 |
| K011215 | 0.75 | 1.85 | 0.54 | 0.57 | 0.11 | 0.55 | 0.48 | 0.54 | 0.57 | 0.57 | 1.46 | 0.57 |
| K011216 | 0.90 | 1.80 | 0.56 | 0.58 | 0.12 | 0.57 | 0.50 | 0.53 | 0.51 | 0.57 | 1.51 | 0.57 |
| K011217 | 0.81 | 1.87 | 0.54 | 0.57 | 0.12 | 0.53 | 0.49 | 0.54 | 0.54 | 0.56 | 1.47 | 0.56 |
| K011218 | 0.87 | 1.77 | 0.56 | 0.59 | 0.11 | 0.55 | 0.48 | 0.52 | 0.55 | 0.58 | 1.51 | 0.58 |
| K011219 | 1.18 | 1.81 | 0.55 | 0.56 | 0.11 | 0.57 | 0.41 | 0.56 | 0.41 | 0.70 | 1.57 | 0.70 |
| K011220 | 0.99 | 1.99 | 0.50 | 0.54 | 0.12 | 0.53 | 0.36 | 0.55 | 0.42 | 0.64 | 1.53 | 0.64 |
| K011221 | 1.10 | 1.81 | 0.55 | 0.98 | 0.08 | 0.32 | 0.16 | 0.45 | 0.37 | 0.52 | 1.76 | 0.52 |
| K011222 | 0.91 | 1.26 | 0.79 | 1.34 | 0.09 | 0.40 | 0.16 | 0.44 | 0.30 | 0.92 | 1.68 | 0.92 |
| K011223 | 0.79 | 0.97 | 1.03 | 2.04 | 0.06 | 0.40 | 0.15 | 0.45 | 0.31 | 0.95 | 1.77 | 0.95 |
| K011224 | 0.77 | 0.85 | 1.18 | 2.12 | 0.08 | 0.43 | 0.16 | 0.45 | 0.28 | 1.03 | 2.21 | 1.03 |
| K011225 | 0.96 | 0.69 | 1.45 | 2.51 | 0.12 | 0.42 | 0.18 | 0.43 | 0.46 | 0.88 | 2.63 | 0.88 |
| K011226 | 0.85 | 0.91 | 1.10 | 1.92 | 0.08 | 0.36 | 0.17 | 0.42 | 0.29 | 0.84 | 1.80 | 0.84 |
| K011227 | 0.95 | 1.24 | 0.80 | 1.88 | 0.07 | 0.36 | 0.16 | 0.44 | 0.29 | 0.86 | 2.07 | 0.86 |
| K011199 | 0.76 | 0.95 | 1.05 | 2.24 | 0.08 | 0.36 | 0.19 | 0.46 | 0.31 | 1.05 | 1.74 | 1.05 |
| K011200 | 0.95 | 0.88 | 1.13 | 1.75 | 0.08 | 0.39 | 0.20 | 0.47 | 0.38 | 0.91 | 1.78 | 0.91 |
| K011201 | 0.91 | 0.72 | 1.39 | 2.15 | 0.08 | 0.39 | 0.22 | 0.48 | 0.31 | 0.92 | 1.91 | 0.92 |
| K011202 | 1.26 | 1.25 | 0.80 | 1.37 | 0.08 | 0.41 | 0.21 | 0.47 | 0.35 | 0.89 | 1.98 | 0.89 |
| K011203 | 0.88 | 0.85 | 1.18 | 2.06 | 0.08 | 0.38 | 0.21 | 0.48 | 0.30 | 0.88 | 1.78 | 0.88 |
| K011204 | 1.21 | 1.45 | 0.69 | 1.34 | 0.08 | 0.41 | 0.25 | 0.50 | 0.39 | 1.03 | 1.99 | 1.03 |
| K011205 | 1.38 | 1.50 | 0.66 | 1.14 | 0.08 | 0.39 | 0.23 | 0.51 | 0.45 | 0.91 | 1.91 | 0.91 |
| K011206 | 1.24 | 1.54 | 0.65 | 1.09 | 0.06 | 0.36 | 0.25 | 0.50 | 0.35 | 0.84 | 1.93 | 0.84 |

(continued on next page)

Molecular geochemical data (I): Saturates (continued)

| Sample ID | Pr/Ph | n C ₁₇ /Pr | Pr/n C ₁₇ | Ph/n C ₁₈ | C ₃₀ dia/(C ₃₀ dia+C ₃₀ qβ) Hopanes | β/(β+αα) C ₂₉ Steranes | C ₂₉ ααα 20S/(20S+20R) Steranes | 22S/(22S+22R) C ₃₂ Hopanes | Steranes/Hopanes | C ₂₇ Dia/C ₂₈ Reg Steranes | C ₃₁ /C ₃₂ Homohopanes | C ₂₇ /C ₂₈ αββ Steranes |
|-----------|-------|-----------------------|----------------------|----------------------|---|--------------------------------------|---|--|------------------|---|---|--|
| K011207 | 0.92 | 0.78 | 1.29 | 1.71 | 0.09 | 0.40 | 0.21 | 0.48 | 0.34 | 0.85 | 1.80 | 0.85 |
| K011208 | 0.94 | 0.99 | 1.01 | 1.48 | 0.09 | 0.39 | 0.21 | 0.48 | 0.38 | 0.94 | 1.78 | 0.94 |
| K011209 | 0.82 | 0.79 | 1.26 | 1.93 | 0.09 | 0.40 | 0.25 | 0.50 | 0.44 | 0.93 | 2.27 | 0.93 |
| K011210 | 0.92 | 0.65 | 1.54 | 2.04 | 0.08 | 0.42 | 0.24 | 0.49 | 0.38 | 1.06 | 1.79 | 1.06 |
| K011211 | 0.87 | 0.70 | 1.42 | 1.87 | 0.07 | 0.41 | 0.24 | 0.49 | 0.34 | 1.03 | 1.67 | 1.03 |
| K012477 | 1.49 | 0.81 | 1.24 | 1.35 | 0.08 | 0.31 | 0.34 | 0.56 | 0.30 | 0.59 | 1.65 | 0.59 |
| K012478 | 1.03 | 0.56 | 1.77 | 1.95 | 0.07 | 0.29 | 0.30 | 0.55 | 0.32 | 0.57 | 1.74 | 0.57 |
| K012479 | 1.07 | 0.64 | 1.56 | 1.87 | 0.09 | 0.34 | 0.36 | 0.56 | 0.26 | 0.62 | 1.62 | 0.62 |
| K012480 | 1.10 | 0.66 | 1.53 | 1.61 | 0.07 | 0.32 | 0.32 | 0.55 | 0.30 | 0.57 | 1.67 | 0.57 |
| K012481 | 1.19 | 0.65 | 1.55 | 1.57 | 0.09 | 0.33 | 0.33 | 0.56 | 0.34 | 0.67 | 1.58 | 0.67 |
| K012482 | 1.79 | 1.09 | 0.92 | 0.71 | 0.06 | 0.50 | 0.52 | 0.58 | 0.99 | 1.94 | 2.04 | 1.94 |

Appendix

Molecular geochemical data (II): Aromatics

| Sample ID | TA(II)/TA(I+II) | MPI 1 | 9-/1-MPhen | (2-MPhen+3-MPhen)/ (1-MPhen+9-MPhen) | DBT/Phen | C ₁ -DBT/C ₁ -Phen | C ₁ -DBF/C ₁ -Phen | C ₁ -DBF/C ₁ -DBT | C ₁ -Phen/Phen | C ₁ -DBT/DBT | C ₁ -DBF/DBF |
|-----------|-----------------|-------|------------|---|----------|--|--|---|---------------------------|-------------------------|-------------------------|
| K011188 | 0.43 | 0.56 | 1.31 | 0.56 | 0.14 | 0.20 | 0.05 | 0.26 | 3.19 | 4.78 | 7.20 |
| K011189 | 0.48 | 0.48 | 1.26 | 0.51 | 0.19 | 0.23 | 0.11 | 0.48 | 2.49 | 3.14 | 6.05 |
| K011190 | 0.58 | 0.49 | 1.23 | 0.55 | 0.21 | 0.24 | 0.15 | 0.60 | 2.26 | 2.57 | 5.19 |
| K012302 | 0.68 | 0.48 | 1.29 | 0.53 | 0.25 | 0.26 | 0.14 | 0.53 | 2.25 | 2.37 | 4.43 |
| K011191 | 0.70 | 0.47 | 1.25 | 0.54 | 0.23 | 0.27 | 0.16 | 0.61 | 2.13 | 2.44 | 4.56 |
| K011192 | 0.65 | 0.47 | 1.22 | 0.53 | 0.25 | 0.27 | 0.16 | 0.58 | 2.17 | 2.36 | 4.69 |
| K011193 | 0.60 | 0.47 | 1.24 | 0.53 | 0.24 | 0.27 | 0.16 | 0.58 | 2.17 | 2.43 | 4.40 |
| K011194 | 0.61 | 0.46 | 1.17 | 0.53 | 0.22 | 0.27 | 0.16 | 0.61 | 2.18 | 2.69 | 5.00 |
| K011195 | 0.62 | 0.45 | 1.22 | 0.51 | 0.23 | 0.28 | 0.16 | 0.58 | 2.14 | 2.58 | 4.22 |
| K011196 | 0.39 | 0.52 | 1.22 | 0.51 | 0.15 | 0.20 | 0.05 | 0.24 | 3.16 | 4.11 | 6.05 |
| K012303 | 0.41 | 0.59 | 1.27 | 0.55 | 0.15 | 0.20 | 0.03 | 0.16 | 3.81 | 4.85 | 6.99 |
| K011197 | 0.39 | 0.55 | 1.27 | 0.52 | 0.13 | 0.20 | 0.04 | 0.21 | 3.74 | 5.53 | 5.49 |
| K012304 | 0.61 | 0.47 | 1.29 | 0.53 | 0.25 | 0.26 | 0.14 | 0.55 | 2.22 | 2.34 | 4.45 |
| K012305 | 0.51 | 0.50 | 1.27 | 0.56 | 0.21 | 0.24 | 0.12 | 0.49 | 2.27 | 2.61 | 6.47 |
| K012430 | 0.44 | 0.62 | 1.10 | 0.63 | 0.15 | 0.22 | 0.06 | 0.26 | 3.13 | 4.59 | 8.91 |
| K012306 | 0.41 | 0.62 | 1.23 | 0.63 | 0.12 | 0.17 | 0.03 | 0.16 | 3.14 | 4.25 | 4.68 |
| K011198 | 0.43 | 0.64 | 1.21 | 0.63 | 0.08 | 0.14 | 0.04 | 0.28 | 3.44 | 5.54 | 2.23 |
| K012431 | 0.49 | 0.45 | 1.30 | 0.51 | 0.21 | 0.24 | 0.15 | 0.65 | 2.12 | 2.40 | 4.50 |
| K012432 | 0.48 | 0.45 | 1.30 | 0.52 | 0.21 | 0.23 | 0.16 | 0.68 | 2.14 | 2.37 | 4.53 |
| K012433 | 0.49 | 0.46 | 1.29 | 0.52 | 0.21 | 0.23 | 0.16 | 0.67 | 2.14 | 2.39 | 4.63 |
| K012434 | 0.48 | 0.45 | 1.29 | 0.51 | 0.21 | 0.23 | 0.15 | 0.65 | 2.13 | 2.39 | 4.50 |
| K012435 | 0.50 | 0.45 | 1.26 | 0.52 | 0.20 | 0.22 | 0.14 | 0.65 | 2.09 | 2.34 | 4.46 |
| K012436 | 0.45 | 0.46 | 1.27 | 0.52 | 0.19 | 0.21 | 0.15 | 0.71 | 2.13 | 2.41 | 4.65 |
| K012437 | 0.33 | 0.50 | 1.31 | 0.53 | 0.18 | 0.20 | 0.10 | 0.52 | 2.62 | 2.99 | 5.11 |
| K012438 | 0.48 | 0.45 | 1.29 | 0.52 | 0.21 | 0.23 | 0.15 | 0.67 | 2.08 | 2.32 | 4.18 |
| K012439 | 0.47 | 0.45 | 1.30 | 0.51 | 0.20 | 0.23 | 0.15 | 0.65 | 2.13 | 2.36 | 4.37 |
| K012440 | 0.51 | 0.45 | 1.28 | 0.52 | 0.21 | 0.23 | 0.16 | 0.69 | 2.07 | 2.32 | 4.35 |
| K012441 | 0.28 | 0.54 | 1.32 | 0.52 | 0.15 | 0.19 | 0.06 | 0.32 | 3.35 | 4.02 | 8.31 |
| K012442 | 0.30 | 0.55 | 1.31 | 0.56 | 0.15 | 0.20 | 0.06 | 0.31 | 2.99 | 3.90 | 11.74 |
| K012443 | 0.29 | 0.56 | 1.33 | 0.54 | 0.13 | 0.17 | 0.05 | 0.29 | 3.49 | 4.69 | 6.85 |
| K012444 | 0.28 | 0.56 | 1.32 | 0.51 | 0.12 | 0.15 | 0.04 | 0.26 | 4.23 | 5.55 | 6.85 |
| K012445 | 0.31 | 0.51 | 1.31 | 0.53 | 0.11 | 0.16 | 0.11 | 0.67 | 2.65 | 3.77 | 6.68 |
| K012446 | 0.48 | 0.45 | 1.28 | 0.52 | 0.20 | 0.22 | 0.15 | 0.68 | 2.07 | 2.32 | 4.22 |
| K012447 | 0.48 | 0.45 | 1.27 | 0.52 | 0.20 | 0.22 | 0.15 | 0.66 | 2.10 | 2.34 | 4.28 |
| K012448 | 0.47 | 0.45 | 1.27 | 0.52 | 0.19 | 0.22 | 0.15 | 0.68 | 2.08 | 2.38 | 4.25 |
| K012449 | 0.48 | 0.45 | 1.27 | 0.52 | 0.20 | 0.22 | 0.15 | 0.68 | 2.08 | 2.33 | 4.31 |
| K012450 | 0.47 | 0.45 | 1.28 | 0.52 | 0.19 | 0.21 | 0.15 | 0.72 | 2.08 | 2.40 | 4.17 |
| K011228 | 0.45 | 0.56 | 1.36 | 0.59 | 0.24 | 0.33 | 0.10 | 0.29 | 2.80 | 3.93 | 3.82 |
| K011229 | 0.47 | 0.57 | 1.35 | 0.56 | 0.21 | 0.30 | 0.05 | 0.18 | 3.32 | 4.68 | 2.38 |
| K011230 | 0.49 | 0.55 | 1.38 | 0.55 | 0.27 | 0.33 | 0.08 | 0.25 | 3.04 | 3.61 | 5.18 |
| K011231 | 0.70 | 0.48 | 1.38 | 0.53 | 0.33 | 0.37 | 0.15 | 0.40 | 2.43 | 2.70 | 4.11 |

(continued on next page)

Appendix

Molecular geochemical data (II): Aromatics (continued)

| Sample ID | TA(I)/TA(I+II) | MPI 1 | 9-/1-MPhen | (2-MPhen+3-MPhen)/ (1-MPhen+9-MPhen) | DBT/Phen | C ₁ -DBT/C ₁ -Phen | C ₁ -DBF/C ₁ -Phen | C ₁ -DBF/C ₁ -DBT | C ₁ -Phen/Phen | C ₁ -DBT/DBT | C ₁ -DBF/DBF |
|-----------|----------------|-------|------------|---|----------|--|--|---|---------------------------|-------------------------|-------------------------|
| K011232 | 0.67 | 0.48 | 1.37 | 0.53 | 0.30 | 0.34 | 0.15 | 0.43 | 2.40 | 2.67 | 3.92 |
| K011233 | 0.64 | 0.50 | 1.36 | 0.53 | 0.36 | 0.34 | 0.19 | 0.55 | 2.56 | 2.46 | 4.04 |
| K012421 | 0.62 | 0.47 | 1.40 | 0.50 | 0.26 | 0.31 | 0.14 | 0.45 | 2.51 | 2.96 | 4.26 |
| K012422 | 0.71 | 0.46 | 1.37 | 0.50 | 0.31 | 0.34 | 0.13 | 0.39 | 2.40 | 2.71 | 4.22 |
| K011234 | 0.46 | 0.53 | 1.37 | 0.51 | 0.24 | 0.29 | 0.06 | 0.22 | 3.25 | 3.98 | 2.98 |
| K012423 | 0.47 | 0.52 | 1.41 | 0.50 | 0.24 | 0.29 | 0.08 | 0.27 | 3.33 | 4.00 | 7.29 |
| K012424 | 0.71 | 0.46 | 1.37 | 0.50 | 0.34 | 0.37 | 0.13 | 0.36 | 2.41 | 2.60 | 4.99 |
| K011235 | 0.46 | 0.50 | 1.37 | 0.54 | 0.27 | 0.33 | 0.12 | 0.36 | 2.47 | 3.01 | 3.37 |
| K011236 | 0.71 | 0.49 | 1.36 | 0.52 | 0.35 | 0.37 | 0.18 | 0.47 | 2.49 | 2.65 | 4.22 |
| K011237 | 0.46 | 0.54 | 1.31 | 0.56 | 0.23 | 0.30 | 0.08 | 0.26 | 2.76 | 3.57 | 5.19 |
| K011238 | 0.70 | 0.48 | 1.39 | 0.53 | 0.34 | 0.38 | 0.15 | 0.38 | 2.37 | 2.62 | 3.94 |
| K011239 | 0.36 | 0.59 | 1.35 | 0.58 | 0.19 | 0.28 | 0.08 | 0.30 | 3.28 | 4.80 | 2.86 |
| K012425 | 0.97 | 0.76 | 0.67 | 1.02 | 0.05 | 0.04 | 0.72 | 17.48 | 2.01 | 1.75 | 2.69 |
| K011240 | 0.98 | 0.81 | 0.72 | 1.03 | 0.06 | 0.05 | 0.63 | 12.43 | 2.22 | 1.74 | 2.80 |
| K011241 | 0.95 | 0.74 | 0.71 | 0.95 | 0.10 | 0.06 | 0.59 | 9.71 | 2.12 | 1.30 | 3.20 |
| K011242 | 0.96 | 0.64 | 0.94 | 0.85 | 0.27 | 0.28 | 0.35 | 1.23 | 1.86 | 1.95 | 3.01 |
| K011243 | 0.66 | 0.62 | 1.30 | 0.67 | 0.29 | 0.34 | 0.20 | 0.60 | 2.71 | 3.15 | 4.32 |
| K011244 | 0.62 | 0.62 | 1.29 | 0.65 | 0.30 | 0.35 | 0.17 | 0.48 | 2.93 | 3.49 | 5.58 |
| K011245 | 0.66 | 0.62 | 1.27 | 0.63 | 0.28 | 0.33 | 0.14 | 0.42 | 3.15 | 3.63 | 6.37 |
| K011246 | 0.65 | 0.61 | 1.26 | 0.65 | 0.28 | 0.33 | 0.17 | 0.51 | 2.77 | 3.32 | 5.11 |
| K012426 | 0.83 | 0.61 | 1.29 | 0.72 | 0.04 | 0.09 | 0.17 | 1.92 | 2.25 | 4.60 | 3.63 |
| K012427 | 0.92 | 0.64 | 1.29 | 0.78 | 0.03 | 0.06 | 0.16 | 2.86 | 2.18 | 3.83 | 3.70 |
| K011247 | 0.85 | 0.71 | 1.19 | 0.94 | 0.13 | 0.12 | 0.19 | 1.55 | 1.98 | 1.82 | 3.59 |
| K011248 | 0.91 | 0.71 | 0.97 | 0.85 | 0.10 | 0.08 | 0.22 | 2.76 | 2.35 | 1.90 | 4.46 |
| K011249 | 0.93 | 0.70 | 0.67 | 0.76 | 0.12 | 0.08 | 0.25 | 2.92 | 2.77 | 1.88 | 4.44 |
| K011250 | 0.89 | 0.70 | 0.61 | 0.78 | 0.12 | 0.08 | 0.27 | 3.32 | 2.73 | 1.78 | 4.23 |
| K012428 | 0.93 | 0.67 | 0.62 | 0.72 | 0.09 | 0.06 | 0.26 | 3.98 | 2.86 | 1.96 | 4.30 |
| K011251 | 0.90 | 0.71 | 0.63 | 0.77 | 0.13 | 0.08 | 0.26 | 3.24 | 2.86 | 1.78 | 4.48 |
| K012429 | 0.69 | 0.75 | 0.81 | 0.75 | 0.13 | 0.11 | 0.17 | 1.61 | 3.45 | 2.96 | 8.04 |
| K011252 | 0.81 | 0.69 | 1.07 | 0.80 | 0.07 | 0.10 | 0.19 | 1.89 | 2.44 | 3.22 | 4.02 |
| K011253 | 0.91 | 0.54 | 1.20 | 0.64 | 0.23 | 0.29 | 0.17 | 0.59 | 2.10 | 2.67 | 3.42 |
| K011254 | 0.66 | 0.60 | 1.28 | 0.64 | 0.28 | 0.33 | 0.17 | 0.51 | 2.71 | 3.20 | 6.87 |
| K012451 | 0.66 | 0.61 | 1.41 | 0.63 | 0.04 | 0.10 | 0.04 | 0.41 | 2.98 | 8.11 | 6.20 |
| K012452 | 0.68 | 0.61 | 1.38 | 0.63 | 0.01 | 0.05 | 0.04 | 0.81 | 3.01 | 12.36 | 6.42 |
| K012453 | 0.68 | 0.61 | 1.38 | 0.63 | 0.01 | 0.04 | 0.04 | 0.92 | 2.98 | 17.07 | 7.28 |
| K012454 | 0.70 | 0.61 | 1.37 | 0.63 | 0.06 | 0.14 | 0.03 | 0.25 | 2.99 | 7.27 | 7.88 |
| K012455 | 0.71 | 0.61 | 1.35 | 0.63 | 0.02 | 0.08 | 0.04 | 0.48 | 2.92 | 11.39 | 6.69 |
| K012456 | 0.70 | 0.61 | 1.36 | 0.63 | 0.01 | 0.05 | 0.04 | 0.70 | 2.91 | 15.50 | 7.28 |
| K012457 | 0.70 | 0.61 | 1.36 | 0.63 | 0.04 | 0.10 | 0.04 | 0.39 | 2.97 | 7.23 | 7.06 |
| K012458 | 0.69 | 0.61 | 1.36 | 0.63 | 0.00 | 0.03 | 0.04 | 1.42 | 2.96 | 18.70 | 7.70 |
| K012459 | 0.68 | 0.61 | 1.36 | 0.63 | 0.01 | 0.05 | 0.03 | 0.66 | 2.95 | 16.66 | 7.73 |

(continued on next page)

Appendix

Molecular geochemical data (II): Aromatics (continued)

| Sample ID | TA(I)/TA(I+II) | MPI 1 | 9-/1-MPhen | (2-MPhen+3-MPhen)/ (1-MPhen+9-MPhen) | DBT/Phen | C ₁ -DBT/C ₁ -Phen | C ₁ -DBF/C ₁ -Phen | C ₁ -DBF/C ₁ -DBT | C ₁ -Phen/Phen | C ₁ -DBT/DBT | C ₁ -DBF/DBF |
|-----------|----------------|-------|------------|---|----------|--|--|---|---------------------------|-------------------------|-------------------------|
| K012460 | 0.70 | 0.61 | 1.36 | 0.63 | 0.02 | 0.07 | 0.04 | 0.52 | 2.94 | 13.23 | 8.34 |
| K012461 | 0.68 | 0.60 | 1.32 | 0.63 | 0.07 | 0.16 | 0.04 | 0.25 | 2.88 | 7.03 | 8.40 |
| K012462 | 0.70 | 0.61 | 1.35 | 0.64 | 0.02 | 0.09 | 0.03 | 0.40 | 2.90 | 10.61 | 8.96 |
| K012463 | 0.71 | 0.61 | 1.35 | 0.63 | 0.01 | 0.06 | 0.03 | 0.56 | 2.93 | 14.04 | 7.88 |
| K012464 | 0.71 | 0.60 | 1.33 | 0.63 | 0.01 | 0.06 | 0.04 | 0.64 | 2.81 | 13.39 | 6.37 |
| K012465 | 0.68 | 0.62 | 1.36 | 0.64 | 0.01 | 0.04 | 0.04 | 0.94 | 3.06 | 18.58 | 5.89 |
| K012466 | 0.69 | 0.61 | 1.34 | 0.63 | 0.00 | 0.02 | 0.04 | 2.12 | 2.92 | 20.77 | 6.96 |
| K012467 | 0.70 | 0.60 | 1.34 | 0.63 | 0.02 | 0.07 | 0.03 | 0.47 | 2.84 | 11.10 | 7.94 |
| K012468 | 0.75 | 0.61 | 1.34 | 0.63 | 0.06 | 0.15 | 0.04 | 0.26 | 2.89 | 7.03 | 7.69 |
| K012469 | 0.69 | 0.62 | 1.40 | 0.60 | 0.03 | 0.09 | 0.05 | 0.56 | 3.41 | 9.05 | 4.83 |
| K012470 | 0.71 | 0.61 | 1.35 | 0.62 | 0.01 | 0.06 | 0.04 | 0.76 | 3.07 | 13.42 | 7.03 |
| K012471 | 0.74 | 0.61 | 1.34 | 0.64 | 0.05 | 0.13 | 0.04 | 0.27 | 2.86 | 8.16 | 8.44 |
| K012472 | 0.74 | 0.61 | 1.34 | 0.64 | 0.02 | 0.09 | 0.04 | 0.46 | 2.88 | 10.31 | 6.25 |
| K012473 | 0.74 | 0.60 | 1.34 | 0.63 | 0.06 | 0.15 | 0.04 | 0.25 | 2.87 | 7.07 | 7.19 |
| K012474 | 0.76 | 0.61 | 1.34 | 0.63 | 0.06 | 0.14 | 0.04 | 0.26 | 2.89 | 7.30 | 7.52 |
| K012475 | 0.74 | 0.60 | 1.33 | 0.63 | 0.06 | 0.15 | 0.04 | 0.25 | 2.88 | 7.12 | 7.56 |
| K012476 | 0.75 | 0.61 | 1.34 | 0.64 | 0.04 | 0.12 | 0.04 | 0.29 | 2.87 | 8.22 | 7.08 |
| K011212 | 0.16 | 0.59 | 1.32 | 0.61 | 0.27 | 0.32 | 0.08 | 0.25 | 3.04 | 3.59 | 8.08 |
| K011213 | 0.17 | 0.60 | 1.34 | 0.64 | 0.31 | 0.35 | 0.10 | 0.29 | 2.75 | 3.11 | 11.41 |
| K011214 | 0.17 | 0.58 | 1.38 | 0.62 | 0.30 | 0.36 | 0.10 | 0.28 | 2.70 | 3.20 | 12.46 |
| K011215 | 0.16 | 0.62 | 1.30 | 0.58 | 0.26 | 0.33 | 0.05 | 0.14 | 3.98 | 5.06 | 10.12 |
| K011216 | 0.17 | 0.62 | 1.35 | 0.65 | 0.30 | 0.35 | 0.09 | 0.24 | 2.80 | 3.35 | 9.13 |
| K011217 | 0.17 | 0.62 | 1.32 | 0.58 | 0.29 | 0.30 | 0.06 | 0.19 | 3.83 | 3.94 | 5.90 |
| K011218 | 0.18 | 0.60 | 1.31 | 0.66 | 0.31 | 0.33 | 0.11 | 0.34 | 2.53 | 2.70 | 6.83 |
| K011219 | 0.25 | 0.52 | 1.30 | 0.65 | 0.26 | 0.29 | 0.23 | 0.80 | 1.92 | 2.14 | 3.33 |
| K011220 | 0.24 | 0.54 | 1.35 | 0.67 | 0.33 | 0.35 | 0.22 | 0.63 | 1.94 | 2.10 | 3.23 |
| K011221 | 0.09 | 0.28 | 1.34 | 0.55 | 0.57 | 0.67 | 0.64 | 0.95 | 0.80 | 0.94 | 1.64 |
| K011222 | 0.07 | 0.43 | 1.50 | 0.59 | 0.68 | 0.83 | 0.25 | 0.30 | 1.50 | 1.82 | 1.18 |
| K011223 | 0.06 | 0.37 | 1.56 | 0.53 | 0.66 | 0.83 | 0.25 | 0.31 | 1.33 | 1.68 | 2.20 |
| K011224 | 0.06 | 0.41 | 1.59 | 0.50 | 0.77 | 0.85 | 0.20 | 0.24 | 1.84 | 2.05 | 2.15 |
| K011225 | 0.05 | 0.41 | 1.68 | 0.53 | 0.66 | 0.76 | 0.26 | 0.34 | 1.63 | 1.87 | 2.23 |
| K011226 | 0.06 | 0.42 | 1.62 | 0.54 | 0.55 | 0.64 | 0.24 | 0.38 | 1.63 | 1.90 | 2.42 |
| K011227 | 0.06 | 0.41 | 1.60 | 0.52 | 0.40 | 0.53 | 0.23 | 0.43 | 1.68 | 2.22 | 2.89 |
| K011199 | 0.06 | 0.39 | 1.75 | 0.50 | 0.53 | 0.59 | 0.25 | 0.43 | 1.59 | 1.79 | 1.84 |
| K011200 | 0.05 | 0.39 | 1.93 | 0.48 | 0.57 | 0.54 | 0.24 | 0.45 | 1.76 | 1.69 | 1.83 |
| K011201 | 0.04 | 0.36 | 1.94 | 0.46 | 0.59 | 0.57 | 0.26 | 0.46 | 1.63 | 1.59 | 1.81 |
| K011202 | 0.07 | 0.38 | 1.89 | 0.47 | 0.56 | 0.54 | 0.26 | 0.49 | 1.73 | 1.68 | 1.81 |
| K011203 | 0.06 | 0.35 | 1.86 | 0.45 | 0.59 | 0.61 | 0.33 | 0.54 | 1.56 | 1.61 | 1.94 |
| K011204 | 0.05 | 0.39 | 1.76 | 0.49 | 0.47 | 0.50 | 0.32 | 0.64 | 1.62 | 1.72 | 1.91 |
| K011205 | 0.07 | 0.33 | 1.80 | 0.49 | 0.35 | 0.51 | 0.36 | 0.69 | 1.20 | 1.76 | 1.56 |
| K011206 | 0.05 | 0.39 | 1.80 | 0.48 | 0.48 | 0.53 | 0.26 | 0.48 | 1.70 | 1.90 | 2.32 |

(continued on next page)

Appendix

Molecular geochemical data (II): Aromatics (continued)

| Sample ID | TA(I)/TA(I+II) | MP1 1 | 9-/1-MPhen | (2-MPhen+3-MPhen)/ (1-MPhen+9-MPhen) | DBT/Phen | C ₁ DBT/C ₁ Phen | C ₁ DBF/C ₁ Phen | C ₁ DBF/C ₁ DBT | C ₁ Phen/Phen | C ₁ DBT/DBT | C ₁ DBF/DBF |
|-----------|----------------|-------|------------|---|----------|--|--|---------------------------------------|--------------------------|------------------------|------------------------|
| K011207 | 0.06 | 0.35 | 1.85 | 0.47 | 0.66 | 0.62 | 0.32 | 0.52 | 1.44 | 1.35 | 1.98 |
| K011208 | 0.05 | 0.45 | 1.80 | 0.58 | 0.62 | 0.69 | 0.28 | 0.40 | 1.68 | 1.90 | 1.86 |
| K011209 | 0.06 | 0.45 | 1.94 | 0.52 | 0.69 | 0.69 | 0.23 | 0.34 | 2.02 | 2.02 | 1.66 |
| K011210 | 0.06 | 0.39 | 1.79 | 0.53 | 0.53 | 0.69 | 0.28 | 0.40 | 1.49 | 1.93 | 1.93 |
| K011211 | 0.06 | 0.34 | 1.78 | 0.47 | 0.73 | 0.70 | 0.36 | 0.52 | 1.37 | 1.32 | 1.64 |
| K012477 | 0.07 | 0.42 | 1.21 | 0.60 | 0.22 | 0.26 | 0.21 | 0.79 | 1.40 | 1.72 | 2.71 |
| K012478 | 0.05 | 0.42 | 1.35 | 0.57 | 0.45 | 0.49 | 0.17 | 0.34 | 1.54 | 1.68 | 2.78 |
| K012479 | 0.07 | 0.42 | 1.42 | 0.55 | 0.39 | 0.42 | 0.16 | 0.38 | 1.61 | 1.73 | 2.86 |
| K012480 | 0.06 | 0.42 | 1.44 | 0.54 | 0.48 | 0.50 | 0.16 | 0.33 | 1.66 | 1.74 | 3.02 |
| K012481 | 0.07 | 0.43 | 1.37 | 0.56 | 0.39 | 0.43 | 0.16 | 0.38 | 1.63 | 1.77 | 2.85 |
| K012482 | 0.19 | 0.46 | 1.25 | 0.65 | 0.13 | 0.20 | 0.24 | 1.24 | 1.50 | 2.31 | 3.03 |

Appendix

Molecular geochemical data (III): Carbazoles

| Sample ID | C ₁ Carb/Carb | C ₂ Carb (Shielded/Exposed) | BC ratio |
|-----------|--------------------------|--|----------|
| K011188 | 6.96 | 15.67 | 0.62 |
| K011189 | 3.23 | 5.51 | 0.49 |
| K011190 | 3.07 | 7.29 | 0.47 |
| K012302 | 3.61 | 4.83 | 0.56 |
| K011191 | 3.78 | 5.45 | 0.54 |
| K011192 | 3.76 | 6.06 | 0.55 |
| K011193 | 3.93 | 6.04 | 0.56 |
| K011194 | 5.20 | 11.56 | 0.55 |
| K011195 | 3.26 | 5.45 | 0.52 |
| K011196 | 4.88 | 9.51 | 0.56 |
| K012303 | 4.75 | 12.96 | 0.54 |
| K011197 | 5.79 | 12.14 | 0.58 |
| K012304 | 2.86 | 4.50 | 0.46 |
| K012305 | 2.61 | 3.84 | 0.46 |
| K012430 | 4.20 | 6.45 | 0.45 |
| K012306 | 4.11 | 13.36 | 0.56 |
| K011198 | 4.43 | 9.24 | 0.59 |
| K012431 | 3.30 | 7.77 | 0.33 |
| K012432 | 3.29 | 7.09 | 0.42 |
| K012433 | 3.65 | 9.29 | 0.45 |
| K012434 | 3.34 | 7.17 | 0.44 |
| K012435 | 3.70 | 5.69 | 0.50 |
| K012436 | 3.66 | 6.54 | 0.46 |
| K012437 | 3.99 | 6.12 | 0.46 |
| K012438 | 3.54 | 6.34 | 0.48 |
| K012439 | 3.14 | 5.15 | 0.49 |
| K012440 | 3.06 | 4.49 | 0.46 |
| K012441 | 5.53 | 7.52 | 0.44 |
| K012442 | 4.60 | 5.96 | 0.43 |
| K012443 | 4.45 | 6.22 | 0.40 |
| K012444 | 5.23 | 7.52 | 0.45 |
| K012445 | 4.68 | 7.33 | 0.53 |
| K012446 | 3.97 | 4.80 | 0.54 |
| K012447 | 4.01 | 4.96 | 0.54 |
| K012448 | 3.86 | 4.51 | 0.53 |
| K012449 | 3.90 | 4.58 | 0.54 |
| K012450 | 3.86 | 4.79 | 0.54 |
| K011228 | 4.32 | 4.50 | 0.59 |
| K011229 | 4.31 | 3.95 | 0.58 |
| K011230 | 4.37 | 4.27 | 0.58 |
| K011231 | 4.04 | 6.57 | 0.50 |
| K011232 | 4.03 | 4.02 | 0.58 |
| K011233 | 3.97 | 3.50 | 0.58 |
| K012421 | 4.01 | 3.01 | 0.56 |
| K012422 | 4.40 | 4.16 | 0.58 |
| K011234 | 5.54 | 7.85 | 0.55 |
| K012423 | 4.73 | 4.66 | 0.58 |
| K012424 | 3.96 | 3.98 | 0.55 |
| K011235 | 4.29 | 6.11 | 0.53 |
| K011236 | 4.21 | 4.98 | 0.55 |
| K011237 | 3.91 | 4.93 | 0.57 |
| K011238 | 4.01 | 7.09 | 0.52 |
| K011239 | 4.63 | 5.14 | 0.50 |
| K012425 | 3.51 | 3.86 | 0.53 |
| K011240 | 4.22 | 5.32 | 0.60 |
| K011241 | 3.52 | 5.46 | 0.56 |
| K011242 | 2.76 | 4.04 | 0.63 |
| K011243 | 4.35 | 4.56 | 0.57 |
| K011244 | 2.79 | 8.56 | 0.37 |
| K011245 | 4.73 | 9.56 | 0.63 |
| K011246 | 4.16 | 7.13 | 0.63 |
| K012426 | 3.58 | 3.58 | 0.61 |
| K012427 | 3.29 | 3.38 | 0.62 |
| K011247 | 2.41 | 2.88 | 0.63 |
| K011248 | 2.58 | 3.48 | 0.60 |
| K011249 | 3.10 | 5.05 | 0.56 |
| K011250 | 3.32 | 5.74 | 0.57 |
| K012428 | 4.10 | 4.80 | 0.55 |
| K011251 | 3.87 | 5.72 | 0.55 |
| K012429 | 3.81 | 6.55 | 0.57 |

Molecular geochemical data (III): Carbazoles (continued)

| Sample ID | C ₁ Carb/Carb | C ₂ Carb (Shielded/Exposed) | BC ratio |
|-----------|--------------------------|--|----------|
| K011252 | 2.90 | 3.63 | 0.64 |
| K011253 | 2.95 | 2.45 | 0.66 |
| K011254 | 4.84 | 5.87 | 0.67 |
| K012451 | 3.62 | 8.69 | 0.56 |
| K012452 | 3.80 | 7.10 | 0.62 |
| K012453 | 3.64 | 7.12 | 0.60 |
| K012454 | 3.76 | 8.24 | 0.55 |
| K012455 | 3.74 | 6.49 | 0.61 |
| K012456 | 3.74 | 7.91 | 0.60 |
| K012457 | 3.76 | 6.49 | 0.60 |
| K012458 | 3.90 | 7.59 | 0.60 |
| K012459 | 3.92 | 6.62 | 0.61 |
| K012460 | 3.85 | 6.88 | 0.61 |
| K012461 | 1.30 | 3.83 | 0.28 |
| K012462 | 3.74 | 7.35 | 0.60 |
| K012463 | 3.78 | 6.18 | 0.61 |
| K012464 | 4.15 | 6.23 | 0.64 |
| K012465 | 3.92 | 6.99 | 0.62 |
| K012466 | 3.77 | 6.23 | 0.62 |
| K012467 | 3.56 | 5.14 | 0.62 |
| K012468 | 2.66 | 4.28 | 0.48 |
| K012469 | 3.89 | 7.60 | 0.60 |
| K012470 | 3.81 | 7.11 | 0.62 |
| K012471 | 3.57 | 6.34 | 0.53 |
| K012472 | 3.61 | 6.87 | 0.60 |
| K012473 | 2.16 | 4.01 | 0.41 |
| K012474 | 3.20 | 5.77 | 0.49 |
| K012475 | 2.26 | 4.20 | 0.35 |
| K012476 | 3.56 | 5.80 | 0.54 |
| K011212 | 6.05 | 11.73 | 0.61 |
| K011213 | 5.11 | 13.96 | 0.49 |
| K011214 | 5.14 | 14.31 | 0.68 |
| K011215 | 8.36 | 21.21 | 0.60 |
| K011216 | 5.99 | 16.18 | 0.62 |
| K011217 | 3.32 | 14.07 | 0.65 |
| K011218 | 3.03 | 9.20 | 0.62 |
| K011219 | 4.93 | 9.84 | 0.55 |
| K011220 | 2.98 | 9.11 | 0.50 |
| K011221 | 3.62 | 9.22 | 0.53 |
| K011222 | 3.21 | 6.84 | 0.51 |
| K011223 | 2.76 | 6.50 | 0.52 |
| K011224 | 3.10 | 7.53 | 0.46 |
| K011225 | 2.97 | 6.63 | 0.49 |
| K011226 | 2.98 | 6.89 | 0.50 |
| K011227 | 2.52 | 4.72 | 0.51 |
| K011199 | 2.41 | 6.02 | 0.51 |
| K011200 | 2.26 | 6.46 | 0.41 |
| K011201 | 2.37 | 8.57 | 0.36 |
| K011202 | 2.40 | 7.28 | 0.38 |
| K011203 | 2.52 | 6.76 | 0.37 |
| K011204 | 1.91 | 5.22 | 0.43 |
| K011205 | 1.91 | 5.99 | 0.42 |
| K011206 | 1.98 | 7.09 | 0.45 |
| K011207 | 2.06 | 6.56 | 0.37 |
| K011208 | 1.95 | 8.06 | 0.38 |
| K011209 | 1.89 | 6.14 | 0.42 |
| K011210 | 2.04 | 8.82 | 0.43 |
| K011211 | 2.33 | 9.28 | 0.40 |
| K012477 | 2.30 | 5.43 | 0.55 |
| K012478 | 2.38 | 4.56 | 0.51 |
| K012479 | 2.18 | 4.96 | 0.54 |
| K012480 | 2.06 | 4.32 | 0.50 |
| K012481 | 2.30 | 5.26 | 0.53 |
| K012482 | 2.02 | 4.10 | 0.50 |

Molecular geochemical data (IV): Ternary systems I

| Sample ID | Steranes | | | Methylphenanthrenes | | | Methyl dibenzothiophenes | | | | C ₁ Phen-C ₁ DBF-C ₁ DBT | | | C ₁ Phen-C ₁ Carb-C ₁ DBT | | |
|-----------|---------------------------------|---------------------------------|---------------------------------|---------------------|-------------|---------------|--------------------------|--------------|------------|-------------------------|---|------------------------|-------------------------|--|------------------------|--|
| | C ₂₇ αβ Steranes [%] | C ₂₈ αβ Steranes [%] | C ₂₉ αβ Steranes [%] | 9-MPhen [%] | 1-MPhen [%] | 2+3-MPhen [%] | 4-MDBT [%] | 2+3-MDBT [%] | 1-MDBT [%] | C ₁ Phen [%] | C ₁ DBF [%] | C ₁ DBT [%] | C ₁ Phen [%] | C ₁ Carb [%] | C ₁ DBT [%] | |
| K011188 | 38.15 | 26.98 | 34.88 | 36.32 | 27.81 | 35.87 | 56.40 | 26.73 | 16.87 | 79.63 | 4.19 | 16.19 | 82.13 | 1.17 | 16.70 | |
| K011189 | 36.62 | 25.03 | 38.34 | 36.80 | 29.23 | 33.97 | 61.56 | 23.28 | 15.16 | 74.27 | 8.39 | 17.33 | 78.15 | 3.61 | 18.24 | |
| K011190 | 34.08 | 27.44 | 38.48 | 35.64 | 28.98 | 35.38 | 61.38 | 24.69 | 13.93 | 71.91 | 10.53 | 17.56 | 78.13 | 2.79 | 19.08 | |
| K012302 | 35.89 | 26.20 | 37.91 | 36.78 | 28.50 | 34.72 | 58.95 | 26.43 | 14.62 | 71.46 | 9.87 | 18.68 | 73.51 | 7.27 | 19.21 | |
| K011191 | 39.76 | 25.73 | 34.51 | 36.23 | 28.92 | 34.86 | 60.60 | 24.65 | 14.75 | 69.90 | 11.38 | 18.72 | 76.10 | 3.52 | 20.38 | |
| K011192 | 40.54 | 26.02 | 33.44 | 35.93 | 29.45 | 34.63 | 60.53 | 25.51 | 13.96 | 69.92 | 11.10 | 18.98 | 74.56 | 5.20 | 20.24 | |
| K011193 | 40.12 | 25.54 | 34.34 | 36.09 | 29.18 | 34.73 | 60.46 | 25.10 | 14.44 | 70.07 | 11.01 | 18.93 | 74.77 | 5.03 | 20.20 | |
| K011194 | 39.15 | 25.21 | 35.64 | 35.29 | 30.17 | 34.53 | 59.58 | 25.44 | 14.97 | 69.98 | 11.33 | 18.69 | 76.44 | 3.14 | 20.42 | |
| K011195 | 38.35 | 26.66 | 34.99 | 36.40 | 29.73 | 33.87 | 60.38 | 25.80 | 13.81 | 69.65 | 11.18 | 19.17 | 75.07 | 4.27 | 20.66 | |
| K011196 | 35.77 | 27.71 | 36.52 | 36.28 | 29.86 | 33.86 | 59.03 | 25.60 | 15.37 | 80.38 | 3.79 | 15.83 | 80.20 | 4.01 | 15.79 | |
| K012303 | 33.59 | 27.35 | 39.06 | 36.08 | 28.42 | 35.50 | 56.79 | 27.78 | 15.43 | 81.54 | 2.51 | 15.95 | 78.93 | 5.63 | 15.44 | |
| K011197 | 36.66 | 27.01 | 36.34 | 36.89 | 29.09 | 34.02 | 57.90 | 27.08 | 15.01 | 80.79 | 3.40 | 15.82 | 78.72 | 5.87 | 15.41 | |
| K012304 | 35.45 | 26.47 | 38.08 | 36.93 | 28.57 | 34.50 | 59.26 | 26.33 | 14.41 | 71.18 | 10.18 | 18.65 | 77.89 | 1.71 | 20.40 | |
| K012305 | 35.89 | 23.89 | 40.22 | 35.79 | 28.19 | 36.02 | 60.17 | 25.93 | 13.89 | 73.49 | 8.73 | 17.77 | 79.34 | 1.48 | 19.19 | |
| K012430 | 34.30 | 27.13 | 38.57 | 32.11 | 29.19 | 38.70 | 56.78 | 27.29 | 15.92 | 78.25 | 4.51 | 17.25 | 80.78 | 1.42 | 17.81 | |
| K012306 | 34.43 | 27.07 | 38.49 | 33.78 | 27.53 | 38.69 | 55.59 | 28.14 | 16.27 | 83.88 | 2.27 | 13.85 | 79.82 | 7.00 | 13.18 | |
| K011198 | 31.23 | 26.93 | 41.84 | 33.71 | 27.75 | 38.54 | 60.59 | 22.45 | 16.96 | 85.17 | 3.26 | 11.57 | 80.91 | 8.09 | 11.00 | |
| K012431 | 36.58 | 26.30 | 37.11 | 37.31 | 28.74 | 33.95 | 59.46 | 25.88 | 14.66 | 71.84 | 11.12 | 17.04 | 78.59 | 2.77 | 18.64 | |
| K012432 | 36.69 | 26.10 | 37.21 | 37.20 | 28.66 | 34.14 | 59.08 | 25.90 | 15.03 | 72.02 | 11.29 | 16.68 | 75.75 | 6.70 | 17.55 | |
| K012433 | 36.32 | 25.76 | 37.92 | 37.13 | 28.71 | 34.15 | 59.18 | 25.98 | 14.84 | 71.91 | 11.26 | 16.83 | 77.10 | 4.86 | 18.04 | |
| K012434 | 35.94 | 26.20 | 37.86 | 37.19 | 28.83 | 33.98 | 59.31 | 25.82 | 14.86 | 72.22 | 10.91 | 16.87 | 78.85 | 2.73 | 18.42 | |
| K012435 | 34.64 | 25.69 | 39.67 | 36.71 | 29.10 | 34.19 | 59.57 | 25.72 | 14.71 | 73.18 | 10.56 | 16.26 | 79.05 | 3.39 | 17.56 | |
| K012436 | 34.88 | 25.95 | 39.18 | 36.71 | 28.90 | 34.39 | 60.11 | 25.16 | 14.73 | 73.23 | 11.09 | 15.67 | 79.79 | 3.13 | 17.08 | |
| K012437 | 35.21 | 25.46 | 39.33 | 37.21 | 28.30 | 34.49 | 59.06 | 25.74 | 15.21 | 76.54 | 8.02 | 15.44 | 82.17 | 1.25 | 16.58 | |
| K012438 | 35.50 | 26.72 | 37.78 | 37.12 | 28.87 | 34.01 | 59.32 | 25.75 | 14.93 | 72.27 | 11.13 | 16.60 | 78.36 | 3.65 | 17.99 | |
| K012439 | 36.43 | 25.91 | 37.66 | 37.29 | 28.73 | 33.97 | 59.22 | 25.70 | 15.08 | 72.90 | 10.64 | 16.46 | 78.82 | 3.38 | 17.80 | |
| K012440 | 36.11 | 26.39 | 37.50 | 37.05 | 28.86 | 34.09 | 59.64 | 25.70 | 14.66 | 71.91 | 11.48 | 16.61 | 74.23 | 8.63 | 17.15 | |
| K012441 | 33.21 | 26.12 | 40.67 | 37.52 | 28.34 | 34.14 | 57.87 | 26.15 | 15.98 | 80.33 | 4.78 | 14.89 | 83.39 | 1.15 | 15.46 | |
| K012442 | 33.99 | 26.46 | 39.55 | 36.34 | 27.83 | 35.83 | 58.53 | 26.14 | 15.33 | 79.49 | 4.88 | 15.63 | 82.82 | 0.90 | 16.28 | |
| K012443 | 31.96 | 26.65 | 41.39 | 37.13 | 27.81 | 35.06 | 58.87 | 25.72 | 15.41 | 81.54 | 4.20 | 14.27 | 84.26 | 0.99 | 14.74 | |
| K012444 | 34.61 | 25.72 | 39.67 | 37.78 | 28.64 | 33.58 | 57.96 | 25.85 | 16.19 | 83.90 | 3.31 | 12.79 | 84.91 | 2.15 | 12.94 | |
| K012445 | 33.37 | 26.92 | 39.72 | 36.94 | 28.23 | 34.82 | 61.05 | 24.15 | 14.80 | 78.92 | 8.45 | 12.63 | 83.00 | 3.71 | 13.29 | |
| K012446 | 36.38 | 26.43 | 37.19 | 36.85 | 28.86 | 34.29 | 59.20 | 25.70 | 15.10 | 72.69 | 11.09 | 16.23 | 72.44 | 11.39 | 16.17 | |
| K012447 | 35.67 | 26.48 | 37.85 | 36.84 | 29.03 | 34.13 | 59.36 | 25.55 | 15.08 | 73.11 | 10.73 | 16.16 | 75.08 | 8.32 | 16.60 | |
| K012448 | 35.86 | 26.12 | 38.02 | 36.84 | 28.95 | 34.20 | 59.74 | 25.35 | 14.91 | 73.05 | 10.94 | 16.00 | 68.46 | 16.54 | 15.00 | |
| K012449 | 36.04 | 26.51 | 37.45 | 36.84 | 29.00 | 34.15 | 59.66 | 25.37 | 14.98 | 72.82 | 11.02 | 16.16 | 69.15 | 15.50 | 15.35 | |
| K012450 | 36.15 | 25.89 | 37.96 | 36.88 | 28.83 | 34.29 | 60.06 | 25.12 | 14.82 | 73.17 | 11.20 | 15.63 | 66.70 | 19.05 | 14.25 | |
| K011228 | 33.86 | 23.55 | 42.59 | 36.28 | 26.65 | 37.07 | 58.12 | 27.98 | 13.91 | 70.05 | 6.78 | 23.17 | 70.46 | 6.23 | 23.31 | |
| K011229 | 39.59 | 27.12 | 33.29 | 36.91 | 27.30 | 35.79 | 57.38 | 28.33 | 14.29 | 74.03 | 3.88 | 22.09 | 71.65 | 6.97 | 21.38 | |
| K011230 | 30.86 | 28.25 | 40.89 | 37.32 | 27.08 | 35.60 | 58.30 | 27.75 | 13.95 | 71.08 | 5.80 | 23.12 | 71.73 | 4.94 | 23.33 | |
| K011231 | 38.52 | 26.46 | 35.02 | 37.96 | 27.57 | 34.47 | 58.46 | 27.53 | 14.01 | 65.96 | 9.77 | 24.27 | 66.86 | 8.55 | 24.60 | |

(continued on next page)

Appendix

Molecular geochemical data (IV): Ternary systems I (continued)

| Sample ID | Steranes | | | Methylphenanthrenes | | | Methyl dibenzothiophenes | | | | C ₁ Phen-C ₁ DBF-C ₁ DBT | | | C ₁ Phen-C ₁ Carb-C ₁ DBT | | |
|-----------|---------------------------------|---------------------------------|---------------------------------|---------------------|-------------|---------------|--------------------------|--------------|------------|-------------------------|---|------------------------|-------------------------|--|------------------------|--|
| | C ₂₇ αβ Steranes [%] | C ₂₈ αβ Steranes [%] | C ₂₉ αβ Steranes [%] | 9-MPhen [%] | 1-MPhen [%] | 2+3-MPhen [%] | 4-MDBT [%] | 2+3-MDBT [%] | 1-MDBT [%] | C ₁ Phen [%] | C ₁ DBF [%] | C ₁ DBT [%] | C ₁ Phen [%] | C ₁ Carb [%] | C ₁ DBT [%] | |
| K011232 | 40.42 | 27.19 | 32.40 | 37.89 | 27.64 | 34.47 | 60.53 | 25.81 | 13.66 | 67.46 | 9.79 | 22.75 | 63.15 | 15.55 | 21.30 | |
| K011233 | 40.39 | 27.58 | 32.03 | 37.72 | 27.73 | 34.55 | 59.25 | 26.38 | 14.37 | 65.46 | 12.23 | 22.31 | 58.99 | 20.90 | 20.11 | |
| K011241 | 37.27 | 27.43 | 35.30 | 38.91 | 27.86 | 33.23 | 59.83 | 25.70 | 14.47 | 68.94 | 9.59 | 21.47 | 60.43 | 20.75 | 18.82 | |
| K011242 | 39.06 | 26.15 | 34.79 | 38.61 | 28.27 | 33.13 | 59.06 | 26.63 | 14.32 | 67.62 | 9.10 | 23.29 | 51.66 | 30.54 | 17.80 | |
| K011234 | 35.13 | 24.33 | 40.55 | 38.14 | 27.94 | 33.92 | 57.78 | 27.50 | 14.72 | 73.63 | 4.68 | 21.69 | 70.84 | 8.29 | 20.87 | |
| K011243 | 37.30 | 27.25 | 35.45 | 38.94 | 27.57 | 33.49 | 58.42 | 26.78 | 14.80 | 73.41 | 5.60 | 20.99 | 68.12 | 12.40 | 19.48 | |
| K0112424 | 39.32 | 26.76 | 33.92 | 38.68 | 28.13 | 33.19 | 58.47 | 27.06 | 14.47 | 66.74 | 8.77 | 24.49 | 50.75 | 30.63 | 18.62 | |
| K011235 | 46.05 | 22.71 | 31.25 | 37.53 | 27.48 | 34.99 | 58.67 | 27.33 | 14.00 | 68.89 | 8.20 | 22.91 | 66.08 | 11.96 | 21.97 | |
| K011236 | 38.40 | 27.31 | 34.30 | 37.85 | 27.86 | 34.29 | 58.11 | 27.63 | 14.26 | 64.55 | 11.35 | 24.10 | 61.69 | 15.28 | 23.03 | |
| K011237 | 31.90 | 29.53 | 38.57 | 36.32 | 27.66 | 36.02 | 57.55 | 27.82 | 14.63 | 72.66 | 5.71 | 21.63 | 66.28 | 13.99 | 19.73 | |
| K011238 | 40.45 | 26.10 | 33.45 | 38.12 | 27.44 | 34.44 | 58.65 | 27.18 | 14.17 | 65.59 | 9.54 | 24.87 | 70.95 | 2.15 | 26.90 | |
| K011239 | 46.07 | 22.93 | 31.00 | 36.26 | 26.94 | 36.80 | 58.82 | 26.86 | 14.31 | 73.68 | 6.03 | 20.29 | 70.60 | 9.96 | 19.44 | |
| K0112425 | 18.96 | 20.65 | 60.39 | 19.83 | 29.65 | 50.53 | 51.42 | 40.74 | 7.85 | 56.73 | 40.93 | 2.34 | 53.80 | 43.98 | 2.22 | |
| K011240 | 19.76 | 22.07 | 58.17 | 20.66 | 28.65 | 50.69 | 49.82 | 43.19 | 6.99 | 59.57 | 37.42 | 3.01 | 88.58 | 6.94 | 4.48 | |
| K011241 | 15.48 | 20.57 | 63.95 | 21.35 | 29.93 | 48.72 | 52.38 | 41.00 | 6.63 | 60.76 | 35.57 | 3.67 | 84.43 | 10.48 | 5.09 | |
| K011242 | 20.39 | 22.79 | 56.82 | 26.29 | 27.84 | 45.87 | 56.07 | 31.67 | 12.26 | 61.25 | 21.34 | 17.41 | 64.12 | 17.65 | 18.23 | |
| K011243 | 37.13 | 27.83 | 35.04 | 33.79 | 26.08 | 40.13 | 56.28 | 29.93 | 13.79 | 64.92 | 13.12 | 21.97 | 71.75 | 3.96 | 24.28 | |
| K011244 | 37.36 | 27.18 | 35.46 | 34.13 | 26.47 | 39.41 | 55.55 | 30.63 | 13.83 | 65.71 | 11.16 | 23.13 | 72.99 | 1.32 | 25.69 | |
| K011245 | 38.15 | 27.07 | 34.78 | 34.29 | 27.07 | 38.65 | 54.18 | 31.31 | 14.50 | 68.24 | 9.42 | 22.34 | 67.95 | 9.80 | 22.25 | |
| K011246 | 35.60 | 26.18 | 38.23 | 33.83 | 26.86 | 39.31 | 54.91 | 30.70 | 14.38 | 66.48 | 11.35 | 22.17 | 64.75 | 13.66 | 21.59 | |
| K0112426 | 38.27 | 21.80 | 39.93 | 32.70 | 25.43 | 41.87 | 61.46 | 25.52 | 13.02 | 79.57 | 13.44 | 6.99 | 66.20 | 27.98 | 5.82 | |
| K0112427 | 41.58 | 17.46 | 40.96 | 31.62 | 24.54 | 43.84 | 60.34 | 27.07 | 12.58 | 82.10 | 13.26 | 4.64 | 60.44 | 36.15 | 3.42 | |
| K011247 | 29.50 | 19.10 | 51.40 | 28.13 | 23.54 | 48.33 | 58.57 | 32.22 | 9.20 | 76.33 | 14.38 | 9.29 | 75.95 | 14.80 | 9.25 | |
| K011248 | 33.98 | 19.10 | 46.91 | 26.64 | 27.46 | 45.91 | 59.58 | 32.96 | 7.45 | 77.24 | 16.71 | 6.05 | 77.45 | 16.47 | 6.07 | |
| K011249 | 15.01 | 20.66 | 64.32 | 22.87 | 34.03 | 43.10 | 54.57 | 36.70 | 8.73 | 75.23 | 18.45 | 6.31 | 83.36 | 9.64 | 7.00 | |
| K011250 | 11.36 | 19.98 | 68.66 | 21.42 | 34.89 | 43.68 | 54.71 | 36.76 | 8.52 | 74.11 | 19.90 | 5.99 | 84.97 | 8.16 | 6.87 | |
| K0112428 | 12.16 | 18.46 | 69.38 | 22.35 | 35.78 | 41.87 | 55.12 | 35.21 | 9.66 | 75.61 | 19.49 | 4.90 | 53.60 | 42.92 | 3.47 | |
| K011251 | 12.08 | 20.33 | 67.60 | 21.79 | 34.74 | 43.48 | 55.04 | 36.04 | 8.92 | 74.69 | 19.34 | 5.97 | 86.18 | 6.93 | 6.88 | |
| K0112429 | 36.01 | 27.18 | 36.81 | 25.50 | 31.66 | 42.84 | 55.06 | 32.98 | 11.95 | 77.89 | 13.63 | 8.48 | 87.83 | 2.61 | 9.56 | |
| K011252 | 26.10 | 24.60 | 49.30 | 28.66 | 26.76 | 44.58 | 64.88 | 25.10 | 10.02 | 77.74 | 14.57 | 7.69 | 81.32 | 10.63 | 8.04 | |
| K011253 | 35.47 | 25.29 | 39.23 | 33.38 | 27.76 | 38.85 | 59.02 | 27.56 | 13.43 | 68.29 | 11.76 | 19.95 | 76.20 | 1.54 | 22.27 | |
| K011254 | 35.65 | 25.62 | 38.73 | 34.25 | 26.80 | 38.95 | 56.24 | 29.69 | 14.07 | 66.73 | 11.17 | 22.10 | 67.20 | 10.55 | 22.26 | |
| K0112451 | 35.91 | 28.75 | 35.33 | 35.89 | 25.49 | 38.62 | 79.38 | 15.06 | 5.55 | 87.31 | 3.68 | 9.01 | 87.37 | 3.62 | 9.01 | |
| K0112452 | 36.14 | 28.58 | 35.27 | 35.65 | 25.85 | 38.50 | 81.64 | 12.99 | 5.38 | 90.98 | 4.04 | 4.98 | 86.06 | 7.11 | 4.82 | |
| K0112453 | 34.60 | 28.69 | 36.71 | 35.60 | 25.85 | 38.55 | 83.81 | 11.55 | 4.64 | 92.74 | 3.48 | 3.78 | 89.31 | 7.05 | 3.64 | |
| K0112454 | 34.24 | 30.40 | 35.36 | 35.54 | 25.97 | 38.49 | 76.52 | 17.53 | 5.94 | 85.24 | 2.93 | 11.84 | 84.06 | 4.26 | 11.67 | |
| K0112455 | 34.55 | 29.11 | 36.34 | 35.20 | 26.10 | 38.70 | 81.14 | 13.95 | 4.91 | 89.81 | 3.30 | 6.89 | 86.21 | 7.18 | 6.61 | |
| K0112456 | 36.39 | 27.87 | 35.74 | 35.38 | 25.94 | 38.68 | 80.57 | 14.20 | 5.23 | 91.60 | 3.46 | 4.95 | 86.44 | 8.89 | 4.67 | |
| K0112457 | 36.11 | 28.13 | 35.76 | 35.32 | 25.99 | 38.68 | 79.30 | 15.12 | 5.58 | 87.30 | 3.56 | 9.14 | 82.67 | 8.67 | 8.65 | |
| K0112458 | 36.84 | 27.98 | 35.18 | 35.35 | 26.02 | 38.63 | 84.46 | 10.77 | 4.77 | 94.21 | 3.40 | 2.39 | 88.48 | 9.27 | 2.24 | |
| K0112459 | 34.91 | 28.98 | 36.10 | 35.31 | 25.97 | 38.72 | 82.19 | 12.93 | 4.88 | 92.01 | 3.18 | 4.81 | 88.96 | 6.39 | 4.65 | |

(continued on next page)

Molecular geochemical data (IV): Ternary systems I (continued)

| Sample ID | Steranes | | | Methylphenanthrenes | | | Methyl dibenzothiophenes | | | | C ₁ Phen-C ₁ DBF-C ₁ DBT | | | C ₁ Phen-C ₁ Carb-C ₁ DBT | | |
|-----------|---------------------------------|---------------------------------|---------------------------------|---------------------|-------------|---------------|--------------------------|--------------|------------|-------------------------|---|------------------------|-------------------------|--|------------------------|--|
| | C ₂₇ αβ Steranes [%] | C ₂₈ αβ Steranes [%] | C ₂₉ αβ Steranes [%] | 9-MPhen [%] | 1-MPhen [%] | 2+3-MPhen [%] | 4-MDBT [%] | 2+3-MDBT [%] | 1-MDBT [%] | C ₁ Phen [%] | C ₁ DBF [%] | C ₁ DBT [%] | C ₁ Phen [%] | C ₁ Carb [%] | C ₁ DBT [%] | |
| K012460 | 35.58 | 29.04 | 35.39 | 35.44 | 26.02 | 38.54 | 81.72 | 13.45 | 4.84 | 90.62 | 3.21 | 6.18 | 84.05 | 10.22 | 5.73 | |
| K012461 | 35.58 | 29.18 | 35.25 | 34.94 | 26.38 | 38.67 | 76.14 | 18.11 | 5.74 | 83.48 | 3.25 | 13.27 | 85.25 | 1.20 | 13.55 | |
| K012462 | 34.97 | 29.62 | 35.41 | 35.06 | 26.03 | 38.90 | 81.19 | 14.02 | 4.80 | 89.34 | 3.06 | 7.60 | 84.51 | 8.31 | 7.19 | |
| K012463 | 36.76 | 28.25 | 34.99 | 35.15 | 26.02 | 38.83 | 81.58 | 13.52 | 4.90 | 91.41 | 3.08 | 5.51 | 86.41 | 8.38 | 5.21 | |
| K012464 | 37.07 | 28.13 | 34.81 | 35.03 | 26.29 | 38.68 | 82.61 | 12.61 | 4.78 | 91.04 | 3.50 | 5.45 | 79.27 | 15.98 | 4.75 | |
| K012465 | 35.36 | 28.10 | 36.54 | 35.13 | 25.85 | 39.01 | 79.51 | 14.86 | 5.63 | 92.82 | 3.48 | 3.70 | 86.06 | 10.51 | 3.43 | |
| K012466 | 36.02 | 28.70 | 35.28 | 35.08 | 26.17 | 38.75 | 81.43 | 12.51 | 6.06 | 95.00 | 3.40 | 1.60 | 87.25 | 11.28 | 1.47 | |
| K012467 | 35.85 | 28.64 | 35.51 | 35.13 | 26.31 | 38.56 | 82.57 | 12.75 | 4.68 | 90.54 | 3.02 | 6.44 | 81.78 | 12.40 | 5.82 | |
| K012468 | 37.95 | 28.73 | 33.32 | 36.11 | 26.13 | 38.76 | 76.61 | 17.78 | 5.61 | 84.27 | 3.25 | 12.48 | 84.50 | 2.99 | 12.51 | |
| K012469 | 35.32 | 29.80 | 34.88 | 36.41 | 25.98 | 37.61 | 75.92 | 17.06 | 7.02 | 88.02 | 4.31 | 7.67 | 88.46 | 3.84 | 7.70 | |
| K012470 | 35.64 | 29.93 | 34.43 | 35.48 | 26.19 | 38.33 | 78.43 | 15.38 | 6.19 | 91.11 | 3.83 | 5.06 | 89.31 | 5.73 | 4.96 | |
| K012471 | 37.01 | 29.35 | 33.64 | 34.90 | 25.96 | 39.13 | 78.24 | 16.59 | 5.17 | 85.71 | 3.08 | 11.21 | 83.59 | 5.47 | 10.93 | |
| K012472 | 36.44 | 30.02 | 33.54 | 34.91 | 26.05 | 39.04 | 81.14 | 13.98 | 4.87 | 88.83 | 3.53 | 7.64 | 83.08 | 9.78 | 7.15 | |
| K012473 | 36.24 | 28.94 | 34.82 | 35.09 | 26.25 | 38.66 | 76.84 | 17.64 | 5.52 | 84.06 | 3.23 | 12.71 | 85.41 | 1.67 | 12.91 | |
| K012474 | 37.88 | 28.00 | 34.12 | 35.06 | 26.16 | 38.78 | 76.95 | 17.61 | 5.44 | 84.66 | 3.16 | 12.18 | 84.77 | 3.03 | 12.91 | |
| K012475 | 37.77 | 28.36 | 33.88 | 35.11 | 26.33 | 38.57 | 76.40 | 17.99 | 5.61 | 83.85 | 3.18 | 12.97 | 85.28 | 1.52 | 13.20 | |
| K012476 | 36.64 | 28.72 | 34.63 | 34.96 | 26.13 | 38.91 | 78.59 | 16.18 | 5.22 | 86.40 | 3.06 | 10.54 | 83.15 | 6.70 | 10.14 | |
| K01212 | 35.45 | 28.96 | 35.58 | 35.42 | 26.82 | 37.75 | 54.85 | 27.91 | 17.24 | 71.25 | 5.71 | 23.04 | 74.83 | 0.98 | 24.20 | |
| K011213 | 35.70 | 27.89 | 36.40 | 34.98 | 26.07 | 38.95 | 54.21 | 28.89 | 16.90 | 68.85 | 7.05 | 24.10 | 73.55 | 0.70 | 25.75 | |
| K011214 | 35.60 | 28.11 | 36.29 | 35.81 | 25.89 | 38.29 | 55.27 | 28.40 | 16.33 | 68.65 | 6.79 | 24.56 | 73.39 | 0.34 | 26.26 | |
| K011215 | 35.63 | 28.53 | 35.84 | 35.77 | 25.80 | 36.73 | 55.02 | 28.70 | 16.28 | 72.45 | 3.30 | 24.26 | 74.43 | 0.66 | 24.92 | |
| K011216 | 35.33 | 28.83 | 35.83 | 34.76 | 25.76 | 39.48 | 53.64 | 29.45 | 16.91 | 69.55 | 5.91 | 24.53 | 73.53 | 0.53 | 25.94 | |
| K011217 | 35.91 | 28.47 | 35.62 | 35.92 | 27.26 | 36.82 | 51.14 | 31.20 | 17.66 | 73.76 | 4.28 | 21.96 | 76.63 | 0.55 | 22.82 | |
| K011218 | 36.16 | 28.31 | 35.53 | 34.17 | 26.14 | 39.70 | 54.45 | 28.87 | 16.68 | 69.11 | 7.92 | 22.97 | 74.05 | 1.33 | 24.62 | |
| K011219 | 35.46 | 28.29 | 36.25 | 34.24 | 26.32 | 39.44 | 57.00 | 26.52 | 16.48 | 65.88 | 15.16 | 18.96 | 74.57 | 3.97 | 21.46 | |
| K011220 | 35.41 | 28.19 | 36.40 | 34.28 | 25.47 | 40.25 | 54.64 | 28.59 | 16.77 | 63.50 | 14.10 | 22.40 | 73.56 | 0.49 | 25.94 | |
| K011221 | 35.18 | 31.23 | 33.59 | 36.94 | 27.64 | 35.42 | 31.81 | 22.41 | 45.79 | 43.40 | 27.60 | 29.00 | 56.65 | 5.50 | 37.86 | |
| K011222 | 37.86 | 27.25 | 34.89 | 37.80 | 25.18 | 37.02 | 21.58 | 17.76 | 60.65 | 48.02 | 12.07 | 39.91 | 42.84 | 21.56 | 35.60 | |
| K011223 | 37.74 | 30.16 | 32.09 | 39.78 | 25.51 | 34.72 | 20.11 | 16.58 | 63.30 | 47.99 | 12.17 | 39.83 | 45.71 | 16.35 | 37.94 | |
| K011224 | 39.37 | 27.30 | 33.33 | 40.92 | 25.74 | 33.33 | 20.94 | 17.01 | 62.05 | 48.64 | 9.87 | 41.49 | 46.23 | 14.34 | 39.43 | |
| K011225 | 38.36 | 25.82 | 35.82 | 41.00 | 24.44 | 34.56 | 25.44 | 20.14 | 54.42 | 49.63 | 12.75 | 37.62 | 48.98 | 13.89 | 37.13 | |
| K011226 | 36.78 | 28.94 | 34.28 | 40.04 | 24.70 | 35.25 | 24.21 | 19.25 | 56.54 | 53.21 | 12.79 | 34.00 | 51.21 | 16.06 | 32.73 | |
| K011227 | 35.45 | 32.55 | 32.00 | 40.43 | 25.23 | 34.34 | 24.17 | 17.00 | 58.84 | 56.85 | 12.99 | 30.16 | 44.57 | 31.78 | 23.64 | |
| K011199 | 38.49 | 31.24 | 30.27 | 42.37 | 24.26 | 33.38 | 25.16 | 19.96 | 54.89 | 54.15 | 13.68 | 32.17 | 55.60 | 11.37 | 33.03 | |
| K011200 | 36.29 | 27.39 | 36.32 | 44.43 | 23.06 | 32.51 | 25.74 | 20.69 | 53.57 | 56.03 | 13.67 | 30.30 | 62.14 | 4.25 | 33.60 | |
| K011201 | 37.73 | 26.36 | 35.91 | 45.21 | 23.26 | 31.53 | 25.60 | 20.74 | 53.66 | 54.47 | 14.25 | 31.28 | 60.41 | 4.90 | 34.69 | |
| K011202 | 35.10 | 31.38 | 33.52 | 44.55 | 23.63 | 31.82 | 26.28 | 19.85 | 53.87 | 55.40 | 14.64 | 29.96 | 58.36 | 10.08 | 31.56 | |
| K011203 | 36.93 | 27.72 | 35.35 | 44.75 | 24.02 | 31.23 | 26.37 | 21.35 | 52.28 | 51.49 | 17.10 | 31.41 | 58.52 | 5.79 | 35.69 | |
| K011204 | 37.39 | 27.79 | 34.81 | 42.67 | 24.27 | 33.06 | 28.68 | 19.68 | 51.63 | 54.96 | 17.61 | 27.43 | 55.30 | 17.11 | 27.59 | |
| K011205 | 38.56 | 28.28 | 33.16 | 43.23 | 24.05 | 32.72 | 28.73 | 19.39 | 51.88 | 53.47 | 19.00 | 27.53 | 56.30 | 14.71 | 28.99 | |
| K011206 | 38.77 | 26.43 | 34.80 | 43.27 | 24.09 | 32.65 | 27.79 | 20.01 | 52.20 | 55.89 | 14.30 | 29.81 | 57.50 | 11.84 | 30.66 | |

(continued on next page)

Molecular geochemical data (IV): Ternary systems I (continued)

| Sample ID | Steranes | | | Methylphenanthrenes | | | Methyl dibenzothiophenes | | | C ₁ Phen - C ₁ DBF - C ₁ DBT | | | C ₁ Phen - C ₁ Carb - C ₁ DBT | | |
|-----------|------------------------------------|------------------------------------|------------------------------------|---------------------|----------------|------------------|--------------------------|-----------------|---------------|---|---------------------------|---------------------------|--|----------------------------|---------------------------|
| | C ₂₇ αβ Steranes [%] | C ₂₈ αβ Steranes [%] | C ₂₉ αβ Steranes [%] | 9-MPhen [%] | 1-MPhen [%] | 2+3-MPhen [%] | 4-MDBT [%] | 2+3-MDBT [%] | 1-MDBT [%] | C ₁ Phen [%] | C ₁ DBF [%] | C ₁ DBT [%] | C ₁ Phen [%] | C ₁ Carb [%] | C ₁ DBT [%] |
| K011207 | 36.61 | 27.46 | 35.93 | 44.20 | 23.94 | 31.86 | 26.33 | 20.28 | 53.39 | 51.48 | 16.54 | 31.98 | 57.74 | 6.40 | 35.86 |
| K011208 | 37.19 | 26.27 | 36.54 | 40.79 | 22.66 | 36.55 | 22.70 | 20.59 | 56.71 | 50.65 | 14.15 | 35.20 | 55.92 | 5.21 | 38.86 |
| K011209 | 37.82 | 26.28 | 35.90 | 43.34 | 22.32 | 34.34 | 23.26 | 21.96 | 54.78 | 52.04 | 12.21 | 35.75 | 55.23 | 6.83 | 37.94 |
| K011210 | 36.73 | 29.23 | 34.04 | 41.99 | 23.52 | 34.49 | 24.02 | 20.81 | 55.17 | 50.81 | 14.14 | 35.06 | 55.70 | 5.87 | 38.43 |
| K011211 | 38.82 | 25.78 | 35.40 | 43.59 | 24.52 | 31.89 | 24.82 | 20.92 | 54.26 | 48.61 | 17.49 | 33.90 | 55.74 | 5.38 | 38.88 |
| K012477 | 34.21 | 29.14 | 36.65 | 34.20 | 28.33 | 37.47 | 33.77 | 17.92 | 48.31 | 67.92 | 14.11 | 17.97 | 61.94 | 21.67 | 16.39 |
| K012478 | 36.89 | 29.09 | 34.01 | 36.54 | 27.12 | 36.34 | 28.40 | 21.43 | 50.17 | 60.36 | 10.13 | 29.51 | 63.10 | 6.05 | 30.85 |
| K012479 | 33.14 | 33.07 | 33.78 | 37.89 | 26.66 | 35.45 | 29.36 | 19.85 | 50.79 | 63.51 | 9.97 | 26.52 | 56.11 | 20.46 | 23.43 |
| K012480 | 34.95 | 32.51 | 32.54 | 38.21 | 26.58 | 35.20 | 28.47 | 20.51 | 51.02 | 60.14 | 9.80 | 30.06 | 61.63 | 7.56 | 30.81 |
| K012481 | 35.32 | 30.79 | 33.89 | 37.05 | 27.08 | 35.88 | 29.26 | 19.88 | 50.86 | 62.77 | 10.26 | 26.98 | 60.00 | 14.21 | 25.79 |
| K012482 | 49.33 | 23.86 | 26.81 | 33.78 | 26.94 | 39.28 | 38.32 | 18.06 | 43.63 | 69.43 | 16.95 | 13.62 | 73.61 | 11.94 | 14.44 |

| Sample ID | | Methylidibenzofurans | | | | | | | | | | Methylcarbazoles | | | Dimethylcarbazoles | | | | Benzocarbazoles | | |
|-----------|-------|----------------------------|---------------------------|---------------------------|---------------|-----------------|---------------|----------------|------------------|----------------|-------------------------|-------------------------|-------------------------|---------------------|---------------------|---------------------|----------------------------|---------------------------|---------------------------|--|--|
| | | C ₁ Carb [%] | C ₁ DBF [%] | C ₁ DBT [%] | 4-MDBT [%] | 2+3-MDBT [%] | 1-MDBT [%] | 1-MCarb [%] | 3+2-MCarb [%] | 4-MCarb [%] | 1,8-Dimethylcarb [%] | 2,7-Dimethylcarb [%] | 1,3-Dimethylcarb [%] | Benzo[a]carb [%] | Benzo[b]carb [%] | Benzo[c]carb [%] | C ₁ Carb [%] | C ₁ DBF [%] | C ₁ DBT [%] | | |
| K011188 | 5.28 | 19.46 | 75.26 | 43.35 | 30.77 | 25.88 | 73.00 | 20.31 | 6.69 | 73.47 | 5.28 | 21.25 | 60.00 | 2.84 | 37.16 | | | | | | |
| K011189 | 11.76 | 28.79 | 59.45 | 34.59 | 35.80 | 29.61 | 52.80 | 30.11 | 17.09 | 57.72 | 10.12 | 32.16 | 47.92 | 3.04 | 49.05 | | | | | | |
| K011190 | 8.38 | 34.34 | 57.28 | 39.05 | 30.79 | 30.16 | 56.65 | 27.98 | 15.37 | 61.69 | 7.14 | 31.17 | 46.33 | 1.29 | 52.38 | | | | | | |
| K012302 | 19.85 | 27.71 | 52.44 | 37.46 | 33.32 | 29.22 | 53.36 | 29.89 | 16.74 | 48.78 | 16.69 | 34.54 | 54.29 | 2.42 | 43.29 | | | | | | |
| K011191 | 9.70 | 34.14 | 56.16 | 39.93 | 31.65 | 28.42 | 54.86 | 29.38 | 15.76 | 56.54 | 12.87 | 30.59 | 53.04 | 2.68 | 44.28 | | | | | | |
| K011192 | 13.96 | 31.75 | 54.30 | 36.52 | 32.64 | 30.85 | 56.33 | 27.88 | 15.79 | 57.27 | 9.66 | 33.08 | 53.71 | 2.52 | 43.77 | | | | | | |
| K011193 | 13.61 | 31.77 | 54.63 | 35.73 | 33.80 | 30.48 | 61.03 | 23.90 | 15.07 | 52.35 | 16.00 | 31.65 | 55.27 | 1.65 | 43.08 | | | | | | |
| K011194 | 8.75 | 34.43 | 56.82 | 40.33 | 31.26 | 28.41 | 73.74 | 17.55 | 8.70 | 56.75 | 9.53 | 33.71 | 54.69 | 1.10 | 44.22 | | | | | | |
| K011195 | 11.56 | 32.57 | 55.87 | 38.59 | 31.92 | 29.49 | 54.04 | 30.37 | 15.60 | 55.17 | 13.02 | 31.81 | 51.38 | 2.08 | 46.53 | | | | | | |
| K011196 | 17.00 | 16.04 | 66.96 | 42.15 | 32.04 | 25.81 | 66.82 | 21.43 | 11.75 | 54.15 | 10.44 | 35.42 | 53.85 | 3.89 | 42.26 | | | | | | |
| K012303 | 23.98 | 10.34 | 65.69 | 34.90 | 36.93 | 28.17 | 72.10 | 18.26 | 9.64 | 59.46 | 6.24 | 34.30 | 51.35 | 4.26 | 44.39 | | | | | | |
| K011197 | 23.88 | 13.46 | 62.66 | 39.85 | 34.14 | 26.01 | 70.32 | 19.07 | 10.62 | 54.83 | 8.21 | 36.96 | 55.90 | 3.40 | 40.70 | | | | | | |
| K012304 | 5.14 | 33.49 | 61.37 | 37.72 | 33.28 | 29.00 | 47.68 | 36.43 | 15.89 | 50.36 | 18.68 | 30.95 | 44.71 | 1.97 | 53.32 | | | | | | |
| K012305 | 4.91 | 31.33 | 63.77 | 36.66 | 34.74 | 28.60 | 42.67 | 38.17 | 19.16 | 45.90 | 19.75 | 34.35 | 45.16 | 2.88 | 51.96 | | | | | | |
| K012430 | 5.93 | 19.49 | 74.58 | 34.73 | 35.98 | 29.29 | 65.37 | 21.97 | 12.67 | 59.55 | 10.79 | 29.66 | 44.19 | 2.31 | 53.50 | | | | | | |
| K012306 | 31.32 | 9.68 | 59.00 | 36.69 | 37.08 | 26.23 | 70.06 | 19.66 | 10.28 | 57.03 | 5.53 | 37.43 | 54.22 | 3.95 | 41.83 | | | | | | |
| K011198 | 36.48 | 13.95 | 49.57 | 41.67 | 25.56 | 32.77 | 65.42 | 21.35 | 13.23 | 56.89 | 9.92 | 33.19 | 57.20 | 2.22 | 40.58 | | | | | | |
| K012431 | 8.26 | 36.23 | 55.51 | 37.34 | 33.99 | 28.67 | 55.21 | 30.89 | 13.90 | 55.61 | 9.72 | 34.68 | 32.40 | 0.87 | 66.72 | | | | | | |
| K012432 | 18.54 | 32.88 | 48.58 | 37.45 | 34.02 | 28.53 | 57.68 | 29.16 | 13.16 | 56.88 | 10.55 | 32.57 | 42.07 | 0.76 | 57.17 | | | | | | |
| K012433 | 13.90 | 34.53 | 51.58 | 37.38 | 34.00 | 28.62 | 63.90 | 24.98 | 11.12 | 58.76 | 8.24 | 33.01 | 44.20 | 0.79 | 55.01 | | | | | | |
| K012434 | 8.25 | 36.04 | 55.71 | 37.31 | 34.06 | 28.64 | 57.30 | 29.71 | 13.00 | 56.77 | 10.02 | 33.21 | 43.38 | 0.94 | 55.68 | | | | | | |
| K012435 | 10.48 | 35.25 | 54.27 | 36.70 | 34.71 | 28.60 | 55.64 | 29.59 | 14.76 | 53.13 | 14.85 | 32.03 | 49.16 | 1.05 | 49.79 | | | | | | |
| K012436 | 9.69 | 37.43 | 52.88 | 37.31 | 34.36 | 28.33 | 54.81 | 30.06 | 15.13 | 55.35 | 11.93 | 32.72 | 45.23 | 1.09 | 53.68 | | | | | | |
| K012437 | 4.73 | 32.56 | 62.71 | 36.79 | 35.23 | 27.98 | 62.48 | 24.82 | 12.70 | 51.43 | 14.20 | 34.37 | 44.23 | 3.11 | 52.65 | | | | | | |
| K012438 | 10.83 | 35.80 | 53.38 | 37.25 | 34.33 | 28.42 | 57.59 | 28.53 | 13.88 | 54.05 | 12.86 | 33.08 | 47.72 | 1.18 | 51.10 | | | | | | |
| K012439 | 10.33 | 35.20 | 54.47 | 37.33 | 34.35 | 28.32 | 53.80 | 31.98 | 14.22 | 54.95 | 14.78 | 30.27 | 48.55 | 1.61 | 49.84 | | | | | | |
| K012440 | 22.93 | 31.49 | 45.57 | 37.09 | 34.25 | 28.66 | 49.18 | 34.66 | 16.16 | 50.17 | 18.67 | 31.16 | 45.30 | 1.39 | 53.31 | | | | | | |
| K012441 | 5.34 | 23.00 | 71.67 | 36.13 | 35.38 | 28.48 | 70.79 | 19.25 | 9.96 | 46.55 | 13.23 | 40.22 | 42.06 | 5.37 | 52.57 | | | | | | |
| K012442 | 4.03 | 22.85 | 73.12 | 35.28 | 36.30 | 28.43 | 63.11 | 24.67 | 12.22 | 49.80 | 13.31 | 36.90 | 40.59 | 6.37 | 53.04 | | | | | | |
| K012443 | 4.95 | 21.60 | 73.45 | 35.09 | 35.98 | 28.93 | 60.37 | 25.83 | 13.80 | 53.58 | 12.27 | 34.15 | 37.52 | 7.01 | 55.47 | | | | | | |
| K012444 | 11.66 | 18.17 | 70.17 | 35.72 | 35.90 | 28.39 | 66.50 | 21.67 | 11.83 | 51.86 | 11.00 | 37.14 | 43.46 | 3.55 | 52.99 | | | | | | |
| K012445 | 14.34 | 34.33 | 51.33 | 36.80 | 34.91 | 28.29 | 65.36 | 21.42 | 13.22 | 55.59 | 11.29 | 33.12 | 51.95 | 2.33 | 45.71 | | | | | | |
| K012446 | 29.51 | 28.61 | 41.88 | 37.23 | 33.78 | 28.98 | 54.63 | 28.69 | 16.67 | 51.68 | 17.76 | 30.56 | 52.39 | 2.82 | 44.79 | | | | | | |
| K012447 | 23.16 | 30.66 | 46.19 | 37.01 | 34.23 | 28.76 | 55.83 | 27.75 | 16.43 | 52.19 | 17.87 | 29.93 | 52.91 | 2.43 | 44.66 | | | | | | |
| K012448 | 39.57 | 24.54 | 35.89 | 36.94 | 34.39 | 28.67 | 53.72 | 30.06 | 16.23 | 51.12 | 18.94 | 29.94 | 52.03 | 2.62 | 45.36 | | | | | | |
| K012449 | 37.52 | 25.33 | 37.15 | 36.97 | 34.07 | 28.97 | 55.20 | 28.40 | 16.40 | 51.01 | 19.08 | 29.91 | 52.40 | 2.66 | 44.94 | | | | | | |
| K012450 | 43.78 | 23.48 | 32.74 | 37.07 | 33.98 | 28.95 | 55.55 | 28.14 | 16.31 | 51.83 | 18.60 | 29.57 | 52.76 | 2.50 | 44.74 | | | | | | |
| K011228 | 17.14 | 18.76 | 64.09 | 38.26 | 35.07 | 26.67 | 51.93 | 26.90 | 21.16 | 57.07 | 9.64 | 33.28 | 55.07 | 6.82 | 38.12 | | | | | | |
| K011229 | 21.72 | 11.70 | 66.59 | 37.17 | 37.49 | 25.34 | 48.90 | 28.46 | 22.64 | 49.94 | 16.39 | 33.67 | 54.62 | 5.10 | 40.28 | | | | | | |
| K011230 | 14.48 | 17.14 | 68.38 | 37.79 | 33.49 | 28.72 | 47.58 | 29.64 | 22.78 | 52.47 | 14.59 | 32.94 | 54.43 | 5.36 | 40.21 | | | | | | |
| K011231 | 19.85 | 23.01 | 57.14 | 39.53 | 31.85 | 28.63 | 58.96 | 24.67 | 16.37 | 56.36 | 9.36 | 34.28 | 48.82 | 2.36 | 48.82 | | | | | | |

(continued on next page)

Molecular geochemical data (IV): Ternary systems II (continued)

| Sample ID | C ₁ Carb - C ₁ DBF - C ₁ DBT | | | Methylidibenzofurans | | | Methylcarbazoles | | | 1,8-, 2,7-, 1,3-Dimethylcarbazole | | | Benzocarbazoles | | |
|-----------|---|------------------------|------------------------|----------------------|--------------|------------|------------------|---------------|-------------|-----------------------------------|----------------------|----------------------|------------------|------------------|------------------|
| | C ₁ Carb [%] | C ₁ DBF [%] | C ₁ DBT [%] | 4-MDBT [%] | 2+3-MDBT [%] | 1-MDBT [%] | 1-MCarb [%] | 3+2-MCarb [%] | 4-MCarb [%] | 1,8-Dimethylcarb [%] | 2,7-Dimethylcarb [%] | 1,3-Dimethylcarb [%] | Benzo[a]carb [%] | Benzo[b]carb [%] | Benzo[c]carb [%] |
| K011232 | 33.80 | 19.91 | 46.29 | 39.94 | 31.35 | 28.71 | 47.32 | 30.09 | 22.59 | 47.17 | 14.85 | 37.98 | 55.12 | 4.54 | 40.34 |
| K011233 | 40.17 | 21.18 | 38.65 | 39.71 | 31.38 | 28.91 | 45.72 | 31.02 | 23.26 | 44.12 | 20.58 | 35.30 | 55.40 | 4.97 | 39.63 |
| K012421 | 43.25 | 17.52 | 39.22 | 41.03 | 30.93 | 28.04 | 44.98 | 30.47 | 24.55 | 41.05 | 29.16 | 29.79 | 55.08 | 2.47 | 42.45 |
| K012422 | 55.24 | 12.57 | 32.19 | 40.60 | 31.56 | 27.85 | 54.06 | 26.40 | 19.55 | 43.80 | 23.02 | 33.18 | 55.98 | 2.79 | 41.22 |
| K011234 | 24.63 | 13.38 | 61.99 | 38.66 | 35.85 | 25.49 | 65.68 | 20.79 | 13.53 | 40.67 | 10.16 | 49.17 | 53.93 | 2.80 | 43.26 |
| K012423 | 33.44 | 14.02 | 52.55 | 41.87 | 33.16 | 24.97 | 54.77 | 26.10 | 19.13 | 39.56 | 20.71 | 39.73 | 56.40 | 2.68 | 40.93 |
| K012424 | 54.77 | 11.92 | 33.30 | 40.36 | 31.86 | 27.78 | 52.49 | 28.47 | 19.04 | 44.83 | 23.35 | 31.81 | 53.23 | 2.89 | 43.88 |
| K011235 | 28.61 | 18.83 | 52.57 | 38.80 | 34.40 | 26.80 | 58.07 | 24.78 | 17.15 | 42.27 | 13.88 | 43.85 | 51.34 | 3.15 | 45.51 |
| K011236 | 31.09 | 22.06 | 46.85 | 40.57 | 32.34 | 27.09 | 55.71 | 26.56 | 17.43 | 49.94 | 17.44 | 32.61 | 53.57 | 3.23 | 43.20 |
| K011237 | 35.95 | 13.37 | 50.69 | 39.12 | 34.89 | 26.00 | 56.36 | 25.20 | 18.44 | 49.93 | 19.13 | 41.84 | 54.86 | 2.96 | 42.18 |
| K011238 | 5.45 | 26.22 | 68.33 | 39.69 | 31.90 | 28.40 | 57.33 | 26.12 | 16.55 | 57.81 | 10.46 | 31.73 | 50.55 | 2.72 | 46.73 |
| K011239 | 28.31 | 16.43 | 55.26 | 37.89 | 37.65 | 24.46 | 53.16 | 27.13 | 19.71 | 48.04 | 13.01 | 38.95 | 47.67 | 4.82 | 47.51 |
| K012425 | 51.73 | 45.66 | 2.61 | 34.29 | 47.67 | 18.04 | 46.85 | 40.44 | 12.70 | 39.27 | 26.18 | 34.55 | 42.64 | 19.51 | 37.86 |
| K011240 | 10.35 | 82.98 | 6.68 | 33.73 | 47.53 | 18.74 | 49.71 | 40.56 | 9.73 | 48.65 | 16.76 | 34.60 | 44.78 | 24.78 | 30.44 |
| K011241 | 16.12 | 76.04 | 7.84 | 34.71 | 45.33 | 19.96 | 47.12 | 39.52 | 13.36 | 45.13 | 13.59 | 41.28 | 44.15 | 15.87 | 36.97 |
| K011242 | 30.31 | 38.38 | 31.31 | 34.25 | 45.10 | 20.66 | 43.64 | 38.66 | 17.69 | 44.32 | 18.34 | 37.33 | 55.65 | 11.48 | 32.87 |
| K011243 | 9.27 | 33.92 | 56.81 | 36.09 | 40.33 | 23.58 | 53.30 | 25.52 | 21.18 | 52.81 | 12.71 | 34.48 | 54.35 | 5.30 | 40.35 |
| K011244 | 3.35 | 31.46 | 65.19 | 36.40 | 39.41 | 24.19 | 50.31 | 36.18 | 13.51 | 63.89 | 6.40 | 29.70 | 34.00 | 7.97 | 58.04 |
| K011245 | 23.66 | 22.63 | 53.70 | 35.99 | 39.13 | 24.88 | 62.31 | 22.00 | 15.69 | 60.87 | 7.06 | 32.07 | 60.05 | 3.97 | 35.98 |
| K011246 | 29.50 | 23.87 | 46.63 | 36.66 | 38.67 | 24.87 | 59.64 | 23.26 | 17.10 | 56.97 | 13.11 | 29.92 | 61.27 | 3.26 | 35.47 |
| K012426 | 62.21 | 24.86 | 12.94 | 36.17 | 38.59 | 25.24 | 48.88 | 27.42 | 23.70 | 46.04 | 22.86 | 31.10 | 57.75 | 4.58 | 37.68 |
| K012427 | 73.28 | 19.79 | 6.93 | 35.60 | 38.45 | 25.95 | 48.33 | 28.10 | 23.57 | 43.59 | 25.61 | 30.80 | 58.74 | 5.65 | 35.61 |
| K011247 | 38.58 | 37.31 | 24.11 | 33.64 | 39.80 | 26.56 | 40.98 | 34.63 | 24.39 | 44.63 | 22.58 | 32.79 | 57.07 | 9.02 | 33.91 |
| K011248 | 41.92 | 42.63 | 15.45 | 33.22 | 39.94 | 26.84 | 43.56 | 32.21 | 24.23 | 48.52 | 14.72 | 36.75 | 55.22 | 8.25 | 36.53 |
| K011249 | 26.00 | 55.13 | 18.86 | 33.30 | 41.65 | 25.05 | 46.36 | 36.78 | 16.87 | 46.94 | 11.47 | 41.59 | 48.97 | 12.55 | 38.49 |
| K011250 | 21.56 | 60.28 | 18.16 | 33.11 | 42.26 | 24.63 | 47.45 | 38.81 | 13.74 | 46.27 | 11.55 | 42.17 | 48.71 | 13.94 | 37.35 |
| K012428 | 71.29 | 22.94 | 5.77 | 34.18 | 40.97 | 24.86 | 49.78 | 37.42 | 12.80 | 41.37 | 20.30 | 38.33 | 46.70 | 14.66 | 38.64 |
| K011251 | 19.19 | 61.76 | 19.05 | 33.11 | 41.89 | 25.00 | 47.72 | 37.89 | 14.39 | 48.06 | 11.77 | 40.17 | 47.55 | 14.06 | 38.40 |
| K012429 | 9.48 | 55.79 | 34.73 | 34.31 | 42.38 | 23.32 | 59.42 | 26.28 | 14.31 | 49.80 | 14.10 | 36.10 | 53.16 | 6.01 | 40.83 |
| K011252 | 31.35 | 44.93 | 23.71 | 33.99 | 39.14 | 26.88 | 46.31 | 30.73 | 22.95 | 46.37 | 19.95 | 33.67 | 59.38 | 6.65 | 33.97 |
| K011253 | 4.17 | 35.53 | 60.30 | 36.76 | 36.97 | 26.27 | 51.39 | 26.91 | 21.70 | 44.36 | 26.28 | 29.36 | 62.64 | 4.99 | 32.37 |
| K011254 | 23.94 | 25.53 | 50.53 | 37.60 | 36.70 | 25.70 | 55.38 | 24.84 | 19.78 | 51.85 | 12.09 | 36.07 | 64.66 | 3.22 | 32.12 |
| K012451 | 22.19 | 22.57 | 55.24 | 41.80 | 22.87 | 35.33 | 66.51 | 20.00 | 13.49 | 72.07 | 8.16 | 19.76 | 55.56 | 0.73 | 43.71 |
| K012452 | 44.88 | 24.69 | 30.44 | 41.40 | 24.66 | 33.94 | 59.13 | 22.27 | 18.60 | 63.81 | 8.02 | 28.16 | 61.11 | 1.09 | 37.80 |
| K012453 | 50.21 | 23.86 | 25.93 | 40.94 | 22.03 | 37.03 | 60.58 | 21.54 | 17.88 | 64.24 | 11.66 | 24.10 | 59.69 | 1.09 | 39.21 |
| K012454 | 22.65 | 15.34 | 62.01 | 40.85 | 22.23 | 36.92 | 64.55 | 19.66 | 15.79 | 69.78 | 8.33 | 21.89 | 54.97 | 0.80 | 44.23 |
| K012455 | 42.33 | 18.69 | 38.99 | 40.73 | 22.19 | 37.08 | 59.20 | 22.30 | 18.50 | 63.26 | 11.04 | 25.70 | 60.14 | 1.06 | 38.81 |
| K012456 | 52.86 | 19.40 | 27.75 | 40.96 | 22.05 | 36.99 | 62.15 | 20.87 | 16.98 | 71.06 | 8.56 | 20.38 | 59.47 | 0.86 | 39.67 |
| K012457 | 41.89 | 16.30 | 41.80 | 40.68 | 25.20 | 34.12 | 61.68 | 20.45 | 17.87 | 61.38 | 14.53 | 24.09 | 59.96 | 0.81 | 39.24 |
| K012458 | 63.04 | 21.71 | 15.25 | 41.29 | 21.75 | 36.97 | 64.04 | 19.26 | 16.70 | 64.06 | 10.97 | 24.97 | 59.73 | 0.68 | 39.59 |
| K012459 | 45.26 | 21.76 | 32.98 | 40.66 | 21.30 | 38.04 | 63.78 | 19.42 | 16.80 | 63.94 | 14.98 | 21.08 | 60.01 | 0.81 | 39.18 |

(continued on next page)

Molecular geochemical data (IV): Ternary systems II (continued)

| Sample ID | C ₁ Carb - C ₁ DBF - C ₁ DBT | | | Methylidibenzofurans | | | Methylcarbazoles | | | 1,8-, 2,7-, 1,3-Dimethylcarbazole | | | | Benzocarbazoles | | |
|-----------|---|------------------------|------------------------|----------------------|--------------|------------|------------------|---------------|-------------|-----------------------------------|----------------------|----------------------|------------------|------------------|------------------|--|
| | C ₁ Carb [%] | C ₁ DBF [%] | C ₁ DBT [%] | 4-MDBT [%] | 2+3-MDBT [%] | 1-MDBT [%] | 1-MCarb [%] | 3+2-MCarb [%] | 4-MCarb [%] | 1,8-Dimethylcarb [%] | 2,7-Dimethylcarb [%] | 1,3-Dimethylcarb [%] | Benzo[a]carb [%] | Benzo[b]carb [%] | Benzo[c]carb [%] | |
| K012460 | 54.01 | 15.72 | 30.27 | 40.59 | 21.56 | 37.85 | 61.13 | 21.29 | 17.57 | 62.79 | 12.16 | 25.05 | 60.05 | 0.82 | 39.13 | |
| K012461 | 6.65 | 18.38 | 74.98 | 41.23 | 22.31 | 36.45 | 35.73 | 42.35 | 21.93 | 33.60 | 19.91 | 46.49 | 27.71 | 2.40 | 69.89 | |
| K012462 | 45.18 | 15.74 | 39.08 | 40.44 | 21.88 | 37.67 | 61.40 | 20.83 | 17.77 | 68.02 | 9.73 | 22.25 | 59.76 | 0.89 | 39.35 | |
| K012463 | 50.76 | 17.64 | 31.59 | 40.41 | 21.28 | 38.31 | 58.44 | 22.42 | 19.14 | 60.70 | 13.58 | 25.71 | 60.05 | 0.97 | 38.99 | |
| K012464 | 67.19 | 12.84 | 19.97 | 40.42 | 22.17 | 37.41 | 57.69 | 22.42 | 19.90 | 62.77 | 11.19 | 26.04 | 63.74 | 0.80 | 35.46 | |
| K012465 | 61.25 | 18.77 | 19.99 | 41.05 | 22.76 | 36.19 | 60.56 | 21.52 | 17.92 | 59.62 | 11.32 | 29.06 | 61.32 | 1.07 | 37.62 | |
| K012466 | 71.06 | 19.68 | 9.26 | 40.60 | 21.78 | 37.62 | 59.15 | 21.49 | 19.36 | 61.30 | 10.83 | 27.87 | 61.04 | 0.97 | 37.98 | |
| K012467 | 59.21 | 13.00 | 27.79 | 39.88 | 21.80 | 36.33 | 55.34 | 23.36 | 21.30 | 62.13 | 10.72 | 27.15 | 61.07 | 1.09 | 37.84 | |
| K012468 | 15.94 | 17.38 | 66.68 | 41.12 | 22.73 | 36.15 | 47.49 | 33.07 | 19.45 | 64.87 | 12.10 | 23.03 | 48.04 | 0.48 | 51.48 | |
| K012469 | 24.18 | 27.30 | 48.52 | 41.89 | 28.68 | 29.43 | 61.35 | 20.87 | 17.78 | 60.34 | 9.33 | 30.32 | 59.37 | 1.21 | 39.42 | |
| K012470 | 39.67 | 26.00 | 34.33 | 41.47 | 25.09 | 33.44 | 59.11 | 21.96 | 18.93 | 63.40 | 7.85 | 28.75 | 61.09 | 0.90 | 38.01 | |
| K012471 | 28.20 | 15.47 | 56.33 | 40.97 | 21.59 | 37.45 | 64.48 | 21.20 | 14.33 | 68.39 | 11.42 | 20.19 | 53.00 | 0.70 | 46.29 | |
| K012472 | 48.34 | 16.33 | 35.33 | 40.99 | 22.46 | 36.55 | 61.19 | 20.71 | 18.10 | 67.59 | 9.16 | 23.24 | 59.34 | 0.97 | 39.69 | |
| K012473 | 9.36 | 18.39 | 72.26 | 41.29 | 22.48 | 36.23 | 36.59 | 41.41 | 22.00 | 51.02 | 15.95 | 33.04 | 41.03 | 0.84 | 58.13 | |
| K012474 | 16.46 | 17.19 | 66.35 | 41.06 | 22.03 | 36.91 | 57.39 | 26.65 | 15.96 | 68.68 | 7.30 | 24.02 | 48.95 | 0.76 | 50.29 | |
| K012475 | 8.48 | 18.02 | 73.51 | 41.14 | 22.19 | 36.67 | 41.89 | 37.22 | 20.90 | 41.31 | 20.72 | 37.98 | 34.98 | 1.21 | 63.82 | |
| K012476 | 33.87 | 14.88 | 51.25 | 40.06 | 22.29 | 37.65 | 61.47 | 20.74 | 17.79 | 66.87 | 12.68 | 20.45 | 53.19 | 0.95 | 45.86 | |
| K011212 | 3.13 | 19.25 | 77.62 | 38.87 | 36.43 | 24.70 | 56.91 | 36.18 | 6.91 | 51.10 | 9.52 | 39.37 | - | - | - | |
| K011213 | 2.07 | 22.15 | 75.78 | 39.85 | 35.77 | 24.38 | 68.91 | 21.99 | 9.10 | 65.27 | 7.92 | 26.81 | - | - | - | |
| K011214 | 1.02 | 21.44 | 77.54 | 38.21 | 36.05 | 25.74 | 58.09 | 35.65 | 6.26 | 47.48 | 5.41 | 47.12 | - | - | - | |
| K011215 | 2.27 | 11.70 | 86.04 | 39.12 | 34.99 | 25.89 | 61.00 | 25.29 | 13.72 | 54.39 | 3.60 | 42.01 | - | - | - | |
| K011216 | 1.62 | 19.11 | 79.27 | 38.51 | 36.38 | 25.11 | 62.24 | 28.92 | 8.84 | 55.04 | 7.15 | 37.81 | - | - | - | |
| K011217 | 1.98 | 15.98 | 82.04 | 39.15 | 36.30 | 24.55 | 60.46 | 29.08 | 10.46 | 55.57 | 6.91 | 37.53 | - | - | - | |
| K011218 | 3.86 | 24.65 | 71.49 | 39.52 | 36.40 | 24.08 | 59.65 | 28.80 | 11.54 | 52.44 | 11.31 | 36.24 | - | - | - | |
| K011219 | 9.32 | 40.28 | 50.40 | 42.39 | 33.98 | 23.63 | 61.36 | 27.66 | 10.98 | 56.99 | 8.27 | 34.74 | 52.96 | 3.49 | 43.56 | |
| K011220 | 1.16 | 38.19 | 60.66 | 39.34 | 35.90 | 24.75 | 40.53 | 45.17 | 14.30 | 48.65 | 6.93 | 44.42 | 48.15 | 4.41 | 47.43 | |
| K011221 | 6.92 | 45.39 | 47.69 | 41.63 | 31.72 | 26.65 | 60.84 | 26.45 | 12.72 | 44.40 | 8.83 | 46.77 | 52.43 | 1.42 | 46.15 | |
| K011222 | 31.73 | 15.85 | 52.41 | 36.59 | 35.02 | 28.39 | 60.23 | 25.60 | 14.17 | 40.85 | 12.70 | 46.45 | 49.95 | 1.48 | 48.57 | |
| K011223 | 24.82 | 17.60 | 57.58 | 35.55 | 33.46 | 30.99 | 55.52 | 27.15 | 17.32 | 41.69 | 10.87 | 47.44 | 50.02 | 3.01 | 46.97 | |
| K011224 | 22.71 | 14.85 | 62.44 | 34.85 | 34.51 | 30.64 | 62.63 | 21.99 | 15.39 | 45.73 | 11.63 | 42.63 | 45.18 | 1.31 | 53.51 | |
| K011225 | 21.84 | 19.79 | 58.37 | 35.29 | 33.07 | 31.64 | 59.49 | 24.88 | 15.63 | 41.35 | 13.33 | 45.32 | 48.43 | 1.67 | 49.90 | |
| K011226 | 26.28 | 20.15 | 53.57 | 33.81 | 35.62 | 30.82 | 61.46 | 22.72 | 15.82 | 40.29 | 13.59 | 46.13 | 49.12 | 1.24 | 49.64 | |
| K011227 | 48.44 | 15.52 | 36.04 | 35.67 | 35.48 | 28.85 | 51.50 | 29.09 | 19.40 | 37.33 | 18.81 | 43.86 | 48.84 | 3.48 | 47.68 | |
| K011199 | 19.46 | 24.04 | 56.51 | 35.93 | 33.58 | 30.49 | 56.73 | 25.58 | 15.69 | 39.83 | 18.65 | 41.52 | 49.51 | 2.45 | 48.04 | |
| K011200 | 8.02 | 28.60 | 63.38 | 37.41 | 33.57 | 29.02 | 55.08 | 28.85 | 16.08 | 40.10 | 15.88 | 44.02 | 40.06 | 1.42 | 58.53 | |
| K011201 | 8.85 | 28.53 | 62.62 | 37.97 | 32.20 | 29.84 | 57.97 | 25.89 | 16.14 | 41.23 | 9.02 | 49.75 | 35.99 | 1.23 | 62.78 | |
| K011202 | 17.67 | 27.02 | 55.31 | 40.40 | 32.06 | 27.55 | 59.39 | 23.76 | 16.86 | 41.75 | 10.45 | 47.80 | 37.28 | 1.58 | 61.14 | |
| K011203 | 9.50 | 31.90 | 58.59 | 39.34 | 32.09 | 28.57 | 56.97 | 26.63 | 16.39 | 38.88 | 13.10 | 48.02 | 36.87 | 1.37 | 61.76 | |
| K011204 | 27.41 | 28.39 | 44.20 | 40.09 | 30.82 | 29.09 | 48.96 | 30.85 | 20.18 | 38.77 | 16.06 | 45.18 | 40.90 | 3.79 | 55.31 | |
| K011205 | 23.09 | 31.40 | 45.50 | 40.57 | 31.41 | 28.02 | 49.76 | 31.20 | 19.04 | 41.69 | 13.59 | 44.72 | 40.77 | 3.53 | 55.70 | |
| K011206 | 20.70 | 25.71 | 53.59 | 38.45 | 31.83 | 29.72 | 51.75 | 30.01 | 18.24 | 40.07 | 11.39 | 48.54 | 43.91 | 2.65 | 53.44 | |

(continued on next page)

Molecular geochemical data (IV): Ternary systems II (continued)

| Sample ID | C ₁ Carb - C ₁ DBF - C ₁ DBT | | | Methylidibenzofurans | | | Methylcarbazoles | | | 1,8-, 2,7-, 1,3-Dimethylcarbazole | | | | Benzocarbazoles | | |
|-----------|---|------------------------|------------------------|----------------------|--------------|------------|------------------|---------------|-------------|-----------------------------------|----------------------|----------------------|------------------|------------------|------------------|--|
| | C ₁ Carb [%] | C ₁ DBF [%] | C ₁ DBT [%] | 4-MDBT [%] | 2+3-MDBT [%] | 1-MDBT [%] | 1-MCarb [%] | 3+2-MCarb [%] | 4-MCarb [%] | 1,8-Dimethylcarb [%] | 2,7-Dimethylcarb [%] | 1,3-Dimethylcarb [%] | Benzo[a]carb [%] | Benzo[b]carb [%] | Benzo[c]carb [%] | |
| K011207 | 10.53 | 30.49 | 58.98 | 37.66 | 32.36 | 29.98 | 54.41 | 28.03 | 17.56 | 39.26 | 14.19 | 46.55 | 36.92 | 1.21 | 61.87 | |
| K011208 | 8.73 | 26.16 | 65.11 | 40.31 | 31.63 | 28.06 | 55.82 | 27.73 | 16.46 | 43.41 | 12.23 | 44.36 | 37.38 | 0.71 | 61.92 | |
| K011209 | 11.82 | 22.45 | 65.72 | 38.95 | 31.55 | 29.49 | 53.69 | 28.71 | 17.60 | 39.01 | 18.42 | 42.57 | 41.97 | 1.05 | 56.98 | |
| K011210 | 9.81 | 25.92 | 64.27 | 43.92 | 31.12 | 24.96 | 59.11 | 24.86 | 16.03 | 43.22 | 10.58 | 46.20 | 42.52 | 0.98 | 56.50 | |
| K011211 | 8.36 | 31.19 | 60.45 | 39.59 | 32.05 | 28.36 | 65.92 | 20.25 | 13.83 | 41.98 | 13.73 | 44.30 | 39.92 | 0.85 | 59.23 | |
| K012477 | 42.56 | 25.27 | 32.17 | 38.46 | 35.24 | 26.30 | 54.86 | 30.77 | 14.37 | 40.93 | 16.47 | 42.61 | 53.95 | 2.62 | 43.43 | |
| K012478 | 12.73 | 22.31 | 64.96 | 37.59 | 34.75 | 27.66 | 46.59 | 37.31 | 16.10 | 43.80 | 12.63 | 43.56 | 49.74 | 2.46 | 47.80 | |
| K012479 | 38.83 | 16.71 | 44.46 | 37.38 | 34.27 | 28.35 | 51.64 | 33.48 | 14.88 | 44.47 | 12.79 | 42.74 | 51.82 | 3.23 | 44.95 | |
| K012480 | 15.62 | 20.74 | 63.63 | 38.08 | 33.90 | 28.02 | 45.77 | 38.26 | 15.97 | 43.12 | 17.82 | 39.06 | 48.70 | 2.05 | 49.25 | |
| K012481 | 28.54 | 19.69 | 51.77 | 37.66 | 33.80 | 28.54 | 53.16 | 32.32 | 14.52 | 45.10 | 13.08 | 41.83 | 51.04 | 2.94 | 46.01 | |
| K012482 | 26.93 | 40.52 | 32.55 | 40.69 | 34.54 | 24.77 | 40.17 | 42.69 | 17.15 | 41.24 | 12.13 | 46.63 | 48.26 | 4.17 | 47.57 | |

Appendix

Appendix: (2) Analytics overview

Analytics overview

| Sample ID | CNS | Rock-Eval | Solvent extraction | SPE separation | GC-MS saturates | GC-MS aromatics | GC-MS carbazoles | Molecular sieving |
|-----------|-----|-----------|--------------------|----------------|-----------------|-----------------|------------------|-------------------|
| K011188 | ✓ | ✓ | ✓ | ✓ | ✓ | ✓ | ✓ | ✓ |
| K011189 | ✓ | ✓ | ✓ | ✓ | ✓ | ✓ | ✓ | X |
| K011190 | ✓ | ✓ | ✓ | ✓ | ✓ | ✓ | ✓ | X |
| K012302 | ✓ | ✓ | ✓ | ✓ | ✓ | ✓ | ✓ | X |
| K011191 | ✓ | ✓ | ✓ | ✓ | ✓ | ✓ | ✓ | X |
| K011192 | ✓ | ✓ | ✓ | ✓ | ✓ | ✓ | ✓ | X |
| K011193 | ✓ | ✓ | ✓ | ✓ | ✓ | ✓ | ✓ | ✓ |
| K011194 | ✓ | ✓ | ✓ | ✓ | ✓ | ✓ | ✓ | X |
| K011195 | ✓ | ✓ | ✓ | ✓ | ✓ | ✓ | ✓ | X |
| K011196 | ✓ | ✓ | ✓ | ✓ | ✓ | ✓ | ✓ | X |
| K012303 | ✓ | ✓ | ✓ | ✓ | ✓ | ✓ | ✓ | X |
| K011197 | ✓ | ✓ | ✓ | ✓ | ✓ | ✓ | ✓ | X |
| K012304 | ✓ | ✓ | ✓ | ✓ | ✓ | ✓ | ✓ | X |
| K012305 | ✓ | ✓ | ✓ | ✓ | ✓ | ✓ | ✓ | X |
| K012430 | ✓ | ✓ | ✓ | ✓ | ✓ | ✓ | ✓ | X |
| K012306 | ✓ | ✓ | ✓ | ✓ | ✓ | ✓ | ✓ | X |
| K011198 | ✓ | ✓ | ✓ | ✓ | ✓ | ✓ | ✓ | X |
| K012431 | ✓ | ✓ | ✓ | ✓ | ✓ | ✓ | ✓ | X |
| K012432 | ✓ | ✓ | ✓ | ✓ | ✓ | ✓ | ✓ | X |
| K012433 | ✓ | ✓ | ✓ | ✓ | ✓ | ✓ | ✓ | X |
| K012434 | ✓ | ✓ | ✓ | ✓ | ✓ | ✓ | ✓ | X |
| K012435 | ✓ | ✓ | ✓ | ✓ | ✓ | ✓ | ✓ | X |
| K012436 | ✓ | ✓ | ✓ | ✓ | ✓ | ✓ | ✓ | X |
| K012437 | ✓ | ✓ | ✓ | ✓ | ✓ | ✓ | ✓ | X |
| K012438 | ✓ | ✓ | ✓ | ✓ | ✓ | ✓ | ✓ | X |
| K012439 | ✓ | ✓ | ✓ | ✓ | ✓ | ✓ | ✓ | X |
| K012440 | ✓ | ✓ | ✓ | ✓ | ✓ | ✓ | ✓ | X |
| K012441 | ✓ | ✓ | ✓ | ✓ | ✓ | ✓ | ✓ | X |
| K012442 | ✓ | ✓ | ✓ | ✓ | ✓ | ✓ | ✓ | X |
| K012443 | ✓ | ✓ | ✓ | ✓ | ✓ | ✓ | ✓ | X |
| K012444 | ✓ | ✓ | ✓ | ✓ | ✓ | ✓ | ✓ | X |
| K012445 | ✓ | ✓ | ✓ | ✓ | ✓ | ✓ | ✓ | X |
| K012446 | ✓ | ✓ | ✓ | ✓ | ✓ | ✓ | ✓ | X |
| K012447 | ✓ | ✓ | ✓ | ✓ | ✓ | ✓ | ✓ | X |
| K012448 | ✓ | ✓ | ✓ | ✓ | ✓ | ✓ | ✓ | X |
| K012449 | ✓ | ✓ | ✓ | ✓ | ✓ | ✓ | ✓ | X |
| K012450 | ✓ | ✓ | ✓ | ✓ | ✓ | ✓ | ✓ | X |
| K011228 | ✓ | ✓ | ✓ | ✓ | ✓ | ✓ | ✓ | X |
| K011229 | ✓ | ✓ | ✓ | ✓ | ✓ | ✓ | ✓ | X |
| K011230 | ✓ | ✓ | ✓ | ✓ | ✓ | ✓ | ✓ | X |
| K011231 | ✓ | ✓ | ✓ | ✓ | ✓ | ✓ | ✓ | ✓ |
| K011232 | ✓ | ✓ | ✓ | ✓ | ✓ | ✓ | ✓ | X |
| K011233 | ✓ | ✓ | ✓ | ✓ | ✓ | ✓ | ✓ | X |
| K012421 | ✓ | ✓ | ✓ | ✓ | ✓ | ✓ | ✓ | X |
| K012422 | ✓ | ✓ | ✓ | ✓ | ✓ | ✓ | ✓ | X |
| K011234 | ✓ | ✓ | ✓ | ✓ | ✓ | ✓ | ✓ | ✓ |
| K012423 | ✓ | ✓ | ✓ | ✓ | ✓ | ✓ | ✓ | X |
| K012424 | ✓ | ✓ | ✓ | ✓ | ✓ | ✓ | ✓ | X |
| K011235 | ✓ | ✓ | ✓ | ✓ | ✓ | ✓ | ✓ | X |
| K011236 | ✓ | ✓ | ✓ | ✓ | ✓ | ✓ | ✓ | X |
| K011237 | ✓ | ✓ | ✓ | ✓ | ✓ | ✓ | ✓ | X |
| K011238 | ✓ | ✓ | ✓ | ✓ | ✓ | ✓ | ✓ | X |
| K011239 | ✓ | ✓ | ✓ | ✓ | ✓ | ✓ | ✓ | X |
| K012425 | ✓ | ✓ | ✓ | ✓ | ✓ | ✓ | ✓ | X |
| K011240 | ✓ | ✓ | ✓ | ✓ | ✓ | ✓ | ✓ | X |
| K011241 | ✓ | ✓ | ✓ | ✓ | ✓ | ✓ | ✓ | X |
| K011242 | ✓ | ✓ | ✓ | ✓ | ✓ | ✓ | ✓ | X |
| K011243 | ✓ | ✓ | ✓ | ✓ | ✓ | ✓ | ✓ | X |
| K011244 | ✓ | ✓ | ✓ | ✓ | ✓ | ✓ | ✓ | ✓ |
| K011245 | ✓ | ✓ | ✓ | ✓ | ✓ | ✓ | ✓ | X |
| K011246 | ✓ | ✓ | ✓ | ✓ | ✓ | ✓ | ✓ | X |
| K012426 | ✓ | ✓ | ✓ | ✓ | ✓ | ✓ | ✓ | X |
| K012427 | ✓ | ✓ | ✓ | ✓ | ✓ | ✓ | ✓ | X |
| K011247 | ✓ | ✓ | ✓ | ✓ | ✓ | ✓ | ✓ | X |
| K011248 | ✓ | ✓ | ✓ | ✓ | ✓ | ✓ | ✓ | X |
| K011249 | ✓ | ✓ | ✓ | ✓ | ✓ | ✓ | ✓ | X |
| K011250 | ✓ | ✓ | ✓ | ✓ | ✓ | ✓ | ✓ | X |

(continued on next page)

Appendix

Analytics overview (continued)

| Sample ID | CNS | Rock-Eval | Solvent extraction | SPE separation | GC-MS saturates | GC-MS aromatics | GC-MS carbazoles | Molecular sieving |
|-----------|-----|-----------|--------------------|----------------|-----------------|-----------------|------------------|-------------------|
| K012428 | ✓ | ✓ | ✓ | ✓ | ✓ | ✓ | ✓ | × |
| K011251 | ✓ | ✓ | ✓ | ✓ | ✓ | ✓ | ✓ | ✓ |
| K012429 | ✓ | ✓ | ✓ | ✓ | ✓ | ✓ | ✓ | × |
| K011252 | ✓ | ✓ | ✓ | ✓ | ✓ | ✓ | ✓ | × |
| K011253 | ✓ | ✓ | ✓ | ✓ | ✓ | ✓ | ✓ | × |
| K011254 | ✓ | ✓ | ✓ | ✓ | ✓ | ✓ | ✓ | × |
| K012451 | ✓ | ✓ | ✓ | ✓ | ✓ | ✓ | ✓ | × |
| K012452 | ✓ | ✓ | ✓ | ✓ | ✓ | ✓ | ✓ | × |
| K012453 | ✓ | ✓ | ✓ | ✓ | ✓ | ✓ | ✓ | × |
| K012454 | ✓ | ✓ | ✓ | ✓ | ✓ | ✓ | ✓ | × |
| K012455 | ✓ | ✓ | ✓ | ✓ | ✓ | ✓ | ✓ | ✓ |
| K012456 | ✓ | ✓ | ✓ | ✓ | ✓ | ✓ | ✓ | × |
| K012457 | ✓ | ✓ | ✓ | ✓ | ✓ | ✓ | ✓ | × |
| K012458 | ✓ | ✓ | ✓ | ✓ | ✓ | ✓ | ✓ | × |
| K012459 | ✓ | ✓ | ✓ | ✓ | ✓ | ✓ | ✓ | × |
| K012460 | ✓ | ✓ | ✓ | ✓ | ✓ | ✓ | ✓ | × |
| K012461 | ✓ | ✓ | ✓ | ✓ | ✓ | ✓ | ✓ | × |
| K012462 | ✓ | ✓ | ✓ | ✓ | ✓ | ✓ | ✓ | × |
| K012463 | ✓ | ✓ | ✓ | ✓ | ✓ | ✓ | ✓ | × |
| K012464 | ✓ | ✓ | ✓ | ✓ | ✓ | ✓ | ✓ | × |
| K012465 | ✓ | ✓ | ✓ | ✓ | ✓ | ✓ | ✓ | × |
| K012466 | ✓ | ✓ | ✓ | ✓ | ✓ | ✓ | ✓ | × |
| K012467 | ✓ | ✓ | ✓ | ✓ | ✓ | ✓ | ✓ | × |
| K012468 | ✓ | ✓ | ✓ | ✓ | ✓ | ✓ | ✓ | × |
| K012469 | ✓ | ✓ | ✓ | ✓ | ✓ | ✓ | ✓ | × |
| K012470 | ✓ | ✓ | ✓ | ✓ | ✓ | ✓ | ✓ | × |
| K012471 | ✓ | ✓ | ✓ | ✓ | ✓ | ✓ | ✓ | × |
| K012472 | ✓ | ✓ | ✓ | ✓ | ✓ | ✓ | ✓ | × |
| K012473 | ✓ | ✓ | ✓ | ✓ | ✓ | ✓ | ✓ | × |
| K012474 | ✓ | ✓ | ✓ | ✓ | ✓ | ✓ | ✓ | × |
| K012475 | ✓ | ✓ | ✓ | ✓ | ✓ | ✓ | ✓ | × |
| K012476 | ✓ | ✓ | ✓ | ✓ | ✓ | ✓ | ✓ | × |
| K011212 | ✓ | ✓ | ✓ | ✓ | ✓ | ✓ | ✓ | × |
| K011213 | ✓ | ✓ | ✓ | ✓ | ✓ | ✓ | ✓ | × |
| K011214 | ✓ | ✓ | ✓ | ✓ | ✓ | ✓ | ✓ | × |
| K011215 | ✓ | ✓ | ✓ | ✓ | ✓ | ✓ | ✓ | × |
| K011216 | ✓ | ✓ | ✓ | ✓ | ✓ | ✓ | ✓ | ✓ |
| K011217 | ✓ | ✓ | ✓ | ✓ | ✓ | ✓ | ✓ | × |
| K011218 | ✓ | ✓ | ✓ | ✓ | ✓ | ✓ | ✓ | × |
| K011219 | ✓ | ✓ | ✓ | ✓ | ✓ | ✓ | ✓ | × |
| K011220 | ✓ | ✓ | ✓ | ✓ | ✓ | ✓ | ✓ | × |
| K011221 | ✓ | ✓ | ✓ | ✓ | ✓ | ✓ | ✓ | × |
| K011222 | ✓ | ✓ | ✓ | ✓ | ✓ | ✓ | ✓ | × |
| K011223 | ✓ | ✓ | ✓ | ✓ | ✓ | ✓ | ✓ | × |
| K011224 | ✓ | ✓ | ✓ | ✓ | ✓ | ✓ | ✓ | × |
| K011225 | ✓ | ✓ | ✓ | ✓ | ✓ | ✓ | ✓ | × |
| K011226 | ✓ | ✓ | ✓ | ✓ | ✓ | ✓ | ✓ | × |
| K011227 | ✓ | ✓ | ✓ | ✓ | ✓ | ✓ | ✓ | × |
| K011199 | ✓ | ✓ | ✓ | ✓ | ✓ | ✓ | ✓ | × |
| K011200 | ✓ | ✓ | ✓ | ✓ | ✓ | ✓ | ✓ | × |
| K011201 | ✓ | ✓ | ✓ | ✓ | ✓ | ✓ | ✓ | × |
| K011202 | ✓ | ✓ | ✓ | ✓ | ✓ | ✓ | ✓ | × |
| K011203 | ✓ | ✓ | ✓ | ✓ | ✓ | ✓ | ✓ | × |
| K011204 | ✓ | ✓ | ✓ | ✓ | ✓ | ✓ | ✓ | × |
| K011205 | ✓ | ✓ | ✓ | ✓ | ✓ | ✓ | ✓ | × |
| K011206 | ✓ | ✓ | ✓ | ✓ | ✓ | ✓ | ✓ | × |
| K011207 | ✓ | ✓ | ✓ | ✓ | ✓ | ✓ | ✓ | × |
| K011208 | ✓ | ✓ | ✓ | ✓ | ✓ | ✓ | ✓ | × |
| K011209 | ✓ | ✓ | ✓ | ✓ | ✓ | ✓ | ✓ | × |
| K011210 | ✓ | ✓ | ✓ | ✓ | ✓ | ✓ | ✓ | × |
| K011211 | ✓ | ✓ | ✓ | ✓ | ✓ | ✓ | ✓ | × |
| K012477 | ✓ | ✓ | ✓ | ✓ | ✓ | ✓ | ✓ | × |
| K012478 | ✓ | ✓ | ✓ | ✓ | ✓ | ✓ | ✓ | × |
| K012479 | ✓ | ✓ | ✓ | ✓ | ✓ | ✓ | ✓ | × |
| K012480 | ✓ | ✓ | ✓ | ✓ | ✓ | ✓ | ✓ | × |
| K012481 | ✓ | ✓ | ✓ | ✓ | ✓ | ✓ | ✓ | × |
| K012482 | ✓ | ✓ | ✓ | ✓ | ✓ | ✓ | ✓ | × |

Eidesstattliche Erklärung

Eidesstattliche Erklärung

Nachname, Vorname(n): Panitz, Florian Maximilian

Adresse: Holtenauer Str. 64

PLZ, Ort: 24105, Kiel

Matrikelnummer: 5654

Hiermit versichere ich an Eides statt, dass ich die vorliegende Arbeit selbständig und ohne fremde Hilfe angefertigt und keine anderen als die angegebenen Quellen und Hilfsmittel verwendet habe. Alle wörtlich oder sinngemäß von anderen Autoren übernommen Abschnitte, auch solche aus dem Internet, wurden durch Zitate kenntlich gemacht. Weiterhin versichere ich, dass diese Dissertation noch nicht als Abschlussarbeit an anderer Stelle vorgelegen hat oder veröffentlicht wurde.

Die Arbeit wurde unter Einhaltung der Regeln guter wissenschaftlicher Praxis der Deutschen Forschungsgemeinschaft verfasst.

Mir wurde kein akademischer Grad entzogen.

Mir sind sowohl die Bedeutung dieser eidesstattlichen Erklärung, als auch die strafrechtlichen Konsequenzen einer unwahren eidesstattlichen Versicherung bekannt und bewusst.

Datum, Unterschrift